

PREDICTION OF HIGH IMPACT PRECIPITATION EVENTS
OVER BANGLADESH AND ITS SURROUNDING AREA USING
NWP MODELS

BY

MD. ABDULLAH ELIAS AKHTER

Roll No. 0555751

SESSION: July-2005



**A thesis submitted in partial fulfillment of the requirements
for the degree of Doctor of Philosophy in Physics**



**DEPARTMENT OF PHYSICS
KHULNA UNIVERSITY OF ENGINEERING & TECHNOLOGY
KHULNA, BANGLADESH**

MARCH 2012

Declaration

This is to certify that the thesis work entitled "*Prediction of High Impact Precipitation Events over Bangladesh and its surrounding areas using NWP Models*" has been carried out by *Md. Abdullah Elias Akhter* in the department of *Physics*, Khulna University of Engineering & Technology, Khulna, Bangladesh. The above research work or any part of this work has not been submitted anywhere for the award of any degree or diploma.



Signature of Supervisor
Name: *Dr. Md. Mahbub Alam*
Designation: *Professor*



Signature of Candidate
Name: *Md. Abdullah Elias Akhter*
Roll No: 0555751

Signature of Co-Supervisor
Name: *Dr. Mohammad Arif Hossain*
Designation: *Professor*

KHULNA UNIVERSITY OF ENGINEERING & TECHNOLOGY
DEPARTMENT OF PHYSICS

CERTIFICATION OF THESIS WORK

A THESIS ON


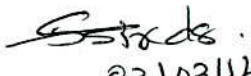


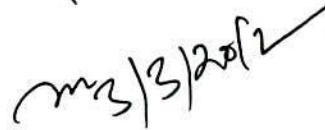
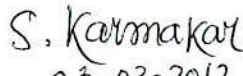
**Prediction of High Impact Precipitation Events over Bangladesh and its Surrounding Area
Using NWP Models**

By

Md. Abdullah Elias Akhter

has been accepted as satisfactory in partial fulfillment for the degree of Doctor of Philosophy in Physics and certify that the student has demonstrated a satisfactory knowledge in the field covered by his thesis in an oral examination held on March 03, 2012.

Board of Examiners

- | | | | |
|----|--|-------------------|---|
| 1. | Prof. Dr. Md. Mahbub Alam Department of Physics KUET, Khulna-9203 | Supervisor |  3/3/2012 |
| 2. | Prof. Dr. Mohammad Arif Hossain Department of Mathematics KUET, Khulna-9203 | Co-supervisor | |
| 3. | Head Department of Physics KUET, Khulna-9203 | Member |  03/03/12 |
| 4. | Prof. Dr. Shibendra Shekher Sikder Department of Physics KUET, Khulna-9203 | Member |  03/03/12 |
| 5. | Dr. D. A. Quadir CSO (Rtd), SPARSO Mohakas Biggyan Bhawan Agargaon, Sher - E - Bangla Nagar Dhaka - 1207 | Member |  |
| 6. | Prof. Dr. Md. Abdul Mannan Chowdhury Department of Physics Jahangir Nagar University Savar, Dhaka - 1207 | Member |  03/3/2012 |
| 7. | Dr. Samarendra Karmakar Director (Rtd), SAARC Meteorological Research Centre (SMRC) 63 Jafrabad, Dhaka - 1206, Bangladesh | Member (External) |  03-03-2012 |
| 8. | Dr. Madan Lall Shrestha Academician Nepal Academy of Science and Technology | Member (External) | |

DR. SAMARENDRA KARMAKAR
MSc., MS., Ph.D.

Former Director
Bangladesh Meteorological Department &
SAARC Meteorological Research Centre
Former Permanent Representative of Bangladesh with WMO
Former Faculty Member, BRAC University
Former Faculty Member, Galaxy Flying Academy Ltd.
Former Vice Principal, United College of Aviation, Science and Management
Cell: 01199065734, 01813583511

**Report on the examination
of the Ph. D. Thesis:**

**“Prediction of high impact precipitation events over Bangladesh and
its surrounding area using NWP models”**

**By
Abdullah Elias Akhter**

Comments:

The chapters presented in the **Ph. D. Thesis** are examined critically and the following comments are made:

1. Chapter 1: Introduction

Introduction is written in a well manner.

2. Chapter 2: Literature Review

A number of relevant literatures are reviewed in the thesis. The notation for the numbers should be same in all cases and better to give in superscripts form/or as per the University formats (if any).

3. Chapter 3: Methodology

Methodology has been discussed in a well manner. Physics of the two models, MM5 and WRF models are discussed critically. Different parameterization schemes have also been discussed and presented nicely.

4. Chapter 4: Simulation of heavy rainfall events using MM5 and WRF

Three heavy rainfall events have been studied with the help of two models MM5 and WRF. These are:

- (i) Heavy rainfall events of 1-3 July 2008
- (ii) Heavy rainfall events of 09-11 June 2007
- (iii) Heavy rainfall event of 1-3 May 2009

Two latest important Numerical Weather Prediction (NWP) models, MM5 and WRF, have been used to simulate a number of important different meteorological parameters. These parameters are mean sea level pressure, rain with vector wind, relative humidity with vector wind, and vertical structure of

vertical velocity, divergence, relative vorticity, relative humidity and mixing ratio along the centre of the most developed cloud.

The models MM5 and WRF have been able to capture well the above mentioned meteorological parameters with variability in spatial and temporal distributions. The results are shown in graphical forms with their horizontal and vertical distributions. It has been found that the model simulated parameters are favourable for the incidents of heavy rainfall in some parts of Bangladesh. The variability in intensity along with spatial and temporal distributions of the parameters depends on the resolution of the model, domains selection and use of initial data with its quality and source as well as the assimilation of local data. The assimilation of local data is cumbersome still now and the scientists are engaged to do this job.

In the present thesis, the author has simulated rainfall for 3 domains for different cases under the study. The results differ from domain to domain and from model to model, and also from case to case. However, both the models have well captured the heavy rainfall with difference in magnitudes.

Mr. Abdullah has nicely described the results and presented in a well manner.

5. Chapter 5: Simulation of Tropical Cyclone events using WRF and MM5 Model

The MM5 and WRF Models have been used to simulate a number of important different meteorological parameters associated with tropical cyclones Sidr, Aila and Rashmi those formed in the Bay of Bengal. These parameters are mean sea level pressure, rain with vector wind, relative humidity with vector wind, and vertical structures of vertical velocity, divergence, relative vorticity, relative humidity and mixing ratio along the centre of the most developed cloud, tracks of the cyclones, minimum central pressure, etc.

The parameters which are favourable for the genesis of tropical cyclones and their movement are well captured by the two models. But the magnitudes of the parameters differ from model to model, domain to domain and also vary from place to place. The wind speed associated with cyclone Sidr is simulated to be 60 m/s at 850 hPa level at 00 UTC on 15 November 2007. The central pressures and the tracks of the cyclones have also deviations.

The diagrams given in this chapter are well prepared and described. The vertical structure of mixing ratio, humidity, vorticity, and other parameters are presented in the diagrams and narrated nicely.

6. Chapter 6: Sensitivity tests

For the simulation of heavy precipitation events and tropical cyclone (TC) events, both of the models are run for 72 hours. Final Reanalysis (FNL) data ($1^0 \times 1^0$) from National Centre for Environment Prediction (NCEP) is used as initial and lateral boundary conditions (LBCs) which is updated at six hourly interval i.e. the model is initialized with 00, 06, 12 and 18 UTC initial field of corresponding date.

Two domains are considered: first one is mother domain and another one is nested domain inside the mother domain. Nested domain covers the Bangladesh region. Ratio of the resolution of the two domains is 3:1 respectively. The horizontal grid resolution of the mother domain is 90 km and nested domain is 30 km respectively.

It is found from the results that AK CP is better for daily rainfall prediction and KF2 is better for total rainfall prediction.

Simulated track are parallel to each other and they are deviated mainly in the longitudinal position. Landfall times are different for different RPS options and those are obtained earlier than those of the observed. Landfall times for the cyclones are found to vary by a few hours.

This chapter is also described nicely.

7. Chapter 7: Conclusions

The conclusions based on the present study are appropriate and presented in a well manner.

Remarks:

Based on the work presented in the thesis, Ph. D. Degree may be conferred upon Mr. Abdullah Elias Akhter.

S. Karmakar
16-01-2012

(Dr. Samarendra Karmakar)

Director (Retired)

Bangladesh Meteorological Department (BMD)

and

SAARC Meteorological Research Centre (SMRC)

Agargaon, Sher-E-Bangla Nagar, Dhaka – 1207

Present Address:

63, Jafrabad (2nd Floor)

Durga Mandir Gali, Shankar, Dhaka-1207



NEPAL ACADEMY OF SCIENCE & TECHNOLOGY

CENTRAL OFFICE

NAST

To,
Prof. Md. Toyebur Rahman,
Controller of Examinations
Khulna University of Engineering and Technology (KUET)
Khulna, BANGLADESH



Dear Sir,

First of all, I would like to appreciate for trusting me to be an examiner to evaluate the Ph. D. Thesis of Mr. Md. Abdullah Elias Akhter. The topic of the Thesis is very timely and important for country like Bangladesh, where many heavy impact weather systems affect every year. Such research will help to understand these weather phenomena and help to predict them so that proper management and prevention can be taken in time. The application of this research helps to minimize the loss of life and property and so helps in the developing process of the country.

After going through the Thesis, I found that the student worked satisfactorily on his thesis and so may be awarded the Ph. D. degree.

Regards,

Madan Lall Shrestha, Ph. D.
Academician
Nepal Academy of Science and Technology (NAST)
P. O. Box 19444
Kathmandu, NEPAL

Acknowledgements

Countless thanks to the Almighty Allah for his divine blessings to finish this job. First and foremost I would like to express my profound sense of sincere gratitude to my supervisor Professor Dr. Md. Mahbub Alam, Department of Physics, Khulna University of Engineering & Technology and my joint-supervisor Professor Dr. Mohammad Arif Hossain, Department of Mathematics, Khulna University of Engineering & Technology, for their continuous guidance, excellent cooperation, fruitful comments and suggestions and encouragement for the completion of the research work in proper and smooth way. I am very grateful to them for giving me the opportunity to carry out research under their constructive guidance, exact supervision, generous support, ceaseless effort and vast knowledge.

It is a matter of great pleasure for me to record the deepest sense of gratitude to Professor Dr. Shibendra Shekher Sikder, Head, Department of Physics, Khulna University of Engineering & Technology, who has given me a strong support in various ways during the entire period of my study in this department.

I am indebted to Prof. Dr. Md. Abdul Mannan Choudury, Department of Physics, Jahangirnagar University and Professor Dr. D. A. Quadir, Head of the Department of Physics, Uttara University who are also the Honourable Members of the Doctoral Scrunity Committee (DSC) for their constant help and suggestions in improving the thesis. Both of them were very kind to enquire about the progress of my work routinely and always advised and encourage me.

I gratefully acknowledge Mr. Md. Zaidur Rahman, Assistant Professor, Department of Mathematics, Khulna University of Engineering & Technology, for his cooperation regarding writing the thesis.

I wish to express my thanks to Dr. Jolly Sultana, Mr. Md. Kamrul Hasan Reza, and Mr. Asaduzzaman, Mr. Md. Mr. Torikul Islam, Mrs. Nipa Debnath and Mr. Sujit Kumer Shill, Department of Physics, Khulna University of Engineering & Technology, for their invaluable suggestions and inspiration during my study in this department.

My thanks are due to research staff of SMRC and Bangladesh Meteorological Department (BMD) for providing necessary data with other necessary help. Thanks are due to the Ministry of Science and Information & Communication Technology, Bangladesh for their financial grant in the form of project and fellowship.

Moreover, I am immensely grateful to my parents, my wife, my kids as well as all of my in-laws for their sacrifice, pure inspiration and providing me lots of time-wise supports during this period

I also wish to thank the authority of Khulna University of Engineering & Technology, for providing me with the necessary permission and financial assistance for conducting this thesis work.



DEDICATED
TO
MY PARENTS, WIFE AND KIDS

ABSTRACT

Bangladesh is a disaster prone country. Almost every year, the country experience disasters of one kind or another - such as tropical cyclones, storm surges, coastal erosion, floods due to heavy rainfall and droughts - causing heavy loss of life and property and jeopardizing the development activity. Because of south-westerly wind, high amount of moisture come to the Bangladesh region from the warm surface of the Bay of Bengal and heavy rainfall occurs by convection in our region. Tropical cyclone also forms over the warm oceans and ravage life and property especially over the coastal belt due to extremely strong winds and associate storm surges at the time of landfall. The Bay of Bengal is highly vulnerable to tropical cyclogenesis. To save the life and minimize the damage it is necessary to make advance warning and prediction of both the heavy rainfall and tropical cyclone quite ahead of time. Therefore a study has been conducted to investigate the formation and vertical structure of the heavy rainfall events and structure, intensity and track with landfall time of the tropical cyclone events.

In the present study, two state-of-the-art mesoscale models MM5 and WRF-ARW have been used to evaluate their performances in the simulation of heavy precipitation events and tropical cyclone (TC) and its impact on Bangladesh and its surrounding areas. Three test cases for the heavy rainfall events are considered and the cases are during 1-3 May 2009, 1-3 July 2008 and 9-14 June 2007. First one is the pre-monsoon seasonal case and last two are the monsoon seasonal test cases. On the other hand, three test cases for the TCs are considered and the cases are TC Aila, 23-27 May 2009; TC Sidr, 11-17 November 2007 and TC Rashmi, 24-28 October 2008.

For TC prediction, one nested domain is used inside the mother domain with horizontal resolution mothe and nested domain are 90 and 30 km respectively. On the other hand, for heavy rainfall events, two nested domains are used inside the mother domain with the resolution of mother domain is 90 km that for two nested domains are 30 and 10 km respectively.

For MM5 model, in this present study Medium Range Forecast (MRF) PBL scheme, Kain - Fritsch (KF) cumulus parameterization (CP) scheme, Dudhia Simple Ice microphysical Scheme for moisture anticipation, Cloud Radiation Schemes for radiation calculation and 5- Layer Soil model to predict soil temperature is used as model physics. Model equations in the surface flux form and solved on Arakawa B grid. Leapfrog time integration scheme with time splitting technique is used in model integration.

For WRF model, the modified Kain - Fritsch cumulus parameterization scheme, WRF Single-Moment (WSM) 3-class simple ice scheme, Transfer Model (RRTM) scheme, Dudhia scheme short wave scheme, Yonsei University Scheme (YSU) Planetary Boundary Layer (PBL) parameterization which is the next generation MRF-PBL is used as model physics..

For the heavy rainfall events Mean Seal Level Pressure (MSLP), wind with rain, wind with humidity, rainfall, vertical structure of vertical velocity, divergence, relative vorticity, relative humidity and mixing ratio have been simulated and analyzed to understand the convective activity of the precipitation system by both the models. Both of the models would simulate the convective activity of the precipitation events fairly well. Amount of precipitation are more than those of the observed by TRMM in monsoon and than pre-monsoon.

On the other hand, for the TC events MSLP, wind (vector, radial, tangential, vertical wind), vorticity, temperature anomaly, relative humidity, mixing ratio, rainfall and tracks have been analyzed to understand the structure and behavior of the cyclones by the models. Both the models would simulate the cyclonic nature at the lower and anti-cyclonic nature at the upper levels. Simulations of intensity are more or less than the observed but realistic to observed except for TC Sidr. Amount of precipitation are more than those of the observed by TRMM.

To understand the knowledge about the sensitivity of various physics options of the MM5 model, model was run for various sensitivity cases: sensitivity study on PBL with CP is both for heavy precipitation events and TC events, sensitivity study on microphysics, radiation are only for TC Aila.

In case of sensitivity on PBL with CP for heavy precipitation events, it is observed that some schemes have overestimated the rainfall and someone has underestimated that. The options for simulations of heavy rainfall events with MM5 have been found dependable on resolution and location of the area. According to our study, no single option may be considered as the most suitable among the 10 options for the assessment of rainfall over Bangladesh but it can be understood that AK CP is better for daily rainfall prediction and KF2 is better for total rainfall prediction. More case studies are necessary to make final commend for our region.

The PBL option with CP play very vital role on the track and intensity of TC. No one combination plays the best in the three TC cases but PBL MRF with KF CP plays better among the 10 combination in the three TC cases. Sensitivity test on microphysical parameterization option and radiation parameters options is done only for TC Aila. It is

seen that they have their own impact on the simulation of track and intensity of TC Aila. The present study has investigated only one cyclone, and more cases should be examined to supplement these results. It is suggested that it would be desirable to make sensitivity experiments with all possible combinations of the schemes of the physical processes. Other sensitivity tests like horizontal resolution, bogusging vortex may be done to improve the performance of the two models. Then the two models would be used as an operational purpose for the simulation of all kind of heavy precipitation events.

Table of content

| | | |
|---------|--|----|
| 1. | Introduction | |
| 1.1 | Introduction | 1 |
| 1.2 | Objective of our present research | 3 |
| 1.3 | Social and Economic benefit of the research work | 3 |
| 1.4 | Structure of the thesis | 4 |
| 2. | Literature review | |
| 2.1.1 | Numerical weather prediction model | 6 |
| 2.1.2 | Historical development of NWP | 7 |
| 2.2 | Description of MM5 Modeling System | 9 |
| 2.2.2 | Current Release | 11 |
| 2.2.3 | Features of the Modeling System | 11 |
| 2.2.4 | Program Functions | 13 |
| 2.2.5 | MM5 Model physics Options | 14 |
| 2.2.6 | Data and Model setup | 16 |
| 2.3 | Description of WRF model | 18 |
| 2.3.1 | Introduction | 19 |
| 2.3.2 | Advanced Research WRF | 20 |
| 2.3.3 | Major Features of the ARW System, Version 3 | 21 |
| 2.3.4 | Model Physics | 22 |
| 2.3.4.1 | Microphysics | 25 |
| 2.3.4.2 | Cumulus parameterization | 26 |
| 2.3.4.3 | Surface layer | 27 |
| 2.3.4.4 | Land-surface model | 28 |

| | | |
|-----------|---|----|
| 2.3.4.5 | Planetary boundary layer | 28 |
| 2.3.4.6 | Atmospheric radiation | 29 |
| 2.3.4.6.1 | Longwave radiation | 30 |
| 2.3.4.6.2 | Shortwave radiation | 31 |
| 2.4.1 | Formation of cloud | 32 |
| 2.4.2 | The different types of cloud in atmosphere | 33 |
| 2.4.3 | The classification of rainfall | 34 |
| 2.5.1 | Introduction on Tropical cyclone | 35 |
| 2.5.2 | Tropical Cyclone Formation | 36 |
| 2.5.2.1 | Climatological Conditions of Tropical Cyclone Formation | 37 |
| 2.5.2.2 | Large Scale Conditions associated with Tropical Cyclone Formation | 38 |
| 2.5.3 | Life Cycle of Tropical Cyclone | 39 |
| 2.5.4 | The Mature Cyclone | 40 |
| 2.5.4.1 | Pressure | 40 |
| 2.5.4.2 | Cloud Pattern | 40 |
| 2.5.4.3 | Wind fields | 40 |
| 2.5.4.4 | Precipitation | 41 |
| 2.5.4.5 | The eye of the cyclone | 41 |
| 2.5.5 | Cyclones of North Indian Ocean | 41 |
| 2.5.6 | Movement and track | 42 |
| 2.5.6.1 | Cyclone track prediction | 43 |
| 2.5.7 | Rainfall distribution around a tropical cyclone | 44 |
| 2.5.7.1 | Rainfall Measurement | 46 |
| 2.5.7.2 | Rainfall Analysis and Forecasting | 47 |
| 2.5.8 | Tropical Cyclone Speed | 48 |

| | | |
|---------|--|----|
| 2.5.8.1 | Direction of Tropical Cyclone Motion | 49 |
| 2.5.8.2 | Variability of Tropical Cyclone Motion | 49 |
| 2.5.9 | Tropical Cyclone Intensity | 50 |
| 2.5.10 | Tropical Cyclone Warning | 51 |
| 2.5.11 | Prevention | 51 |
| 2.6 | Previous studies on rainfall and tropical cyclones | 51 |
| | | |
| 3. | Methodology | 54 |
| 3.1. | Selection of Model | 54 |
| 3.2. | Experiments on simulation of events | 54 |
| 3.3. | Domain Model Physics | 54 |
| 3.3.1 | Domain set up | 54 |
| 3.3.2 | Model Physics | 55 |
| 3.3.2a | Model Physics for MM5 | 55 |
| 3.3.2b | Model Physics for WRF | 56 |
| 3.4 | Initial Data Source | 56 |
| 3.5. | Synoptic feature of the selected heavy rainfall | 57 |
| 3.5.1. | Heavy rainfall case 1 (1-3 July, 2008) | 57 |
| 3.5.2. | Heavy rainfall case 2 (9-11 June, 2007) | 57 |
| 3.5.3. | Heavy rainfall case 3 (1-3 May, 2009) | 57 |
| 3.6. | Synoptic feature of the selected tropical Cyclones (TC) | 57 |
| 3.6.1. | Severe cyclonic storm Aila (23-27 May 2009) | 57 |
| 3.6.2. | Super cyclone Sidr (11-16 November 2007) | 59 |
| 3.6.3. | Cyclonic storm Rashmi (24-28 October 2008) | 60 |
| 4.1 | Simulation of heavy rainfall events of 1-3 July 2008 using MM5 and WRF | 66 |
| 4.1.1 | Mean Sea Level Pressure | 66 |
| 4.1.2 | Study Rainfall with Wind | 66 |



| | | |
|-------|---|-----|
| 4.1.3 | Study Humidity with Wind | 77 |
| 4.1.4 | Validation of rainfall | 84 |
| 4.1.5 | Vertical profile of vertical velocity | 88 |
| 4.1.6 | Vertical profile of divergence | 89 |
| 4.1.7 | Vertical profile of vorticity | 90 |
| 4.1.8 | Vertical profile of relative humidity | 92 |
| 4.1.9 | Vertical profile of mixing ratio | 94 |
| 4.2 | Simulation of heavy rainfall events of 9-11 June 2007 using MM5 and WRF | 96 |
| 4.2.1 | Mean Sea Level Pressure | 96 |
| 4.2.2 | Study Rainfall with Wind | 96 |
| 4.2.3 | Study Humidity with Wind | 107 |
| 4.2.4 | Validation of rainfall | 114 |
| 4.2.5 | Vertical profile of vertical velocity | 119 |
| 4.2.6 | Vertical profile of divergence | 122 |
| 4.2.7 | Vertical profile of vorticity | 123 |
| 4.2.8 | Vertical profile of relative humidity | 125 |
| 4.2.9 | Vertical profile of mixing ratio | 126 |
| 4.3 | Simulation of heavy rainfall events of 1-3 May 2009 using MM5 and WRF | 129 |
| 4.3.1 | Mean Sea Level Pressure | 129 |
| 4.3.2 | Study Rainfall with Wind | 130 |
| 4.3.3 | Study Humidity with Wind | 141 |
| 4.3.4 | Validation of rainfall | 148 |
| 4.3.5 | Vertical profile of vertical velocity | 152 |

| | | |
|-------|---|-----|
| 4.3.6 | Vertical profile of divergence | 152 |
| 4.3.7 | Vertical profile of vorticity | 156 |
| 4.3.8 | Vertical profile of relative humidity | 158 |
| 4.3.9 | Vertical profile of mixing ratio | 160 |
| 4.4 | Summary of Rainfall Events | 164 |
| 5.1 | Simulation of Tropical Cyclone Sidr using MM5 and WRF Model | 166 |
| 5.1.1 | Distribution of Pressure field | 166 |
| 5.1.2 | Distribution of Wind field | 167 |
| 5.1.3 | Distribution of Vorticity field | 177 |
| 5.1.4 | Temperature anomaly | 185 |
| 5.1.5 | Distribution of Relative humidity | 187 |
| 5.1.6 | Water vapor mixing ratio | 190 |
| 5.1.7 | Distribution of Rainfall pattern | 193 |
| 5.1.8 | Track pattern | 197 |
| 5.2 | Simulation of Tropical Cyclone Aila using MM5 and WRF Model | 201 |
| 5.2.1 | Distribution of Pressure field | 201 |
| 5.2.2 | Distribution of Wind field | 205 |
| 5.2.3 | Distribution of Vorticity field | 217 |
| 5.2.4 | Temperature anomaly | 223 |
| 5.2.5 | Distribution of Relative humidity | 225 |
| 5.2.6 | Water vapor mixing ratio | 228 |
| 5.2.7 | Distribution of Rainfall pattern | 232 |
| 5.2.8 | Track pattern | 235 |

| | | | |
|--------|--|---|-----|
| 5.3 | Simulation of Tropical Cyclone Rashmi using MM5 and WRF Model | | 238 |
| 5.3.1 | Distribution of Pressure field | | 238 |
| 5.3.2 | Distribution of Wind field | | 243 |
| 5.3.3 | Distribution of Vorticity field | | 253 |
| 5.3.4 | Temperature anomaly | | 258 |
| 5.3.5 | Distribution of Relative humidity | | 261 |
| 5.3.6 | Water vapor mixing ratio | | 263 |
| 5.3.7 | Distribution of Rainfall pattern | | 265 |
| 5.3.8 | Track pattern | | 269 |
| 5.4 | Summary of the Tropical Cyclone Events | 1 | 272 |
| 6. | Sensitivity Test | | 276 |
| 6.1 | Selection of Model | | 276 |
| 6.2 | Experiment on simulation of different heavy precipitation and TC events | | 276 |
| 6.3 | Initial data source | | 276 |
| 6.4 | Sensitivity study on PBL with Cumulus Parameterization | | 276 |
| 6.4.1 | Domain set up | | 276 |
| 6.4.2 | Model physics | | 277 |
| 6.4.3 | Results, Discussion and conclusions of sensitivity of PBL with CP on heavy precipitation events | | 278 |
| 6.4.4. | Results, Discussion and conclusions of sensitivity of PBL with CP on heavy precipitation events | | 286 |
| 6.5 | Sensitivity study of Microphysics for TC Aila | | 293 |
| 6.5.1 | Domain set up | | 293 |
| 6.5.2 | Model physics | | 294 |

| | | |
|-------|--|-----|
| 6.5.3 | Results, Discussion and conclusions of sensitivity of Microphysics on TC Aila | 295 |
| 6.6 | Sensitivity study of Radiation parameterization on TC Aila | 296 |
| 6.6.1 | Domain set up | 296 |
| 6.6.2 | Model physics | 297 |
| 6.6.3 | Results, Discussion and conclusions of sensitivity of Radiation parameterization on TC Aila | 297 |
| 7. | Conclusions | 300 |
| | References | 305 |

CHAPTER 1
INTRODUCTION

1.1 INTRODUCTION

Bangladesh has a peculiar geographical condition with the Himalayas in the north and the Bay of Bengal in the south. The hilly areas are situated to the northeast in the eastern margin of the Sylhet plains, and in the southeastern part of the country in the Chittagong and Chittagong Hill tracts regions. The world's largest mangrove forest called Sundarban is located in the southwestern coastal zone. Bangladesh is a delta of the great river Ganges, Brahmapurta and Meghna (GBM) and most of the areas are low lying flood planes except Barined tracts and Modhupur tracts situated in the north-west and north-central regions of Bangladesh respectively.

Bangladesh has a mild winter and hot summer. The annual statistics show that that 70.6% of the country average rainfall occurs during the southwest monsoon season and 18.9% during pre-monsoon seasons. The winter and post-monsoon show about 1.5 and 9% of the annual average rainfall. There are considerable spatial variations. The northeast part of Bangladesh experiences very high rainfall of about Bangladesh enjoys generally a sub-tropical monsoon climate. There are four prominent seasons in a year namely; winter (December - February), pre-monsoon (March – May), monsoon (June – September) and post monsoon (October – November). Winter, which is quite pleasant begins in December and ends in February. The average annual rainfall varies from 1429 to 4338 mm. About 80% of the total rainfall of the country occurs during monsoon. The maximum rainfall is recorded in the coastal areas of Chittagong (in the south-east) and northern part of Sylhet district (in the north-east of Bangladesh), while the minimum is observed in the western and northwestern parts of the country. Monsoon rainfall is very essential for agriculture. The agricultural and land-use practices depend on the rainfall pattern and water availability.

The country is prone to disasters like floods and droughts, tropical cyclones, norwesters/tornadoes. Variability of rainfall causes floods and droughts. The excess rainfall in Bangladesh and in the upper catchments of the Bangladesh rivers causes floods in Bangladesh. It is to mention that 92% of the Catchments of Ganges, Brahmaputra and Meghan lies outside Bangladesh and the runoff from these areas pass through Bangladesh which accounts for the 8% of the catchments. The severe floods cause the damages to crops, infrastructure, power supply, economic activities and overall livelihood of the affected areas. Besides, the heavy rainfall events cause flash floods and landslides. The latter is very common in Chittagong districts. The deficit rainfall for a long period causes severe droughts affecting the agricultural crops, lack of water recourses for fisheries and livelihood of the people in various ways.

Normally, in the pre-monsoon season, when the warm and moist air blows from the sea to the land in the lower level and the subtropical cool air blows from the westerly direction over this moisture laden hot air mass creating a situation of high instability in the troposphere favouring the convective processes to occur frequently. Due to this convection, the other disasters come from the severe thunderstorms, squall lines, nor'westers, meso-scale convective clouds and tornadoes which are of localized nature and are relatively short lived but causes damages to lives and properties over the areas where they occur. The horizontal scale of these systems is within the range 1-100 km. The Bay of Bengal is highly suitable for tropical cyclogenesis. One of the linked features of the tropical cyclone is the storm surges, which is responsible for major damages due to a tropical cyclone. The strong wind of the tropical cyclone exerts frictional force on the water surface which is proportional to the square of the wind speed. This frictional force causes high gravity waves with heights of up to 10-12 meter or more. These waves cause water to flow inland and lash every thing in its path. The human casualties of the cyclones of 12 November 1970, 29 April 1991 and 15 November 2007 were 300000, 138882 and 3363 respectively due to the rampages of these killer cyclones. The shocks of these losses in the economy and livelihood are irreparable and it takes a long time to settle the victims back to normal life.

Prediction of rainfall associated with precipitation events is a challenging task for the scientists dealing in this profession. The rainfall in monsoon seasons are mainly associated with the activities of monsoon trough, which is a east west oriented low pressure area with axis extending from central Pakistan to the head of the Bay of Bengal along the *Gangetic* valley parallel to the foot hills of the Himalayas. The monsoon depressions, land depressions and meso-scale convective systems generate within the monsoon trough and cause heavy rainfall. Sometimes these systems originate more frequently and become unusually active to produce damaging floods.

The formation, intensification and movement of the monsoon depressions/ land depressions and the spatial temporal variability of the monsoon trough itself are very important aspects, which need to be studied. Again, the formation, intensification and movement of the tropical cyclone are also very important aspects, which need to be studied. One of the most powerful and advanced tools of such research is the Numerical Weather Prediction (NWP) Models. The objective of the present research is to predict the high impact precipitation events over Bangladesh and its surrounding areas using NWP models. For the proposed investigation the high-resolution model MM5 and WRF are used and the descriptions of these models are written in the chapter 2.

Initially a number of high impact precipitation events (three rainfall events and tropical cyclones events) those occurred in the recent decades were identified using observed data. The above mentioned models have been set up for predicting these impact events. The model has been run using NECP FNL reanalysis data ($1^0 \times 1^0$ resolution) as the initial field for different meteorological parameters. The model predicted results have been compared with observed data from JTWC. Predicted rainfalls are also compared with the rainfall obtained from TRMM and BMD rain-gauge data.

Attempts have been done to adjust the physical parameterization schemes and boundary layer parameterization to improve the performance of the models. Some sensitivity tests are also performed to test the model ability to predict meteorological parameters.

1.2 Objectives and Scope of the Research Work

The objective of the present research is to predict the high impact precipitation events over Bangladesh and its surrounding areas using NWP models. The present study has been conducted with the following objectives:

- To investigate the performance of MM5 and WRF model.
- To setup the models and their various optional parameters to study the heavy precipitation event over Bangladesh and its surroundings.
- To investigate the physics and dynamics related to formation, evolution and horizontal and vertical structure of heavy rainfall events.
- To investigate the model performance in respect of prediction of the tracks with landfall time and positions of Tropical Cyclone (TC) events using different initial conditions.
- Sensitivity test of PBL with CP on heavy rainfall events and TC events
- Sensitivity test of Microphysics of models on TC events
- Sensitivity test of Microphysics of model on TC events

1.3 Social and Economic Benefit of the Research Work.

The economic activities of the country, especially the agriculture, are dependent on the rainfall. Besides, the tropical cyclones, tornadoes and other meso-scale activities cause

severe damage to lives, properties, infrastructures and environment. The weather activities of the country of Bangladesh are dominated by the southwest monsoon. In addition to this, Bangladesh is supposed to become the worst victim of the impacts of global warming and associated climate change. The climate change induced enhancement of natural disasters will cause its people to suffer innumerable loss to resources and livelihood.

Tropical cyclone can neither be destroyed nor be prevented, but the damages can be minimized by proper management practices which include preparedness, rescue operation and rehabilitation. Again, variability of rainfall causes floods and droughts. The effect of these can be minimized by proper management practices which include preparedness, rescue operation and rehabilitation. Again, agriculture plan can be made suitable using the prediction of above convective activity.

To identify the impacts of precipitation events, it is of prime necessity to understand the knowledge to predict them earlier their formation. So, this requires research on the prediction of high impact precipitation events over Bangladesh and its surroundings using NWP models to save the valuable life and assets. It also helps the policy maker to develop the country especially in the agriculture sector.

1.4 Structure of the Thesis

The thesis has been constructed with the following structure:

Abstract is the gist of the research work performed for this dissertation.

Chapter 1 contains general introduction. It describes the geographical settings of Bangladesh and adjacent land masses, climate and disaster of Bangladesh, objectives and scope of the study and explains how the research results will be of social and economic benefit.

Chapter 2 contains an overview of the historical development of NWP models, description of MM5 and WRF models, description of high impact precipitation events (heavy rainfall and tropical cyclone), previous work associated with high impact precipitation events by NWP models (MM5 and WRF models)

Chapter 3 deals with model setup, initialization of MM5 and WRF models.

Chapter 4 contains the results and discussions of the study of rainfall events. It deals with the formation, evolution, and structure of heavy rainfall over Bangladesh and its surroundings area based on MM5 and WRF models results.

Chapter 5 contains the results and discussions of the study of tropical cyclone events. It deals with the formation, evolution, structure, track and landfall of selected tropical cyclones Bay of Bengal based on MM5 and WRF models results.

Chapter 6 deals with a few sensitivity tests using different model physics to predict rainfall and tropical cyclone events to understand how model physics behave on meteorological parameters.

In Chapter 7, the conclusion of the research findings have been brought in with a few recommendations for future research in this subject.

CHAPTER 2
LITERATURE REVIEW

2.1.1 Numerical Weather Prediction Models

Models use systems of differential equations based on the laws of physics, fluid motion, and chemistry, and use a coordinate system which divides the planet into a 3D grid. Winds, heat transfer, solar radiation, relative humidity, and surface hydrology are calculated within each grid cell, and the interactions with neighboring cells are used to calculate atmospheric properties in the future.

Numerical weather prediction uses mathematical models of the atmosphere and oceans to predict the weather based on current weather conditions. Though first attempted in the 1920s, it was not until the advent of computer simulation in the 1950s that numerical weather predictions produced realistic results. A number of global and regional forecast models are run in different countries worldwide, using current weather observations relayed from radiosondes or weather satellites as inputs to the models.

Mathematical models based on the same physical principles can be used to generate either short-term weather forecasts or longer-term climate predictions; the latter are widely applied for understanding and projecting climate change. The improvements made to regional models have allowed for significant improvements in tropical cyclone track and air quality forecasts; however, atmospheric models perform poorly at handling processes that occur in a relatively constricted area, such as wildfires.

Manipulating the vast datasets and performing the complex calculations necessary to modern numerical weather prediction requires some of the most powerful supercomputers in the world. Even with the increasing power of supercomputers, the forecast skill of numerical weather models only extends to about six days. Factors affecting the accuracy of numerical predictions include the density and quality of observations used as input to the forecasts, along with deficiencies in the numerical models themselves. Although post-processing techniques such as model output statistics (MOS) have been developed to improve the handling of errors in numerical predictions, a more fundamental problem lies in the chaotic nature of the partial differential equations used to simulate the atmosphere. It is impossible to solve these equations exactly, and small errors grow with time (doubling about every five days). In addition, the partial differential equations used in the model need to be supplemented with parameterizations for solar radiation, moist processes (clouds and precipitation), heat exchange, soil, vegetation, surface water, and the effects of terrain. In an effort to quantify the large amount of inherent uncertainty remaining in numerical predictions, ensemble forecasts have been used since the 1990s to help gauge the confidence in the forecast, and to obtain useful results farther into the future than otherwise possible. This approach analyzes multiple forecasts created with an individual forecast model or multiple models.



2.1.2 History of Numerical Weather Prediction Models

The history of numerical weather prediction began in the 1920s through the efforts of Lewis Fry Richardson, who used procedures originally developed by Vilhelm Bjerknes[1] to produce by hand a six-hour forecast for the state of the atmosphere over two points in central Europe, taking at least six weeks to do so [1][2]. It was not until the advent of the computer and computer simulations that computation time was reduced to less than the forecast period itself. The ENIAC was used to create the first weather forecasts via computer in 1950 [3,4]; in 1954, Carl-Gustav Rossby's group at the Swedish Meteorological and Hydrological Institute used the same model to produce the first operational forecast (i.e. routine predictions for practical use) [5]. Operational numerical weather prediction in the United States began in 1955 under the Joint Numerical Weather Prediction Unit (JNWPU), a joint project by the U.S. Air Force, Navy and Weather Bureau [6]. In 1956, Norman Phillips developed a mathematical model which could realistically depict monthly and seasonal patterns in the troposphere; this became the first successful climate model [7][8]. Following Phillips' work, several groups began working to create general circulation models [9]. The first general circulation climate model that combined both oceanic and atmospheric processes was developed in the late 1960s at the NOAA Geophysical Fluid Dynamics Laboratory [10].

As computers have become more powerful, the size of the initial datasets has increased and newer atmospheric models have been developed to take advantage of the added available computing power. These newer models include more physical processes in the simplifications of the equations of motion in numerical simulations of the atmosphere [5]. In 1966, West Germany and the United States began producing operational forecasts based on primitive-equation models, followed by the United Kingdom in 1972 and Australia in 1977 [1, 11]. The development of limited area (regional) models facilitated advances in forecasting the tracks of tropical cyclones as well as air quality in the 1970s and 1980s [12,13]. By the early 1980s models began to include the interactions of soil and vegetation with the atmosphere, which led to more realistic forecasts [14].

The output of forecast models based on atmospheric dynamics is unable to resolve some details of the weather near the Earth's surface. As such, a statistical relationship between the output of a numerical weather model and the ensuing conditions at the ground was developed in the 1970s and 1980s, known as model output statistics (MOS) [15, 16]. Starting in the 1990s, model ensemble forecasts have been used to help define the forecast uncertainty and to extend the window in which numerical weather forecasting is viable farther into the future than otherwise possible [17, 18, 19].

Many research groups and agencies have developed their own global general circulation models as well as local/limited area models. Some of the better known numerical models are:

Global models

- GFS Global Forecast System (previously AVN)-developed by NOAA
- NOGAPS-developed by the US Navy to compare with the GFS
- GEM Global Environmental Multiscale-developed by the Meteorological Service of Canada (MSC)
- ECMWF-a model run by the European Centre for Medium-Range Weather Forecasts
- UKMO developed by the UK Met Office
- GME developed by the German Weather Service, DWD
- FSU GSM Florida State University Global Spectral Model

Regional models

- WRF - The Weather Research and Forecasting Model was developed cooperatively by NCEP and the meteorological research community. WRF has several configurations, including:
 - WRF-NMM - The WRF Nonhydrostatic Mesoscale Model is the primary short-term weather forecast model for the U.S.
 - ARW - Advanced Research WRF developed primarily at the U.S. National Center for Atmospheric Research (NCAR)
 - AHW - Advance Hurricane WRF
- MM5 - The Fifty Generation Penn State/NCAR Mesoscale Model
- QLM - Quasi-Lagrangian Limited Area Model
- FSU NRAM - Florida State University Nested Regional Spectral Model
- NAM - North American Mesoscale Model
- HIRLAM - High Resolution Limited Area Model
- GEM-LAM - Global Environmental Multiscale Limited Area Model, the high resolution (2.5 km) GEM by the Meteorological Service of Canada (MSC)
- ALADIN - The high-resolution limited-area hydrostatic and non-hydrostatic model developed and operated by several European and North African countries under the leadership of Meteo-France.

2.2: Description of MM5 Modeling System

2.2.1: Brief Description

The PSU/NCAR mesoscale model is a limited-area, nonhydrostatic or hydrostatic (Version 2 only), terrain-following sigma-coordinate model designed to simulate or predict mesoscale and regional-scale atmospheric circulation. It has been developed at Penn State and NCAR as a community mesoscale model and is continuously being improved by contributions from users at several universities and government laboratories.

The Fifth-Generation NCAR / Penn State Mesoscale Model (MM5) is the latest in a series that developed from a mesoscale model used by Anthes at Penn State in the early 70's that was later documented by Anthes and Warner [20]. Since that time, it has undergone many changes designed to broaden its usage. A detailed description of MM5 can also be found in Grell *et al.* [21] and Dudhia *et al.*[22]. These include (i) a multiple-nest capability, (ii) nonhydrostatic dynamics, which allows the model to be used at a few-kilometer scale, (iii) multitasking capability on shared- and distributed-memory machines, (iv) a four-dimensional data-assimilation capability, and (v) more physics options.

The model MM5 is supported by several auxiliary programs, which are referred to collectively as the MM5 modeling system.

A schematic diagram (Fig.2.2a.) is provided to facilitate discussion of the complete modeling system. It is intended to show the order of the programs and the flow of the data, and to briefly describe their primary functions. Documentation for various programs in the modeling system is available online.

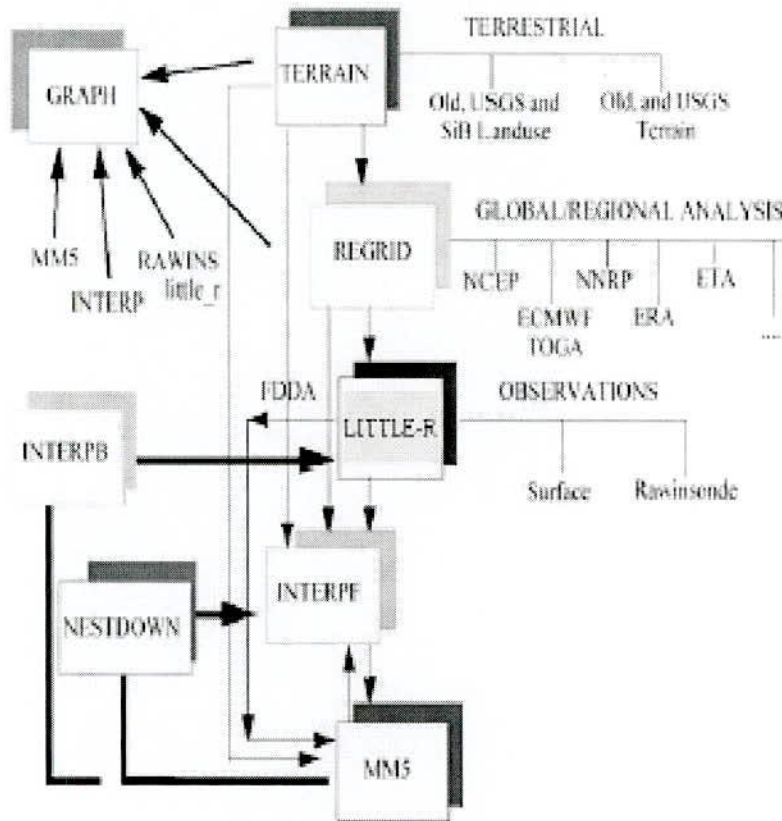


Fig.2.2a: MM5 modeling system flow chart

Terrestrial and isobaric meteorological data are horizontally interpolated (programs TERRAIN and REGRID) from a latitude-longitude mesh to a variable high-resolution domain on either a Mercator, Lambert conformal, or polar stereographic projection. Since the interpolation does not provide mesoscale detail, the interpolated data may be enhanced (program RAWINS or little_r) with observations from the standard network of surface and rawinsonde stations using either a successive-scan Cressman technique or multiquadric scheme. Program INTERPF performs the vertical interpolation from pressure levels to the sigma coordinate system of MM5. Sigma surfaces near the ground closely follow the terrain, and the higher-level sigma surfaces tend to

approximate isobaric surfaces. Since the vertical and horizontal resolution and domain size are variable, the modeling package programs employ parameterized dimensions requiring a variable amount of core memory. Some peripheral storage devices are also used.

Since MM5 is a regional model, it requires an initial condition as well as lateral boundary condition to run. To produce lateral boundary condition for a model run, one needs gridded data to cover the entire time period that the model is integrated.

2.2.2: Current Release

The current release for the MM5 modeling system is Version 3. MM5 Version 2, or V2 is also available. I used Version 3.7.

2.2.3: Features of the Modeling System

- Globally re-locatable
 - Three map projections:
 - Polar stereographic;
 - Lambert conformal;
 - Mercator.
 - Support different true latitudes.
 - Variable resolution terrain elevation, landuse, soil type, deep soil temperature, vegetation fraction, and land-water mask datasets are provided (the new global 30 sec terrain data may be obtained from USGS anonymous ftp site).
- Flexible and multiple nesting capability
 - Can be configured to run from global scale down to cloud scale in one model

- Parallelize on distributed-memory machines:
 - IBM SP2, Cray T3E, SGI Origin 2000, HP-SPP2000, Fujitsu VPP, Sun and Linux clusters
 - Well-documented, and user-support available.

2.2.4: Program Functions

- TERRAIN
 - Define model domain and map projection
 - Generate terrain, and landuse category data on model grids
 - Generate vegetation/soil category data for MM5 model's land-surface model option (V3 only)
 - Calculate map-scale factors and Coriolis parameter for the model (V3 only)
- REGRID / (DATAGRID V2 only)
 - Generate first-guess pressure-level fields on model grids from another model dataset
 - Calculate map-scale factors and Coriolis parameter for the model (V2 only)
- RAWINS / LITTLE_R

Perform objective analysis: blend first-guess fields with radiosonde and surface observations

- INTERPF / (INTERP V2 only)

Interpolate pressure-level data from either RAWINS/LITTLE_R or REGRID/ (DATAGRID V2) to model's sigma coordinate

- MM5

Perform time integration

- NESTDOWN

- Generate fine mesh model input from coarse mesh model output (1-way option).

Capability of changing vertical sigma levels.

- Generate fine mesh model input from coarse mesh model input

- INTERPB

- Interpolate model sigma-level data to pressure levels

- Generate first guess for RAWINS/LITTLE_R

- Generate intermediate files for REGRID/regridder

- GRAPH/RIP

Generate plots from the output of modeling system programs (based on NCAR Graphics)

2.2.5: MM5 Model Physics Options

- Precipitation physics

- Cumulus parameterization schemes:

- Anthes-Kuo
- Grell
- Kain-Fritsch
- New Kain-Fritsch (including shallow convection physics)
- Betts-Miller

- Arakawa-Schubert

Among the above Anthes-Kuo (AK), Grell, Kain-Fritsch (KF), New Kain-Fritsch (KF-2), and Betts –Miller (BM) are documented in Anthes[23], Grell [24], Kain and Fritsch [25], Kain [26] and Betts and Miller [27].

- Resolvable-scale microphysics schemes:
 - Removal of supersaturation
 - Hsie's warm rain scheme
 - Dudhia's simple ice scheme
 - Reisner's mixed-phase scheme
 - Reisner's mixed-phase scheme with graupel
 - NASA/Goddard microphysics with hail/graupel
 - Schultz mixed-phase scheme with graupel
- Planetary boundary layer process parameterization
 - Bulk formula
 - Blackadar scheme
 - Burk-Thompson (Mellor-Yamada 1.5-order/level-2.5 scheme)
 - Eta TKE scheme [28]
 - MRF scheme [29]
 - Gayno-Seaman scheme
- Surface layer process parameterization
 - fluxes of momentum, sensible and latent heat
 - ground temperature prediction using energy balance equation

- variable land use categories (defaults are 13, 16 and 24)
- 5-layer soil model
- OSU land-surface model (V3.1 - V3.5)
- Noah land-surface model (since V3.6)
- Pleim-Xiu land-surface model (V3 only)
- Atmospheric radiation schemes
 - Simple cooling
 - Dudhia's long- and short-wave radiation scheme
 - NCAR/CCM2 radiation scheme

2.2.6: Data and Model Setup

MM5 model flow diagram is shown in figure below. In the case of post-processing of the model output, Grid Analysis and Display System (GrADS) is used. Terrestrial data are required for TERRAIN program and meteorological data are required for REGRED program.

2.2.6.1 Terrain Data

The data available as input to the program TERRAIN include terrain elevation, landuse/vegetation, land-water mask, soil types, vegetation fraction and deep soil temperature.

Most data are available at six resolutions

: 1 degree, 30, 10, 5 and 2 minutes, and 30 seconds. Here is the list of available data:

1. Elevation data at six resolutions from USGS: 1-degree, 30-, 10-, 5-, 2-minutes (5 files) and 30-second (33 tiles directly from USGS). All lower resolution data (1 degree to 2 minutes) are created from the 30 seconds USGS data.

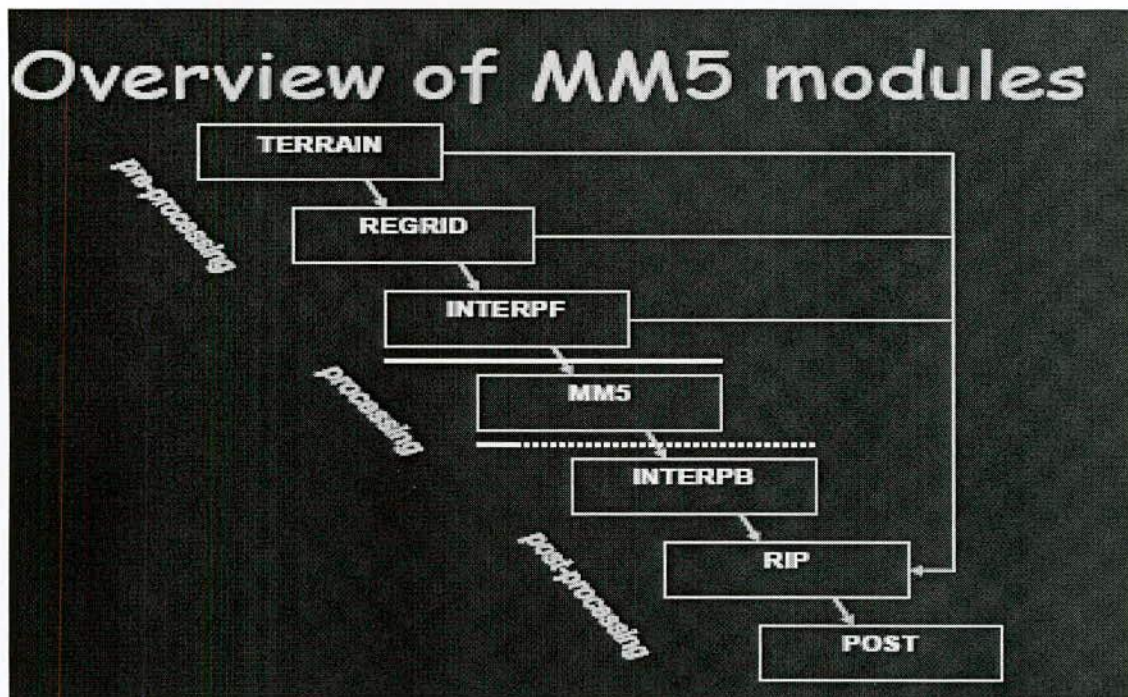


Figure 2.2: MM5 model flow diagram

2. Three types of source vegetation/land-use data available:

- (a) 13-category, global coverage with the resolution of 1-degree, 30- and 10-minute (3 files);
- (b) 17-category, North-American coverage with the resolution of 1-degree, 30-, 10-, 5-, 2-minutes and 30 seconds (6 files);
- (c) 25-category, global coverage with the resolution of 1-degree, 30-, 10-, 5-, 2-minutes and 30-seconds (6 files; all lower resolution data are created from 30 sec data from USGS version 2 land cover data).

3. Two types of land-water mask data:

(a) 17-category, North-American coverage with the resolution of 1-degree, 30-, 10-, 5-, 2-minutes and 30seconds (6 files);

(b) 25-category, global coverage with the resolution of 1-degree, 30-, 10-, 5-, 2-minutes and 30-seconds (6 files).

4. For LSM option in MM5, the soil, vegetation fraction, and annual deep soil temperature are needed. The source data files are:

(a) 17-category, six resolutions of global soil data (6 files);

(b) 12 monthly, 10-minute, global vegetation fraction data (1 file);

(c) 1-degree, global annual deep soil temperature (1 file).

2.2.6.2: REGRED Data:

NCEP Final Analysis (GRIB, 1 degree resolution) ,1999 SEP15 – CON, were used.

2.3 Description of WRF Model

Weather Research and Forecasting (WRF) is a next generation meso-scale numerical weather forecasting community model. Its simulation capacity is very high and can simulate meteorological phenomena ranging from meters to thousands of kilometers. This chapter focuses on the few important features of the Advance Research WRF (ARW) model using NCAR TECHNICAL NOTE NCAR/TN-475+STR Shamarock *et al.* [30].

2.3.1 Introduction

The Weather Research and Forecasting (WRF) model is a numerical weather prediction (NWP) and atmospheric simulation system designed for both research and operational applications. WRF is supported as a common tool for the university/research and operational communities to promote closer ties between them and to address the needs of both. The development of WRF has been a multi-agency effort to build a next-generation mesoscale forecast model and data

assimilation system to advance the understanding and prediction of mesoscale weather and accelerate the transfer of research advances into operations. The WRF effort has been a collaborative one among the National Center for Atmospheric Research's (NCAR) Mesoscale and Microscale Meteorology (MMM) Division, the National Oceanic and Atmospheric Administration's (NOAA) National Centers for Environmental Prediction (NCEP) and Earth System Research Laboratory (ESRL), the Department of Defense's Air Force Weather Agency (AFWA) and Naval Research Laboratory (NRL), the Center for Analysis and Prediction of Storms (CAPS) at the University of Oklahoma, and the Federal Aviation Administration (FAA), with the participation of university scientists.

WRF reflects flexible, state-of-the-art, portable code that is efficient in computing environments ranging from massively-parallel supercomputers to laptops. Its modular, single-source code can be configured for both research and operational applications. Its spectrum of physics and dynamics options reflects the experience and input of the broad scientific community. Its WRF-Var variational data assimilation system can ingest a host of observation types in pursuit of optimal initial conditions, while its WRF-Chem model provides a capability for air chemistry modeling.

WRF is maintained and supported as a community model to facilitate wide use internationally, for research, operations, and teaching. It is suitable for a broad span of applications across scales ranging from large-eddy to global simulations. Such applications include real-time NWP, data assimilation development and studies, parameterized-physics research, regional climate simulations, air quality modeling, atmosphere-ocean coupling, and idealized simulations. As of this writing, the number of registered WRF users exceeds 6000, and WRF is in operational and research use around the world.

The principal components of the WRF system are depicted in Figure 2.3.1. The WRF Software Framework (WSF) provides the infrastructure that accommodates the dynamics solvers, physics packages that interface with the solvers, programs for initialization, WRF-Var, and WRF-Chem. There are two dynamics solvers in the WRF: the Advanced Research WRF (ARW) solver (originally referred to as the Eulerian mass or "em" solver) developed primarily at NCAR, and the NMM (Nonhydrostatic Mesoscale Model) solver developed at NCEP. Community support for the former is provided by the MMM Division of NCAR and that for the latter is provided by the Developmental Testbed Center (DTC).

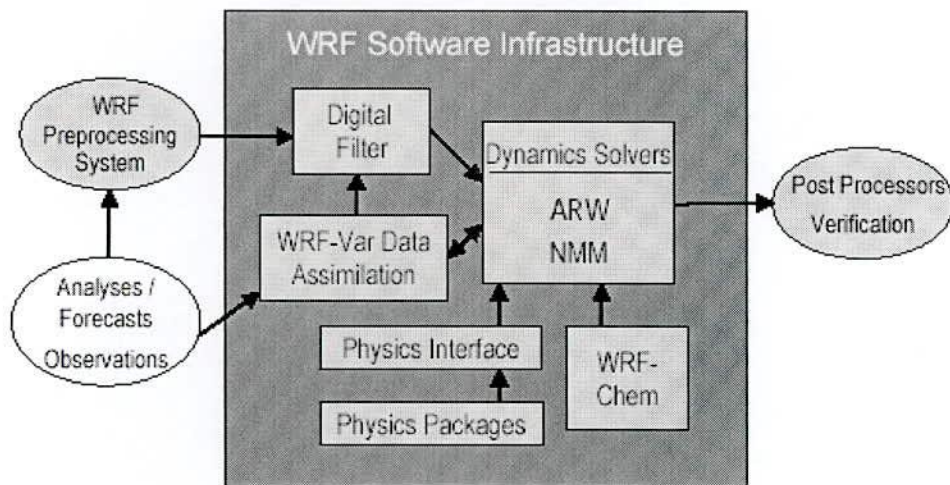


Figure 2.3.1: WRF system components.

2.3.2 Advanced Research WRF

The ARW is the ARW dynamics solver together with other components of the WRF system compatible with that solver and used in producing a simulation. Thus, it is a subset of the WRF modeling system that, in addition to the ARW solver, encompasses physics schemes, numerics/dynamics options, initialization routines, and a data assimilation package (WRF-Var). The ARW solver shares the WSF with the NMM solver and all other WRF components within the framework. Physics packages are largely shared by both the ARW and NMM solvers, although specific compatibility varies with the schemes considered. The association of a component of the WRF system with the ARW subset does not preclude it from being a component of WRF configurations involving the NMM solver. The following section highlights the major features of the ARW, Version 3, and reflects elements of WRF Version 3, which was first released in April 2008.

This technical note focuses on the scientific and algorithmic approaches in the ARW, including the solver, physics options, initialization capabilities, boundary conditions, and grid-nesting techniques.

2.3.3 Major Features of the ARW System, Version 3

ARW Solver

- Equations: Fully compressible, Euler nonhydrostatic with a run-time hydrostatic option available. Conservative for scalar variables.
- Prognostic Variables: Velocity components u and v in Cartesian coordinate, vertical velocity w , perturbations potential temperature, perturbation geopotential, and perturbation surface pressure of dry air. Optionally, turbulent kinetic energy and any number of scalars such as water vapor mixing ratio, rain/snow mixing ratio, cloud water/ice mixing ratio, and chemical species and tracers.
- Vertical Coordinate: Terrain-following, dry hydrostatic-pressure, with vertical grid stretching permitted. Top of the model is a constant pressure surface.
- Horizontal Grid: Arakawa C-grid staggering.
- Time Integration: Time-split integration using a 2nd- or 3rd-order Runge-Kutta scheme with smaller time step for acoustic and gravity-wave modes. Variable time step capability.
- Spatial Discretization: 2nd- to 6th-order advection options in horizontal and vertical.
- Turbulent Mixing and Model Filters: Sub-grid scale turbulence formulation in both coordinate and physical space. Divergence damping, external-mode filtering, vertically implicit acoustic step off-centering. Explicit filter option.
- Initial Conditions: Three dimensional for real-data, and one-, two- and three-dimensional for idealized data. Digital filtering initialization (DFI) capability is available (real-data cases).
- Lateral Boundary Conditions: Periodic, open, symmetric, and specified options available.
- Top Boundary Conditions: Gravity wave absorbing (diffusion, Rayleigh damping, or implicit Rayleigh damping for vertical velocity). Constant pressure level at top boundary along a material surface. Rigid lid option.
- Bottom Boundary Conditions: Physical or free-slip.
- Earth's Rotation: Full Coriolis terms included.
- Mapping to Sphere: Four map projections are supported for real-data simulation: polar stereographic, Lambert conformal, Mercator, and latitude-longitude (allowing rotated pole). Curvature terms included.
- Nesting: One-way interactive, two-way interactive, and moving nests. Multiple levels and integer ratios.
- Nudging: Grid (analysis) and observation nudging capabilities available.
- Global Grid: Global simulation capability using polar Fourier filter and periodic east-west conditions.

Model Physics

- Microphysics: Schemes ranging from simplified physics suitable for idealized studies to sophisticated mixed-phase physics suitable for process studies and NWP.
- Cumulus parameterizations: Adjustment and mass-flux schemes for mesoscale modeling.
- Surface physics: Multi-layer land surface models ranging from a simple thermal model to full vegetation and soil moisture models, including snow cover and sea ice.
- Planetary boundary layer physics: Turbulent kinetic energy prediction or non-local K schemes.
- Atmospheric radiation physics: Long wave and shortwave schemes with multiple spectral bands and a simple shortwave scheme suitable for climate and weather applications. Cloud effects and surface fluxes are included.

WRF-Var System

- WRF-Var merged into WRF software framework.
- Incremental formulation of the model-space cost function.
- Quasi-Newton or conjugate gradient minimization algorithms.
- Analysis increments on unstaggered Arakawa-A grid.
- Representation of the horizontal component of background error B via recursive filters (regional) or power spectra (global). The vertical component is applied through projection onto climatologically-averaged eigenvectors of vertical error. Horizontal/vertical errors are non-separable (horizontal scales vary with vertical eigenvector).
- Background cost function (J_b) preconditioning via a control variable transform U defined as $B = UUT$.
- Flexible choice of background error model and control variables.
- Climatological background error covariances estimated via either the NMC-method of averaged forecast differences or suitably averaged ensemble perturbations.
- Unified 3D-Var (4D-Var under development), global and regional, multi-model capability.

WRF-Chem

- Online (or “inline”) model, in which the model is consistent with all conservative transport done by the meteorology model.
- Dry deposition, coupled with the soil/vegetation scheme.
- Aqueous phase chemistry coupled to some of the microphysics and aerosol schemes.

- Three choices for biogenic emissions: No biogenic emissions; Online calculation of biogenic emissions; Online modification of user specified biogenic emissions (e.g., EPA Biogenic Emissions Inventory System (BEIS)).
- Two choices for anthropogenic emissions: No anthropogenic emissions and user-specified anthropogenic emissions.
- Two choices for gas-phase chemical reaction calculations: RADM2 chemical mechanism and CBM-Z mechanism.
- Several choices for gas-phase chemical reaction calculations through the use of the Kinetic Pre-Processor (KPP).
- Three choices for photolysis schemes: Madronich scheme coupled with hydrometeors, aerosols, and convective parameterizations; Fast-J Photolysis scheme coupled with hydrometeors, aerosols, and convective parameterizations; FTUV scheme coupled with hydrometeors, aerosols, and convective parameterizations.
- Choices for aerosol schemes: The Modal Aerosol Dynamics Model for Europe (MADE/SORGAM); Model for Simulating Aerosol Interactions and Chemistry (MOSAIC); and The GOCART aerosol model (experimental).
- A tracer transport option in which the chemical mechanism, deposition, etc., has been turned off.

WRF Software Framework

- Highly modular, single-source code for maintainability.
- Two-level domain decomposition for parallel and shared-memory generality.
- Portable across a range of available computing platforms.
- Support for multiple dynamics solvers and physics modules.
- Separation of scientific codes from parallelization and other architecture-specific issues.
- Input/Output Application Program Interface (API) enabling various external packages to be installed with WRF, thus allowing WRF to easily support various data formats.
- Efficient execution on a range of computing platforms (distributed and shared memory, vector and scalar types). Support for accelerators (e.g., GPUs).
- Use of Earth System Modeling Framework (ESMF) and interoperable as an ESMF component.
- Model coupling API enabling WRF to be coupled with other models such as ocean, and land models using ESMF, MCT, or MCEL.



2.3.4 Model Physics

This chapter outlines the physics options available in the ARW. The WRF physics options fall into several categories, each contains several choices. The physics categories are (1) microphysics, (2) cumulus parameterization, (3) planetary boundary layer (PBL), (4) land-surface model, and (5) radiation.

The physics section is insulated from the rest of the dynamics solver by the use of physics drivers. These are between solver-dependent routines: a pre-physics preparation and post-physics modifications of the tendencies. The physics preparation involves filling arrays with physics-required variables that include the temperature, pressure, heights, layer thicknesses, and other state variables in MKS units at half-level grid points and on full levels. The velocities are also de-staggered so that the physics part is independent of the dynamical solver's velocity staggering. Physics packages compute tendencies for the velocity components (un-staggered), potential temperature, and moisture fields. The solver-dependent post-physics step will re-stagger these tendencies as necessary, couple tendencies with coordinate metrics, and convert to variables or units appropriate to the dynamics solver.

In the first Runge-Kutta step, prior to the acoustic steps, tendencies are computed for radiation, surface, PBL, and cumulus physics. These tendencies are then held fixed through the Runge-Kutta steps. Microphysics is computed after the last Runge-Kutta step in order to maintain proper saturation conditions at the end of the time-step. The initialization of the physics is called prior to the first model step. This initialization may include reading in data files for physics tables or calculating look-up tables of functions. Each physics module includes an initialization routine for this purpose. Often physics packages will have many of their own constants that should also be included in their own module, while common physical constants are passed in from the physics drivers.

2.3.4.1 Microphysics

Microphysics includes explicitly resolved water vapor, cloud, and precipitation processes. The model is general enough to accommodate any number of mass mixing-ratio variables, and other quantities such as number concentrations. Four-dimensional arrays with three spatial indices and one species index are used to carry such scalars. Memory, i.e., the size of the fourth dimension in these arrays, is allocated depending on the needs of the scheme chosen, and advection of the species also applies to all those required by the microphysics option. In the current version of the ARW, microphysics is carried out at the end of the time-step as an adjustment process, and so

does not provide tendencies. The rationale for this is that condensation adjustment should be at the end of the time-step to guarantee that the final saturation balance is accurate for the updated temperature and moisture. However, it is also important to have the latent heating forcing for potential temperature during the dynamical sub-steps, and this is done by saving the microphysical heating as an approximation for the next time-step.

Currently, the sedimentation process is accounted for inside the individual microphysics modules, and, to prevent instability in the calculation of the vertical flux of precipitation, a smaller time step is allowed. The saturation adjustment is also included inside the microphysics. In the future, however, it might be separated into an individual subroutine to enable the remaining microphysics to be called less frequently than the model's advection step for efficiency.

Different schemes of microphysics option available in ARW are discuss as follows:

- a. Kessler scheme: A warm-rain (i.e. no ice) scheme used commonly in idealized cloud modeling studies [31].
- b. Purdue Lin scheme: A sophisticated scheme that has ice, snow and graupel processes, suitable for real-data high-resolution simulations. All parameterization production terms are based on Lin *et al.* [32] and Rutledge and Hobbs [33] with some modifications.
- c. WRF Single-Moment 3-class (WM3) scheme: A simple efficient scheme with ice and snow processes suitable for meaoscale grid sizes which follows Hong *et al.* [34].
- d. WRF Single-Moment 5-class (WSM5) scheme: A slightly more sophisticated version of (c) that allows for mixed-phase processes and super-cooled water [34, 35].
- e. Eta microphysics: The operational microphysics in NCEP models: A simple efficient scheme with diagnostic mixed-phase processes [36].
- f. WRF Single-Moment 6-class (WSM6) scheme: A scheme with ice, snow and graupel processes suitable for high-resolution simulations [37,34,37].
- g. Goddard microphysics scheme: A scheme with ice, snow and graupel processes suitable for high-resolution simulations [38].
- h. Thompson et al. scheme: A new scheme with ice, snow and graupel processes suitable for high-resolution simulations [39].
- i. Morrison double-moment scheme: Double-moment ice, snow, rain and graupel for cloud-resolving simulations [40].

2.3.4.2 Cumulus Parameterization

These schemes are responsible for the sub-grid-scale effects of convective and/or shallow clouds. The schemes are intended to represent vertical fluxes due to unresolved updrafts and downdrafts and compensating motion outside the clouds. They operate only on individual columns where the scheme is triggered and provide vertical heating and moistening profiles. Some schemes additionally provide cloud and precipitation field tendencies in the column, and future schemes may provide momentum tendencies due to convective transport of momentum. The schemes all provide the convective component of surface rainfall.

Cumulus parameterizations are theoretically only valid for coarser grid sizes, (e.g., greater than 10 km), where they are necessary to properly release latent heat on a realistic time scale in the convective columns. Where the assumptions about the convective eddies being entirely sub-grid-scale break down for finer grid sizes, sometimes these schemes have been found to be helpful in triggering convection in 5-10 km grid applications. Generally, they should not be used when the model can resolve the convective eddies itself (e.g., <5 km grid).

The available cumulus parameterization options in the ARW are as following:

- a. Kain-Fritsch scheme: Deep and shallow convection sub-grid scheme using a mass flux approach with downdrafts and Convective Available Potential Energy (CAPE) removal time scale. The modified version of the Kain-Fritsch scheme [41] is based on Kain and Fritsch [42] and Kain and Fritsch schemes [43].
- b. Betts-Miller-Janjic scheme: Operational Eta scheme. Column moist adjustment scheme relaxing towards a well-mixed profile [44, 45].
- c. Grell-Devenyi ensemble scheme: Multi-closure, multi-parameter, ensemble method with typically 144 sub-grid members [46].
- d. Grell 3d ensemble cumulus scheme: Scheme for higher resolution domains allowing for subsidence in neighboring columns.
- e. Old Kain-Fritsch scheme: Deep convection scheme using a mass flux approach with downdrafts and CAPE removal time scale.

2.3.4.3 Surface Layer

The surface layer schemes calculate friction velocities and exchange coefficients that enable the calculation of surface heat and moisture fluxes by the land-surface models and surface stress in the planetary boundary layer scheme. Over water surface, the surface fluxes and surface diagnostic fields are computed in the surface layer scheme itself. The schemes provide no tendencies, only the stability-dependent information about the surface layer for the land-surface and PBL schemes. Currently, each surface layer option is tied to particular boundary-layer options, but in the future more interchangeability and options may become available. It may be noted that some boundary layer schemes (YSU and MRF) require the thickness of the surface layer in the model to be representative of the actual surface layer (e.g. 50-100 meters).

- a. MM5 similarity: Based on Monin-Obukhov [47] with Carslon-Boland viscous sub-layer and standard similarity functions from look-up tables.
- b. Eta similarity: Used in Eta model [48,49]. Based on Monin- Obukhov [47] with Zilitinkevich [50] thermal roughness length and standard similarity functions from look-up tables.
- c. Pleim-Xiu surface layer: This scheme is based on similarity theory and includes parameterizations of a viscous sub-layer in the form of quasi-laminar boundary layer resistance accounting for differences in the diffusivity of heat, water vapor, and trace chemical species [51].

2.3.4.4 Land-Surface Model

The land-surface models (LSMs) use atmospheric information from the surface layer scheme, radiative forcing from the radiation scheme, and precipitation forcing from the microphysics and convective schemes, together with internal information on the land's state variable and land-surface properties, to provide heat and moisture fluxes over land points and sea-ice points. These fluxes provide a lower boundary condition for the vertical transport done in the PBL schemes (or the vertical diffusion scheme in the case where a PBL scheme is not run, such as in large-eddy mode). The land-surface models have various degrees of sophistication in dealing with thermal and moisture fluxes in multiple layers of the soil and also may handle vegetation, root, and canopy effects and surface snow-cover prediction. The land-surface model provides no tendencies, but does update the land's state variables which include the ground (skin)

temperature, soil temperature profile, soil moisture profile, snow cover, and possible canopy properties. There is no horizontal interaction between neighboring points in the LSM, so it can be regarded as a one-dimensional column model for WRF land grid-point, and many LSMs can be run in a stand-alone mode.

The different land surface schemes options available in ARW are as followings.

- a. 5-layer thermal diffusion: Soil temperature only scheme, using five layers.
- b. Noah Land Surface Model: Unified NCEP/NCAR/AFWA scheme with soil temperature and moisture in four layers, fractional snow cover and frozen soil physics [52].
- Urban canopy model: 3-category UCM option. This can be run as an option with the Noah LSM.
- c. Rapid Update Cycle (RUC) Land Surface Model: RUC operational scheme with soil temperature and moisture in six layers, multi-layer snow and frozen soil physics [53,54].
- d. Pleim-Xiu Land Surface Model: Two-layer scheme with vegetation and sub-grid tiling [55,56]

2.3.4.5 Planetary Boundary Layer

The planetary boundary layer (PBL) is responsible for vertical sub-grid-scale fluxes due to eddy transports in the whole atmospheric column, not just the boundary layer. Thus, when a PBL scheme is activated, explicit vertical diffusion is de-activated with the assumption that the PBL scheme will handle this process. The most appropriate horizontal diffusion choices are those based on horizontal deformation or constant horizontal eddy viscosity values where horizontal and vertical mixing are treated independently. The surface fluxes are provided by the surface layer and land-surface schemes. The PBL schemes determine the flux profiles within the well-mixed boundary layer and the stable layer, and thus provide atmospheric tendencies of temperature, moisture (including clouds), and horizontal momentum in the entire atmospheric column. Most PBL schemes consider dry mixing, but can also include saturation effects in the vertical stability that determines the mixing. The schemes are one-dimensional, and assume that there is a clear scale separation between sub-grid eddies and resolved eddies. This assumption will become less clear at grid sizes below a few hundred meters, where boundary layer eddies may start to be resolved, and in these situations the scheme should be replaced by a fully three-

dimensional local sub-grid turbulence scheme such as the Turbulent Kinetic Energy (TKE) diffusion scheme.

PBL Schemes options available in ARW model are discussed below:

- a. Medium Range Forecast Model (MRF) scheme: Older version of YSU with implicit treatment of entrainment layer as part of non-local-K mixed layer. This scheme is described by Hong and Pan [57].
- b. Yonsei University (YSU) scheme: The Yonsei University PBL [58] is the next generation of the MRF. Non-local-K scheme with explicit entrainment layer and parabolic K profile in unstable mixed layer.
- c. Mellor-Yamada Janjic (MYJ) scheme: Eta operational scheme. One-dimensional prognostic turbulent kinetic energy scheme with local vertical mixing [59, 48,49].
- d. Asymmetrical Convective Model version 2 (Acm2) PBL: Asymmetric Convective Model with non-local upward mixing and local downward mixing [60].

2.3.4.6 Atmospheric Radiation

The radiation schemes provide atmospheric heating due to radiative flux divergence and surface downward longwave and shortwave radiation for the ground heat budget. Longwave radiation includes infrared or thermal radiation absorbed and emitted by gases and surfaces. Upward longwave radiative flux from the ground is determined by the surface emissivity that in turn depends upon land-use type, as well as the ground (skin) temperature. Shortwave radiation includes visible and surrounding wavelengths that make up the solar spectrum. Hence, the only source is the Sun, but processes include absorption, reflection, and scattering in the atmosphere and at surfaces. For shortwave radiation, the upward flux is the reflection due to surface albedo. Within the atmosphere the radiation responds to model-predicted cloud and water vapor distributions, as well as specified carbon dioxide, ozone, and (optionally) trace gas concentrations. All the radiation schemes in WRF currently are column (one-dimensional) schemes, so each column is treated independently, and the fluxes correspond to those in infinite horizontally uniform planes, which is a good approximation if the vertical thickness of the model

layers is much less than the horizontal grid length. This assumption would become less accurate at high horizontal resolution.

2.3.4.6.1 Longwave Radiation

a. Rapid Radiative Transfer Model (RRTM) scheme: This RRTM, which is taken from MM5, is based on Mlawer *et al.*, [61] and is a spectral-band scheme using the correlated-k method. An accurate scheme using looking tables for efficiency. Accounts for multiple bands, trace gases, and microphysics species.

b. GFDL scheme: Eta operational radiation scheme. This longwave radiation scheme is from Geophysical Fluid Dynamical Laboratory (GFDL). An older multi-band scheme with carbon dioxide, ozone and microphysics effects.

c. CAM3 longwave scheme: A spectral-band scheme used in the NCAR Community Atmosphere Model (CAM 3.0) for climate simulations [62]. It allows for aerosols and trace gases.

2.3.4.6.2 Shortwave Radiation

a. **MM5 (Dudhia) scheme:** This scheme is base on Dudhia [63] and is taken from MM5. Simple downward integration allowing efficiently for clouds and clear-sky absorbtion and scattering. When used in high-resolution simulations, sloping and shadowing effects may be considered.

b. **Goddard shortwave:** Two-stream multi-band scheme with ozone from climatology and cloud effects based on Chou and Suarez [64].

c. **GFDL shortwave:** Eta operational scheme. This shortwave radiation is a GFDL version of the Lacis and Hansen [65] parameterization. It has two stream Two-stream multi-band scheme with zone from climatology and cloud effects.

d. **CAM3 shortwave scheme:** A spectral-band scheme used in the NCAR Community Atmosphere Model (CAM 3.0) for climate simulation [62].It allows for aerosols and trace gases.

2.3.5 Post-processing Utilities

There are a number of visualization tools available to display WRF-ARW model data. Model data in netCDF (Network Common Data Form) format can essentially be displayed using any tool capable of displaying this data format.

Currently the following post-processing utilities are supported: NCL, RIP4, ARWpost (converter to GrADS and Vis5D), WPP, and VAPOR.

Short description of above mentioned utilities are as follows:

- **NCL:** The NCAR Command Language (NCL) is a free interpreted language designed specifically for scientific data processing and visualization. NCL has robust file input and output. It can read in netCDF, HDF4, HDF4-DOS, GriB (Gridded Binary), binary and ASCII data. The graphics are world class and highly customizable.
- **RIP4:** RIP (which stands for Read/Interpolate/Plot) is a Fortran program that invokes NCAR Graphics routines for the purpose of visualizing output from gridded meteorological data sets, primarily from mesoscale numerical models. RIP4 can currently only read data in netCDF format.
- **ARWpost (converter to GrADS and Vis5D):** The ARWpost package reads in WRF-ARW model data and creates output in either GrADS or Vis5D format. The converter can read in WPS geogrid and metgrid data, and WRF-ARW unput and output files. It can read data in netCDF and GRIBI format.
- **WPP:** It can read data in netCDF and binary format.
- **VAPOR:** VAPOR is the visualization and Analysis platform for Ocean, Atmosphere, and Solar Researchers. VAPOR was developed at NCAR to provide interactive visualization and analysis of numerically simulated fluid dynamics.

For the present study, ARWpost is used to convert the out readable to GrADS and then the GrADS (Grid Analysis and Display System) visualization tools are used as post-processing utilities to display and read the WRF-ARW model data.

2.4.1 Formation of Cloud

CLOUDS are formed by the lifting of damp air which then cools adiabatically by expansion as it encounters continuously falling pressures at higher levels in the atmosphere. The relative humidity consequently rises and eventually the air becomes saturated with water vapour. Further cooling produces a supersaturated vapour, but the excess vapor condenses on to some of the multitude of tiny particles suspended in the air to form a cloud composed of minute water droplets. The growth of these droplets tends to oppose further increase in the super saturation, which reaches a peak value of usually less than 1 per cent and then decreases. In the absence of foreign particles and ions, much higher super saturations are required for droplet condensation. Although we are never concerned with this process in natural clouds, we begin with a discussion of homogeneous nucleation of water vapour because it represents the simplest form of condensation process. Moreover, it provides the most straightforward illustration of the theoretical approach to nucleation problems in general, some examples of which will be discussed later.

2.4.2 The different Types of Clouds in the Atmosphere

Clouds are classified into a system that uses Latin words to describe their appearance and the height of cloud base. This classification is due to the English chemist Luke Howard in 1803. The Latin words used are: cirrus, that means "curl of hair"; stratus, that means layer"; cumulus : "heap"; and nimbus: "rain"[66].

Cloud types are divided in 4 groups. The first three groups of clouds are identified based upon the height of cloud base above the ground:

- high level clouds, from 5 to 13 km
- mid-level clouds, from 2 to 6 km
- low level clouds, from 0 to 2 km above the ground

The fourth group consists of vertically developed clouds: such clouds are so thick that they cannot be classified according to their level above the ground.

High level clouds

High level clouds are named cirrus, cirrostratus and cirrocumulus. They are so high in the sky that they are made of millions of tiny ice crystals, rather than water droplets found at lower altitude. Indeed, their temperature is less than -40°C !

Cirrus (Ci)

Cirrus clouds are curly, featherlike and will often be the first clouds to appear in a clear, blue sky. Shape and moving of cirrus clouds can be an indication of strength and direction of high altitude winds. Such clouds never produce rain or snow at the surface.

Cirrocumulus (Cc)

They take the form of small white balls that are individual or in long rows, high in the sky. When the puffs are in rows, they give the cloud a rippling appearance that resemble the scales of a fish and distinguishes it from a Cirrus or a Cirrostratus.

Cirrostratus (Cs)

These sheet-like, nearly transparent clouds form above 6 km. Cirrostratus clouds are so thin that the sun and moon can be seen clearly through the cloud. When sun or moonlight passes through the ice crystals of a cirrostratus cloud, the light is bent in such a way that a halo may form. Cirrostratus clouds often signal an approaching precipitation event.

Mid-level clouds

Such clouds with the prefix "alto" have bases between 2 to 6 km and are named Altostratus and Altocumulus.

Altostratus (As):

Altostratus clouds are composed of water droplets and ice crystals. They cover the entire sky over an area that usually extends over hundreds of square kilometres. Sun appears as if behind frosted glass: don't look for your shadow on the ground, you won't find it ! And do not forget your umbrella... Although altostratus clouds bring very little precipitation, they often indicate increasing and likelihood of precipitation.

Altocumulus (Ac):

These clouds are white, grey, or both white and grey, they are puffy or like fuzzy bubbles in long rows. They generally have dark, shadowed undersides. Altocumulus without shading may

sometimes be confused with cirrocumulus. In case of doubt, hold your hand at arm's length: if the puff is smaller than one finger width, you are looking at a cirrocumulus cloud!

Low level clouds

Between the ground and 2000 m height, clouds are most generally composed of water droplets and are called stratus, stratocumulus and nimbostratus.

Stratus (St):

Stratus clouds form a low layer that cover the sky like a blanket. They develop horizontally as opposed to the vertically developed cumulus cloud. They can form only a few meters above t

Stratocumulus (Sc):

They are grey with dark shading and spread in a puffy layer. They do not produce rain. They often form after a rainstorm.

Nimbostratus (Ns):

Such clouds form a dark grey, wet looking cloudy layer, associated with falling rain or snow. They can also be considered as mid-level clouds as their thickness can be of about 3000 m! They totally mask the sun.

Vertically developed clouds: cumulus and cumulonimbus

Cumulus (Cu)

Cumulus clouds look like white balls of cotton wool. They are usually isolated with blue sky between the clouds, and they sometimes have funny forms. As they are due to thermal convection (see the chapter "formation processes"), they have flat bases and lumpy tops.

Cumulonimbus (Cb):

Here is the king of clouds. The top of such a cloud can reach 12 km (much higher than the Everest!) and is commonly topped with anvil-shaped head. Rarely, cumulonimbus clouds can reach altitudes up to 18 km and penetrate into the stratosphere. Lower level of cumulonimbus is made mostly of water droplets, whereas at higher elevation, ice crystals dominate as the temperature is well below 0°C. Updraft and gusty wind associated with Cb is more than 100 km/h. If you like rain, thunder, lightning and even tornadoes, cumulonimbus are your friends! If not, just run quickly to your house

2.4.3 The classification of rainfall

The classification of rainfall used by the BMD/WMO is tabulated in Table 2.4.3.

Table 2.4.3: BMD/WMO Classification of rainfall

| Type of rain | Range in mm/Day |
|-----------------------|-----------------|
| Light rain | 4.57 – 9.64 |
| Moderate rain | 9.65 – 22.34 |
| Moderately heavy rain | 22.35 – 44.19 |
| Heavy rain | 44.20 – 88.90 |

2.5.1 Introduction on Tropical Cyclone

A cyclone is an area of intense low pressure where strong winds blow around a centre in anti clockwise direction in the Northern Hemisphere and clockwise direction in the Southern Hemisphere. The term cyclone is derived from the Greek word “Kyklos”. The cyclones are classified as (a) Tropical cyclone and (b) Extra tropical cyclone. The tropical cyclones identified by different local names in different regions, viz. Hurricane , Cyclone, Baguio , Typhoon , Willy - Willy etc. The habit of labeling tropical cyclones with girls and other names persists since 1941.

Tropical cyclones form from initial convective disturbances known as cloud clusters. As they evolve from a loosely organized state into mature, intense storms, they pass through several characteristic stages. A uniform terminology does not exist to describe these stages over the different regions of the globe. General agreement exists that a key stage in the formation process is when the system reaches sustained surface winds exceeding 17.5 m/s (34 kt). Such systems are referred to as tropical cyclones. Another agreed threshold is sustained surface winds of 33 m/s (64 kt), which referred to as severe tropical cyclones.

Cyclonic disturbances in the North Indian Ocean are classified according to their intensity. The following nomenclature is in use:

- | | |
|--|--------------------------------------|
| 1. Low: | Wind speed <31 km/hr. |
| 2. Well marked low: | Wind speed equals to 31 km/hr. |
| 3. Depression: | Wind speed ranges from 32-48 km /hr. |
| 4. Deep depression: | Wind speed ranges from 49-62 km/hr. |
| 5. Cyclonic Strom: | Wind speed ranges from 63-88 km/hr. |
| 6. Severe Cyclonic Strom: | Wind speed ranges from 89-117 km/hr. |
| 7. Severe Cyclonic Strom with a core of hurricane intensity: | Winds =118-220 km/hr |
| 8. Super Cyclone: | Wind \geq 221 km/hr. |

2.5.2 Tropical Cyclone Formation

2.5.2.1 Climatological Conditions for Tropical Cyclone Formation

The first global climatology of tropical cyclone genesis by Gray [67, 68 and 69] demonstrates that the distribution of genesis may relate to six environmental factors;

- i) large values of low level positive relative vorticity.
- ii) a location at least a few degrees poleward of the equator, giving a significant value of planetary vorticity;
- iii) weak vertical shear of the horizontal winds;
- iv) sea-surface temperatures (SSTs) exceeding 26°C, and a deep thermocline;

- v) conditional instability through a deep atmospheric layer ; and
- vi) large values of relative humidity in the lower and middle troposphere.

The first three factors are factors of the horizontal dynamics, while the last three are thermodynamic parameters. Gray defined the product of (i), (ii) and (iii) to be the dynamic potential for cyclone development, while the product of (iv), (v) and (vi) may be considered the thermodynamic potential. As discussed by Gray [68] the thermodynamic parameters vary slowly in time and would be expected to remain above any threshold values necessary for tropical cyclone development throughout cyclonic season. On the other hand, the dynamic potential can change dramatically through synoptic activity. Thus, it was hypothesized by Gray that cyclones form only during periods when the dynamic potential is perturbed to a value above its regional climatological mean.

Frank [70] reduced the list to four parameters by combining (i) and (ii) into the absolute vorticity at low levels deleting (v) and adding mean upward vertical motion to (vi). Following Palmen [71], it has been generally accepted that tropical cyclones only form when the underlying sea surface temperature (SST) exceeds 26⁰C. Palmen hypothesized that the temperature criterion is one of threshold rather than proportionality. Through a more comprehensive study, Raper [72] concluded that higher SST's has no direct impact on the frequencies of tropical cyclones.

2.5.2.2 Large Scale Conditions associated with Tropical Cyclone Formation

Tropical cyclones form only over tropical oceans where upper air observations are sparse, which has made it difficult to document the structure and evolution of the flow during the formation process. Consequently, much of the early understanding of formation was gained from case studies based on innovative use of the existing data networks [73, 74 and 75]. Subsequent studies that exploited improved observational systems have led to further refinement and detail in documentation of the tropical cyclone formation process. However, no well-accepted closed theory of formation exists.

The observational studies have isolated a number of synoptic-scale aspects that have an important role in the formation process:

- i) Tropical cyclones form from pre-existing disturbances containing abundant deep convection;
- ii) The pre-existing disturbances must acquire a warm core thermal structure throughout the troposphere;
- iii) Formation is preceded by an increase (spin-up) of lower tropospheric relative vorticity over a horizontal scale of approximately 1000 to 2000 km;
- iv) A necessary condition for cyclone formation is a large-scale environment with small vertical shear of the horizontal wind;
- v) An early indicator that cyclone formation has begun is the appearance of curved banding features of the deep convection in the incipient disturbance;
- vi) The inner core of the cyclone may originate as a mid-level meso-vortex that has formed in association with a pre-existing mesoscale area of altostratus (i.e., a Mesoscale Convective System or MCS); and
- vii) Formation often occurs in conjunction with an interaction between the incipient disturbance and an upper-tropospheric trough.

We observe universally that tropical storms form only within pre-existing disturbances. An initial disturbance, therefore, forms part of the starting mechanism. A weak circulation, low pressure and a deep moist layer are present at the beginning. The forecaster need not look into areas which contain no such circulations. These statements by Riehl [76] have stood the test of time. The structure of these tropical “cloud clusters” has been documented by many authors (e.g. Ruprecht and Gray [77], Johnson [78] and Houze. The cloud clusters have an upper tropospheric warm core and mean (averaged over a 4° latitude-longitude square) upward velocities of about 100 hPa/day (McBride and Gray [79] and Lee [80]). Although the diameter of the convective area is typically only a few hundred km, the rotational circulation associated with the systems usually extend over a diameter of approximately 1000 - 1500 km.

2.5.3 Life Cycle of Tropical Cyclones

The life span of tropical cyclones with full cyclonic intensity averages at about 6 days. Some storms last only a few hours; a few as long as two weeks. The evolution of the average storm from birth to death has been divided into four stages [81].

Formative stage: Tropical storm form only in pre-existing weather systems. Deepening can be a slow process, requiring days for the organization of a large area with diffuse winds. It can also produce a well-formed eye within 12 hours. Wind speed usually remains below hurricane force in the formative stage. Unusual fall of pressure over 24 hours by 2 - 3 hPa or more takes place in the centre of the vorticity concentration.

Immature Stage: A large number of formative cyclones die within 24 hours. Others travel long distances as shallow depressions. Wind of cyclonic force forms a tight band around the centre. The cloud and rain pattern changes from disorganized squalls to narrow organized bands, spiraling inward. Only a small area is as yet involved, though there may be a large outer envelop. The eye is usually visible but ragged and irregular in shape.

Mature Stage: The force of cyclonic winds may blow within a 30 – 50 km radius during immature stage. This radius can increase to over 300 km in mature storms. On the average, the mature stage occupies the longest part of the cycle and most often lasts for several days. The eye is prominent and circular and the cloud pattern is almost circular and smooth. The surface pressure at the centre is no longer falling and the maximum wind speeds no longer increasing. At this stage, heating from convective clouds furnishes the largest amount of energy for cyclone maintenance. Pressure gradient is largest at the surface. Wind speed range is between 128 – 322 km/hr.

Terminal stage: Nearly, all cyclones weaken substantially upon entering land, because they lose the energy source furnished by the underlying ocean surface. The decay is especially rapid where the land is mountainous. Movement of a cyclone over land cuts off the surface energy source and increases the surface friction, especially when the land is mountainous. Some cyclones die out over sea and this event can be related to their moving over a cold ocean current or being invaded by a surface cold air mass behind a cold front or by a cold centre at high levels moving over their top.

2.5.4 The Mature Cyclone

The description of a composite picture in all its facets from the ocean surface to the upper troposphere of the mature cyclone is written below:

2.5.4.1 Pressure

Within 200 km of the cyclone centre, the pressure field and its isobars are very nearly circular and symmetric around the eye. The most reliable and widely used surface instrument yielding quantitative data is the barometer. Ordinarily, surface pressure varies little more than 0.3% (3mb) in the tropics. The central pressure of cyclones, however, may be 5% or even 10% below average sea-level pressure. A cyclone with 950 mb central pressure is always rated a severe storm.

2.5.4.2 Cloud Pattern

Cloud photographs obtained from weather satellite have revealed that a cyclone seedling initially appears as a cluster of rain clouds. A mature cyclone has a well-organized cloud pattern. It is possible to deduce the wind speed from the size and degree of organization of this cloud. The clouds, especially at the outer edges, form long streets that spiral inward. The most intense part is situated off centre to the right of the direction of motion, which is toward north-northwest. Usually central dot denoting the eye is visible.

2.5.4.3 Wind Fields

When a cyclone lies embedded we may term a steering current of large scale, the speed of the steering current and of vortex are largely additive. To the right of the direction of motion of the centre, the direction of vortex motion and steering current coincide. On the left they are opposed to each other. Thus, speeds are almost invariably higher to the right than to the left of the direction of motion in moving cyclone. Streamlines spiral inward to the ring of strongest wind. The spiral observed in all cyclones.

2.5.4.4 Precipitation

Individual rain gauge measurements give only a poor approximation of precipitation in cyclones. The wind drives rain horizontally and picks up water already fallen to the ground. Even slight topographic features such as buildings, lakes and small hills influence precipitation. Rainfall at any station depends on its location with respect to cyclonic path, intensity and celerity.



2.5.4.5 The eye of the cyclone

The centre of the cyclone is revealed as a ‘singular point’; pressure stops falling, wind stops blowing hard, rainfall ceases, clouds lighten or disappear so that the satellite photograph shows a central small hole, and the ocean motion are confused. Eye diameter varies from 5 to over 60km, depending on rate of strong propagation. Though the eye is usually pictured as circular, it sometimes becomes elongated. Sometimes it is diffused with a double structured appearance. Modern observation specially radar, have proved that an eye does not remain in steady state but is constantly undergoing transformation.

2.5.5 Cyclones of North Indian Ocean

Most North Indian Ocean cyclones form within the inter tropical convergence zone ITCZ. Formation may occur either as reintensification of westward-propagating disturbances or from in-situ disturbances that develop within the trough. The zone of formation shift meridionally between 5°-20°N following the annual migration of the ITCZ.

Although only about 7% of the global tropical cyclone [82] occur in the North Indian Ocean and they are most deadly. The shallow waters of the Bay of Bengal, the low flat coastal terrain and the funneling shape of the coastline can lead to devastating losses of life and property due to the surge from a storm of even moderate intensity. The Buckerganj cyclone of 1876 and the Bhola cyclone of 1970 each killed more than 200,000 people in Bangladesh. More than 138,000 people were killed by a storm surge of cyclone 1991 in Bangladesh.

About 10 cyclones [83] form in the North Indian Ocean basin each year, with variation from 3 to 16 during the period 1891-1991. The average annual frequency of cyclonic storms is about 3. The annual number of cyclonic storms is about 26.56% of the annual number of cyclonic disturbances. The average annual number of severe cyclones is about 1.48 which is 14.81% [83] of the annual number of cyclonic disturbances. Alam *et al.* [84, 85] observed that on the average 7.77 storms and depressions and 3.46 storms formed in the Bay of Bengal during 1974 – 1999. The average annual number of cyclonic disturbances is about 2. That indicates five to six times more tropical cyclones occur in the Bay of Bengal as in the Arabian Sea.

The seasonal variation has a bimodal distribution with the primary maximum in November and a secondary maximum in May. That is, the intervening period of the summer monsoon is a relatively suppressed period of tropical cyclone formation. McBride [86] attributed this suppression to the close interrelation between tropical cyclones and monsoon depressions. The two types of systems have almost identical structure of the larger scale vortex, and both systems form over warm tropical oceans. During the May and June cyclone season, system develops this large scale vortex structure in the ITCZ/ monsoon trough and remain over the ocean long enough to develop an inner core structure and so become tropical cyclones. When the ITCZ/ monsoon trough is located further north and closer to land in August, the systems still form over warm waters, but they then track northwest into the Indian subcontinent and so remain monsoon depressions (i.e. with no inner – core structure).

2.5.6 Movement and track

Cyclones have two motions: one is wind speed called intensity of cyclone and another is translational speed of the cyclone. The path of motion is referred to as a tropical cyclone's track. The translational speed or movement of cyclone is different for different cyclones. A cyclone also does not move with same speed through its whole trajectory. The movement speed of cyclones in the Northwest Pacific Ocean and western side of the North Atlantic Ocean is maximum and it is least in the North Indian Ocean (Arabian Sea and Bay of Bengal). The translational speed of a mature tropical cyclone in Bay of Bengal is about 8-10 knots [87].

Once formed, tropical cyclones tend to move westward and pole-ward. If they do not dissipate over land or cold water, they usually recurve pole-ward and eastward, often moving into middle and high latitudes before finally dissipating or transforming to extra-tropical cyclones which, unlike their tropical cousins, derive their energy from the potential energy stored in the pole-to-equator temperature gradient [88]. The motions and tracks of tropical cyclones are controlled by different factors. Some are discussed below:

- **Steering winds:** It has been found that the tropical cyclone movement is steered by the upper tropospheric wind overlying the system. This is called the steering wind.

- Coriolis effect: The Coriolis force adds additional vorticity to the cyclonic system and turns the east-west moving systems towards north in the northern hemisphere and towards south in the southern hemisphere.
- Interaction with the mid-latitude westerlies: When the tropical cyclone moving poleward comes under the mid-latitude westerlies, it takes turn towards the east.

2.5.6.1 Cyclone track prediction

Cyclone track prediction techniques are grossly classified as

- a) Simple techniques
- b) Statistical models and
- c) Dynamical models



Persistence, climatology and analog techniques fall in the simple track prediction category. There are number of Statistical models to predict cyclone tracks. Barotropic models and baroclinic models of regional and global scales are of dynamical types.

It may be assumed that the entire tropical cyclone system has considerable inertia that can not be turned rapidly. If the vortex, large scale flow, and the interaction process do not change, future motion should resemble the past motion and thus persistence model developed. In climatological track prediction models it is assumed that the present storm will move with the average direction and speed of all past storms near that location.

A combination of persistence plus climatology may be expected to provide an improvement over the separate techniques. A statistical combination of CLImatology and PERsistence (CLIPER) developed for the Atlantic region by Neumann [89] has been extended to other basins [90, 91]. Predictors such as the present latitude and, longitude, the components of the recent motion of the storm and the intensity are used. Least squares to fitting of the basic predictors and various polynomial combinations is used in CLIPER derive regression equations for future latitudinal/longitudinal displacements in 12-h increments.

The basic assumption of the analog techniques is that a given storm will move in the mean speed and direction of all storms that occurred in that region within some time interval centered on the current day. The analog technique also includes a persistence aspect. In the HURRICANE ANalog

(HURRAN) scheme by Hope and Neumann [92] each selected analog is translated to the position of the existing storms and started at the heading and speed of the current storm. The predictand in the statistical models is the tropical cyclone components motion over some future time interval. Statistical models derive their variance reducing potential from one or more of four sources of predictive information: "climatology; persistence; analyzed environmental data; or numerically forecast environmental data". When synoptic data is used the model then it is termed as Statistical-synoptic (e.g. NHC-72) and when dynamical models data is used then the Statistical model is termed as Statistical – dynamical model (e.g. NHC-73). NHC -83 has a hybridized form of CLIPER type, Statistical synoptic and statistical dynamical model.

Barotropic models have their capability to achieve higher horizontal resolution to better resolve the storm structure and the interaction between the vortex and its environment. The barotropic model is useful for situation in which the lower tropospheric flow in the tropics is more barotropic and limited period of times. To achieve higher horizontal resolution to better resolve the strong structure and the interaction between the vortex and its environment barotropic model is preferred. A barotropic model is useful for situation in which the lower tropospheric flow in the tropics is more barotropic for limited periods of time. VICBAR developed by Hurricane Research Division of U.S.A is a barotropic model and used for operational track forecasting Bureau of Meteorology Research Center of Australia also uses its own barotropic model. It is found that with respect to CLIPER both of them works better.

Baroclinic models are of two categories (i) regional models and (ii) global models. Many countries have their own regional baroclinic models and they are of different resolution. One of the major problems of the regional baroclinic model is to assign its lateral boundary conditions. In some situation the lateral boundary conditions are assigning through its global counter part.

On the other hand major meteorological research centre has their own global models. Most of these global models handles all over the environmental factors that have their role to the local weather for example land ocean interaction, land use pattern, topography, sea surface temperature, incoming and outgoing solar radiation along with pressure, wind field temperature etc. The global models differ in terms of resolution also in terms of the model physics. With the enhancement of number of layers along the verticals and the number of grid points in the Lat-

long direction the requirement of computational capacity goes higher and higher. So forecasters use low resolution global models to assign boundary conditions to a high resolution regional model.

2.5.7 Rainfall Distribution around a Tropical Cyclone

Rainfall is found to be strongest in their inner core, within a degree of latitude of the center, with lesser amounts farther away from the center [76]. Most of the rainfall in hurricanes is concentrated within its radius of gale-force winds. The chart to the right was developed by Riehl in [76] using meteorological equations which assume a gale radius of about 210 statute miles/300 km, a fairly symmetric cyclone, and does not consider the effect hills and mountains would have on the rainfall distribution, or vertical wind shear. As seen in the statistics from China, local amounts can exceed this chart by a factor of two due to topography. Rain is a source of precipitation which forms when separate drops of water fall to the Earth's surface from clouds. Larger tropical cyclones have larger rain shields, which can lead to higher rainfall amounts farther from the cyclone's center. This is generally due to the longer time frame rainfall falls at any one spot in a larger system, as long as forward motion is similar to that of a smaller system. Some of the difference seen concerning rainfall between larger and small storms could be the increased sampling of rainfall within a larger tropical cyclone when compared to that of a compact cyclone; in other words, the difference could be the result of a statistical problem.

Quantitative prediction of tropical cyclone rainfall is very difficult for three reasons:

- i) Rainfall itself is difficult to measure accurately, which hinders both operational analysis of rainfall and the development of improved forecasting aids;
- ii) Current errors in track prediction mean that accurate rainfall estimates cannot necessarily be transformed into precise predictions, this is especially a problem when a cyclone is moving near regions of significant orography;
- iii) Interactions between tropical cyclones and other weather systems are themselves complicated and poorly understood, so that heavy rain in areas of large-scale ascent and high humidity are difficult to predict;
- iv) Even within clearly defined threat areas, mesoscale processes, which are poorly understood and difficult to monitor, may determine the distribution of heavy rainfall.

As with other aspects of tropical cyclone structure forecasting, operational numerical models generally lack the resolution and physical processes to predict rainfall accurately and explicitly but they are rapidly being improved. They may be especially useful in determining threat areas in complicated situations.

Research on tropical cyclone rainfall has tended towards intensive examination of a few cases. Improvements in forecasting ability, especially of regional peculiarities, would be well served by the development of a simple archive of the relevant synoptic features and resulting rainfall for a wide variety of cases. Were this available, forecasters would be able to classify each new situation within the range of typical patterns and perhaps make a more accurate prediction of the heavy rain threat area.

2.5.7.1 Rainfall Measurement

Rainfall is very difficult to measure accurately, especially for small areas, heavy rain, and short periods of time. Three methods are commonly used:

Rain Gauges: Rain gauges are very simple and direct. Unfortunately, convective rainfall is extremely variable in the horizontal, so a rain gauge network must be very dense. Otherwise a local extreme can be misinterpreted as the amount for an entire region. High winds such as found in tropical cyclones may also cause turbulence around the gauge and lessen its catch unless special shielding is used. Rain gauge networks are of most value in providing the ground truth, however limited, for indirect radar and satellite estimates.

Radar: Radar can continuously cover a 400 km radius circle over all conditions, unless blocked by terrain. It is less prone to sampling problems than gauges because of its continuous spatial coverage and implicit averaging over an area determined by the pulse length and beam width. Radar measures the strength of radio pulses scattered back to the radar by precipitation particles, which is related to their size and type (rain, snow, hail) by a rather complex equation. The size and type of particles is in turn related to rain rate by a less clearly known relationship, based on empirical 'Z-R relationships' determined by comparing radar and rain gauge measurements. The relationship varies according to the radar and type of weather system.

Satellite Imagery: Satellite imagery can be used to estimate rainfall by empirical relationships based on the shape, texture and (infrared) black-body temperature of the tops of clouds. Although the relationships are not overly accurate, the large area and frequent time coverage make this a useful initial estimate of tropical cyclone rainfall over the ocean.

Satellite Microwave Measurements: Satellite microwave measurements use either radiometers measuring upwelling microwave radiation, or active "radars" in space, which work on the same principle as ground-based radars. Several systems are currently being tested and show significant promise for quantitative determination of tropical cyclone rainfall. Their operational use is untested at this stage, however.

2.5.7.2 Rainfall Analysis and Forecasting

Because of the meteorological complexity, measurement limitations, and lack of objective aids, analysis and forecasting of heavy rain associated with tropical cyclones can at best be indicative of likely outcomes. A suggested mode of operation is to first classify the situation as uncomplicated or complicated.

Uncomplicated situations satisfy the following conditions:

- i) The tropical cyclone is relatively well developed;
- ii) The tropical cyclone is a day or less from landfall and is moving rapidly enough such that its precipitating region will pass over a given point completely within a day or less;
- iii) There are no topographic features within the path of the tropical cyclone which are significant enough to appreciably alter the rainfall;
- iv) There are no significant nearby weather systems, including frontal zones, jet streams, or upper-level cut-off lows, which are likely to interact with the tropical cyclone during its passage inland.

Unfortunately, the majority of forecast situations near landfall involves rapid changes in the character and structure of the precipitation as the system moves inland and interacts with orography and other weather systems. Simple extrapolation procedures will not work very well and the situation is therefore complicated. About the best the forecaster can do in advance is identifying a general threat area based on the locations of the tropical cyclone and surrounding

weather systems. The actual locations of heavy rain must then be identified as the event proceeds in order to identify areas which are accumulating dangerous amounts of rainfall. In the absence of dominating terrain, mesoscale processes such as the development of new convective cells at the merger of old convective outflow boundaries generally determine where within the threat area the heavy rain actually falls. If these mesoscale focusing mechanisms are quasi-stationary, extremely heavy rain may fall even though the convective elements are moving quickly.

2.5.8 Tropical Cyclone Speed

Wide ranges in tropical cyclone translational speeds are observed, both within and across ocean basins. Some of the more significant aspects of translational speeds are:

- i) Predominance of slow tropical cyclones over the north Indian basin and the more equatorial portions of the Southern Hemisphere west of 160°E ;
- ii) A marked lack of slow tropical cyclones over the North Atlantic and the western North Pacific basins;
- iii) The fastest cyclones predominate only in the high latitudes of the North Atlantic and the western North Pacific basins, where average speeds occasionally exceed 40 kt (75 km h^{-1}), but a qualification is needed here on the inclusion of extratropical systems;
- iv) A comparatively small range of speeds are observed over the eastern North Pacific basin.

2.5.8.1 Direction of Tropical Cyclone Motion

The mean directions of motion show that the classical recurvature patterns occur over the North Atlantic and the western North Pacific basins, and to a lesser extent in the southwestern Indian Ocean. The cyclones over the eastern North Pacific typically dissipate before recurvature into the westerlies. In both the north Indian Ocean and northern and western Australia regions cyclones often encounter land and dissipate before or during recurvature. The near-equatorial approach of mid-latitude westerlies in the southwest Pacific leads to a predominantly eastward motion of tropical cyclones.

2.5.8.2 Variability of Tropical Cyclone Motion

Analyses of tropical cyclone position forecast errors demonstrate that they are highly dependent on the tropical cyclone translational speeds and variability thereof. The greatest forecast errors are typically associated with rapidly moving or highly variable tropical cyclones. Thus, indications of the steadiness of cyclone motion, combined with knowledge of the mean translational errors provide a useful means of comparing forecast errors.

The vector speeds are always less than the scalar speeds and the proportion of speed reduction compared with the scalar means indicates the degree of variability in tropical cyclone motion. Thus, the western part of the eastern North Pacific basin has highly consistent tropical cyclone motions, whereas the recurvature latitudes of the North Atlantic and the western North Pacific as well as the equatorial regions of the Southern Hemisphere experience highly variable motion. A climatological measure of speed variability therefore can be obtained by algebraically dividing vector speeds by scalar speeds

The global variation in tropical-cyclone motion steadiness, as defined by the above index multiplied by 100 and rounded off the nearest integer value. Note that the higher the index, the more consistent the motion, and perfectly steady cyclones would rate 100. Three ranges of steadiness have been arbitrarily defined with indices greater than 90 being rated high; 60-90 indicate average steadiness and systems below 60 are rated as erratic.

Noteworthy the regions of erratic motion (some less than 40) in the Australian / southwest Pacific region and the remarkably consistent tracks in the eastern North Pacific basin. Relatively low steadiness values also are found over the recurvature latitudes of the North Atlantic and the western North Pacific basins.

2.5.9 Tropical Cyclone Intensity

The Dvorak (1984) analysis is the worldwide standard for tropical cyclone intensity monitoring in the absence of aircraft reconnaissance and is the most common method of intensity forecasting as well. An important part of the technique is a climatological development rate, which provides a basis for estimating intensity changes.

Previous research indicates that 75% of all western North Pacific tropical cyclones deeper than 920 hPa have experienced a period of rapid intensification of 42 hPa d^{-1} or more. Extreme deepening rates of nearly 100 hPa d^{-1} have been observed. All tropical cyclones, even the weaker ones, should therefore be regarded as potentially serious.

One conceptual model of tropical cyclones at sea is that they are self-amplifying systems. They will intensify until they reach a Maximum Potential Intensity (MPI) unless their surroundings disrupt them, as is frequently (and fortunately) the case. The potential intensity is primarily a function of Sea Surface Temperature (SST) and tropopause temperature, so passage over colder water (or land) reduces the MPI. Strong vertical shear of the environmental flow is the most common factor limiting intensification in tropical and subtropical latitudes at sea. Tropical cyclones with a compact core of maximum winds and strongest convection are thought to intensify more rapidly, as are those that are well below their potential intensity. Another commonly held view is that interactions with upper-level troughs, either of tropical or subtropical nature, may further tropical cyclone intensification under the right conditions.

The threat of rapid intensification resulting in a very destructive tropical cyclone should therefore be considered greatest for compact, well-organised circulations with warm SST, a high tropopause, and relatively low vertical shear of the environmental flow. The Dvorak method contains detailed procedures for evaluating the satellite signature of a tropical cyclone in terms of its current and near-future intensity. Work sheets designed to modify the Dvorak forecast development rate based on other information are then presented and discussed.

2.5.10 Tropical Cyclone Warnings

There are two general types of tropical cyclone warnings: those for land areas and coastal waters and those for the high seas (sometimes referred to as marine warnings).

2.5.11 Prevention

In 1947 a group of scientist under the leadership of the Nobel laureate Irving Langmuir seeded a hurricane with ice nuclei to test it could be modified and make less destructive. Because of the risks involved in trying to change the behavior of hurricanes approaching land, only half a dozen hurricane-seeding tests have been conducted. The most encouraging ones were carried out on

August 18 to 20, 1969, when hurricane Debbie was seeded with silver iodide by aeroplanes of Project Storm fury, a joint research program of the National Oceanic and Atmosphere Administration and the U.S Navy. Following both periods of seeding, the peak winds within the hurricane decreased substantially at the aircraft flight level of about 3600m. Mathematical analysis by project scientist indicated that ice-nuclei seeding of a hurricane outside the zone of maximum winds should cause a reduction of peak speed. These results persuaded some scientists that it might be possible to weaken hurricanes by seeding them, but there still are many uncertainties. It is considered essential that more experiments over the open ocean be performed before seeding hurricanes about to populated areas.

2.6 Previous studies on Heavy Rainfall and Tropical Cyclones

A number of cumulus parameterization (CP) schemes have been developed over the years but all of them have certain limitations [93, 94, 95, 96 and 97]. Convection has long been recognized as a process of central importance in the development of many weather events. The scale of convective clouds is too small to be resolved by numerical models and hence need to be parameterized in terms of variables defined at the grid points. With increasing computer resources, in the last half decade, many of these NWP centers started using higher resolution models for prediction of cyclone and cold front to reduce errors associated with finite differencing [98] and for better representation of topographical features and sub-grid scale physical processes.

Convective activities in the tropic play an important role. The Asian monsoon, in particular, is composed of diurnal cycle [99] and intraseasonal variation [100, 101]. During summer, the Bay of Bengal is characterized as cloudiest oceanic area [102]. The monsoon wind carries water vapor from the Bay of Bengal to the inland and produces convective systems in and around Bangladesh and about 6000 mm rainfall occurred during summer monsoon[103]. There are variation of rainfall with respect to place and time[104]. So, it will be useful if we can estimate the amount of rainfall at different place of Bangladesh. Kataoka[105] have used MM5 to study the diurnal variation of precipitation. Akhter *et al.* [106] has tried to select a suitable combination of PBL and CP scheme to simulate rainfalls over Bangladesh.

Ahsan *et al.* [107] simulate heavy rainfall events using MM5 model. Role of cumulus parameterization schemes is tested by Odury *et al.* [108,109]. During summer monsoon period, one of the main synoptic conditions for occurrence of heavy rainfall over Bangladesh and

neighborhood is the southwesterly flow streaming from the head Bay of Bengal into Bangladesh [110]. TRMM overestimates the summer monsoon rainfall [111].

The most crucial aspects in developing and maintaining of tropical cyclones in any basin are the heat and moisture fluxes from the warm ocean surface and release of latent heat from cumulus clouds. These driving mechanisms are now well understood and represented through physical processes by known parameters called "parameterization". Rao and Prasad [112] emphasized that Planetary Boundary Layer (PBL) processes and convection processes in free atmosphere are crucial in modeling tropical cyclone. He further emphasized that PBL processes and Conditionally Instability of Second Kind (CISK) mechanism proposed by Charney and Eliassen [113] are the important physical processes for the intensification of a low pressure into a cyclonic storm. Though the dynamical and physical processes are well understood and represented in numerical models, prediction of movement of these systems is still not clear due to representation of vortex in the initial condition with coarse resolution grid over data sparse oceanic region, where formation of tropical cyclones take place. In some studies [114, 115, 116, 117, 118] bogus vortices are adopted to overcome this poor representation of vortices in the initial analysis. One of the reasons for this poor representation may be due to coarse resolution of initial condition such as NCEP reanalysis ($2.5^{\circ} \times 2.5^{\circ}$) and FNL analysis ($1^{\circ} \times 1^{\circ}$).

To simulate track and structure of cyclones, several numerical models have been deployed by many researchers in the world. Some of these are Typhoon Model (TYM) for Western North Pacific [119], Quasi-Lagrangian Model (QLM) for North Atlantic, Eastern North Pacific [120] and Bay of Bengal [117, 112 and 121], Geophysical Fluid Dynamics Model (GFDL) [122, 115] for North Atlantic and Eastern North Pacific, BMRC model for Australia [123], etc. Liu *et al.* [124] utilized NCAR MM5 model to simulate track, storm intensity and inner core structure of Andrew-1992 with triple nested grid with 6 km horizontal resolution.

Davis and Bosart [125] utilized MM5 model to simulate genesis of hurricane Diana-1984 and documented that physics play an important role during transformation from marginal storm to hurricane intensity. Barun [126] employed MM5 model to simulate asymmetrical structure of eye and eyewall of BOB-1991 hurricane. Mohanty *et al.* [127] simulated Orissa super cyclone using MM5 with horizontal resolution 30 km. He reported that model is able to predict intensity of the storm up to 48 hrs and underestimate between 48 hrs and 72 hrs. He further emphasized that delayed landfall could be due to overestimation of the intensity of the system. Rao and Rao [128] simulated the same Orissa super cyclone using MM5 with options of Grell, MRF and simple ice for parameterization schemes of convection, planetary boundary layer and explicit moisture. They reported that the cyclone is better simulated by the model but intensity was

underestimated. Trivedi *et al.* [129] documented some improvement of track prediction of Orissa super cyclone with assimilation of synthetic vortex into the initial analysis.

Using MM5, Yang and Ching [130] studied sensitivity of different parameterization schemes by applying to Typhoon Toraji-2001. It revealed that Grell convection scheme and Goddard Graupel cloud microphysics scheme give better track; whereas warm rain scheme gives lowest central surface pressure and MRF planetary boundary layer gives the intensity and track in agreement with the observations. Lin *et al.* [131] studied super cyclonic storm Nargis (2008), which developed in the Bay of Bengal and devastated low-lying coastal areas of Myanmar. They utilized Price-Weller-Pinkel [132] ocean mixed layer model to study air-sea interaction during rapid intensification of Nargis. It is documented that rapid intensification from a weak category-1 storm to an intense category-4 storm within 24 hrs is mainly due to pre-existing warm ocean anomaly in the Bay of Bengal.

CHAPTER 3
METHODOLOGY

3.1 Selection of Model

In the present study two state-of-the-art mesoscale models MM5 and WRF-ARW have been used to evaluate their performances for the simulation of heavy precipitation events and tropical cyclone events.

3.2 Experiments on Simulation of different Heavy Precipitation and TC events

Two types of events i.e. heavy rainfall and tropical cyclone events have been considered for the simulation of different meteorological parameters to understand the genesis, characteristics and structure of the systems. Three test cases have been considered for the heavy rainfall events and the events are Case 1 (1-3 July 2008), Case 2 (9-11 June 2007) and Case 3 (1-3 May 2009). On the other hand, three test cases have been considered for the tropical cyclone events and the cases are Case 1 (Tropical Cyclone Aila, 23-27 May 2009), Case 2 (Tropical Cyclone Sidr, 11-17 November 2007) and Case 3 (Tropical Cyclone Rashmi 24-28 October 2008).

3.3 Domain and Model Physics

Domain and model physics set up are the one of the vital things for the simulation of any event in Numerical Weather Prediction Model. Set up of them are explained in the following sub-sections.

3.3.1 Domain Set Up

For the heavy precipitation events, three domains are taken: first one is mother domain and other two are nested domains in the mother domain. Inner most domains will cover the Bangladesh region. Ratio of the resolution of the three domains is 9:3:1 respectively. The horizontal grid resolution of the mother domain is 90 km and those for two nested domains are 30 km and 10 km respectively. The dimension of the models MM5 and WRF are summarized in Table 3.3.1.1. There is little variation in the dimension between two models.

Table 3.3.1.1: Dimension of the domain for heavy precipitation events

| Domain | MM5 | | WRF | |
|--------|-------------|--------------|-------------|--------------|
| | Latitude °N | Longitude °E | Latitude °N | Longitude °E |
| 1 | 4.21-39.51 | 62.98-101.02 | 8.73-32.07 | 60.62-103.06 |
| 2 | 18.20-29.06 | 80.52-96.43 | 12.70-28.58 | 80.25-99.02 |
| 3 | 20.41-27.71 | 87.98-93.82 | 20.08-27.39 | 86.80-93.63 |

For the TC events, two domains are taken: first one is mother domain and the other one nested domain in the mother domain. Inner most domains cover the whole cyclone path including Bangladesh region. Ratio of the resolution of the two domains is 3:1 respectively. The horizontal grid resolution of the mother and nested domains are 90 km and 30 km respectively. The dimension of the model for the models MM5 and WRF are summarized in Table 3.3.1.2. There is little variation in the dimension between two models.

Table 3.3.1.2: Dimension of the domain for tropical cyclone prediction

| Domain | MM5 | | WRF | |
|--------|-------------|--------------|-------------|--------------|
| | Latitude °N | Longitude °E | Latitude °N | Longitude °E |
| 1 | -0.22-37.94 | 67.36-108.64 | -1.58-38.94 | 66.10-110.02 |
| 2 | 5.36-28.71 | 81.66-99.20 | 4.19-28.50 | 81.25-99.17 |

3.3.2 Model Physics

3.3.2a. Model physics for MM5

In our present study Medium Range Forecast (MRF) PBL scheme, Kain - Fritsch (KF) cumulus parameterization (CP) scheme, Dudhia Simple Ice microphysical Scheme for moisture anticipation, Cloud Radiation Schemes for radiation calculation and 5- Layer Soil model to predict soil temperature are used as model physics and are summarized in Table 3.3.2.1. Model equations in the surface flux form are solved on Arakawa B grid. Leapfrog time integration scheme with time splitting technique is used in model integration.

Table 3.3.2.1: Domain design of the model MM5 Version 3.7

| | |
|-----------------------------------|---|
| Dynamics | Non-hydrostatic with three-dimensional Coriolis force |
| Main prognostic variables | u, v, w, T, p and q |
| Map projection | Lambert conformal mapping |
| Horizontal grid distance | 90 and 30 km for TC; 90, 30 and 10 km for rainfall |
| Number of vertical levels | 23 half sigma levels |
| Horizontal grid system | Arakawa B grid |
| Time integration scheme | Leapfrog scheme with time-splitting technique |
| Radiation parameterization scheme | Cloud |
| PBL parameterization scheme | MRF |
| Cumulus parameterization schemes | KF |
| Microphysics | Simple Ice |
| Soil model | 5-layer soil model |

3.3.2a. Model Physics for WRF

The modified Kain - Fritsch cumulus parameterization scheme is used in this case [41]. The cloud microphysics scheme is WRF Single-Moment (WSM) 3-class simple ice scheme, which is a simple efficient scheme with ice and snow processes suitable for mesoscale grid sizes [34]. It replaces NCEP 3 scheme. The long-wave radiation parameterization is the Rapid Radiative Transfer Model (RRTM) scheme, which is an accurate scheme using look-up tables for efficiency accounts for multiple bands, trace gases, and microphysics species [61]. The short-wave radiation scheme is as per the Dudhia scheme, which allows simple downward integration for efficient cloud and clear-sky absorption and scattering [63]. The Planetary Boundary Layer (PBL) parameterization is the Yonsei University Scheme (YSU) [58], which is the next generation MRF-PBL. An overview of the model used in this study is provided in Table 1.

Table 1: Domain design of the model WRF

| | |
|---------------------------------|--|
| Dynamics | Nonhydrostatic |
| Horizontal grid distance | 90 and 30 km for TC; 90, 30 and 10 km for rainfall |
| Integration time step | 240 s |
| Map projection | Mercator |
| Horizontal grid system | Arakawa-C grid |
| Vertical co-ordinate | Sigma co-ordinates 28 σ levels |
| Time integration scheme | Third-order Runge-Kutta scheme |
| Spatial Differencing scheme | Second to Sixth order schemes |
| Radiation parameterizations | RRTM, Dudhia scheme |
| Surface layer parameterizations | Monin-Obukhov scheme, thermal diffusion scheme |
| Cumulus parameterization | Kain- Fritsch schemes |
| PBL parameterization | YSU scheme |
| Microphysics | WSM 3 simple ice scheme |
| Land surface | Unified Noah Land surface Model |

3.4 Initial Data Source

For the simulation of heavy precipitation events and tropical cyclone (TC) events, both the models are run for 72 hours. Final Reanalysis (FNL) data ($1^0 \times 1^0$) from National Centre for Environment Prediction (NCEP) is used as initial and lateral boundary conditions (LBCs) which is updated at six hourly interval i.e. the model is initialized with 00, 06, 12 and 18 UTC initial field of corresponding date.

3.5 Synoptic Features of the Selected Heavy Rainfall Events

3.5.1. Heavy Rainfall case 1 (1-3 May, 2009)

There was a low pressure system over West Bengal and adjoining area persists with its associated trough extended to North Bay on 1 May 2009. On 2 May the low also was over West Bengal and adjoining Bihar and one of its associated troughs extended to North Bay. Due to this low rain occurred at maximum places over Bangladesh and highest rainfall was recorded at Sylhet – Srimongal region. On 3 May the low shifted over Orissa and adjoining West Bengal extending its trough to the south western part of Bangladesh. Heavy rainfall occurred over many places of Bangladesh, e.g. Mymensingh 81 mm, Feni 78 mm, Chittagong 62 mm and Comilla 35 mm.

3.5.2. Heavy Rainfall case 2 (9-14 June, 2007)

At 09 June 2007, a low formed over sub-Himalayan West Bengal and adjoining area with its trough extended to Northeast Bay. Monsoon was moderate to strong elsewhere over North Bay. Southwest monsoon swept up to southern part of Rajshahi Division and it was likely to sweep over rest of the country during next 12 – 18 hours. At 10 June 2007, the low was over eastern Uttar Pradesh and adjoining area. Southwest monsoon was set on all over Bangladesh. Monsoon was active over Bangladesh and strong to vigorous over North Bay. At 11 June 2007, monsoon axis ran through Bihar to Assam across central part of Bangladesh. One of its associated troughs extended to northwest Bay. Monsoon was active over Bangladesh and strong to vigorous elsewhere over North Bay.

3.5.3 Heavy Rainfall case 3 (1-3 July, 2008)

Monsoon axis ran through Phnjab, Horiyana, Uttar Prodesh, Bihar, West Bengal and thence northeastwards of Assam across central part of Bangladesh on 1 July 2008. Its associated trough extended to North Bay. Steep pressure gradient persisted over North Bay. Monsoon was active over Bangladesh and moderate to strong over North Bay. On 2 July 2008, monsoon axis ran through Phnjab, Horiyana, Uttar Prodesh, Bihar, West Bengal to Assam across central part of Bangladesh. One of its associated troughs extended to Northwest Bay. Monsoon was active over Bangladesh and moderate to strong elsewhere over North Bay. On the following day, Monsoon axis was seen to run through Phnjab, Horiyana, Uttar Prodesh, Bihar, West Bengal to Assam across central part of Bangladesh. One of its associated troughs extended to Northwest Bay. Monsoon was fairly active over Bangladesh and moderate elsewhere over North Bay.

3.6 Synoptic Features of the Selected Tropical Cyclones (TC)

3.6.1 Severe Cyclonic Storm Aila (23-27 May 2009)

At 06 UTC of 23 May 2009 the system was in the state of depression and was centered near 16.5°N , 88°E i.e. about 600 km south of Sagar Island. The track of the system is shown in Figure 3.6.1.1. The track and other parameters of the system are tabulated in the Table 2. The depression moved mainly in a northerly direction and intensified into deep depression and at 03 UTC of 24 May was near 18.0°N , 88.5°E . At 12 UTC of 24 May it was intensified into a cyclonic storm and named as Aila and was centered near 18.5°N , 88.5°E . It continued to move in a northerly direction and intensified into a severe cyclonic storm at 06 UTC of 25 May and was centered over northwest Bay of Bengal near 21.5°N 88.0°E close to Sagar Island. The system crossed West Bengal coast close to the east of Sagar Island between 0800 to 0900 UTC as a severe cyclonic storm with wind speed of 100 to 110 kph. The lowest estimated central pressure was about 967 hPa at the time of landfall. After the landfall, the system continued to move in a northerly direction, gradually weakened into a **cyclonic storm** and at 1500 UTC of 25 May was centered over Gangetic West Bengal, close to Kolkata. While it continued its northerly movement, it further weakened into a **deep depression** and at 0300 UTC of 26 May it was over Sub-Himalayan west Bengal close to Malda. It weakened into a **depression** and at 0060 UTC of 26 May was close to Bagdogra. It weakened further and became less marked on 27 May (Figure 3.6.1.1).

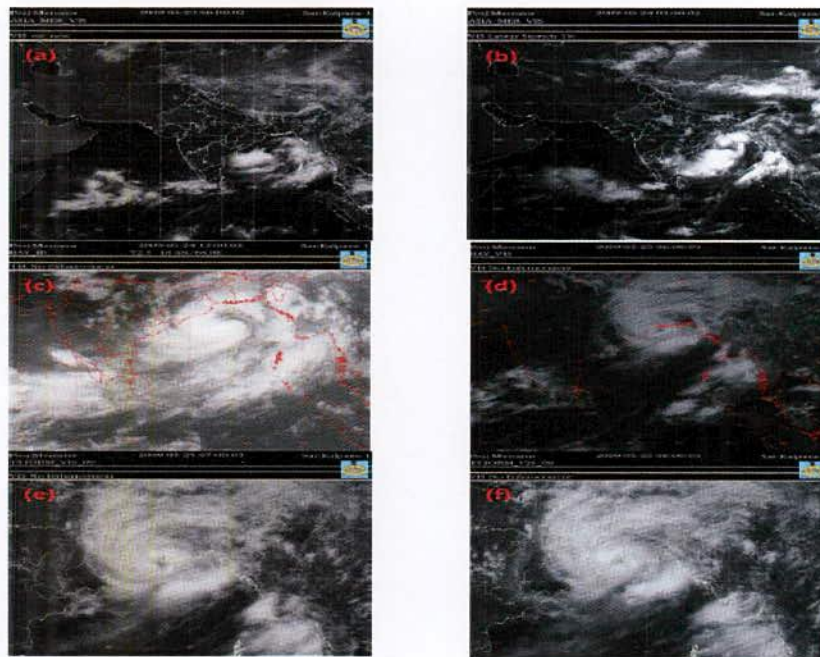
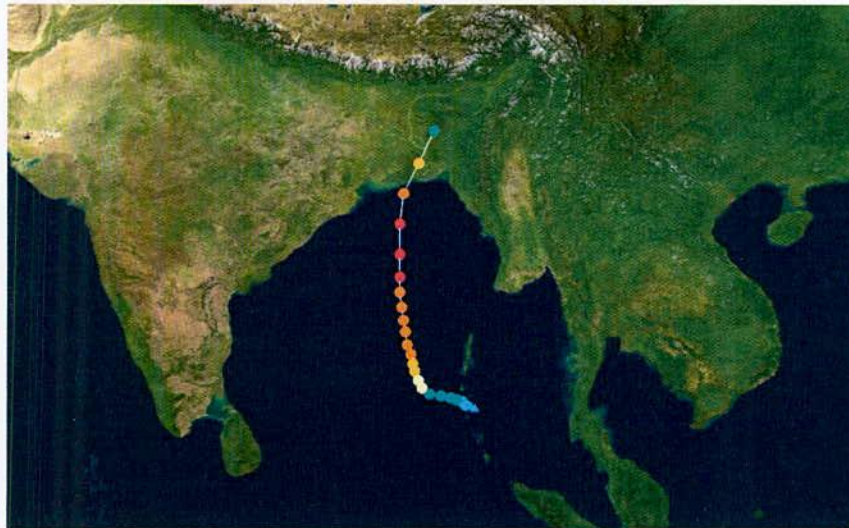


Figure 3.6.1.1: INSAT imageries of the system at different stages of intensification and landfall a) Depression, (b) deep depression, (c) cyclonic storm, (d) severe cyclonic storm, (e) prior to landfall and (f) during landfall

3.6.2 Super cyclone Sidr (09-16 November 2007)

Super cyclonic storm Sidr, also known as 06B, was one of the strongest TCs to hit Bangladesh. This was the fourth TC formed in the North Indian Ocean cyclone season in 2007. A disturbed weather developed over the Andaman Sea near Nicobar Islands on 09th November and deepened into a depression over the same area on 11th. It was further strengthened into a deep depression on the same day and moved slowly in northwestward direction. On 12th the system was developed into a cyclonic storm and moved further in the same direction and quickly intensified into a severe cyclonic storm on the same day. It was developed into a very severe cyclonic storm on 13th and continued moving northward. On 15th morning it was deepened into a super cyclonic storm with the maximum sustained winds around 245 km/h and hit Bangladesh as category 4 strength near Sundarbans forest around 1600 to 1700 UTC on 15th (Figures 3.6.2.1 & 3.6.2.2) November 2007. It weakened quickly after the landfall and moved northeastward direction.



[Saffir-Simpson Hurricane Scale](#)

Figure 3.6.2.1: Observed track of super cyclonic storm Sidr (wikipedia)

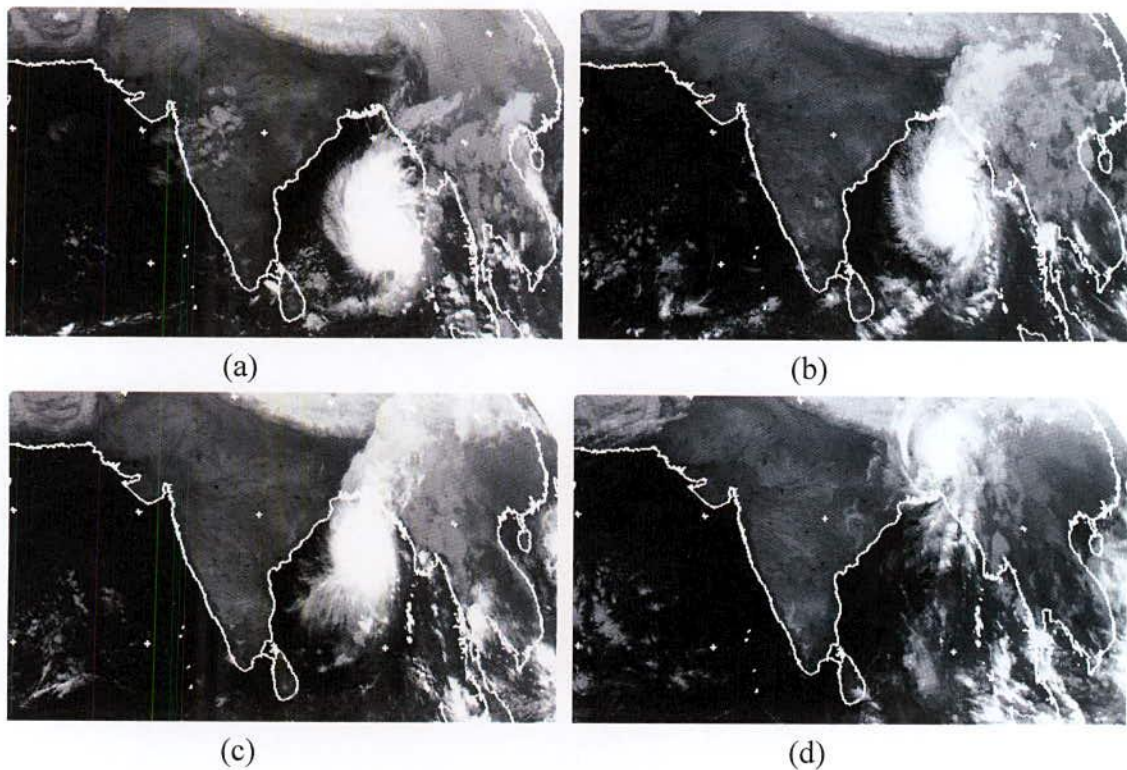


Figure 3.6.2.2: Satellite pictures of super cyclonic storm Sidr as obtained from EUMETSAT Meteosat 7 (Courtesy: Dundee website) (a) at 0000 UTC on 13th November 2007, (b) at 0000 UTC on 14th November 2007, (c) at 0000 UTC on 15th November 2007 and (d) at 0000 UTC on 16th November 2007.

3.6.3 Cyclonic Storm Rashmi (24-28 October 2008)

Southwest monsoon withdrew from the entire country, Bay of Bengal and Arabian Sea on 15th October 2008. Simultaneously, the northeast monsoon set in over peninsular India and adjoining Bay of Bengal and Arabian Sea. In addition, during the second half of October the ITCZ over Indian region was active with development of cyclonic storm over the Bay of Bengal, a deep depression and a low pressure area over the Arabian Sea. A trough on equatorial easterlies in lower levels roughly ran along 100°E up to 10°N on 16th, along 95°E up to 15°N on 17th, along 92°E up to 15°N on 18th and along 88°E up to 15°N on 19th. It was seen as trough of low pressure extending from southwest Bay of Bengal to North Bay of Bengal on 20th and from southwest Bay of Bengal to west central Bay of Bengal off Tamilnadu and Andhra Pradesh coast during 21st to 23rd. The associated cyclonic circulation extended up to mid tropospheric level on 23rd. Under its influence, a low pressure area formed over the west central Bay of Bengal off Andhra Pradesh coast on 24th. A trough from this system extended up to coastal Bangladesh across North Bay of Bengal. A trough of westerlies at 500 hPa level roughly ran along 86°E to the north of 20°N. A convective cloud cluster was seen over west central Bay of Bengal on 23rd which subsequently led to the

development of low level cyclonic circulation over the same area in 23rd evening. A vortex was seen in the satellite imagery of 0600 UTC of 24th with centre near 16°N and 85°E.

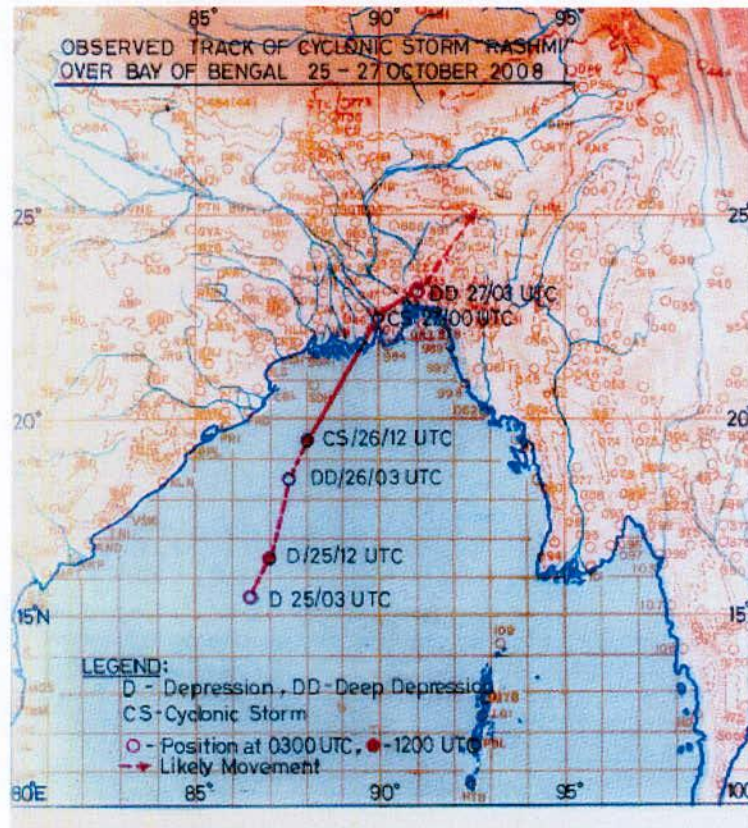


Figure 3.6.3.1a: Observed Track of cyclonic storm, "RASHMI" during 25-27 October 2008



Figure 3.6.3.1b: Track of cyclonic storm, "RASHMI" during 25-27 October 2008

The environmental conditions continued to be favorable for the cyclogenesis over the Bay of Bengal region from the beginning of the second fortnight with warmer SST (29-30°C) over central Bay of Bengal and adjoining areas, low to moderate vertical wind shear (10-20 knots), decreasing wind shear and depth of moisture extending up to mid tropospheric level. Under the influence of all the above, the low pressure area concentrated into a depression and lay centred at 0300 UTC of 25th near latitude 16.5°N and longitude 86.5°E. The track of the system is shown in Figure 3.6.3.1a - 3.6.3.1b. The satellite imageries at 0300 UTC 25th suggested organized convections and curved band pattern of cloud was association with the

system (Fig. 3.6.3.2a). The intensity was estimated to be 1.5 with sustained maximum wind speed of 25 knots and estimated central pressure of 1004 hPa. The lowest cloud top temperature was about -60°C .

The intense convection due to the system was sheared to the west of the system centre. The 24 hours wind shear tendency was about -5 to -10 knots. The lower level vorticity and upper level divergence increased during past 24 hours. The system lay close to the south of the upper tropospheric ridge which roughly ran along 18°N and to the periphery of the anticyclonic circulation centred over Myanmar. The trough of westerlies at 500 hPa level roughly ran along 87°E and hence influenced the movement of the system.

Under the influence of the above, the depression moved north-northwestwards and further intensified into a deep depression and lay centred at 0000 UTC of 26th over west central and adjoining northwest Bay of Bengal near lat. 18°N and long. 87°E . The sustained maximum wind speed was estimated to be about 30 knots. The convection according to satellite imagery further organized and curved band pattern of the system continued with T 2.0 (Fig. 3.6.3.2b). The lowest cloud top temperature due to convection was about -80°C at 0000 UTC of 26th. The low level vorticity and upper level divergence increased further. The vertical wind shear continued to be low to moderate (10-20 knots). The wind shear tendency was negative (-5 to -10 knots) to the north of the system. The system continued to be close to the upper tropospheric ridge and at the periphery of the anticyclonic circulation centred over Myanmar. With the continuance of similar favourable environmental conditions, the system further moved in a north-northeasterly direction, intensified into a cyclonic storm 'RASHMI' and lay centred at 1200 UTC of 26th over the northwest Bay of Bengal near 19.5°N and 88°E , about 350 km south of Kolkata. The satellite estimated intensity of the system was T 2.5 with sustained maximum wind speed of 35 knots. The system moved over the area north of the upper tropospheric ridge. The organized convection changed from curved band pattern to central dense over cast (CDO) pattern (Fig. 3.6.3.2c). The lowest cloud top temperature was about -80°C . The vertical wind shear continued to be low to moderate (10-20 knots) around the system center and wind shear tendency was -5 to -10 knots to the north and northeast of the system center. As the system lay to the north of the system center, it started to move rapidly in a north-northeasterly direction after 1200 UTC of 26th towards Bangladesh coast. However due to favourable environmental condition as discussed earlier, the system further intensified with estimated intensity of T3.0 and sustained maximum wind speed of about 45 knots at 2100 UTC of 26th and lay centred at 2100 UTC of 26th over north Bay of Bengal near 21.5°N and 89.5°E , very close to the coast. The lowest cloud top temperature continued to be -80°C .

The westward propagation of the trough in easterlies, its intensification leading to the formation of cyclonic storm and north-northeastward movement of the system leading to landfall over Bangladesh was also reflected in 24-hours MSLP change and pressure departure. The MSLP fell by about 2 hPa over Andhra Pradesh coast on 23rd and was below

normal by about 2 hPa along north Tamilnadu and Andhra Pradesh coast. It further fell slightly over north coastal Andhra Pradesh, Orissa and West Bengal and increased over Tamil Nadu coast by 1-2 hPa on 24th. It was below normal by about 2-4 hPa along north coastal Andhra Pradesh and south coastal Orissa on 24th. The MSLP further fell by 2-3 hPa over coastal Orissa and fell slightly elsewhere along the east coast on 25th and were below normal by 4-5 hPa along north Andhra Pradesh and Orissa coast. It fell by 2-4 hPa over Orissa, West Bengal and Bangladesh coasts at 0300 UTC of 26th and was below normal by 4-6 hPa along these coasts. The MSLP along Orissa, West Bengal and Bangladesh coast increased from 27th and became above normal gradually. The best track positions of the system are shown in Table 3.6.3.1.

The system crossed Bangladesh coast near 21.8°N and 89.5°E (about 50 km west Khepupara) between 2200 and 2300 UTC of 26th. Due to the land interaction and increase in vertical wind shear and entrainment of cold air the cyclonic storm 'RASHMI' weakened into a deep depression at 0300 UTC of 27th over Bangladesh (Fig. 3.6.3.2d) with disorganization of clouds and lay centred near 23.5°N and 91.0°E close to Maijdi Court. It further weakened into a well marked low pressure area over Meghalaya and neighborhood at 0900 UTC of 27th and become less marked on 28th. The isobaric analysis along with the surface wind at 2100 UTC and 0000 UTC of 27th are presented in Fig. 3.6.3.3 to show the characteristics of pressure and wind during landfall.

Table 3.6.3.1: Best track Positions and other parameters for cyclonic storm RASHMI over Bay of Bengal during 25-27 October 2008

| Date | Time (UTC) | Centre lat. ^o N/ long. ^o E | C.I. NO. | Estimated Central Pressure (hPa) | Estimated Maximum Sustained Surface Wind (kt) | Estimated Pressure drop at the Centre (hPa) | Grade | |
|------------|------------|--|-----------|----------------------------------|---|---|-------|--|
| 25.10.2008 | 0300 | 16.5/86.5 | 1.5 | 1004 | 25 | 3 | D | |
| | 0900 | 17.0/87.0 | 1.5 | 1002 | 25 | 3 | D | |
| | 1200 | 17.5/87.0 | 1.5 | 1002 | 25 | 3 | D | |
| | 1800 | 18.0/87.0 | 1.5 | 1000 | 25 | 3 | D | |
| 26.10.2008 | 0000 | 18.0/87.0 | 2.0 | 1000 | 30 | 5 | DD | |
| | 0300 | 18.5/87.5 | 2.0 | 1000 | 30 | 5 | DD | |
| | 0900 | 18.5/87.5 | 2.0 | 1000 | 30 | 5 | DD | |
| | 1200 | 19.5/88.0 | 2.5 | 996 | 35 | 6 | CS | |
| | 1500 | 20.5/88.5 | 2.5 | 996 | 35 | 6 | CS | |
| | 1800 | 21.0/89.0 | 2.5 | 994 | 35 | 6 | CS | |
| | 2100 | 21.5/89.5 | 3.0 | 984 | 45 | 18 | CS | |
| 27.10.2008 | 0000 | 22.5/90.0 | Over land | 992 | 35 | 10 | CS | |
| | 0300 | 23.0/91.0 | Over land | | 30 | 5 | DD | |
| | 0900 | Weakened into a Well Marked Low pressure area over Meghalaya at 270900 UTC | | | | | | |

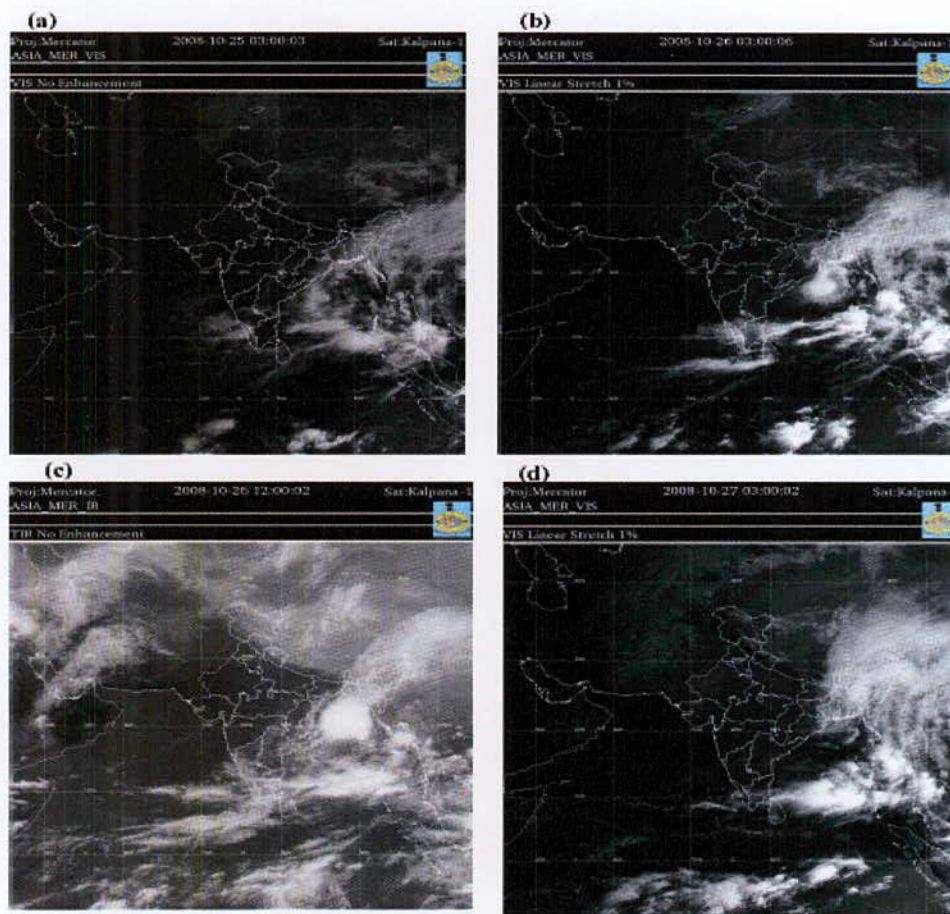


Figure 3.6.3.2(a-d): INSAT imageries of the system at (a) 250300 UTC, (b) 260300 UTC, (c) 261200 UTC and (d) 270300 UTC

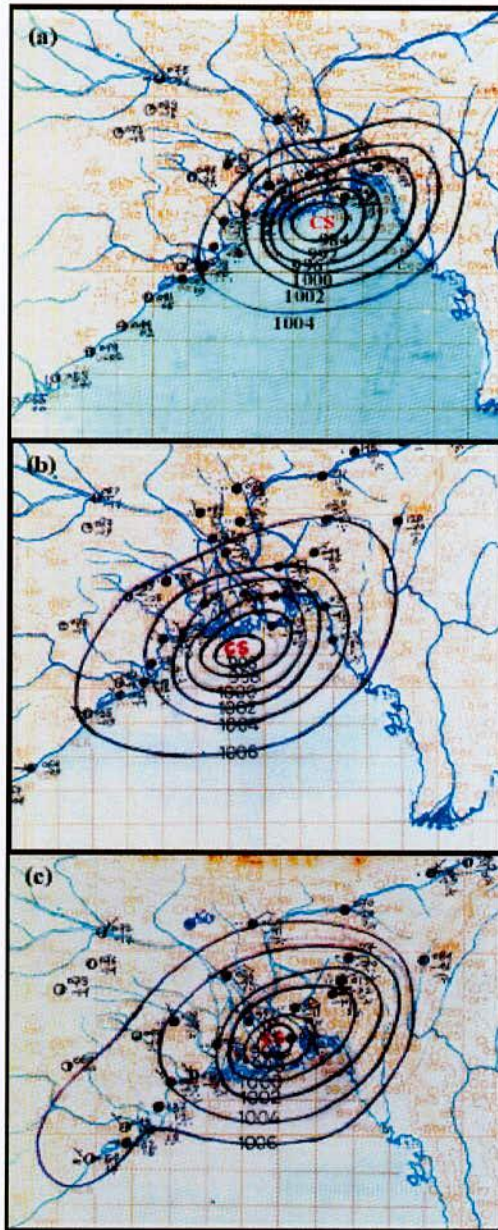


Fig. 3.6.3.3: Isobaric analysis at (a) 18 UTC on 26 October (b) 21 UTC on 26 October and 00 UTC on 27 October indicating the intensity of the system and point of landfall.

CHAPTER 4
SIMULATION OF HEAVY RAINFALL
EVENTS USING MM5 AND WRF MODELS

4.1 Simulation of Heavy Rainfall Events of 1-3 July 2008 using WRF and MM5

To analyze the convective system of 1-3 July 2008 with their vertical structure, the models MM5 and WRF were run for 72 hours based on the initial conditions at 00 UTC of 01 July 2008. All parameters were depicted for 00 UTC of 02 July 2008 for the analysis of the synoptic conditions responsible for producing rain. The first 24 hours was considered as spin up period. The model performance was evaluated by examining the different simulated meteorological parameters i.e. mean sea level pressure, rain with vector wind, relative humidity with vector wind, and vertical structure of vertical velocity, divergence, relative vorticity, relative humidity and mixing ratio at the centre of the most developed cloud. The model derived rainfall for all three domains were compared with that obtained from TRMM and Bangladesh Meteorological Department (BMD) rain-gauge observation data. Surface simulated precipitation was considered as rainfall throughout the study.

4.1.1 Mean Sea Level Pressure (MSLP)

Model simulated MSLPs (hPa) obtained from both the MM5 and WRF models for domain D1, valid for the initial time 00 UTC of 01 July to 00 UTC of 04 July 2008, are presented in Fig. 4.1.1.1a and Fig. 4.1.1.1b respectively. Figures show that the monsoon trough lies parallel to the foot hills of Himalayan Mountain with low pressure 997 and 996 hPa at the center of the system simulated by MM5 and WRF models respectively. The MSLP over Tibet is very high and central pressures are above 1017 and 1016 hPa at 00 UTC of 01 July 2008 simulated by MM5 and WRF models respectively. At 03 UTC of 01 July, the center of the depression changes toward Bangladesh and lies over north-eastern part of Bangladesh having minimum pressure between 988 to 993 hPa for MM5 and 998 to 1002 hPa for WRF model. Its center remains stationary over north-eastern part of Bangladesh and nearby Indian Territory up to 00 UTC of 04 July 2008. It may be due to high pressure over Tibetan plateau and weak heat low. A prominent lowest surface pressure lies over western Bangladesh and adjoining territory of India.

4.1.2 Study of Rainfall with Wind

During summer monsoon period, one of the main synoptic conditions for occurrence of heavy rainfall over Bangladesh and neighborhood is the southwesterly flow streaming from the head Bay of Bengal into Bangladesh [110]. In this case, westerly wind comes from the Arabian Sea into the Indian region and south westerly wind comes from the Bay of Bengal enter into the Bangladesh region. This southwesterly wind carry moisture from the Bay of Bengal and convergence occurred in the southeastern part (hilly region) of Bangladesh. A well marked low pressure area forms over this region and cyclonic circulation is developed over Bangladesh and West Bengal of India. Due to this system heavy rainfall occurred over

Bangladesh and the Bay of Bengal. The detailed analyses of the system are given below using both the MM5 and WRF models and shown in Figures 4.1.2.1 (a-d), 4.1.2.2 (a-b) and 4.1.2.3 (a-b).

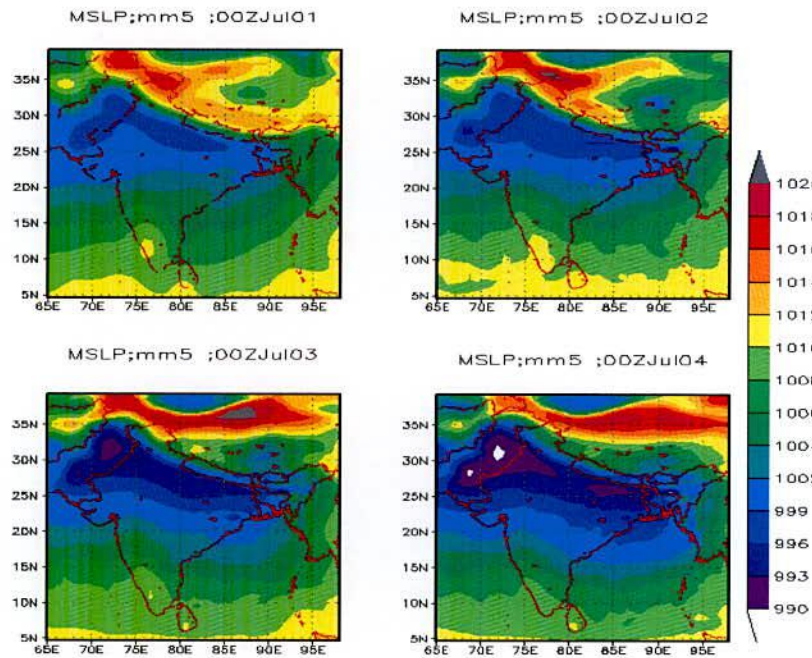


Fig. 4.1.1.1a: MM5 Model simulated MSLP (hPa) from 00 UTC of 01 – 04 July 2008

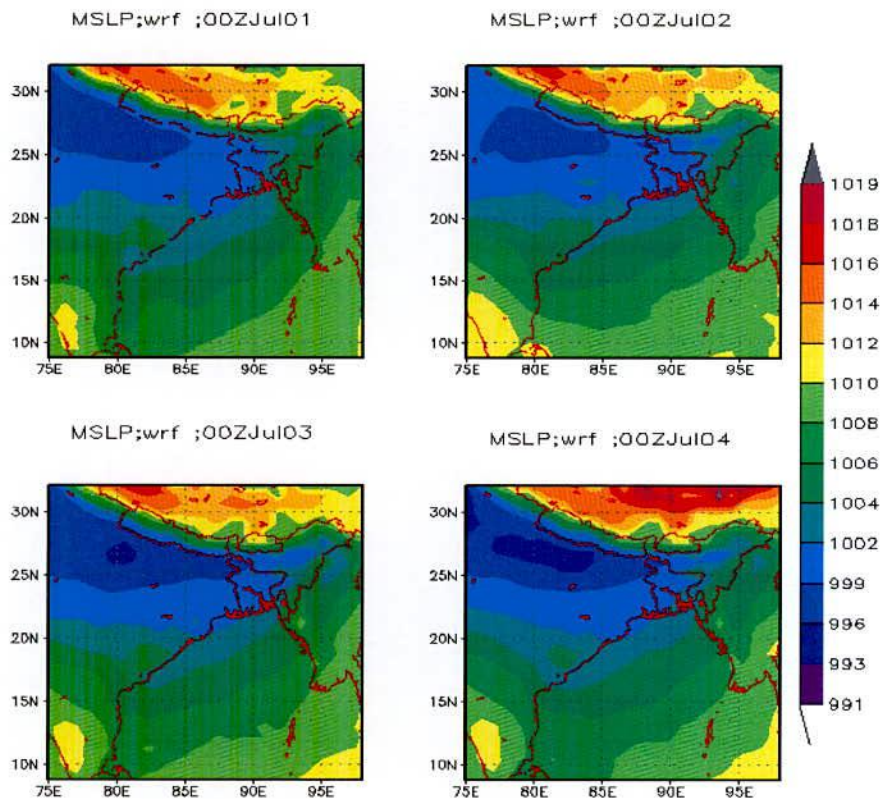


Fig. 4.1.1.1b: WRF Model simulated MSLP (hPa) from 00 UTC of 01 – 04 July 2008

Using MM5 model, the distributions of low level wind at 850 hPa and upper level wind at 500 and 200 hPa levels valid from 00 UTC of 01 July to 00 UTC of 04 July 2008 are presented in Figures 4.1.2.1(a-b), 4.1.2.2a and 4.1.2.3a respectively. The prominent feature is a strong southwesterly (SW'ly) flow transporting high magnitude of moisture from the Bay of Bengal into southeast and central Bangladesh during the whole simulation period. From the Figure 4.1.2.1(a-b), it is seen that the area of convergence (i.e., zone of high convective activity) observed over Bangladesh and neighborhood especially in the northeastern sector of the low pressure region. At time 00 UTC on 02 July, 2008, at level 850 hPa, the amount of moisture is very low. Due to convergence, small cells merge with others cells make clusters. With the advancement of time other cells make another cluster. Clusters merge to form mesoscale convective system (MCS) and rainfall occurs in and outside of Bangladesh. It is seen that vary developed MCS form near the foot hills of Himalayan Mountain and hence heavy rainfall occurred in the north-eastern part of Bangladesh. The cyclonic circulation is observed at 850 hPa level through out the simulation (Figure 4.1.2.1(a-b)). Figures make us clear that rainfall happens because of the combined effect of SW'ly and southerly wind which carrying moisture from Arabian Sea and Bay of Bengal respectively. The southwesterly is prevailed over North Bay of Bengal and southern part of Bangladesh up to 500 hPa level with cyclonic circulation (Figure 4.1.2.2a). Anti-cyclonic circulation is observed at 200 hPa level (Figure 4.1.2.3a). The maximum wind speed for the levels 850, 500 and 200 are 20, 30 and 50 m/s respectively.

Using WRF model, the distributions of 850 hPa, 500 hPa and 200 hPa level wind valid from 00 UTC of 01 July to 00 UTC of 04 July 2008 are presented in Figures 4.1.2.1(e-h), 4.1.2.2b and 4.1.2.3b respectively. Similar features are observed using both the models with different amount of moisture contained and wind speed. The simulation of MCS using WRF model is more than that using the MM5 model. The maximum wind speed at the levels 850, 500 and 200 are 20, 10 and 30 m/s respectively. This maximum wind speed is smaller than those obtained using MM5 model. From the above figures it is clear that the rainfall occurred due to the combined effect of southwesterly and southerly wind which carrying moisture from Arabian Sea and Bay of Bengal respectively.

Figures 4.1.2.4a and 4.1.2.4b are obtained using inner most Domains i.e. Domain 3 of MM5 and WRF models respectively. It is noted that resolution of Domain 3 is 10 km for both the models. Figures show the development of cloud (accumulated rainfall in every 3 hours) with the advancement of time from 00 UTC of 02 July to 21 UTC of 03 July, 2008. It is clear from the Figures 4.1.2.4a and 4.1.2.4b that simulated rainfall obtained from WRF model is more than that obtained from MM5 model.

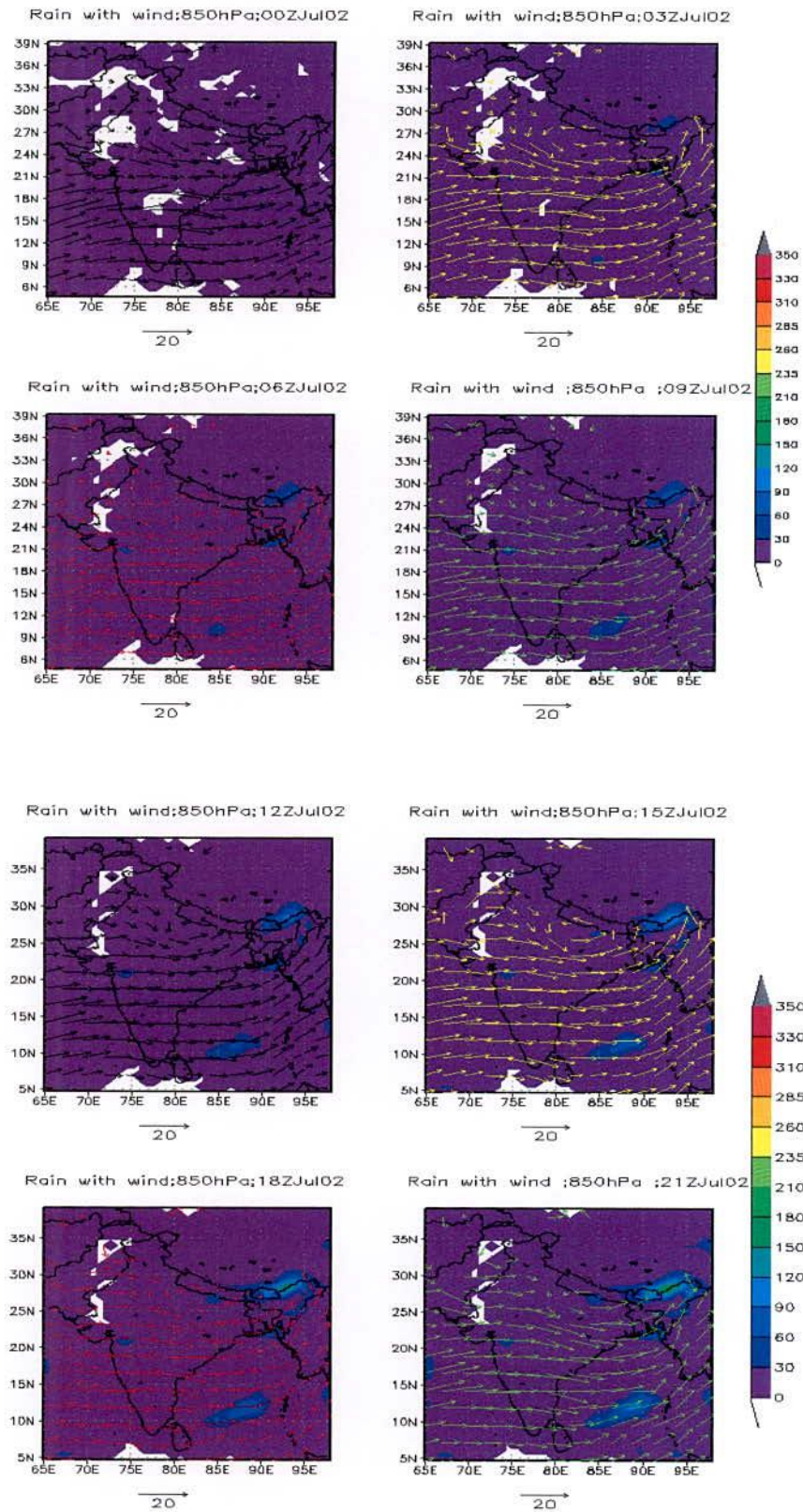


Figure 4.1.2.1a: MM5 Model simulated rain with wind flow (m/s) at 850 hPa valid for time 00 to 21 UTC of 02 July 2008

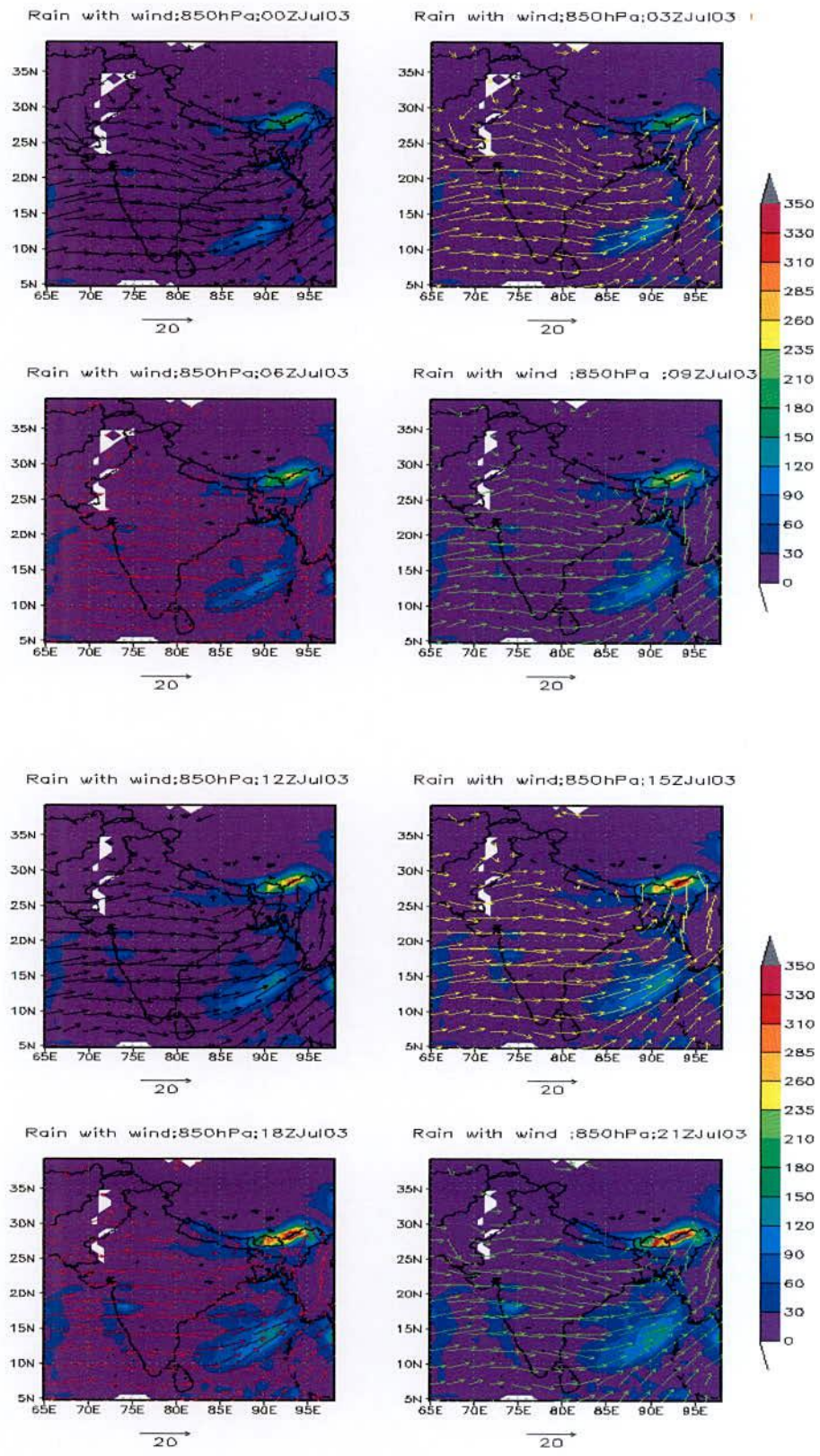


Figure 4.1.2.1b: Same as Figure 4.1.2.1a but valid for 00 to 21 UTC of 03 July 2008

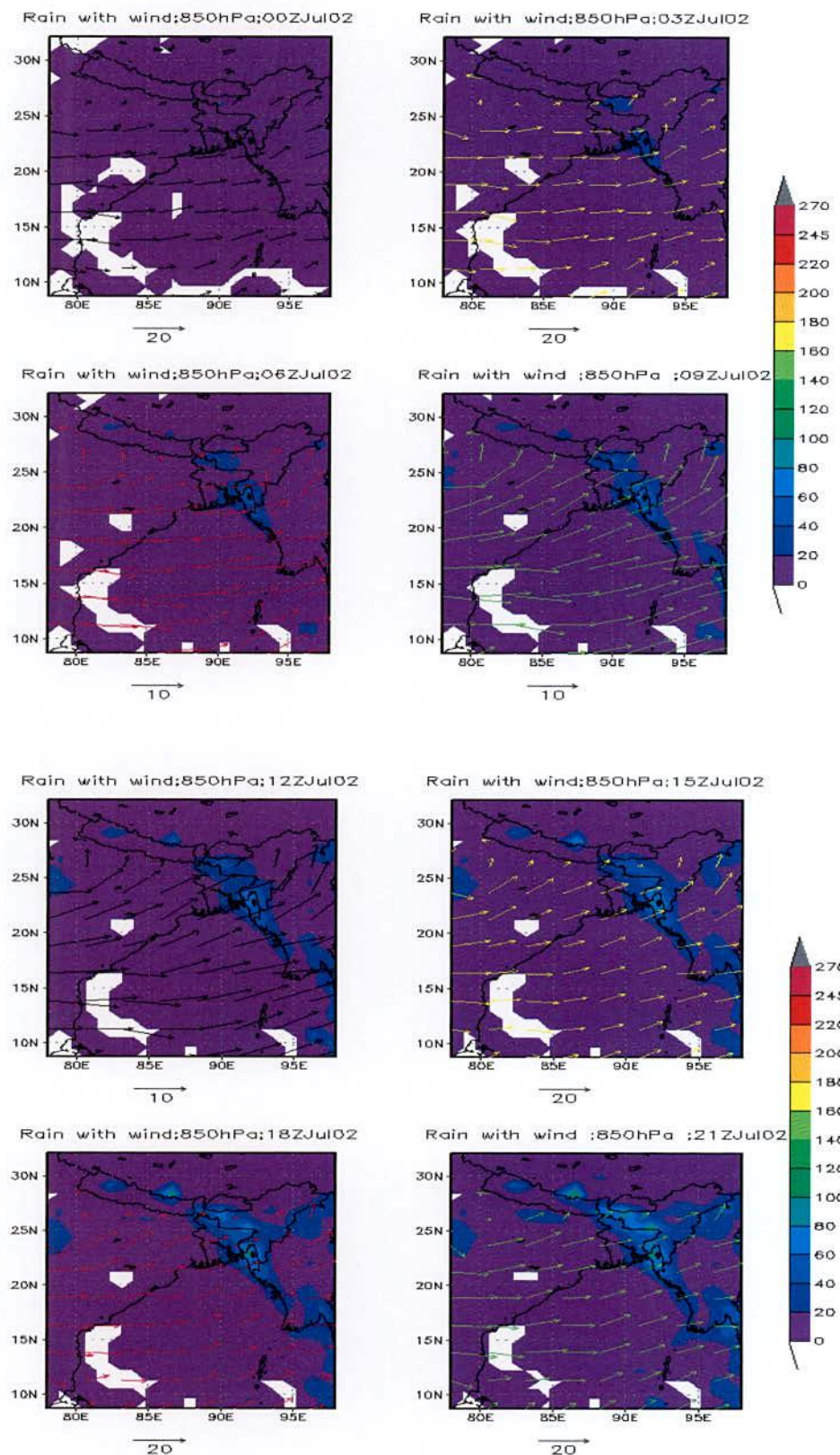


Figure 4.1.2.1c: WRF Model simulated rain with wind flow (m/s) at 850 hPa valid for 00 to 201UTC of 02 July 2008

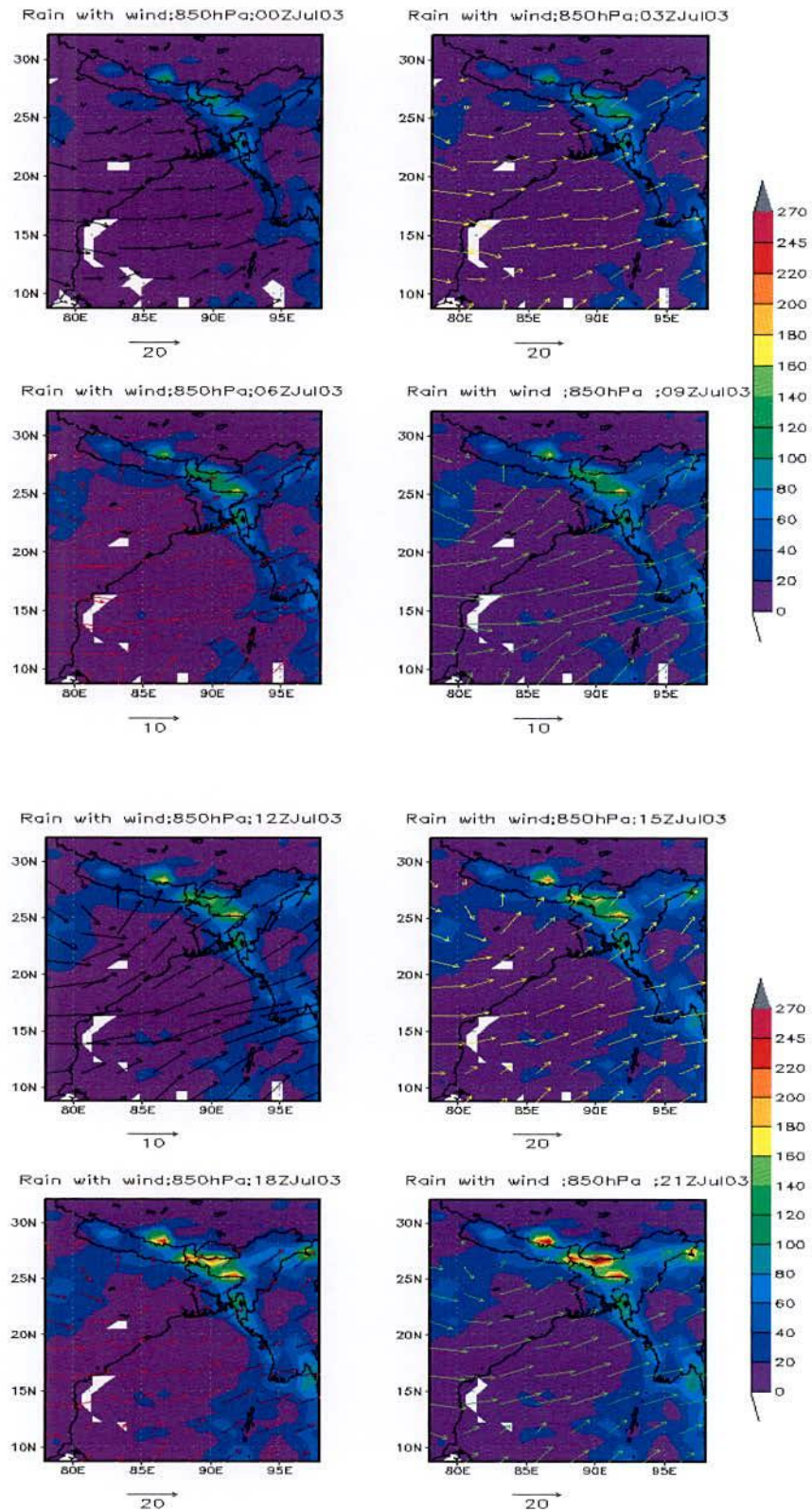


Figure 4.1.2.1d: Same as Figure 4.1.2.1c but valid for 00 to 21 UTC of 03 July 2008

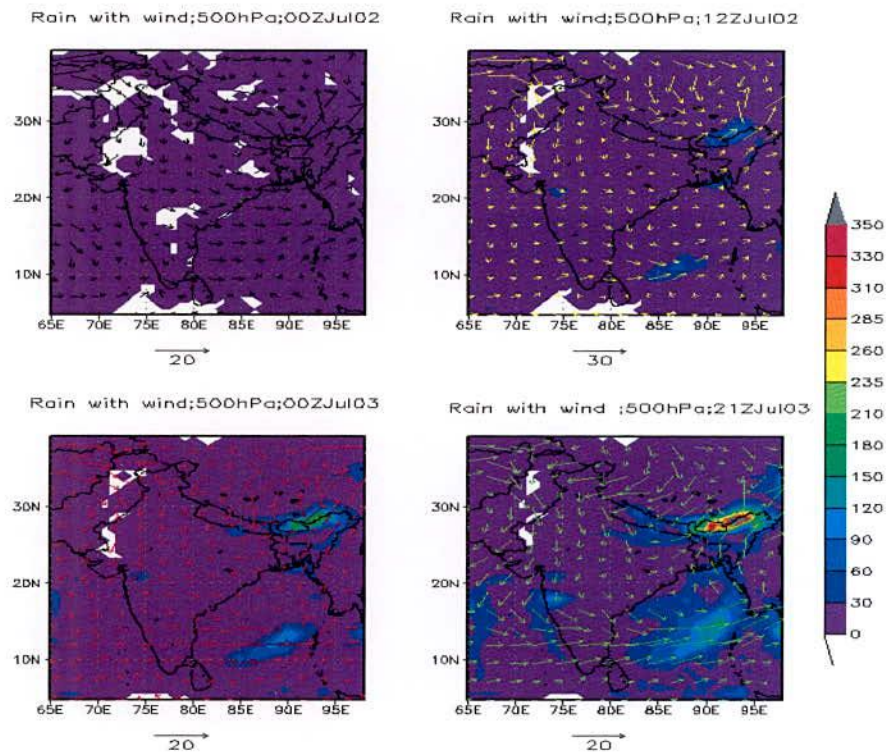


Figure 4.1.2.2a: MM5 Model simulated rainfall with wind flow (m/s) at 500 hPa valid for 00 UTC of 02 July to 21 UTC of 03 July 2008.

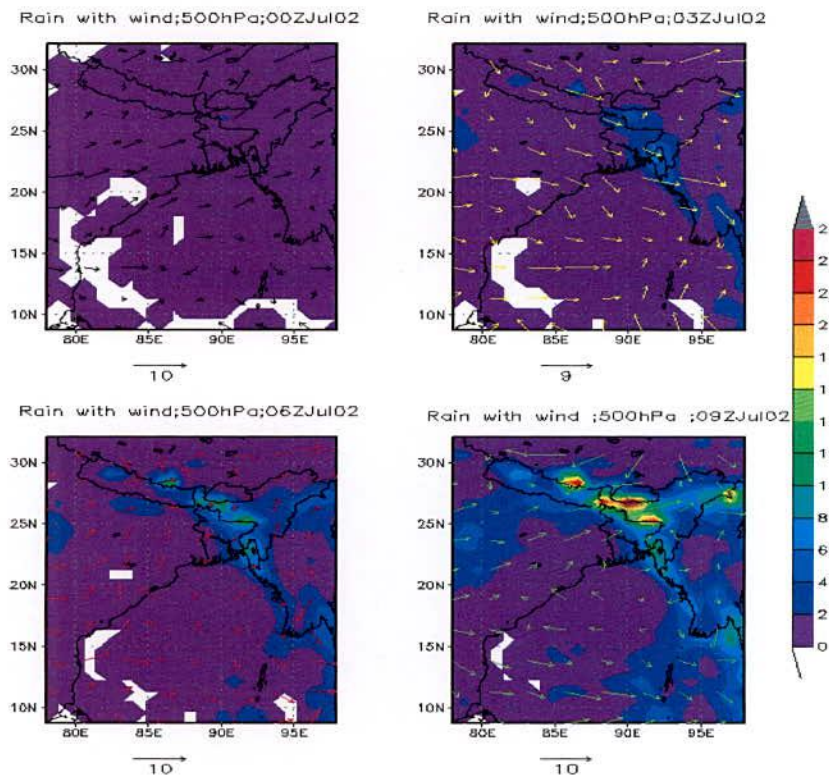


Figure 4.1.2.2b: WRF Model simulated rainfall with wind flow (m/s) at 500 hPa valid for 00 UTC on 02 July to 21 UTC of 03 July 2008

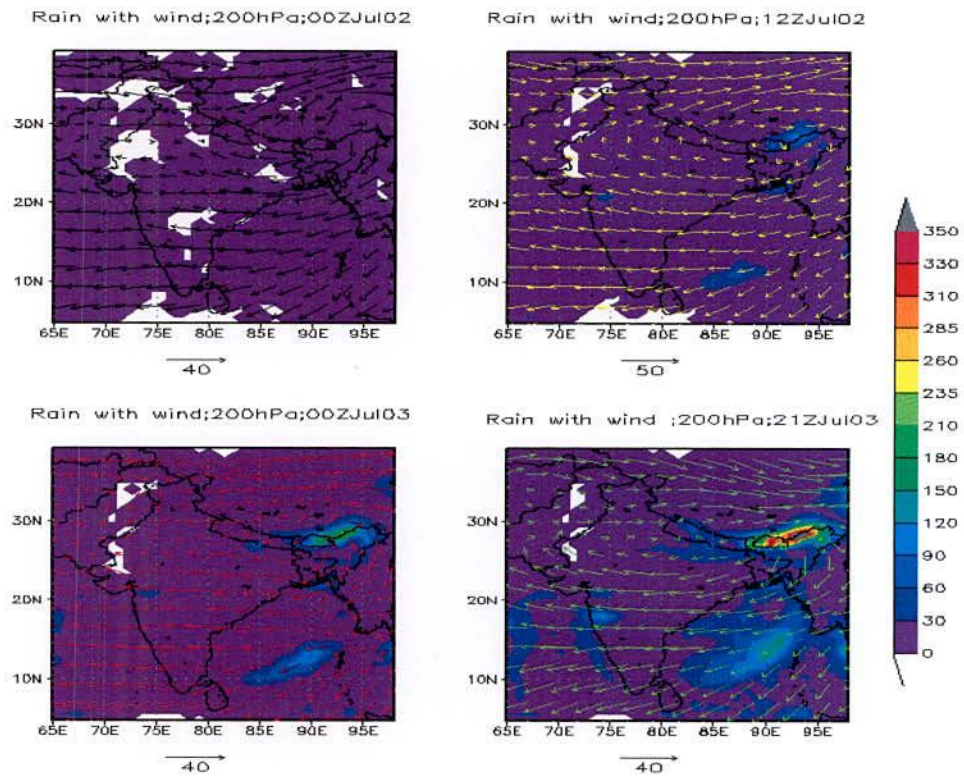


Figure 4.1.2.3a: MM5 Model simulated rainfall with wind flow (m/s) at 200 hPa valid for 00 UTC on 02 July 02 to 21 UTC of 03 July 2008.

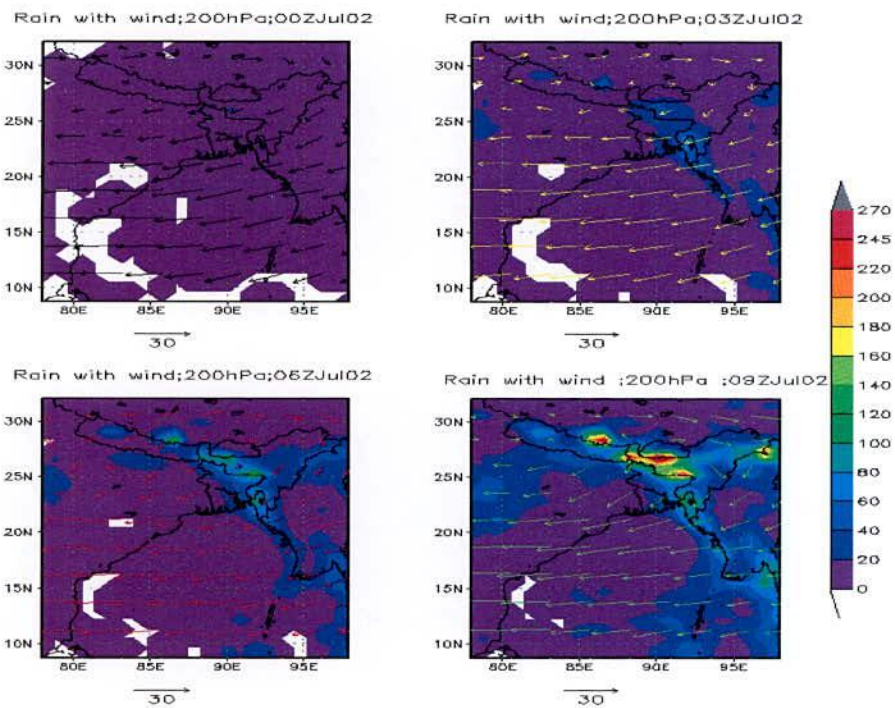


Figure 4.1.2.3b: WRF Model simulated wind flow (m/s) at 200 hPa valid for 00 UTC on 02 July 02 to 21 UTC of 03 July 2008.

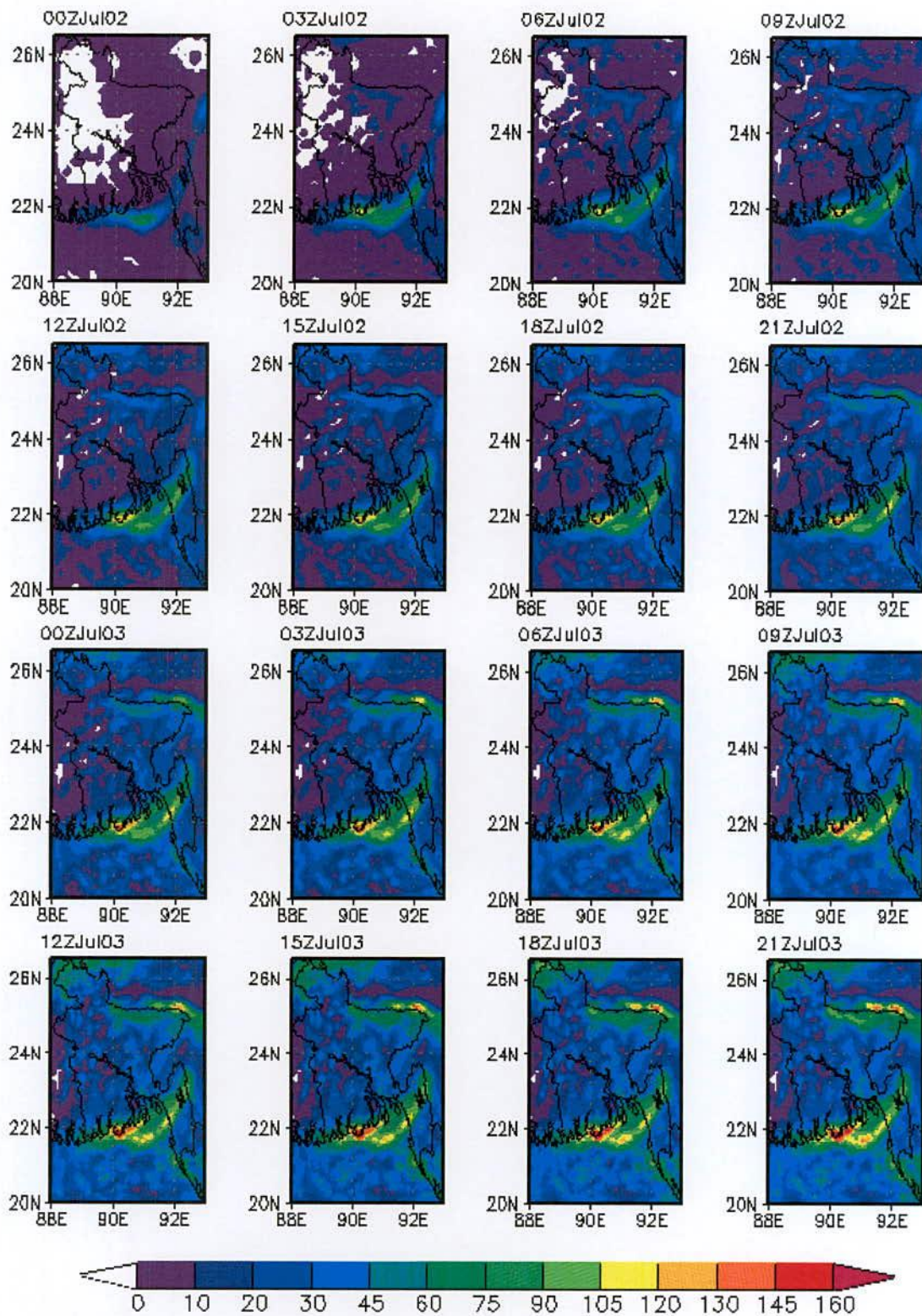


Figure 4.1.2.4a: MM5 Model simulated precipitation field valid for 00 UTC on 02 July to 21 UTC of 03 July 2008 (sequence is top left to right).



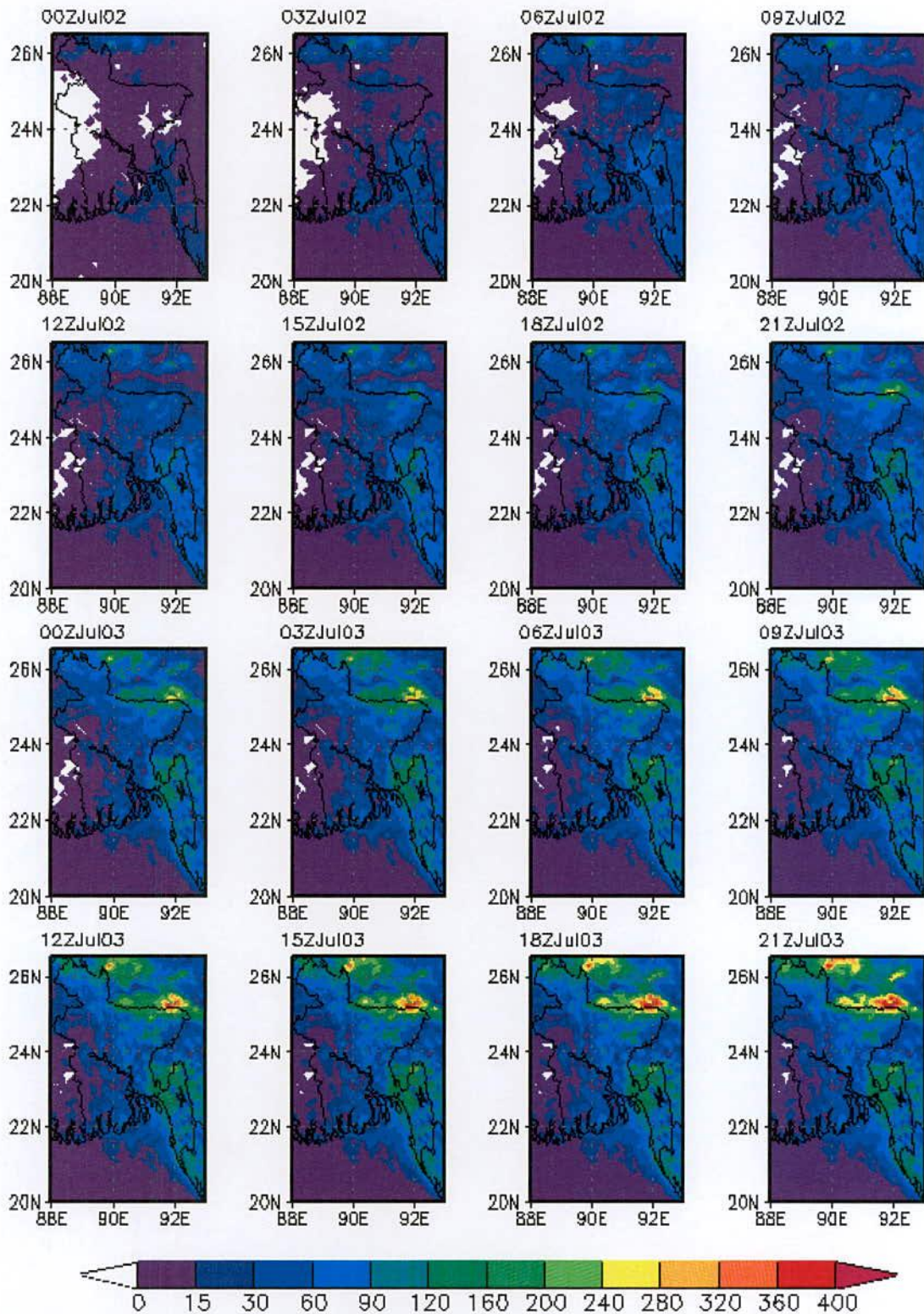


Figure 4.1.2.4b: WRF Model precipitation field valid for 00 UTC on 02 July to 21 UTC of 03 July 2008 (sequence is top left to right).

4.1.3 Study of Relative Humidity (RH) with Wind

The simulated relative humidity with wind shows the southwesterly flow transports of plentiful moisture from the Bay of Bengal and westerly flow transport moisture from the Arabian Sea through the Indian region to the plains of Bangladesh and neighborhood. Using MM5 model, the spatial distribution of relative humidity with wind at 850, 500 and 200 hPa levels from 00 UTC of 02 July to 21 UTC of 03 July 2008 are presented in Figures 4.1.3.1(a-b), 4.1.3.2a and 4.1.3.3a respectively. The significant amount of moisture of the order of 90-100% with cyclonic circulation is simulated over most of the region of Bangladesh at 850 to 500 hPa levels. But the amount of the simulated moisture is less at 200 hPa level with anti-cyclonic circulation. This moisture and circular patterns are in agreement with the climatological patterns during southwest monsoon season.

Using WRF model, the spatial distribution of relative humidity with wind at 850, 500 and 200 hPa levels from 00 UTC of 02 July to 21 UTC of 03 July 2008 are presented in Figures 4.1.3.1(c-d), 4.1.3.2b and 4.1.3.3b respectively. Similar to MM5 model, the WRF Model simulates high amount of moisture (of the order of 90-100%) with cyclonic circulation over most of the regions of Bangladesh at 850 and 500 hPa levels but the less amount of moisture are simulated at 200 hPa level with anti-cyclonic circulation of wind. Simulated wind speed for the levels 500 and 200 hPa are less than those obtained using MM5 model.

From Figures obtained from both the models, it is clear that the amount of relative humidity prevail because of combined effect of southwesterly and southerly winds which are carrying moisture from Arabian Sea and Bay of Bengal respectively.

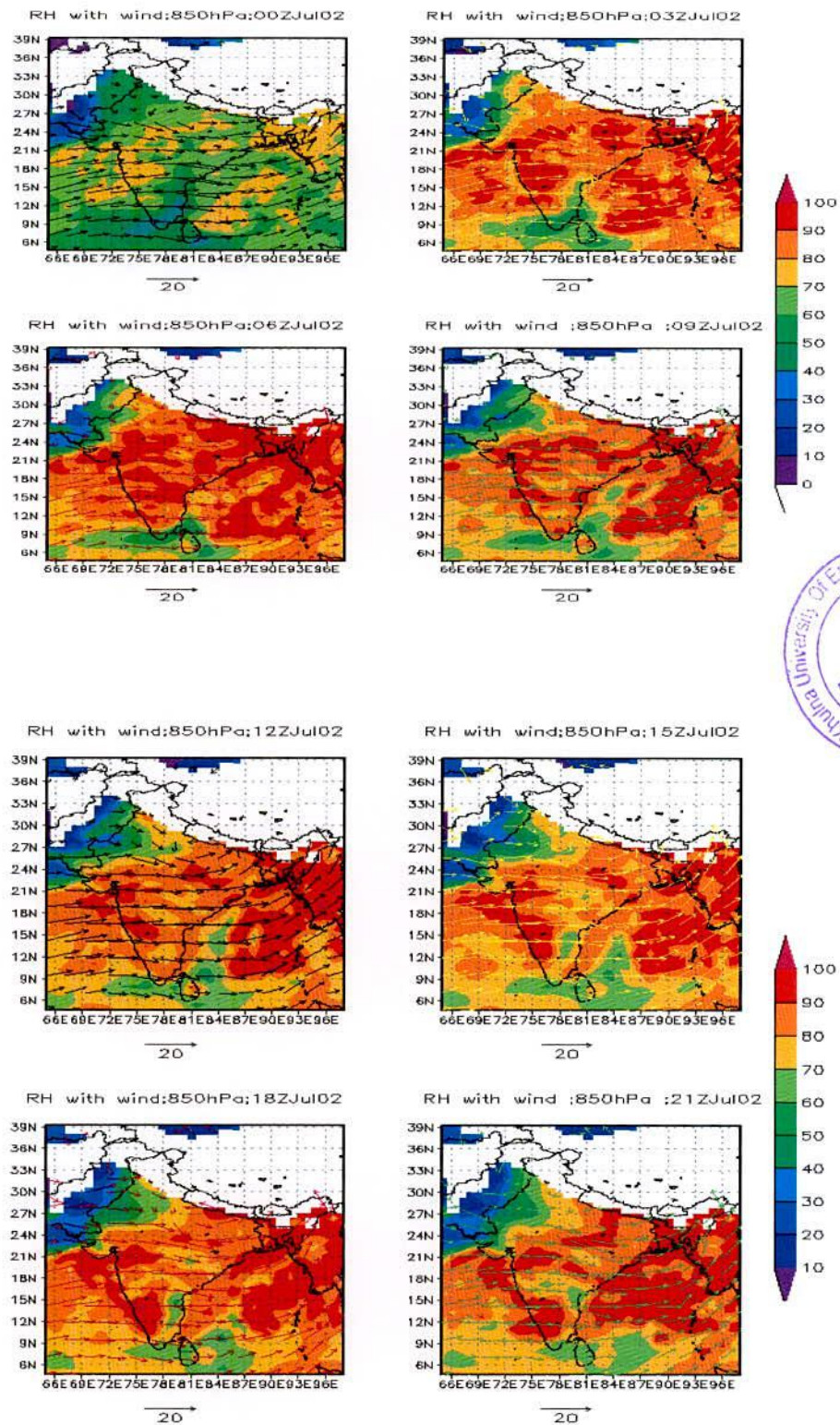


Figure 4.1.3.1a: MM5 simulated RH with wind at 850 hPa level valid for 00 to 21 UTC of 02 July 2008

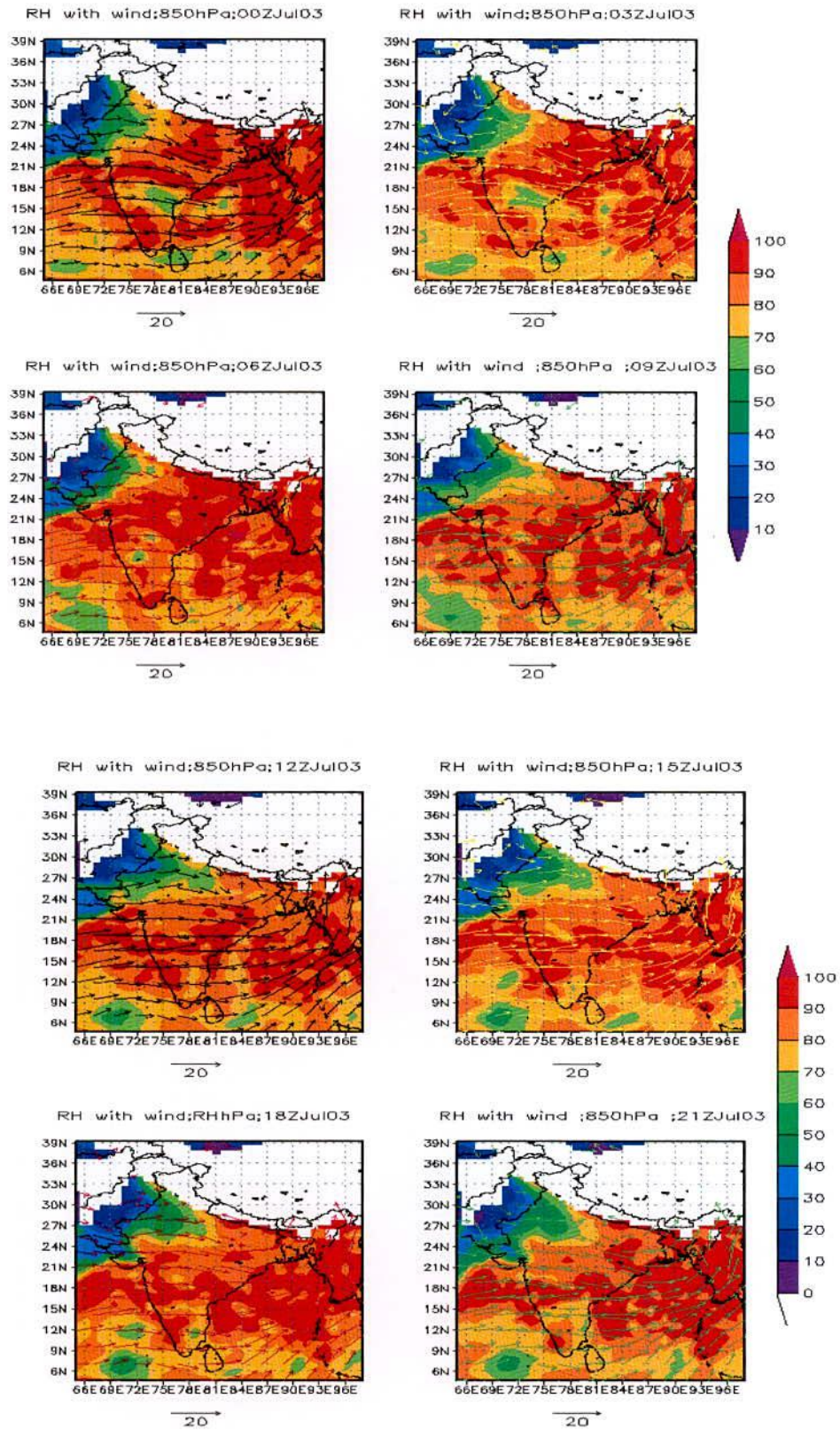


Figure 4.1.3.1b: MM5 simulated RH with wind at 850 hPa level valid for 00 to 21 UTC of 03 July 2008

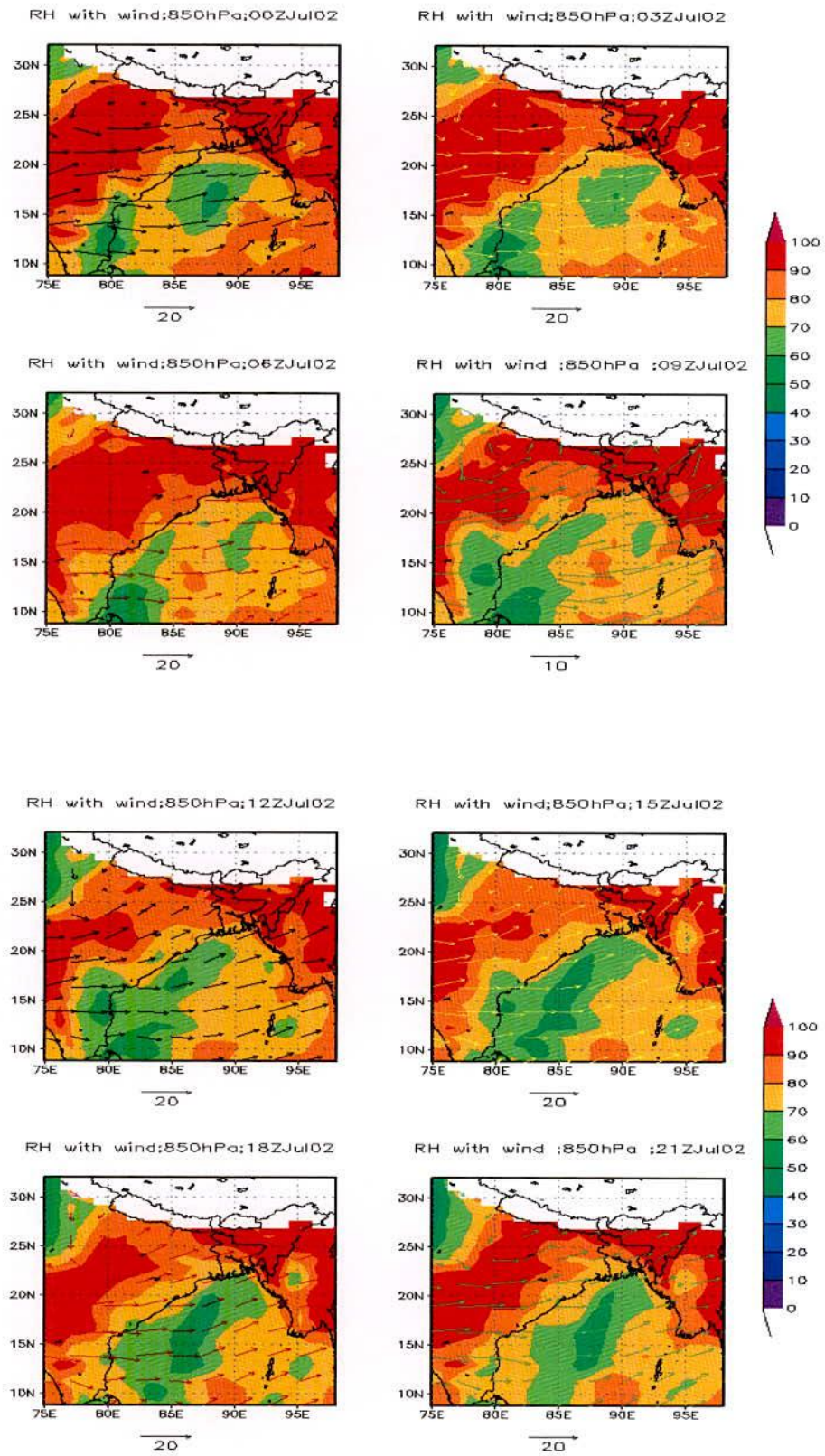


Figure 4.1.3.1c: WRF simulated RH with wind at 850 hPa level valid for 00 to 21 UTC of 02 July 2008

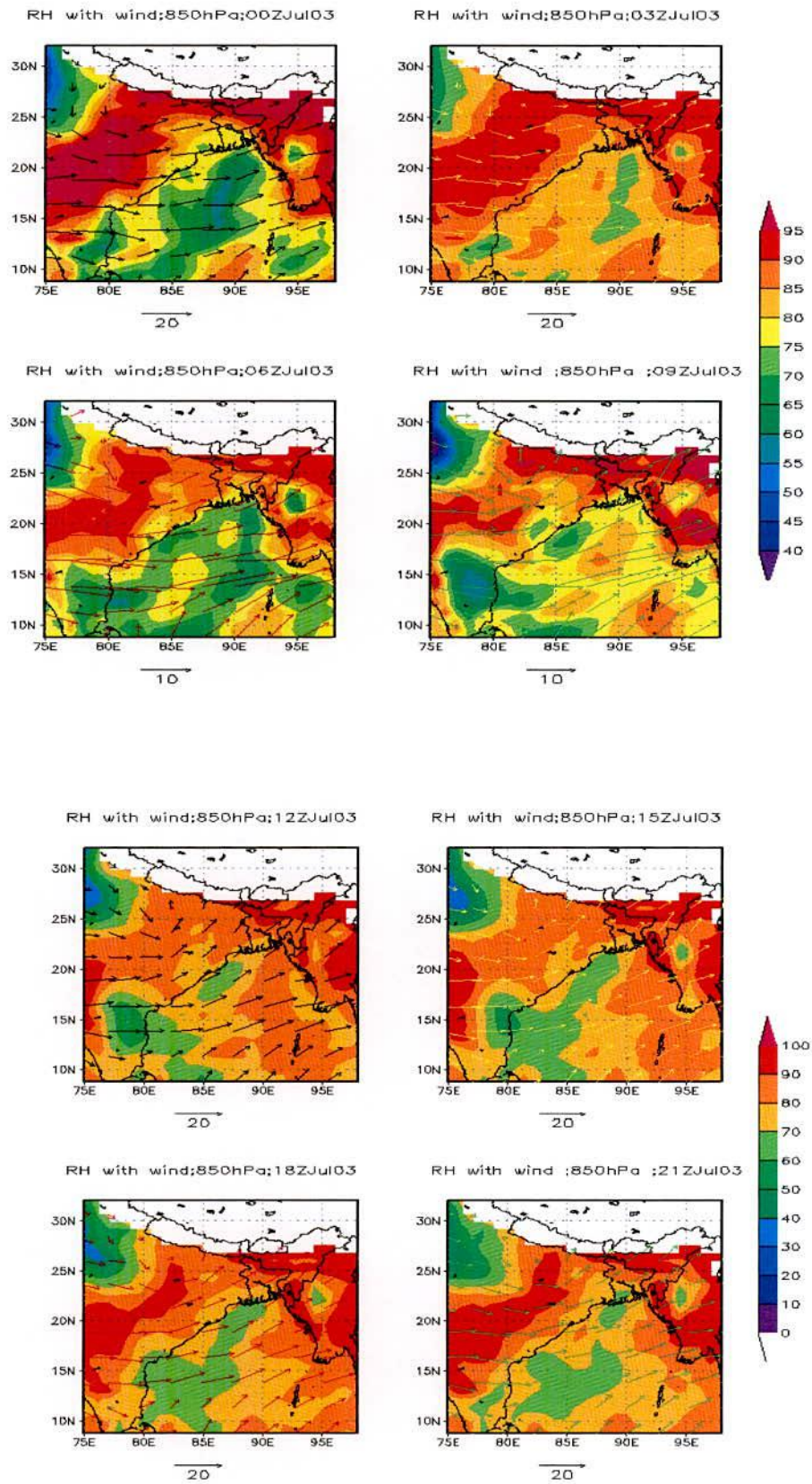


Figure 4.1.3.1d: WRF simulated RH with wind at 850 hPa level valid for 00 to 21 UTC of 03 July 2008

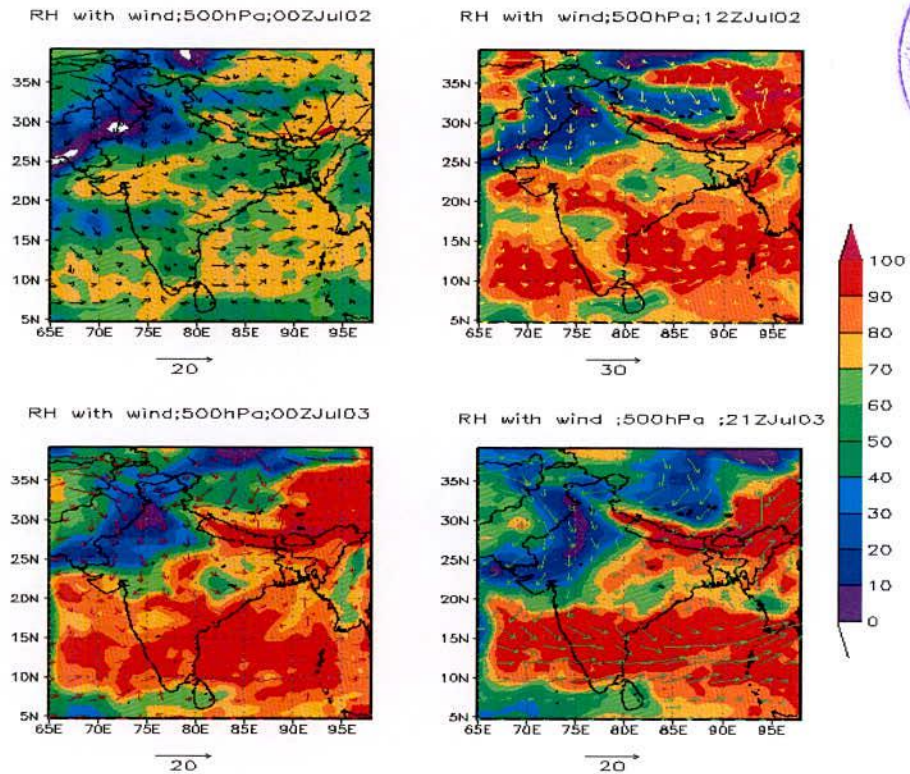


Figure 4.1.3.2a: MM5 model simulated RH with wind at 500 hPa level valid for 00 UTC on 02 July to 21UTC on 03 July 2008.

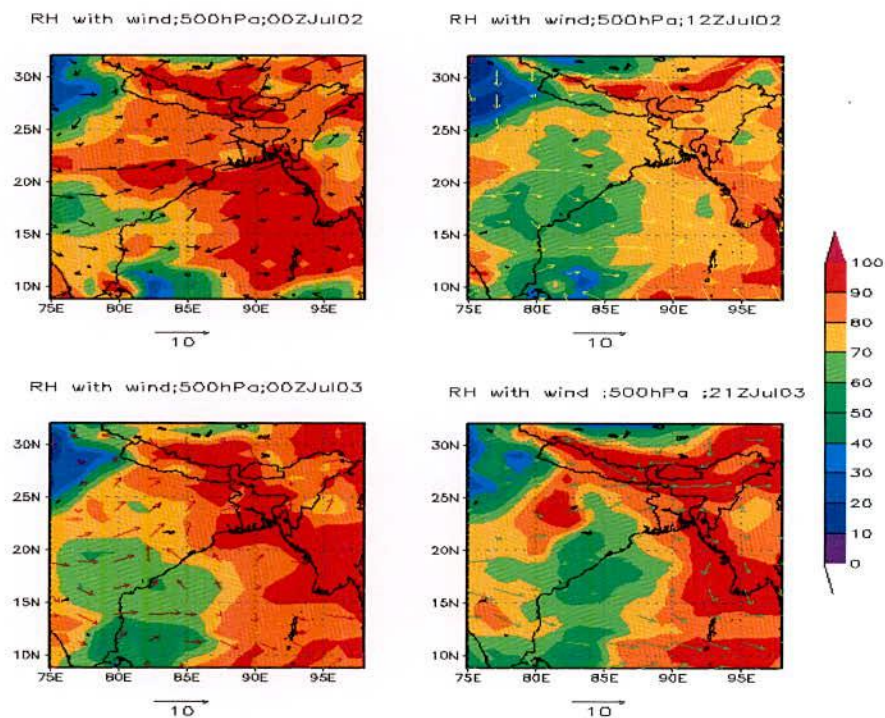


Figure 4.1.3.2b: WRF model simulated RH with wind at 500 hPa level valid for 00 UTC on 02 July to 21UTC on 03 July 2008.

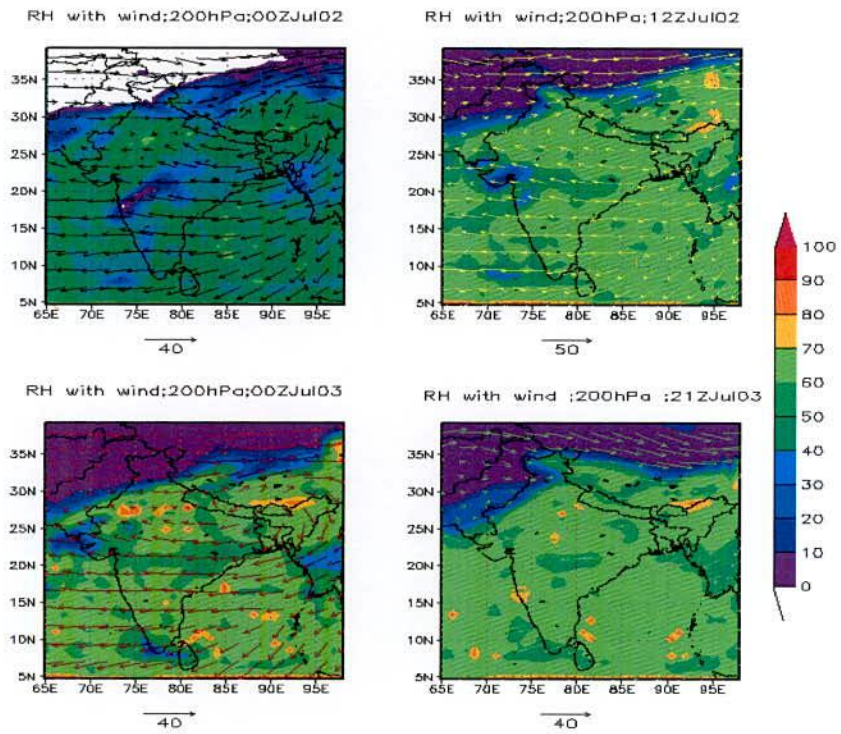


Figure 4.1.3.3a: MM5 model simulated RH with wind at 200 hPa level valid for 00 UTC on 02 to July 21UTC on 03 July 2008.

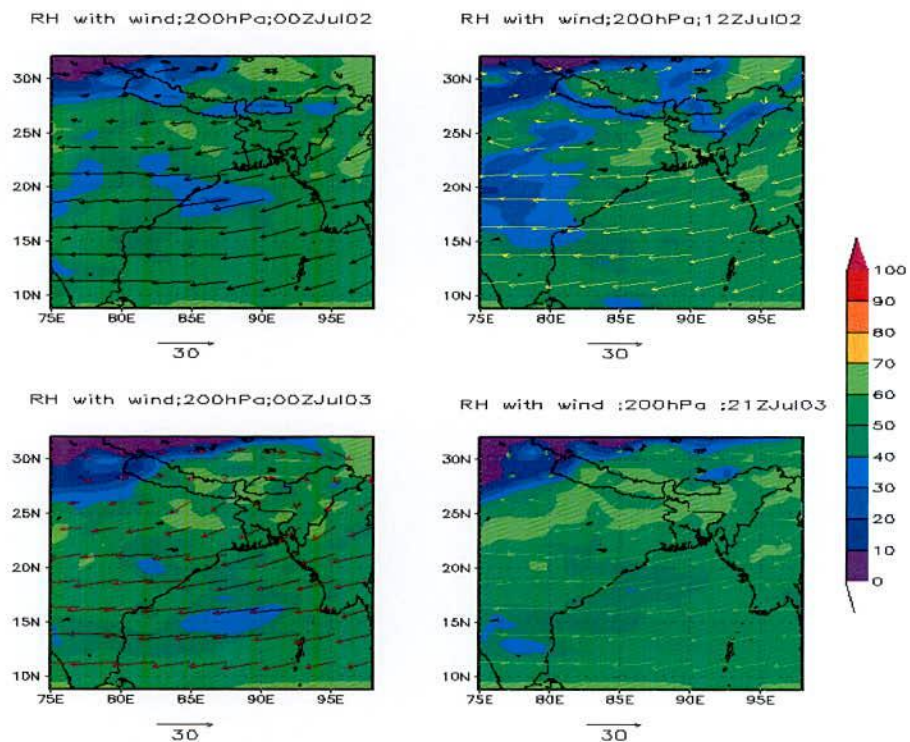


Figure 4.1.3.3b: WRF model simulated RH with wind at 200 hPa level valid for 00 UTC on 02 to July 21UTC on 03 July 2008.

4.1.4 Validation of Rainfall

24-h accumulated rainfalls obtained from the MM5 and WRF Models valid for 01, 02 and 03 July 2008 are shown in Figures 4.1.4.1– 4.1.4.3. Figures are plotted using model simulated 24-h accumulated rainfalls for Domain 1 (90 km resolution), Domain 2 (30 km resolution) and Domain 3 (10 km resolution) with rainfall obtained using TRMM and rain-gauge data. Rain-gauge data is obtained from Bangladesh Meteorological Department (BMD). Model simulated rainfall for both the models are seen at all places of Bangladesh with large spatial variability. For these simulations, Kain- Fritsch cumulus parameterization scheme with MRF PBL for MM5 model and Yonsei University Scheme (YSU) PBL for WRF model are used. It is found that the model simulated rainfall for all the domains of both the models overestimated the rainfall obtained from TRMM observational data. It is noted that TRMM underestimates the summer monsoon rainfall [111] in our region. It is very clear from the Figure 4.1.4.1– 4.1.4.3 that Domain 1 and Domain 3 show the minimum and maximum rainfall respectively than that of other domains for both the models MM5 and WRF. It means that high resolution produces comparatively more rainfall. Domain 3 of WRF model produces more rainfall than that of MM5 model without exception. But Domain 1 and Domain 2 of WRF model produces rainfall more or less than that produces by Domain 1 and Domain 3 of MM5 model. It implies that model produces realistic rainfall at high resolution.

On 01 July 2008, rainfall obtained from both MM5 and WRF models for Domain 3 is comparable to rainfalls obtained from TRMM and rain-gauge data. WRF model produces more rainfall than that of MM5 model and rainfall obtained from WRF model is much closer to that obtained from TRMM and rain-gauge data than that obtained from MM5 model.

On 02 July 2008, rainfall obtained from both MM5 and WRF models for Domain 3 is comparable to rainfalls obtained from rain-gauge data. WRF model produces more rainfall than that of MM5 model and rainfall obtained from WRF model is much closer to that obtained from rain-gauge data than that obtained from MM5 model. In this case rainfall obtained from TRMM data is very poor.

On 03 July 2008, rainfall obtained from both MM5 and WRF models for Domain 3 is comparable closed to rainfalls obtained from rain-gauge data. WRF model produces more rainfall that that of MM5 model and but rainfall obtained from MM5 model is much closer to that obtained from rain-gauge data and than that obtained from WRF model. In this case rainfall obtained from TRMM data is very poor.

From the above discussion, it is clear that rainfall obtained from WRF model is more than that obtained from MM5 model for high resolution domain i.e. Domain 3 without any exception and the Models simulated rainfalls are comparable to those obtained from BMD

rain-gauge with large spatial variability. However, both the models captured well the heavy rainfall event with spatio-temporal variation. It also captured the structure of the convective phenomena of the studied case. Thus simulated rainfall seems to be realistic using both the models.

The horizontal distribution of the cloud structures are shown in Figure 4.1.4.4 and 4.1.4.5 using model MM5 and WRF respectively at stage of high convection i.e. at mature stage of cloud, where 3 hourly precipitation are higher than other moments. Figures show the variation of intensity of cloud with spatial distribution. From the figures, centers of convective activity are identified to understand the vertical structure.

To study the vertical profile of convective system, the vertical structure of vertical velocity, divergence, relative vorticity, relative humidity and mixing ratio are plotted through the centre of the most developed cloud (21.96°N, 90.5°E), (26.95°N, 90.5°E), (27.15°N, 88.98°E) and (26.95°N, 91.94°E) at the time 06 and 15 UTC of 02 July, 03 and 21 UTC of 03 July 2008 respectively for MM5 model and shown in figures in following sections 4.1.5, 4.1.6, 4.1.7, 4.1.8 and 4.1.9. Similarly, the vertical structure of vertical velocity, divergence, relative vorticity, relative humidity and mixing ratio are plotted through the centre of the most developed cloud (23.65°N, 91.99°E), (25.2°N, 91.8°E), (26.875°N, 90.645°E) and (26.7°N, 90.26°E) at the time 06 and 18 UTC of 02 July, 06 and 21 UTC of 03 July 2008 respectively or WRF model are shown in figures in following sections 4.1.5, 4.1.6, 4.1.7, 4.1.8 and 4.1.9.

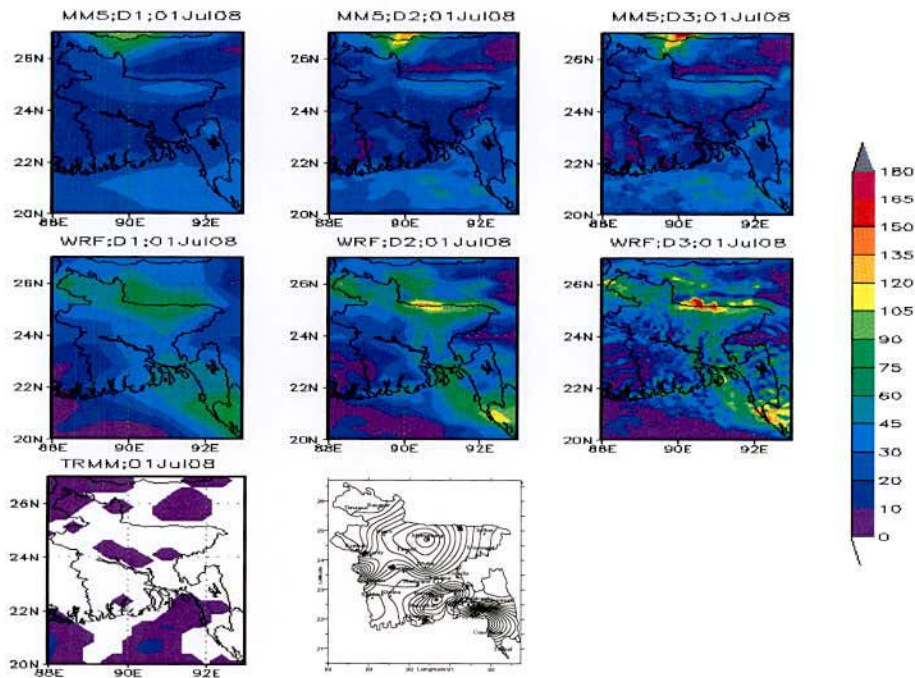


Figure 4.1.4.1: Spatial distribution of model simulated 24-h rainfall (mm) along with rainfall (mm) obtained from TRMM 3B42 V6 and BMD Rain –Gauge data valid for 01 July 2008.

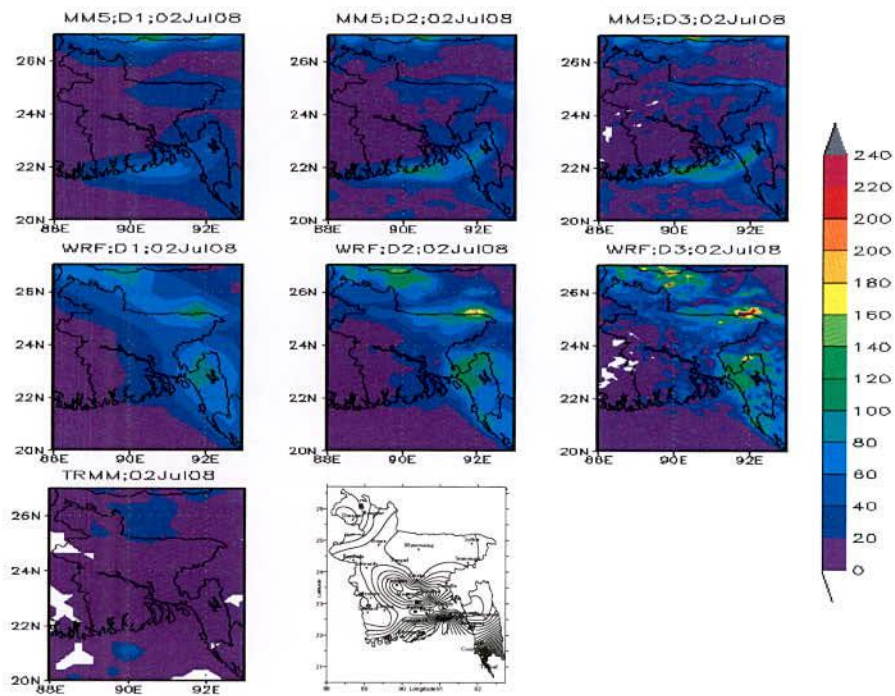


Figure 4.1.4.2: Same as Figures 4.1.4.1 but valid for 02 July 2008.

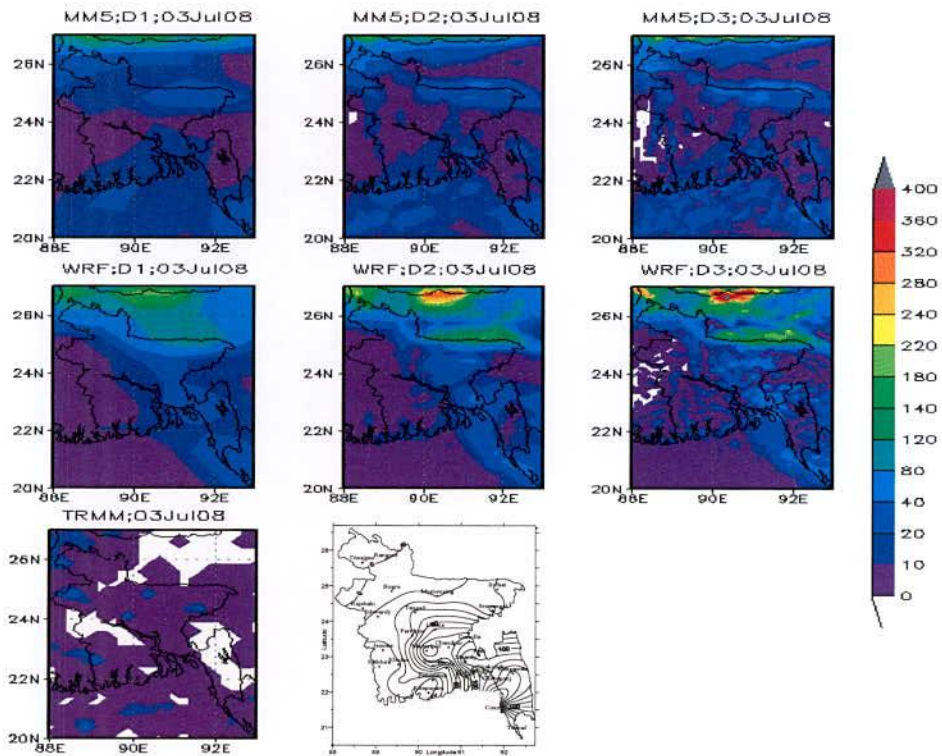


Figure 4.1.4.3: as Figures 4.1.4.1 but valid for 03 July 2008.

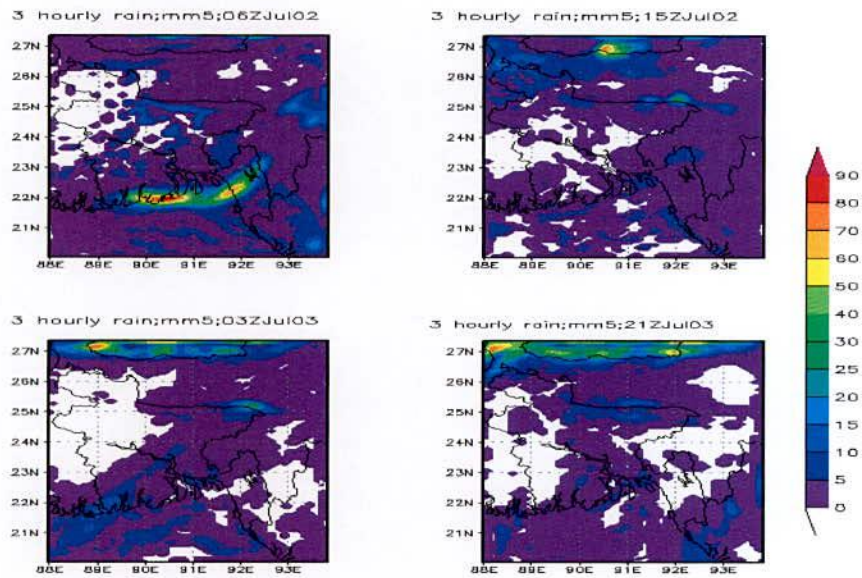


Figure 4.1.4.4: MM5 model simulated horizontal structure of most developed cloud at different times

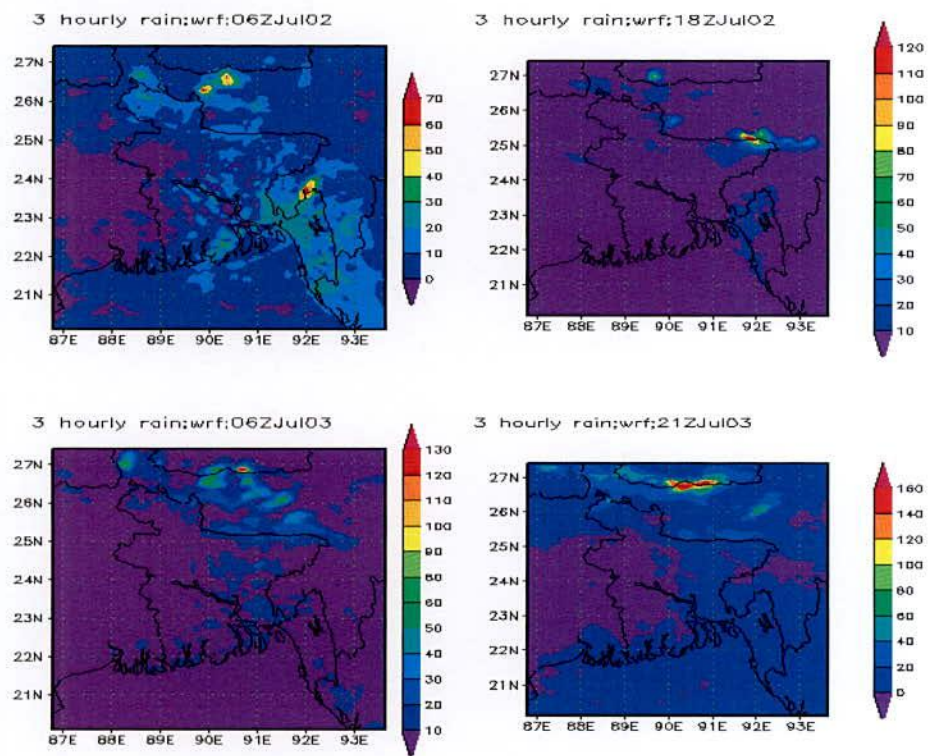


Figure 4.1.4.5: WRF model simulated horizontal structure of most developed cloud at different times

4.1.5 Vertical Structure of Vertical Velocity

To understand the vertical structure of the convective system, the vertical profiles of vertical velocity obtained from MM5 and WRF models are plotted through the centre of the most developed cloud at different times and are shown in Figure 4.1.5.1a and 4.1.5.1b. For MM5 model, times used are at 06 and 15 UTC of 02 July, and 03 and 21 UTC of 03 July 2008. But for WRF model, times used are at time 06 and 18 UTC of 02 July, 06 and 21 UTC of 03 July 2008.

The figures reveal that strong upward motion exists along the centre. The maximum upward vertical velocities for different time are different in magnitude. Their positions are also situated at different levels. Maximum values are 70 cm/s to 140 cm/s and from 70 to 500 cm/s for MM5 and WRF models respectively. Negative value indicates the downward motion. In general, downward motion is not strong. It is also visible in the different levels with areas of small pockets, which could be due to subsidence associated with convection. Values of maximum values of downward motion are from 0 to 20 cm/s and from 0 to 60 cm/s for MM5 and WRF models respectively. So, amount of the maximum values of upward and downward vertical velocity are more in case of MM5 than in case of WRF model.

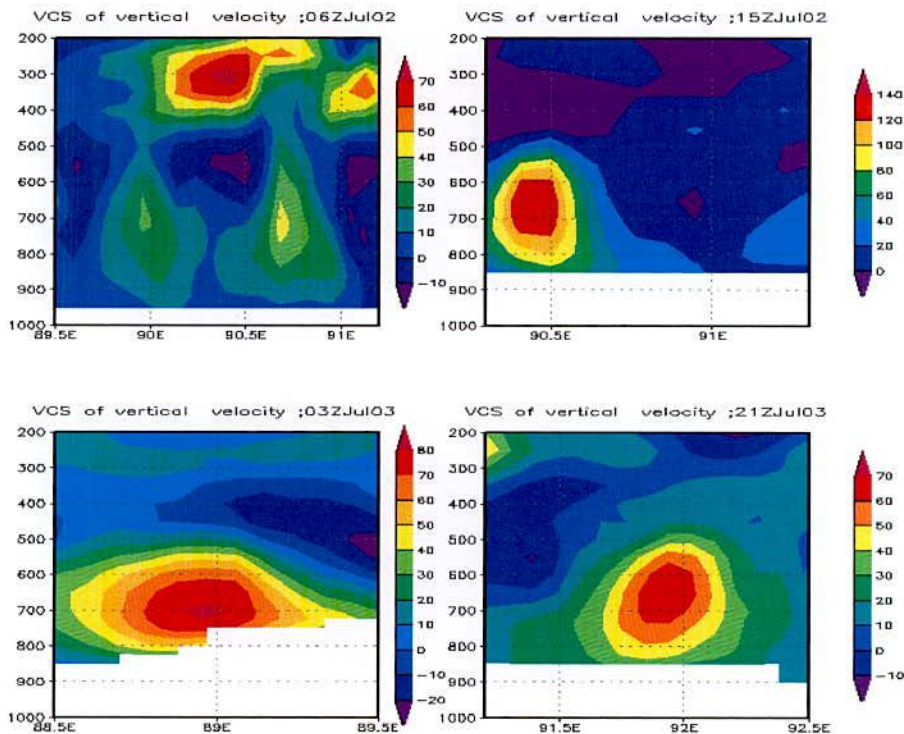


Figure 4.1.5.1a: Vertical structure of vertical velocity obtained from MM5 model through the center at different times.

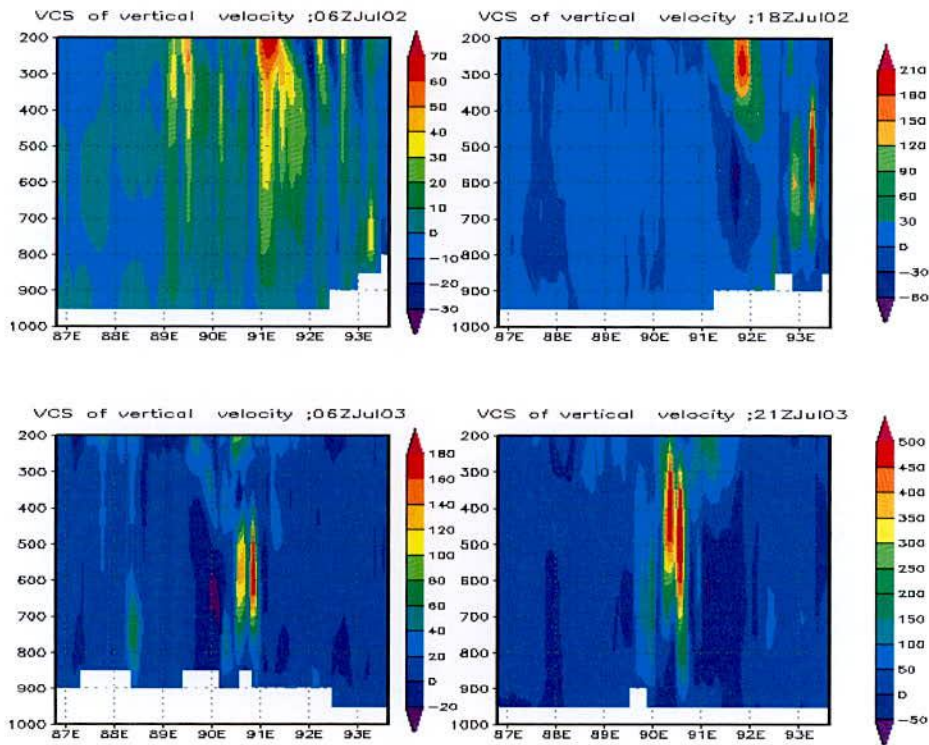


Figure 4.1.5.1b: Vertical structure of vertical velocity obtained from WRF model through the center at different times.

4.1.6 Vertical Structure of Divergence

Divergence is one the important parameters for analyzing the convective system. In general, there are low level convergence and upper level divergence in the convective system. The vertical cross sections of divergence ($\times 10^{-5} \text{ s}^{-1}$) obtained from MM5 and WRF models are plotted through the centre of the most developed cloud at different times and are shown in Figures 4.1.6.1a and 4.1.6.1b. For MM5 model, times used are 06 and 15 UTC of 02 July, and 03 and 21 UTC of 03 July 2008. But for WRF model, times used are 06 and 18 UTC of 02 July, 06 and 21 UTC of 03 July 2008.

In the figure positive and negative values indicate the divergence and convergence respectively. So, well defined convergence areas are available with divergence area at different levels. Low level convergences are available at four different times with upper level divergence. It is seen that divergence area embedded with convergence area. The maximum values of divergence and convergence are $(20 \text{ to } 50) \times 10^{-5} \text{ s}^{-1}$ and $(15 \text{ to } 60) \times 10^{-5} \text{ s}^{-1}$ respectively for MM5 model. Again, the maximum values of divergences and convergences are $(18 \text{ to } 100) \times 10^{-5} \text{ m}^{-1}$ and $(15 \text{ to } 80) \times 10^{-5} \text{ m}^{-1}$ respectively for WRF model.

This state of situation in convection is significant from the point of view of severe convective activity. At time 06 and 21 UTC of 03 July 2008, low level (up to 700 hPa level)

divergences are also available for MM5 model. This state of convection is significant from the point of view of severe convective activity. Again, the maximum values of divergence and convergence obtained using WRF model are more than those obtained from MM5 model. It indicates more precipitation will be obtained from WRF model than that obtained from MM5 model.

4.1.7 Vertical Structure of Relative Vorticity

The vertical profiles of relative vorticity ($\times 10^{-5} \text{ s}^{-1}$) obtained from MM5 and WRF models are plotted through the centre of the most developed cloud at different times and are shown in Figures 4.1.7.1a and 4.1.7.1b. For MM5 model, times used are 06 and 15 UTC of 02 July, and 03 and 21 UTC of 03 July 2008. But for WRF model, times used are 06 and 18 UTC of 02 July, 06 and 21 UTC of 03 July 2008. Relative vorticity is absent in the lower levels at all observed times because of hilly surface area with low pressure and high altitude. It is seen in the figure, strong positive vorticity are observed up to 500 and 200 hPa level with decreasing in magnitude for MM5 and WRF model respectively. There are some variations of the magnitude of maximum positive vorticity at different levels at different times. These values are $(30\sim 50) \times 10^{-5} \text{ s}^{-1}$ and $(10 \sim 40) \times 10^{-5} \text{ s}^{-1}$ for MM5 and WRF models respectively. It is noted that positive vorticity indicates the cyclonic motion in the lower level. Negative vorticity is also observed in the upper levels with different values at different times and positions.

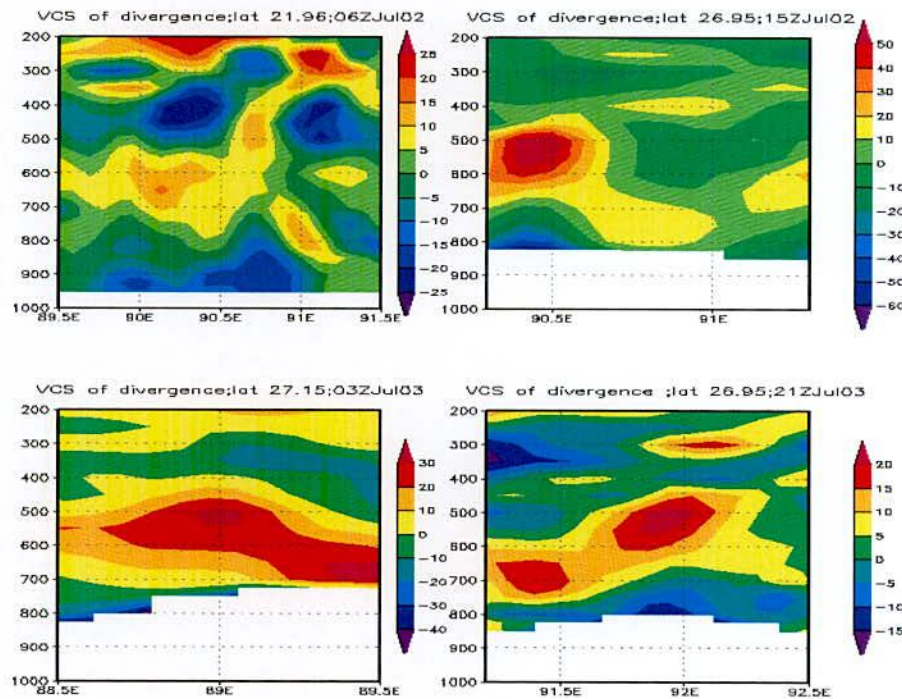


Figure 4.1.6.1a: Vertical structure of divergence (unit: $\times 10^{-5} / \text{s}$) obtained from MM5 model through the center at different times.

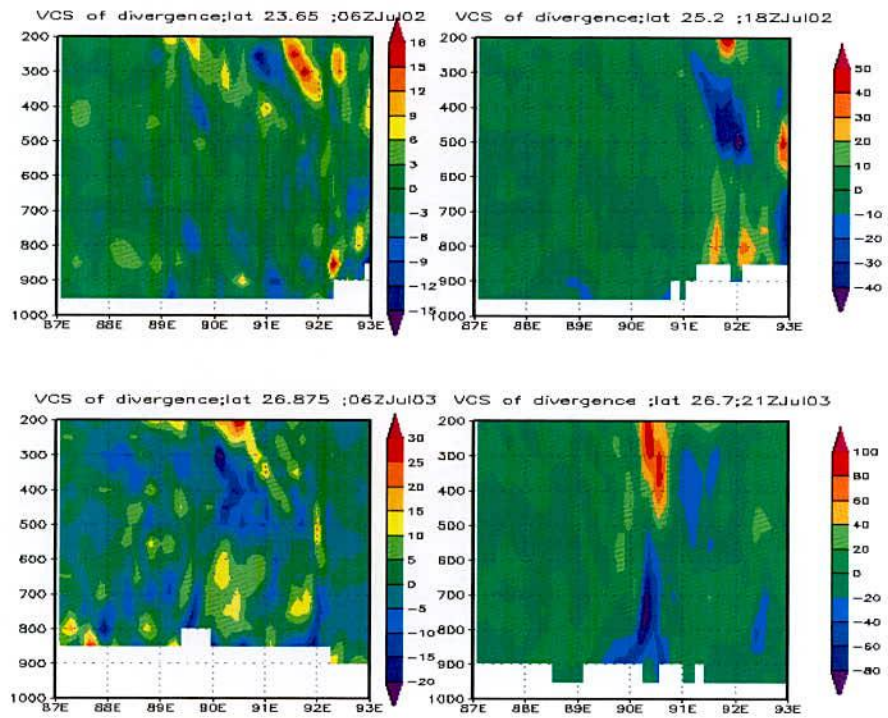


Figure 4.1.6.1b: Vertical structure of divergence (unit: $\times 10^{-5}$ /s) obtained from WRF model through the center at different times

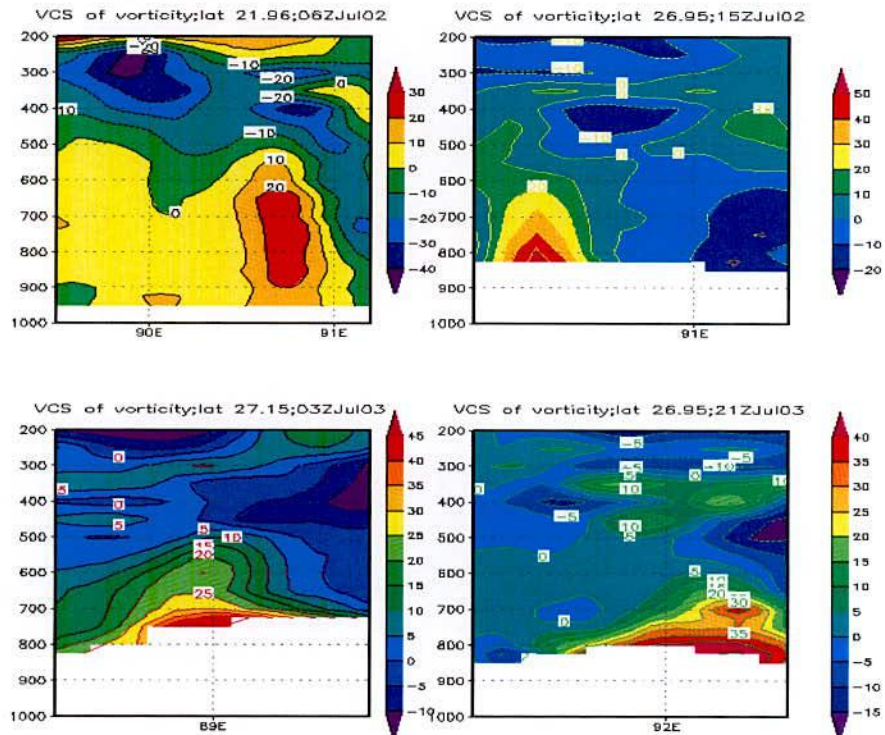


Figure 4.1.7.1a: Vertical structure of relative vorticity ($\times 10^{-5}$ s $^{-1}$) obtained from MM5 model through the center at different times.

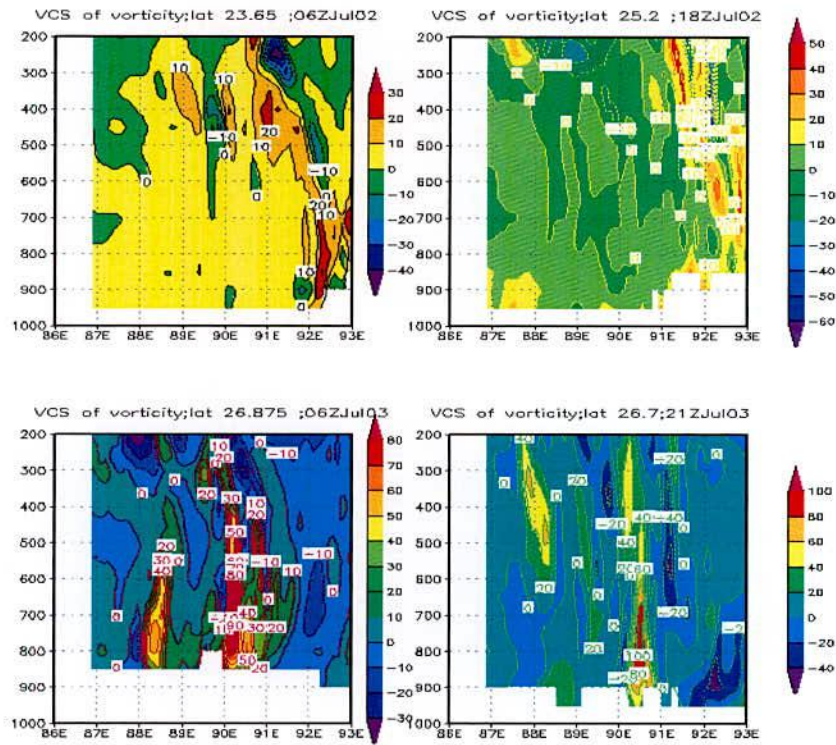


Figure 4.1.7.1b: Vertical structure of relative vorticity ($\times 10^{-5} \text{ s}^{-1}$) obtained from WRF model through the center at different times.

These values are $(10\sim 40) \times 10^{-5} \text{ s}^{-1}$ and $(30 \sim 60) \times 10^{-5} \text{ s}^{-1}$ for MM5 and WRF models respectively. So, low level positive vorticity indicates the convective activity of the system due to westerly and south-westerly wind obtained from both the models.

4.1.8 Vertical Structure of Relative Humidity

The vertical profiles of relative humidity (%) obtained from MM5 and WRF models are plotted through the centre of the most developed cloud at different times and are shown in Figure 4.1.8.1a and 4.1.8.1b. For MM5 model, times used are at 06 and 15 UTC of 02 July, and 03 and 21 UTC of 03 July 2008. But for WRF model, times used are 06 and 18 UTC of 02 July, 06 and 21 UTC of 03 July 2008. For both the models, relative humidity is absent in the lower levels at all observed time because of hilly surface area at high altitude with low pressure. Relative humidity (more than 90%) spreads in outer range of eye wall up to 350 hPa level. High relative humidity is also seen up to 200 hPa level. The vertical profiles of relative humidity satisfy the development of the convective activity.

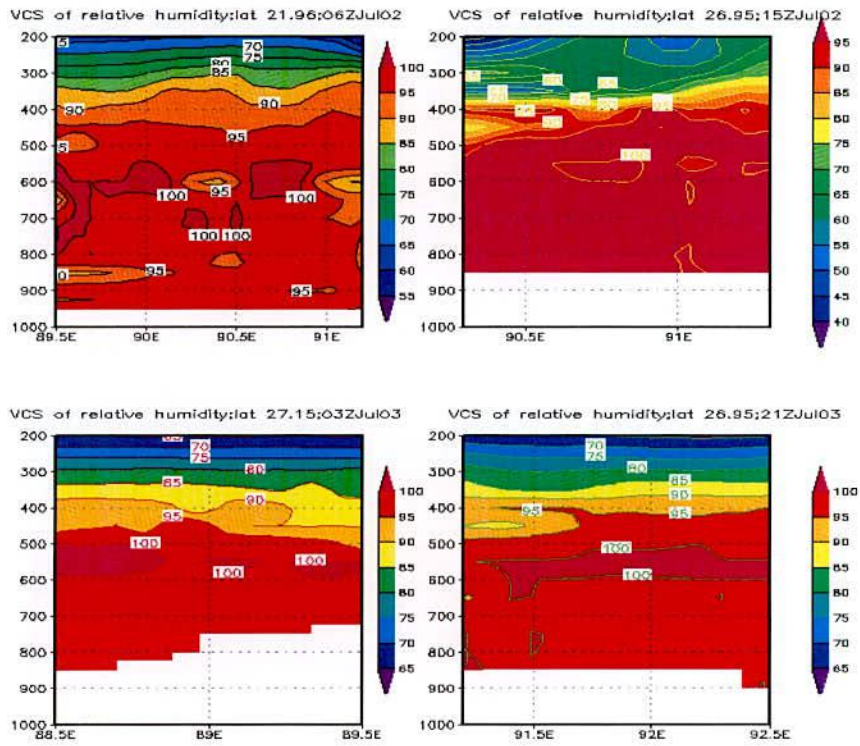


Figure 4.1.8.1a: Vertical structure of relative humidity obtained from MM5 model through the center at different times.

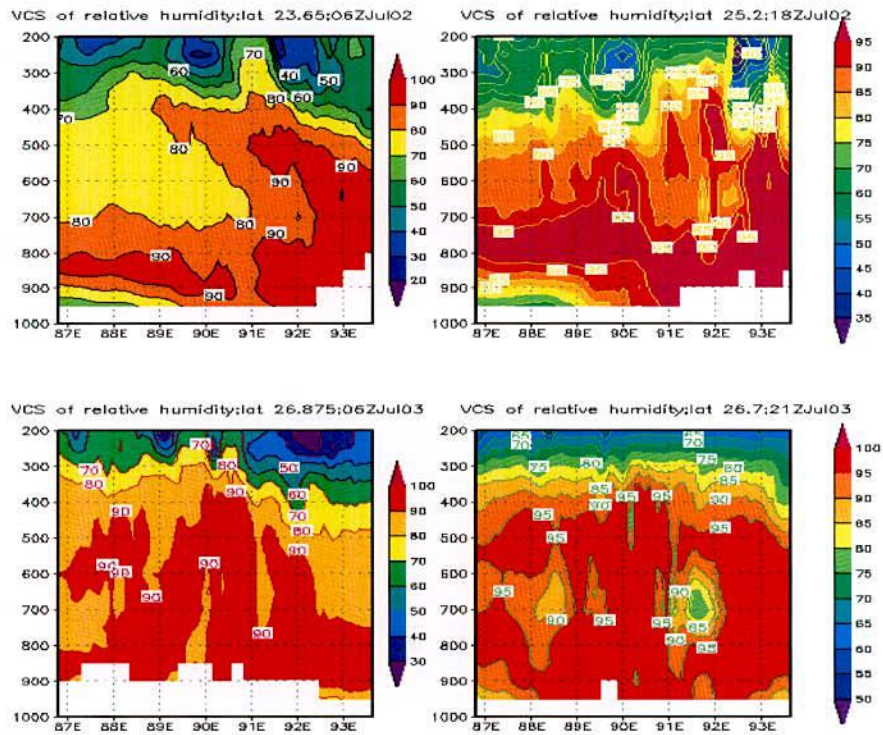


Figure 4.1.8.1b: Vertical structure of relative humidity obtained from WRF model through the center at different times.

4.1.9 Vertical Profile of Mixing Ratio

The vertical profiles of mixing ratio obtained from MM5 and WRF models are plotted through the centre of the most developed cloud at different time and are shown in Figure 4.1.9.1a and 4.1.9.1b. For MM5 model, times used are at 06 and 15 UTC of 02 July, and 03 and 21 UTC of 03 July 2008. But for WRF model, times used are at time 06 and 18 UTC of 02 July, 06 and 21 UTC of 03 July 2008. Mixing ratio is absent in the lower levels at all observed time because of hilly surface area at high altitude with low pressure. It shows that the highest moisture content around 1.8 g/kg or more is found at the centre of the convective system at or above 950 hPa level then it decreases upwards to 350 hPa level or more. It is to be noted that the high moisture flux comes from the southern side covering a large area of the Bay of Bengal which feeds the system along its southeastern side through the boundary layer. A noticeable amount of moisture flux also comes from the south-western side through the Indian sub-continent which feeds the system along its south-western side through the boundary layer.

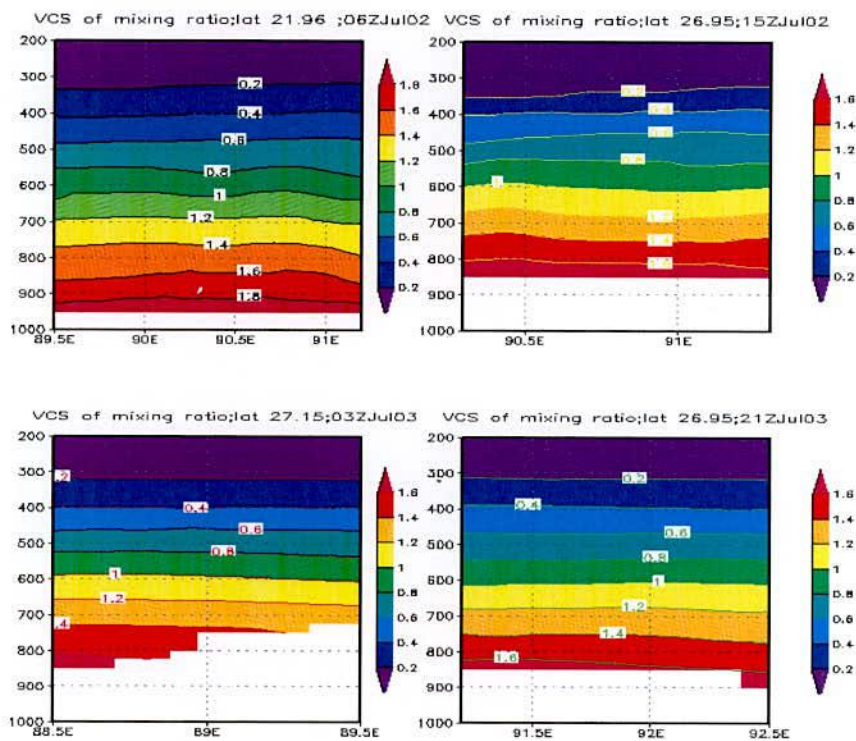


Figure 4.1.9.1a: Vertical structure of mixing ratio ($\times 10^{-2}$) obtained from MM5 model through the center at different times.

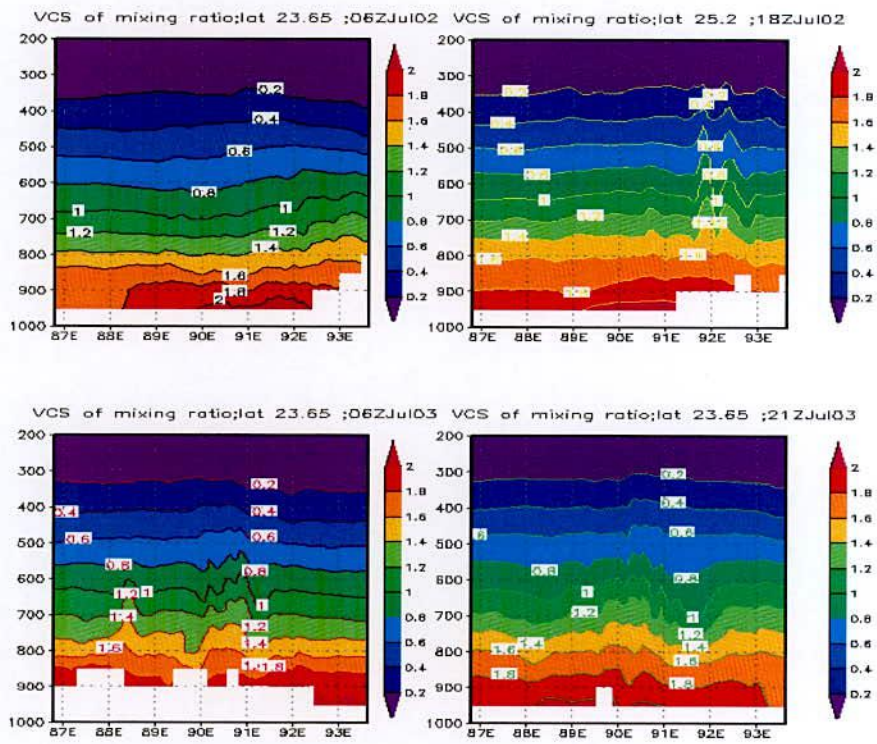


Figure 4.1.9.1b: Vertical structure of mixing ratio ($\times 10^{-2}$) obtained from WRF model through the center at different times.

4.2 Simulation of Heavy Rainfall Events of 09-11 June 2007 using MM5 and WRF Model

To analyze the convective system of 09-11 June 2007 with their vertical structure, the MM5 and WRF models were run for 72 hours based on the initial condition at 00 UTC of 09 June 2007. All parameters were made for 00 UTC of 10 June 2007 for the analysis of the synoptic conditions responsible for producing rain. The first 24 hours was considered as spin up period. The model performance was evaluated by examining the different predicted parameters like mean sea level pressure (MSLP), rain with vector wind, relative humidity with vector wind, and vertical velocity, divergence, relative vorticity, relative humidity and mixing ratio at four different times of most developed cloud. The model derived rainfall for all three domains were compared with that obtained from TRMM and Bangladesh Meteorological Department (BMD) rain-gauge observation data. Surface simulated precipitation was considered as rainfall throughout the study.

4.2.1 Mean Sea Level Pressure (MSLP)

Model simulated MSLPs (hPa) obtained from both the MM5 and WRF models for the domain D1, valid for the initial time 00 UTC of 09 June to 00 UTC of 12 July 2007, are presented in Fig. 4.1.1.1a and Fig. 4.1.1.1b respectively. At initial time 00 UTC of 09 June 2007, the northerly positioned monsoon trough lies parallel to the foot hills of the Himalayan Mountain with low pressure about 996 hPa at the center situated at northern part of India according to the output of MM5 and WRF models. The MSLP over Tibet is very high and central pressures are above 1023 and 1020 hPa simulated by MM5 and WRF models respectively. At this moment, pressure over Bangladesh is from 999 to 1002 hPa for MM5 and WRF models.

The center of the low pressure system changes and extends towards north-western side of Bangladesh with central pressure 993 hPa at time 00 UTC of 10 June 2007 making pressure 996 hPa over other regions of Bangladesh for both the models. Because of this monsoon trough, this state of pressure 993 hPa prevails over most parts of Bangladesh except north-eastern side for the simulation time up to 00 UTC of 11 June 2007 and monsoon trough lies parallel to the foot hills of the Himalayan Mountain over whole (except north-eastern part) Bangladesh and Indian territory for long time. It may be due to this high pressure over Tibetan plateau and weak heat low.

4.2.2 Study of Rainfall with Wind

During summer monsoon period, one of the main synoptic conditions for occurrence of heavy rainfall over Bangladesh and neighborhood is the SW'ly flow streaming from the head of Bay of Bengal into Bangladesh [110].

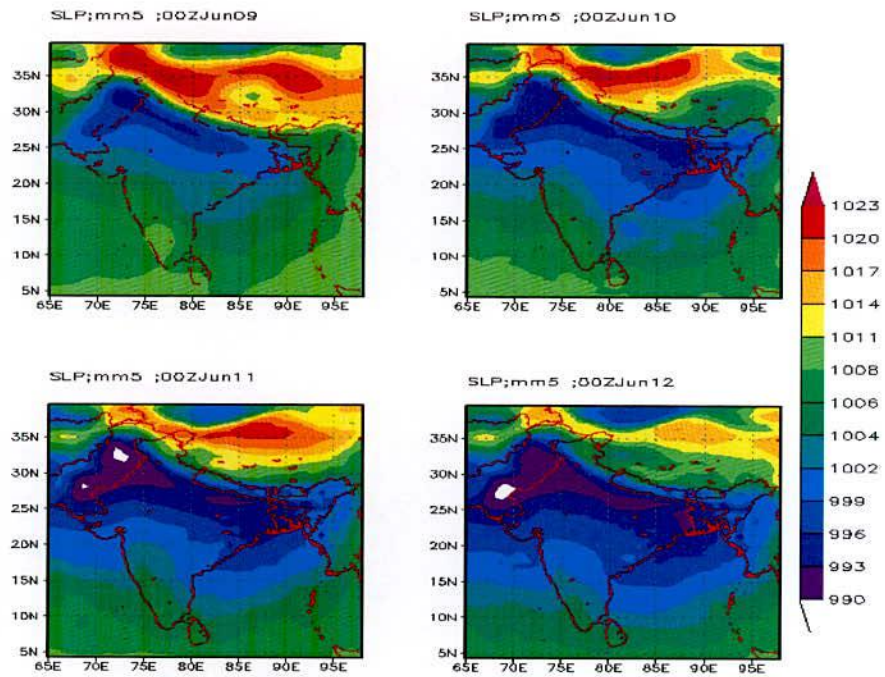


Figure 4.2.1.1a: MM5 Model simulated MSLP (hPa) valid from 00 UTC of 09 June to 00 UTC of 12 June 2007

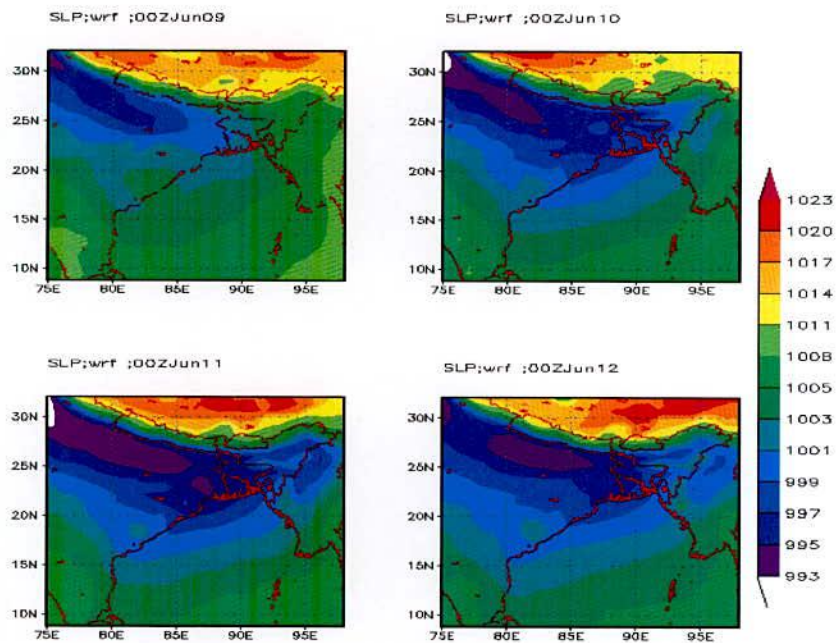


Figure 4.2.1.1b: MM5 Model simulated MSLP (hPa) valid from 00 UTC of 09 June to 00 UTC of 12 June 2007

For the present case, westerly wind comes from the Arabian Sea into the Indian region and SW'ly wind comes from the Bay of Bengal and both of these winds enter into the Bangladesh region. Westerly winds carry moisture from the Arabian Sea and SW'ly winds carry moisture from the Bay of Bengal and convergence occurred in the whole Bangladesh especially near the hilly region. There was a cyclonic circulation developed over Bangladesh and West Bengal of India. A well marked low pressure area forms over this region. Due to this heavy rainfall occurred over Bangladesh and Bay of Bengal. The detailed analyses of the system using both the MM5 and WRF models are given below and shown in Figures 4.2.2.1 (a-d), 4.2.2.2 (a-b) and 4.2.2.3 (a-b).

Using MM5 models, the distributions of low level wind flow at 850 hPa and upper level wind flow at 500 hPa and 200 hPa level valid from 00 UTC of 09 June to 21 UTC of 11 June 2007 are presented in Figures 4.2.2.1(a-b), 4.2.2.2a and 4.2.2.3a respectively. The prominent feature is a strong SW'ly flow transporting high magnitude of moisture from the Bay of Bengal into northeast and central Bangladesh during the whole simulation period. Westerly flow also transports significant amount of moisture from the Arabian Sea through India to main land of Bangladesh. From the Figure 4.2.2.1(a-b), it is seen that the area of convergence (i.e., zone of high convective activity) observed over Bangladesh and neighborhoods. At time 00 UTC on 10 July, 2008, at level 850 hPa, the amount of moisture is very low. Due to convergence, small cells merge with others cells and make clusters. With the advancement of time other cells make another cluster. Clusters merge to form mesoscale convective system (MCS) and rainfall occurs in and outside of Bangladesh. It is seen that very developed MCS form near the foot hills of Himalayan Mountain and hence heavy rainfall occurred in the north-eastern part of Bangladesh. The cyclonic circulation is observed at 850 hPa level wind (Figure 4.2.2.1(a-b)). The wind speed is almost about 20 m/s from 00 UTC of 10 June to 21 UTC of 11 June 2007 with varied amount of 3-hourly rainfalls from 18 to 65 mm. The SW'ly wind speed of about 20 m/s prevails over North Bay of Bengal and south Bangladesh up to 500 hPa level with cyclonic circulation (Figure 4.2.2.2a). Another anticyclonic circulation is also observed at this level over west side of India. Anticyclonic circulation is also observed at 200 hPa level with wind speed range 40 to 50 m/s (Figure 4.2.2.3a).

Using WRF model, the low level wind flow at 850 hPa and upper level wind flow at 500 and 200 hPa level valid from 00 UTC of 09 June to 21 UTC of 11 June 2007 are presented in Figures 4.2.2.1(c-d), 4.2.2.2b and 4.2.2.3b respectively. Similar features are observed using both the models with different amount of moisture content and wind speed. The simulation of MCS using WRF model is more than that using the MM5 model. The maximum wind speed at the levels 850, 500 and 200 are 20, 10 and 30 m/s respectively. This maximum wind speed is smaller than or equal to those obtained using MM5 model.

Figures make us clear that rainfall happens because of the combined effect of SW'ly and southerly wind which carry moisture from Arabian Sea and Bay of Bengal respectively.

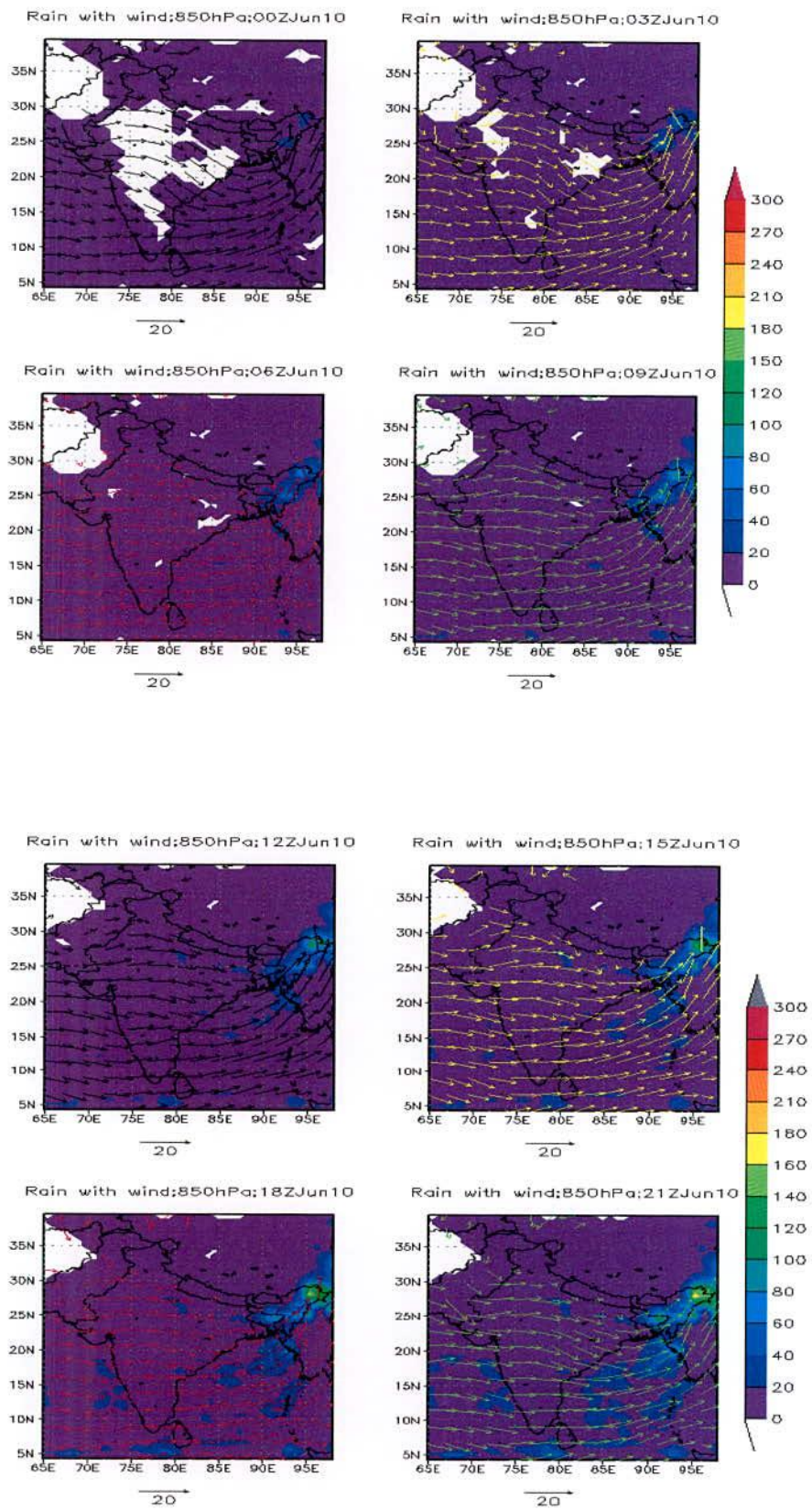


Figure 4.2.2.1a: MM5 Model simulated rain with wind flow (m/s) analysis at 850 hPa valid for time 00 UTC to 21 UTC of 10 June 2007

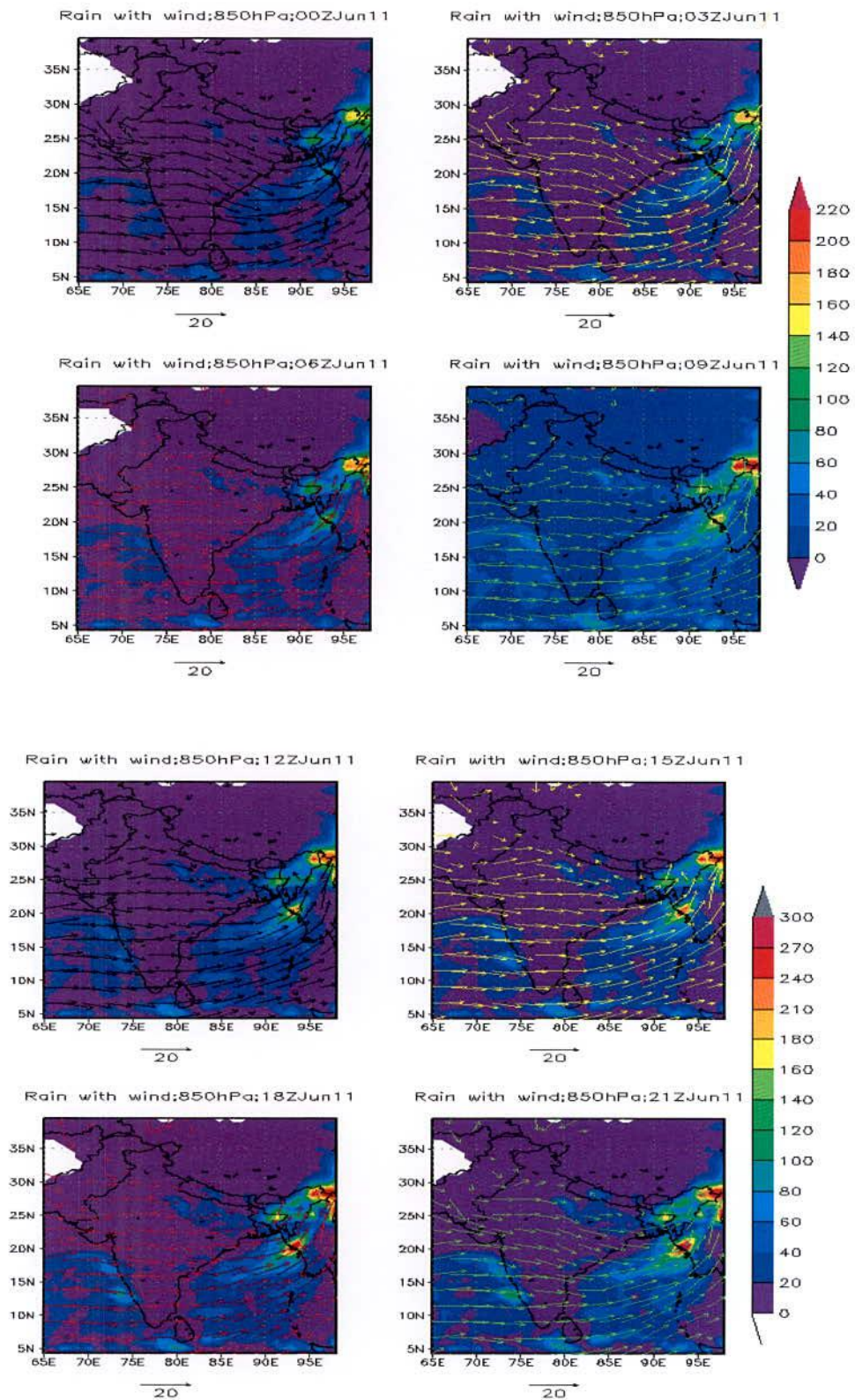


Figure 4.2.2.1b: MM5 Model simulated rain with wind flow (m/s) analysis at 850 hPa valid for time 00 UTC to 21 UTC of 11 June 2007

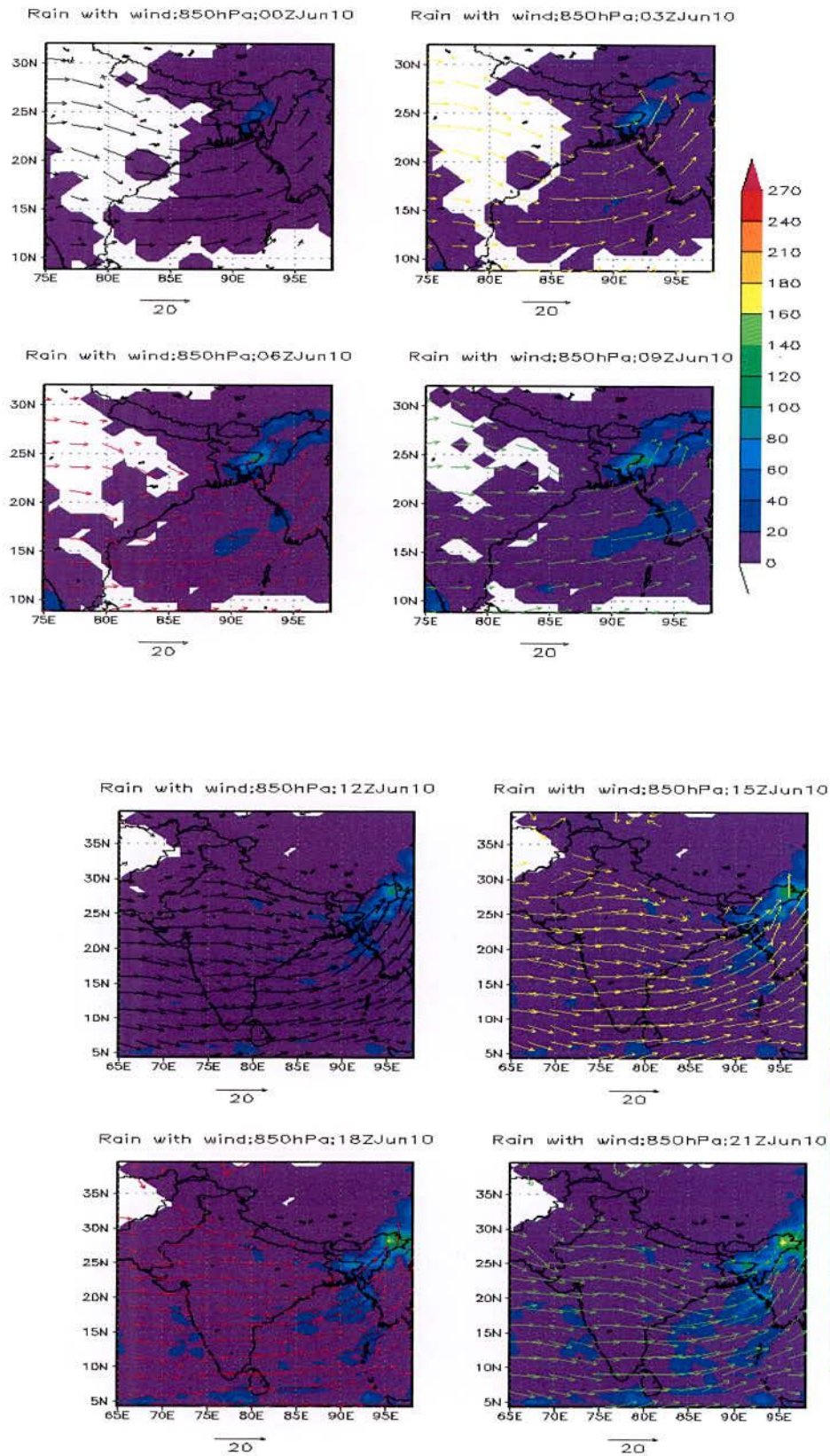


Figure 4.2.2.1c: WRF Model simulated rain with wind flow (m/s) analysis at 850 hPa valid for time 00 UTC to 21 UTC of 10 June 2007

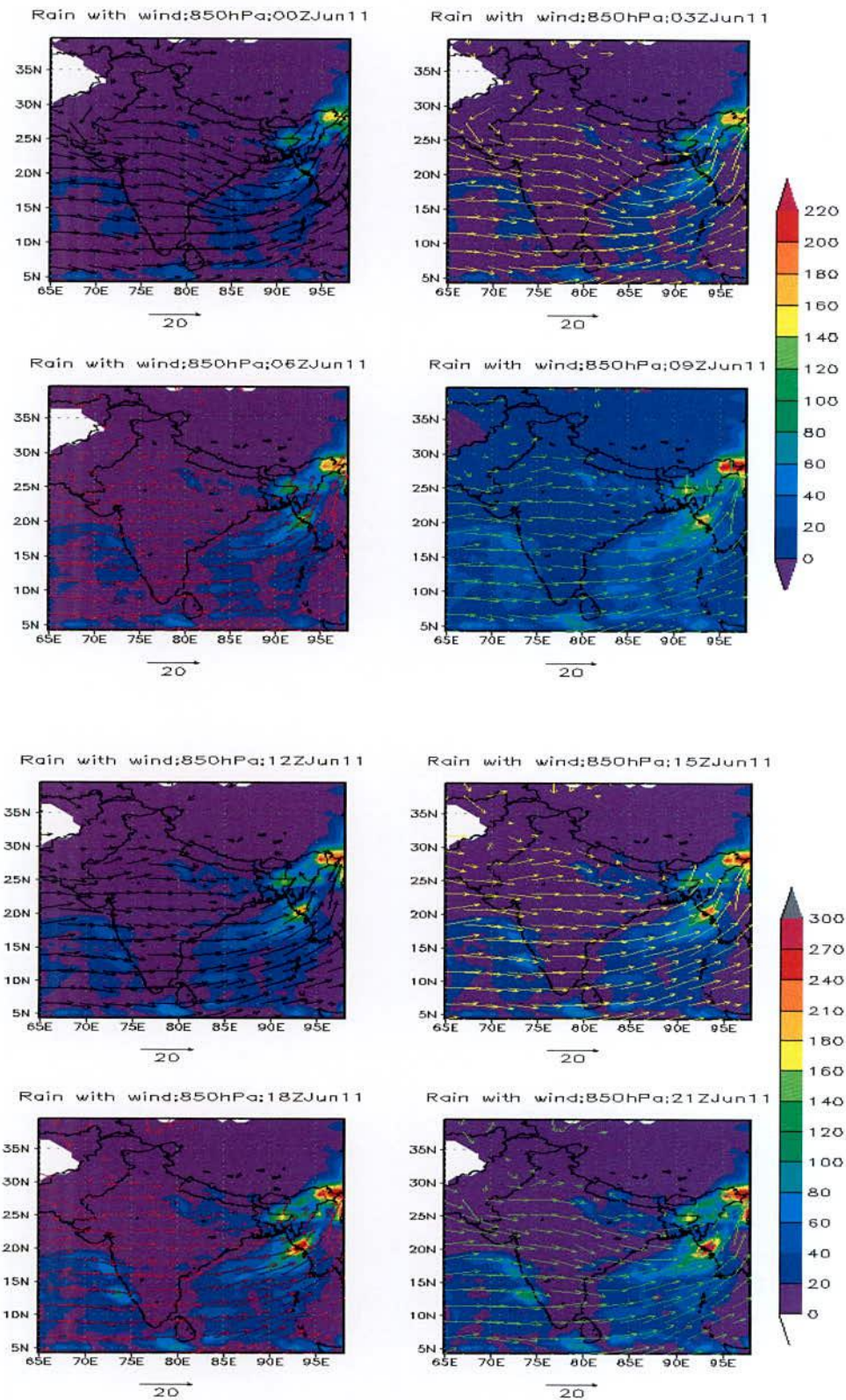


Figure 4.2.2.1d: WRF Model simulated rain with wind flow (m/s) analysis at 850 hPa valid for time 00 UTC to 21 UTC of 11 June 2007

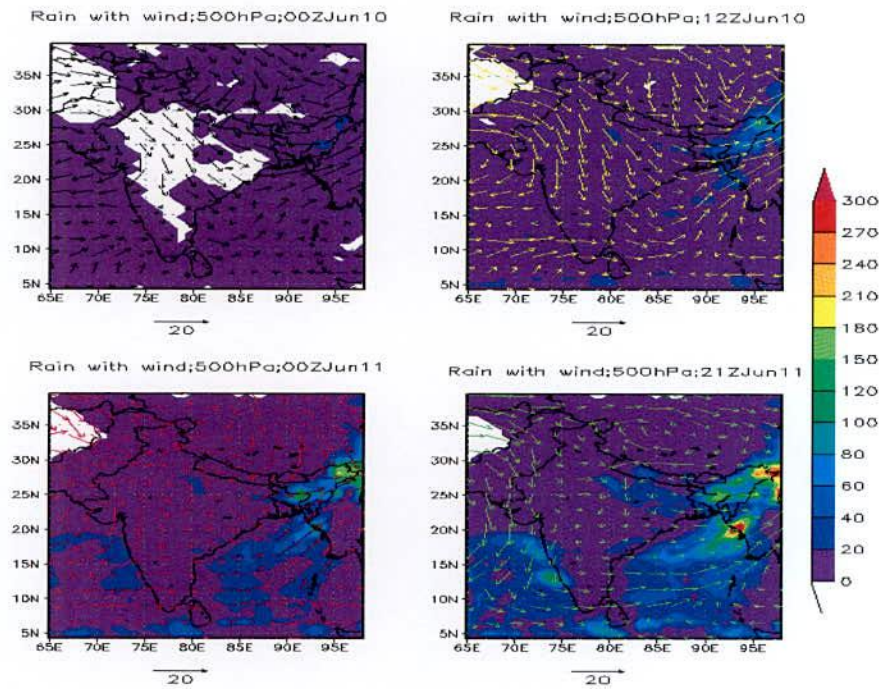


Figure 4.2.2.2a: MM5 Model simulated rain with wind flow (m/s) analysis at 500 hPa valid for time 00 UTC of 10 June to 21 UTC of 11 June 2007

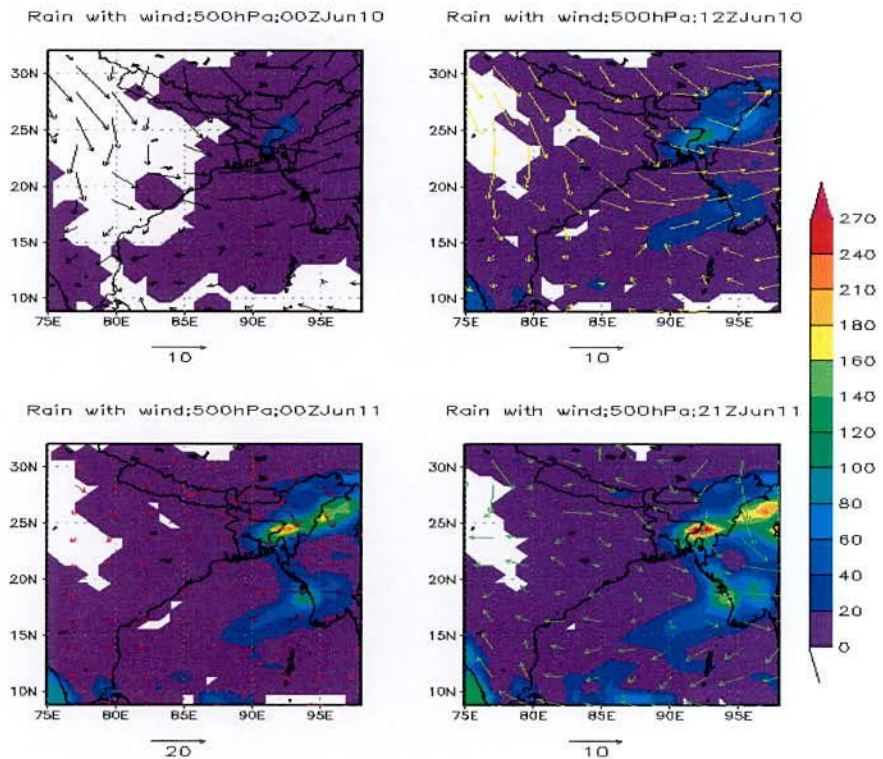


Figure 4.2.2.2b: WRF Model simulated rain with wind flow (m/s) analysis at 500 hPa valid for time 00 UTC of 10 June to 21 UTC of 11 June 2007

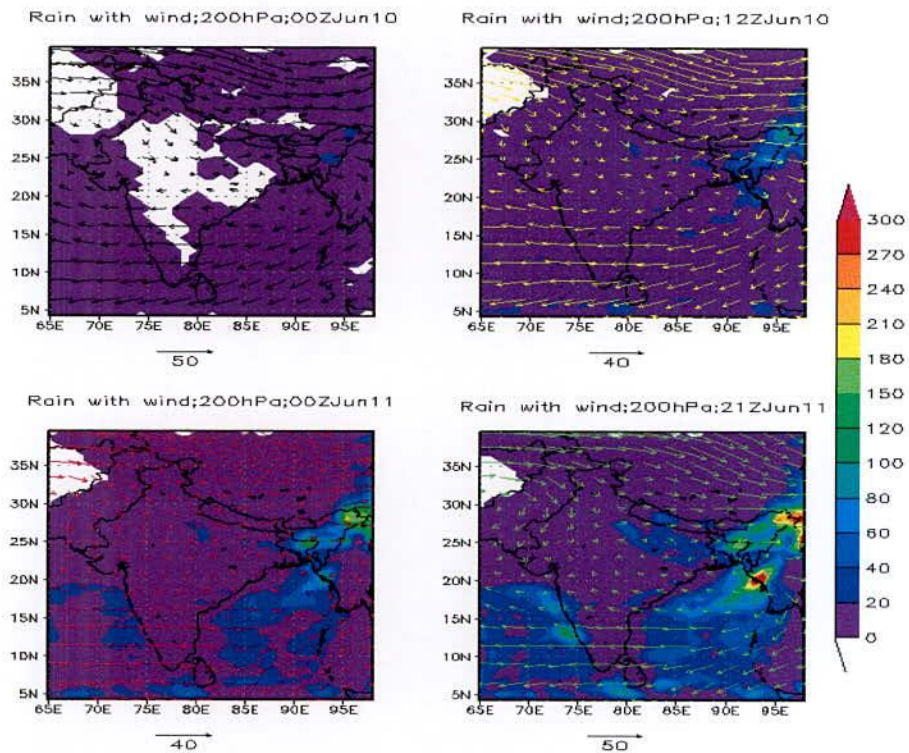


Figure 4.2.2.3a: MM5 Model simulated rain with wind flow (m/s) analysis at 200 hPa valid for time 00 UTC of 10 June to 21 UTC of 11 June 2007

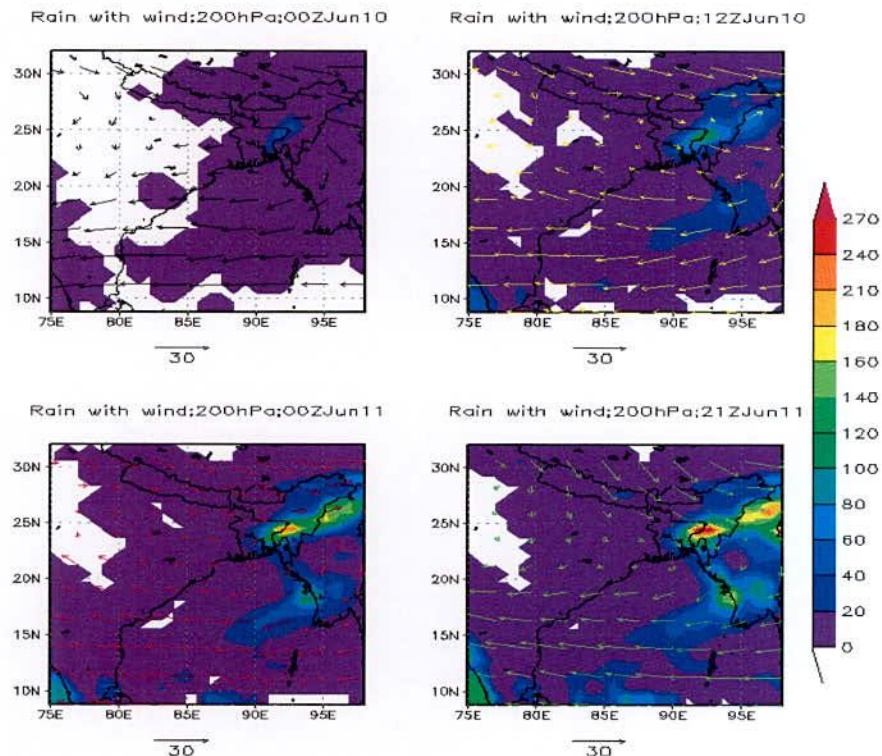


Figure 4.2.2.3b: MM5 Model simulated rain with wind flow (m/s) analysis at 200 hPa valid for time 00 UTC of 10 June to 21 UTC of 11 June 2007

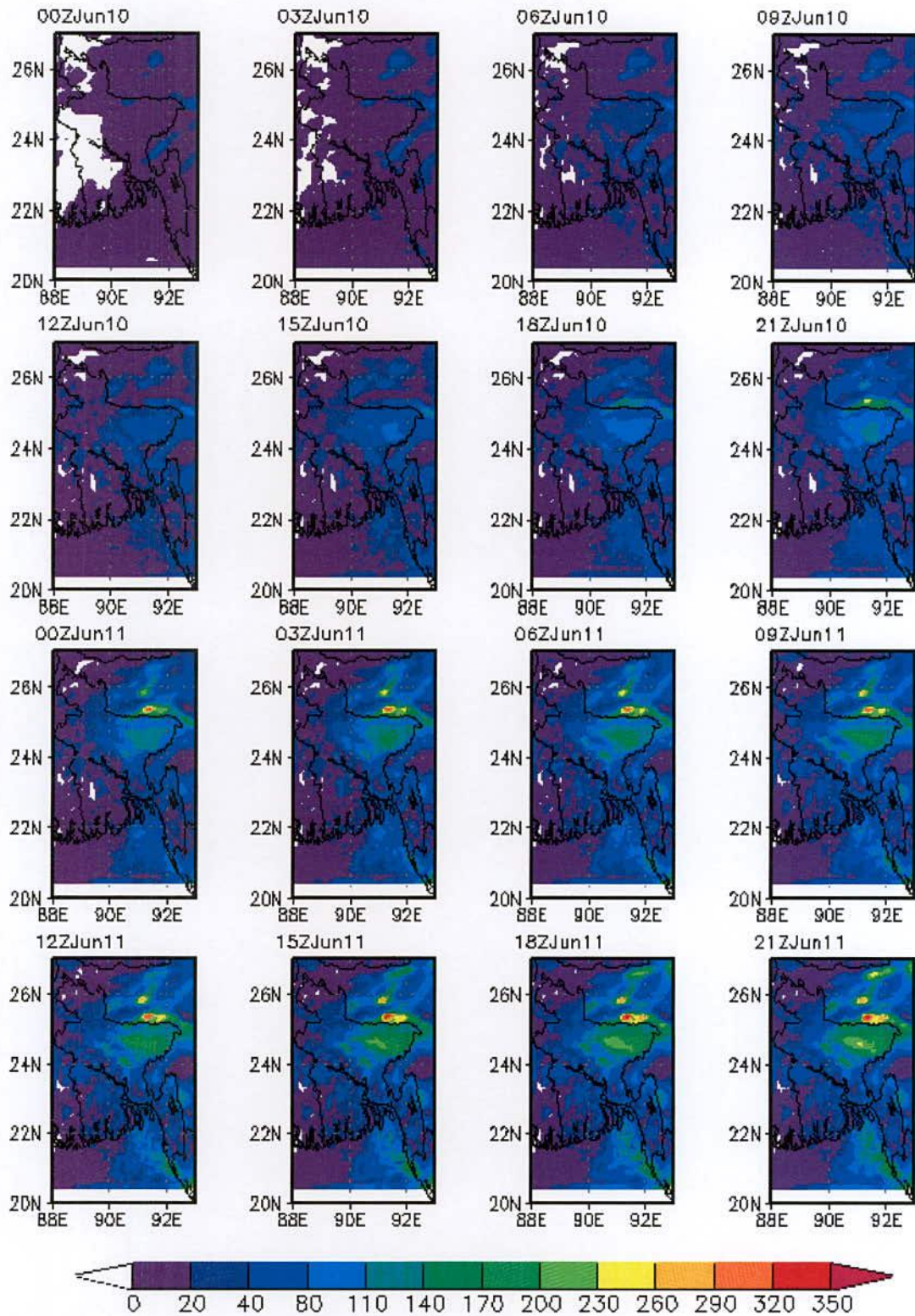


Figure 4.2.2.4a: MM5 Model simulated precipitation field valid from 00 UTC of 10 June to 21 UTC of 11 June 2007. Sequence is top left to right.

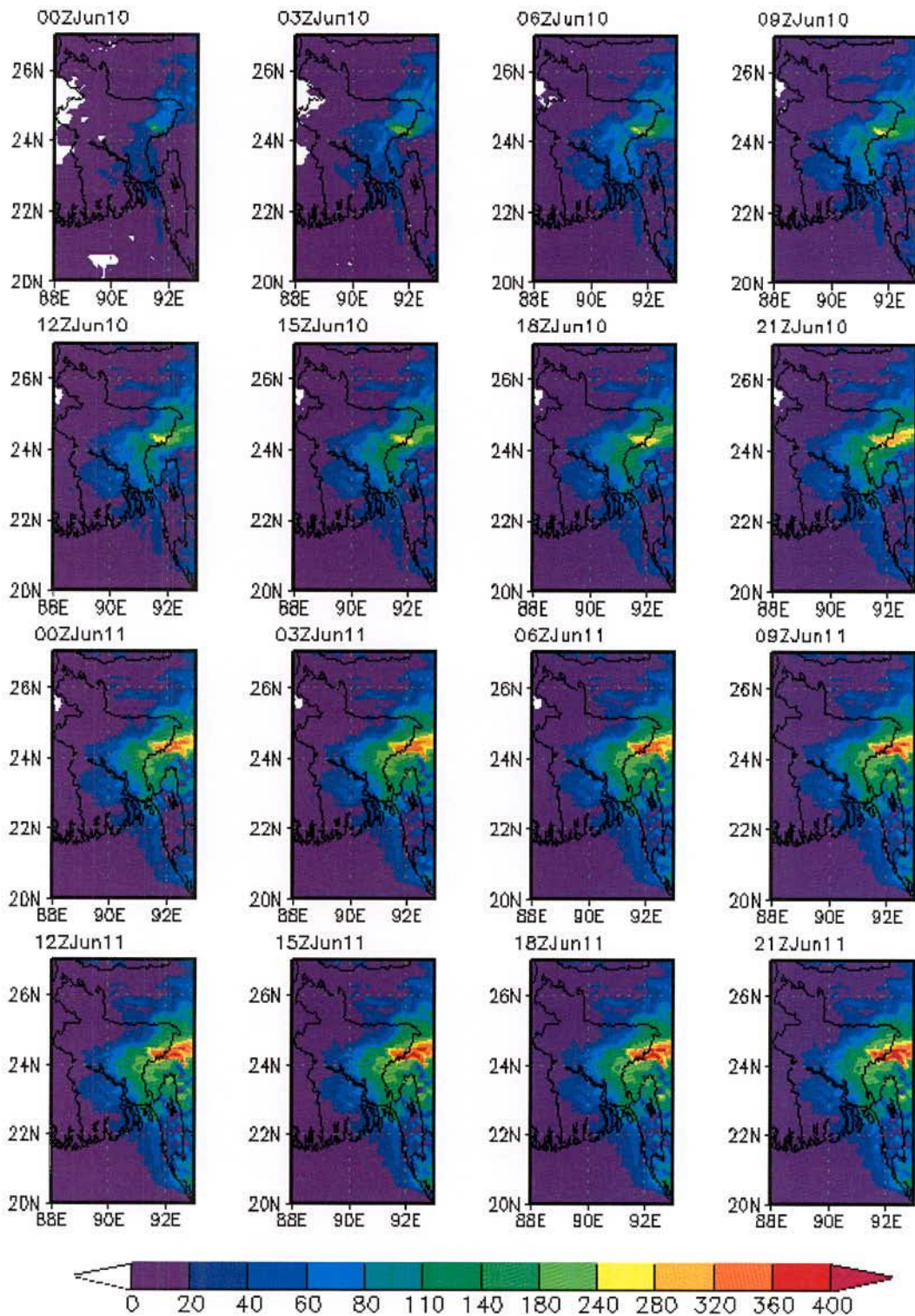


Figure 4.2.2.4b: WRF Model precipitation field valid for 00 UTC of 10 June to 21 UTC of 11 June 2007. Sequence is top left to right

Figures 4.1.2.4a and 4.1.2.4b are obtained using inner most Domains i.e. Domain 3 of MM5 and WRF models. It is noted that resolution of Domain 3 is 10 km for both the models. Figures show the development of cloud i.e. MCS in every 3 hours with the advancement of

time from 00 UTC of 10 June to 21 UTC of 11 June, 2007. It is clear from the Figures 4.2.2.4a and 4.2.2.4b that simulated rainfall obtained from WRF model is more than that obtained from MM5 model.

4.2.3 Study of Relative Humidity with Wind

The simulation of relative humidity and wind shows SW'ly flow transports plentiful of moisture from the Bay of Bengal and westerly flow transport moisture from the Arabian Sea through the Indian region to the plains of Bangladesh and neighborhood. Using MM5 model, the spatial distribution of relative humidity with wind at 850, 500 and 200 hPa levels from 00 UTC of 09 June to 21 UTC of 11 June 2007 are presented in Figures 4.2.3.1(a-b), 4.2.3.2a and 4.2.3.3a respectively. The moisture content of the order of 90-100% over most of the region of Bangladesh at 850 and 500 hPa levels is found with cyclonic circulation of wind for the whole simulation time. But the amount of moisture is less at 200 hPa level with anti-cyclonic circulation of wind. At 850 hPa, the moisture content is very less over the Himalayan Mountain and wind speed almost about 20 m/s from 00 UTC of 10 June to 21 UTC of 11 June 2007. At 500 hPa level, wind speed is about 20 m/s with except little deviation. At 200 hPa level, wind speed is in between 40 to 50 m/s with anti-cyclonic circulation (Figure 4.2.3.3a).

Using WRF model, the spatial distribution of relative humidity with wind at 850, 500 and 200 hPa levels from 00 UTC of 09 June to 21 UTC of 11 June 2007 are presented in Figures 4.2.3.1(c-d), 4.2.3.2b and 4.2.3.3b respectively. The WRF Model simulated high amount of moisture of the order of 90-100% over most of the region of Bangladesh at 850 to 500 hPa levels with cyclonic circulation of wind up to these levels for the whole simulation period. But the contents of moisture are less at 200 hPa level with anti-cyclonic circulation of wind. The wind speed obtained from WRF model are equal to or less than that obtained from MM5 model at all level.

It is to be noted that all the Figures 4.2.3.1(c-d), 4.2.3.2(a-b) and 4.2.3.3(a-b)) show the amount of relative humidity with wind at 850, 500 and 200 hPa levels respectively. Figures make it that amount of humidity prevail because of combined effect of westerly and SW'ly winds carrying moisture from Arabian Sea and Bay of Bengal respectively.

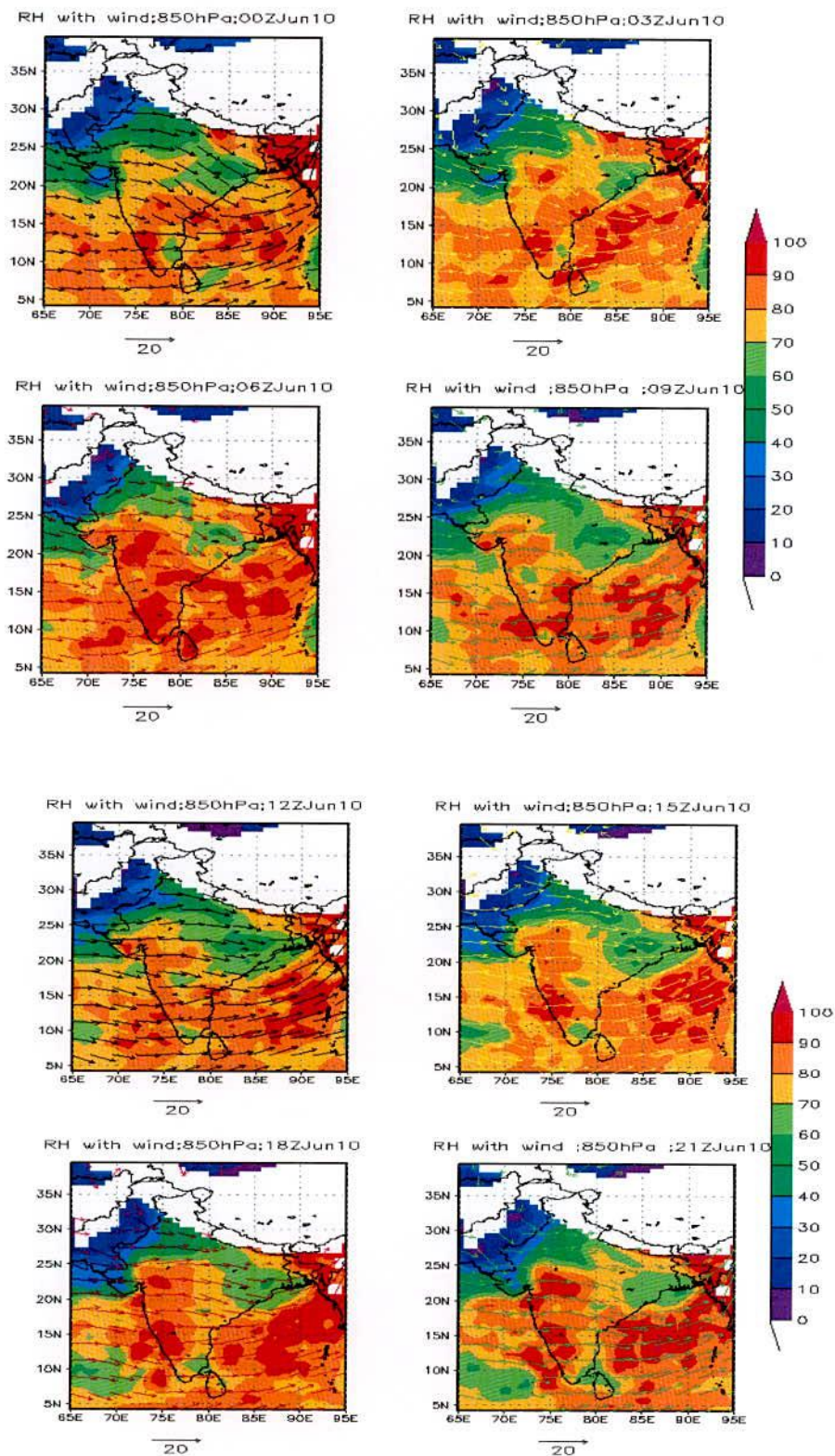


Figure 4.2.3.1a: MM5 Model simulated relative humidity (%) with wind at 850 hPa level valid for 00 to 21 UTC of 10 June 2007

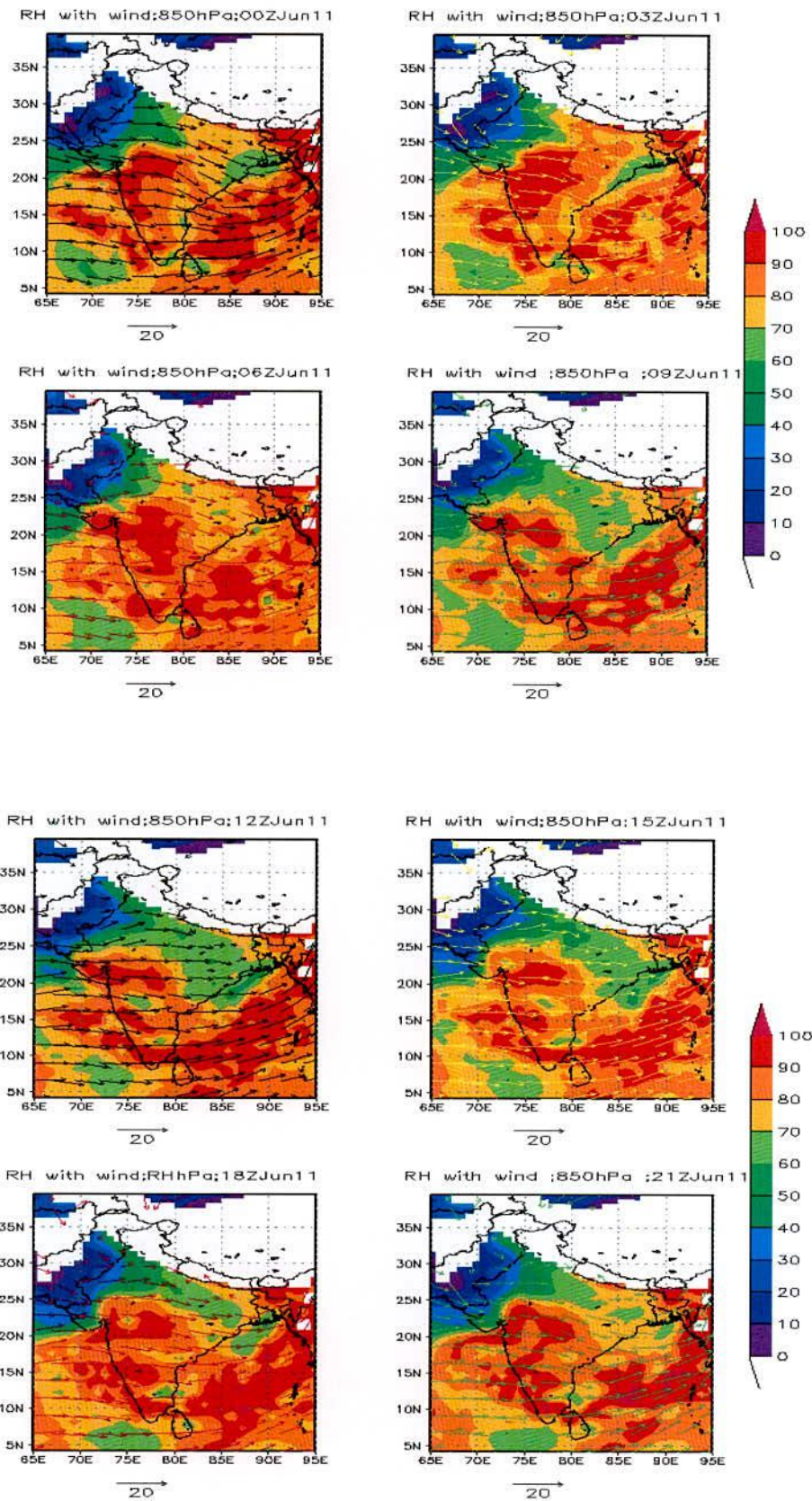


Figure 4.2.2.1b: MM5 Model simulated rain with wind flow (m/s) analysis at 850 hPa valid for time 00 UTC to 21 UTC of 11 June 2007

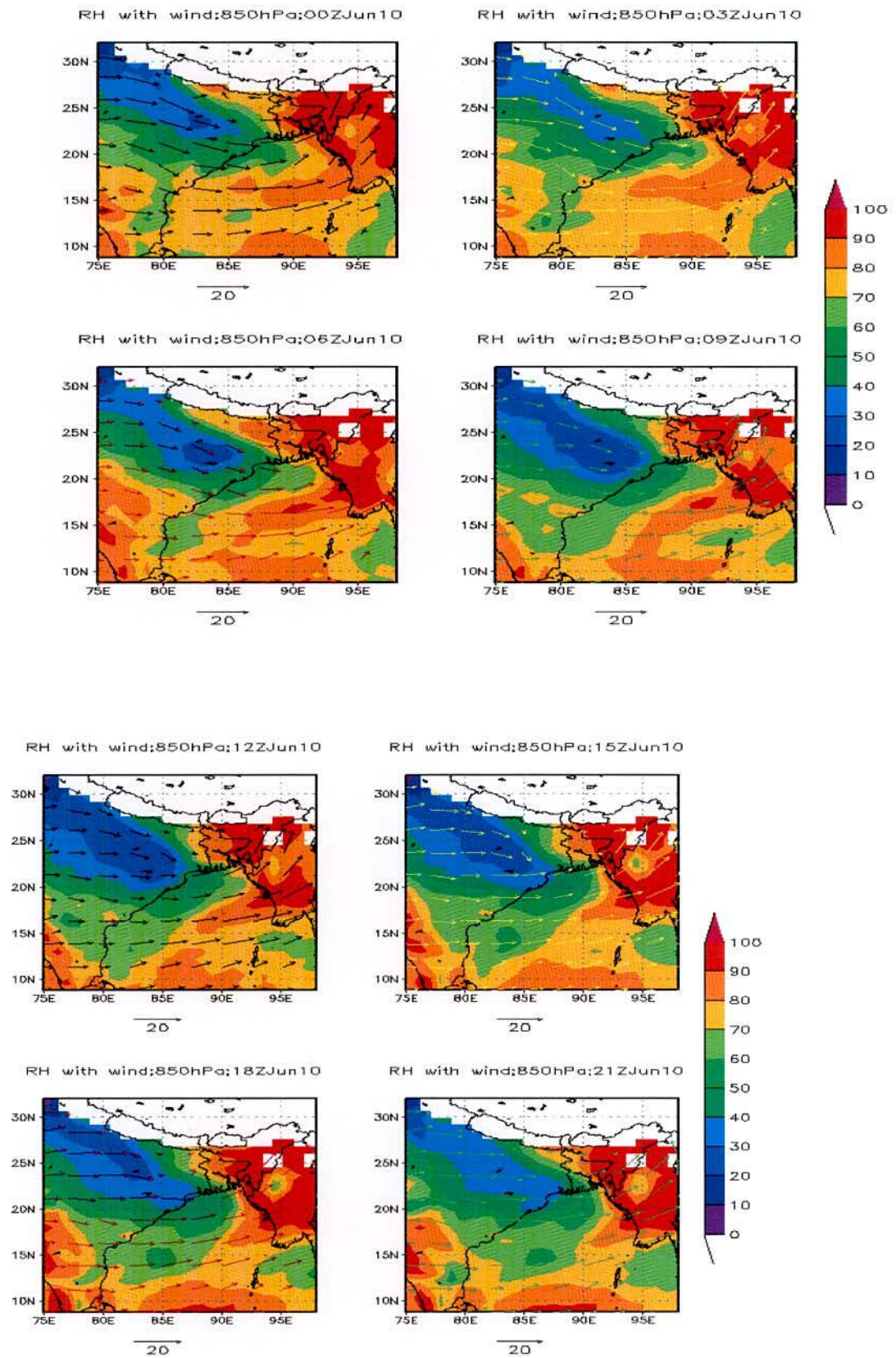


Figure 4.2.3.1c: WRF Model simulated relative humidity (%) with wind at 850 hPa level valid for 00 to 21 UTC of 10 June 2007

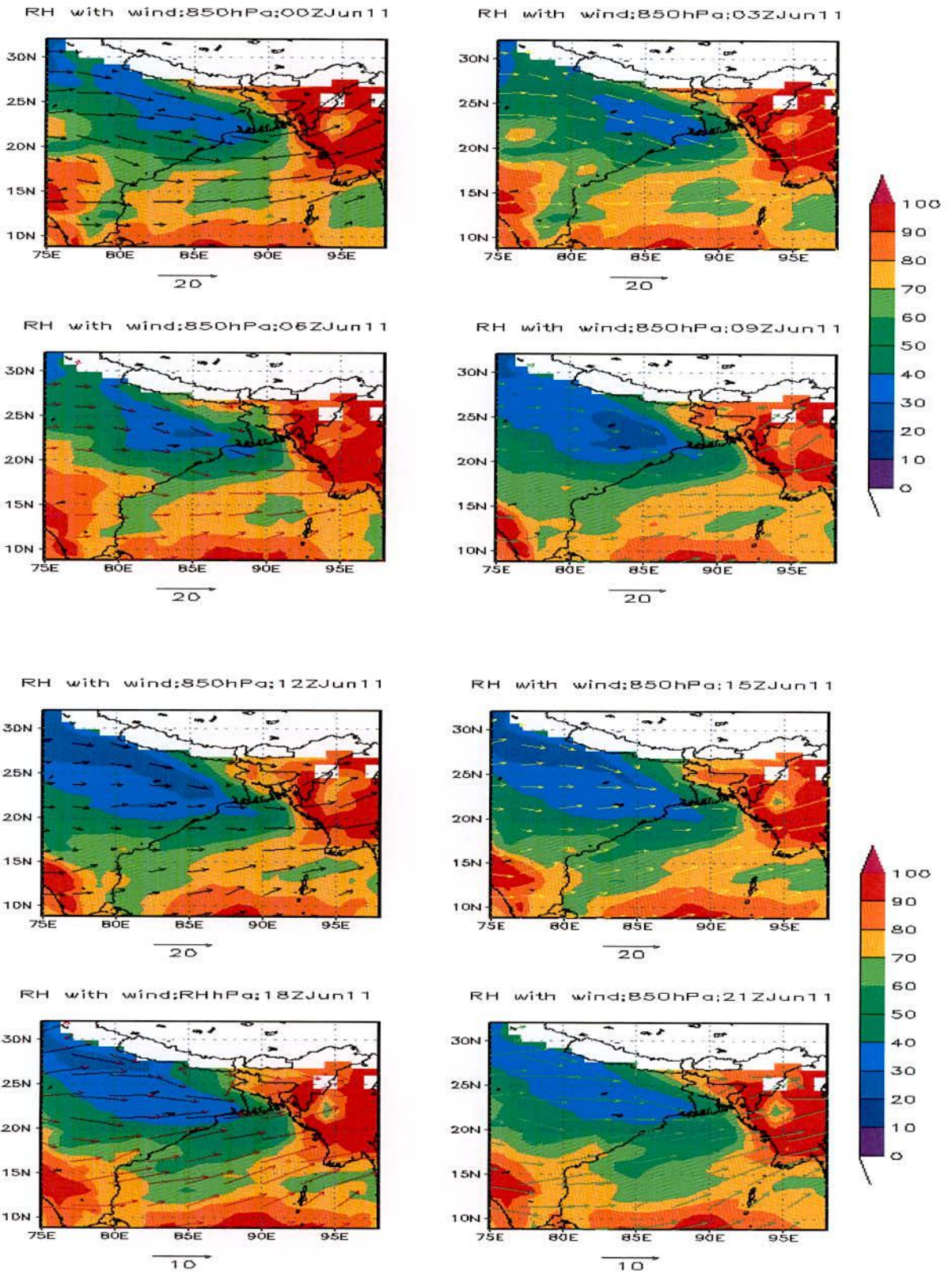


Figure 4.2.3.1d: WRF Model simulated relative humidity (%) with wind at 850 hPa level valid for 00 to 21 UTC of 11 June 2007

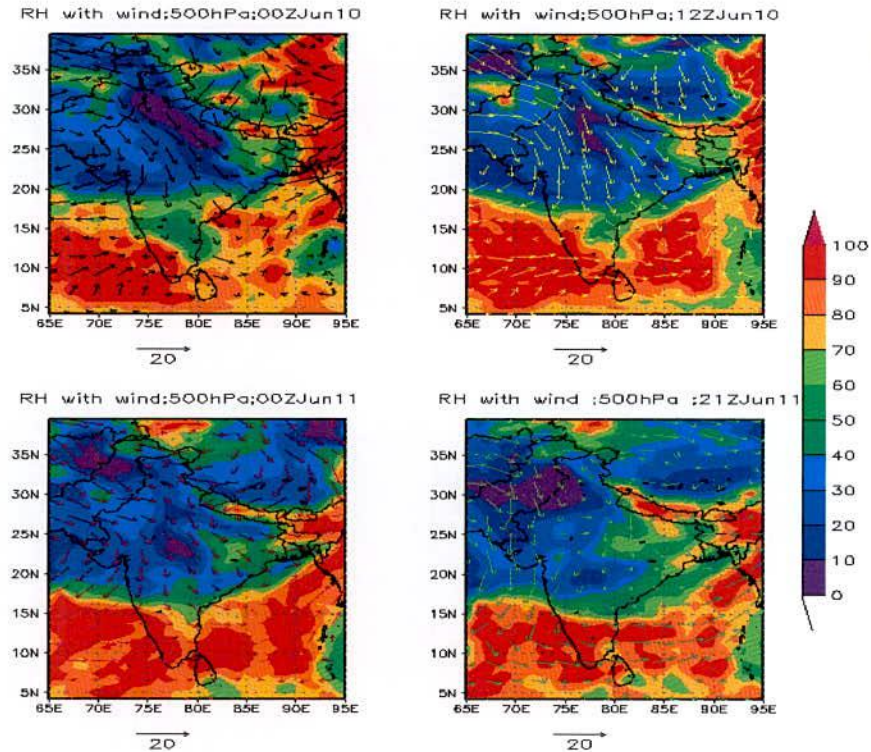


Figure 4.2.3.2a: MM5 Model simulated relative humidity (%) with wind at 500 hPa level valid for 00 UTC of 10 June to 21 UTC of 11 June 2007

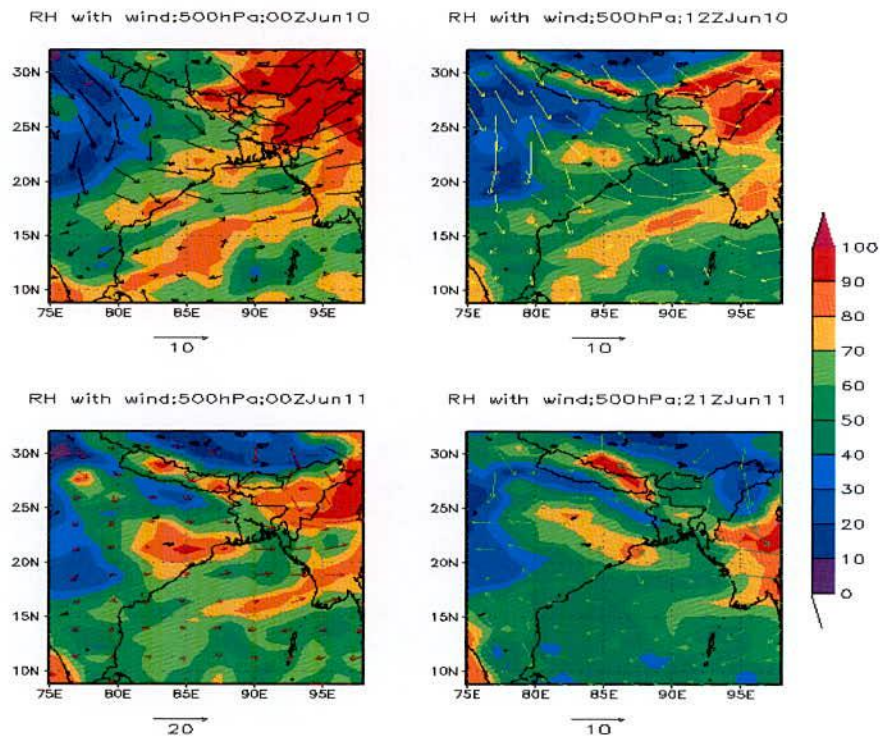


Figure 4.2.3.2b: WRF Model simulated relative humidity (%) with wind at 500 hPa level valid for 00 UTC of 10 June to 21 UTC of 11 June 2007

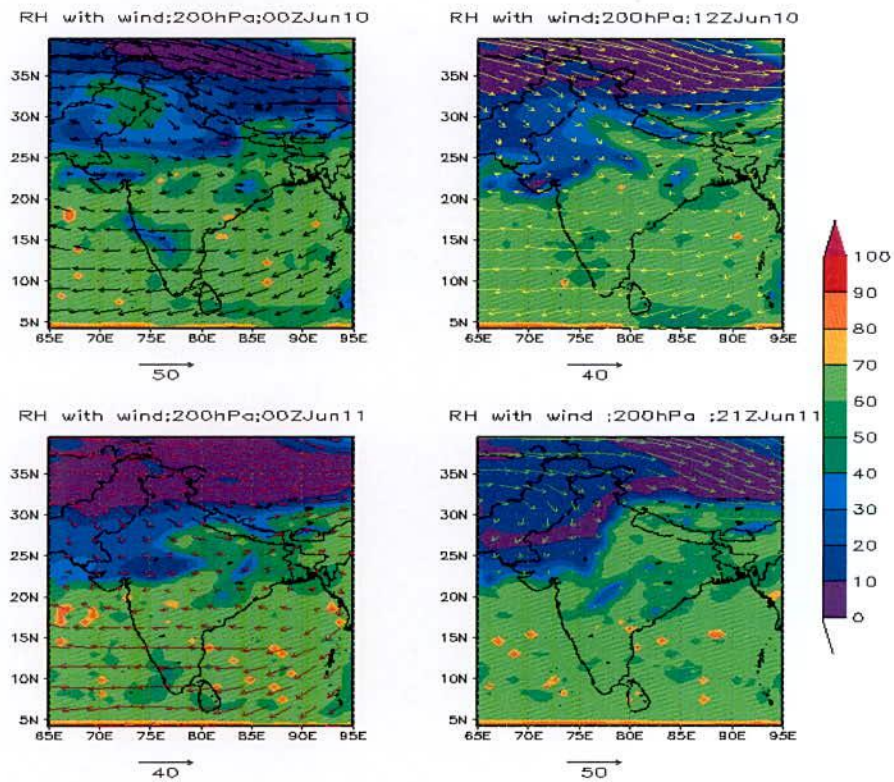


Figure 4.2.3.3a: MM5 Model simulated relative humidity (%) with wind at 200 hPa level valid for 00 UTC of 10 June 21 UTC of 11 June 2007

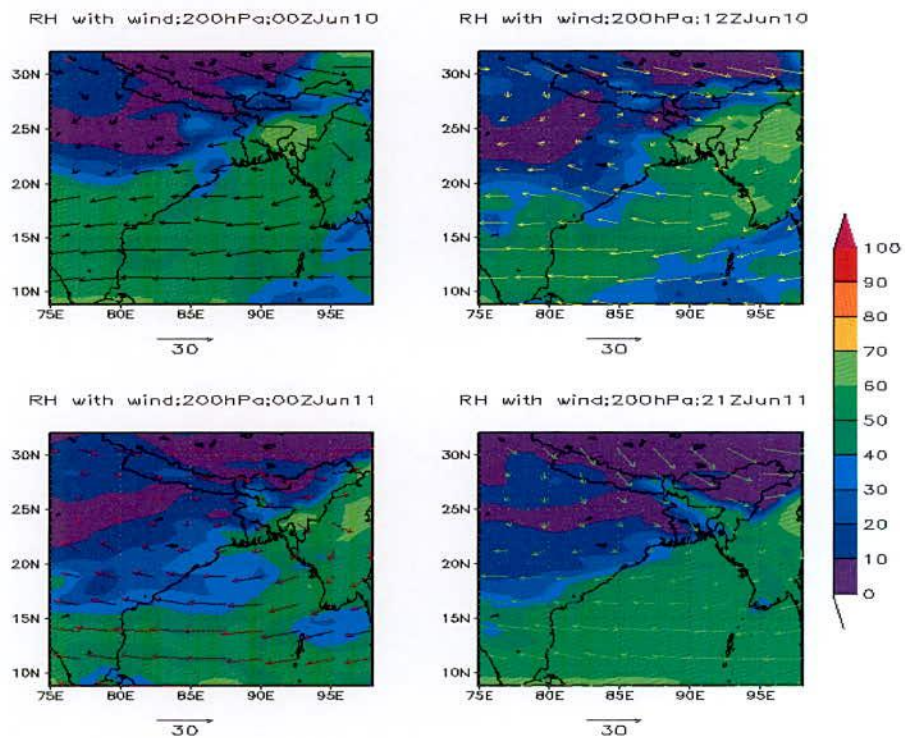


Figure 4.2.3.3b: WRF Model simulated relative humidity (%) with wind at 200 hPa level valid for 00 UTC of 10 June 21 UTC of 11 June 2007

4.2.4 Validation of Rain

24-h accumulated rainfalls obtained from the MM5 and WRF models valid for 09, 10 and 11 June 2007 are shown in Figures 4.2.4.1 – 4.2.4.3 respectively. Figures are plotted using model simulated 24-h accumulated rainfalls for Domain 1 (90 km resolution), Domain 2 (30 km resolution) and Domain 3 (10 km resolution). Figure 4.2.4.4 is plotted using rainfall obtained using TRMM and rain-gauge data. Rain-gauge data is obtained from Bangladesh Meteorological Department (BMD). Model simulated rainfall for both the models are seen at all places of Bangladesh with large spatial variability. For these simulations, Kain-Fritsch cumulus parameterization scheme with MRF PBL for MM5 model and Yonsei University Scheme (YSU) PBL for WRF model are used. It is found that the model simulated rainfall for all the domains of both the models are comparable to the rainfall obtained from TRMM observational data. It is noted that TRMM underestimates the summer monsoon rainfall [111] in this region. Again, Domain 1 shows the minimum rainfall than that of domain 2 and domain 3 and rainfall obtained from WRF model is more than that of MM5 model, but the Models simulated rainfalls are comparable to those obtained from BMD rain-gauge with large spatial variability.

On 09 June 2007, rainfall obtained from both MM5 and WRF models for Domain 3 is comparable to rainfalls obtained from TRMM and rain-gauge data. WRF model produces more rainfall than that of MM5 model. Rainfall obtained from MM5 model is less than the rainfall obtained from rain-gauge but close to that obtained from TRMM and rain-gauge data. Again rainfall obtained from WRF model is higher than that obtained from TRMM and rain-gauge data.

On 10 June 2007, rainfall obtained from both MM5 and WRF models for Domain 3 is comparable to rainfalls obtained from TRMM and rain-gauge data. WRF model produces more rainfall than that of MM5 model. Rainfall obtained from MM5 model is more than the rainfall obtained from rain-gauge but less than that obtained from TRMM. Again rainfall obtained from WRF model is higher than that obtained from rain-gauge data but less than that obtained from TRMM.

On 11 June 2007, rainfall obtained from both MM5 and WRF models for Domain 3 is comparable to rainfalls obtained from TRMM and rain-gauge data. WRF model produces more rainfall than that of MM5 model. Rainfall obtained from MM5 model is less than the rainfall obtained from rain-gauge and TRMM and rain-gauge data. Again rainfall obtained from WRF model is less than that obtained from TRMM and rain-gauge data.

From the above discussion, it is clear that rainfall obtained from WRF model is more than that obtained from MM5 model for high resolution domain i.e. Domain 3 without any

exception and the Models simulated rainfalls are comparable to those obtained from BMD rain-gauge with large spatial variability. However, both the models captured well the heavy rainfall event with spatio-temporal variation. It also captured the structure of the convective phenomena of the studied case. Thus simulated rainfall seems to be realistic using both the models.

The horizontal distribution of the cloud structures are shown in Figure 4.2.4.5 and 4.2.4.6 using model MM5 and WRF respectively at stage of high convection i.e. at mature stage of cloud, where 3 hourly precipitation is higher than other moments. Figures show the variation of intensity of cloud with spatial distribution. From the figures, centers of convective activity are identified to understand the vertical structure.

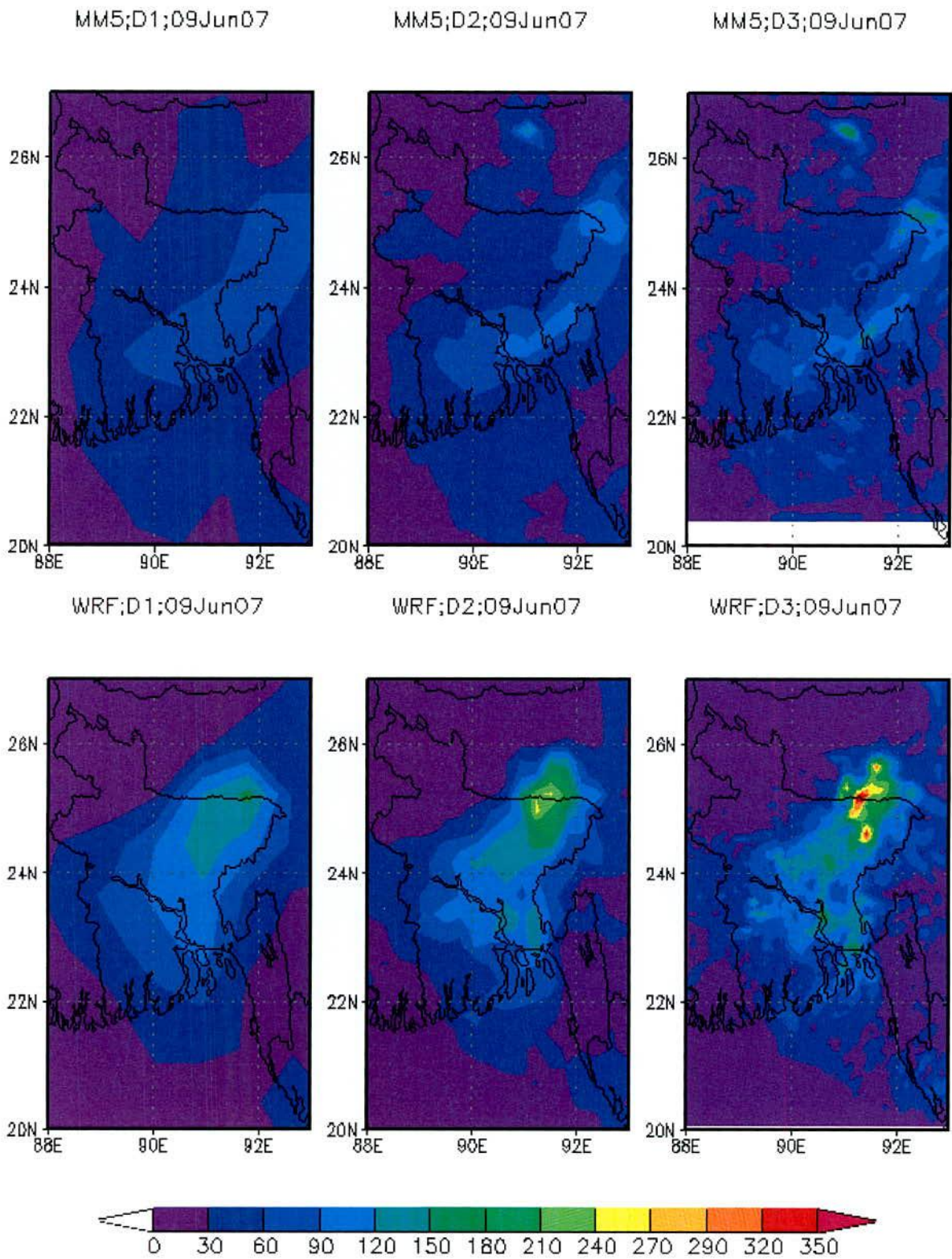


Figure 4.2.4.1: Spatial distribution of MM5 and WRF models simulated 24-h rainfall (mm) valid for 09 June 2007.

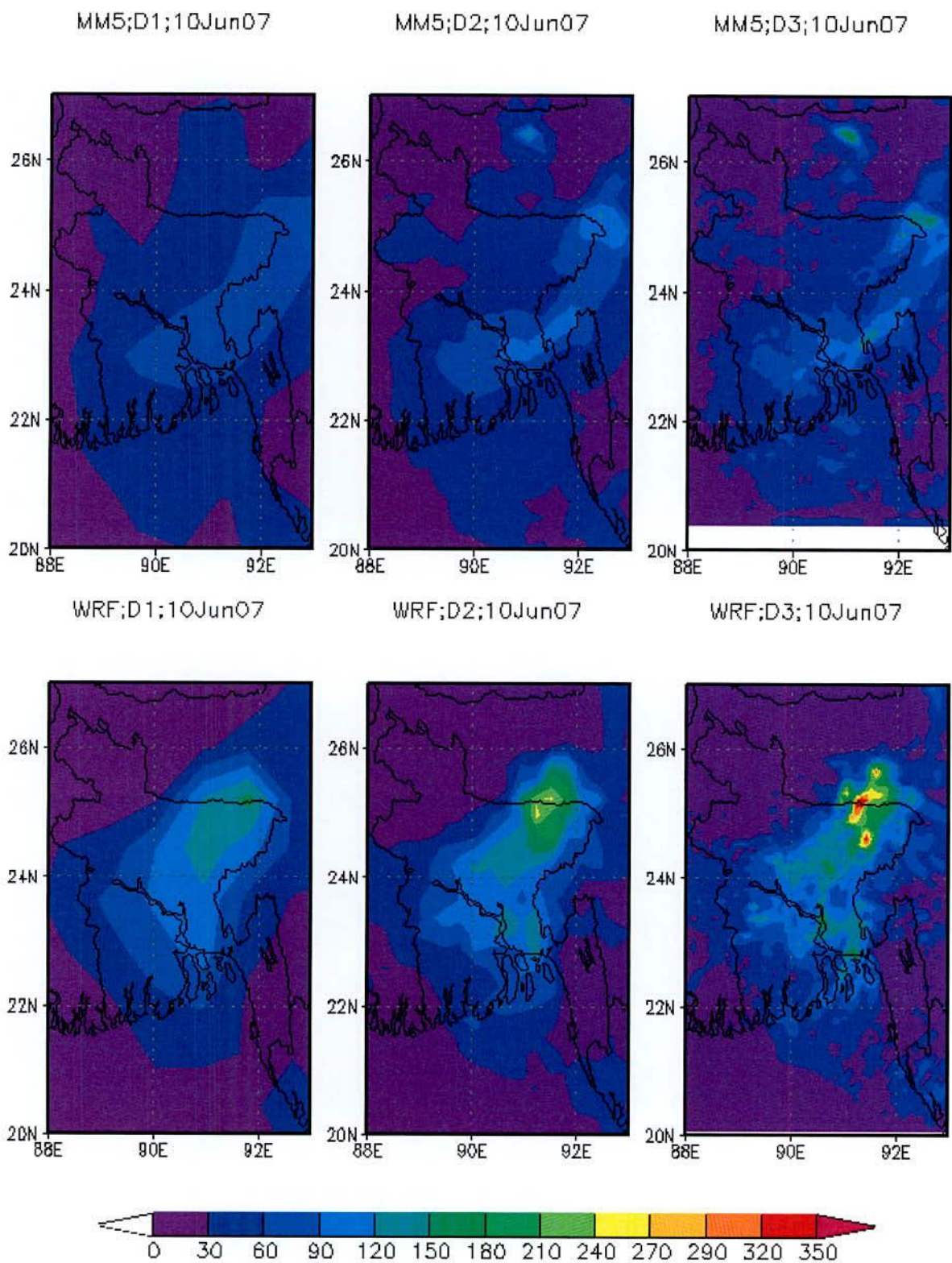


Figure 4.2.4.2: Spatial distribution of MM5 and WRF models simulated 24-h rainfall (mm) valid for 10 June 2007

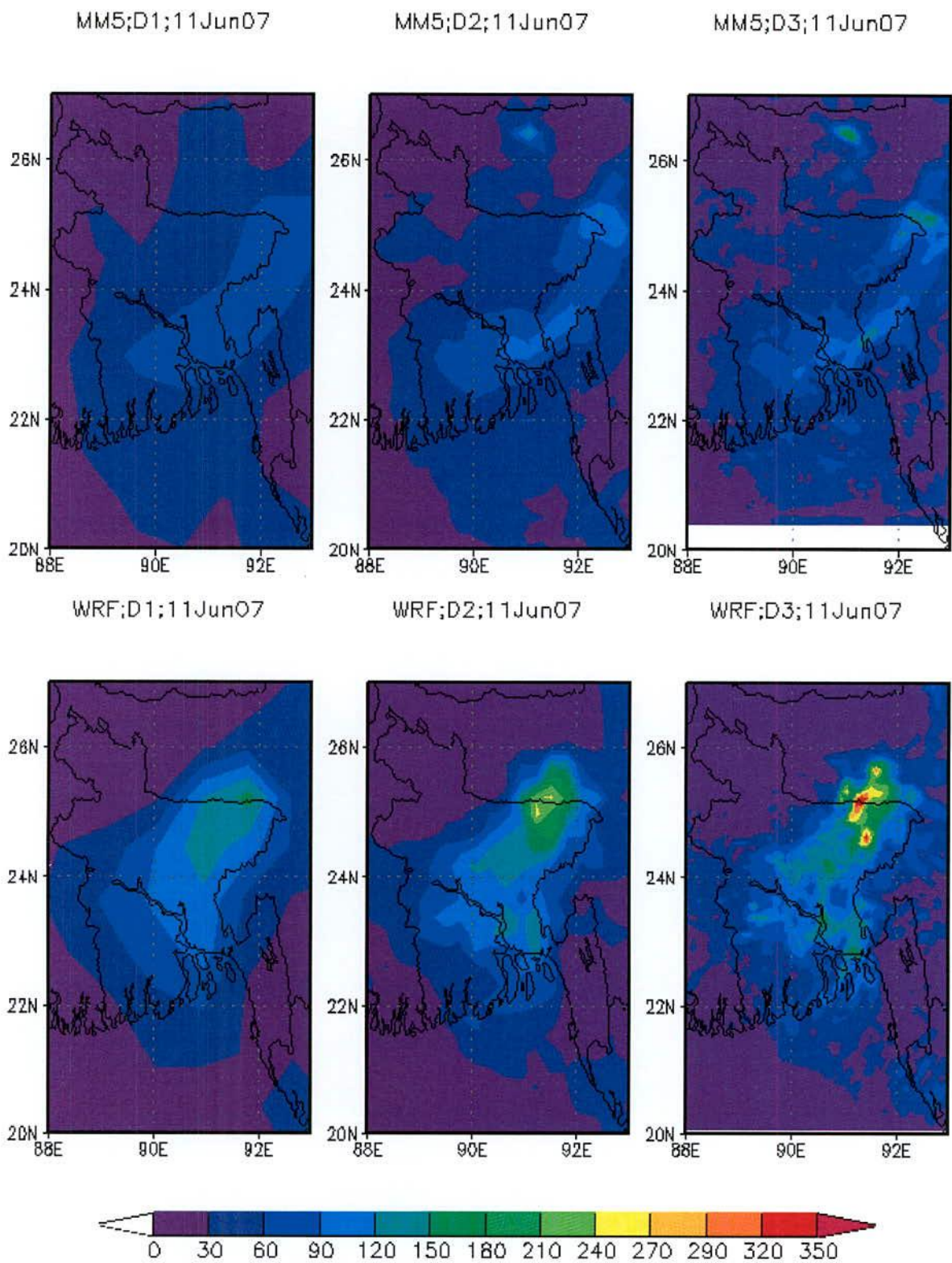


Figure 4.2.4.3: Spatial distribution of MM5 and WRF models simulated 24-h rainfall (mm) valid for 11 June 2007

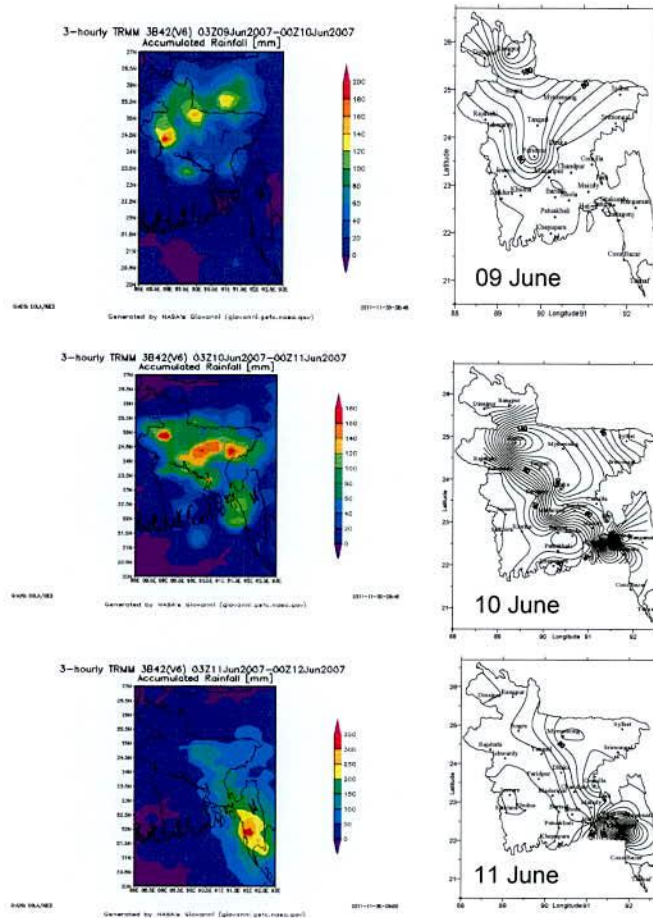


Figure 4.2.1.4.4: Spatial distribution of 24-h accumulated rainfall (mm) obtained from rain-gauge and TRMM 3B42V6 valid for 9, 10 and 11 June 2007.

To study the vertical profile of convective system, the vertical structure of vertical velocity, divergence, relative vorticity, relative humidity and mixing ratio are plotted through the centre of the most developed cloud at $(25.1^{\circ}\text{N}, 93.2^{\circ}\text{E})$, $(25.3^{\circ}\text{N}, 91.00^{\circ}\text{E})$, $(25.95^{\circ}\text{N}, 91.21^{\circ}\text{E})$ and $(21.00^{\circ}\text{N}, 93.35^{\circ}\text{E})$ at the time 03 and 21 UTC of 10 June, and 03 and 09 UTC of 11 June 2007 respectively for MM5 model and shown in figure in following section 4.2.5, 4.2.6, 4.2.7, 4.1.8 and 4.1.9. Similarly, the vertical structure of vertical velocity, divergence, relative vorticity, relative humidity and mixing ratio are plotted through the centre of the most developed cloud at $(24.35^{\circ}\text{N}, 91.52^{\circ}\text{E})$, $(24.25^{\circ}\text{N}, 92.00^{\circ}\text{E})$, $(24.45^{\circ}\text{N}, 92.60^{\circ}\text{E})$ and $(24.10^{\circ}\text{N}, 92.58^{\circ}\text{E})$ for the time of 03 and 06 UTC of 10 June and 00 and 06 UTC of 11 June 2007 respectively for WRF model are shown in figure in following section 4.2.5, 4.2.6, 4.2.7, 4.2.8 and 4.2.9.

4.2.5 Vertical Structure of Vertical Velocity

To understand the vertical structure of the convective system, the vertical profiles of vertical velocity obtained from MM5 and WRF models are plotted through the centre of the most

developed cloud at different time and are shown in Figure 4.2.5.1a and 4.2.5.1b. For MM5 model, figures are plotted at time at 03 and 21 UTC of 10 June, and 03 and 09 UTC of 11 June 2007. But for WRF model; figures are plotted at time for 03 and 06 UTC of 10 June, 00 and 06 UTC of 11 June 2007

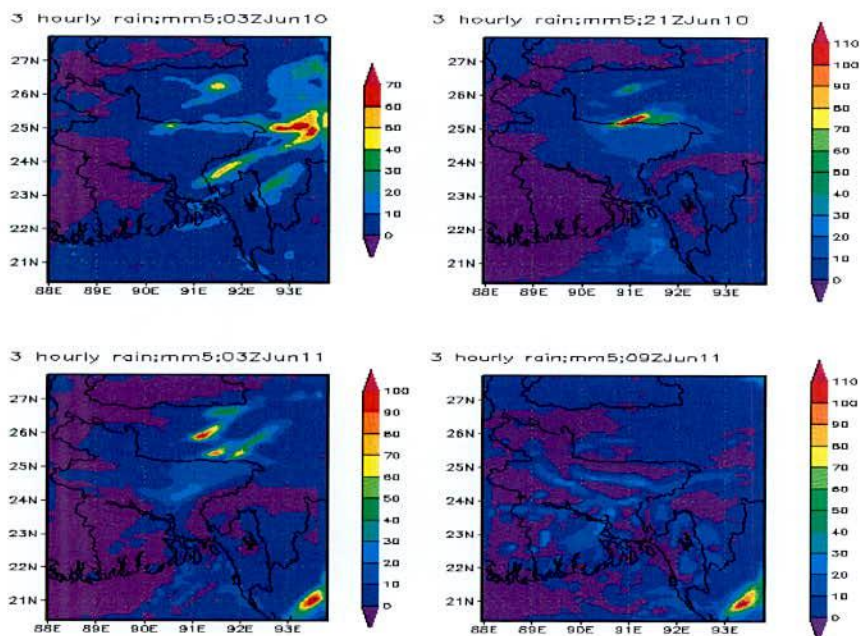


Figure 4.2.4.5: MM5 model simulated horizontal structure of most developed cloud at different time

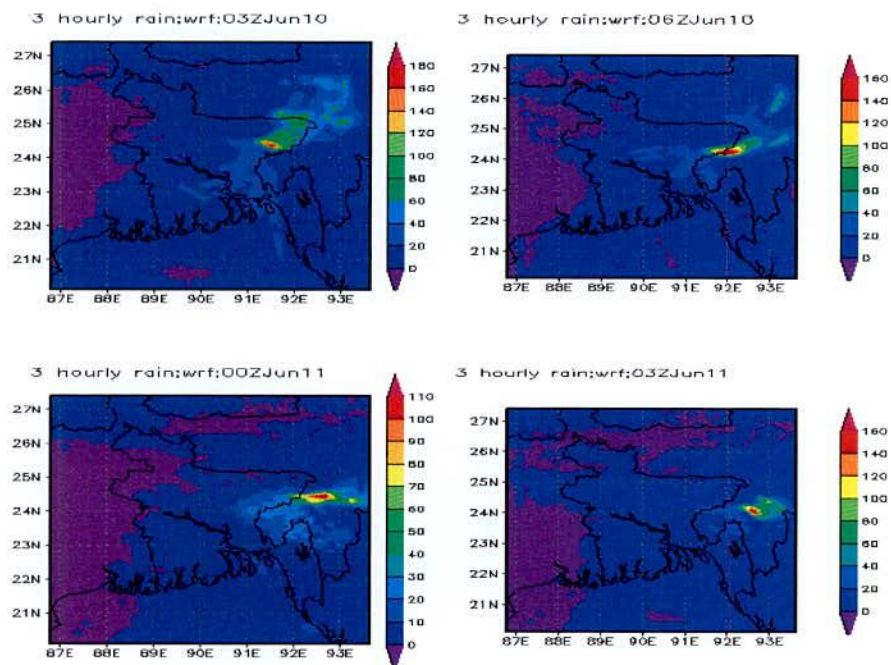


Figure 4.2.4.6: WRF model simulated horizontal structure of most developed cloud at different times.

The figures reveal that strong upward motion exists along the centre. The maximum upward vertical velocities for different times are different in magnitude. Their positions are also situated at different levels. Maximum values obtained for MM5 and WRF models are from 1.00 m/s to 4.50 m/s and from 4.00 to 10.00 m/s respectively. Negative value indicates the downward motion. In general, downward motion is not strong. It is also visible in the different levels with areas of small pockets, which could be due to subsidence associated with convection. Values of maximum values of downward motion obtained from MM5 and WRF models are from 20 to 60 cm/s and from 50 to 100 cm/s respectively. So, amount of the maximum values of upward and downward vertical velocity are more in case of MM5 than in case of WRF model

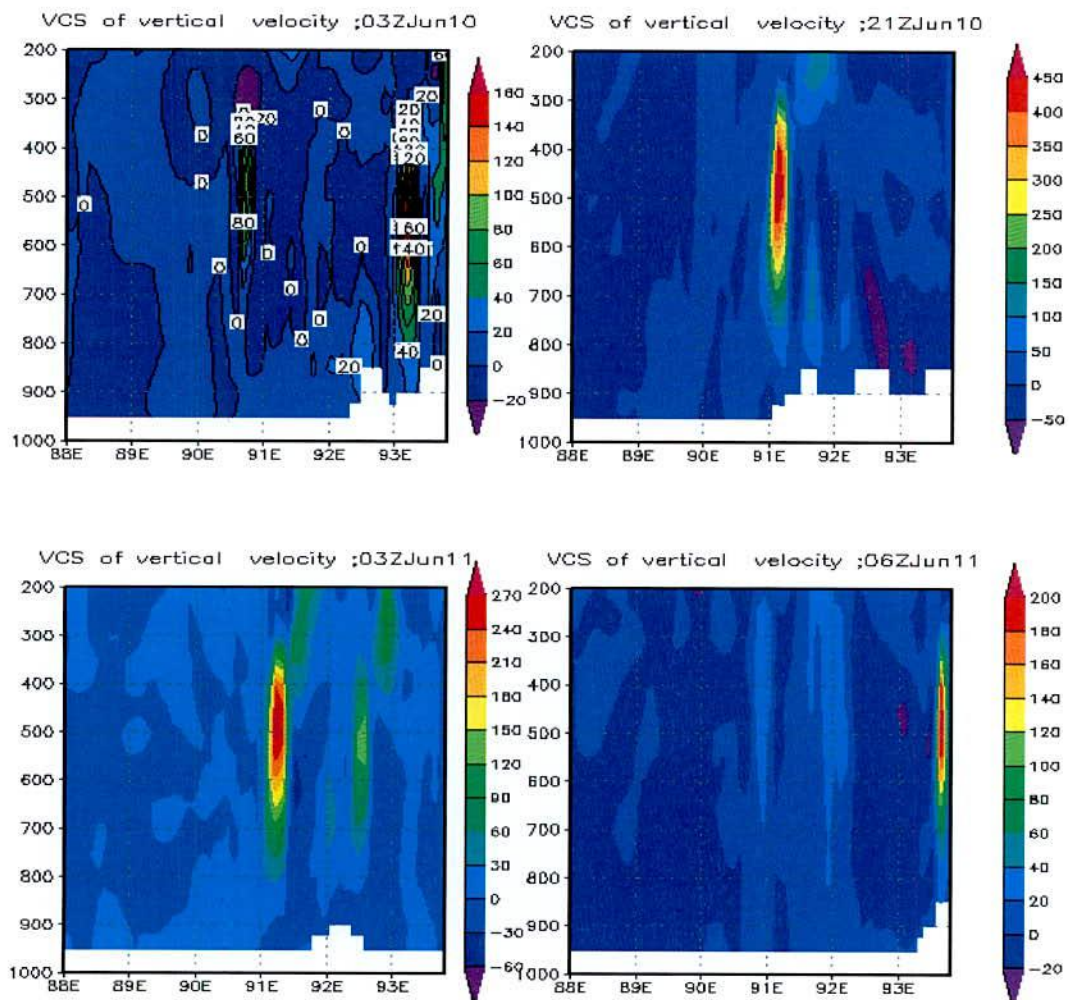


Figure 4.2.5.1a: MM5 Model simulated vertical structure of vertical velocity along the center of most developed cloud at different times.

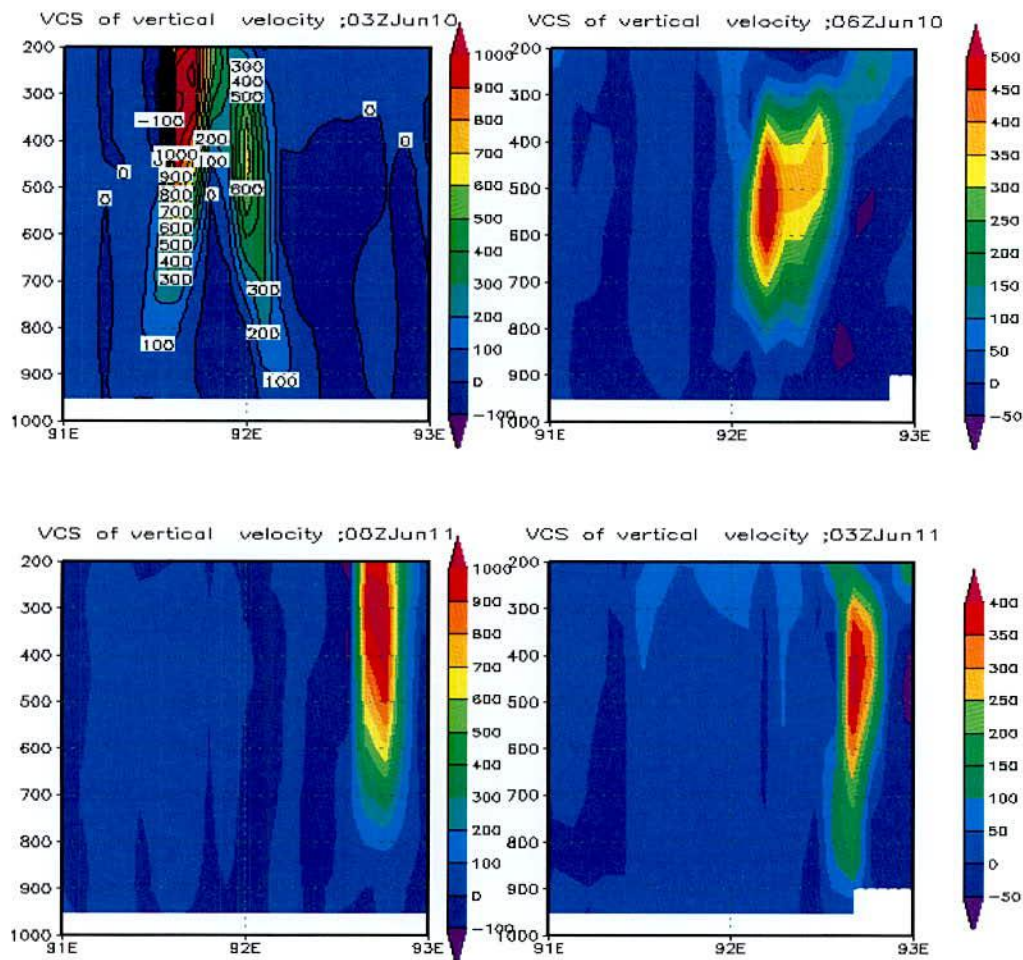


Figure 4.2.5.1b: MM5 Model simulated vertical structure of vertical velocity along the center of most developed cloud at different time.

4.2.6 Vertical Structure of Divergence

Divergence is one of the most important parameters to analysis of the convective system. In general, there are low level convergence and upper level divergence in the convective system. To understand the vertical structure of the convective system, the vertical structure of divergence obtained from MM5 and WRF models are plotted through the centre of the most developed cloud at different time and are shown in Figure 4.2.5.1a and 4.2.5.1b. For MM5 model, figures are plotted at 03 and 21 UTC of 10 June, and 03 and 09 UTC of 11 June 2007. But for WRF model; figures are plotted at 03 and 06 UTC of 10 June, 00 and 06 UTC of 11 June 2007

In the figure, positive and negative values indicate the divergence and convergence respectively. So, well defined convergence areas are available with divergence area at different levels. Low levels convergences are available at four different times with upper levels divergence. It is seen that divergence area is embedded with convergence area. The

maximum values of divergences and convergences are $(40 \text{ to } 100) \times 10^{-5} \text{ s}^{-1}$ and $(30 \text{ to } 50) \times 10^{-5} \text{ s}^{-1}$ respectively for MM5 model. Again, the maximum values of divergences and convergences are $(60 \text{ to } 150) \times 10^{-5} \text{ s}^{-1}$ and $(50 \text{ to } 150) \times 10^{-5} \text{ s}^{-1}$ respectively for WRF model. It is seen from the figures that values of divergence and convergence obtained from WRF model are more than those obtained from MM5 model. It indicates that amount of precipitation obtained from WRF model will be more than that obtained from MM5 model. Again, convergence is more active in the both sides of the centre of the most developed cloud. This state of situation in convection is significant from the point of view of severe convective activity.

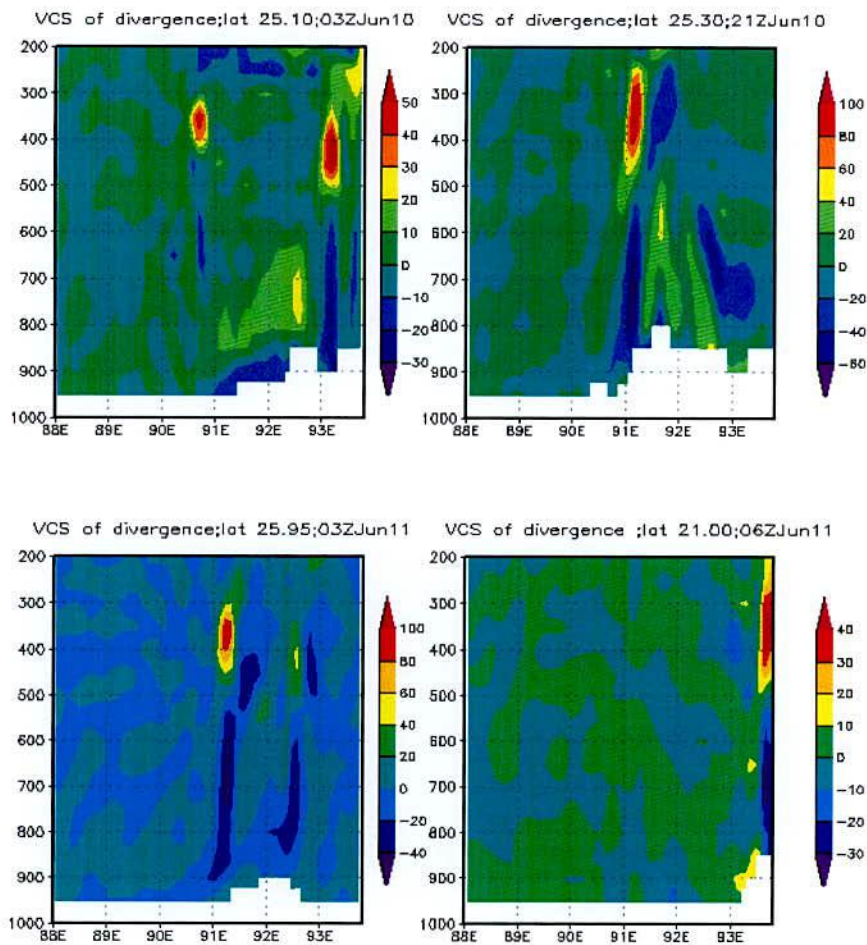


Figure 4.2.6.1a: MM5 Model simulated vertical structure of divergence (unit: $\times 10^{-5} \text{ s}^{-1}$) along the center at different times.

4.2.7 Vertical Structure Relative Vorticity

To understand the vertical structure of the convective system, the vertical structure of relative vorticity obtained from MM5 and WRF models are plotted through the centre of the most developed cloud at different time and are shown in Figure 4.2.5.1a and 4.2.5.1b. For

MM5 model, figures are plotted at 03 and 21 UTC of 10 June, and 03 and 09 UTC of 11 June 2007. But for WRF model; figures are plotted at 03 and 06 UTC of 10 June, 00 and 06 UTC of 11 June 2007

Relative vorticity is absent in the lower levels at all observed time because of hilly surface area with low pressure and high altitude. It is seen in the figure, strong positive vorticity are observed up to 200 hPa level with decreasing in magnitude for both models. There are some variations of the magnitude of maximum positive vorticity at different level at different time. These values are $(100\sim450) \times 10^{-5}\text{s}^{-1}$ and $(60 \sim 130) \times 10^{-5}\text{s}^{-1}$ for MM5 and WRF models respectively. It is noted that positive vorticity indicates the cyclonic motion in the lower level. Negative vorticity are also observed in the upper levels with different values at different times and positions. These values are $(20\sim60) \times 10^{-5}\text{s}^{-1}$ and $(40 \sim 140) \times 10^{-5}\text{s}^{-1}$ for MM5 and WRF models respectively. So, low level positive vorticity obtained from both the models indicates the convective activity of the system and it is due to westerly and south-westerly wind.

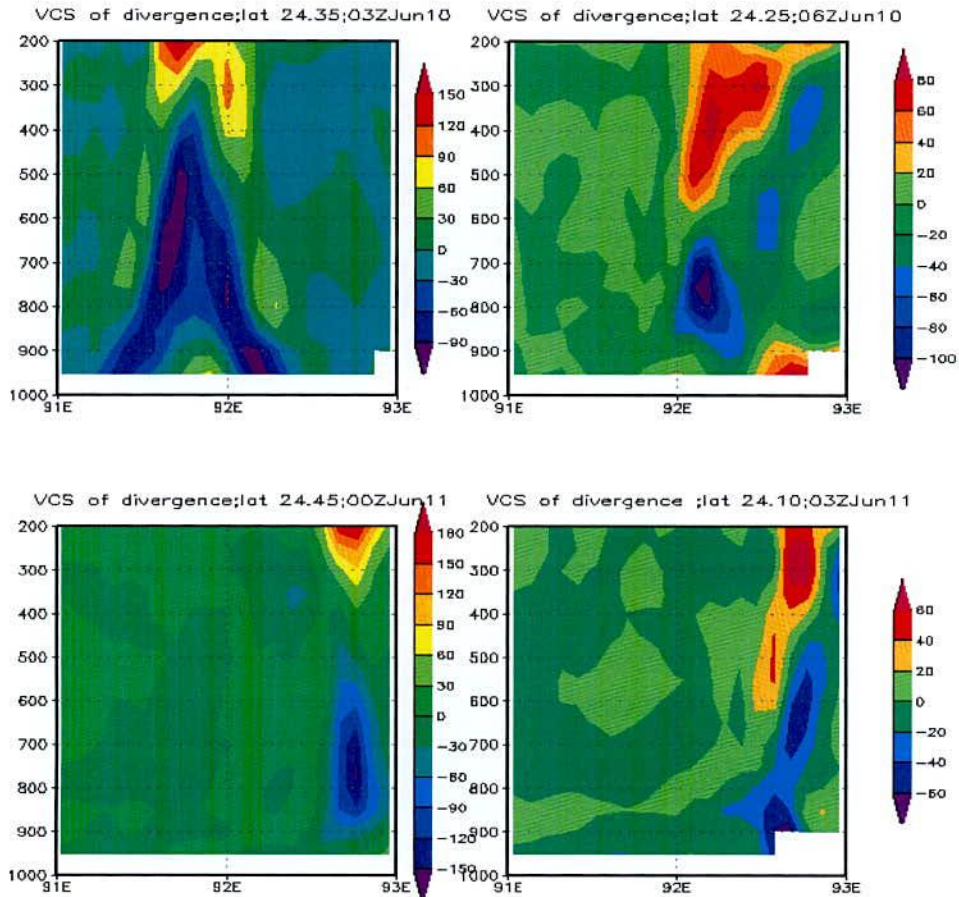


Figure 4.2.6.1b: WRF Model simulated vertical structure of divergence (unit: $\times 10^{-5}\text{s}^{-1}$) along the center at different time

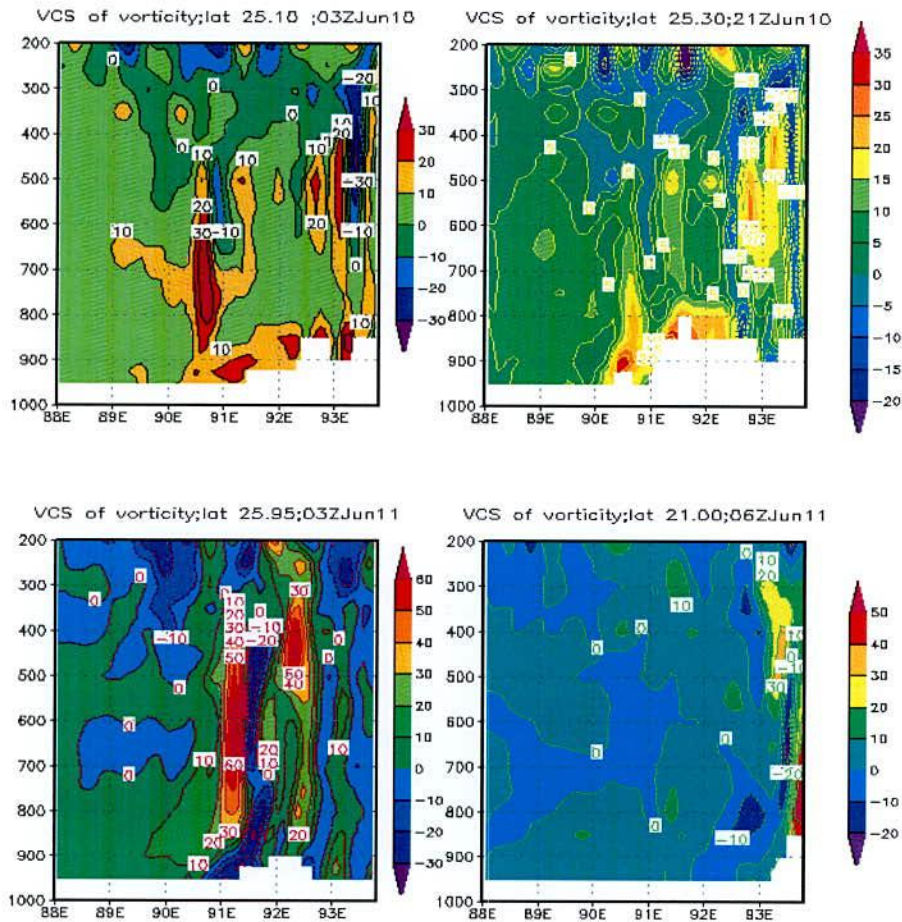


Figure 4.2.7.1a: MM5 Model simulated vertical structure of relative vorticity ($\times 10^{-5} \text{ s}^{-1}$) along the center at different times.

4.2.8 Vertical Structure of Relative Humidity

To understand the vertical structure of the convective system, the vertical structure profiles of relative humidity obtained from MM5 and WRF models are plotted through the centre of the most developed cloud at different time and are shown in Figure 4.2.5.1a and 4.2.5.1b. For MM5 model, figures are plotted at 03 and 21 UTC of 10 June, and 03 and 09 UTC of 11 June 2007. But for WRF model; figures are plotted at 03 and 06 UTC of 10 June, 00 and 06 UTC of 11 June 2007.

For both the models, relative humidity is absent in the lower levels at all observed times because of hilly surface area at high altitude with low pressure. Relative humidity (more than 90%) spreads in outer range of eye wall up to 300 hPa level. High relative humidity is also seen up to 200 hPa level. Due to the presence of hill at the right side of the center of convective state, amount of relative humidity increases at the right side of the centre. Because the westerly and SW'ly winds carry moisture from the Arabian Sea and the Bay of Bengal

respectively and convergence occurs at the foot of the hills. These high magnitudes of vertical structure of humidity satisfy the development of the convective activity of the system.

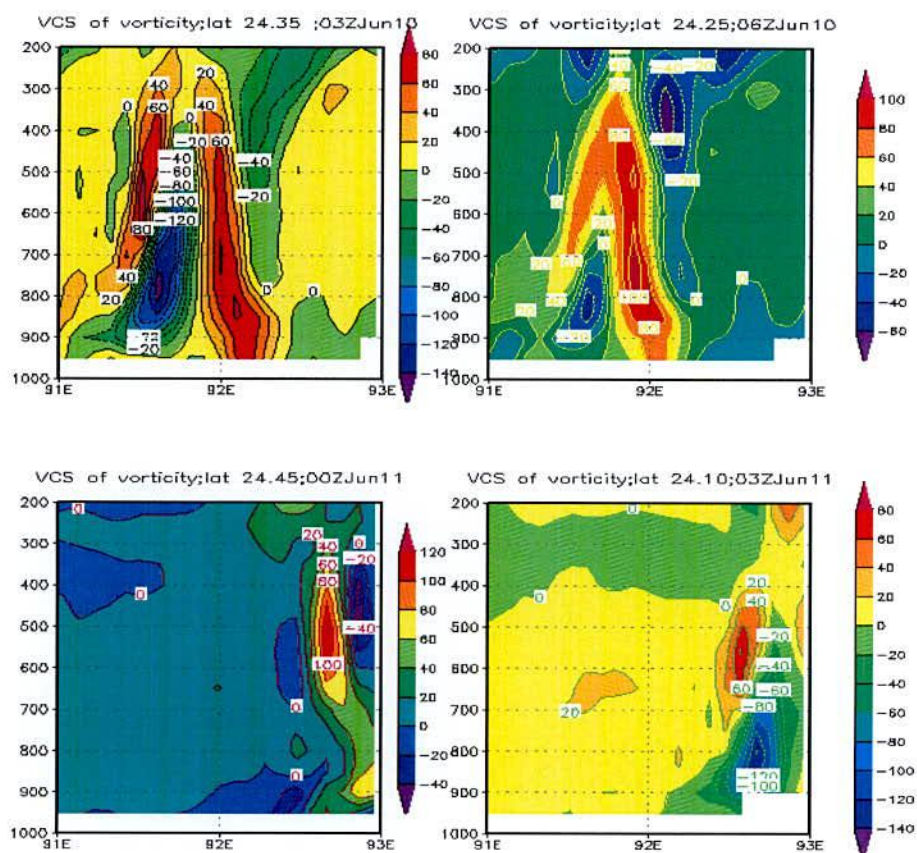


Figure 4.2.7.1b: WRF Model simulated vertical structure of relative vorticity ($\times 10^{-5} \text{ s}^{-1}$) along the center at different times.

4.2.9 Vertical Structure of Mixing Ratio

To understand the vertical structure of the convective system, the vertical profiles of vertical velocity obtained from MM5 and WRF models are plotted through the centre of the most developed cloud at different time and are shown in Figure 4.2.5.1a and 4.2.5.1b. For MM5 model, figures are plotted at 03 and 21 UTC of 10 June, and 03 and 09 UTC of 11 June 2007. But for WRF model; figures are plotted at 03 and 06 UTC of 10 June, 00 and 06 UTC of 11 June 2007

Mixing ratio is absent in the lower levels at all observed time because of hilly surface area at high altitude with low pressure. It shows that the highest moisture content around $1.8 \times 10^2 \text{ kg/kg}$ or more for MM5 and 2.0 g/kg or more for WRF model are found at the centre of the convective system at or above 950 hPa level than it decreases upwards to 300 hPa level or

more. It is to be noted that the high moisture flux comes from the southern side covering a large area of the Bay of Bengal which feeds the system along its southeastern side through the boundary layer. A noticeable amount of moisture flux also comes from the south-western side through the Indian sub-continent which feeds the system along its south-western side through the boundary layer.

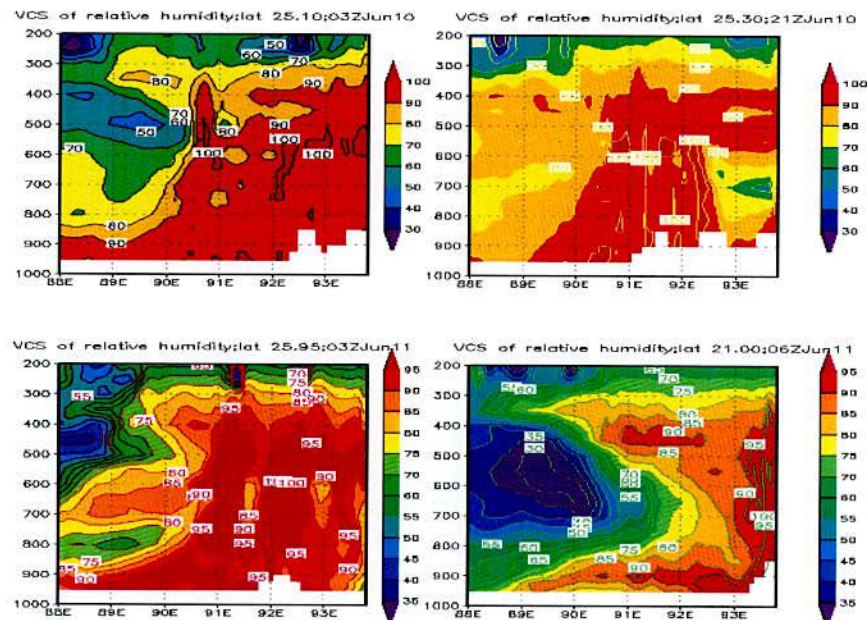


Figure 4.2.8.1a: MM5 Model simulated vertical structure of relative humidity (%) along the center of most developed cloud at different times.

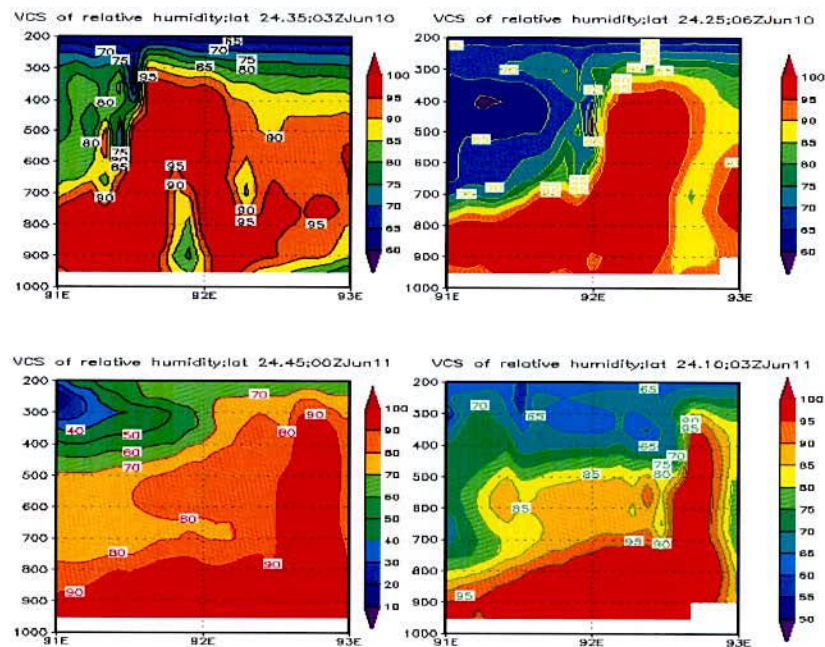


Figure 4.2.8.1b: WRF Model simulated vertical structure of relative humidity (%) along the center of most developed cloud at different times.

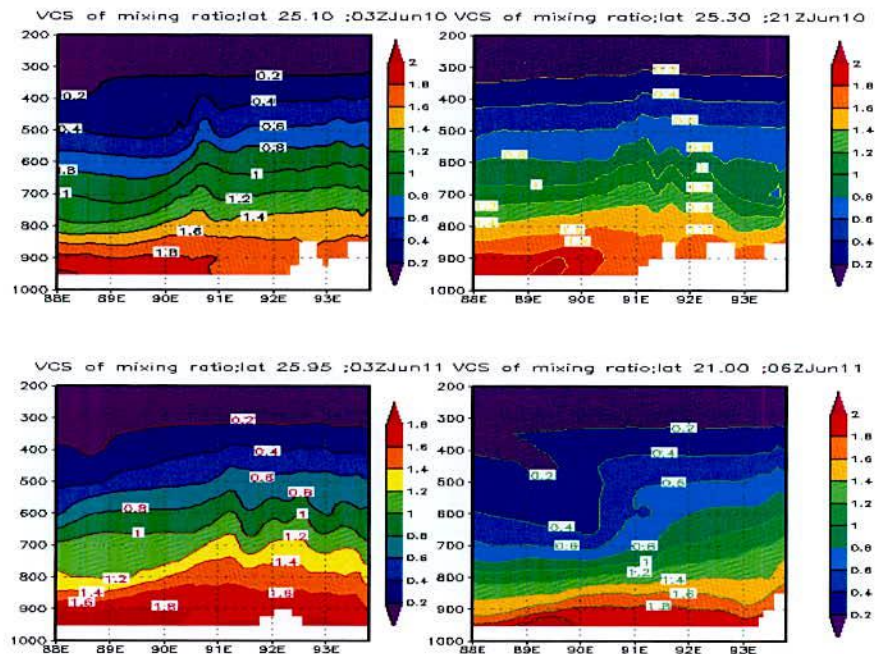


Figure 4.2.9.1a: MM5 Model simulated vertical structure of mixing ratio (kg^{-2}) along the center of most developed cloud at different times.

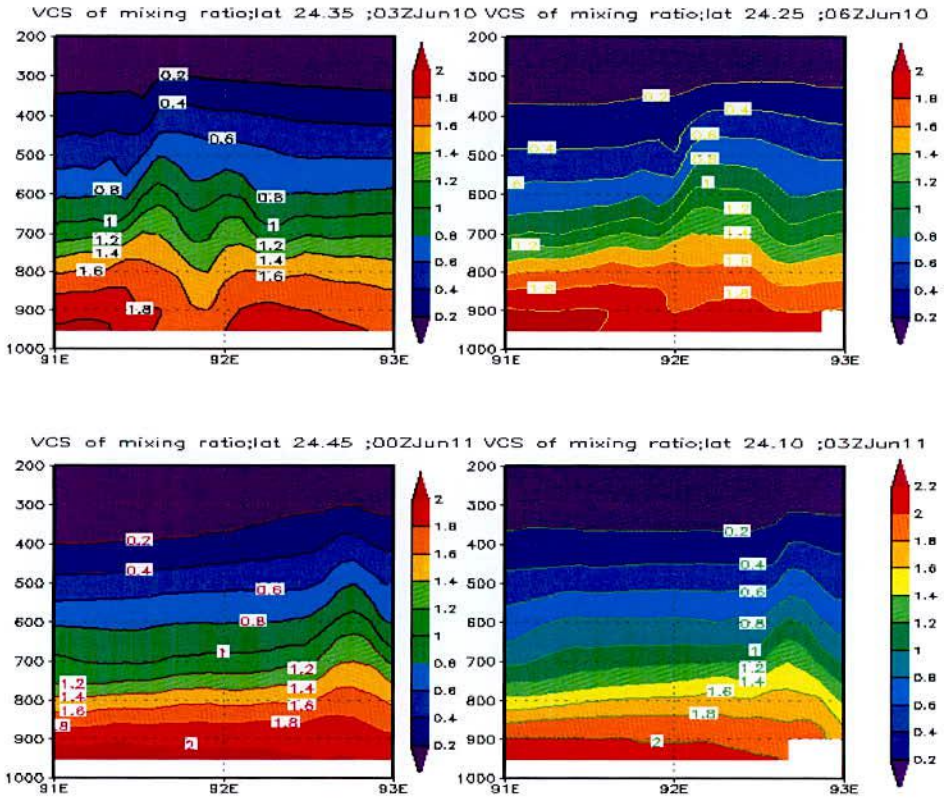


Figure 4.2.9.1b: WRF Model simulated vertical structure of mixing ratio (kg^{-2}) along the center of most developed cloud at different time

4.3 Simulation of Heavy Rainfall Event of 1-3 May 2009 using WRF and MM5

To analyze the convective system of 01-03 May, 2009 with their vertical structure, MM5 model was run for 72 hours based on the initial condition at 00 UTC of 01 May. All parameters were made for 00 UTC of 02 May 2009 for the analysis of the synoptic conditions responsible for producing rain. The first 24 hours was considered as spin up period. The model performance was evaluated by examining the different simulated meteorological parameters i.e. mean sea level pressure, rain with vector wind, relative humidity with vector wind, and vertical structure of vertical velocity, divergence, relative vorticity, relative humidity and mixing ratio at the centre of the most developed cloud. The model derived rainfall for all three domains were compared with that obtained from TRMM and Bangladesh Meteorological Department (BMD) rain-gauge observation data. Surface simulated precipitation was considered as rainfall throughout the study.

4.3.1 Mean Sea Level Pressure (MSLP)

Model simulated MSLPs (hPa) obtained from both the MM5 and WRF models for domain D1, valid for the initial time 00 UTC of 01 May to 00 UTC of 04 May 2009, are presented in Fig. 4.3.1.1a and Fig. 4.3.1.1b respectively. Figures show that the northerly positioned monsoon trough lies parallel to the foot hills of Himalayan Mountains with minimum pressure 1002 hPa at the center of the system simulated by both the MM5 and WRF models. The MSLP over Tibet is very high and central pressures are above 1032 and 1029 hPa at 00 UTC of 01 May 2009 simulated by MM5 and WRF models respectively. At this moment, pressure obtained over Bangladesh is from 1008 to 1011 hPa for MM5 model and from 1005 to 1011 hPa for WRF model. According to result obtained from MM5 model, the center of the depression changes and extended along west-east. One of the centers of the depression is located near the southwest side of Bangladesh with central pressure of 1006 hPa at 00 UTC of 02 May 2009 making pressure 1008 hPa over whole regions of Bangladesh. Because of this depression, pressure of 1008 to 1010 hPa prevails over most of Bangladesh for the whole simulation time up to 00 UTC of 04 May 2009, whereas high pressure of 1022 hPa or more is persisted over Himalayan Mountain and Tibetan plateau. Again, according to result obtained from WRF model, the center of the depression changes and extended along east-west. Low pressure system extended and depression is located near the south-west side of Bangladesh with central pressure of 1005 hPa at 00 UTC of 02 May 2009 making pressure 1008 to 1011 hPa over whole regions of Bangladesh. Because of this depression, pressure 1008 to 1010 hPa prevails over most of the parts of Bangladesh for the whole simulation time up to 00 UTC of 04 May 2009 whereas high pressure of 1024 hPa or more is persisted over Himalayan Mountains and Tibetan plateau.

4.3.2 Study of Rainfall with Wind

One of the main synoptic conditions for occurrence of heavy rainfall over Bangladesh and neighborhood is the SW'ly flow streaming from the head of Bay of Bengal into Bangladesh [1]. For this present study case, westerly wind comes from the Arabian Sea into the Indian region and SW'ly wind comes from the Bay of Bengal and both these winds enter the Bangladesh region. Westerly winds carry moisture from Arabian Sea and SW'ly winds carry moisture from the Bay of Bengal and convergence occurred in Bangladesh especially near the hilly part. Heat flow from the Indian land mass. So, warm and moist environment helps to develop the convective system over Bangladesh. The detailed analyses of the system are given below using both the MM5 and WRF models and shown in Figures 4.3.2.1 (a-d), 4.3.2.2 (a-b) and 4.3.2.3 (a-b).

Using MM5 model, the distributions of low level wind flow at 850 hPa and upper level wind at 500 hPa and 200 hPa levels valid for 00 UTC of 01 May to 21 UTC of 03 May 2009 are presented in Figures 4.3.2.1(a-b), 4.3.2.2a and 4.3.2.3a respectively. The prominent feature is a SW'ly flow transporting moisture from the Bay of Bengal into Bangladesh and heat flow from the India land mass during the whole simulation period. NW'ly flow also transports moisture from Arabian Sea through India to main land of Bangladesh. The area of convergence (i.e., zone of high convective activity) is observed over Bangladesh and neighborhoods. At time 00 UTC on 02 May, 2009, at 850 hPa, the amount of moisture is very low. Due to convergence, small cells merge with others cells and make clusters. With the advancement of time other cells make another cluster. Clusters merge to form mesoscale convective system (MCS) and rainfall occurs in and outside Bangladesh. It is seen that a MCS forms near the foot hills of Himalayan Mountains and hence heavy rainfall occurred in the north-eastern part of Bangladesh. The cyclonic circulation is observed at 850 hPa (Figure 4.3.2.1(a-b)). The wind with varied speed is from 10 to 20 m/s during the 00 UTC of 01 May to 21 UTC of 03 May 2009 with varied amount of 3 hourly rainfalls. Since SW'ly is weak, cyclonic circulation is not observed at 500 hPa. Anticyclonic circulation is observed over north side of the India with wind speed ranges 20 m/s for the whole simulation time (Figure 4.3.2.2a). Anticyclonic circulation is observed at 200 hPa level wind with speed range 40 to 50 m/s (Figure 4.3.2.3a).

Using WRF model, the distributions of 850 hPa, 500 hPa and 200 hPa level wind valid from 00 UTC of 01 May to 00 UTC of 04 May 2009 are presented in Figures 4.3.2.1(c-d), 4.3.2.2b and 4.3.2.3b respectively. Similar features are observed using both the models with different amount of moisture content and wind speed. The simulation of MCS using WRF model is less than that using the MM5 model. The maximum wind speed at the levels 850, 500 and 200 are 10, 10 and 40 m/s respectively. This maximum wind speed is smaller than those obtained by MM5 model. From figures it is clear that the rainfall occurred due to the

combined effect of southwesterly and southerly wind, carrying moisture from Arabian Sea and Bay of Bengal respectively.

Figures 4.3.2.4a and 4.3.2.4b are obtained using inner most Domains i.e. Domain 3 of MM5 and WRF models. It is noted that resolution of Domain 3 is 10 km for both the models. Figures show the development of cloud i.e. MCS in every 3 hours with the advancement of time from 00 UTC of 02 May to 21 UTC of 03 May, 2009. It is clear from the Figures 4.3.2.4a and 4.3.2.4b that simulated rainfall obtained from WRF model is more than that obtained from MM5 model.

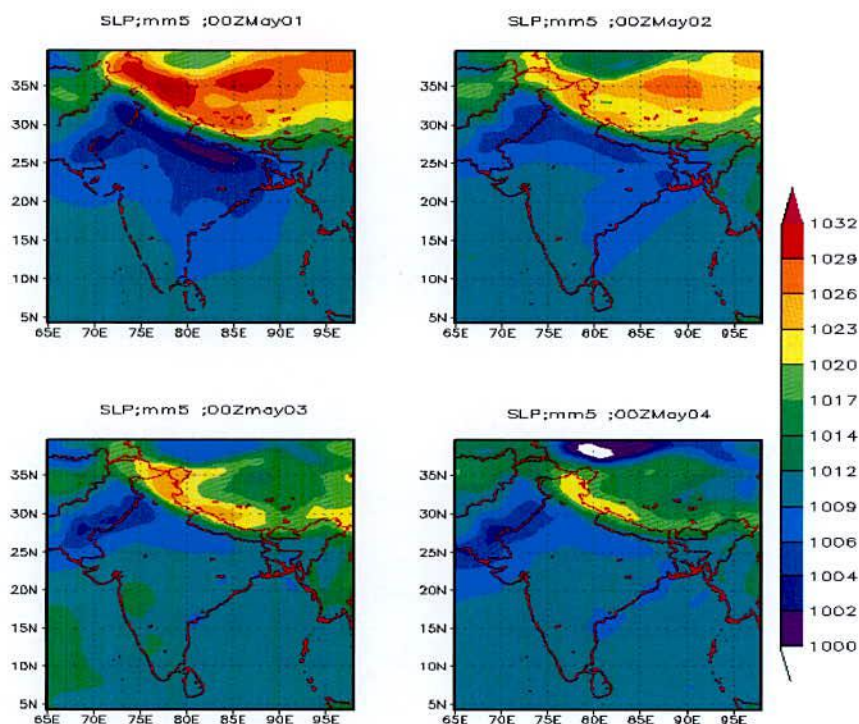


Figure 4.3.1.1a: MM5 Model simulated MSLP (hPa) valid from 00 UTC of 01 May to 00 UTC of 04 May 2009.

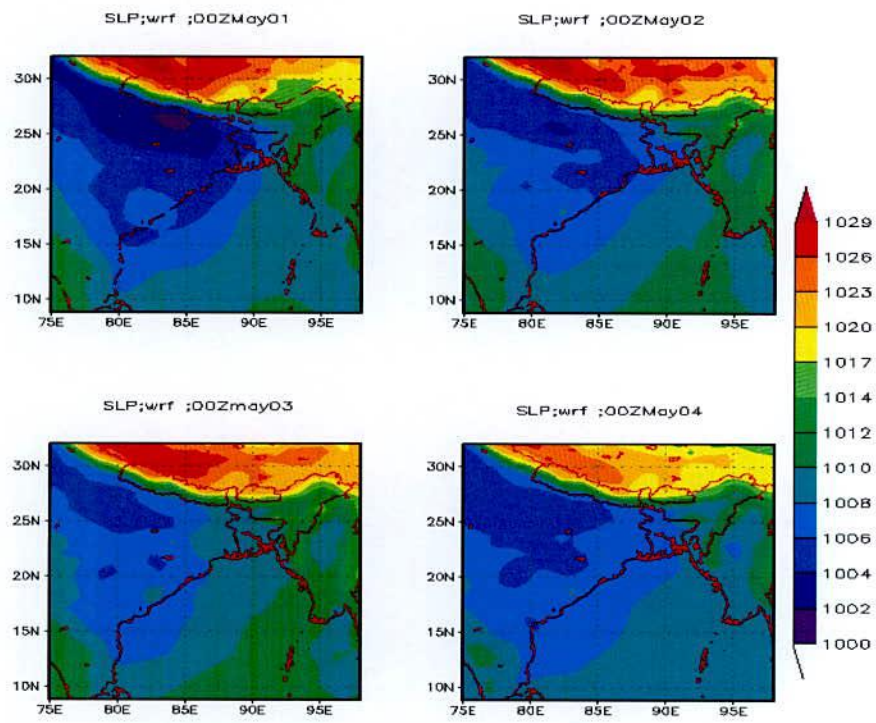


Figure 4.3.1.1b: WRF Model simulated MSLP (hPa) valid from 00 UTC of 01 May to 00 UTC of 04 May 2009.

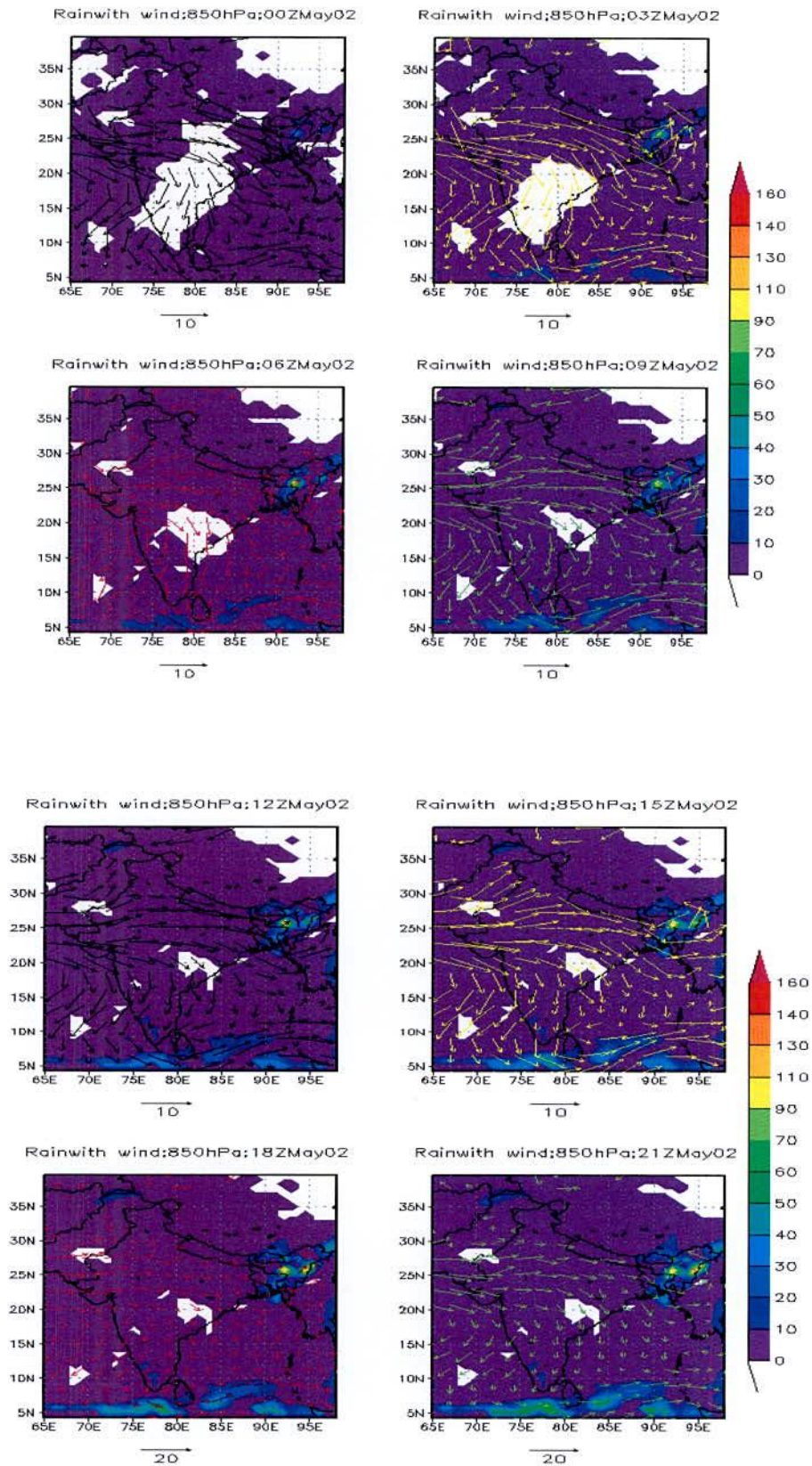


Figure 4.3.2.1a: MM5 Model simulated wind flow (m/s) at 850 hPa valid 00 to 21 UTC of 02 May 2009.

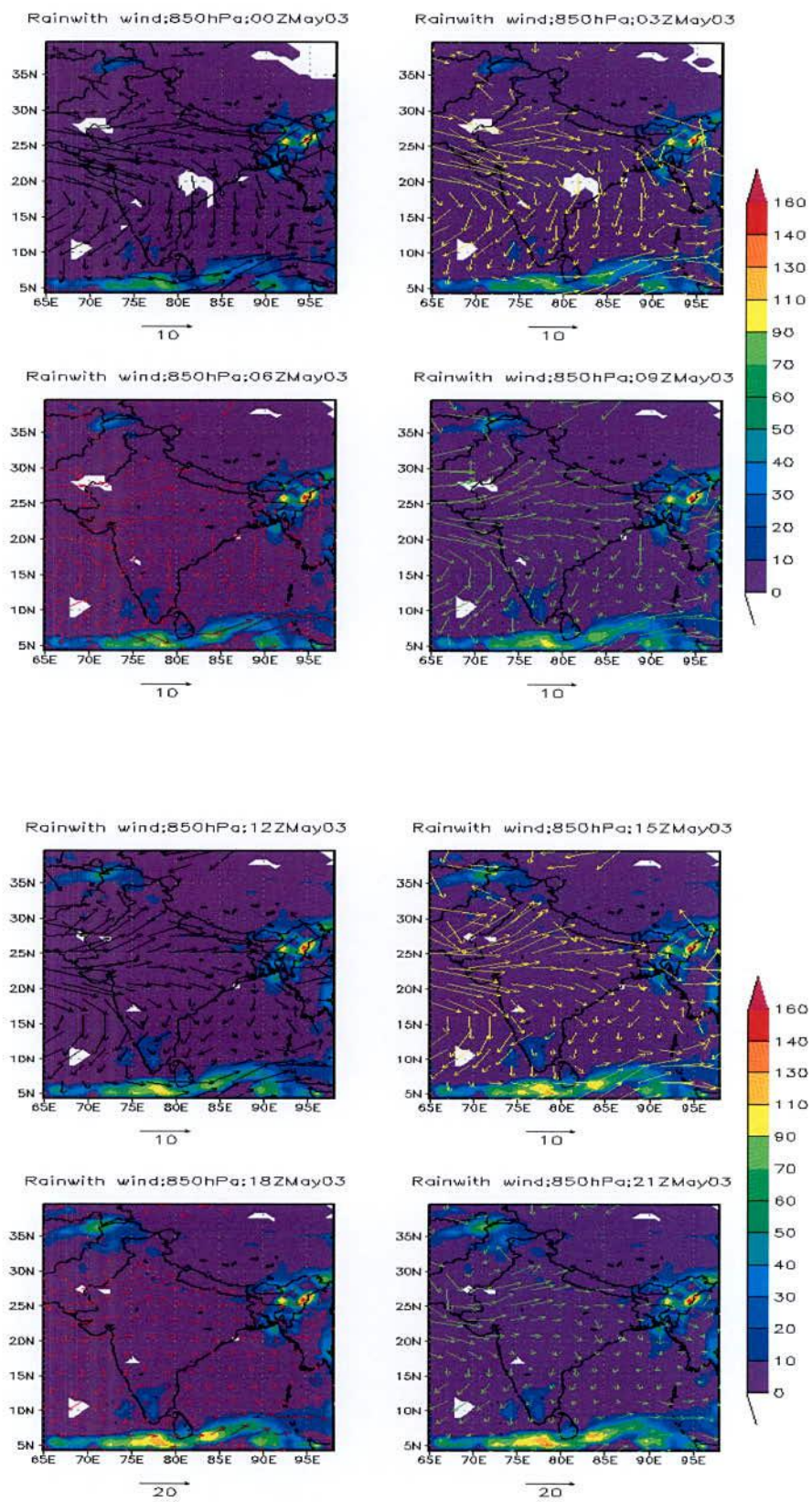


Figure 4.3.2.1b: MM5 Model simulated wind flow (m/s) at 850 hPa valid 00 to 21 UTC of 03 May 2009.

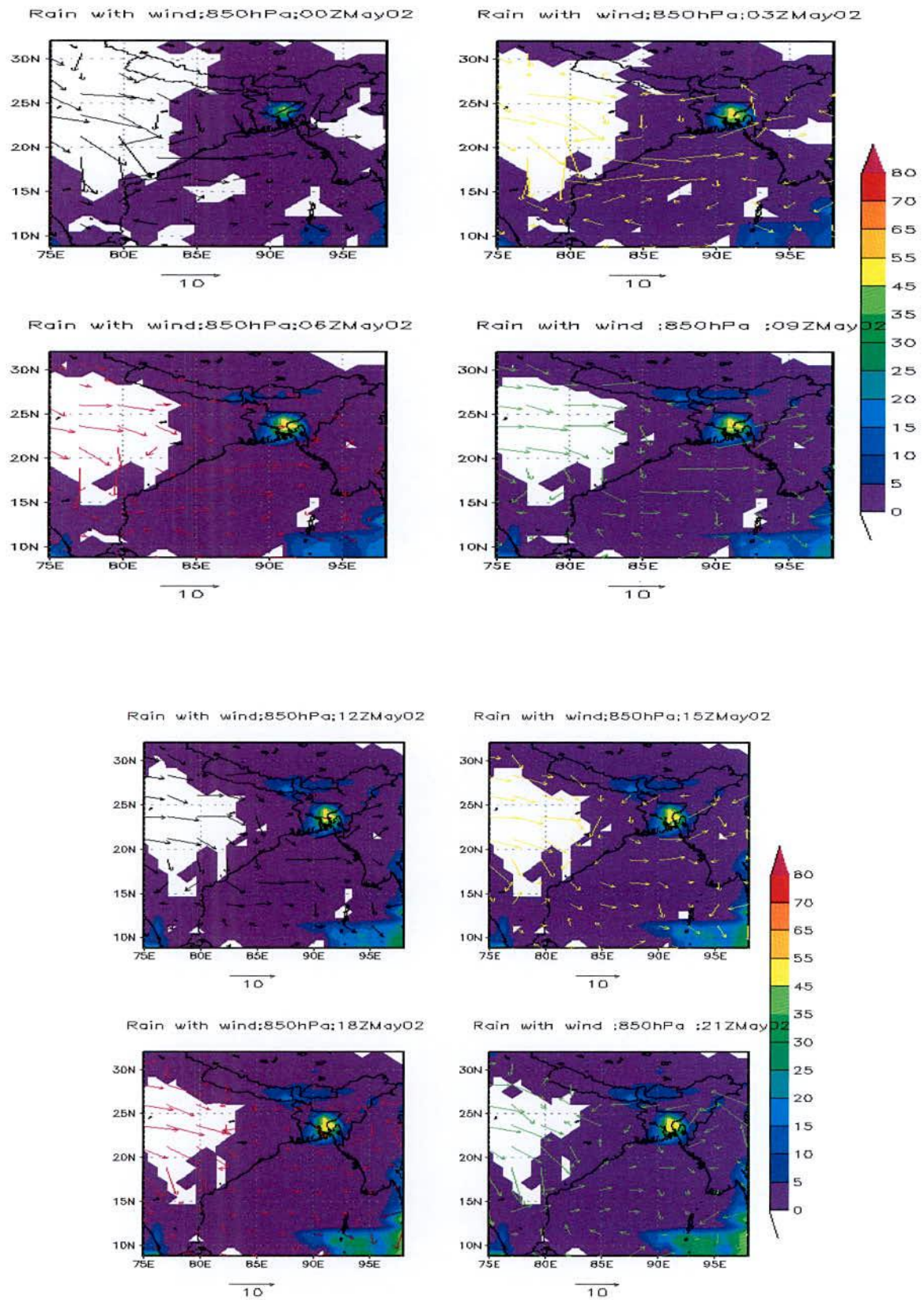


Figure 4.3.2.1c: WRF Model simulated wind flow (m/s) at 850 hPa valid for 00 to 21 UTC of 02 May 2009.

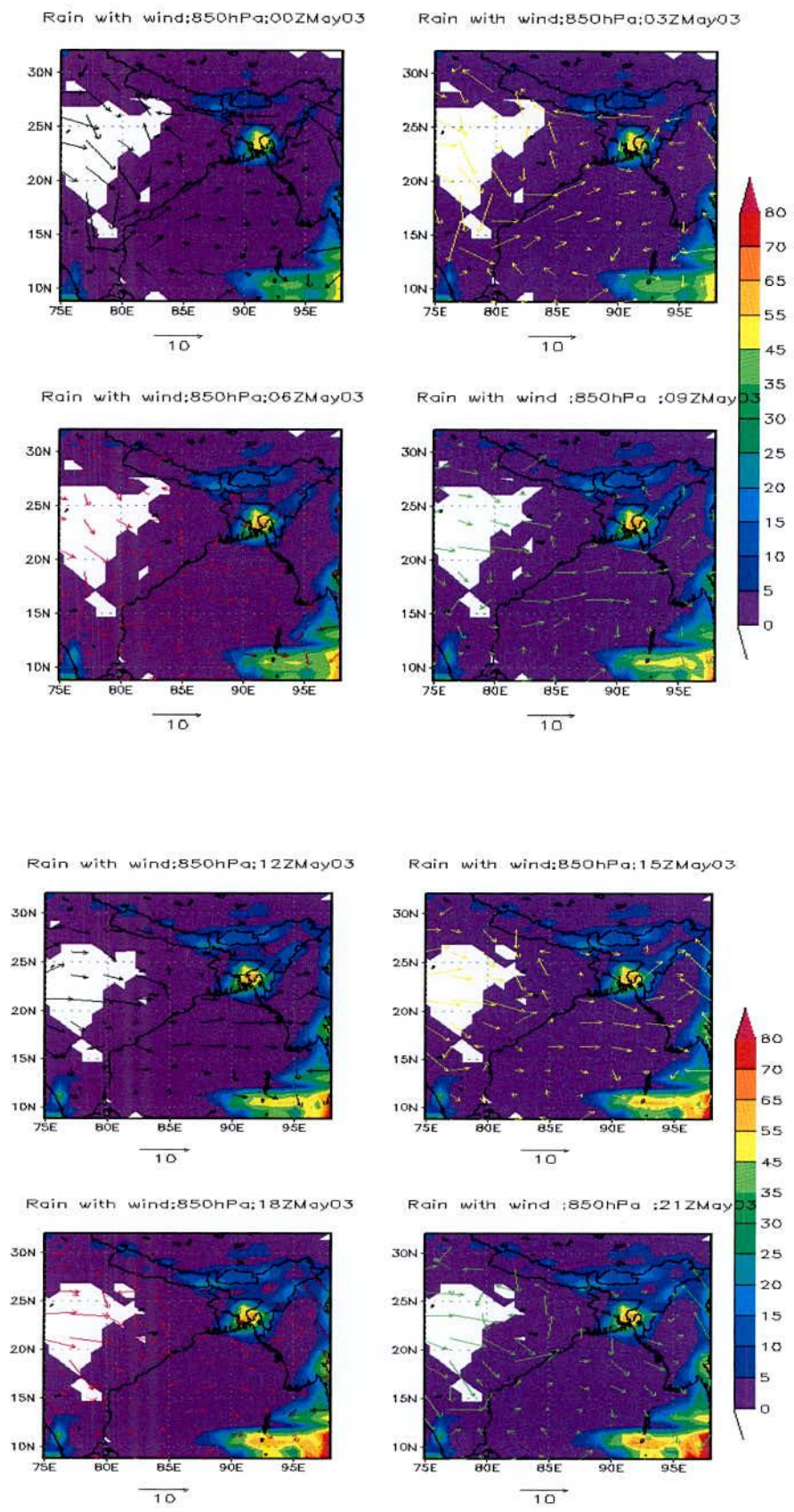


Figure 4.3.2.1d: WRF Model simulated wind flow (m/s) at 850 hPa valid for 00 to 21 UTC of 03 May 2009.

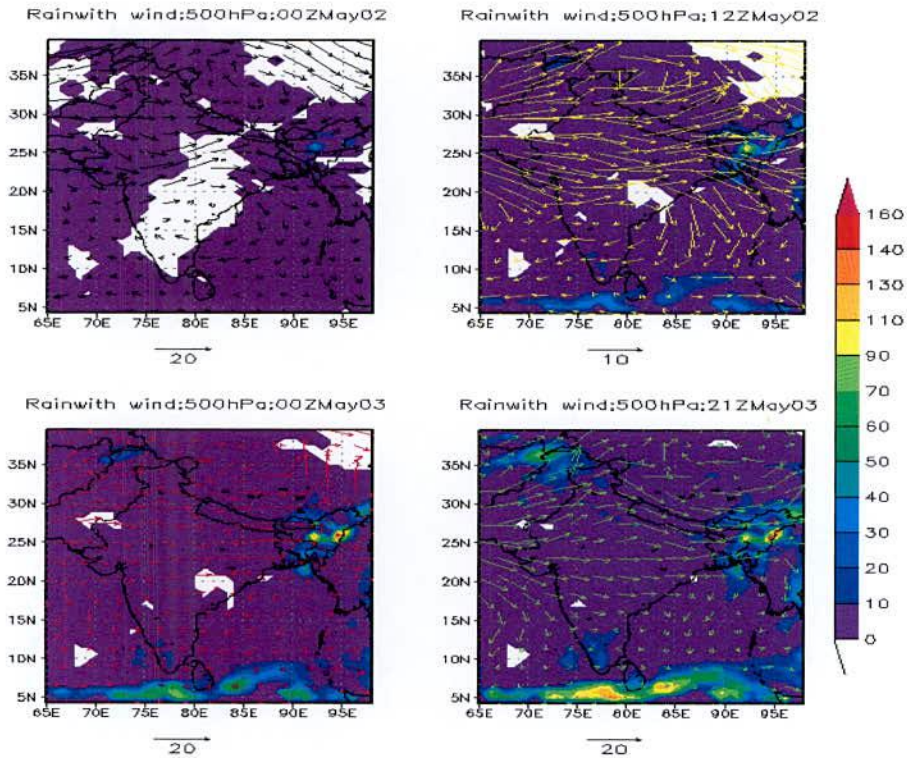


Figure 4.3.2.2a: MM5 Model simulated wind flow (m/s) at 500 hPa valid for 00 UTC of 02 May to 21 UTC of 03 May, 2009.

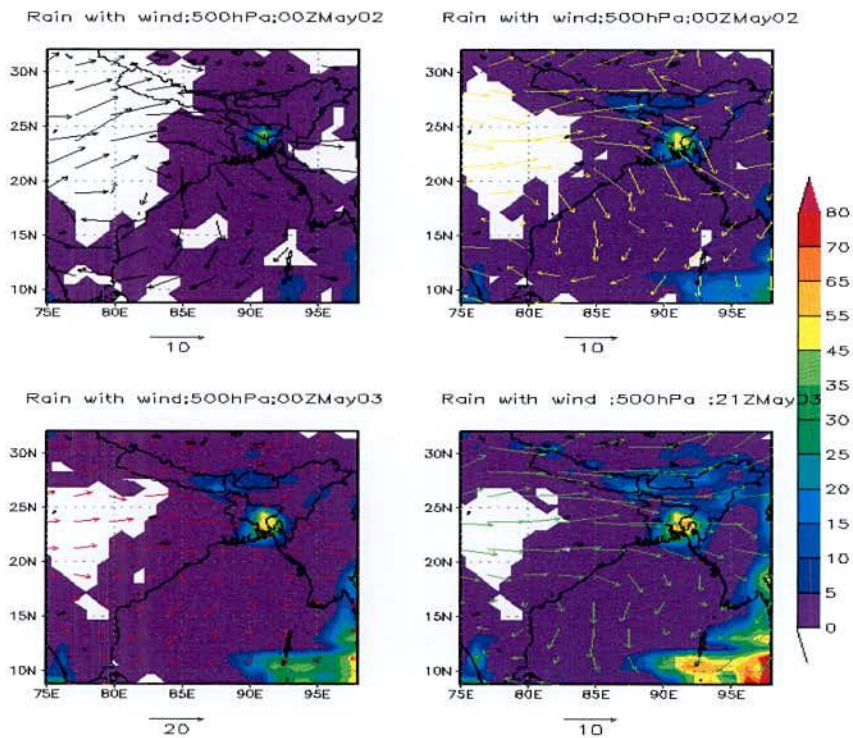


Figure 4.3.2.2b: WRF Model simulated wind flow (m/s) at 500 hPa valid for 12 to 21 UTC of 02 May 2009.

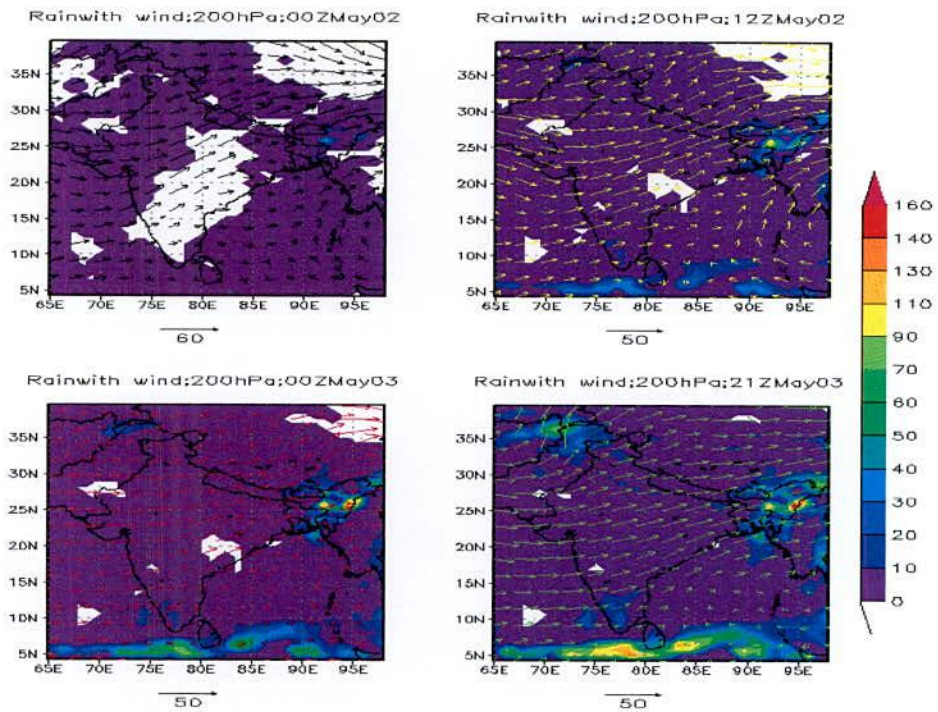


Figure 4.3.2.3a: MM5 Model simulated wind flow (m/s) at 200 hPa valid for 00 UTC of 02 May to 21 UTC of 03 May, 2009.

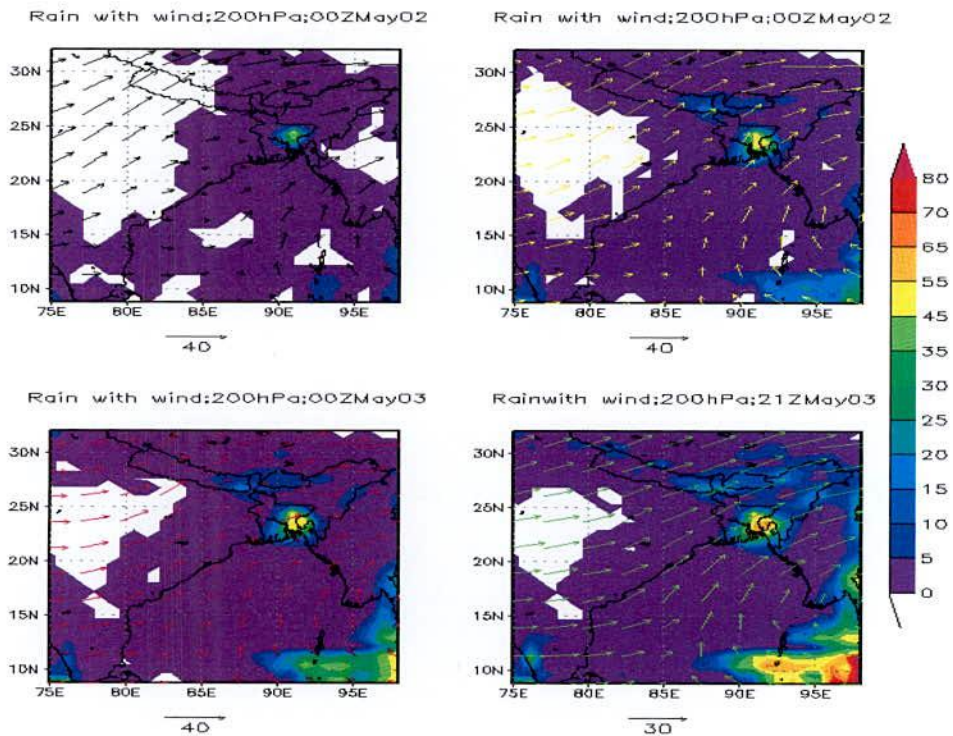


Figure 4.3.2.3b: MM5 Model simulated wind flow (m/s) at 200 hPa valid for 12 to 21 UTC of 03 May 2009

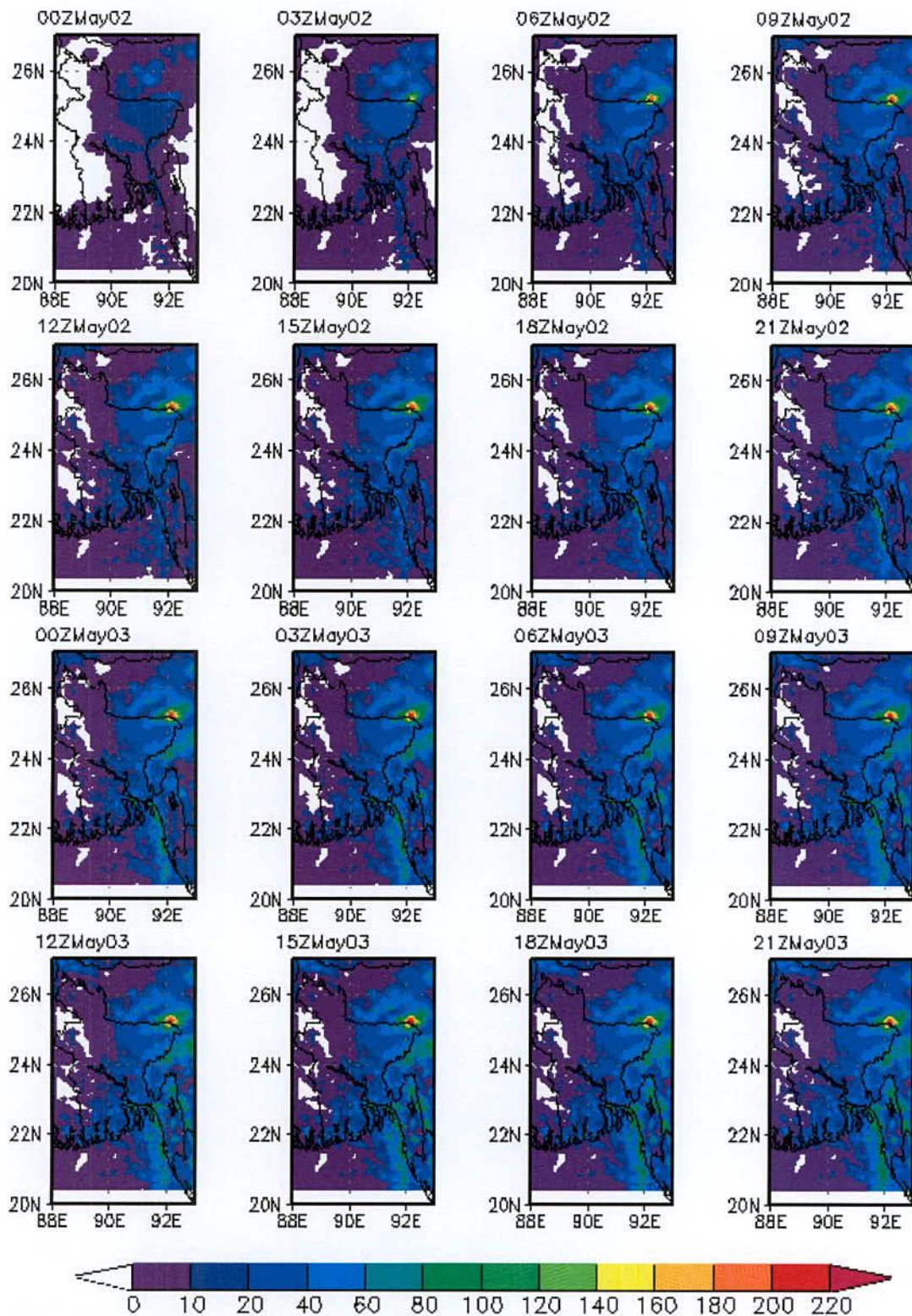


Figure 4.2.2.4a: MM5 Model simulated precipitation field valid from 00 UTC of 02 May to 21 UTC of 03 May 2009. Sequence is top left to right.

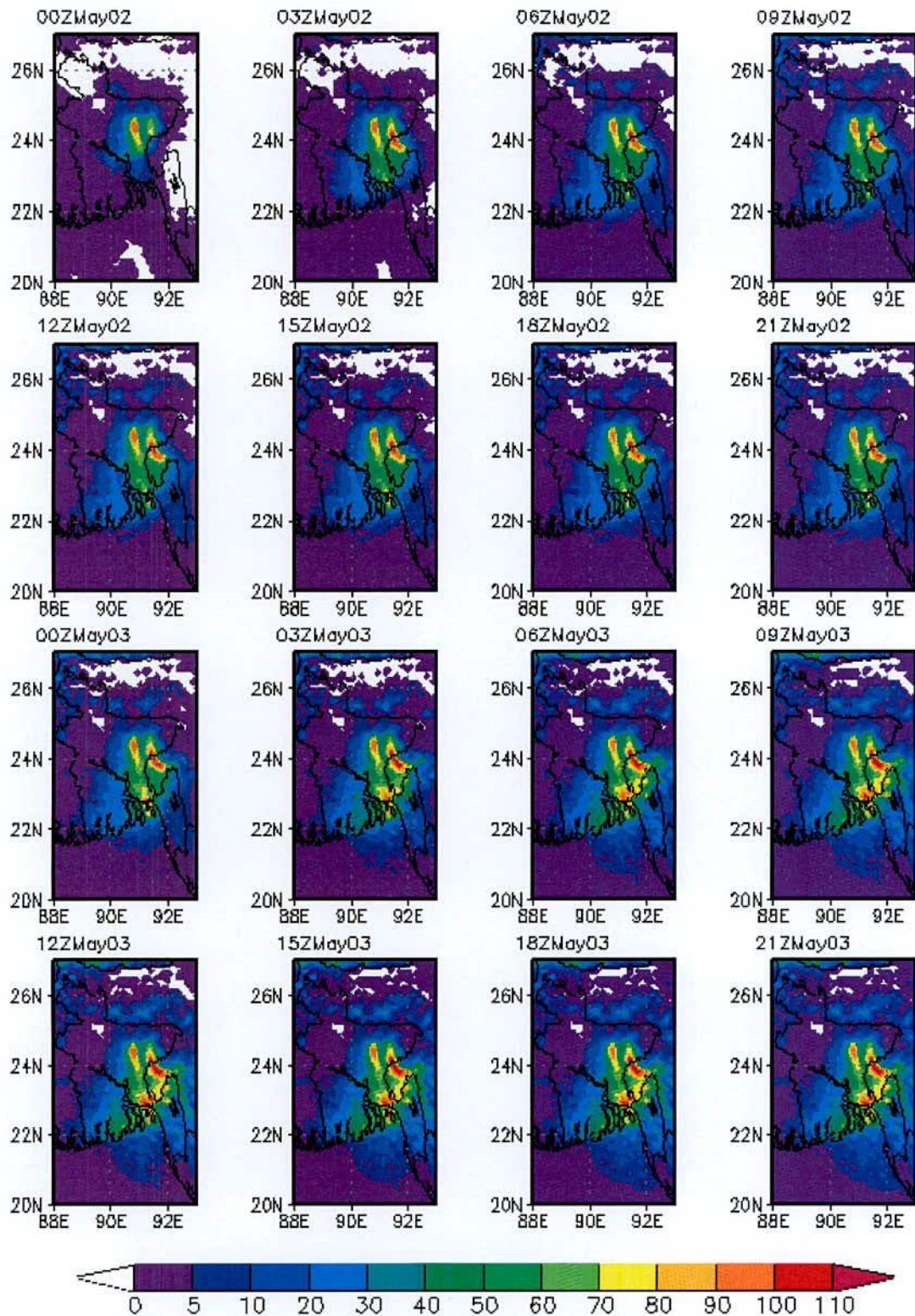


Figure 4.2.2.4b: WRF Model simulated precipitation field valid from 00 UTC of 02 May to 21 UTC of 03 May 2009. Sequence is top left to right.

4.3.3 Study of Relative Humidity with Wind

The simulation of humidity and wind shows SW'ly flow transports of moisture from the Bay of Bengal and westerly flow transport moisture from the Arabian Sea through the Indian region to the plains of Bangladesh and neighborhood. The spatial distribution of relative humidity with wind obtained by MM5 at 850, 500 and 200 hPa levels from 00 UTC of 02 May to 21 UTC of 03 May 2009 are presented in Figures 4.3.3.1(a-b), 4.3.3.2a and 4.3.3.3a respectively. The moisture content of the order of 90-100% at 850 hPa levels is found over most of the region of Bangladesh and is also found with cyclonic circulation of wind for the whole simulation time. The moisture content is almost absent over Himalayan Mountains at 850 hPa level. Comparing with the moisture content at 850 hPa level, the magnitudes moisture are comparatively less at 500 and 200 hPa levels with anti-cyclonic circulation of wind over Bangladesh. It is noted that moisture content at level 200 at few places outside Bangladesh is more than 100 %. For the time from 00 UTC of 02 May to 21 UTC of 03 May 2009, wind speeds are almost about 10-20 m/s, 10-20 m/s and 50-60 m/s at 850, 500 and 200 hPa levels respectively.

The spatial distribution of relative humidity with wind obtained by using WRF model at 850, 500 and 200 hPa levels from 00 UTC of 02 May to 21 UTC of 03 May 2009 are presented in Figures 4.3.3.1(c-d), 4.3.3.2b and 4.3.3.3b respectively. Similar to MM5 model, the WRF Model simulates less amount of moisture (90% or less) with cyclonic circulation over most of the regions of Bangladesh at 850 and 500 hPa levels But the less amount of moisture are simulated at 200 hPa level with anti-cyclonic circulation of wind. Simulated wind speeds for the levels 850, 500 and 200 hPa are equal to or less than those obtained using MM5 model.

It is clear from the figures that amount of humidity prevails because of combined effect of westerly and SW'ly wind, carrying moisture from the Arabian Sea and the Bay of Bengal respectively. The heat flow from the India land mass helps the convective system to intensity.

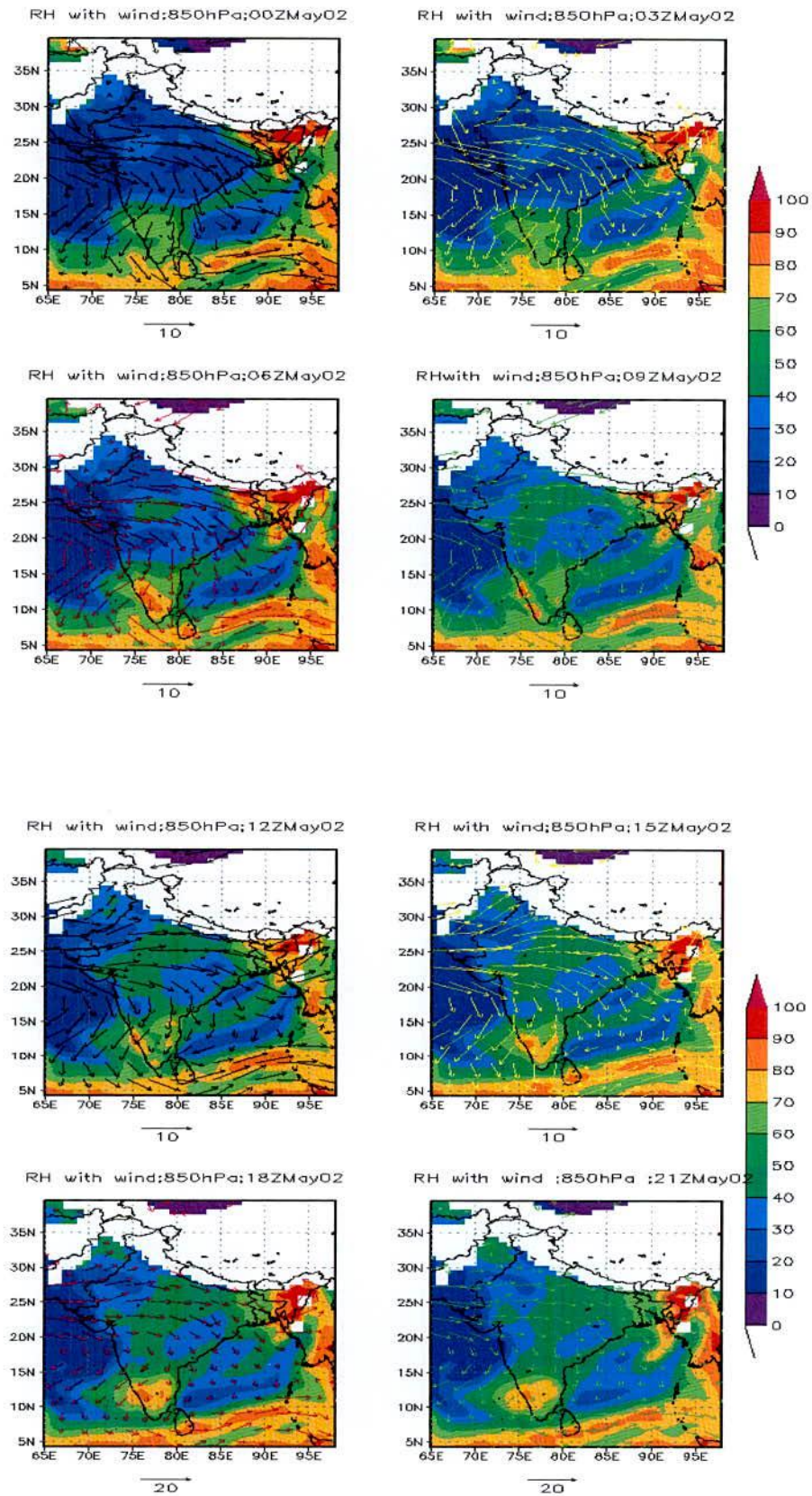


Figure 4.3.3.1a: MM5 Model simulated relative humidity with wind at 850 hPa level valid for 00 to 21 UTC of 02 May 2009.

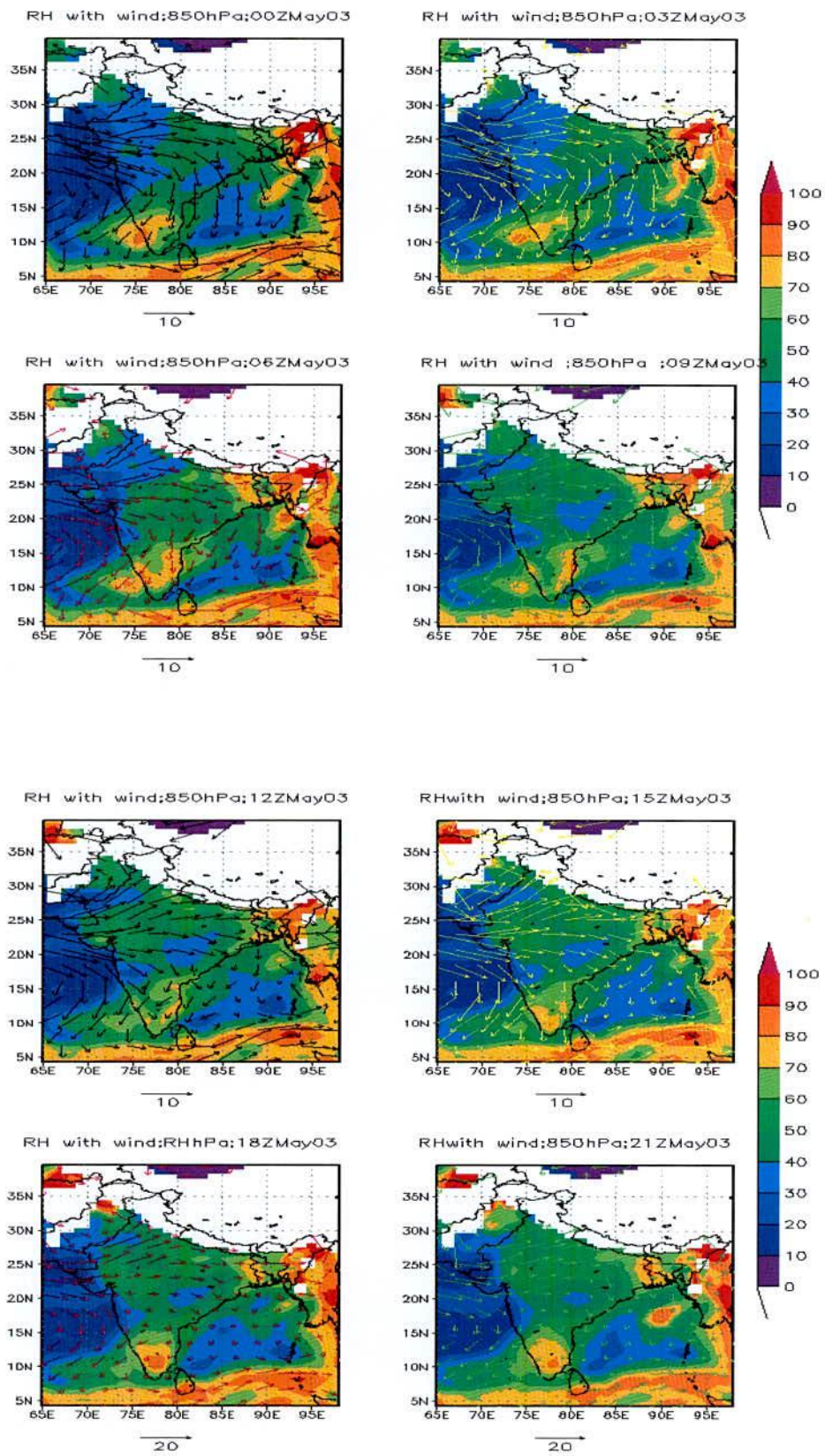


Figure 4.3.3.1b: MM5 Model simulated relative humidity with wind at 850 hPa level valid for 00 to 21 UTC of 02 May 2009.

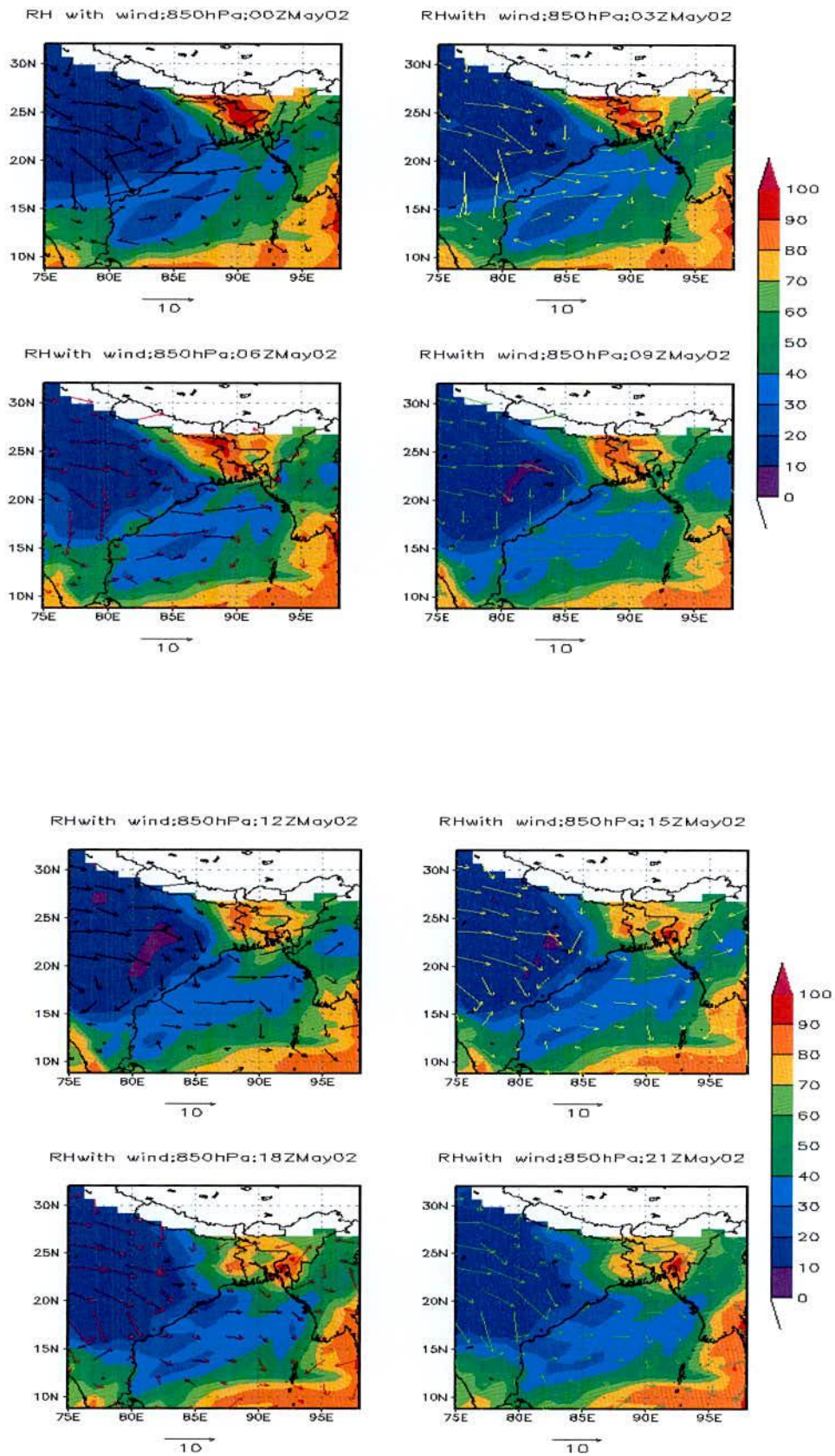


Figure 4.3.3.1c: WRF Model simulated relative humidity with wind at 850 hPa level valid for 00 to 09 UTC of 02 May 2009.

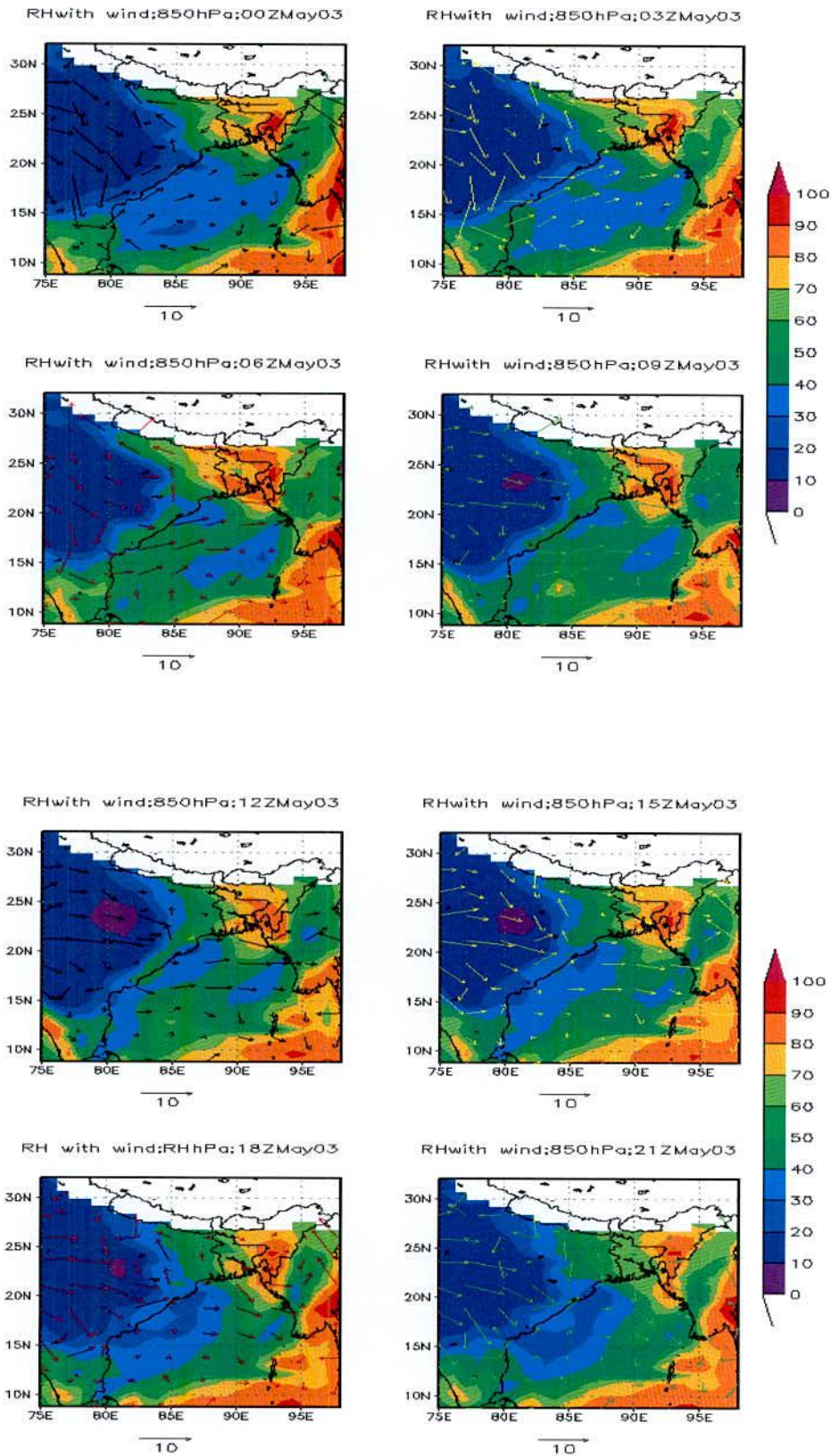


Figure 4.3.3.1d: WRF Model simulated relative humidity with wind at 850 hPa level valid for 00 to 09 UTC of 03 May 2009.

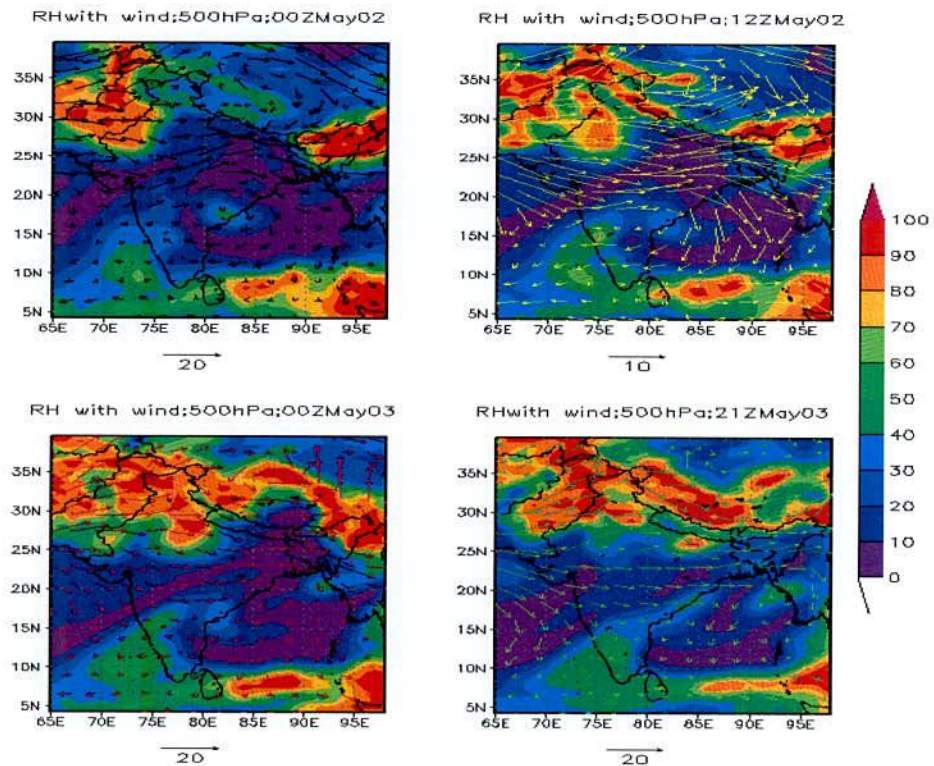


Figure 4.3.3.2a: MM5 Model simulated relative humidity with wind at 500 hPa level valid for 00 UTC of 02 May to 21 UTC of 03 May 2009.

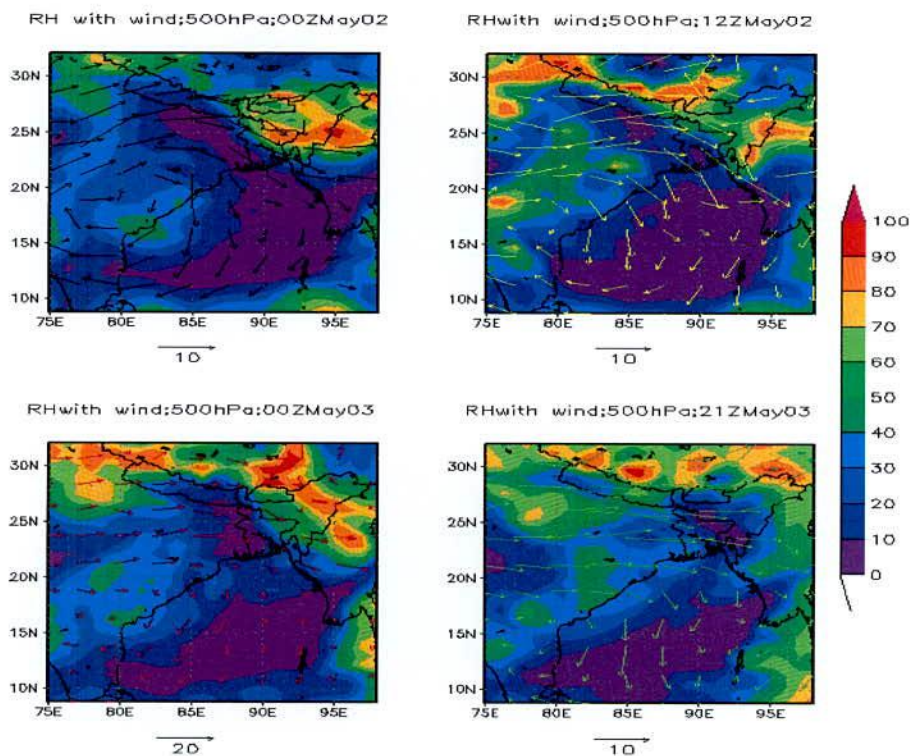


Figure 4.3.3.2b: WRF Model simulated relative humidity with wind at 500 hPa level valid for 00 UTC of 02 May to 21 UTC of 03 May 2009.

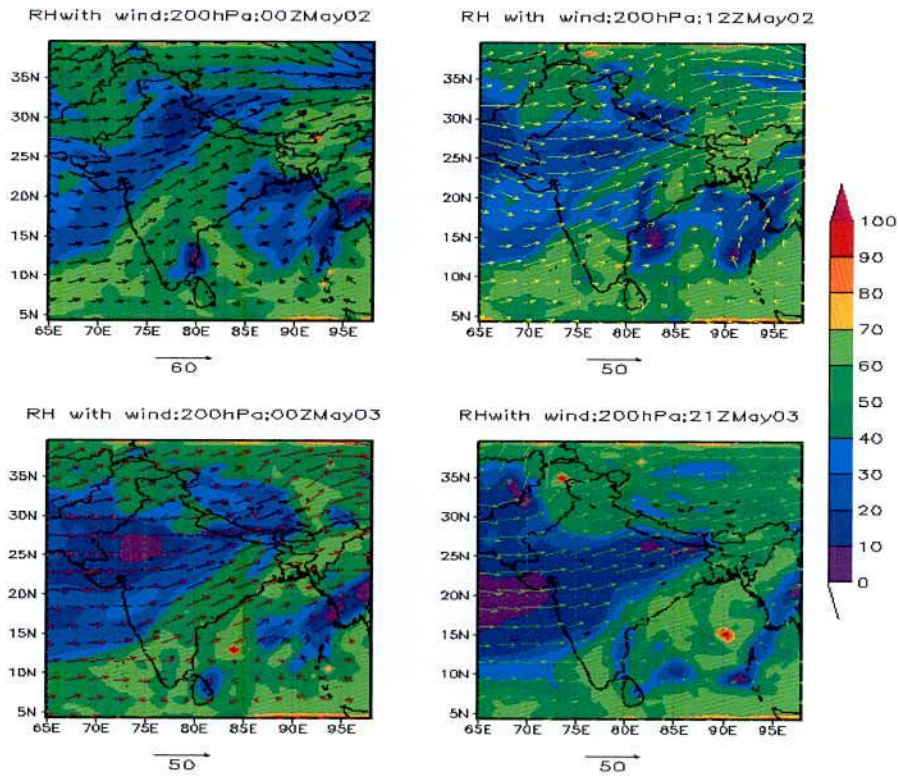


Figure 4.3.3.a: MM5 Model simulated relative humidity with wind at 200 hPa level valid for 00 UTC of 02 May to 21 UTC of 03 May 2009.

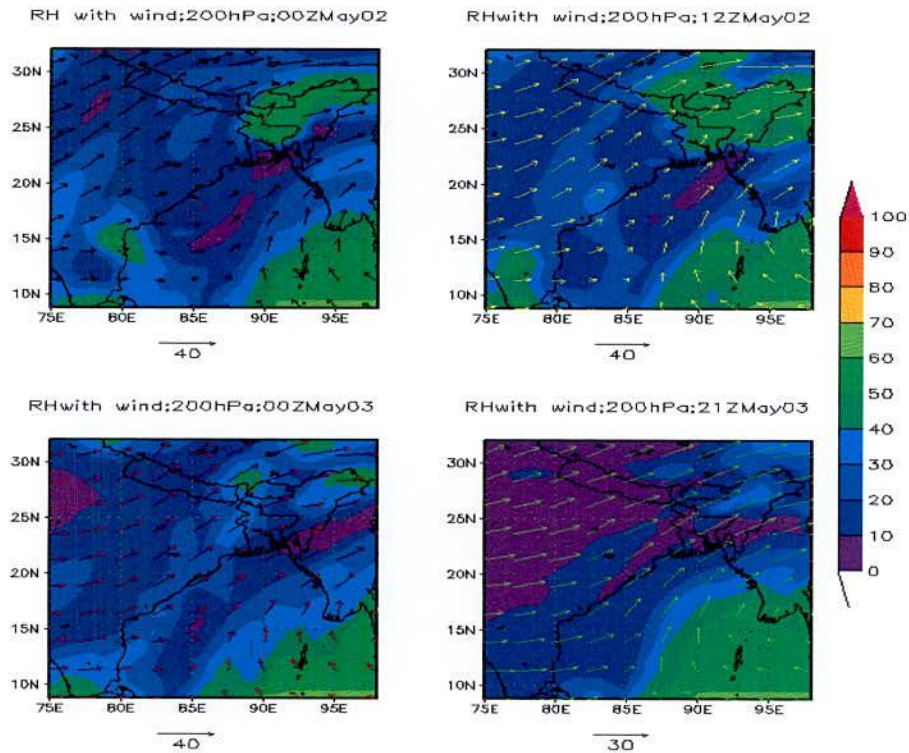


Figure 4.3.3.b: WRF Model simulated relative humidity with wind at 200 hPa level valid for 00 UTC of 02 May to 21 UTC of 03 May 2009

4.3.4 Validation of Rain

24-h accumulated rainfalls obtained from the MM5 and WRF Model valid for 01, 02 and 03 May 2009 are shown in Figures 4.3.4.1– 4.3.4.3. Figures are plotted using model simulated 24-h accumulated rainfalls for Domain 1 (90 km resolution), Domain 2 (30 km resolution) and Domain 3 (10 km resolution) with rainfall obtained using TRMM and rain-gauge data. Rain-gauge data is obtained from Bangladesh Meteorological Department (BMD). Model simulated rainfall for both the models are seen at all places of Bangladesh with large spatial variability. For these simulations, Kain- Fritsch cumulus parameterization scheme with MRF PBL for MM5 model and Yonsei University Scheme (YSU) PBL for WRF model are used.

It is found that the model simulated rainfall for all the domains of both the models is less than or equal to the rainfall obtained from TRMM observational data with exception for Domain 2 and 3 for MM5 model on 02 May 2009. It is noted that TRMM overestimates the pre-monsoon rainfall [111] in this region.

It is very clear from the Figure 4.3.4.1– 4.3.4.3 that Domain 1 and Domain 3 show the minimum and maximum rainfall respectively than that of other domains for both the models MM5 and WRF. It means that high resolution produces comparatively more rainfall. Domain 1, 2 and 3 of WRF model produces equal or less, less, and more or less rainfall than that obtained from Domain 1, 2 and 3 of MM5 model.

On 01 May 2009, WRF model produces more rainfall than that of MM5 model. Rainfall obtained from WRF model is much closer to that obtained from TRMM observational data but rainfall obtained from MM5 model is closer to that obtained from rain-gauge observational data.

On 02 May 2009, MM5 model produces more rainfall than that of WRF model. Rainfall obtained from WRF model is closer to that obtained from TRMM and rain-gauge observation but rainfall obtained from MM5 model is more than that obtained from TRMM and rain-gauge observation

On 03 May 2009, MM5 model produces more rainfall than that of WRF model. Rainfall obtained from MM5 model is less than that obtained from TRMM observational data but more than that obtained from rain –gauge observational data. Rainfall obtained from WRF model is less than that obtained from TRMM and rain-gauge observational data.

From the above discussion, it is clear that rainfall obtained from WRF model is more or less than that obtained from MM5 model for high resolution domain i.e. Domain 3 and the Models simulated rainfalls are comparable to those obtained from BMD rain-gauge with large spatial variability. However, both the models has captured well the heavy rainfall event

with spatio-temporal variation. It also has captured the structure of the convective phenomena of the studied case. Thus simulated rainfall seems to be realistic using both the models

The horizontal distribution of the cloud structures are shown in Figures 4.3.4.4 and 4.3.4.5 using model MM5 and WRF respectively at the stage of high convection i.e. at mature stage of cloud, where 3 hourly precipitation is higher than other moments. Figures show the variation of intensity of cloud with spatial distribution. From the figures, centers of convective activity are identified to understand the vertical structure.

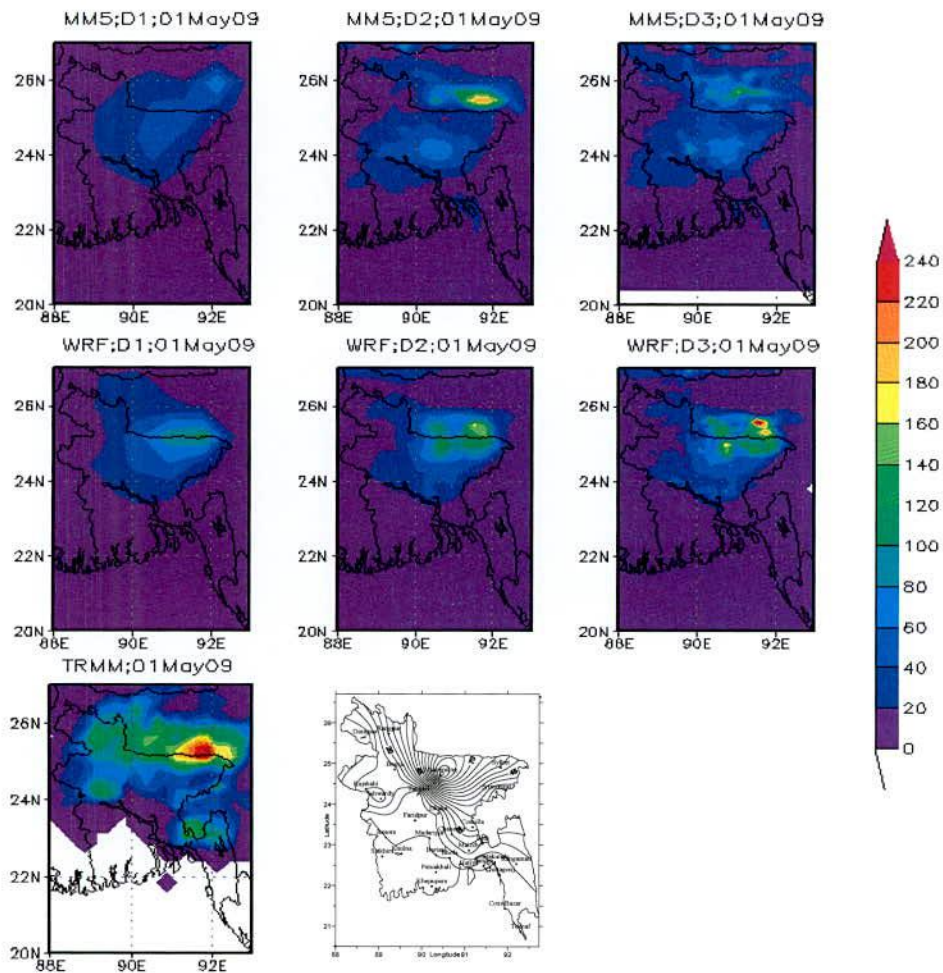


Figure 4.3.4.1: Spatial distribution of MM5 model simulated 24-h accumulated rainfall (mm) and TRMM 3B42V6 observed rainfall (mm) valid for 01 May 2009

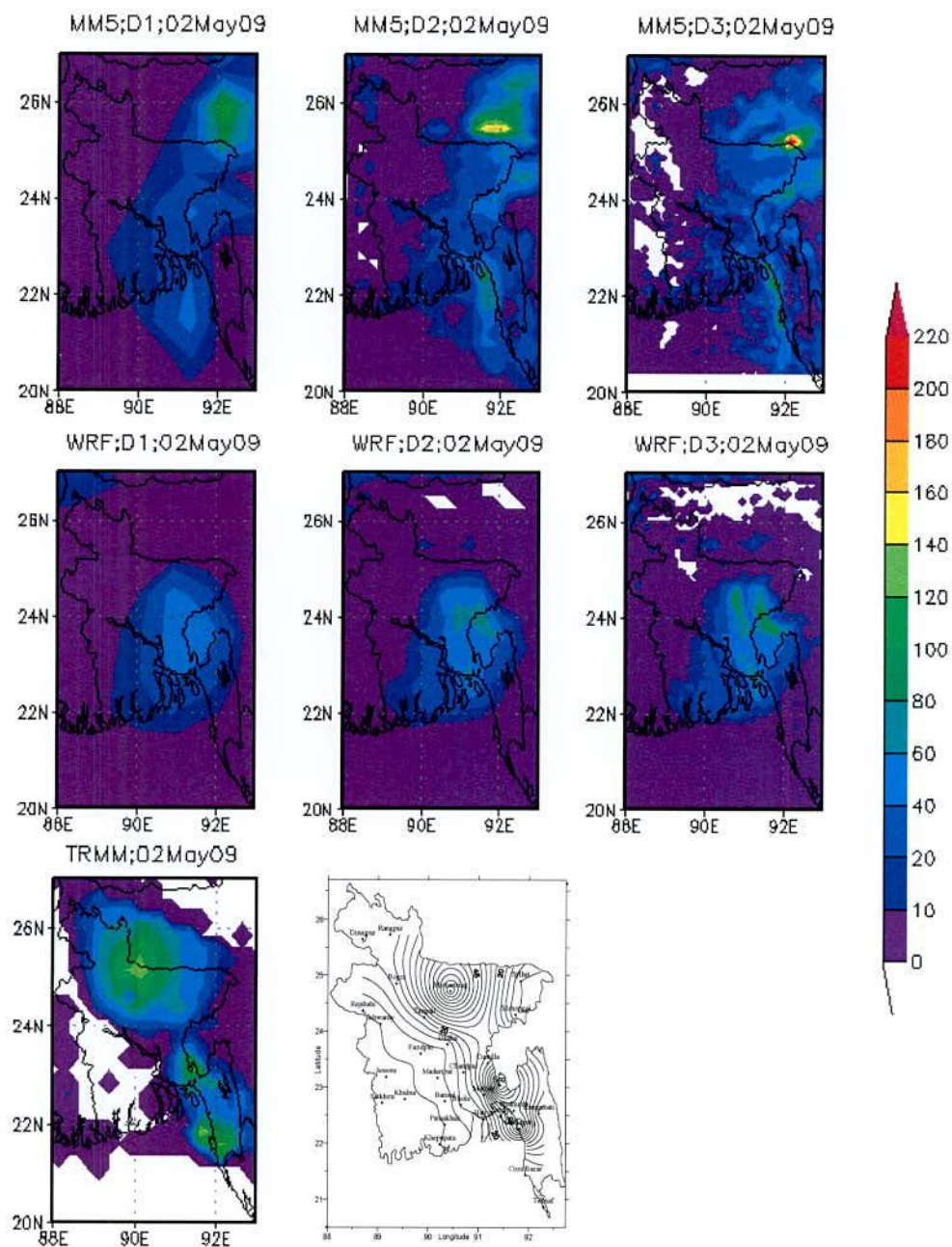


Figure 4.3.4.2: Spatial distribution of MM5 model simulated 24-h accumulated rainfall (mm) and TRMM 3B42V6 observed rainfall (mm) valid for 02 May 2009.

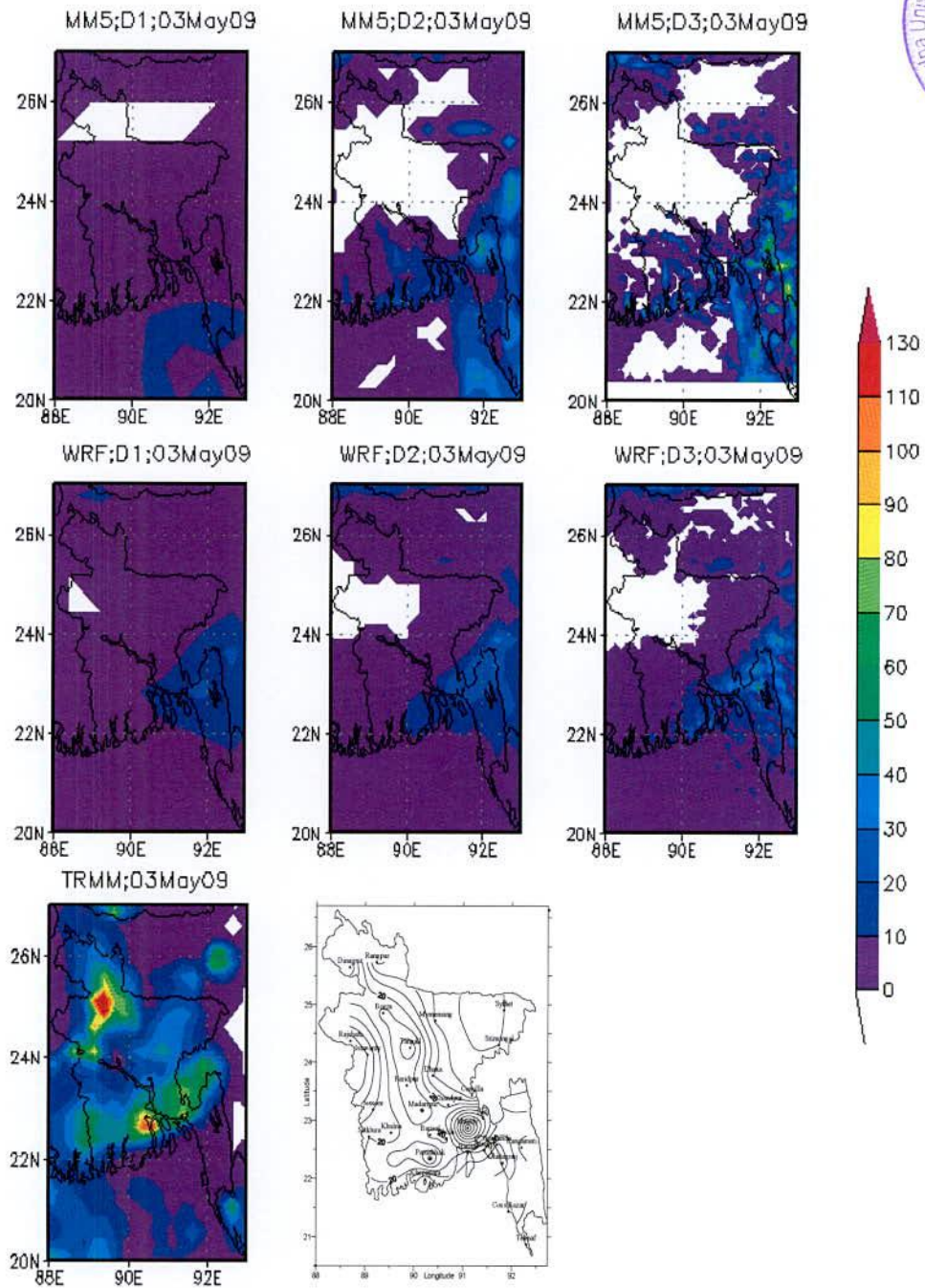


Figure 4.3.1.4.3: Spatial distribution of MM5 model simulated 24-h accumulated rainfall (mm) and TRMM 3B42V6 observed rainfall (mm) valid for 03 May 2009.

To study the vertical profile of convective system, the vertical structure of vertical velocity, divergence, relative vorticity, relative humidity and mixing ratio are plotted through the centre of the most developed cloud at (25.22°N, 92.12°E), (25.20°N, 92.40°E), (22.85°N, 92.40°E) and (22.75°N, 92.50°E) at the time 06 and 09 UTC of 02 May, and 06 and 12 UTC of 03 May 2009 respectively for MM5 model and shown in figure in following section 4.3.5, 4.3.6, 4.3.7, 4.3.8 and 4.3.9. Similarly, the vertical structure of vertical velocity, divergence, relative vorticity, relative humidity and mixing ratio are plotted through the centre of the most developed cloud at (24.32°N, 90.80°E), (23.88°N, 91.61°E), (22.86°N, 91.32°E) and (22.80°N, 92.57°E) at the time 03 and 06 UTC of 02 May, and 03 and 15 UTC of 03 May 2009 respectively for WRF model are shown in figure in following section 4.3.5, 4.3.6, 4.3.7, 4.3.8 and 4.3.9.

4.3.5: Vertical Profile of Vertical Velocity

To understand the vertical structure of the convective system, the vertical profiles of vertical velocity obtained from MM5 and WRF models are plotted through the centre of the most developed cloud at different time and are shown in Figures 4.3.5.1a and 4.3.5.1b. For MM5 model, figures are plotted at 06 and 09 UTC of 02 May, and 06 and 12 UTC of 03 May 2009. But for WRF model; figures are plotted at 03 and 06 UTC on 02 May, and at 03 and 15 UTC on 03 May 2009.

The figures reveal that strong upward motion exists along the centre of the convective system. The maximum upward vertical velocities for different times are different in magnitudes. Their positions are also situated at different levels. Maximum values are 35 cm/s to 550 cm/s and from 15 to 200 cm/s for MM5 and WRF models respectively. Negative value indicates the downward motion. In general, downward motion is not strong. It is also visible in the different levels with areas of small pockets, which could be due to subsidence associated with convection. Maximum values of downward motion are 0 to 100 cm/s and 9 to 150 cm/s for MM5 and WRF models respectively. So, amount of the maximum values of upward and downward vertical velocity are more in case of MM5 than in case of WRF model.

4.3.6 Vertical Profile of Divergence

Divergence ($\times 10^{-5} \text{ s}^{-1}$) is one the important parameters for analysing the convective system. In general, there are low level convergence and upper level divergence in the convective system. To understand the vertical structure of the convective system, the vertical profiles of divergence obtained from MM5 and WRF models are plotted through the centre of the most developed cloud at different times and are shown in Figures 4.3.5.1a and 4.3.5.1b. For MM5 model, figures are plotted at time at 06 and 09 UTC on 02 May, and 06 and 12 UTC on 03

May 2009. But for WRF model, figures are plotted at time for 03 and 06 UTC on 02 May, and 03 and 15 UTC on 03 May 2009.

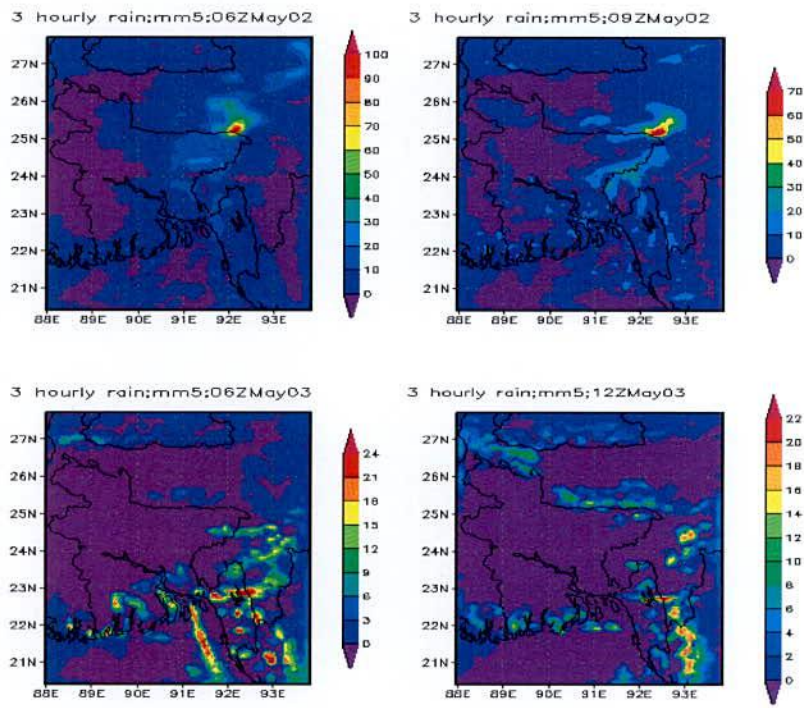


Figure 4.3.4.4: MM5 model simulated horizontal structure of most developed cloud at different times.

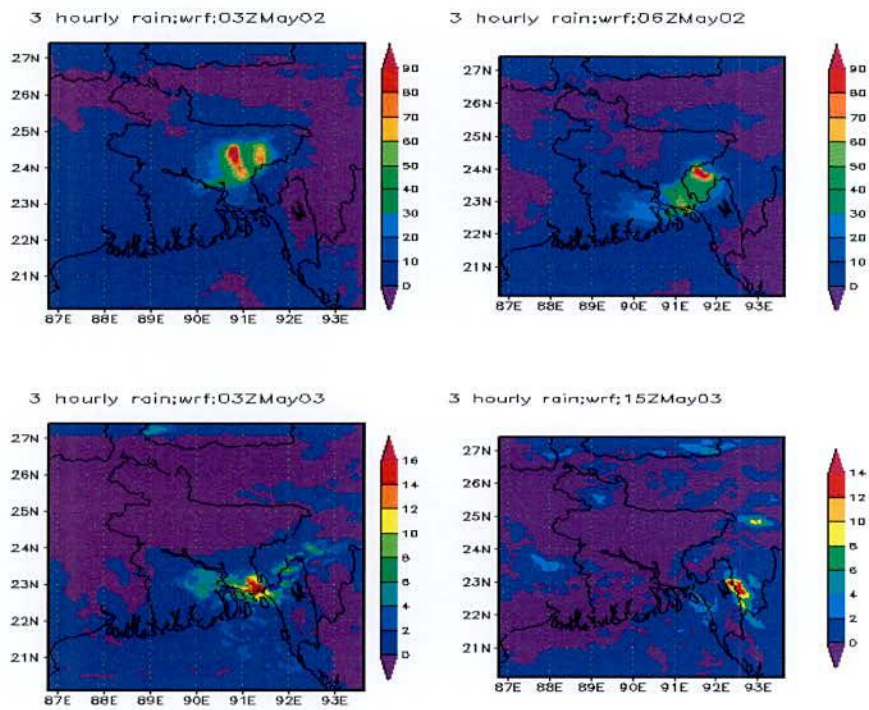


Figure 4.3.4.5: WRF model simulated horizontal structure of most developed cloud at different times.

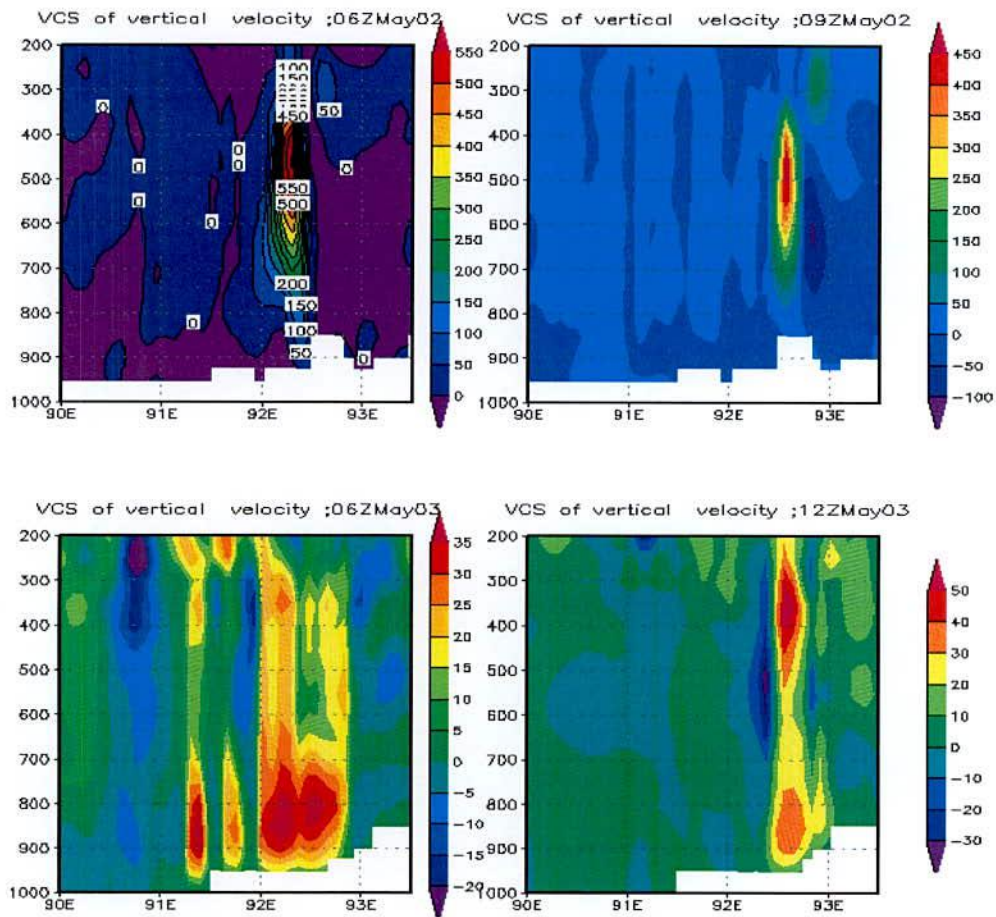


Figure 4.3.5.1a: MM5 Model simulated vertical structure of vertical velocity (cm/s) along the center for different times.

In the figure positive and negative values indicate the divergence and convergence respectively. So, well defined convergence areas are available with divergence area at different levels. Low level convergences are available at four different times with upper level divergence. It is seen that divergence area embedded with convergence area. The maximum values of divergences and convergences are $(15 \text{ to } 150) \times 10^{-5} \text{ s}^{-1}$ and $(25 \text{ to } 90) \times 10^{-5} \text{ s}^{-1}$ respectively for MM5 model. Again, the maximum values of divergences and convergences are $(9 \text{ to } 100) \times 10^{-5} \text{ s}^{-1}$ and $(15 \text{ to } 100) \times 10^{-5} \text{ s}^{-1}$ respectively for WRF model. This state of situation in convection is significant from the point of view of severe convective activity. At 06 and 12 UTC on 03 May 2009, low level (up to 700 hPa) divergences are also available for MM5 model. From WRF model, at 03 and 06 UTC on 02 May 2009, strong upper level convergence and low level divergence are available. At 03 and 15 UTC on 03 May 2009, low level convergence and upper level divergence are also available. This state of convection is significant from the point of view of severe convective activity. Again, the maximum values of divergences obtained using WRF model are less than those obtained from MM5 model. But the maximum values of convergences obtained using WRF model are more than those

obtained from MM5 model. It indicates more precipitation may be obtained from WRF model than that obtained from MM5 model.

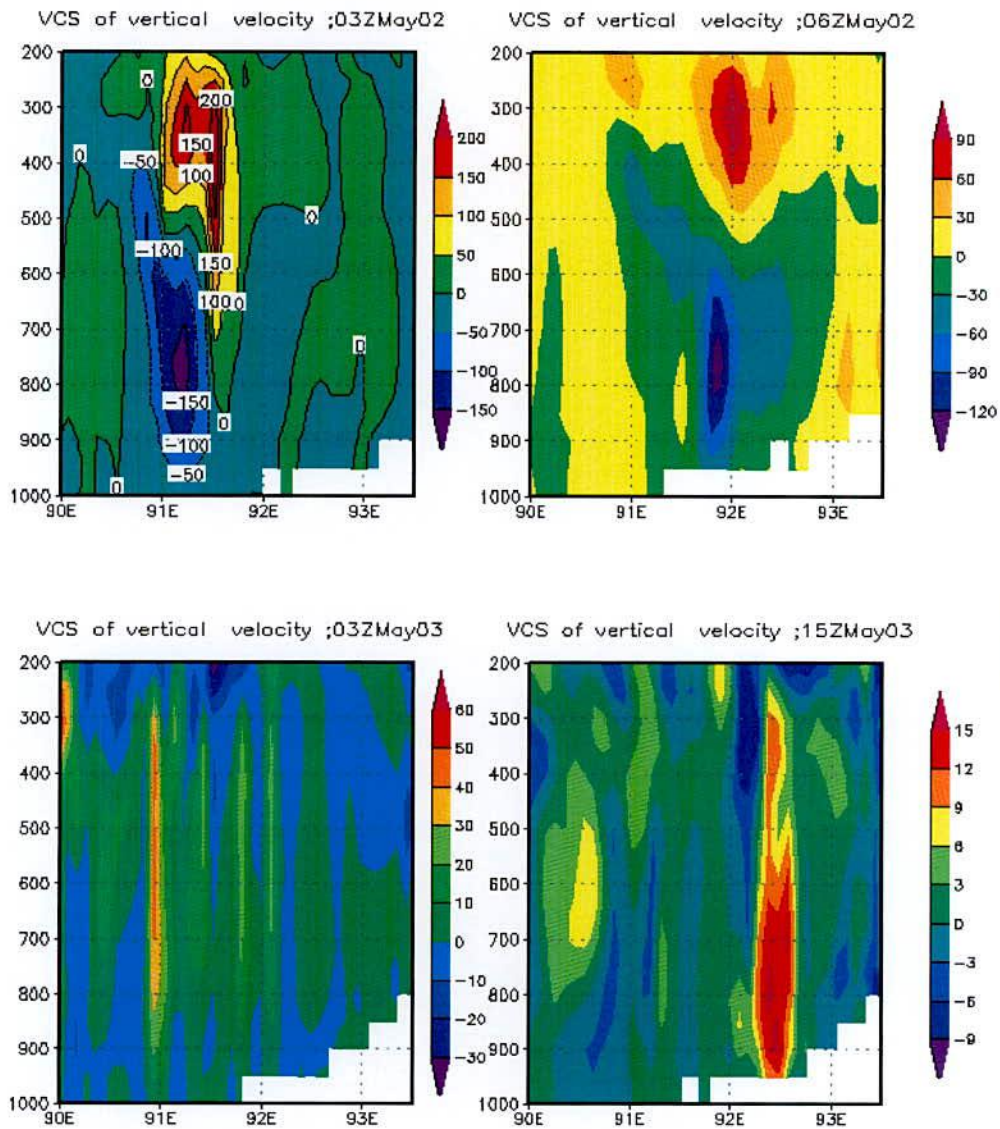


Figure 4.3.5.1b: WRF Model simulated vertical structure of vertical velocity (cm/s) along the center for different times.

4.3.7 Vertical Structure of Relative Vorticity

To understand the vertical structure of the convective system, the vertical profiles of relative vorticity obtained from MM5 and WRF models are plotted through the centre of the most developed cloud at different times and are shown in Figures 4.3.7.1a and 4.3.7.1b. For MM5 model, figures are plotted at 06 and 09 UTC on 02 May and at 06 and 12 UTC on 03 May 2009. But for WRF model, figures are plotted at time for 03 and 06 UTC on 02 May, and 03 and 15 UTC on 03 May 2009.

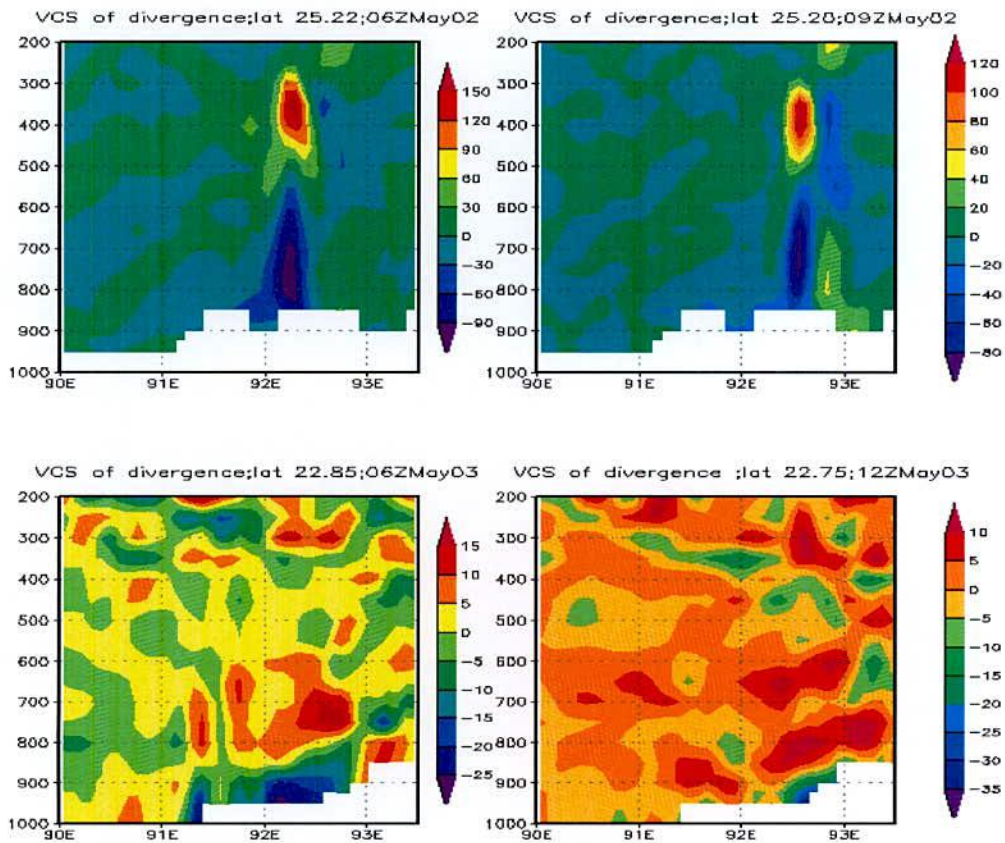


Figure 4.3.6.1a: MM5 Model simulated vertical structure of divergence (unit: $\times 10^{-5} \text{ s}^{-1}$) along the center of most developed cloud at time different times.

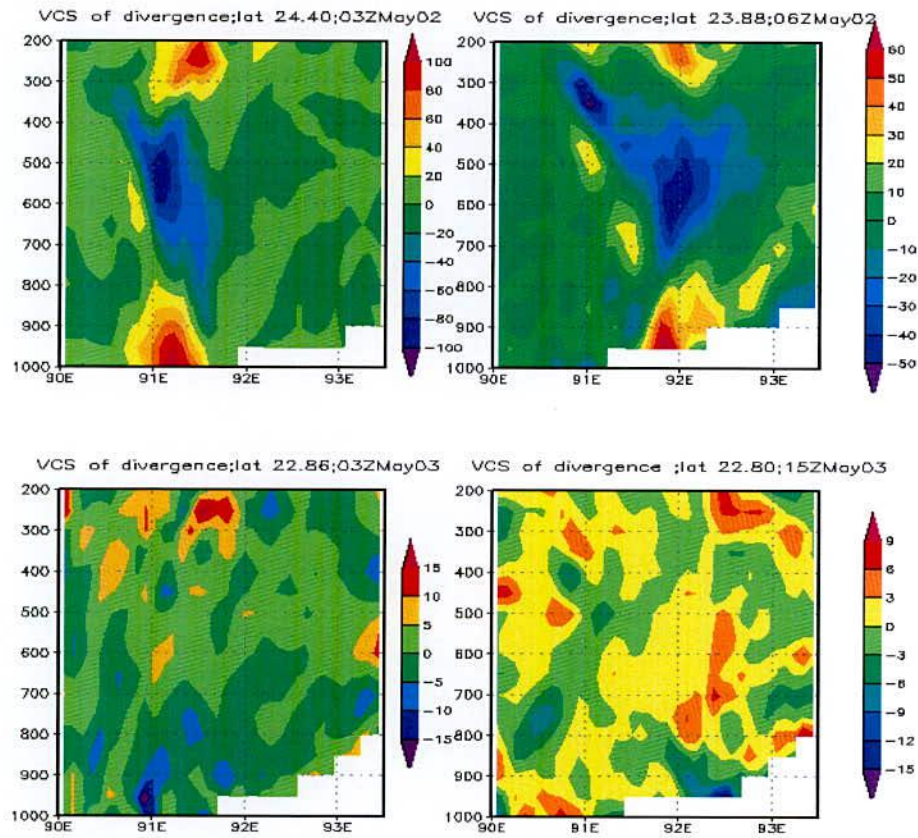


Figure 4.3.6.1b: WRF Model simulated vertical structure of divergence (unit: $\times 10^{-5} \text{s}^{-1}$) along the center of most developed cloud at time different times.

In the figures, strong positive vorticity is observed up to 400 hPa level with decreasing values in magnitude. There are some variations of the magnitude of maximum vorticity at different levels at different times. These values are $(20\sim 60) \times 10^{-5} \text{s}^{-1}$ and $(20\sim 150) \times 10^{-5} \text{s}^{-1}$ for MM5 and WRF models respectively. It is noted that positive vorticity indicates the cyclonic motion in the lower level. Negative vorticity are also observed in the upper levels and far from the center of the convective system. These values are $(20 \sim 50) \times 10^{-5} \text{s}^{-1}$ and $(20 \sim 50) \times 10^{-5} \text{s}^{-1}$ for MM5 and WRF model respectively. This negative vorticity indicates the anticyclonic motion in the upper levels. Some negative vorticity is observed at lower level far from the centre. So, low level positive vorticity indicates the convective activity of the system due to warm westerly wind from India land mass and moist SW'ly wind from the Bay of Bengal.

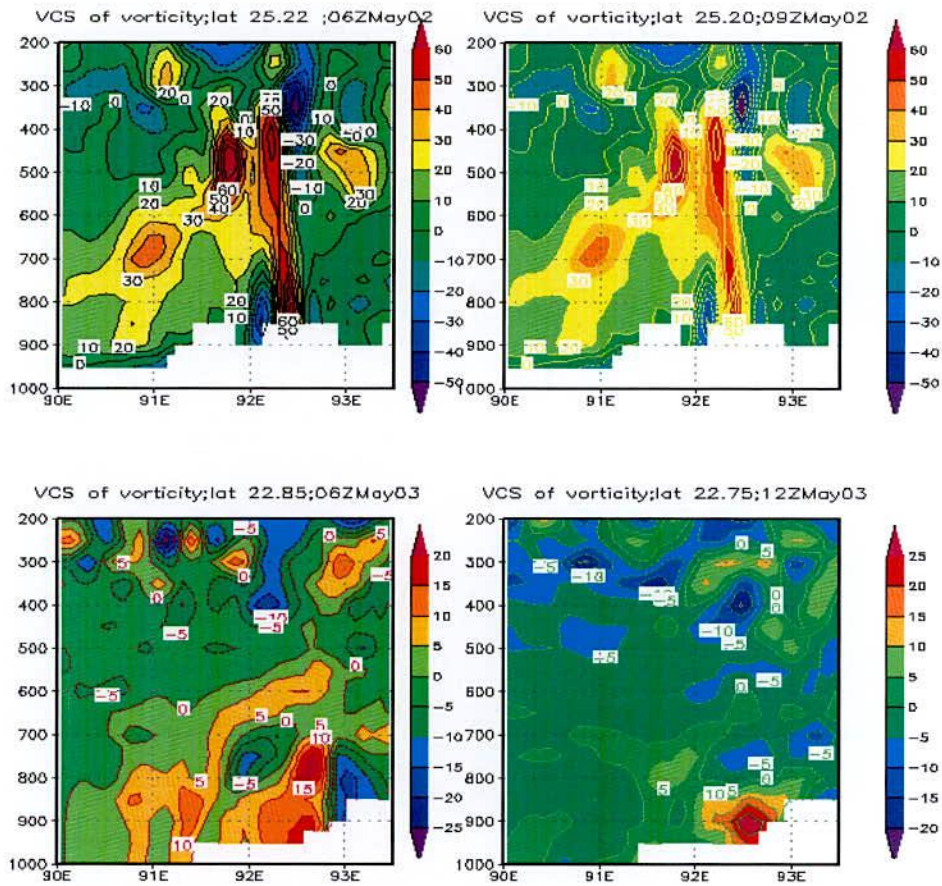


Figure 4.3.7.1a: MM5 Model simulated vertical structure of relative vorticity ($\times 10^{-5} \text{ s}^{-1}$) along the center of most developed cloud at different times.

4.3.8 Vertical Structure of Relative Humidity

To understand the vertical structure of the convective system, the vertical profiles of relative humidity obtained from MM5 and WRF models are plotted through the centre of the most developed cloud at different time and are shown in Figures 4.3.5.1a and 4.3.5.1b. For MM5 model, figures are plotted at 06 and 09 UTC on 02 May and 06 and 12 UTC on 03 May 2009. But for WRF model, figures are plotted at time for 03 and 06 UTC on 02 May and 03 and 15 UTC on 03 May 2009.

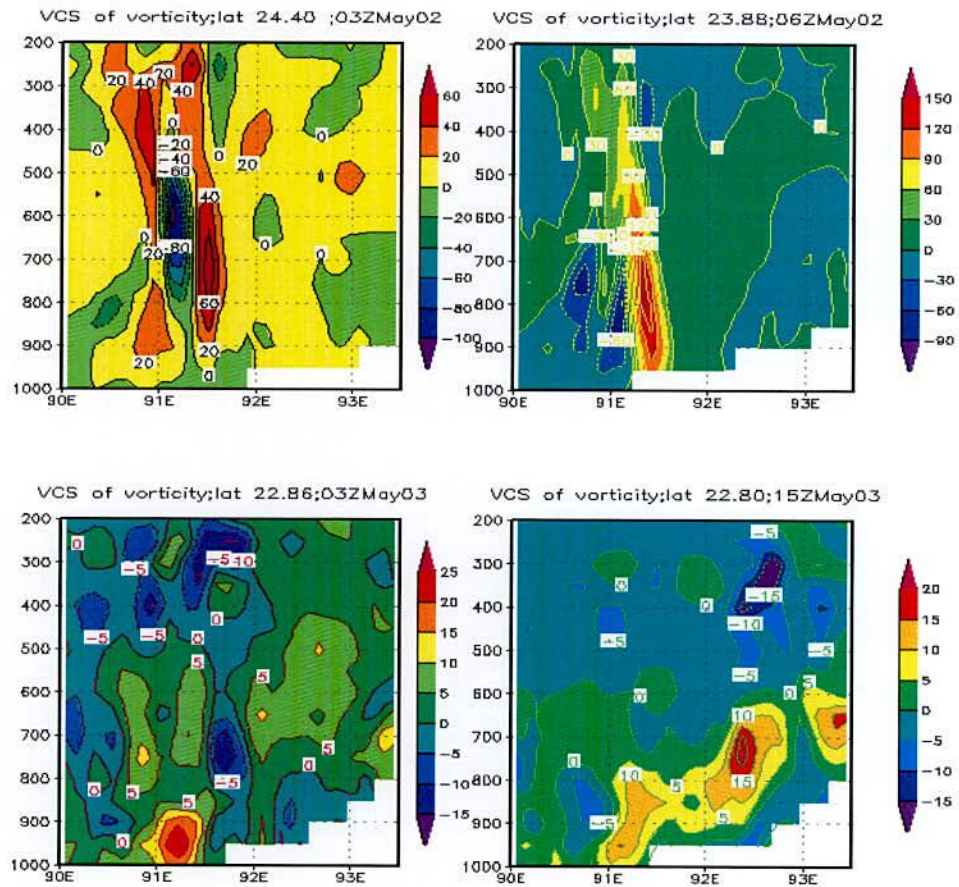


Figure 4.3.7.1b: WRF Model simulated vertical structure of relative vorticity ($\times 10^{-5} \text{ s}^{-1}$) along the center of most developed cloud at different times.

It is noted that high relative humidity (more than 90%) spreads in outer range of eye wall up to 300 hPa level or more and 400 hPa level or more for MM5 and WRF models respectively. High relative humidity is also seen up to 200 hPa level with lower magnitude. Due to the presence of hill at the right side of the center of convective state, amount of relative humidity increases at the right side of the centre. Convergence occurs at the foot of the hill because SW'ly wind carries moisture from the Arabian Sea and westerly carries heat from the land mass of India respectively. These high magnitudes of vertical profile of humidity satisfy the development of the convective activity of the system.

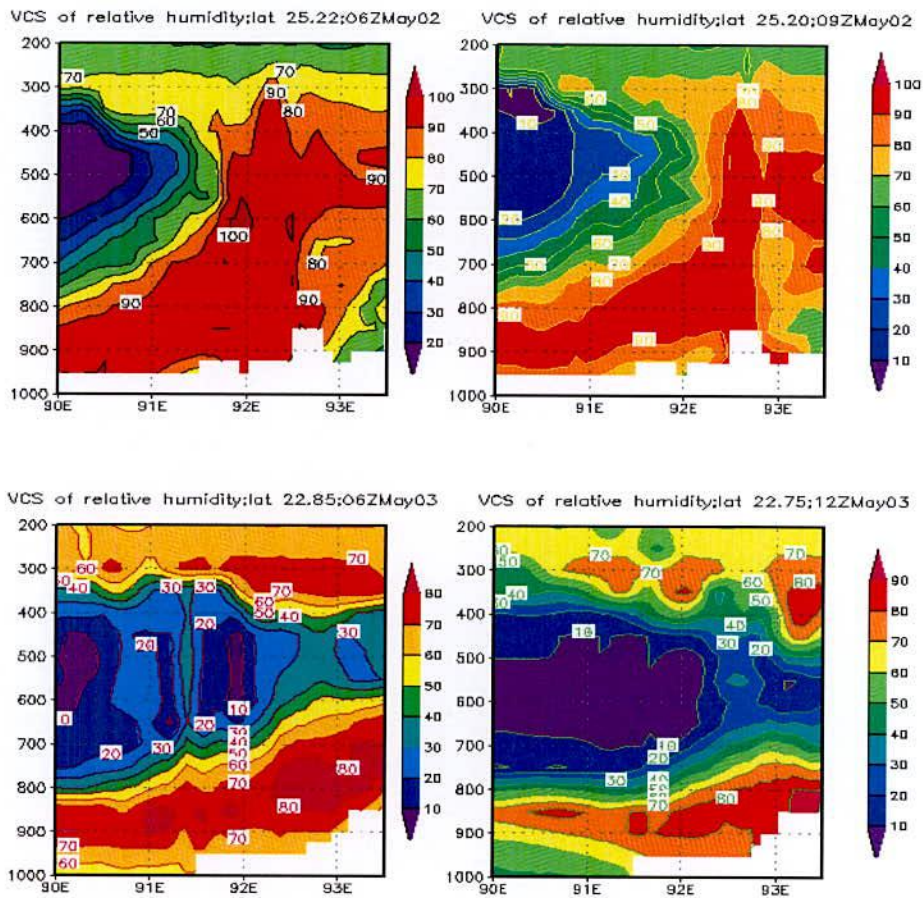


Figure 4.3.8.1a: MM5 Model simulated vertical structure of relative humidity (%) along the center of most developed cloud at different times.

4.3.9 Vertical Structure of Mixing Ratio

To understand the vertical structure of the convective system, the vertical profiles of mixing ratio obtained from MM5 and WRF models are plotted through the centre of the most developed cloud at different times and are shown in Figures 4.3.9.1a and 4.3.9.1b. For MM5 model, figures are plotted at 06 and 09 UTC on 02 May and at 06 and 12 UTC on 03 May 2009. But for WRF model, figures are plotted at 03 and 06 UTC on 02 May and at 03 and 15 UTC on 03 May 2009.

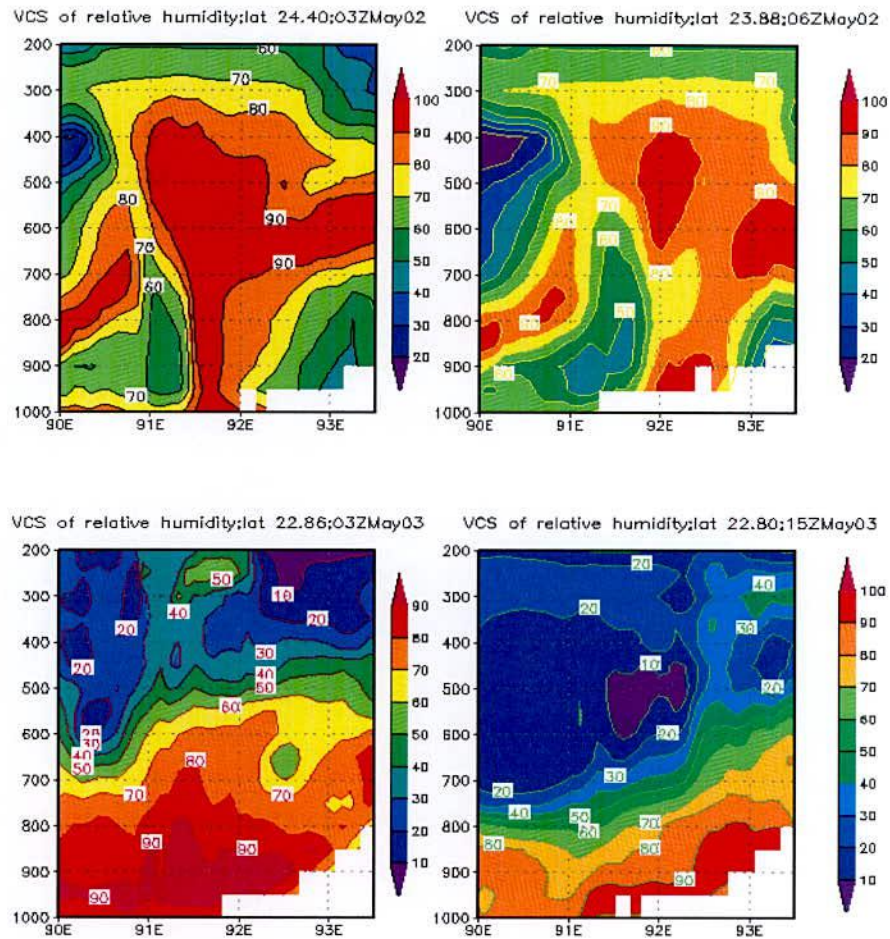


Figure 4.3.8.1b: MM5 Model simulated vertical structure of relative humidity (%) along the center of most developed cloud at different times.

Mixing ratio is absent in the lower levels at all observed times because of hilly surface area at high altitude with low pressure. It shows that the highest moisture content around 1.8 g/kg or more is found at the centre of the convective system at or above 950 hPa level then it decreases upwards to 350 hPa level or more. It is to be noted that the high moisture flux comes from the southern side covering a large area of the Bay of Bengal, which feeds the system along its southeastern side through the boundary layer. A noticeable amount of moisture flux also comes from the south-western side through the Indian sub-continent, which feeds the system along its south-western side through the boundary layer.



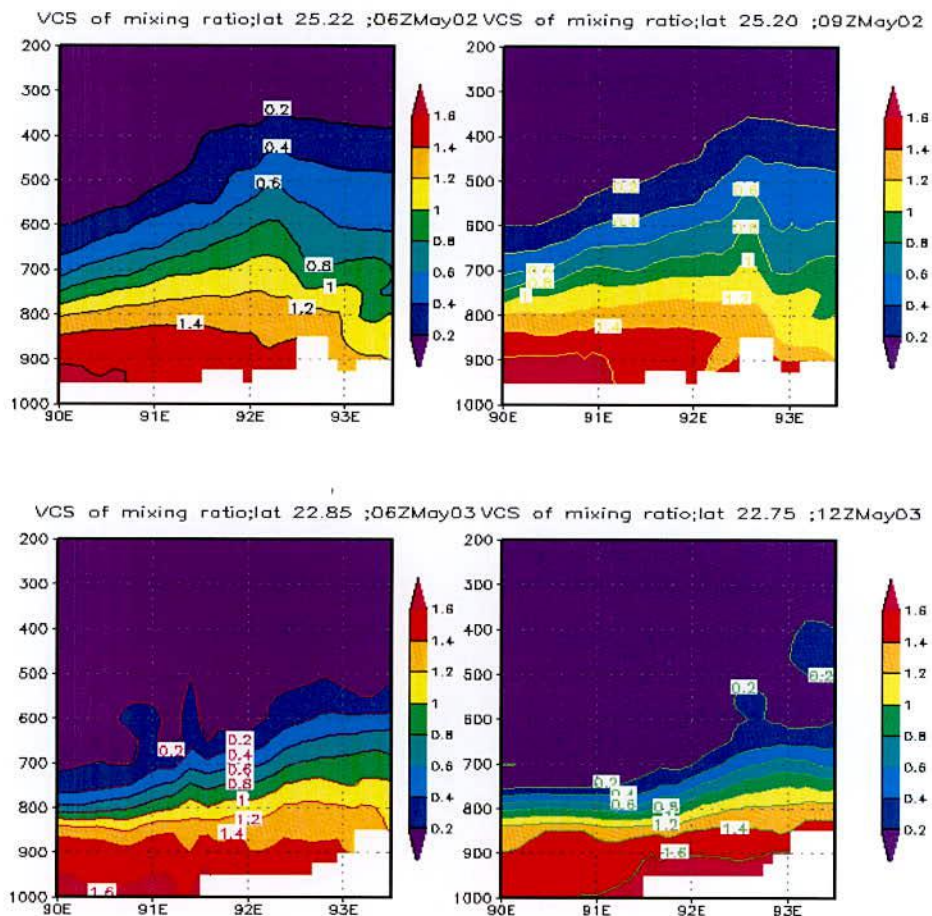


Figure 4.3.9.1a: MM5 Model simulated vertical structure of mixing ratio (g/kg) along the center of most developed cloud at different times.

Figures obtained from both the models show that water vapor mixing ratio is absent in the lower levels at all observed time because of hilly surface area at high altitude with low pressure. The maximum amount of moisture content more than around 1.8 g/kg or more is found at the centre of the convective system at 950 hPa levels, then it decreases upwards up to 400 hPa level or more. It is noted that the high moisture flux comes from the southern side covering a large area of the Bay of Bengal, which feeds the system along its southeastern side through the boundary layer. A noticeable amount of heat flux also comes from the Indian land mass, which helps to develop the convective activity.

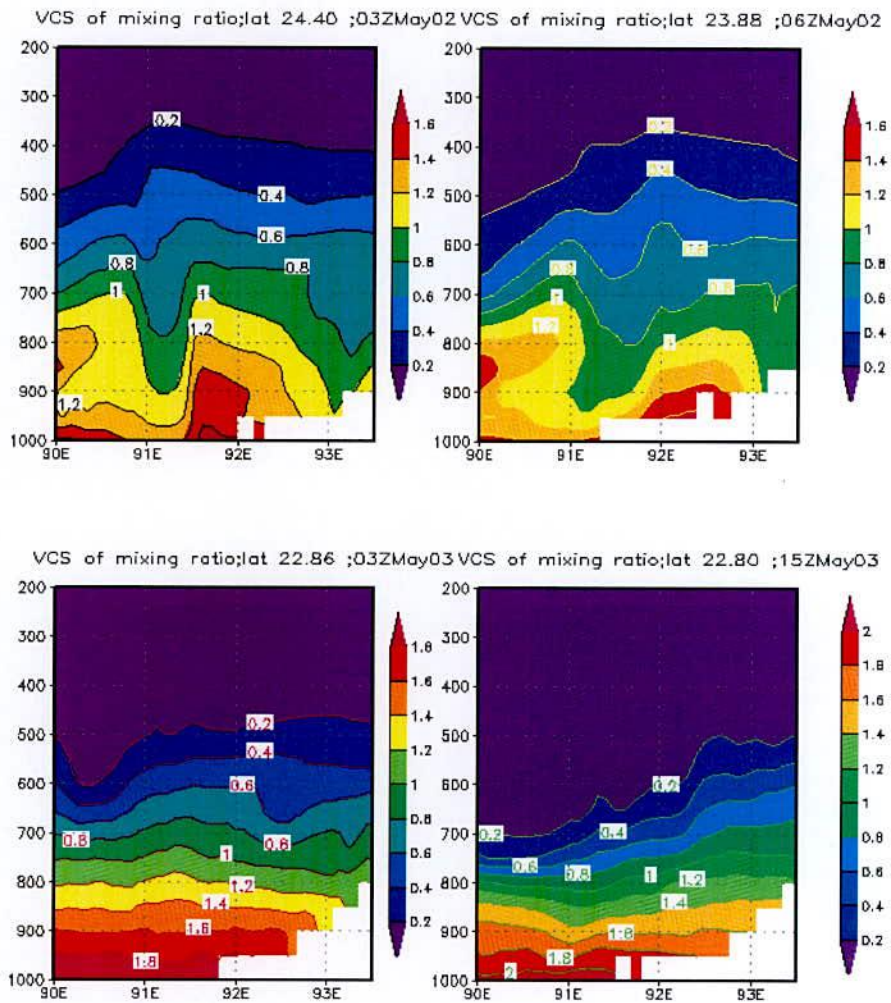


Figure 4.3.9.1b: WRF Model simulated vertical structure of mixing ratio (g/kg^2) along the center of most developed cloud at different times.

4.4: Summary of Rainfall Events

For the heavy precipitation events MSLP, wind with rain, wind with humidity, rainfall and vertical structure of vertical velocity, divergence, relative vorticity, relative humidity (RH) and mixing ratio has been analyzed to understand the convective activity of the precipitation system by both the models.

MSLP simulated by MM5 and WRF models for all the heavy precipitation events are also same. Low pressure systems persist during the simulation period and satisfy the environment for convection. Southwesterly wind is the carrier of moisture from the Bay of Bengal and westerly in association with heat help the development of convective system. RH at 850 hPa levels is always equal or more than 90%. Cyclonic and anti-cyclonic circulations are simulated in all cases by both of the models at 850 and 200 hPa levels respectively. For heavy convective systems (June 07 and July 08) cyclonic circulation are also observed at 500 hPa where for the weak convective system (May 09) anti-cyclonic circulation is simulated by both of models. So, both of the modes can simulate synoptic features clearly and fairly.

Vertical structure of RH, mixing ratio, divergence, vorticity and vertical velocity simulated by both of the models are also consistence with the formation of convection. Both of the models can simulate the features well.

For calculating 24 hours accumulated rainfall over Bangladesh and its surrounding areas, three domains D1, D2 and D3 are used with resolutions 90 km, 30 km and 10 km respectively. The Models (MM5 and WRF) simulated 24 hours accumulated rainfall over Bangladesh and its surrounding areas are tabulated in the Table 4.4.1-4.4.3 with rainfall obtained from TRMM and rain-gauge data. Amount of precipitation simulated by both of the models are comparable with TRMM and Rain Gauge observational data with spatial and temporal variation. For different resolutions of the domains, amount of rainfall are different for different domains. For increasing the resolution of the grid size rainfall obtained from WRF Model is also increased. Simulations of rainfalls are almost same for the two models. KF CP with MRF PBL in MM5 and YSU PBL in WRF Model can simulate the convective features fairly well.

Table 4.4.1 Rainfall for 09-11 June, 2007

| Date | MM5 model | | | WRF Model | | | TRMM | rain-gauge |
|---------|-----------|-----|-----|-----------|-----|-----|------|------------|
| | D1 | D2 | D3 | D1 | D2 | D3 | | |
| 09 June | 80 | 140 | 180 | 160 | 240 | 180 | 180 | 263 |
| 10 June | 110 | 140 | 240 | 180 | 270 | 300 | 350 | 195 |
| 11 June | 240 | 330 | 220 | 80 | 140 | 270 | 350 | 425 |

Table 4.4.2 Rainfall for 01-03 July, 2008

| Date | rainfall obtained from MM5 model (cm) | | | WRF Model | | | TRMM | rain-gauge |
|---------|---------------------------------------|-----|-----|-----------|-----|-----|------|------------|
| | D1 | D2 | D3 | D1 | D2 | D3 | | |
| 01 July | 110 | 140 | 160 | 80 | 12 | 180 | 18 | 171 |
| 02 July | 140 | 160 | 200 | 110 | 180 | 240 | 60 | 367 |
| 03 July | 160 | 240 | 270 | 180 | 330 | 400 | 55 | 179 |

Table 4.4.3: Rainfall for 01-03 May 2009

| Date | MM5 model | | | WRF Model | | | TRMM | rain-gauge |
|--------|-----------|-----|-----|-----------|-----|-----|------|------------|
| | D1 | D2 | D3 | D1 | D2 | D3 | | |
| 01 May | 100 | 200 | 140 | 100 | 160 | 240 | 240 | 93 |
| 02 May | 110 | 160 | 220 | 50 | 80 | 100 | 1440 | 81 |
| 03 May | 30 | 45 | 90 | 22 | 33 | 55 | 130 | 62 |

CHAPTER 5
SIMULATION OF TROPICAL CYCLONE
EVENTS USING MM5 AND WRF MODELS

5.1 Simulation of Tropical Cyclone (TC) Sidr using WRF and MM5 Model

To analyze the evolution and structure of TC Sidr, the MM5 model was run for 96 hrs with the initial field at 00 UTC of 12 November 2007. But after 84 hrs of simulation at 12 UTC of 15 November 2007, the system attained at the state of highest intensity. Again, the WRF model was run for 96 hrs with the initial field at 00 UTC of 13 November 2007. After 72 hrs of simulation at 00 UTC of 16 November 2007 the system attained at the state of highest intensity. Different meteorological parameters obtained from both the models are discussed for the evolution and structure of the TC Sidr in the following sub-section. Model simulated results are compared with available data obtained from Joint Typhoon Warning Centre (JTWC).

5.1.1 Pressure Field

Minimum sea level pressure (MSLP) of a TC is of great importance as it helps to measure the intensity of a TC. Since TCs develop over vast oceanic areas, where observations are sparse or not available, it is of great difficulty to make any validation of model simulated MSLP with real observable data from sea before the landfall. But now meteorologists are able to estimate MSLP and maximum sustained wind (MSW) using interpretations of satellite products. MM5 and WRF Model simulated and observed MSLPs of TC Sidr starting from 00 UTC of 13 November 2007 is presented as in Figure 5.1.1.1. It appears from the Figure 5.1.1.1 that the MM5 model simulated MSLP gradually drops (without any oscillation) with time and attains peak intensity with minimum pressure 961 hPa at 00 UTC of 15 November 2007 and thereafter MSLP increases gradually. Finally just before the landfall the MSLP is 966 hPa at 12 UTC of 15 November 2007. Again, WRF model simulated MSLP gradually drops (having little bit oscillation) with time and attains peak intensity with minimum pressure 977 hPa at 03, 15 and 18 UTC on 15 November 2007 and thereafter MSLP increases gradually. Finally just before the landfall the MSLP is 987 hPa at 00 UTC of 16 November 2007. On the other hand, the observed MSLP 918 hPa is obtained at 18 UTC of 14 November and remain same up to 06 UTC of 15 November 2007 and thereafter MSLP increases gradually. Landfall of the system occurs at 12 UTC of 15 November with observed value of MSLP 926 hPa. It is noted that landfall time obtained from MM5 model simulated is same to that of observed cases with different MSLP but landfall time obtained from WRF model is different to observed time with different value of MSLP. The variation of model simulated MSLP compare to that of observed with time shows that both the models simulate realistic temporal variation of MSLP but simulated values are higher than observed values.

The distribution of sea level pressures (SLP) for the TC Sidr at 00 UTC of 13, 14, 15 November and 12 UTC of 15 November 2007 (i.e. before landfall) for MM5 model and at 00

UTC of 13, 14, 15 and 16 November 2007 (i.e. before landfall) for WRF model have been shown in Figures 5.1.1.2a and 5.1.1.2b. Figure demonstrate that the intensity of the TC increases as the MSLP drops with time up to its peak intensity and TC changes its position with time. The isobar has circular arrangement around the TC centre with some asymmetric features in the outer periphery. The contour interval is different in magnitude or different position because of different intensity of the system. At mature stage the contour intervals are 5 and 3 hPa obtained from MM5 and WRF model respectively. Using MM5 model, the lowest simulated 961 hPa and observed by JTWC 926 hPa MSLPs are obtained at 00 UTC of 15 November and 18 UTC of 14 November 2007 (Figures 5.1.1.1 and 5.1.1.2a) respectively. But just before the landfall at 12 UTC of 15 November 2007 simulated and observed MSLPs are 966 hPa and 926 hPa respectively. At this stage, considering the outermost closed isobar, the system's horizontal size is estimated as 8.0° in the east west and 9.5° in the north-south direction demonstrating a little bit spatial asymmetry in its horizontal structure. Again, using WRF model, the lowest simulated minimum central pressure (MCP) (977 hPa) at the centre of the eye of the TC Sidr is found at 03 UTC of 15 November 2007 (Figure 5.1.2.1.2). But at 00 UTC of 16 November 2007 the simulated MCP of the centre is 987 hPa. At this stage, considering the outermost closed isobar, the system's horizontal size is estimated as 5.0° in the east west direction and 7.5° in the north-south demonstrating a spatial asymmetry in its horizontal structure.

The distribution of the SLP of the TC Sidr along east-west cross section passing through its centre at (20.541°N and 90.734°E) at time 12 UTC of 15 November 2007 for MM5 and through its centre at (21.462°N and 89.453°E) at time 00 UTC of 16 November 2007 have been shown in Figures 5.1.1.3a and 5.1.1.3b respectively. The figures demonstrate the moderate pressure gradient around the centre with maximum gradient at around 15-20 km from the centre for both the models. Thus the radius of the TC eye is found to be below 15 km according to the simulation from both the models.

5.1.2 Wind Fields

Maximum wind speed (MWS) directly devastates the affected area at the time of landfall. On the other hand it is the most active driving force for generating storm surge over the area of landfall. So, it is the most important parameter of TC for measuring its intensity. Now a days, spaced based satellite technology is doing a great job to estimate MWS and other important meteorological parameters because in-situ observations are not widely available over the ocean to determine or to estimate the intensity of the system.

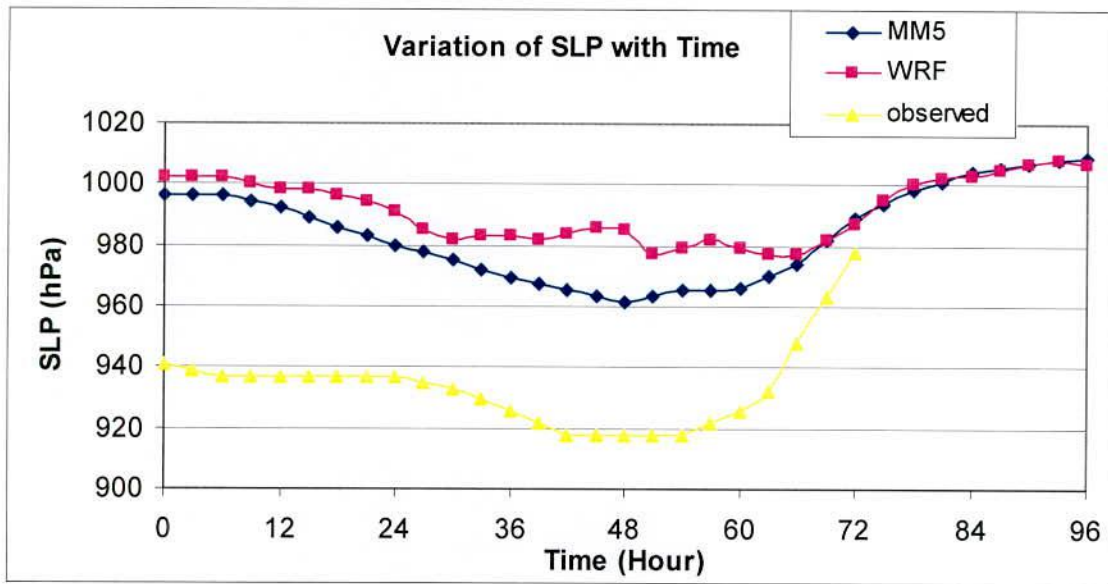


Figure 5.1.1.1: Evolution of MM5 and WRF model simulated and observed minimum central pressure of the eye of the TC Sidr with time.

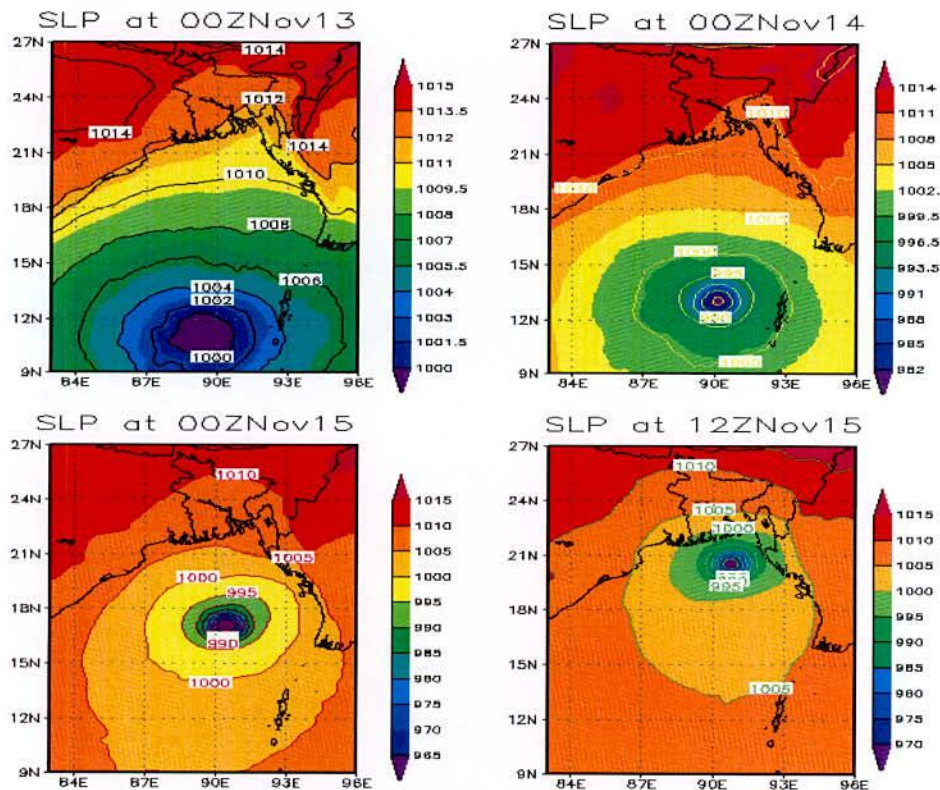


Figure 5.1.1.2a: MM5 Model simulated SLP of TC Sidr at 00 UTC of 13, 14, 15 and 12 UTC of 15 November 2007.

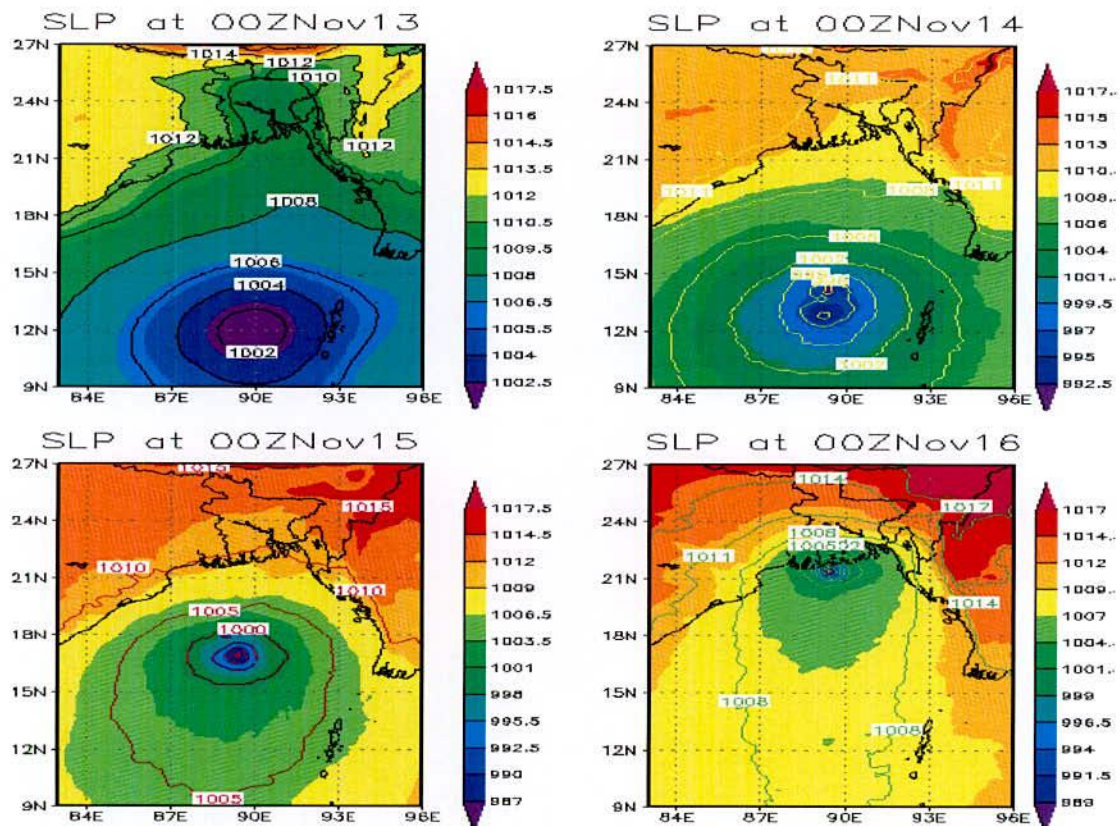


Figure 5.1.1.2b: WRF Model simulated SLP of TC Sidr at 00 UTC of 13, 14, 15 and 16 November 2007

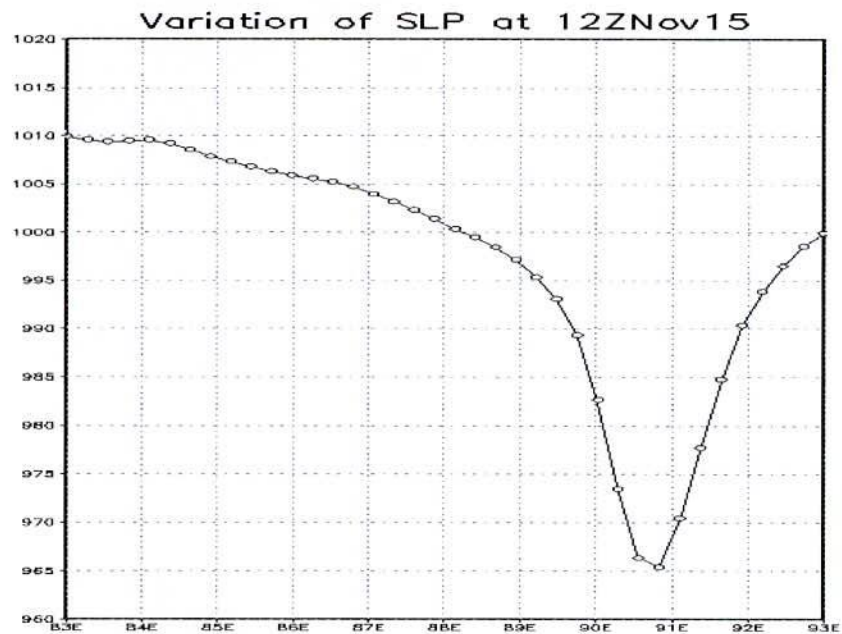


Figure 5.1.1.3a: East West cross sectional view of simulated SLP of TC Sidr obtained from MM5 model through the centre (21.463°N 89.453°E) at 12 UTC of 15 November 2007.

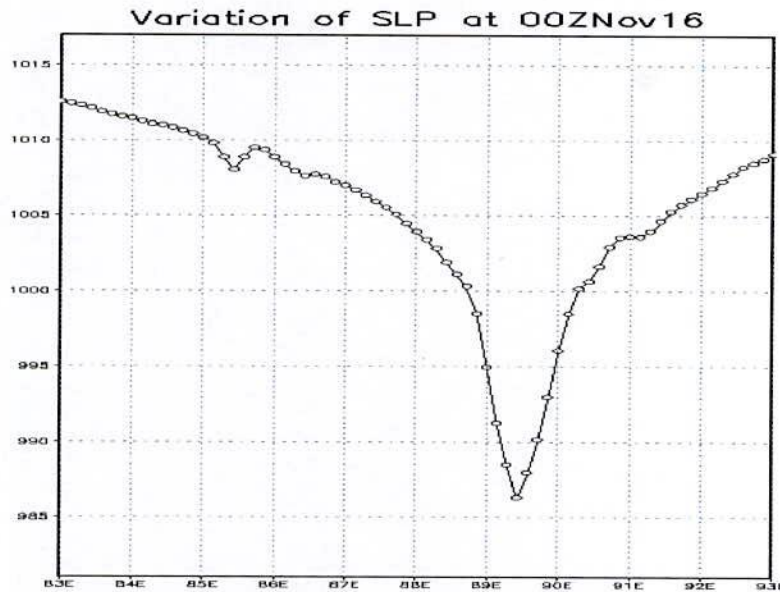


Figure 5.1.2.3b: East West cross sectional view of simulated SLP of TC Sidr obtained from MM5 model through its centre (21.463°N and 89.453°E) at 00 UTC of 16 November 2007.

Figure 5.1.2.1 shows the temporal variations of MM5 and WRF model simulated MWS and observed winds of TC Sidr. The model simulated MWS are obtained at the standard meteorological height of 10 m. The model simulated MWS obtained from MM5 are lower than the observed values all through the simulated time except for the landfall time when the simulated values are almost matched with that observed value. Again, the model simulated MWS obtained from WRF are higher than the observed values all through the simulated time. The simulated highest MWS is obtained at 00 UTC on 15 November for MM5 model and at 18 UTC of 15 November for WRF where as that for observed is obtained at 18 UTC of 14 November 2007 retains this value up to 18 UTC on 15 November 2007.

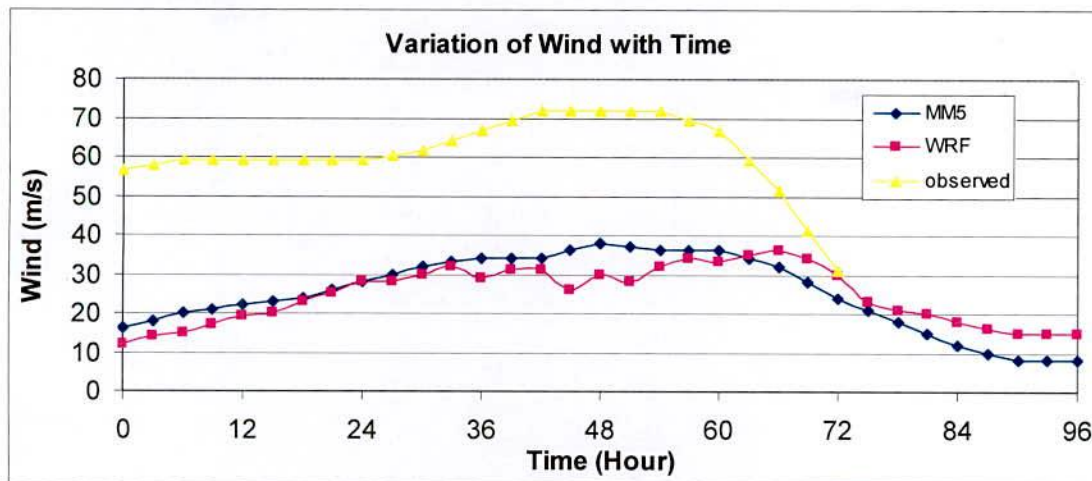


Figure 5.1.2.1: Observed and MM5 and WRF model simulated wind speed (m/s) of TC Sidr with time.

.The distribution of surface (10 m) wind for the TC Sidr at 00 UTC on 13, 14, 15 November and 12 UTC on 15 November 2007 (i.e. before landfall) for MM5 model and at 00 UTC on 13, 14, 15 and 16 November 2007 (i.e. before landfall) for WRF model have been shown in Figures 5.1.2.2a and 5.1.2.2b. Figures show that the wind field of the TC is highly asymmetric in the horizontal distribution. The distribution of surface wind of Sidr for both the models at 00 UTC on 13 November 2007 (i.e. at the initial time of simulation) is shown in Figures 5.1.2.2a and 5.1.2.2b when the TC was in the sea. Figures show that the pattern has an asymmetric wind distribution with strong wind bands in the front left and right sides, close to the centre of north directed moving storm. The wind flow in the core region shows a near circular feature with minimum wind speed at the centre. Maximum speed at this time is 16 and 12 m/s for the MM5 and WRF models respectively. At 00 UTC on 14 and 15 November 2007, TC is organized with strong wind band around and the wind flow in the core region shows asymmetric feature with minimum wind at the centre. Maximum winds at these stages are 27 and 35 m/s for MM5 model and 27 and 30 m/s for WRF model.

For MM5 model, at 15 UTC on 15 November 2007 (i.e. just before the landfall), a strong wind band (wind speed > 30 m/s) having strongest wind exceeding 35 m/s is found around the system centre. It may be noted that the model has generated lower winds of 36 m/s (130 km/hr) than the observed winds of around 140 km/hr but just before landfall (i.e. at 15 UTC on 15 November 2007) both simulated and observed winds are close to each other. Figure 5.1.2.2 shows the landfall feature of surface wind distribution where the winds is much less in the front side compared to other of the cyclonic system. It is due to frictional force of landmass. Similar feature is seen for WRF model at 00 UTC on 16 November 2007 but the maximum wind speed obtained from WRF model is smaller than that of MM5 model.

The distribution of the surface wind of the TC Sidr along east-west cross section passing through its centre (20.541°N) at 12 UTC on 15 November 2007 for MM5 model and at centre (21.462°N and 89.453°E) at 00 UTC on 16 November 2007 for WRF model are shown in Figures 5.1.2.3a and 5.1.2.3b. Figures demonstrate that a calm region is found inside the eye of the system and maximum wind is found in the eye wall. The radius of maximum wind of the TC Sidr is found to be just lower than 70 km/hr according to the simulation.

The horizontal distribution of vector and magnitude of the wind field for 850, 500, 300 and 200 hPa at 12 UTC on 15 November 2007 (i.e. before landfall) for MM5 and 00 UTC on 15 November 2007 (i.e. before landfall) have shown in Figures 5.1.2.4a and 5.1.2.4b respectively.

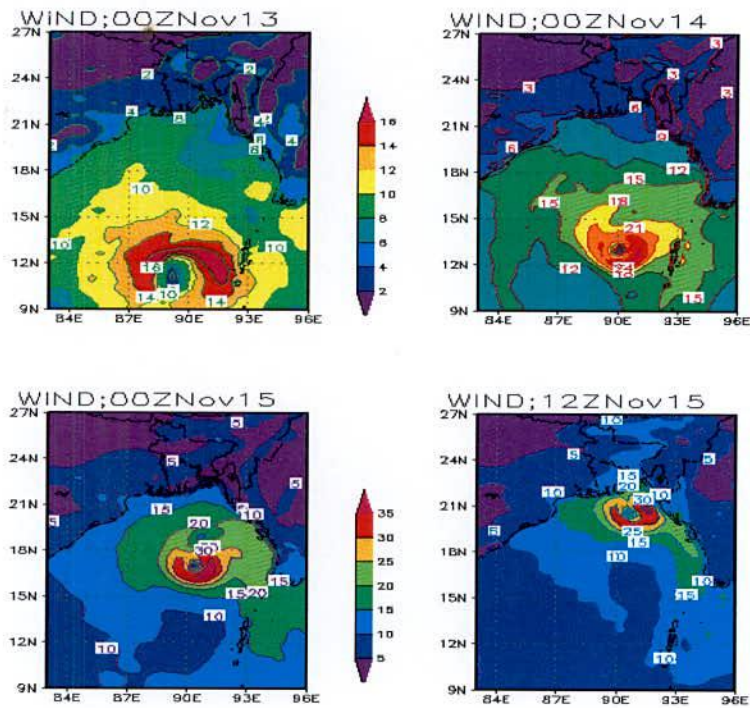


Figure 5.1.2.2a: MM5 model simulated Wind speed (m/s) at 00Z on 13, 14, 15 November and 12 UTC on 15 November 2007 of TC Sidr at 10m.

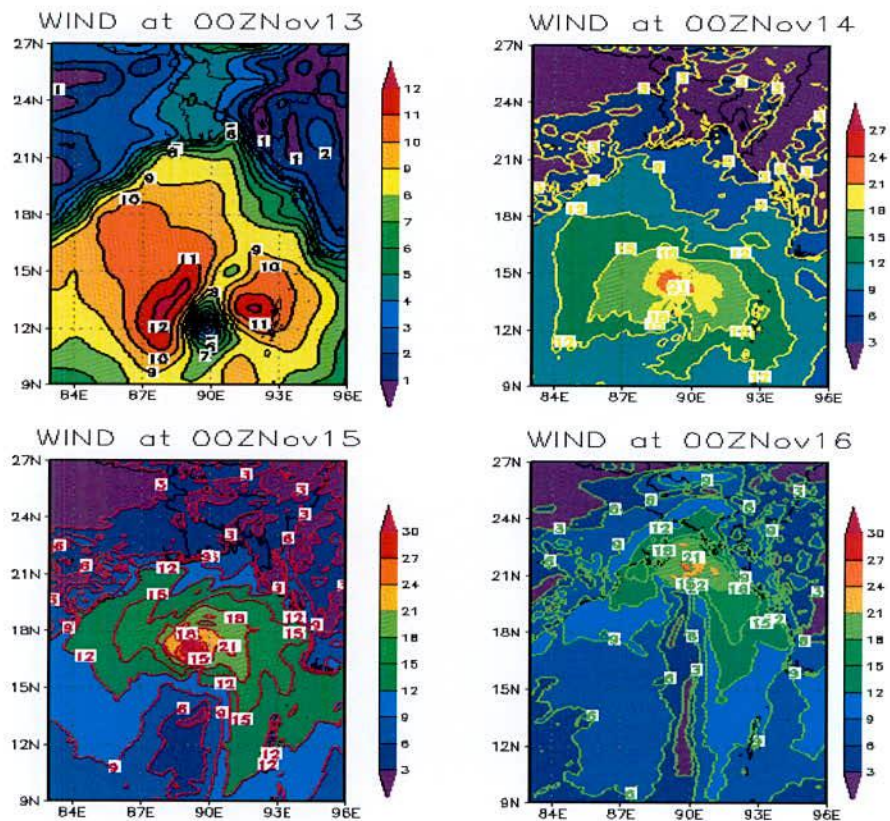


Figure 5.1.2.2b: WRF model simulated Wind speed (m/s) at 00Z on 13, 14, 15 and 16 November 2007 of TC Sidr at 10m.

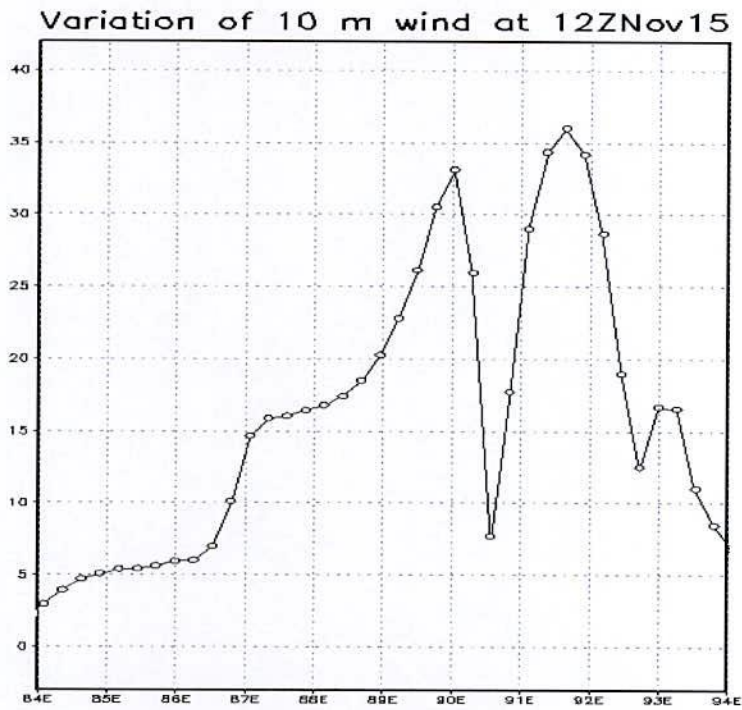


Figure 5.1.2.3a: East West cross sectional view of MM5 model simulated wind speed (m/s) of TC Sidr along the centre (20.541°N) at 12 UTC on 15 November 2007.

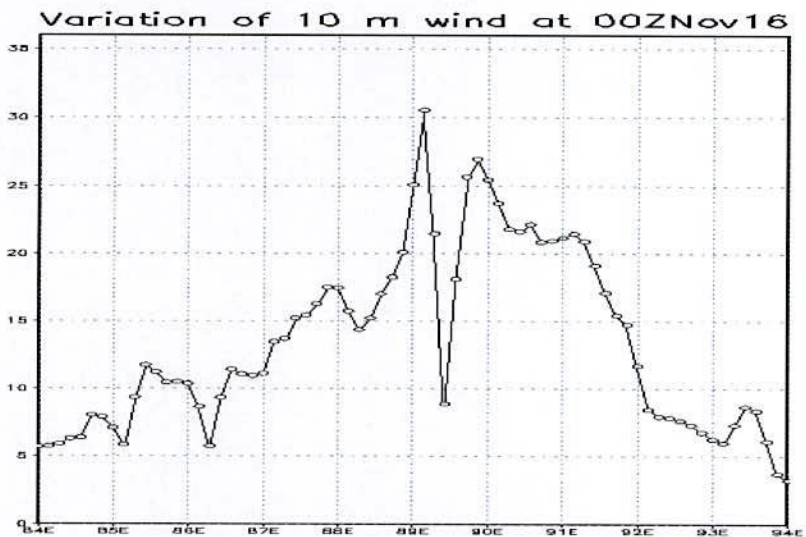


Figure 5.1.2.3b: East-West cross sectional view of WRF model simulated wind speed (m/s) of TC Sidr along its centre (21.462°N) at 00 UTC on 16 November 2007.

Figures show that a well organized cyclonic circulation with strong winds encircling the centre is found at 850 and 500 hPa levels. At 300 hPa wind shows little bit cyclonic circulation in the right side of the TC and weak outflow in the left side. At 200 hPa level strong outflow is evident from the central part of the TC except at 00 UTC on 13 November

2007 (i.e. at initial time not shown in figure). Model derived maximum winds obtained from MM5 and WRF models for different times are tabulated in Table 5.1.2.4a and 5.1.2.4b respectively. MM5 model derived maximum winds obtained just before landfall (12 UTC of 15 November 2007) are about 60, 50, 50 and 25 m/s at 850, 500, 300 and 200 hPa levels respectively. Again, WRF model derived maximum winds just before landfall (00 UTC of 16 November 2007) are about 50, 40, 30 and 20 m/s at 850, 500, 300 and 100 hPa levels respectively. Magnitude of wind obtained from WRF model is higher than that obtained from MM5 model. It is noted that the strong wind is confined to the right of the direction of the movement of the system. So, model derived results shown in Figures 5.1.2.4a and 5.1.2.4b satisfy the inflow in the lower levels and outflow in the upper levels.

Table 5.1.2.1a: MM5 model simulated wind speed (m/s) at 00 UTC of 13, 14, 15 and 16 November 2007 at different pressure levels of TC Sidr

| Pressure level (hPa) | Wind Speed (m/s) at | | | |
|-------------------------|-----------------------|-----------------------|-----------------------|-----------------------|
| | 00 UTC 13 November | 00 UTC 14 November | 00 UTC 15 November | 12 UTC 15 November |
| 850 | 20 | 40 | 60 | 60 |
| 500 | 20 | 30 | 50 | 50 |
| 300 | 40 | 40 | 40 | 50 |
| 200 | 50 | 60 | 50 | 50 |

Table 5.1.2.1b: WRF MM5 model simulated wind speed (m/s) at 00 UTC of 13, 14, 15 and 16 November 2007 at different pressure levels of TC Sidr

| Pressure level (hPa) | Wind Speed (m/s) at 00 UTC of | | | |
|-------------------------|-------------------------------|-------------|-------------|-------------|
| | 13 November | 14 November | 15 November | 16 November |
| 850 | 20 | 40 | 50 | 50 |
| 500 | 20 | 40 | 50 | 40 |
| 300 | 40 | 40 | 40 | 30 |
| 200 | 50 | 50 | 50 | 40 |

Figures 5.1.2.5a and 5.1.2.5b show the vertical profile of radial wind, tangential wind, vertical velocity and horizontal wind of the system at 12 UTC on 15 November 2007 (i.e. just before landfall) for MM5 model and 00 UTC on 16 November 2007 (i.e. just before landfall) for WRF model respectively. MM5 and WRF model simulated radial wind, tangential wind, vertical velocity and horizontal wind (cm/s) of TC Sidr at different times are tabulated in the Tables 5.1.2.5a and 5.1.2.5b respectively.

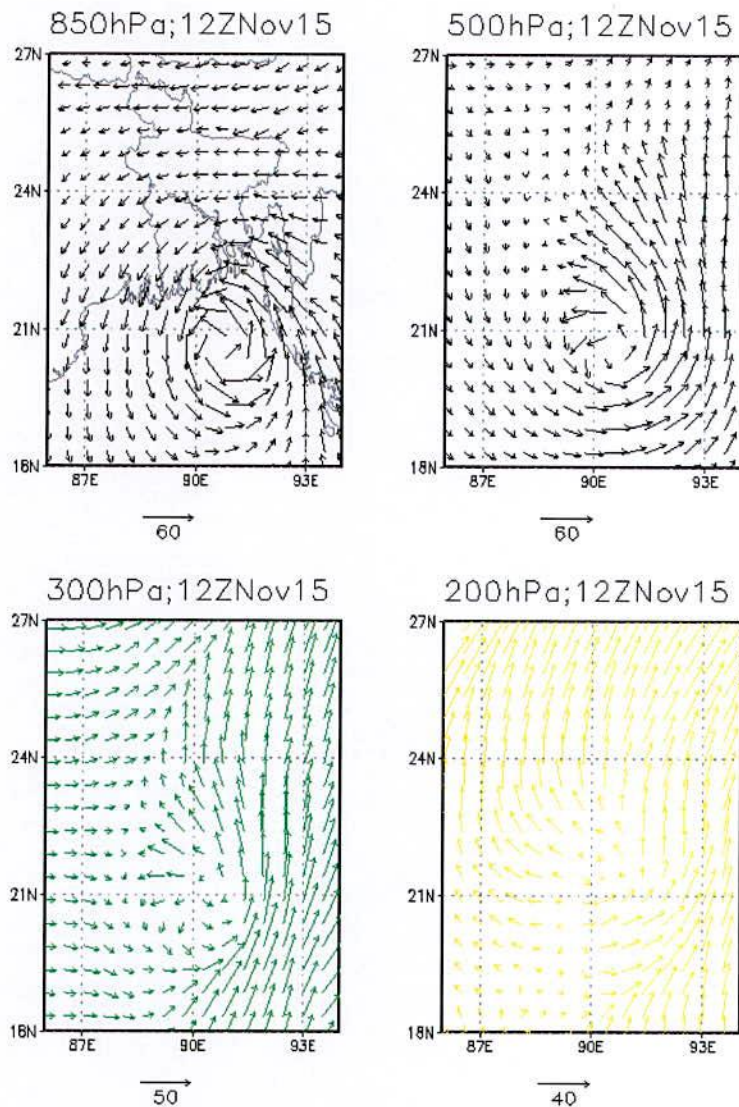


Figure 5.1.2.4a: MM5 Model simulated wind vector at 850, 500, 300 and 200 hPa level at 12 UTC on 15 November 2007.

The system is much more organized except at 00 UTC on 13 November, 2007 (i.e. at initial time; not shown in figure) and it also clearly show that the system has strong inflow in the lower level which bring the air to the system through the boundary level and lower level and outflow in the upper level.

Figures 5.1.2.5a and 5.1.2.5b demonstrate that the tangential wind flows towards northerly direction at the eastern side of the system and southerly direction at the western side. The strong wind with different speed (tabulated in Tables 5.1.2.5a and 5.1.2.5b) is confined to the different levels in the lower troposphere and extended up to 200 hPa level at right and left side of the system.

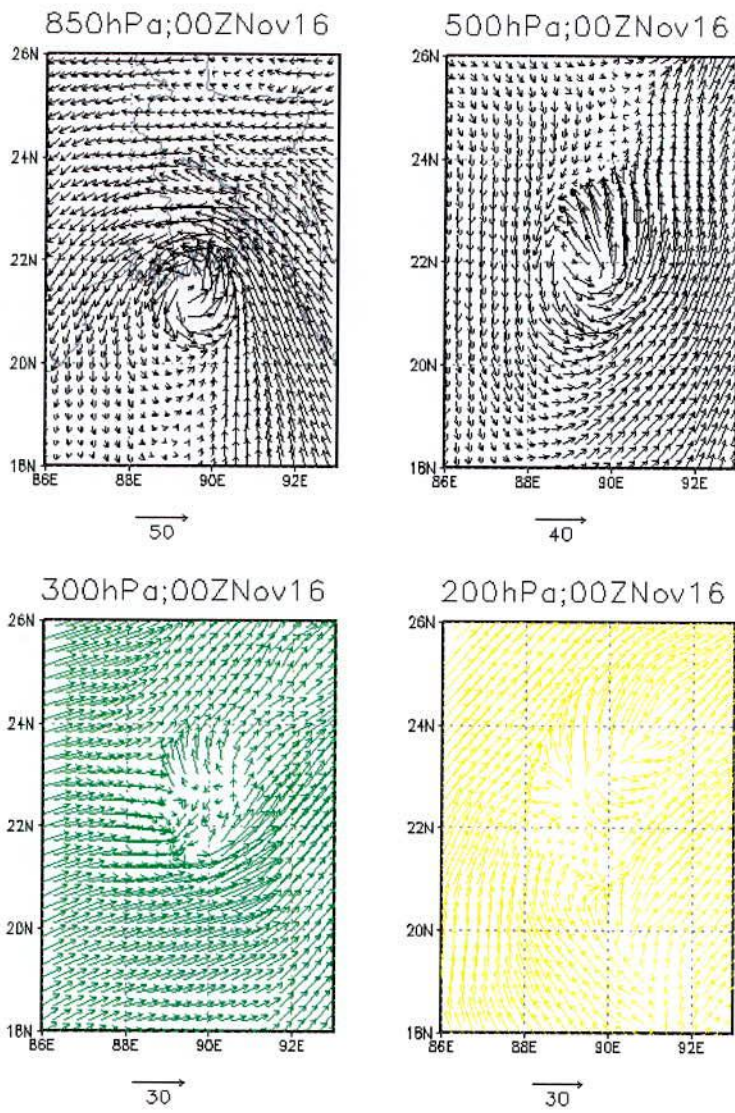


Figure 5.1.2.4b: WRF Model simulated wind vector at 850, 500, 300 and 200 hPa level a at 00 UTC on 16 November 2007.

From the Tables 5.1.25a and 5.1.2.5b, it is seen that the values of vertical motion are different in magnitude for different time and it reveals that strong upward motion of about 120 cm/s at 12 UTC of 15 November 2007 for MM5 model and about 200 cm/s at 00 UTC of 15 November 2007 for WRF model exists along the eye wall and other parts of the system which feed moisture into the system. It is noted that Sidr has very strong updraft motion at the eye wall throughout mid and upper troposphere. In general downward motion is not strong. The downward motion is visible in the central parts of the TC and other areas of small pockets, which could be due to subsidence associated with convection.

From the Tables 5.1.25a and 5.1.2.5b, it is seen that the values of horizontal wind at different times are different. Figures 5.1.2.5a and 5.1.2.5b show the distribution of strong winds up to 200 hPa around the centre of TC at 12 UTC on 15 November 2007 for MM5 and 00 UTC on

16 November 2007 for WRF model along the centre of the system. It further confirms that the maximum winds are confined to the right quadrant of the direction of movement of the system. This value decreases with the radial distance from both sides of the eye. Calm wind zone is sharp and narrow and little bit tilted to the west and get expanded towards upper levels. Cyclonic circulation is generally seen up to about 300 hPa level and anticyclonic circulation with divergence fields aloft. This is in agreement with the previous studies of Rao and Prasad (2006) and Goswami *et al.* (2006) on Orissa cyclone. In this case cyclonic circulation is also seen up to about 350 hPa level for MM5 model and up to 300 hPa for WRF model and anticyclonic circulation with divergence fields aloft.

Table 5.1.2.5a: MM5 model simulated radial wind, tangential wind, vertical velocity and horizontal wind (cm/s) of TC Sidr at 00 UTC on 13, 14, 15 November and 12 UTC on 15 November 2007.

| Component of wind | Simulated wind speed (cm/s) at | | | |
|-------------------|--------------------------------|-----------------------|-----------------------|-----------------------|
| | 00 UTC 13 November | 00 UTC 14 November | 00 UTC 15 November | 12 UTC 15 November |
| Radial wind | 1200 | 1200 | 1500 | 2000 |
| Tangential wind | 1500 | 3000 | 5000 | 5000 |
| Vertical velocity | 50 | 60 | 80 | 120 |
| Horizontal wind | 2000 | 4000 | 5000 | 5000 |

Table 5.1.2.5b: WRF model simulated radial wind, tangential wind, vertical velocity and horizontal wind (cm/s) of TC Sidr at 00 UTC on 13, 14, 15 and 16 November 2007.

| Component of wind | Simulated wind speed (cm/s) at 00 UTC of | | | |
|-------------------|--|-------------|-------------|-------------|
| | 13 November | 14 November | 15 November | 16 November |
| Radial wind | 800 | 12 | 2500 | 2500 |
| Tangential wind | 18 | 2500 | 3000 | 3000 |
| Vertical velocity | 0.40 | 70 | 200 | 140 |
| Horizontal wind | 2000 | 2000 | 4000 | 4000 |

5.1.3 Vorticity Field

To know the evolution, the plot of MM5 and WRF models simulated low level relative vorticity at 850 hPa as a function of time is shown in Figure 5.1.3.1. The analysis reveals that there is a gradually rise in the vorticity value in the first 60 hours of the simulation of MM5 model and thereafter the value shows a falling tendency up to 96 hour of model run.

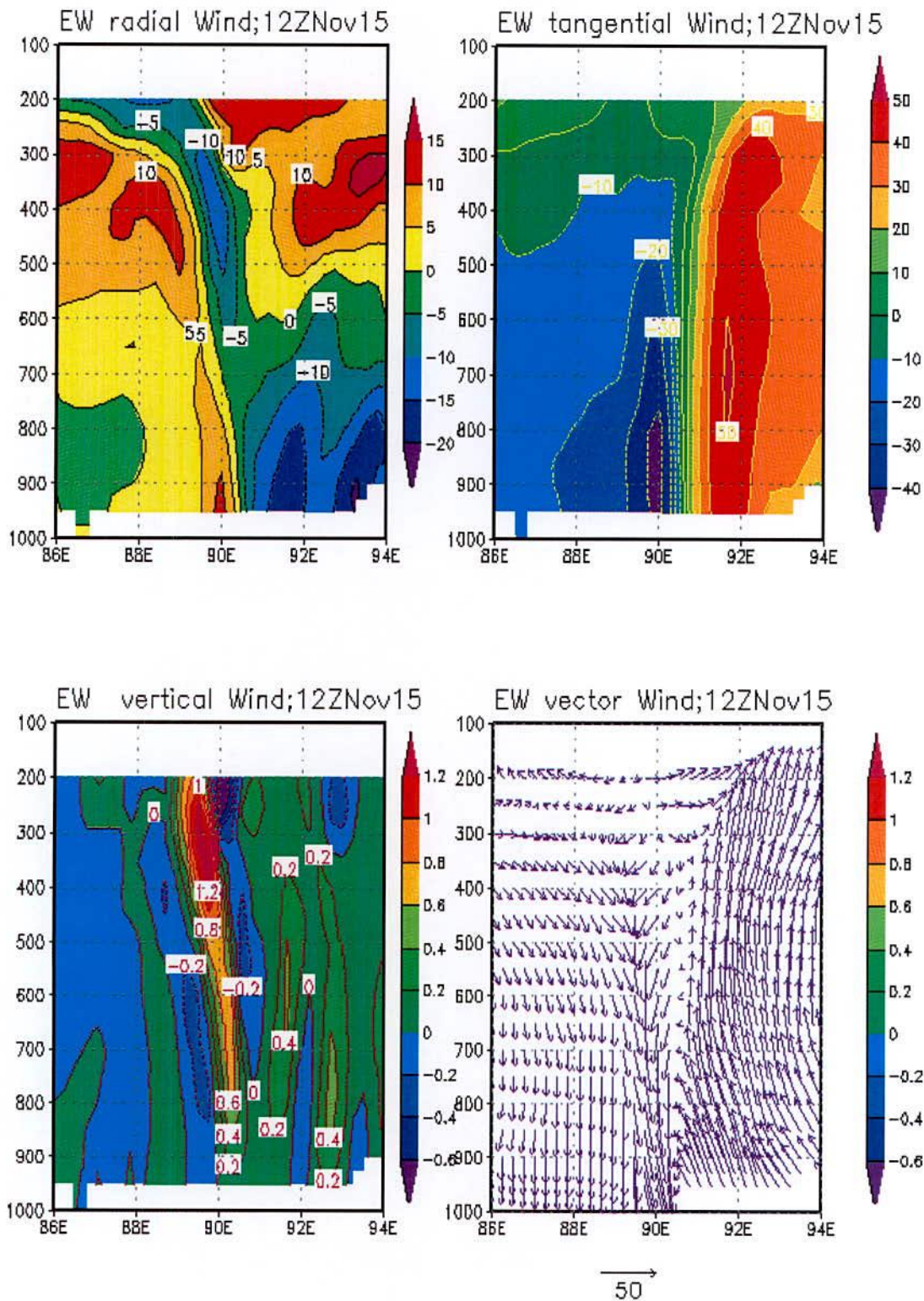


Figure 5.1.2.5a: MM5 model simulated east-west cross section of vertical structure of radial wind, tangential wind, vertical velocity and horizontal wind of TC Sidr along the centre at 12 UTC on 15 November 2007.

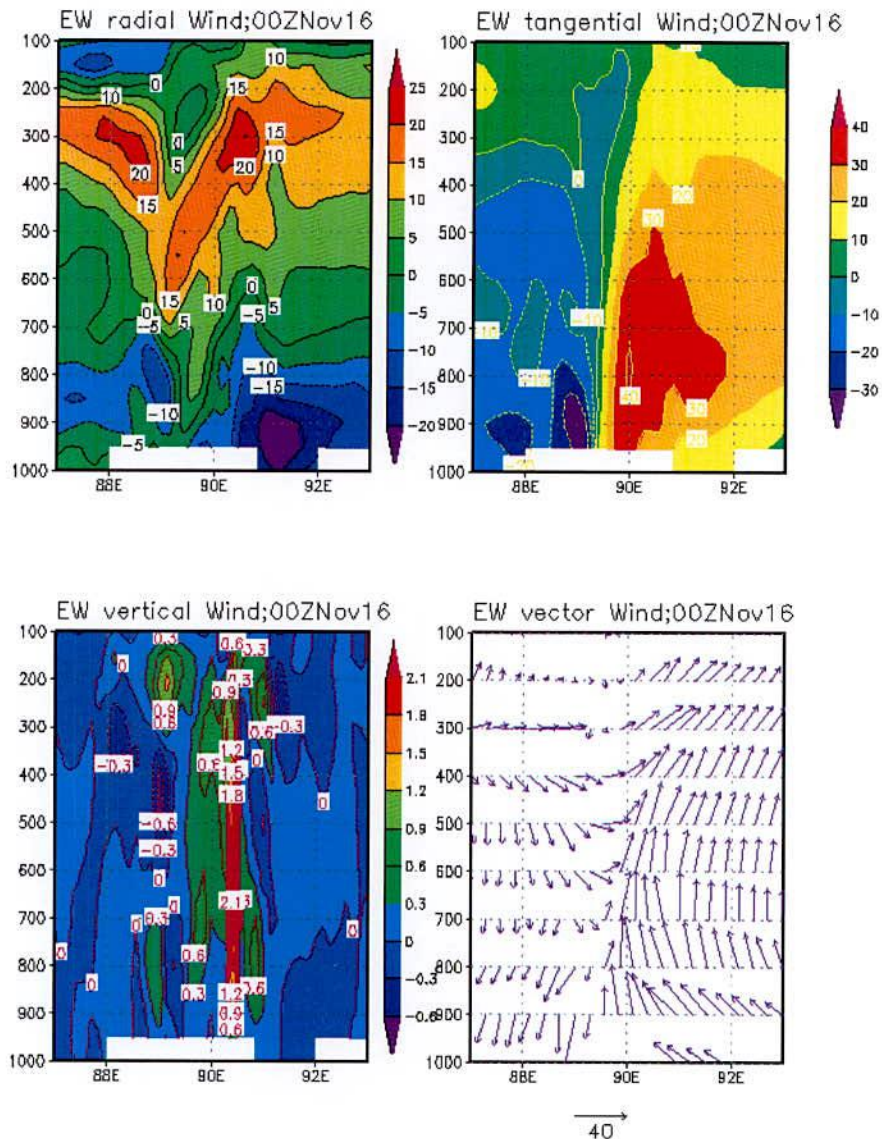


Figure 5.1.2.5b: WRF model simulated east-west cross section of vertical structure of radial wind, tangential wind, vertical velocity and horizontal wind of TC Sidr along the centre at 00 UTC on 16 November 2007

Again output from WRF model reveals that there is a gradually rise of vorticity in the first 24 hours of simulation of the model and then sustains the maximum value with little bit lower value by making several oscillations for next 42 hours duration (24 – 66 hours of forecast). Thereafter the value shows a rapid fall.

The horizontal distribution of the relative vorticity obtained from MM5 model at 12 UTC on 15 November 2007 (i.e. before landfall) and obtained from WRF model at 00 UTC on 16 November 2007 (i.e. before landfall) of TC Sidr at 850, 500, 300 and 200 hPa levels have shown in Figures 5.1.3.2a and 5.1.3.2b respectively.

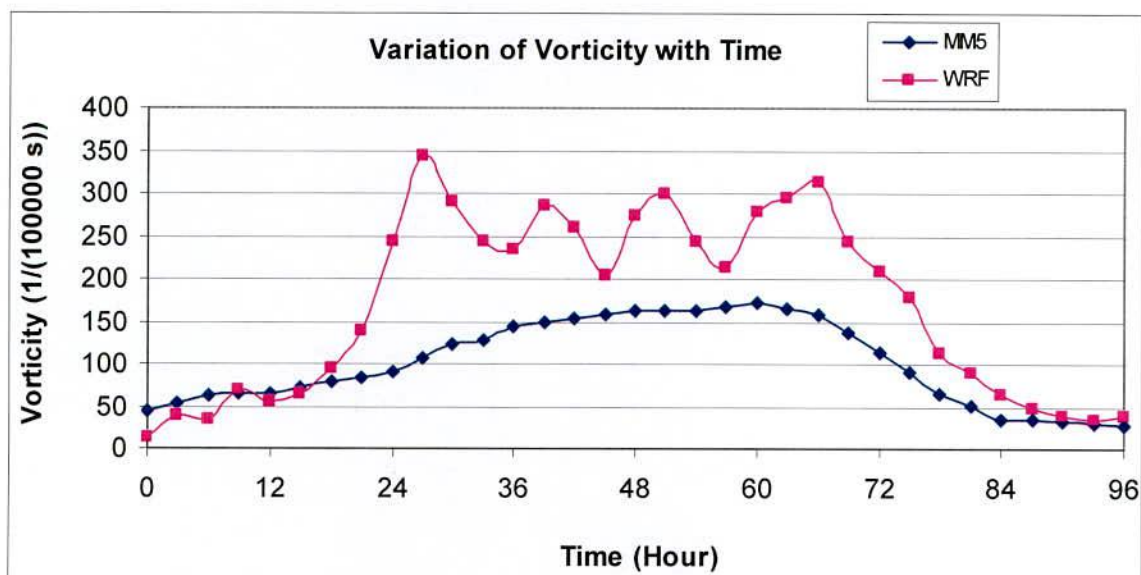


Figure 5.1.3.1: Evolution of MM5 and WRF models simulated vorticity with time of TC Sidr

It is seen from the Figures 5.1.3.2a and 5.1.3.2b that the vorticity obtained from MM5 and WRF models is distributed with maximum value at the centre and these values are tabulated in Tables 5.1.3.1a and 5.1.3ab for MM5 and WRF model respectively. From Tables 5.1.3.1a and 5.1.3.1b, it is clear that these values are increased with the advanced of time except at 12 UTC on 15 November 2007 (i.e. before landfall) for MM5 model and 00 UTC on 16 November 2007 (i.e. just before landfall) for WRF model at different levels. This is due to landmass effect before landfall. The distribution maintains circular pattern with some asymmetric features in the outer periphery except at 00 UTC on 13 November 2007 (i.e. initial time) for both models where symmetrical circular pattern is available at all levels.

At 850 hPa level, (Figures 5.1.3.2a and 5.1.3.2b) negative vorticity fields are found almost in all sides of the centre of the TC which is followed by a positive and negative vorticity fields at 15 UTC of 15 November 2007 (i.e. just before the landfall). Similar phenomenons of negative vorticity are found at 00 UTC on 13, 14 and 15 November 2007 (not shown in figure). The distance of the negative vorticity from the centre are increased due to the intensification of the intensity of TC (not shown). Low level relative vorticity fields confirm the strong cyclonic circulation with different values of the radius at different time in feeding moisture into the system to sustain its intensity.

At 500 and 300 hPa levels the distribution of relative vorticity shows a symmetric character in the horizontal direction. The values of relative vorticity are increased with the intensification of the intensity of the cyclone and then decreased before landfall at time 12

UTC of 15 November for MM5 model and after landfall at 00 UTC of 16 November 2007 at 500 hPa level. But the values of relative vorticity are increased with the development of TC at all stages at 300 hPa level. At 200 hPa level, the weak positive vorticity embedded with negative vorticity field is visible at 200 hPa level. Negative vorticity is found at or near the centre.

Table 5.1.3.1a: MM5 Model simulated maximum vorticity ($\times 10^{-5} \text{ s}^{-1}$) at different pressure levels of TC Sidr at 00 UTC on 13, 14, 15 and 12 UTC on 15 November 2007.

| Pressure level (hPa) | Vorticity ($\times 10^{-5} \text{ s}^{-1}$) at | | | |
|--------------------------|--|--------------------------|--------------------------|--------------------------|
| | 00 UTC of 13 November | 00 UTC of 14 November | 00 UTC of 15 November | 12 UTC of 15 November |
| 850 | 45 | 90 | 160 | 160 |
| 500 | 35 | 55 | 100 | 90 |
| 300 | 20 | 40 | 60 | 60 |
| 200 | 15 | 20 | 50 | 30 |
| Vertical distribution | 35 | 60 | 160 | 160 |

Table 5.1.2.3.1: WRF Model simulated maximum vorticity ($\times 10^{-5} \text{ s}^{-1}$) at different pressure levels of TC Sidr at 00 UTC on 13, 14, 15 and 16 November 2007.

| Pressure level (hPa) | Vorticity ($\times 10^{-5} \text{ s}^{-1}$) at 00 UTC of | | | |
|--------------------------|--|-------------|-------------|-------------|
| | 13 November | 14 November | 15 November | 16 November |
| 850 | 18 | 240 | 270 | 210 |
| 500 | 15 | 240 | 140 | 100 |
| 300 | 12 | 180 | 120 | 70 |
| 200 | 10 | 80 | 70 | 60 |
| Vertical distribution | 18 | 80 | 270 | 210 |

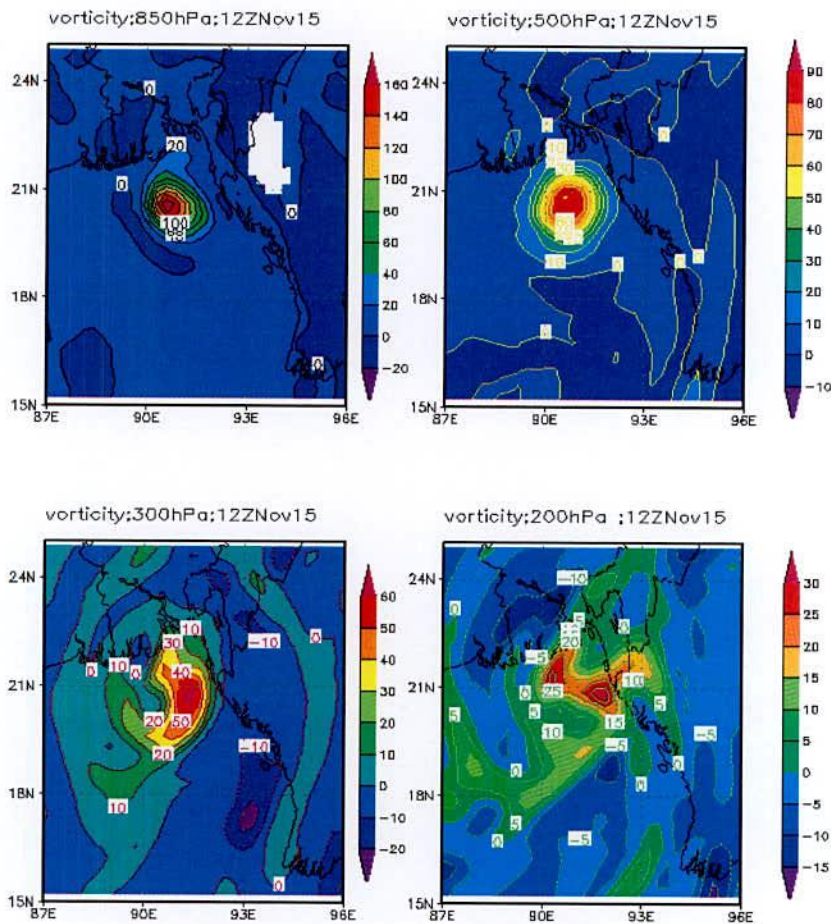


Figure 5.1.3.2a: MM5 model simulated vorticity field associated with Sidr at 850, 500, 300 and 200hPa levels at 12 UTC on 15 November, 2007.

Vertical distribution of relative vorticity through the centre in the east-west direction is shown in Figure 5.1.3.3a and values are tabulated in the Table 5.1.3.1a for MM5 model. The same for WRF model is shown in Figure 5.1.3.3b and values are tabulated in the Table 5.1.3.1b.

According to the output obtained from MM5 model at 00 UTC on 13 November (i.e. the initial time), the positive vorticity is spread over a horizontal distance with strong vorticity at slightly western side of the centre (11.042°N and 89.588°E). This pattern of distribution extends from surface to around 200 hPa level with the exception that the magnitude of the vorticity decreases with height. Similar pattern with higher positive value of vorticity is found at the centre after 24 hours of simulation at 00 UTC on 14 November 2007 along the centre (13.044°N). At 00 UTC on 15 November 2007, the system has the positive vorticity along the centre (17.134°N) up to 200 hPa with highest positive value of vorticity. At 12 UTC on 15

November 2007, the system has the same value of positive vorticity as the previous time at 00 UTC on 15 November 2007 along the centre (20.541°N) up to 200 hPa.

Again, according to the output obtained from WRF model at 00 UTC on 13 November (i.e. the initial time), the positive vorticity is spread over a horizontal distance with strong vorticity at slightly eastern side of the centre (11.861°N and 89.868°E). This pattern of distribution extends from surface to around 150 hPa level with the exception that the magnitude of the vorticity decreases with height. Similar pattern with higher positive vorticity is found at the centre after 24 hours of simulation at 00 UTC on 14 November 2007 along the centre (12.774°N). At 00 UTC on 15 November 2007, the system has the positive vorticity along the centre (16.929°N) up to 200 hPa level with highest positive value. At 00 UTC on 16 November 2007, the system has less positive vorticity than the previous time at 00 UTC on 15 November 2007 along the centre (21.463°N) up to 150 hPa with low magnitude. It may be effect of landmass before landfall.

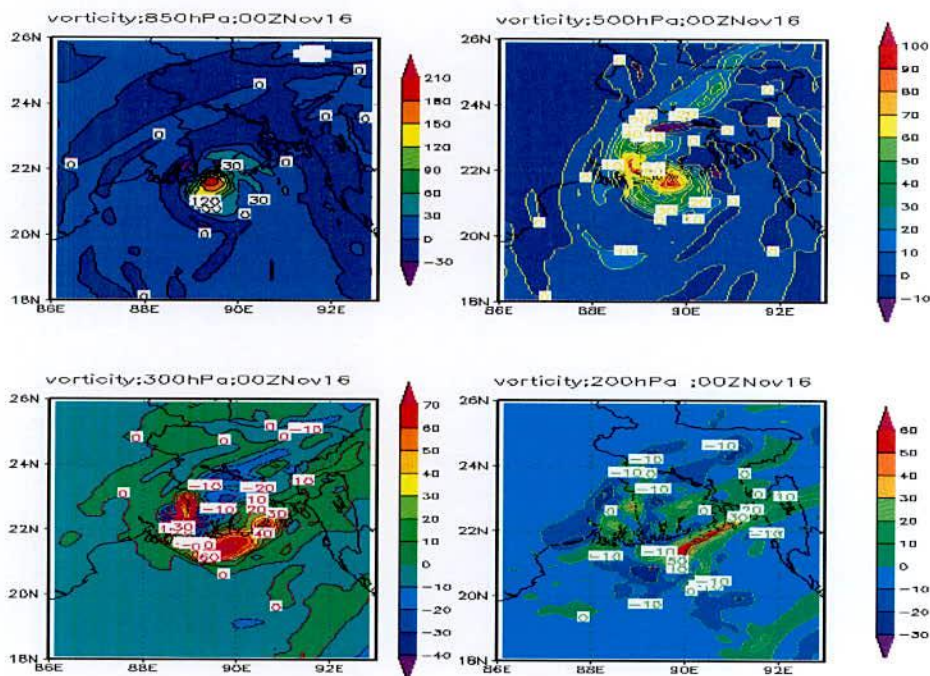


Figure 5.1.3.2b: WRF model simulated vorticity field associated with Sidr at 850, 500,300 and 200 hPa levels at 00 UTC on 16 November 2007.

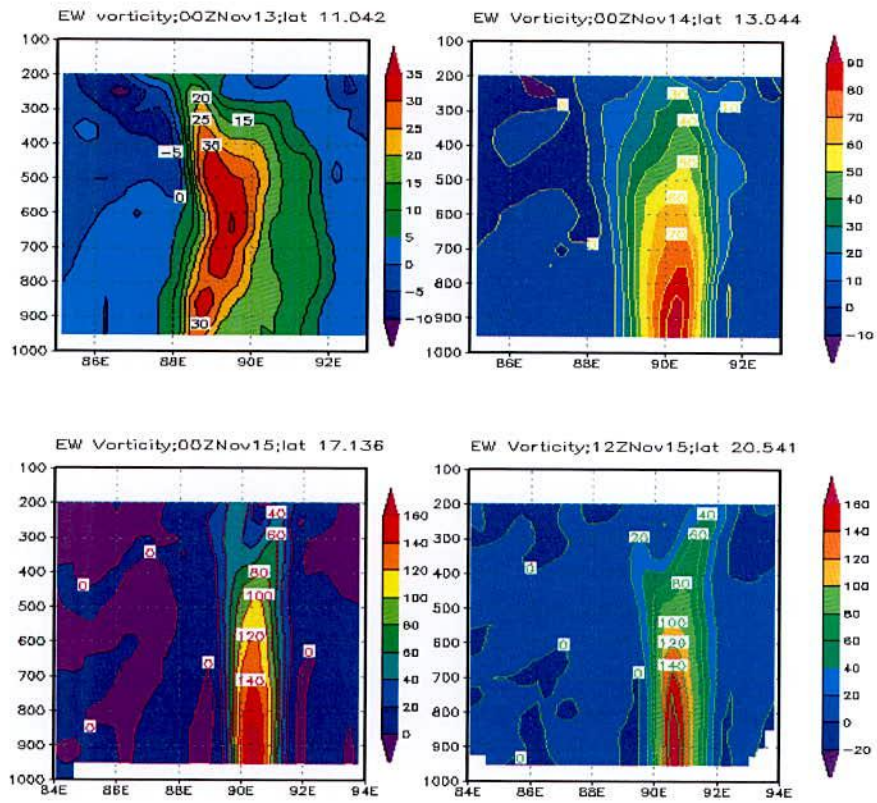


Figure 5.1.3.3a: MM5 model simulated vertical distribution of relative vorticity field in the east-west direction of TC Sidr along the centre at 00 UTC on 13, 14, 15 November and 12 UTC of 15 November 2007.

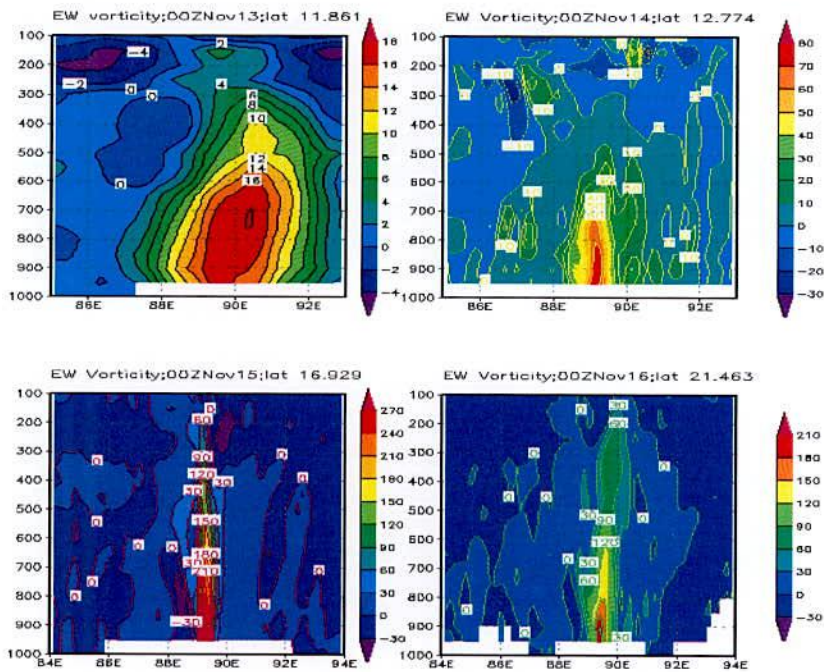


Figure 5.1.3.3b: WRF model simulated vertical distribution of relative vorticity field in the east-west direction of TC Sidr through the centre at 00 UTC on 13, 14, 15 and 16 November 2007.

5.1.4 Temperature Anomaly

The MM5 model simulated temperature anomaly of TC Sidr at 00 UTC on 13, 14, 15 November and 12 UTC of 15 November 2007 (i.e. before landfall) from surface to 100 hPa level is shown in Figure 5.1.4.1a and increase of temperature is given tabulated in Table 5.1.4.1a.

At 00 UTC on 13 November 2007, warm core of 10°C is simulated at 950-200 hPa layer. It is noted that the warm core region is slightly expanded outward at 800-300 hPa level. The greatest anomaly has occurred around 450 hPa level. Negative temperature anomalies are also shown in the upper levels. At 00 UTC of 14 November 2007, warm core of 12°C is simulated at 950-200 hPa layer. It is noted that the warm core region is expanded outward at 700-350 hPa level. The greatest anomaly is simulated by the MM5 model around 500 hPa level. At 00 UTC of 15 November 2007, 14°C warm core is observed at 950-200 hPa layer. It is noted that the warm core region is expanded outward at 600-350 hPa level. The greatest anomaly is simulated around 400 hPa level. At 12 UTC on 15 November 2007, warm core 11°C is observed in 950-200 hPa layer. It is noted that the warm core region is expanded outward at 650-300 hPa level. The greatest anomaly is simulated around 500 hPa level. The simulated temperature anomaly demonstrates that the warm core is visible mainly in the upper troposphere during 13 – 15 November 2007. Negative temperature anomalies at lower levels are due to contamination by heavy precipitation at 00 UTC and 12 UTC of 15 November 2007.

Table 5.1.4.1a: MM5 Model simulated Temperature (°C) anomaly associated with TC Sidr at 00 UTC on 13, 14, 15 November and 12 UTC on 15 November 2007

| Temperature anomaly (°C) | | | |
|--------------------------|--------------------------|--------------------------|--------------------------|
| 00 UTC on 13 November | 00 UTC on 14 November | 00 UTC on 15 November | 12 UTC on 15 November |
| 10 | 12 | 14 | 11 |

Again, the WRF model simulated temperature anomaly of TC Sidr at 00 UTC of 13, 14, 15 and 16 November 2007 from surface to 100 hPa level are shown in Figure 5.1.4.1b and values are tabulated in Table 5.1.4.1b.

Table 5.1.4.1b: WRF Model simulated Temperature (°C) anomaly associated with TC Sidr at 00 UTC on 13, 14, 15 and 16 November 2007.

| Temperature anomaly (°C) at 00 UTC on | | | |
|---------------------------------------|-------------|-------------|-------------|
| 13 November | 14 November | 15 November | 16 November |
| | | | |

| | | | |
|----|---|----|---|
| 10 | 8 | 10 | 8 |
|----|---|----|---|

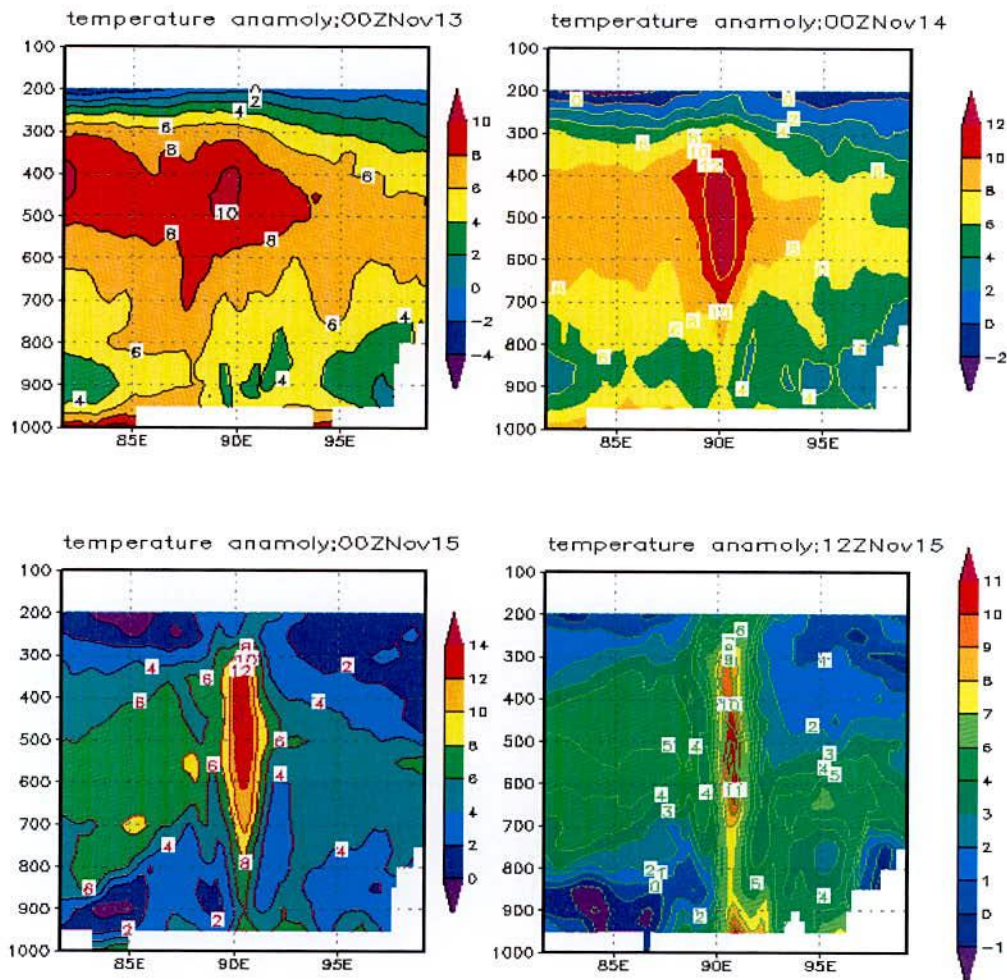


Figure 5.1.4.1a: MM5 model simulated vertical distribution of temperature anomaly in the east-west cross section of TC Sidr through the centre at 00 UTC on 13, 14, 15 November and 12 UTC on 15 November 2007.

At 00 UTC on 13 November 2007, 10°C warm core is observed in the layer between 950-350 hPa. It is noted that the warm core region is slightly expanded outward at 750-350 hPa level. The greatest anomaly is found around 450 hPa level. The simulated temperature anomaly demonstrates that the warm core is visible mainly in the upper troposphere. Negative temperature anomalies are seen at the upper levels. At 00 UTC on 14 November 2007, 8°C warm core is observed in the layer between 950-300 hPa. It is noted that the warm core region is expanded outward at 700-300 hPa level. The greatest anomaly is found around 450 hPa level. The simulated temperature anomaly demonstrates that the warm core is visible mainly in the upper troposphere. At 00 UTC on 15 November 2007, 10°C warm core is observed in the layer between 950-200 hPa. It is noted that the warm core region is expanded outward at 850-200 hPa level. The greatest anomaly is found around 450 hPa level. The

simulated temperature anomaly demonstrates that the warm core is visible mainly at upper troposphere. At 00 UTC on 16 November 2007, 8°C warm core is observed in the layer between 950-300 hPa. The warm core region is expanded outward at 700-300 hPa level. The greatest anomaly is seen around 550 hPa level. The simulated temperature anomaly demonstrates that the warm core is visible mainly at upper troposphere. Negative temperature anomalies at lower levels are due to effect of heavy precipitation.

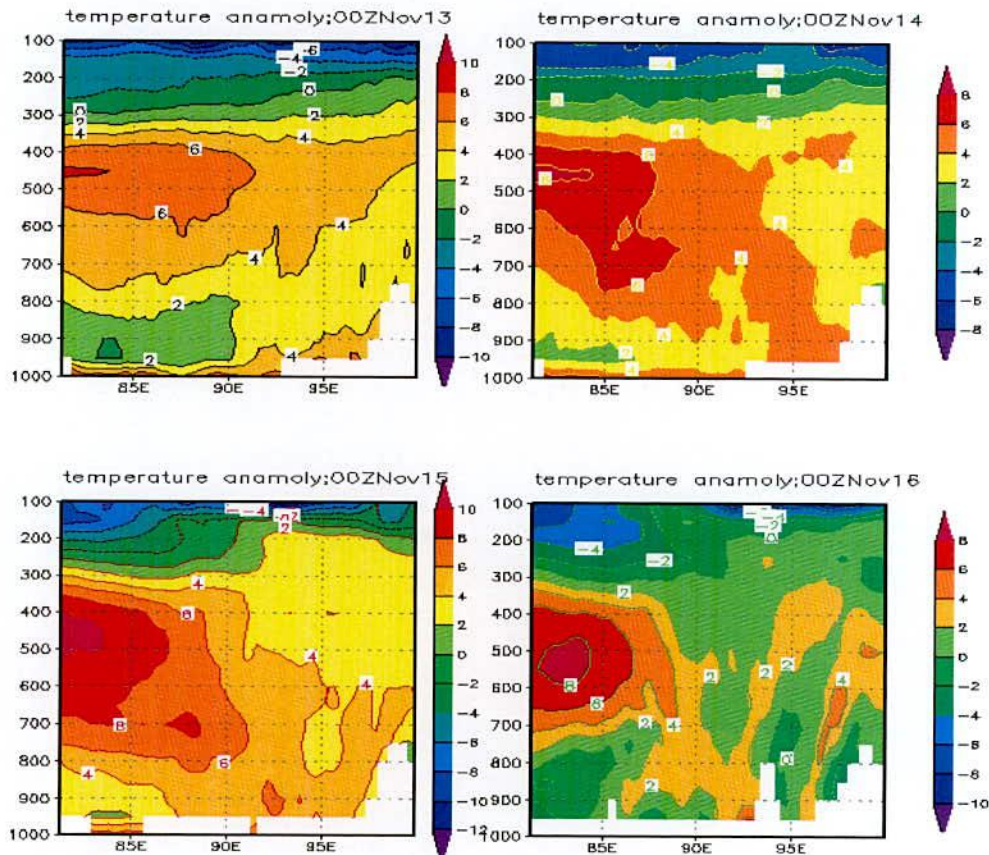


Figure 5.1.4.1b: WRF model simulated vertical distribution of temperature anomaly in the east-west direction of TC Sidr through the centre at 00 UTC on 13, 14, 15 and 16 November 2007.

5.1.5 Relative Humidity

The vertical distribution of MM5 model simulated relative humidity associated with TC Sidr at 00 UTC of 13, 14, 15 November and 12 UTC of 15 November 2007 (i.e. before landfall) from surface to 200 hPa levels are shown in Figure 5.1.5.1a and its values are tabulated in Table 5.1.5.1a. It is seen that high relative humidity (more than 90%) spreads in outer range of eye wall up to 400, 350, 300 and 300 hPa levels at 00 UTC on 13, 14, 15 November and 12 UTC on 15 November 2007 respectively. High relative humidity band are also found in

the rain band of the system situated on both sides of the system throughout 950-750 hPa level.

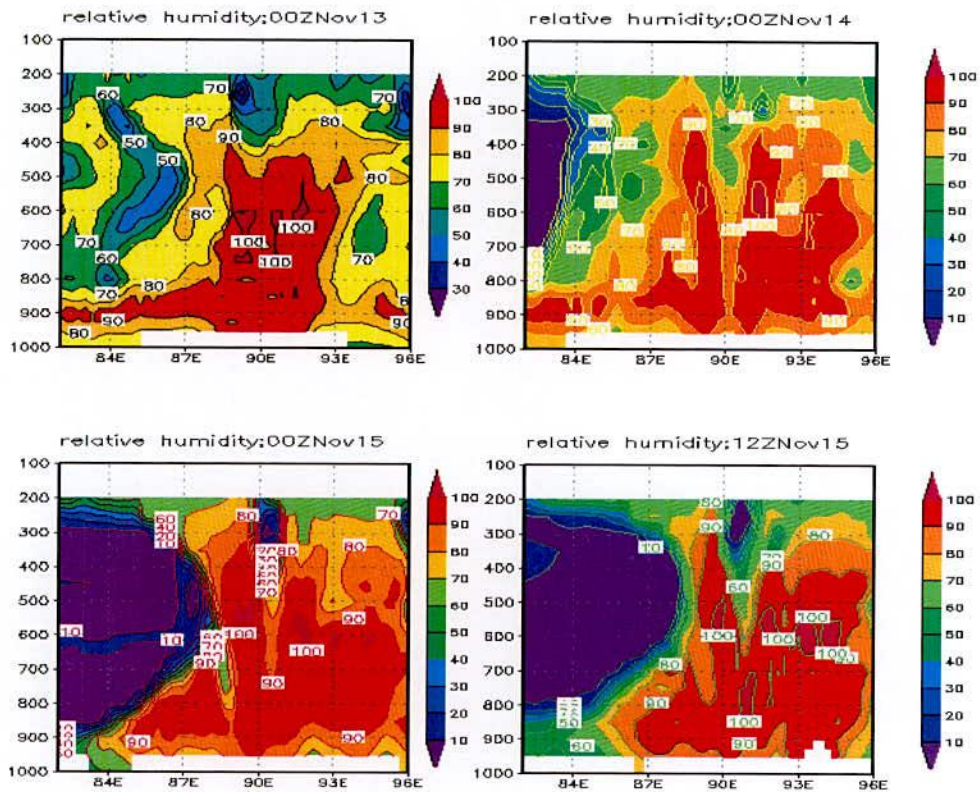


Figure 5.1.5.1a: MM5 model simulated vertical distribution of relative humidity in east-west direction of TC Sidr through the centre at 00 UTC on 13, 14, 15 November and 12 UTC on 15 November 2007.

Table 5.1.5.1a: MM5 model simulated maximum relative humidity (%) of TC Sidr through the centre at 00 UTC on 13, 14, 15 November and 12 UTC on 15 November 2007.

| Simulated maximum relative humidity (%) | | | |
|---|--------------------------|--------------------------|--------------------------|
| 00 UTC on 13 November | 00 UTC on 14 November | 00 UTC on 15 November | 12 UTC on 15 November |
| 100 | 100 | 100 | 100 |

WRF model simulated vertical cross section of relative humidity associated with TC Sidr at 00 UTC on 13, 14, 15 and 16 November 2007 (i.e. before landfall) from surface to 100 hPa levels are shown in Figure 5.1.5.1a and its values are tabulated in Table 5.1.5.1b. It is seen that high relative humidity (more than 90%) spreads in outer range of eye wall up to 550, 550, 500 and 400 hPa levels at 00 UTC of 13, 14, 15 and 16 November 2007 respectively.

High relative humidity bands are also found in the rain band of the system situated on both sides of the system throughout 950-750 hPa levels.

Table 5.1.5.1b: WRF Model simulated maximum relative humidity (%) associated with TC Sidr at 00 UTC on 13, 14, 15 and 16 November 2007.

| Simulated maximum relative humidity (%) at 00 UTC on | | | |
|--|-------------|-------------|-------------|
| 13 November | 14 November | 15 November | 16 November |
| 90 | 100 | 100 | 100 |

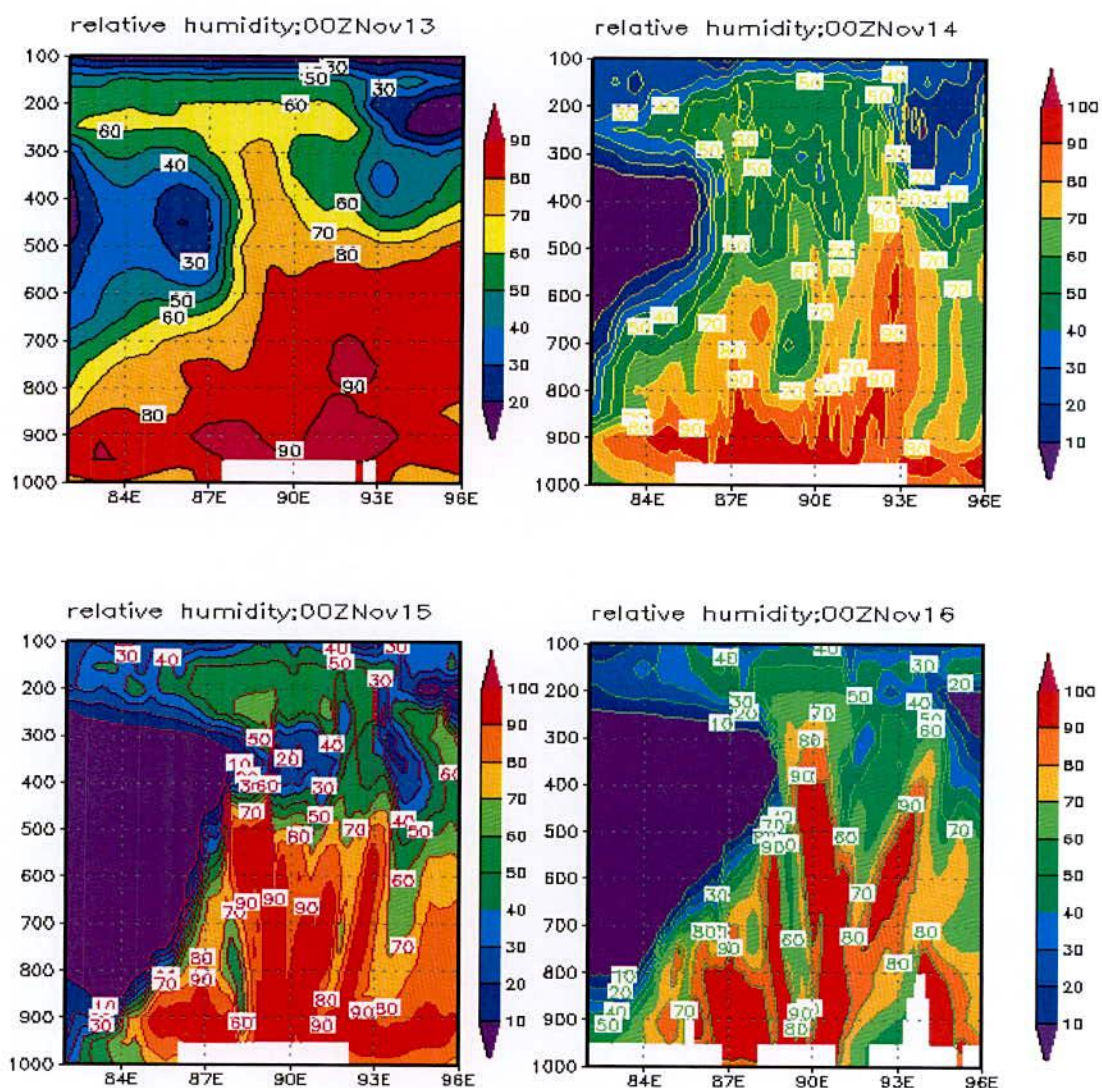


Figure 5.1.5.1b: WRF model simulated vertical distribution of relative humidity in east-west direction of TC Sidr through the centre at 00 UTC on 13, 14, 15 and 16 November 2007

5.1.6 Water Vapor Mixing Ratio

Vertical distribution of MM5 model simulated water vapor mixing ratio in the east-west direction along the centre at 00 UTC on 13, 14, 15 November and 12 UTC on 15 November 2007 (i.e. before landfall) of TC Sidr from surface to 200 hPa levels are shown in Figure 5.1.6.1a. It shows that the highest water vapour mixing ratio around 2.0 g/kg or more is found at the centre of the system at 950 hPa level and it decreases upwards to 500 hPa level or more. It is seen that moisture content distribution has shifted toward eastward with increase of time.

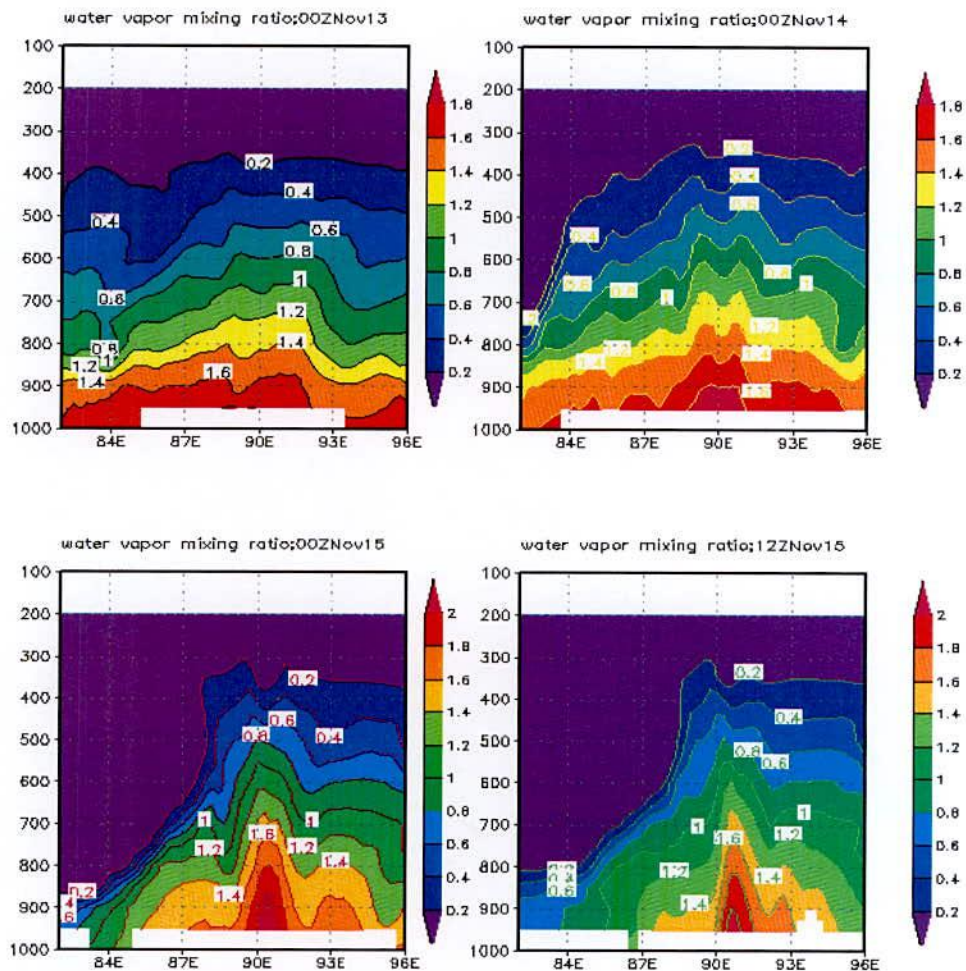


Figure 5.1.6.1a: Vertical distribution of MM5 model simulated water vapor mixing ratio along the east-west cross section of TC Sidr through the center at 00 UTC on 13, 14, 15 November and 12 UTC on 15 November 2007.

Vertical distribution of WRF model simulated water vapor mixing ratio along the east-west cross section of the centre at 00 UTC of 13, 14, 15 and 16 November 2007 associated with TC Sidr from surface to 200 hPa levels is seen in Figure 5.1.6.1b. It shows that the highest

water vapour mixing ratio around 2.0 g/kg or more is found at the centre of the system at 950 hPa level and it decreases upwards to 500 hPa level or more. It is seen that moisture content distribution has shifted toward east with progress of time.

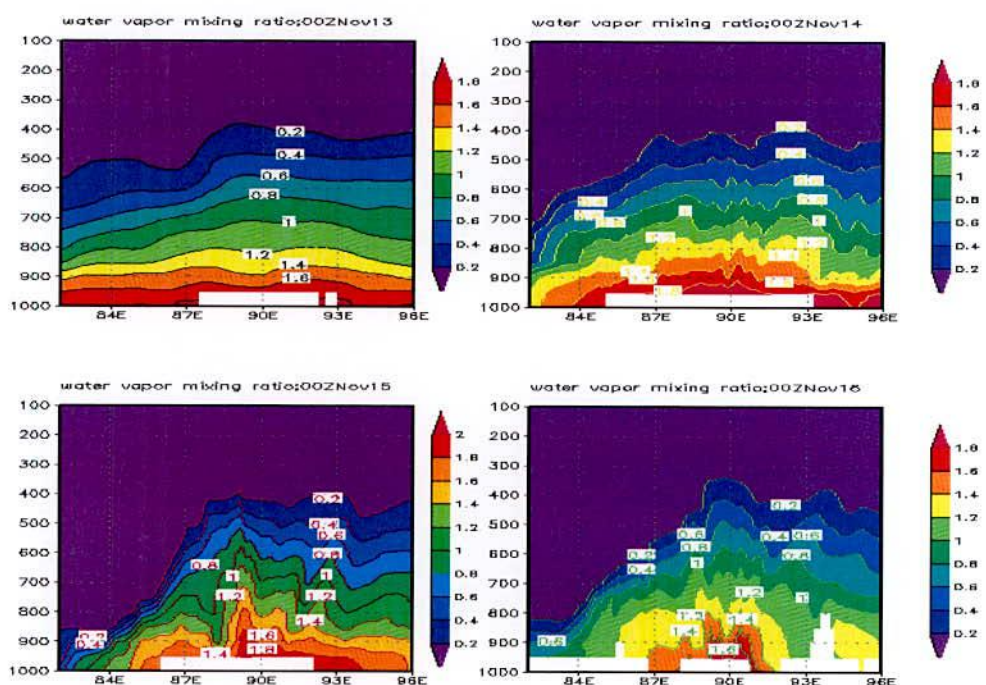


Figure 5.1.6.1b: Vertical distribution of WRF model simulated water vapor mixing ratio along the east-west direction of TC Sidr through the centre at 00 UTC on 13, 14, 15 and 16 November 2007.

The horizontal distribution of water vapor mixing ratio associated with TC Sidr at 950 hPa at 00 UTC on 13, 14, 15 November and 12 UTC of 15 November 2007 (i.e. before landfall) is shown in figure 5.1.6.2a and its values are tabulated in Table 5.1.6.1a. It is found that the high moisture flux comes from the southern side covering a large area of the Bay of Bengal which feeds the system along its southeastern side through the boundary layer. The value of high moisture flux increases slightly with development of the system.

Table 5.1.6.2a: MM5 Model simulated maximum water vapour mixing ratio g/kg of associated with TC Sidr at 00 UTC on 13, 14, 15 November and 12 UTC on 15 November 2007.

| Simulated maximum Water vapor mixing ratio g/kg | | | |
|---|--------------------------|--------------------------|--------------------------|
| 00 UTC on 13 November | 00 UTC on 14 November | 00 UTC on 15 November | 12 UTC on 15 November |
| 1.8 | 1.8 | 2.0 | 2.0 |

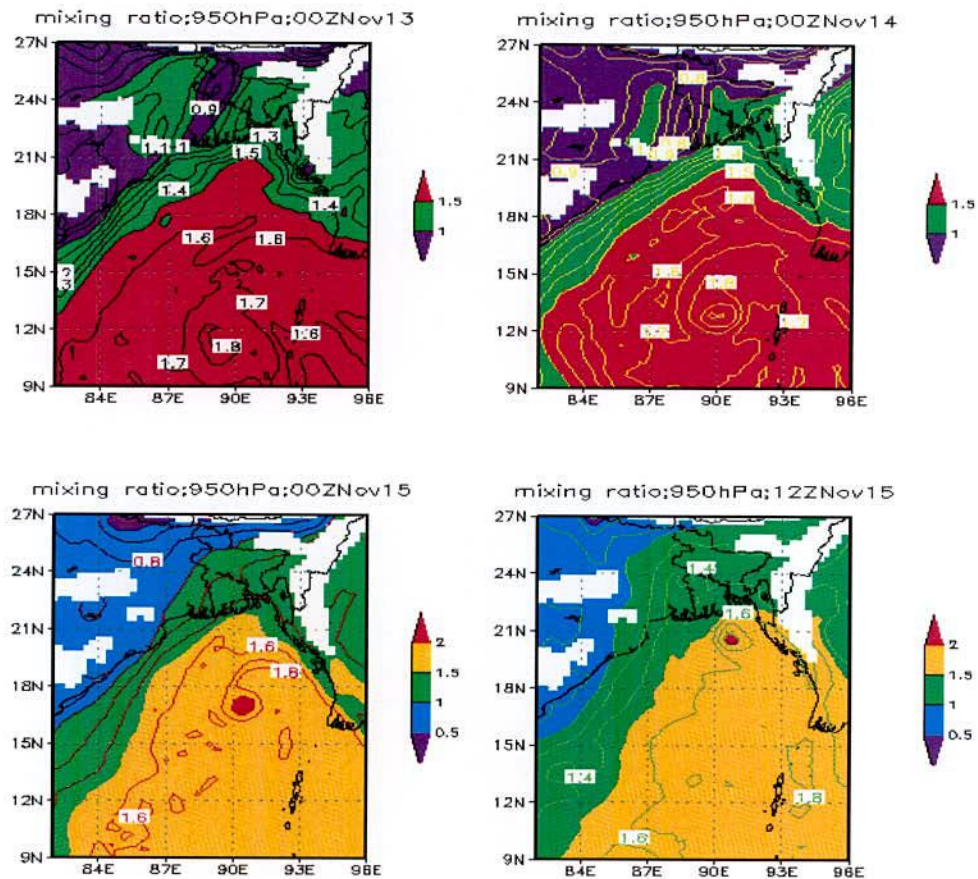


Figure 5.1.6.2a: MM5 model simulated horizontal distribution of water vapor mixing ratio at 950 hPa of TC Sidr at 00 UTC on 13, 14, 15 and 12 UTC of 15 November 2007.

The horizontal distribution of water vapor mixing ratio at 950 hPa at 00 UTC of 13, 14, 15 and 16 November 2007 (i.e. before landfall) of cyclone Sidr has shown in Figure 5.1.2.6.2 and its values are tabulated in Table 5.1.2.6.1. It is noted that the high moisture comes from the south side covering a large area of the Bay of Bengal which feeds the system along its southeastern side through the boundary layer. The value of high moisture increases slightly with development of the system. The value decreases at 00 UTC of 16 November 2007 (i.e. before landfall) due to landmass effect.

Table 5.1.6.2a: WRF Model simulated maximum water vapour mixing ratio g/kg associate with TC Sidr at 00 UTC on 13, 14, 15 and 16 November 2007.

| Simulated maximum value of Water vapor mixing ratio (g/kg) at 00 UTC on | | | |
|---|-------------|-------------|-------------|
| 13 November | 14 November | 15 November | 16 November |
| 1.7 | 2.0 | 2.0 | 1.8 |

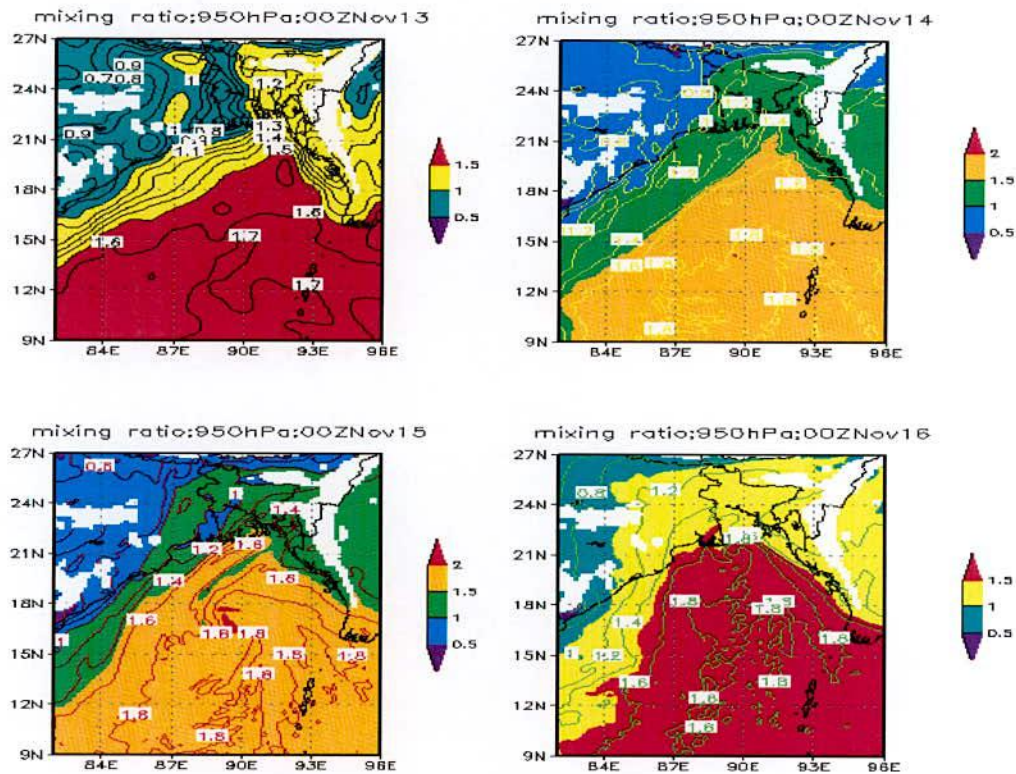


Figure 5.1.6.2b: WRF model simulated horizontal distribution of water vapor mixing ratio associated with TC Sidr at 950 hPa at 00 UTC on 13, 14, 15 and 16 November 2007.

5.1.7 Rainfall Pattern

Figure 5.1.7.1 shows the MM5 and WRF models simulated 24 hrs accumulated rainfall of TC Sidr for the days 13, 14, and 15 November 2007 (i.e. ending at 00 UTC of 14, 15, 16 and 17 November). Again, Figure 5.1.7.2 shows the 24 hrs accumulated rainfall of TC Sidr for the day 13, 14, and 15 November 2007 (i.e. ending at 00 UTC of 14, 15, 16 and 17 November) using TRMM data. On 13 November 2007, the rainfall occurs mainly at the sea and outside south-eastern corner of Bangladesh. MM5 model simulates more rainfall than that simulated by WRF model. MM5 model simulated rainfall is comparable to the rainfall obtained from TRMM data. On 14 November 2007, the rainfall occurs mainly at the sea and south-eastern corner of Bangladesh. Interestingly, there is no rain in some portion of eastern side. MM5 and WRF model simulated rainfall are comparable to rainfall obtained from TRMM data. On 15 November 2007, the rainfall occurs mainly at the sea and whole Bangladesh with heavy rain on some portion in the east side from south to north. The rainfall shows a symmetric character in the horizontal distribution with heavy rainfall at the north-eastern part of Bangladesh. MM5 and WRF model simulated rainfall is comparable to the rainfall obtained from TRMM data with some spatial and temporal variability. Simulated rainfall using both the models is more than the rainfall obtained from TRMM data.

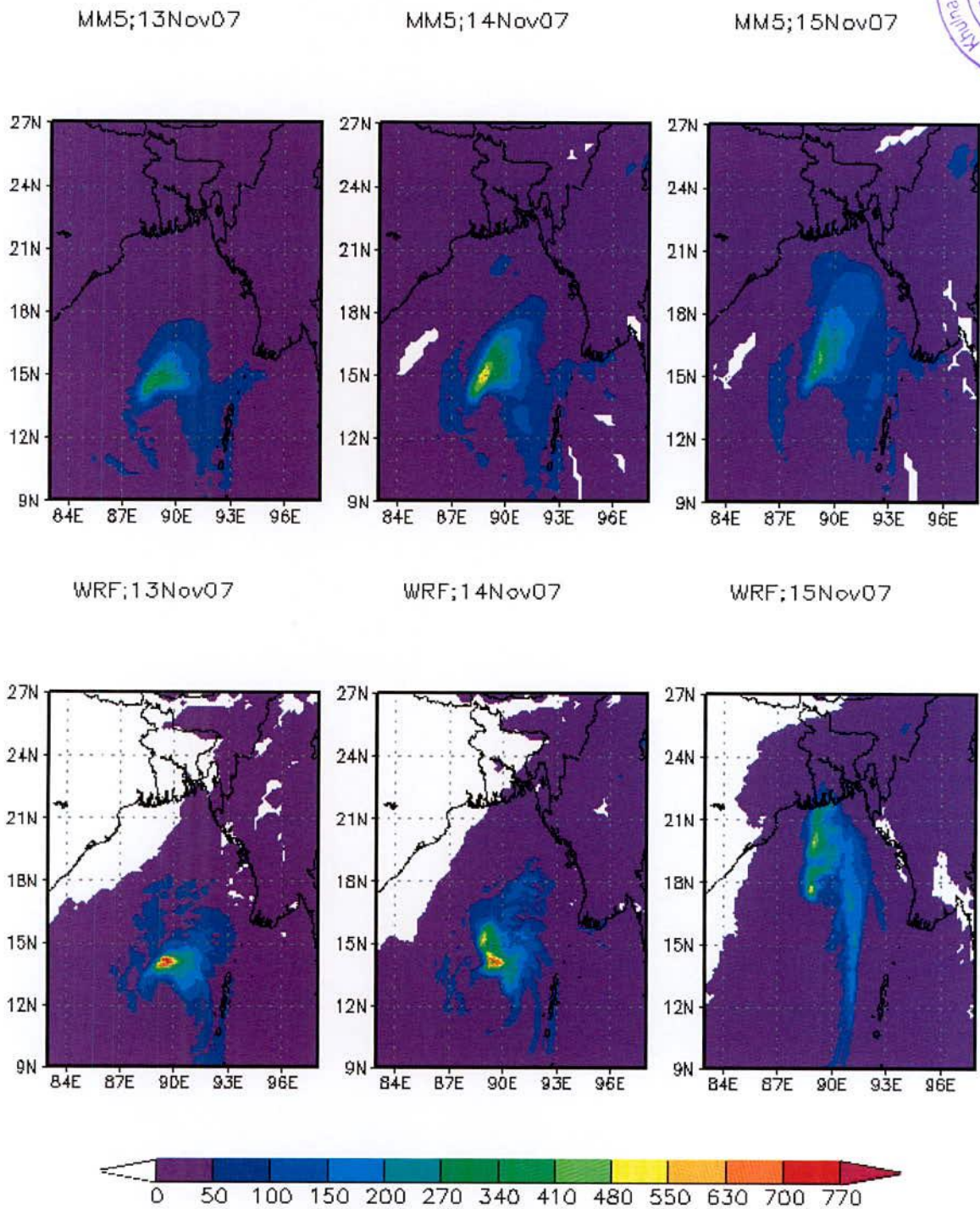


Figure 5.1.7.1: MM5 and WRF Model simulated 24 hours accumulated rainfall (mm) of TC Sidr valid for 13, 14, and 15 November 2007.

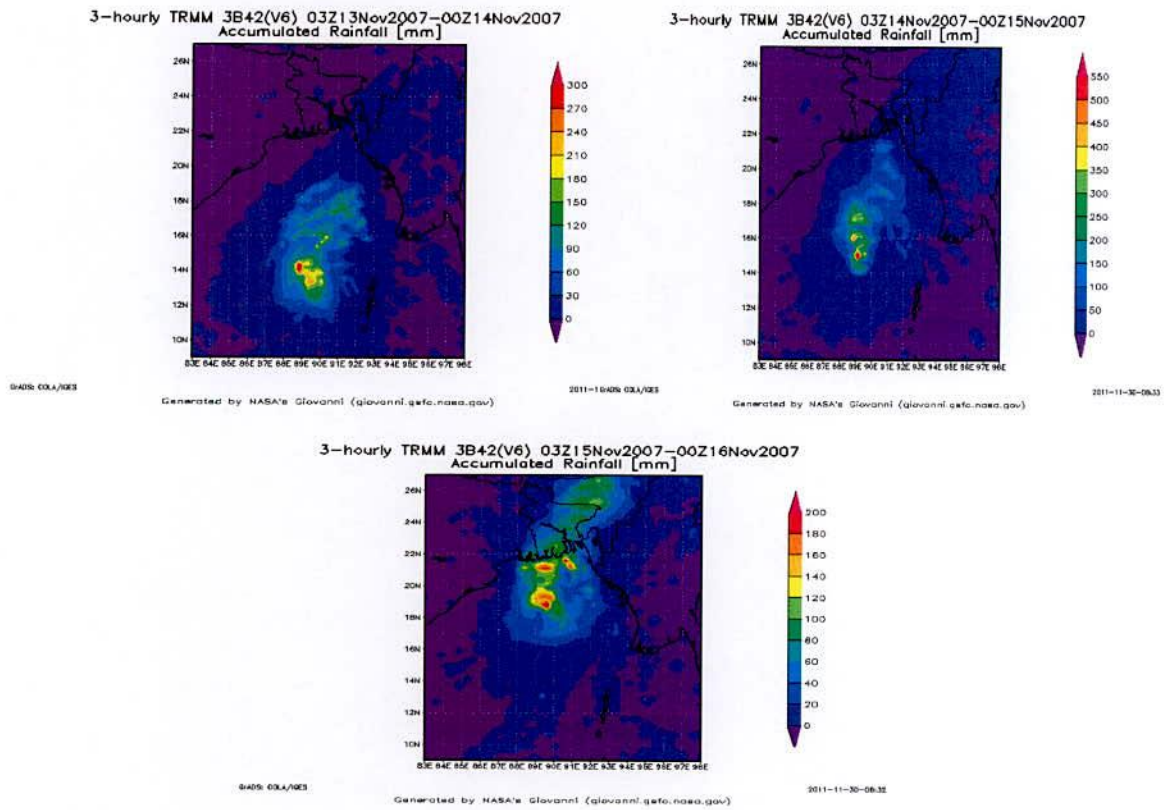


Figure 5.1.7.2: 24 hours accumulated rainfall (mm) of TC Sidr obtained from TRMM data valid for 13, 14, and 15 November 2007.

Figure 5.1.7.3 shows the MM5 and WRF models simulated 24 hrs accumulated rainfall of TC Sidr for the days 15, and 16 November 2007 (i.e. ending at 00 UTC of 16 and 17 November). Again, Figure 5.1.7.4 shows the 24 hrs accumulated rainfall of TC Sidr for the day 15, and 16 November 2007 (i.e. ending at 00 UTC of 16 and 17 November) using TRMM and rain-gauge data. 24 hrs accumulated rainfall of TC Sidr obtained from MM5 and WRF models are comparable with that obtained from TRMM and BMD rain-gauge data with spatial and temporal variability.

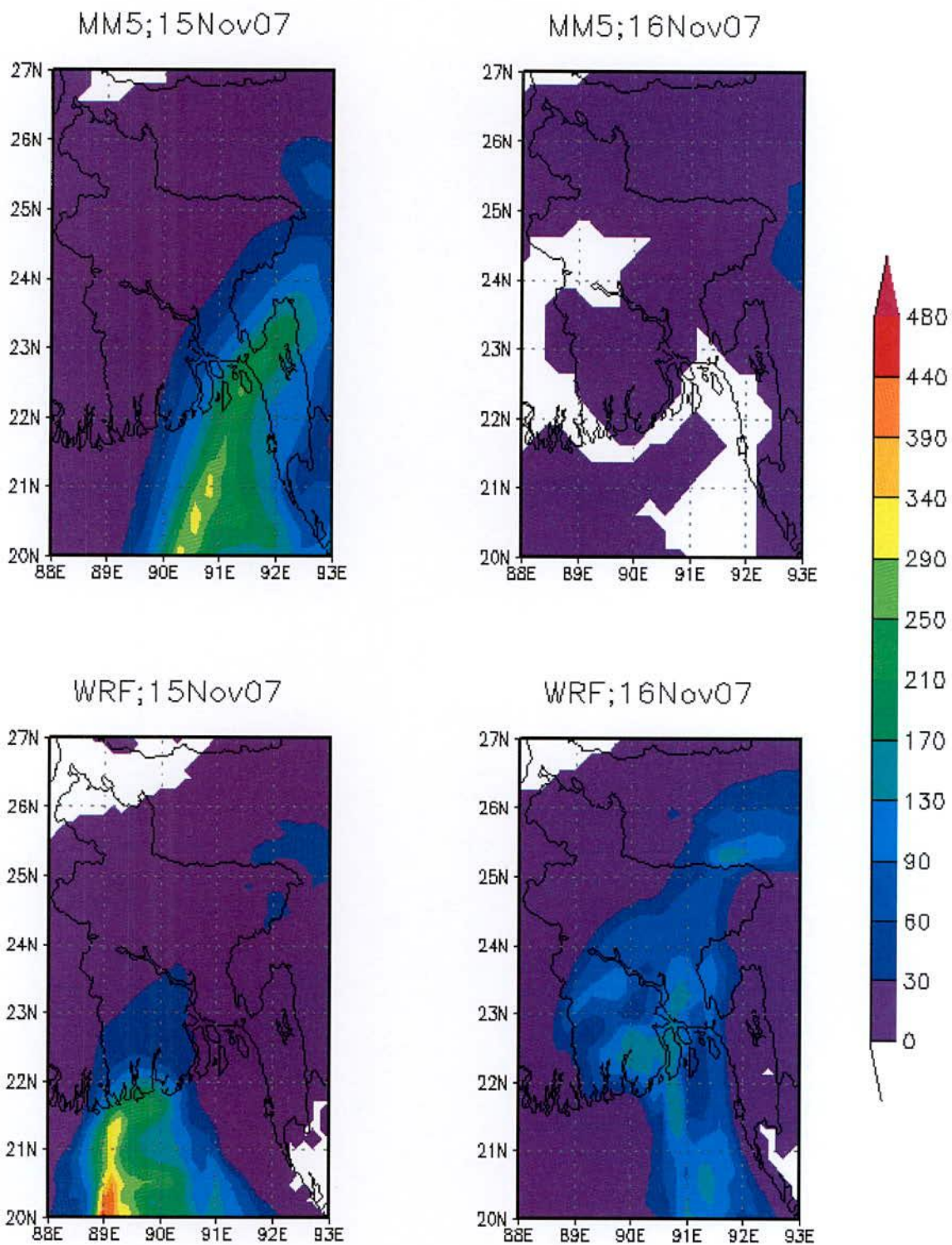


Figure 5.1.7.3: MM5 and WRF Model simulated 24 hours accumulated rainfall (mm) of TC Sidr valid for 15 and 16 November 2007.

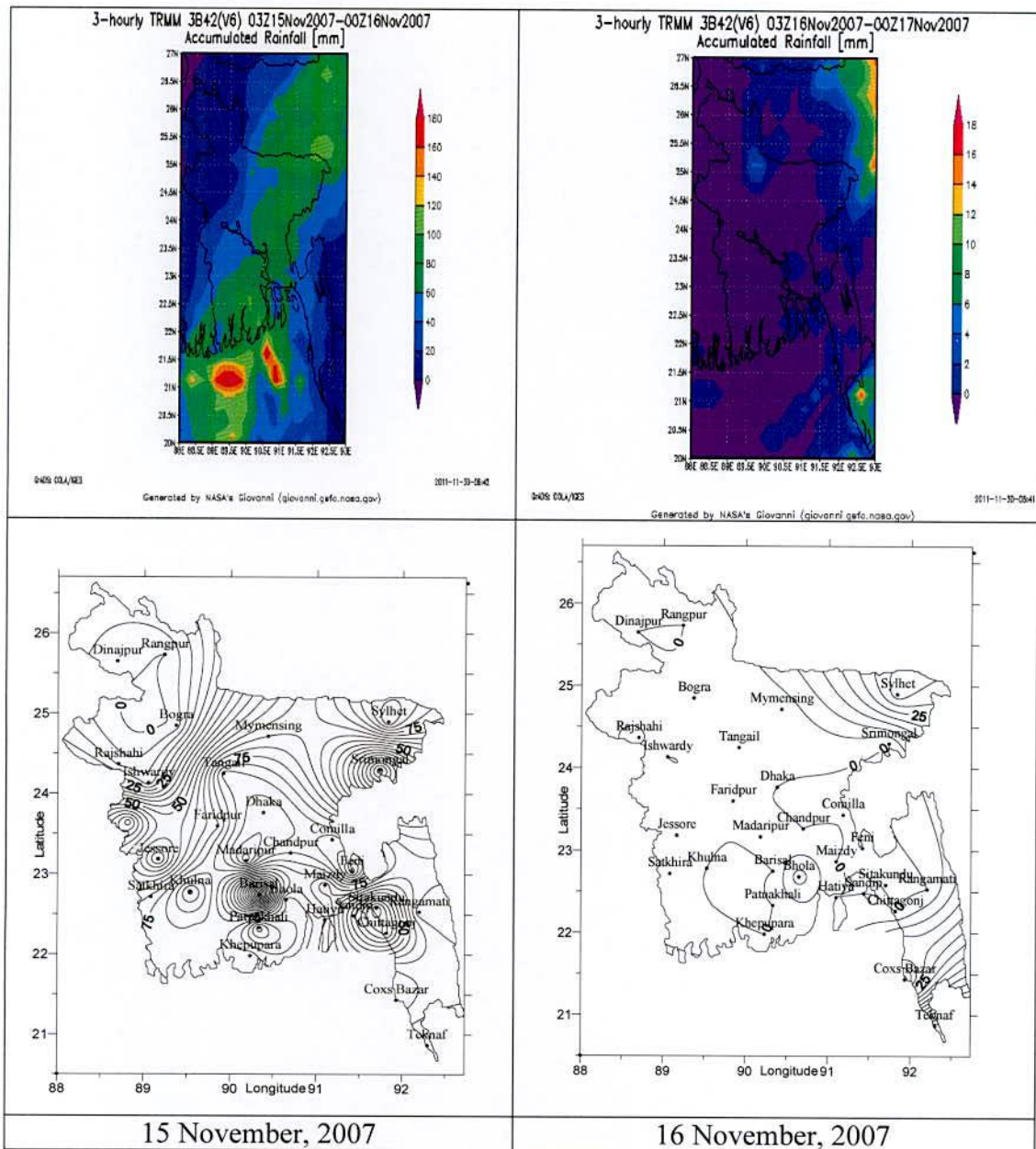


Figure 5.1.7.4: 24 hours accumulated rainfall (mm) of TC Sidr along using TRMM and rain-gauge data valid for 15 and 16 November 2007

5.1.8 Track Pattern

MM5 and WRF models simulated track of TC Sidr along with observed track are plotted in the Figures 5.1.8.1a and 5.1.8.1b respectively. The track forecasts of TC Sidr for 96, 72, 48 and 24 hrs are based on the initial fields of 00 UTC on 13 November, 00 UTC on 14 November, 00 UTC on 15 November and 12 UTC of 15 November respectively.

It is seen from Figure 5.1.8.1a that MM5 model simulated track for 96, 72, 48 and 24 hours are parallel to observed track but it is deviated east and west side of the observed track. It may be because of initial data error. Figure shows that model is able to generate northwest, north and northeast movement of the system very well. It reveals that 24, 48 and 72 hrs tracks are more close to the JTWC best track compared to 96 hrs tracks. However, there are some errors in the positions with respect to time which shows some lag in landfall. The track from 24 hours simulation track is better than that of any others simulation. The landfall position for 24 hrs simulation track is much closed to any other simulation. So, by changing initial data, the simulated track becomes close to the observed track.

It is seen from Figure 5.1.8.1b that WRF model simulated track for 96, 72, 48 and 24 hours are parallel to observed track but it is deviated east and west side of the observed track. It may be because of initial data error. Figure shows that model is able to generate northwest, north and northeast movement of the system very well. It reveals that track obtained from 96 hrs simulation are more close to the JTWC best track compared to the track obtained from 24, 48 and 72 hrs simulation. However, there are some errors in the positions with respect to time which shows some lag in landfall. Simulated landfall time is 00 UTC of 16 November compared to observed landfall time 18 UTC of 15 November using 96 hrs simulation of WRF model based on the initial condition 00 UTC of 13 November, 2007. The track from 96 hours simulation is better than that of any other simulations. The landfall position for 96 hrs simulation track is matched with observed position. So, by changing initial data, the simulated track became close to the observed track.

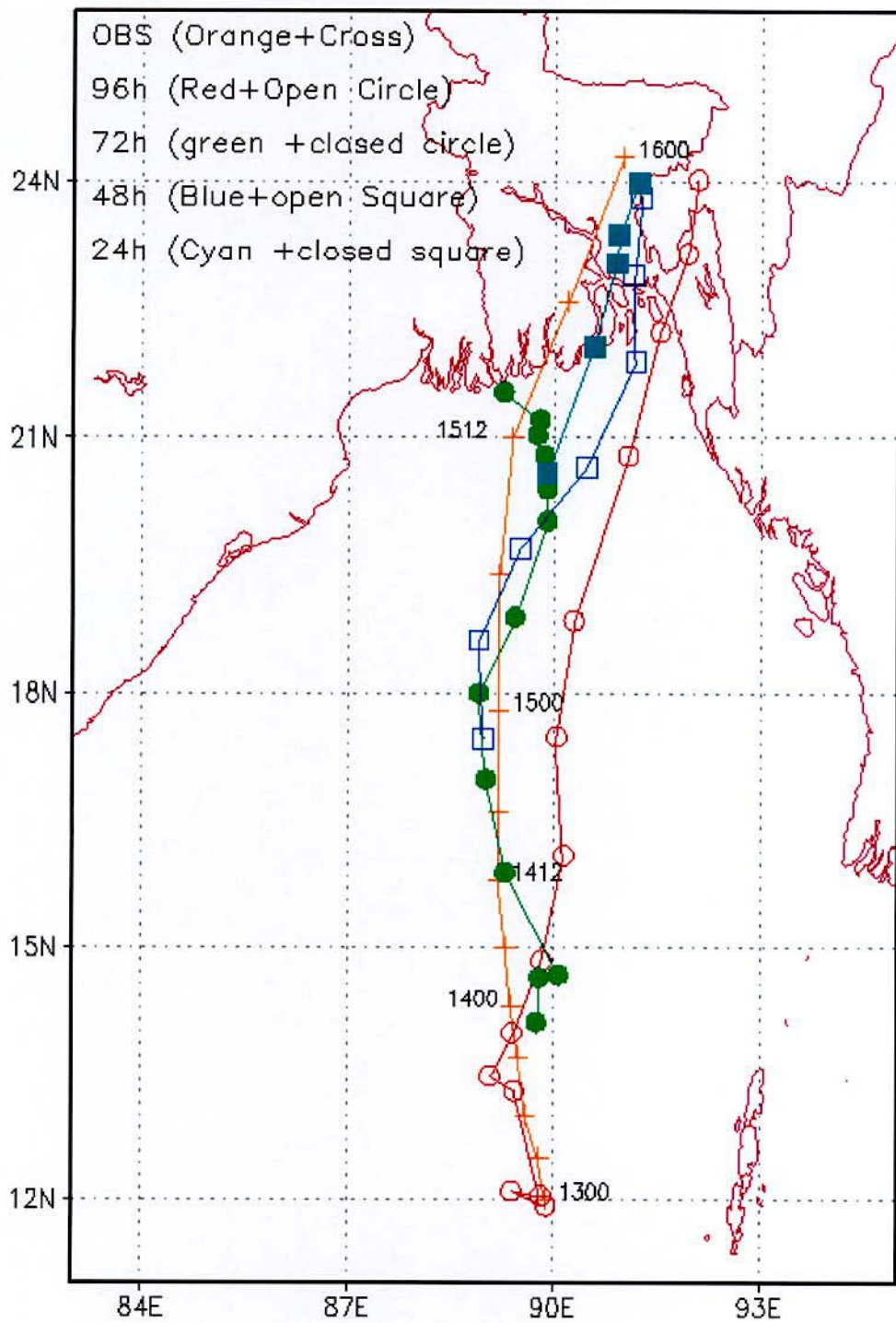


Figure 5.1.8.1a: MM5 model simulated and observed tracks of TC Sidr

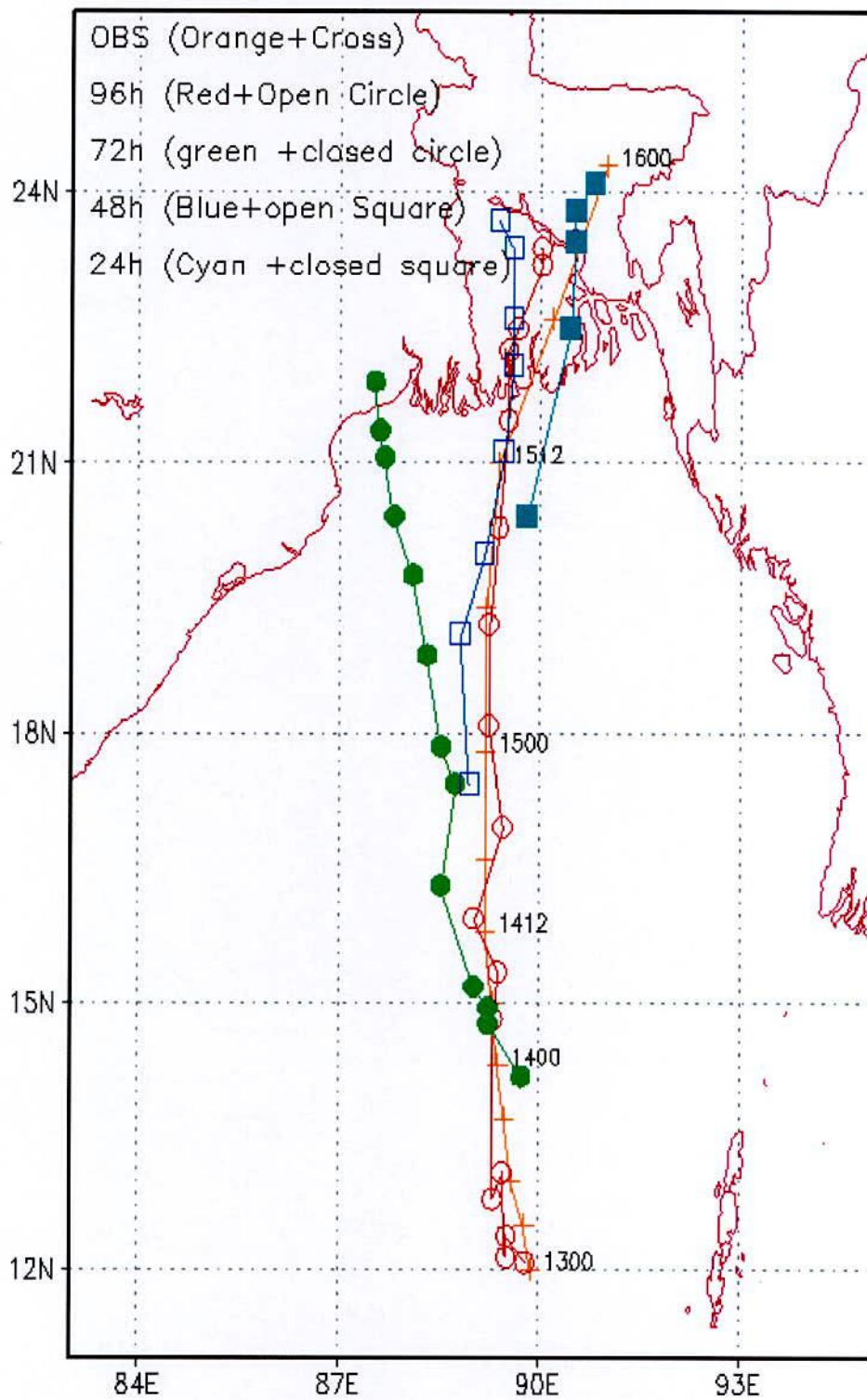


Figure 5.1.8.1b: WRF model simulated and observed tracks of TC Sidr

5.2 Simulation of Tropical Cyclone (TC) Aila using MM5 and WRF Models

To analyze the evolution and structure of TC Aila the MM5 and WRF models were run for 96 hrs from the initial field at 00 UTC of 23 May 2009. But after 51 hrs of simulation of MM5 model at 03 UTC of 25 May 2009 and after 57 hrs of simulation of WRF model at 09 UTC of 25 May 2009 the system attained highest intensity. Using MM5 and WRF models, the different meteorological parameters are discussed for the evolution and structure of the TC Aila in the following sub-section. We compare the MM5 and WRF models simulated data with those obtained from Joint Typhoon Warning Centre (JTWC), which would be treated as observed track hereafter.

5.2.1 Pressure Field

Minimum seal level pressure (MSLP) of a TC is of great importance as it helps to measure the intensity of a cyclone. Since TCs develop over vast oceanic areas, where observations are sparse or not available, it is of great difficulty to make any validation of model simulated MSLP with real observable data from sea before the landfall. But now meteorologists are able to estimate MSLP and maximum sustained wind (MSW) using interpretations of satellite products.

Figure 5.2.1.1 shows the observed and model simulated MSLP of TC Aila. From the figure it is observed that the model simulated and observed MSLP drops gradually with time and attains peak intensity just before the landfall and thereafter MSLP increases. The simulated MSLP using both the models is lower than that of observed. The MM5 and WRF Models simulated and JTWC observed landfall times are 03 UTC, 09 UTC and 06 UTC on 25 May 2009 respectively. The variation of MM5 and WRF models simulated MSLP compare to that of observed with time shows that model simulates realistic temporal variation of MSLP.

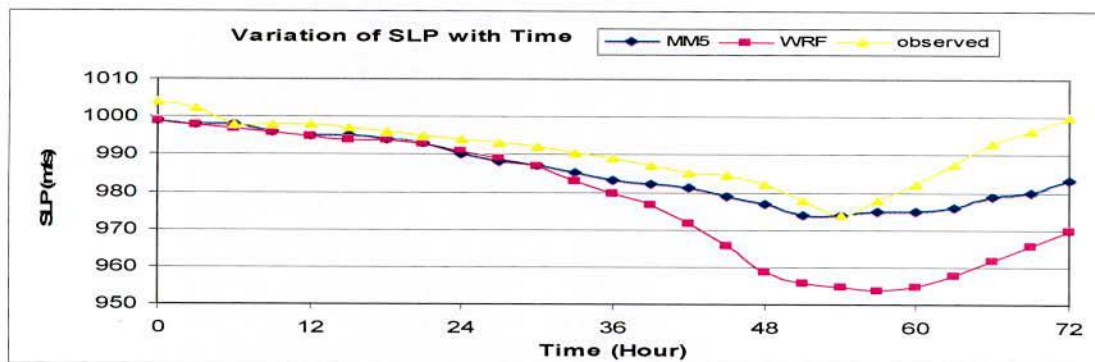


Figure 5.2.1.1: MM5 model simulated and observed central pressure of TC Aila

The distribution of sea level pressure (SLP) of TC Aila obtained from MM5 model at 00 UTC on 23, 24 and 25 May and 03 UTC on 25 May 2009 (i.e. its mature stage) and obtained from WRF model at 00 UTC on 23, 24 and 25 May and 09 UTC on 25 May 2009 (i.e. its mature stage) are shown in Figures 5.2.1.2a and 5.2.1.2b respectively. The figures demonstrate that the intensity of the TC Aila increases as the MSLP drops with time up to its peak intensity and TC changes its position of centre with time. In the figure the isobar has circular arrangement around the cyclone centre with some asymmetric features in the outer periphery. The contour interval is different for different positions. At mature stage the contour interval is 2.5/3.0 and 5 hPa for MM5 and WRF model respectively. The lowest simulated central pressures obtained from MM5 and WRF model are 974 and 955 hPa respectively and they are obtained at 03 and 09 UTC on 25 May respectively, whereas the lowest central is 974 hPa at 06 UTC on 25 May 2009. At mature stage, considering the outermost closed isobar, the system's horizontal size is estimated as 8.0° in the east-west and 9.0° in the north-south direction for MM5 model and as 6.5° in the east-west and 6.0° in the north-south direction for WRF model, demonstrating a little bit spatial asymmetry in its horizontal structure.

The distribution of the sea level pressure of the TC Aila obtained from MM5 model along east-west direction passing through its centre (21.569°N and 90.301°E) at time 03 UTC on 25 May 2009 is shown in Figure 5.2.1.3a. The above mentioned parameter obtained from WRF model through centre (21.357°N and 89.856°E) at time 09 UTC on 25 May 2009 is shown in Figure 5.2.1.3b. The Figures 5.2.1.3a and 5.2.1.3b demonstrate the moderate pressure gradient around the centre with maximum gradient at around 55-60 km from the centre. Thus the radius of the eye of the cyclone is found to be below 55 km according to the simulation.

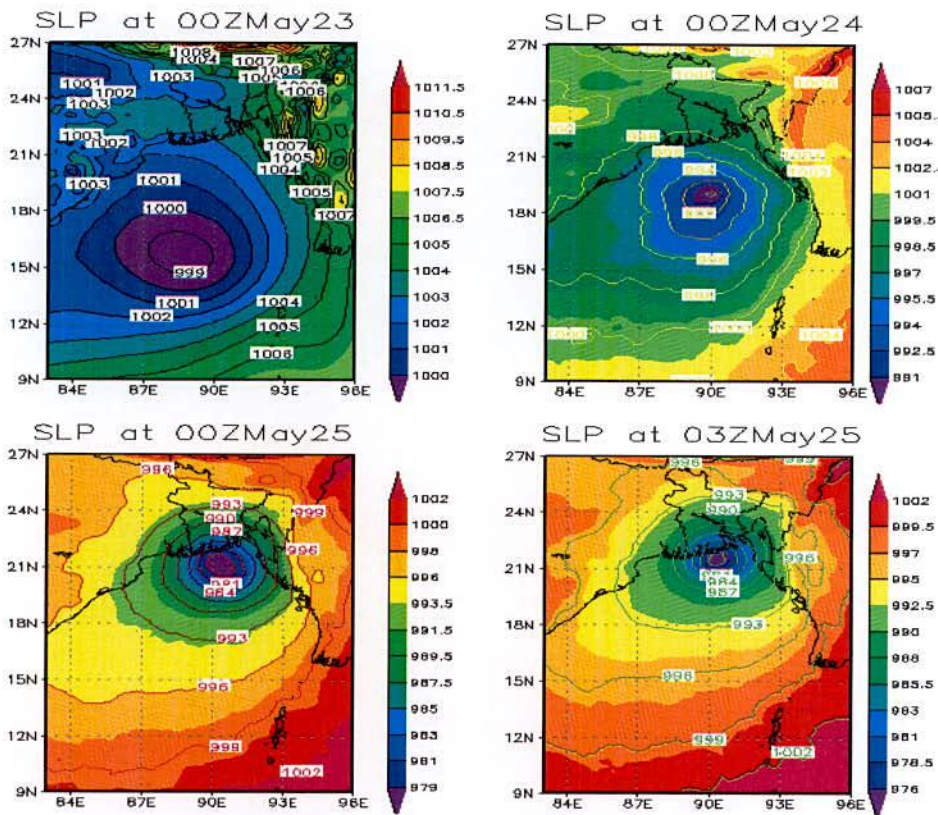


Figure 5.2.1.2a: MM5 model simulated SLP of TC Aila at 00 UTC on 23, 24, 25 May and 03 UTC on 25 May 2009.

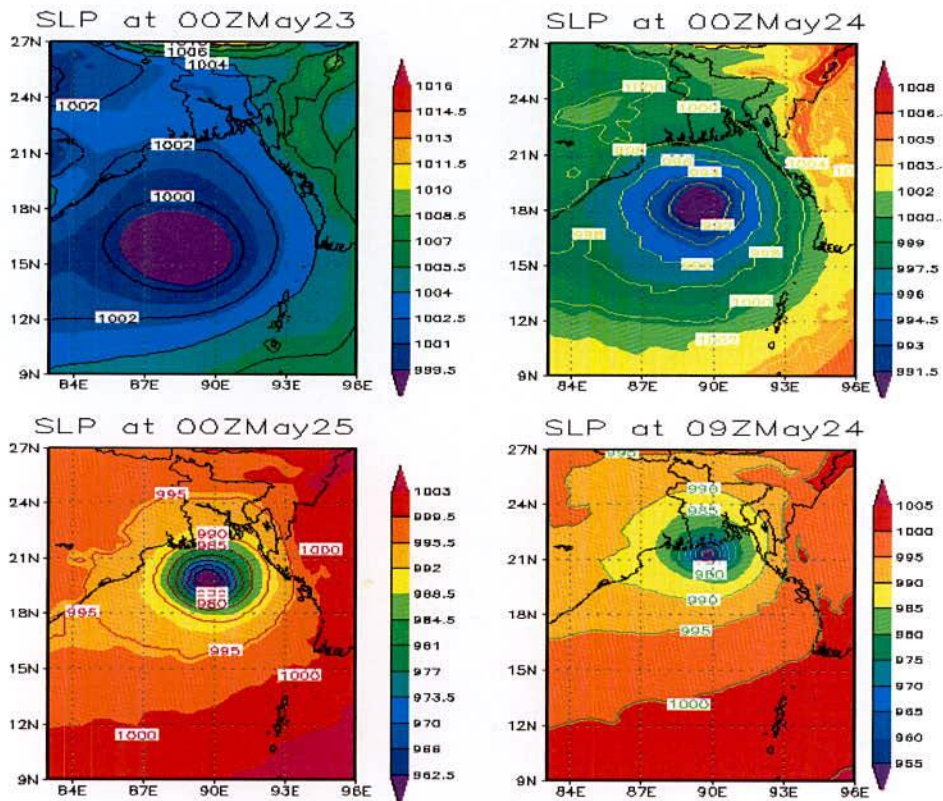


Figure 5.2.1.2b: WRF model simulated SLP of TC Aila at 00 UTC on 23, 24, 25 May and at 09 UTC on 25 May 2009.

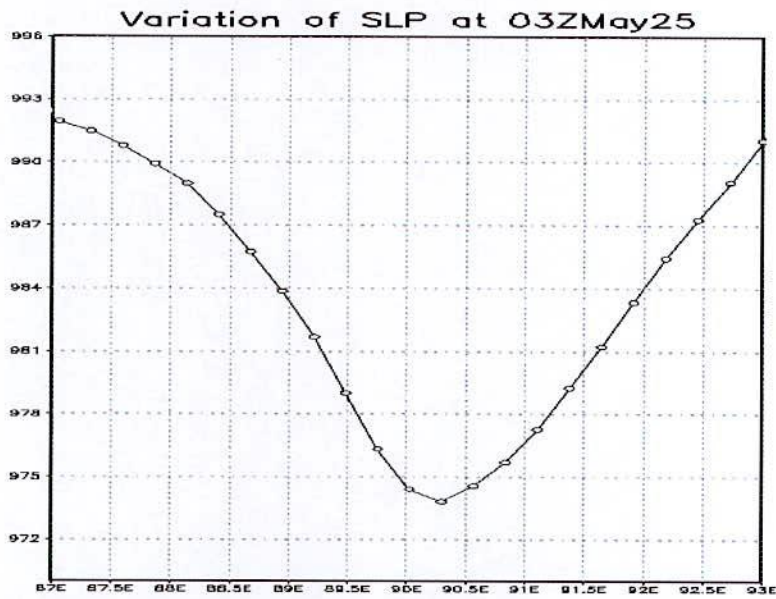


Figure 5.2.1.3a: East West cross sectional view of MM5 model simulated SLP of TC Aila through the centre (21.569°N and 90.301°E) at 03 UTC on 25 May 2009

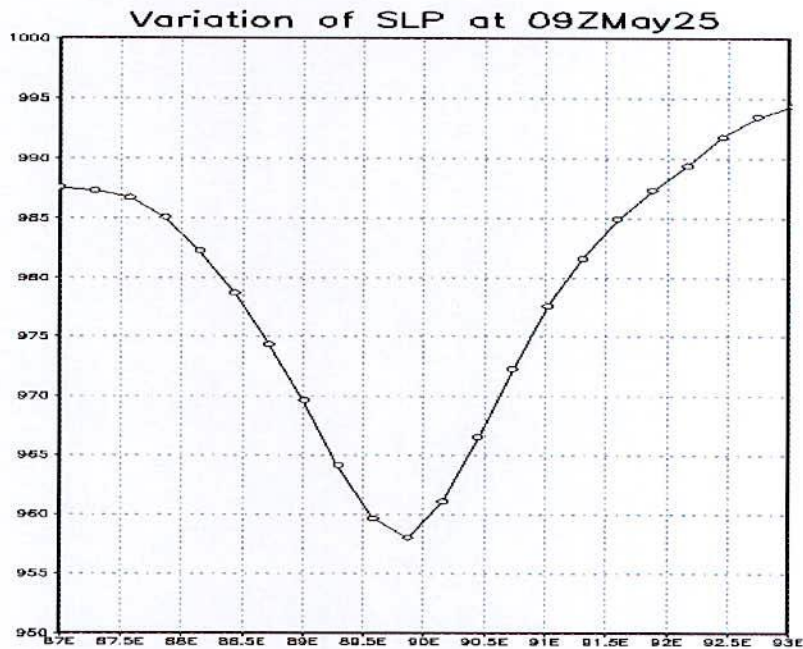


Figure 5.2.1.3b: East West cross sectional view of WRF model simulated SLP of TC Aila through the centre (21.357°N and 89.856°E) at 09 UTC on 25 May 2009.

5.2.2 Wind Field

Maximum wind speed (MWS) directly devastates the affected area at the time of landfall. On the other hand it is the most active driving force of generating storm surge over the area of landfall and along its tracks. So, it is important parameters of tropical cyclone for measuring its intensity. Now a days, spaced based satellite technology is doing a great job to estimate MWS and other important parameters because in-situ observations are not widely available over the ocean to determine or to estimate the intensity of the system.

Figure 5.2.2.1 shows the time variations of MM5 and WRF models simulated MWSs and observed winds of TC Aila. The models simulated MWSs are obtained at the standard meteorological height of 10 m. MM5 model simulated MWSs are lower than the observed values through almost full forecast hours except for the few hours when the predicted values are matched with those observed values. Again, WRF model simulated MWSs are higher than the observed values through almost full forecast hours.

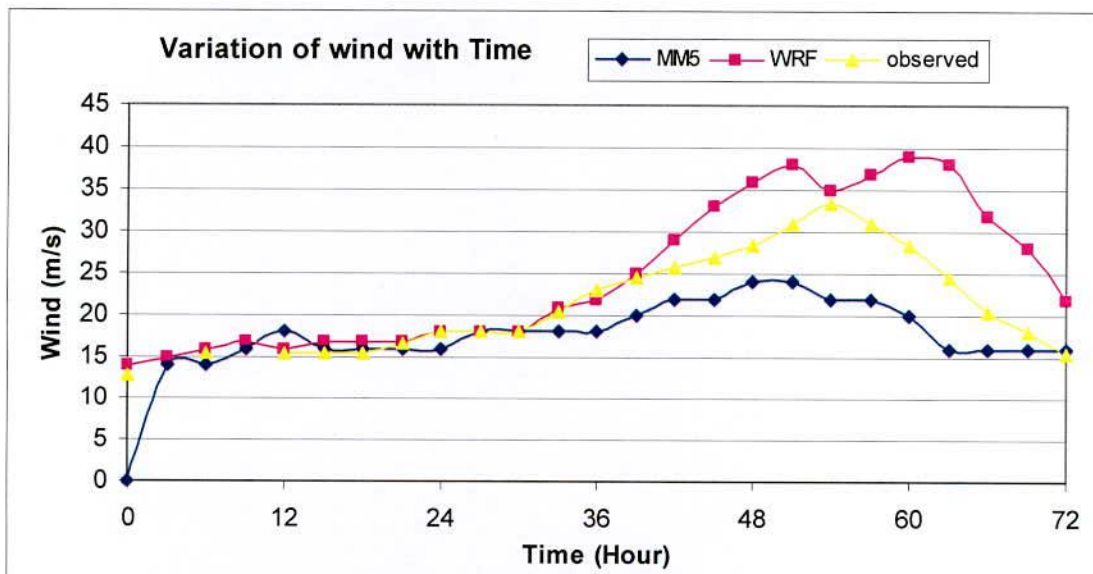


Figure 5.2.2.1: Observed and MM5 and WRF models simulated wind speed (m/s) of TC Aila

The distribution of surface wind of TC Aila obtained from MM5 model at 00 UTC on 23, 24, 25 May and at 03 UTC on 25 May 2009 (i.e. its mature stage) is shown in Figure 5.2.2.2a. The figure shows that the wind field of the cyclone is highly asymmetric in the horizontal distribution. At the initial time of simulation (i.e. 00 UTC on 23 May 2009) the wind speed is zero when the cyclone was in the sea as shown in Figure 5.2.2.2a. After 24 hours of simulation i.e. at 00 UTC on 24 May 2009, the pattern has an asymmetric wind distribution with strong wind bands in the front right side and rear right sides close to the centre of northward moving storm. The wind flow in the core region shows a near circular feature with

minimum wind speed at the centre. At 00 UTC on 25 May 2009 the cyclone is mostly organized and the wind flow in the core region shows a near circular feature with minimum wind speed at the centre. At 03 UTC on 25 May 2009 (i.e. at mature stage), a strong wind band having strongest wind exceeding 24 m/s is found at a distance of around 55 km in the west of the cyclone centre with elongation in northwest-southeast. It may be noted that the model generated horizontal winds of 86 km/hr is lower than the observed winds of around 120 km/hr. It is also noted that, due to frictional force of landmass, the winds is much less in the front side compared to other side of the cyclonic system as seen in the landfall feature of surface wind distribution (Figure 5.2.2.2a).

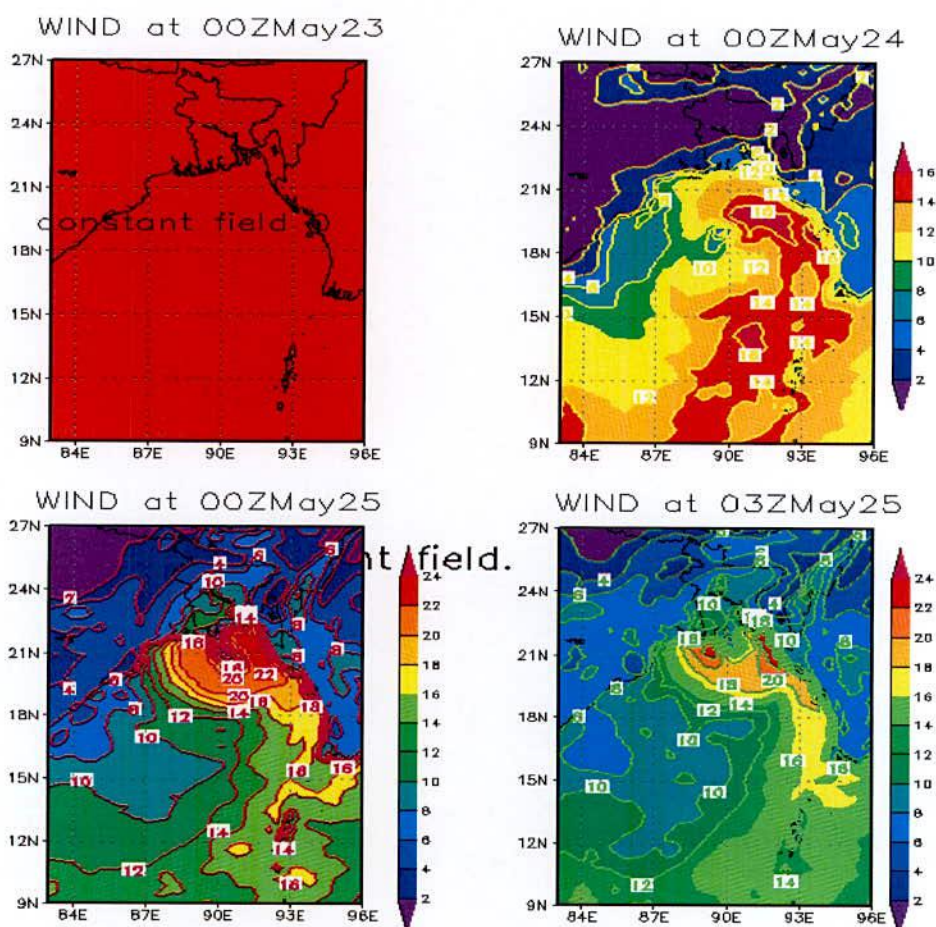


Figure 5.2.2.2a: MM5 model simulated Wind speed (m/s) at 00 UTC on 23, 24, 25 May and at 03 UTC on 25 May 2009 of TC Aila.

The distribution of surface wind of TC Aila obtained from WRF model at 00 UTC on 23, 24 and 25 May and at 09 UTC on 25 May 2009 (i.e. mature stage of TC Aila) is shown in Figure 5.2.2.2b. The figure shows that the wind field of the cyclone is highly asymmetric in the horizontal direction. The distribution of surface wind of Aila at 00 UTC on 23 May 2009 (i.e. at the initial time of simulation) is shown in Figure 5.2.2.2b when the cyclone was in the sea. The figure shows that the pattern has an asymmetric wind distribution with strong wind bands

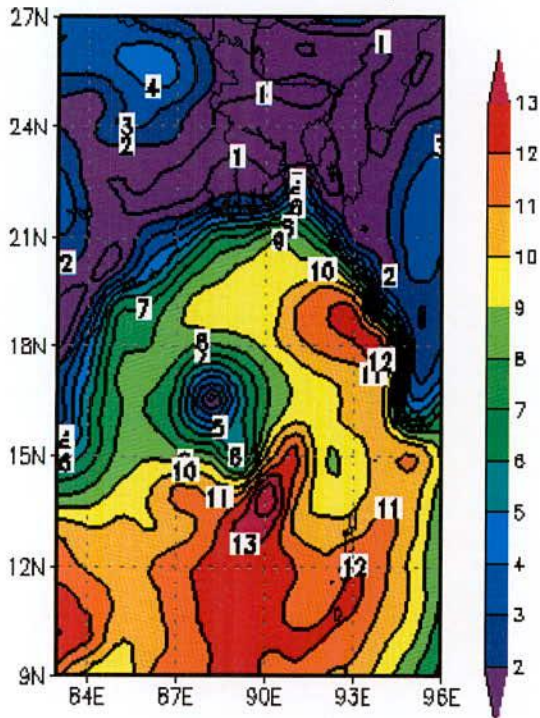
in the front right side, rear left and rear right sides close to the centre of northward moving storm. The wind flow in the core region shows a near circular feature with minimum wind speed at the centre. Similar pattern is also seen at 00 UTC on 24 May 2009. At 00 UTC on 25 May 2009, the TC Aila is almost organized and the wind flow in the core region shows a near circular feature with minimum wind speed at the centre. At 09 UTC on 25 May 2009 (i.e. at mature stage), a strong wind band having strongest wind exceeding 35 m/s is found at a distance of around 55 km south of the system with elongation in the northeast-southwest direction. The model generated horizontal wind speed 126 km/hr is almost the same as the observed winds of around 120 km/hr. Figure 5.2.2.2b (lower right corner) shows the landfall feature of surface wind distribution where the wind is much less in the front side compared to other sides of the cyclonic system.

From the above discussion, it is understood that maximum wind speed obtained from observation is lower than that obtained WRF model and higher than that obtained from MM5.

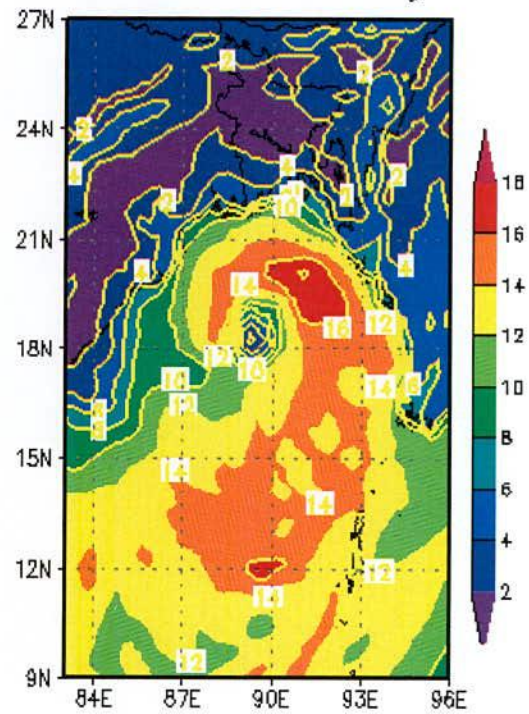
Figure 5.2.2.3a shows the distribution of the surface wind of the TC Aila obtained from MM5 model along east-west cross section passing through its centre ($21.569^{\circ}\text{N } 90.301^{\circ}\text{E}$) at 03 UTC on 25 May 2009. Again, Figure 5.2.2.3b shows the distribution of the surface wind of the TC Aila obtained from WRF model along east-west cross section passing through its centre ($21.357^{\circ}\text{N } 89.856^{\circ}\text{E}$) at 09 UTC on 25 May 2009. Both the figures demonstrate that a calm region is found inside the eye of the system and maximum wind is found in the eye wall. The radius of maximum wind of the TC Aila obtained from MM5 and WRF model is found to be just lower than 55 km according to the simulation.

The horizontal distribution of vector wind field obtained from MM5 model for 850, 500, 300 and 200 hPa at 00 UTC on 23, 24 and 25 May and at 03 UTC on 25 May 2009 (i.e. its mature stage) and obtained from WRF model for 850, 500, 300 and 200 hPa at 00 UTC on 23, 24, 25 May and at 09 UTC on 25 May 2009 (i.e. its mature stage) have shown in Figures 5.2.2.4a and 5.2.2.4b respectively. The Figures 5.2.2.4a and 5.2.2.4b show that a well organized cyclonic circulation with strong winds encircling the centre is found at 850 and 500 hPa levels for both the models. Model derived maximum winds are tabulated in Tables 5.2.2.1a and 5.2.2.1b. MM5 Model derived maximum wind speeds at the mature stage (i. e. at 03 UTC on 25 May) are about 40, 30, 30 and 40 m/s at 850, 500, 300 and 200 hPa levels respectively. The WRF model derived maximum wind speed at the mature stage (at 09 UTC on 25 May) at 850, 500, 300 and 200 hPa levels are about 70, 60, 50 and 40 m/s respectively. It is noted that the strong wind is confined to the right of the direction of the movement of the system for both the model and at level 850 and 500 hPa. At 300 hPa wind shows cyclonic circulation in the right side of the cyclone and weak outflow in the left side. It is very clear in

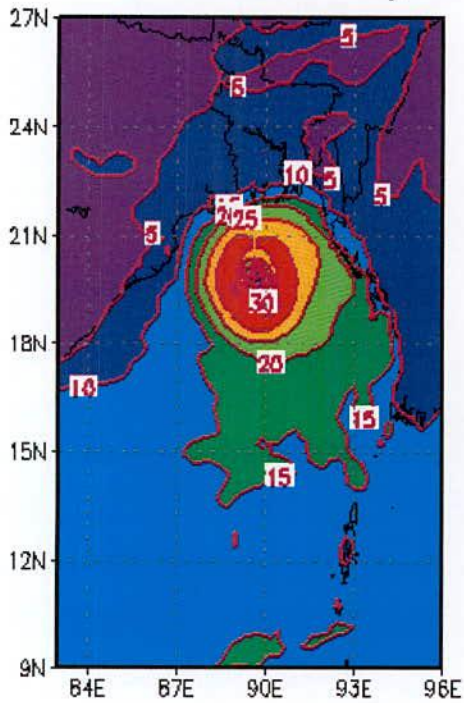
WIND at 00ZMay23



WIND at 00ZMay24



WIND at 00ZMay25



WIND at 09ZMay25

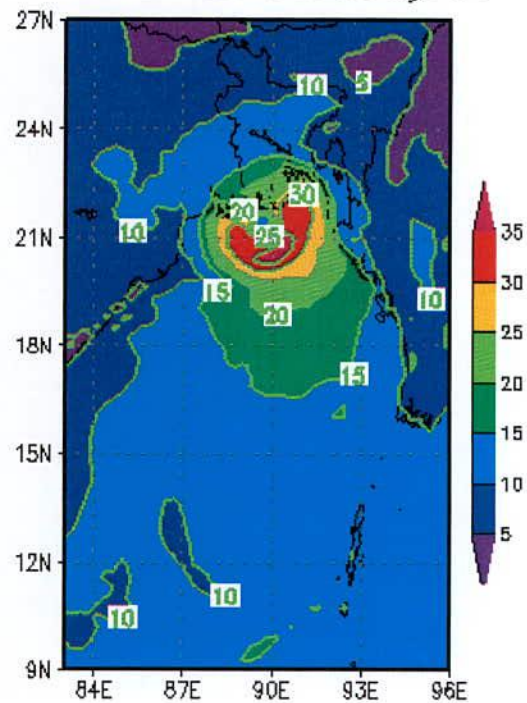


Figure 5.2.2.2b: WRF model simulated Wind speed (m/s) at 00 UTC on 23, 24, 25 May and at 09 UTC on 25 May 2009 of TC Aila

Figure 5.2.2.4a obtained from MM5 model than the Figure 5.2.2.4b obtained from WRF model. At 200 hPa level strong outflow is evident from the central part of the cyclone. So, the results obtained from MM5 and WRF models, demonstrate inflow in the lower level and outflow in the upper levels.

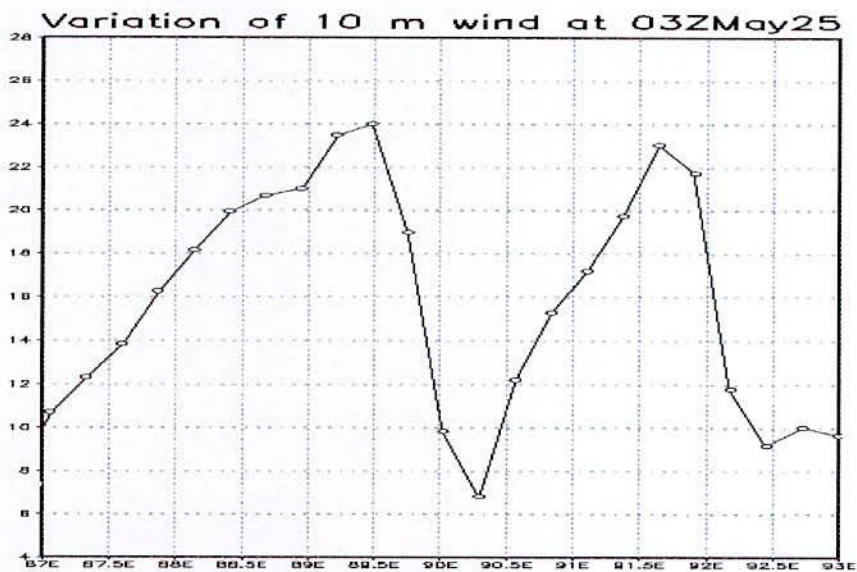


Figure 5.2.2.3a: East-West cross sectional view of MM5 model simulated wind of TC Aila through the centre (21.569°N and 90.301°E) at 03 UTC on 25 May 2009.

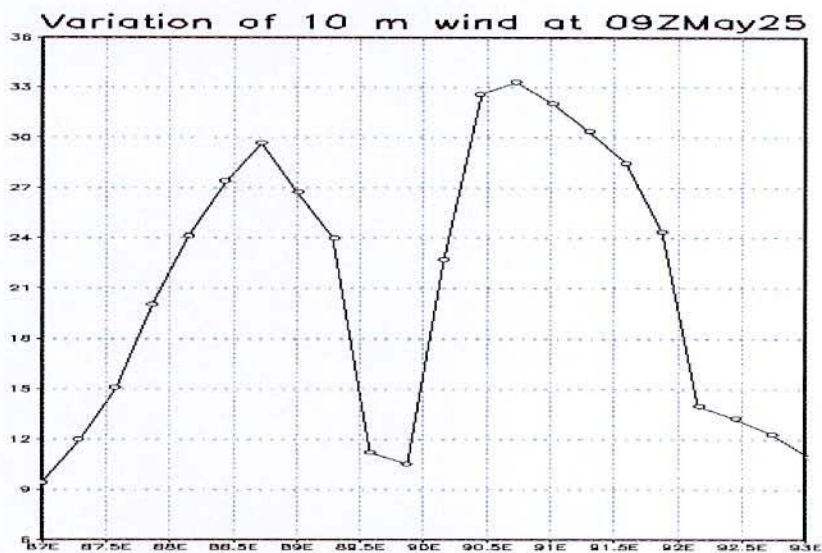


Figure 5.2.2.3b: East-West cross sectional view of WRF model simulated wind of TC Aila through the centre (21.357°N and 89.856°E) at 09 UTC of 25 May 2009

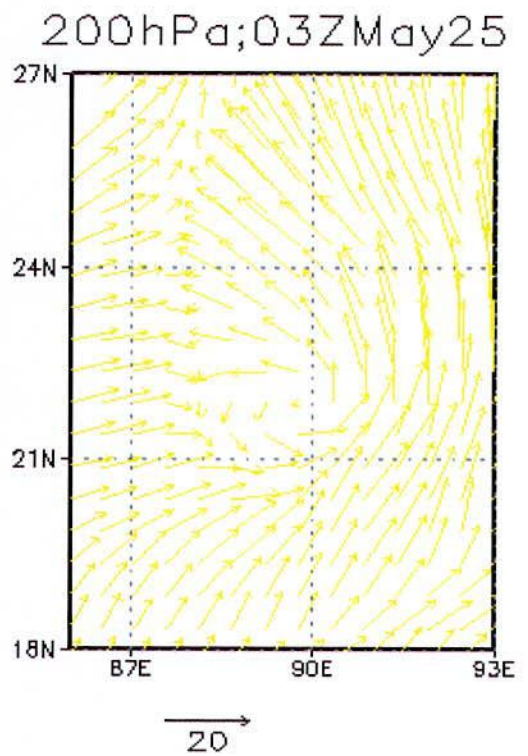
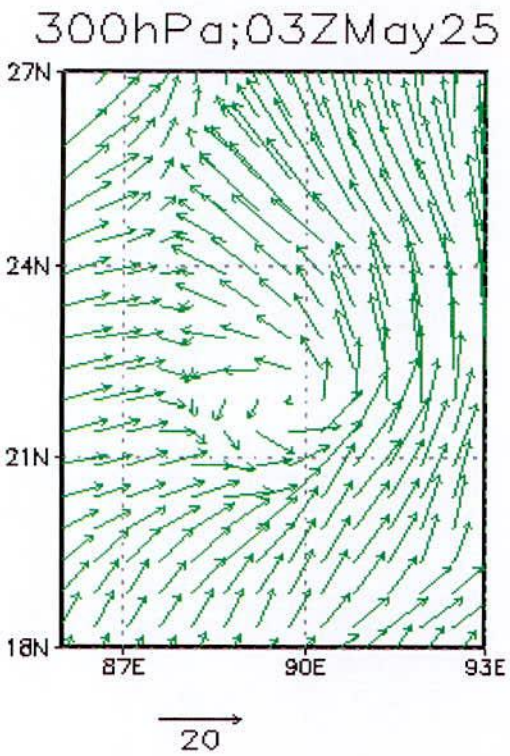
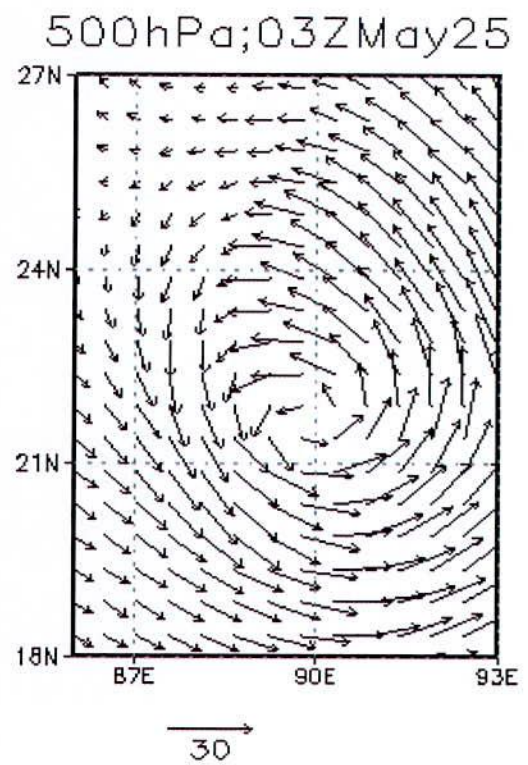
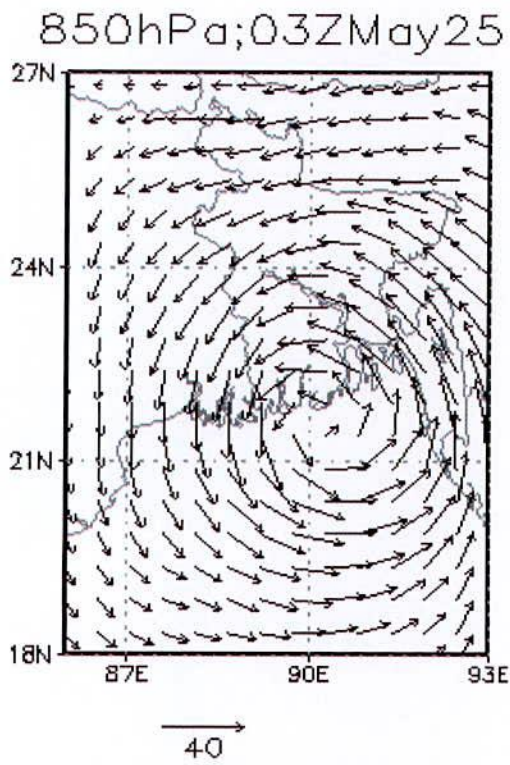


Figure 5.2.2.4a: MM5 model simulated wind vector and magnitude at 850, 500, 300 and 200 hPa levels at 03 UTC on 25 May 2009 of TC Aila.

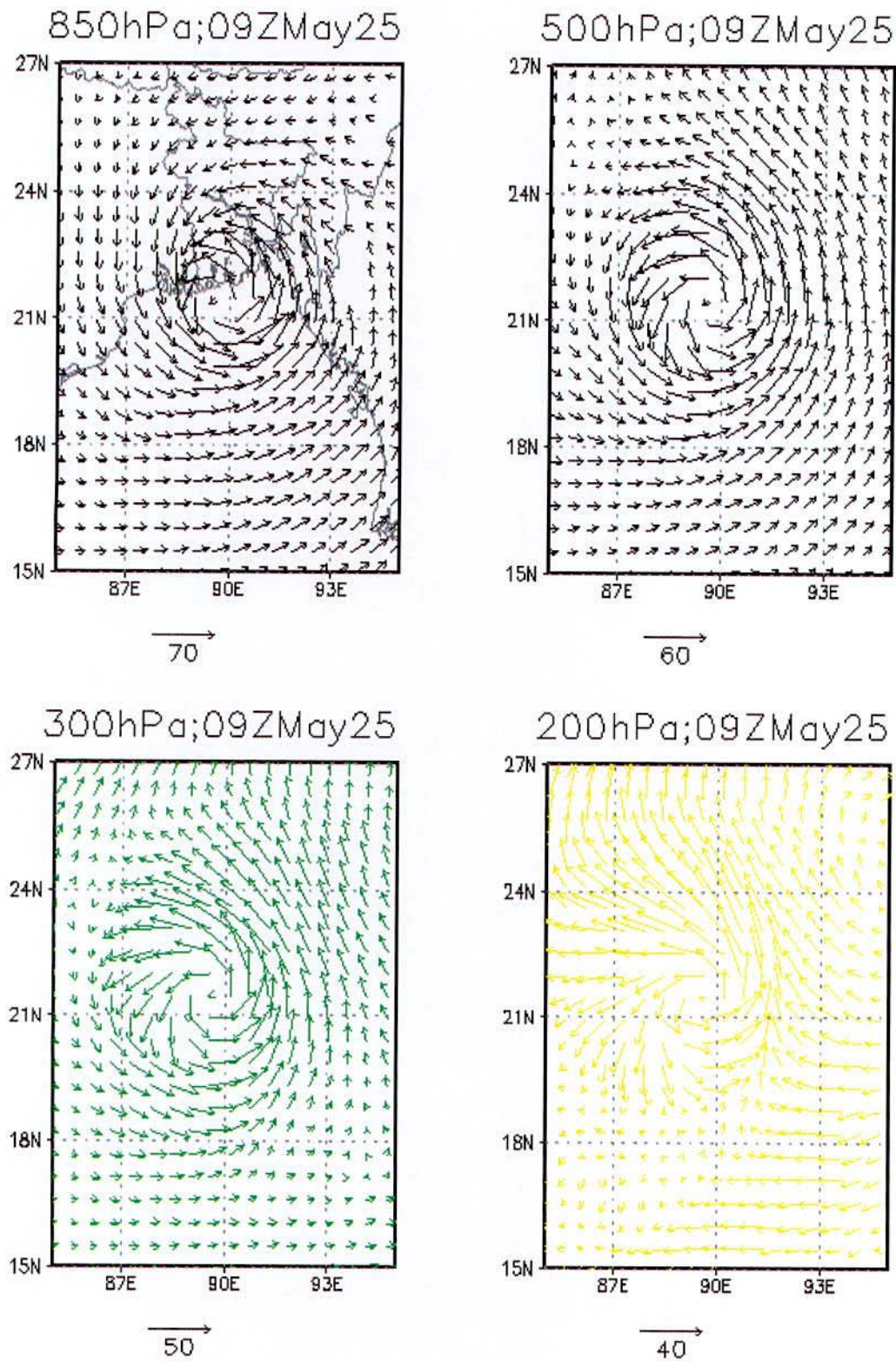


Figure 5.2.2.4b: WRF model simulated wind vector and magnitude at 850, 500, 300 and 200 hPa level at 03 UTC on 25 May 2009 of TC Aila.

Table 5.2.2.1a: MM5 model simulated wind speed (m/s) at different pressure levels of TC Aila on 00 UTC on 23, 24, 25 May and at 03 UTC on 25 May 2009.

| Pressure level (hPa) | MM5 model simulated wind Speed (m/s) at | | | |
|-------------------------|---|---------------------|---------------------|---------------------|
| | 00 UTC of 23 May | 00 UTC of 24 May | 00 UTC of 25 May | 03 UTC of 25 May |
| 850 | 20 | 20 | 40 | 40 |
| 500 | 20 | 20 | 30 | 30 |
| 300 | 10 | 20 | 30 | 30 |
| 200 | 20 | 30 | 40 | 40 |

Table 5.2.2.1b: WRF model simulated wind speed (m/s) at different pressure levels of TC Aila at 00 UTC on 23, 24, 25 May and at 09 UTC on 25 May 2009

| Pressure level (hPa) | WRF model simulated wind Speed (m/s) at | | | |
|-------------------------|---|---------------------|---------------------|---------------------|
| | 00 UTC of 23 May | 00 UTC of 24 May | 00 UTC of 25 May | 09 UTC of 25 May |
| 850 | 20 | 30 | 70 | 70 |
| 500 | 20 | 30 | 50 | 60 |
| 300 | 20 | 20 | 40 | 50 |
| 200 | 20 | 20 | 40 | 40 |

Figure 5.2.2.5a and 5.2.2.5b show the vertical profiles of radial, tangential, vertical and vector wind of the system at 03UTC on 25 May 2009 (i.e. its mature stage) for MM5 and at 09 UTC on 25 May 2009 (i.e. its mature stage) for WRF respectively. The values of the radial, tangential and vertical component of wind for different times are tabulated in Tables 5.2.2.2a and 5.2.2.2b for the MM5 and WRF models respectively. The figure for the radial component of wind indicates that at 03 UTC on 25 May 2009 (i.e. its mature stage), the system is much more organized and it also clearly shows that the system has strong inflow in the lower level and outflow in the upper level. The values of the radial component of wind at mature state obtained from WRF model is higher than that obtained from MM5 model. The figures demonstrate that the tangential wind flows to the northerly direction at the eastern side of the system and southerly direction at the western side. The strong wind with having different speed (tabulated in Table 5.2.2.2a) is confined to the different levels in lower troposphere and extended up to 300 hPa level at the right side and 600 hPa level at the left

side for MM5 model and to 300 hPa level at the right side and 650 hPa level at the left side for WRF model.

From the Table 5.2.2.2a and 5.2.2.2b, the values of vertical velocity are different for different times and it reveals that strong upward motion of about 60 cm/s exists along the eye wall and other parts of the system which feed moisture into the system for MM5 model and about 140 cm/s exists along the eye wall and other parts of the system which feed moisture into the system for WRF model. It is noted that TC Aila has very strong updraft motion exceeding 300 cm/s around the eye wall in the west throughout mid and upper troposphere. The downward motion is visible in the central parts of the cyclone and other areas in between rain bands.

Table 5.2.2.2a: MM5 Model simulated maximum value of radial wind, tangential wind and vertical velocity of TC Aila at 00 UTC on 23, 24, 25 May and 03 UTC on 25 May 2009.

| Component of wind | Simulated Wind Speed (cm/s) at different time | | | |
|-------------------|---|------------------|------------------|------------------|
| | 00 UTC on 23 May | 00 UTC on 24 May | 00 UTC on 25 May | 03 UTC on 25 May |
| Radial wind | 1000 | 1000 | 1200 | 1200 |
| Tangential wind | 1200 | 2000 | 3000 | 2500 |
| Vertical Velocity | 16 | 50 | 35 | 60 |

Table 5.2.2.2b: WRF Model simulated maximum value of radial wind, tangential wind and vertical velocity of TC Aila at 00 UTC on 23, 24, 25 May and 09 UTC on 25 May 2009.

| Component of wind | Simulated Wind Speed (cm/s) at different time | | | |
|-------------------|---|------------------|------------------|------------------|
| | 00 UTC on 23 May | 00 UTC on 24 May | 00 UTC on 25 May | 09 UTC on 25 May |
| Radial wind | 900 | 15 | 3000 | 2000 |
| Tangential wind | 12 | 2000 | 4000 | 5000 |
| Vertical velocity | 0.5 | 50 | 140 | 110 |

Figures of the vertical cross section of wind flow is plotted through latitude 21.569°N at time 03 UTC of 25 May, 2009 for MM5 model and through latitude 21.357°N at 09 UTC on 25 May, 2009 for WRF model.

Strong winds are confined to the lower troposphere, and decreased towards upper levels. It further confirms that the maximum winds are confined, within the entire troposphere, to the right of the direction of the movement of the system. This value decreases with the radial distance from both side of the eye. Calm wind zone is little bit tilted to the west and get expanded towards upper levels. This zone is sharp and narrow and it gets expanded towards upper levels.

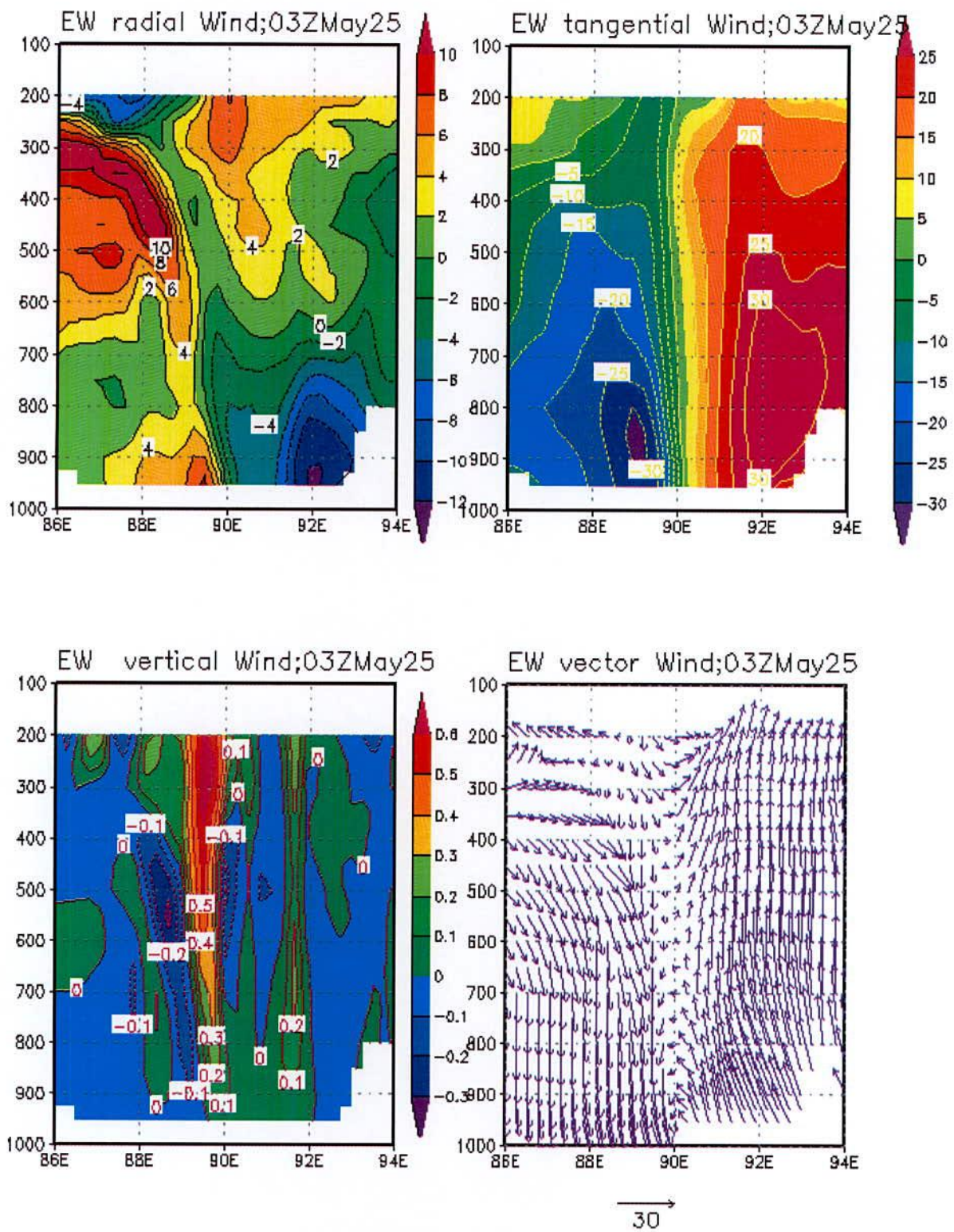


Figure 5.2.2.5a: MM5 model simulated east-west cross section of vertical profile of radial wind at 03 UTC on 25 May 2009 of TC Aila

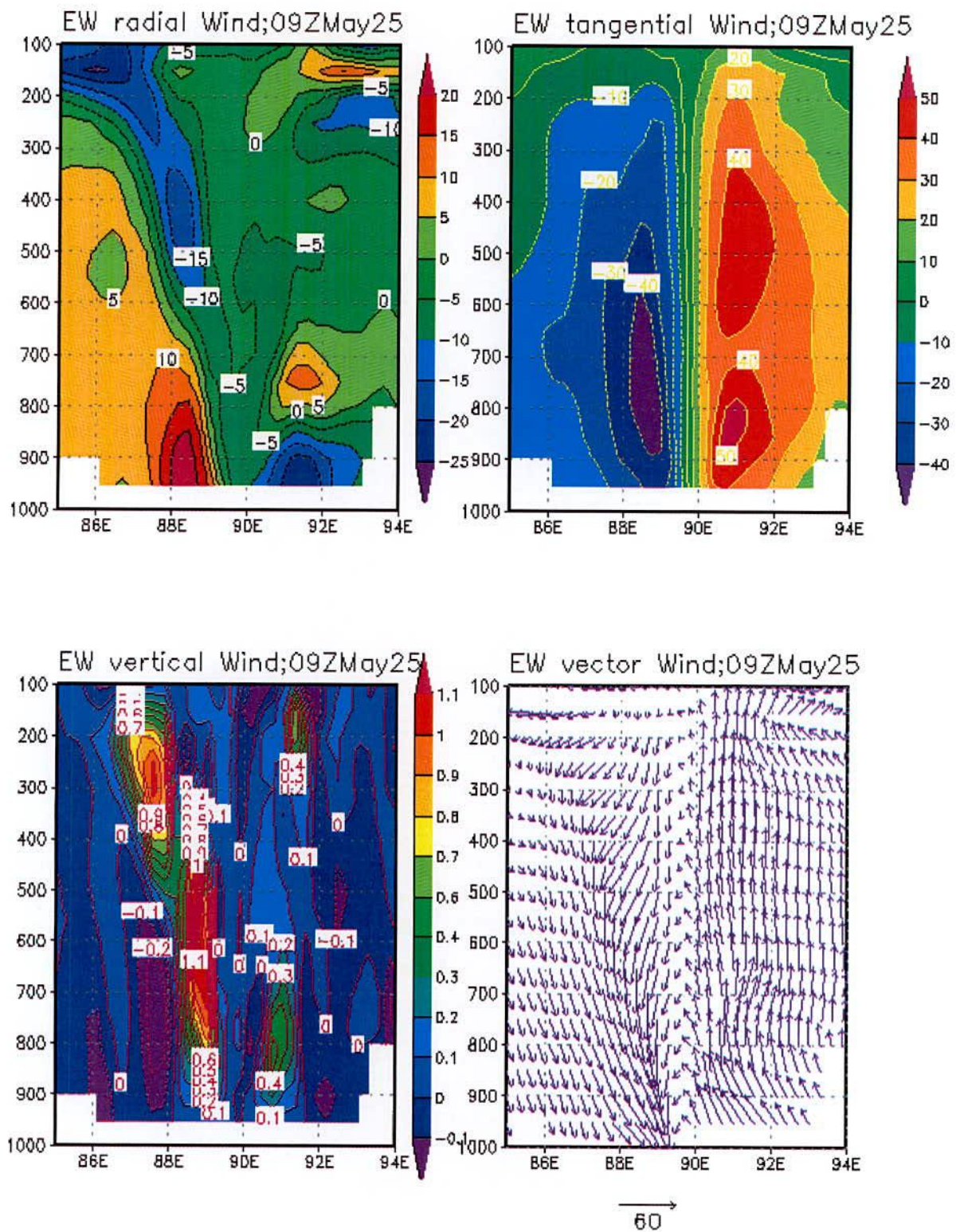


Figure 5.2.2.5b: WRF model simulated east-west cross section of vertical profile of radial wind at 09 UTC on 25 May 2009 of TC Aila.

This is in agreement with the previous studies of Rao and Prasad (2006) and Goswami *et al.* (2006) on Orissa cyclone. Cyclonic circulation is generally seen up to about 300 hPa level and anticyclonic circulation with divergence fields aloft. In this cyclone, there is a variation of the level of cyclonic circulation and is extended even more than 300 hPa level for MM5 and more than 200 hPa for WRF models.

5.2.3 Vorticity Field

The MM5 and WRF models simulated low level relative vorticity at 850 hPa as a function of time is shown in Figure 5.2.3.1. Results obtained from MM5 model shows a sharp rise in the vorticity value in the first 51 hours of simulation of the model and retains the maximum value for 6 hours duration (51 -57 hours of forecast). Thereafter the vorticity decreases up to 72 hours of forecast. Again, results obtained from WRF model shows a sharp rise in the vorticity value in the first 48 hours of simulation of the model and retains the maximum value for 9 hours duration (48-54 hours of forecast). Thereafter the vorticity decreases up to 72 hours of forecast. Maximum value of vorticity obtained from WRF model is more than the value obtained from MM5 model.

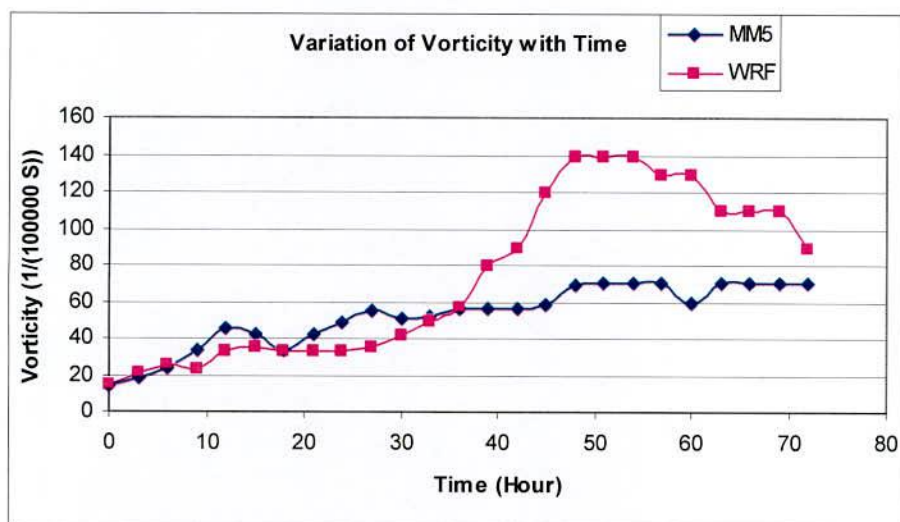


Figure 5.2.3.1: MM5 model simulated Vorticity ($\times 10^{-5}$ /s) with time of TC Aila

The horizontal distribution of the relative vorticity obtained from MM5 model at 03 UTC of 25 May 2009 (i.e. its mature stage) and obtained from WRF model at 09 UTC of 25 May 2009 (i.e. its mature stage) of TC Aila for 850, 500, 300 and 200 hPa levels are shown in Figures 5.2.3.2a and 5.2.3.2b respectively. It is seen from the figures that the vorticity is distributed with maximum value in the centre and these values are tabulated in the Tables

5.2.3.1a and 5.2.3.1b using result obtained from MM5 and WRF models respectively at different times mentioned in the table.

From the Tables 5.2.3.1a and 5.2.3.1b, it is clear that these values increase with the increase of time (i.e. in the development of the cyclone) in all levels except at the 03 UTC of 25 May 2009 in 200 hPa level for MM5 and at the 09 UTC of 25 May 2009 at 850 hPa level for WRF. This may be due to landmass effect before landfall. The distribution maintains circular pattern with some asymmetric features in the outer periphery.

At 850 hPa level, (Figures 5.2.3.2a and 5.2.3.2b) negative vorticity fields are found almost in all sides of the centre of the cyclone which is followed by positive and negative vorticity fields. The distance of the negative vorticity from the centre is increased due to the intensification of the cyclone (not shown). Low level vorticity fields confirm the strong cyclonic circulation at low levels of about 50-55 km radius for MM5 model and about 100-110 km radius for WRF model, feeding moisture into the system to sustain its intensity.

At 500 and 300 hPa, the distribution of relative vorticity also shows a symmetric character in the horizontal distribution. The values of relative vorticity are increased with the development and intensification of cyclone (Tables 5.2.3.1a and 5.2.3.1b). The weak positive vorticity embedded with negative vorticity field is visible at 200 hPa level. It is very clear from the figure that relative vorticity is more organized in the mature stage (i.e. 03 UTC of 25May 2009) at all levels.

The vertical distribution of the relative vorticity at 00 UTC on 23, 24, 25 May and at 03 UTC on 25 May 2009 (i.e. its mature stage) of TC Aila from surface to 200 hPa is shown in Figure 5.2.1.3.5. Negative vorticity bands are located near the positive vorticity at the centre from the initial time to landfall. It is very clear from the Tables 5.2.3.1a and 5.2.3.1b that the values of maximum vorticity obtained from WRF are more than those obtained from MM5 model.

Table 5.2.1.3.1: MM5 Model simulated maximum vorticity ($\times 10^{-5} \text{ s}^{-1}$) at different pressure levels of TC Aila at 00 UTC on 23, 24, 25 May and at 03 UTC on 25 May 2009.

| Pressure level (hPa) | Vorticity ($\times 10^{-5} \text{ s}^{-1}$) at different time | | | |
|-------------------------|---|--------------------|--------------------|--------------------|
| | 00 UTC on 23May | 00 UTC on 24May | 00 UTC on 25May | 03 UTC on 25May |
| 850 | 14 | 45 | 60 | 70 |
| 500 | 12 | 24 | 45 | 50 |
| 300 | 6 | 20 | 30 | 40 |

| | | | | |
|--------------------------------|-----------------------|-----------------------|-----------------------|-----------------------|
| 200 | 4 | 20 | 20 | 15 |
| position of the cyclone centre | 15.845°N and 88.522°E | 19.105°N and 89.983°E | 21.145°N and 90.333°E | 21.569°N and 90.301°E |
| Vertical distribution | 11 | 50 | 70 | 80 |

Table 5.2.2.3.1: WRF Model simulated maximum vorticity ($\times 10^{-5} \text{ s}^{-1}$) at different pressure levels of TC Aila at 00 UTC on 23, 24, 25 May and at 09 UTC on 25 May 2009.

| Pressure level (hPa) | Vorticity ($\times 10^{-5} \text{ s}^{-1}$) at different time | | | |
|--------------------------------|---|--------------------|--------------------|--------------------|
| | 00 UTC on 23May | 00 UTC on 24May | 00 UTC on 25May | 09 UTC on 25May |
| 850 | 15 | 30 | 140 | 120 |
| 500 | 12 | 35 | 70 | 100 |
| 300 | 8 | 25 | 60 | 80 |
| 200 | 4 | 25 | 60 | 70 |
| position of the cyclone centre | 15.898°N, 88.429°E | 18.389°N, 89.379°E | 19.847°N, 89.634°E | 21.357°N, 89.856°E |
| Vertical distribution | 12 | 30 | 140 | 120 |

Vertical distribution of relative vorticity of TC Aila for different times through the centre in the east-west direction are shown in Figure 5.2.3.3a and values are tabulated in the Table 5.2.3.1a for MM5 model and those for WRF model are shown in Figure 5.2.3.3b and values are tabulated in the Table 5.2.3.1b.

According to simulation obtained from MM5 model, the vertical distribution of relative vorticity through the centre (15.845°N and 88.522°E) at 00 UTC on 23 May 2009 (i.e. the initial time) are plotted in the east-west direction (Figure 5.2.3.3a). Figure shows that the positive vorticity is spread over a horizontal distance with strong vorticity at the centre. This pattern of distribution extends from surface to around 200 hPa level with the exception that the magnitude of the vorticity decreases with height. It is noted that the central positive vorticity extends up to 200 hPa level with low magnitude. Similar pattern with higher positive value of vorticity is found at the centre after 24 hours of simulation at 00 UTC on 25 May 2009 along the centre (19.105°N and 89.983°E). At 00 UTC on 25 May 2009, the system has higher value of positive vorticity along the centre (21.145°N and 90.333°E) than the previous time. At 03 UTC on 25 May 2009, the system has the highest value of positive vorticity along the centre (21.569°N and 90.301°E).

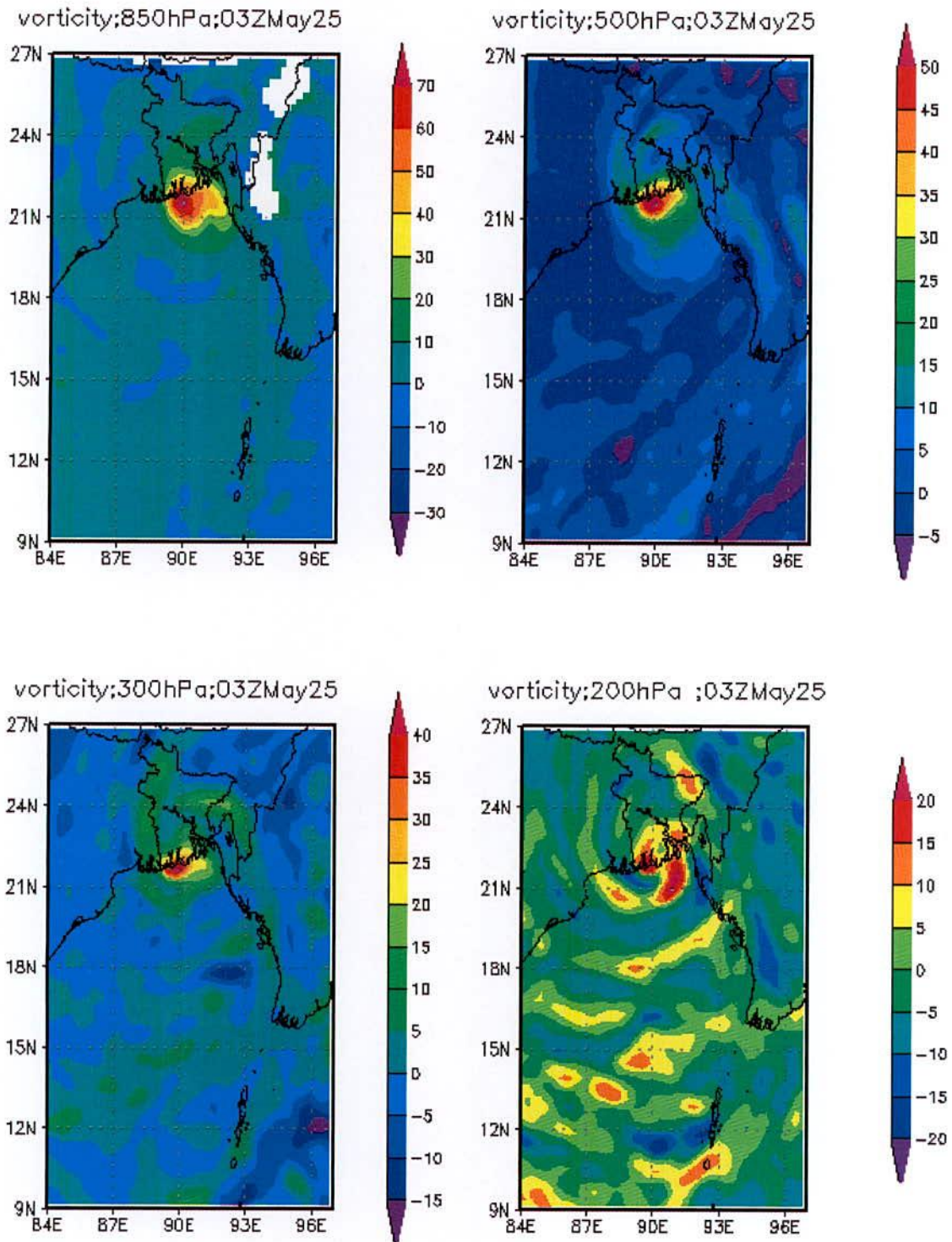


Figure 5.2.3.2a: MM5 model simulated vorticity field at 850, 500, 300 and 200 hPa level at 03 UTC on 25 May 2009 of TC Aila.

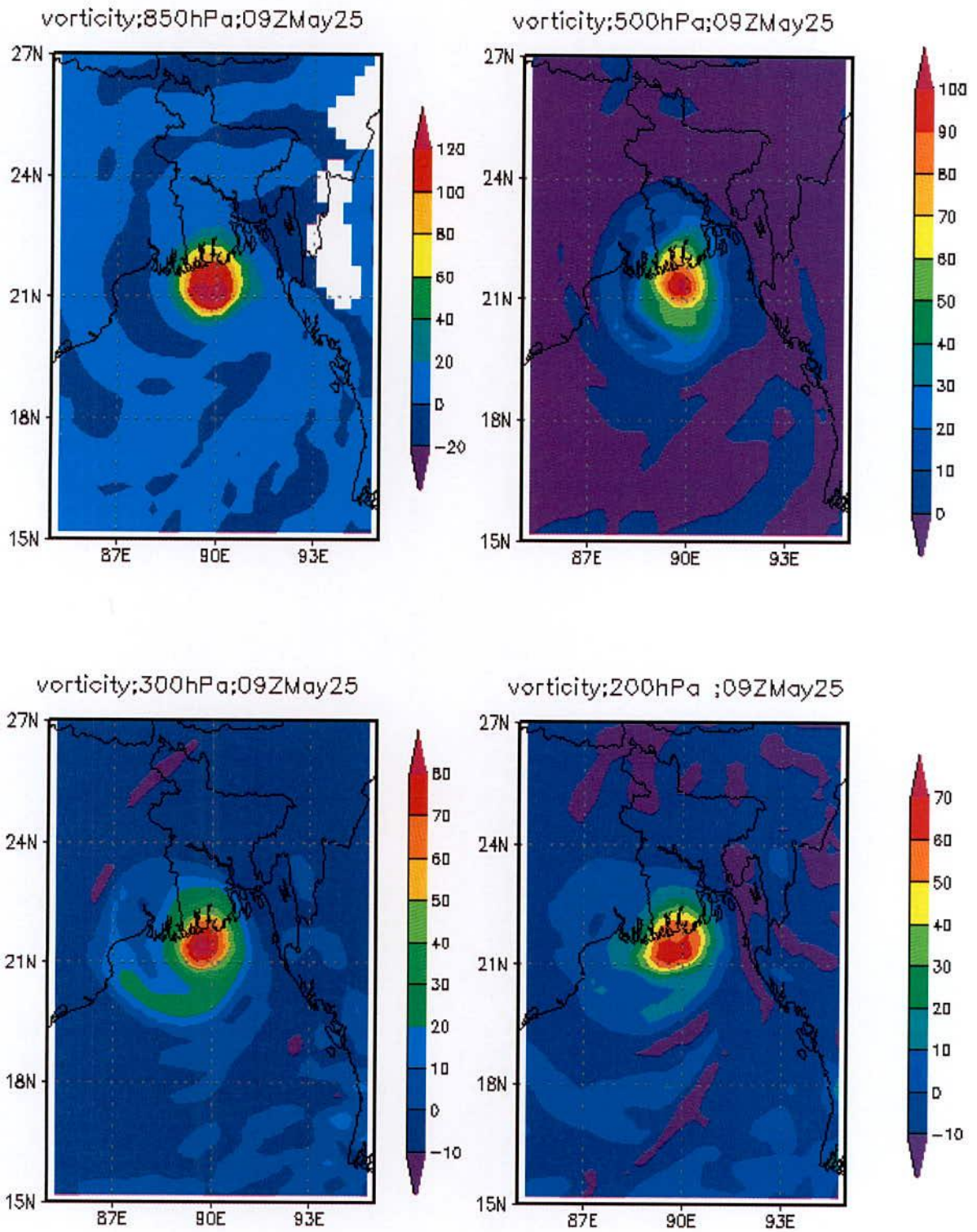


Figure 5.2.3.2b: WRF model simulated vorticity field at 850, 500, 300 and 200 hPa level at 09Z of 25 May 2009 of TC Aila.

According to simulation obtained from WRF model, the vertical distribution of relative vorticity through the centre (15.898°N and 88.427°E) at 00 UTC of 23 May 2009 (i.e. the initial time) are plotted in the east-west direction (Figure 5.2.3.3b). The figure also shows that the positive vorticity is spread over a horizontal distance with strong vorticity at slight western part of the centre. This pattern of distribution extends from surface to around 200 hPa level with the exception that the magnitude of the vorticity decreases with height. It is noted that the central positive vorticity extends up to 100 hPa level with low magnitude. Similar pattern with higher positive value of vorticity is found at the centre after 24 hours of simulation at 00 UTC of 24 May 2009 along the centre (18.389°N and 89.379°E). At 00 UTC of 25 May 2009, the system has the highest value of positive vorticity along the centre (19.847°N and 89.634°E). At 09 UTC of 25 May 2009, the system has slightly lower value of positive vorticity along the centre (21.357°N and 89.856°E) than that at 00 UTC of 25 May 2009. It may be due to landmass effect for landfall

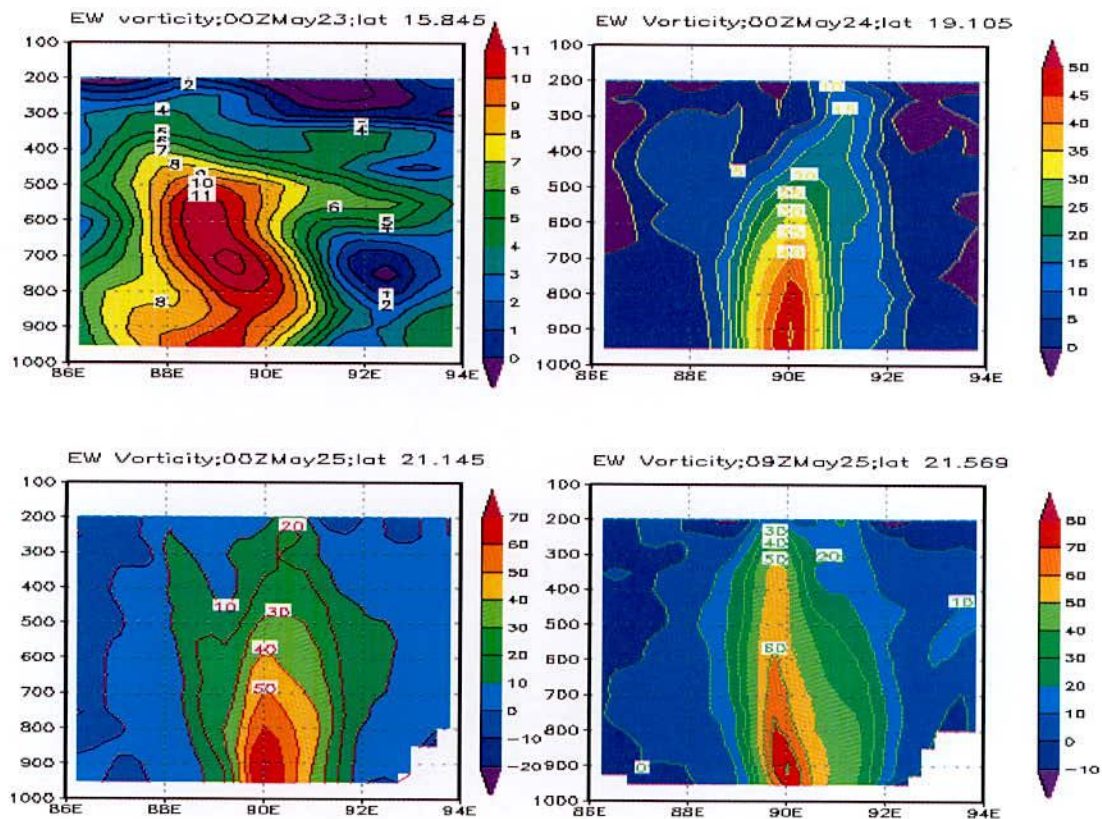


Figure 5.2.3.3a: MM5 model simulated vertical distribution of relative vorticity field along the east-west direction at 00 UTC on 23, 24, 25 May and at 03 UTC on 25 May 2009 of TC Aila.

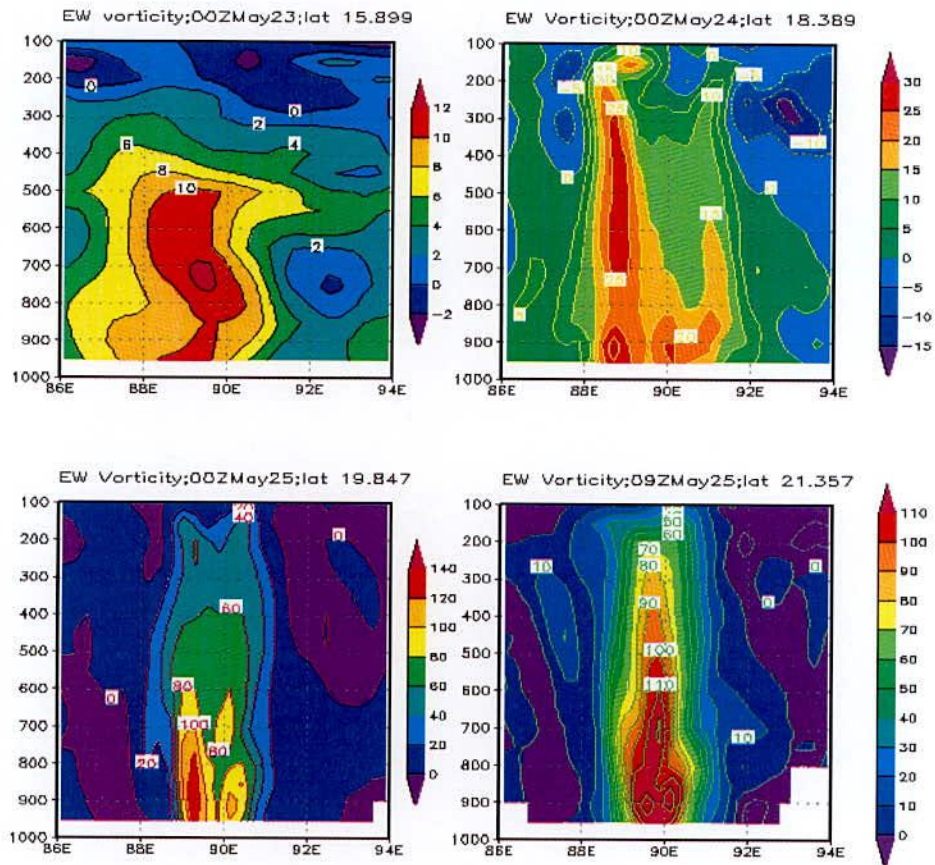


Figure 5.2.3.3b: WRF model simulated vertical distribution of relative vorticity field along the east-west direction at 00 UTC on 23, 24, 25 May and at 09 UTC on 25 May 2009 of TC Aila.

5.2.4 Temperature Anomaly

The MM5 model simulated temperature anomaly ($^{\circ}\text{C}$) of Aila at 00 UTC on 23, 24, 25 May and at 03 UTC on 25 May 2009 (i.e. its mature stage) of TC Aila from surface to 100 hPa is shown in the Figure 5.2.4.1a and the values are tabulated in Table 5.2.4.1a. Again the WRF model simulated temperature anomaly of Aila at 00 UTC of 23, 24 and 25 May and at 09 UTC on 25 May 2009 (i.e. its mature stage) of cyclone Aila from surface to 100 hPa is shown in the Figure 5.2.4.1b and values are tabulated in Table 5.2.4.1b.

According to the simulation obtained from MM5 model, at 00 UTC of 23 May 2009 warm core with 3.5°C is observed at 950-200 hPa layer. It is noted that the warm core region is slightly expanded outward at 700-550 hPa level. The greatest anomaly is occurred around 600 hPa level. The simulated temperature anomaly demonstrates that the warm core is visible mainly in the upper troposphere. Negative temperature anomalies at lower levels are due to contamination by heavy precipitation.

At 00 UTC on 24 May 2009 warm core with 4.0°C is observed at 950-200 hPa layer. The warm core region is expanded outward at 700-500 hPa level. The greatest anomaly is occurred around 600 hPa level. The simulated temperature anomaly demonstrates that the warm core is visible mainly in the upper troposphere. Negative temperature anomalies at lower levels are due to contamination by heavy precipitation.

At 00 UTC of 25 May 2009 warm core 6°C is observed at 950-200 hPa layer. The warm core region is expanded outward at 700-400 hPa level. The greatest anomaly is occurred around 450 hPa level. The simulated temperature anomaly demonstrates that the warm core is visible mainly in the upper troposphere. Negative temperature anomalies at lower levels are due to heavy precipitation.

At 03 UTC of 25 May 2009 warm core 7°C is observed at 950-150 hPa layer. This warm core region is expanded outward at 500-350 hPa level. The greatest anomaly is occurred around 400 hPa level. The simulated temperature anomaly demonstrates that the warm core is visible mainly in the upper troposphere. Negative temperature anomalies at lower levels are due to contamination by heavy precipitation.

Again, according to the simulation obtained from MM5 model, at 00 UTC on 23 May 2009, warm core with 5°C is observed in 800-150 hPa layer and this warm core region is slightly expanded outward at 500-200 hPa level. The maximum temperature anomaly is simulated around 300 hPa level. The simulated temperature anomaly demonstrates that the warm core is visible mainly in the upper troposphere. Negative temperature anomalies at lower levels are due to contamination by heavy precipitation.

At 00 UTC on 24 May 2009, warm core with 6°C is observed in 850-150 hPa layer. It is noted that the warm core region is expanded outward at 700-200 hPa level. The maximum temperature anomaly is simulated around 350 hPa level. The simulated temperature anomaly demonstrates that the warm core is visible mainly in the upper troposphere. Negative temperature anomalies at lower levels are due to contamination by heavy precipitation.

At 00 UTC of 25 May 2009, warm core with 10°C is observed in 900-150 hPa layer. It is noted that the warm core region is expanded outward at 500-300 hPa level. The maximum temperature anomaly is simulated around 350 hPa level. The simulated temperature anomaly demonstrates that the warm core is visible mainly at upper troposphere. Negative temperature anomalies at lower levels are due to contamination by heavy precipitation.

At 09 UTC of 25 May 2009, warm core with 10°C is observed in 900-150 hPa layer. It is noted that the warm core region is expanded outward at 500-300 hPa level. The maximum

temperature anomaly is also simulated around 300 hPa level. The simulated temperature anomaly demonstrates that the warm core is visible mainly at upper troposphere. Negative temperature anomalies at lower levels are due to contamination by heavy precipitation.

Finally, Maximum temperature obtained from WRF model is more that obtained from MM5 model.

Table 5.2.4.1a: MM5 Model simulated Temperature ($^{\circ}$ C) anomaly of TC Aila at 00 UTC on 23, 24, 25 May and at 03 UTC on 25 May 2009.

| Temperature anomaly ($^{\circ}$ C) at different time | | | |
|---|---------------------|---------------------|---------------------|
| 00 UTC on 23 May | 00 UTC on 24 May | 00 UTC on 25 May | 03 UTC on 25 May |
| 3.5 | 4.0 | 6.0 | 7.0 |

Table 5.2.4.1b: WRF Model simulated Temperature ($^{\circ}$ C) anomaly of TC Aila at 00 UTC on 23, 24, 25 May and at 09 UTC on 25 May 2009.

| Temperature anomaly ($^{\circ}$ C) at different time | | | |
|---|---------------------|---------------------|---------------------|
| 00 UTC on 23 May | 00 UTC on 24 May | 00 UTC on 25 May | 09 UTC on 25 May |
| 5 | 6 | 10 | 10 |

5.2.5 Relative Humidity

The vertical cross section of relative humidity obtained from MM5 model at 00 UTC on 23, 24, 25 May and at 03 UTC on 25 May 2009 (i.e. its mature stage) of TC Aila from surface to 200 hPa is shown in Figure 5.2.5.1a and its values are tabulated in Table 5.2.5.1a. It is noted that high relative humidity (more than 90%) spreads in the outer region of eye wall up to 400 hPa level at 00 UTC of 23 May and up to 300 hPa level at 00 UTC of 24, 25 May and 03 UTC on 25 May 2009. High relative humidity bands are also found in the rain band of the system situated at both sides of the system throughout 900-750 hPa level.

The vertical cross section of relative humidity obtained from WRF model at 00 UTC of 23, 24 and 25 May and 09 UTC of 25 May 2009 (i.e. its mature stage) of TC Aila from surface to 100 hPa level has shown in Figure 5.2.5.1b and its values are tabulated in Table 5.2.5.1b. It is noted that higher relative humidity (more than 90%) spreads in outer periphery of the eye

wall up to 400 hPa level at 00 UTC on 23 and 24 May and 300 hPa level at 00 and 09 UTC on 25 May 2009. High relative humidity bands are also found in the rain band of the system situated at both sides of the system throughout 900-750 hPa level.

Table 5.2.5.1a: MM5 Model simulated maximum relative humidity (%) of TC Aila at 00 UTC on 23, 24, 25 May and 03 UTC on 25 May 2009.

| Simulated maximum relative humidity (%) at different time | | | |
|---|---------------------|---------------------|---------------------|
| 00 UTC on 23 May | 00 UTC on 24 May | 00 UTC on 25 May | 03 UTC on 25 May |
| 90 | 100 | 100 | 100 |

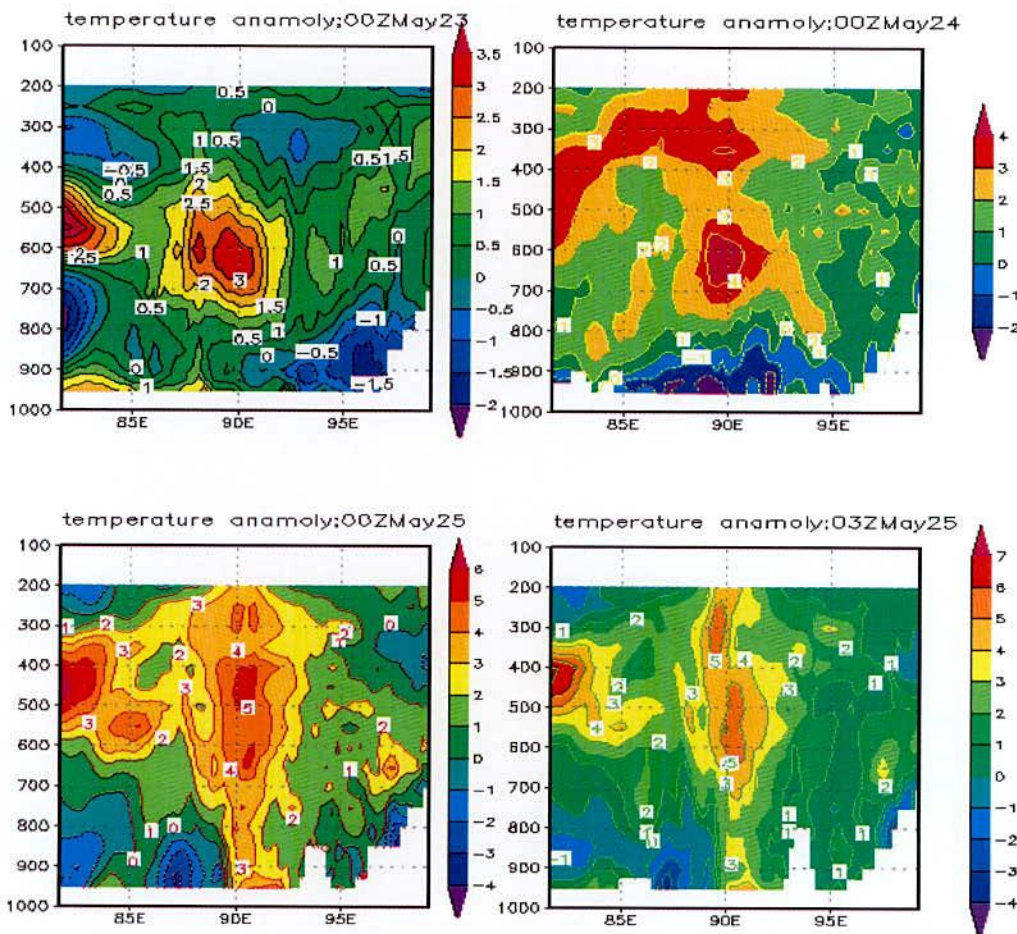


Figure 5.2.4.1a: MM5 model simulated vertical distribution of temperature anomaly along the east-west direction at 00 UTC on 23, 24, 25 May and at 03 UTC on 25 May 2009 of TC Aila.

Table 5.2.5.1b: WRF Model simulated maximum relative humidity (%) of TC Aila at 00 UTC on 23, 24, 25 May and at 09 UTC on 25 May 2009.

| Simulated maximum relative humidity (%) at different time | | | |
|---|---------------------|---------------------|---------------------|
| 00 UTC on 23 May | 00 UTC on 24 May | 00 UTC on 25 May | 09 UTC on 25 May |
| 100 | 90 | 100 | 100 |

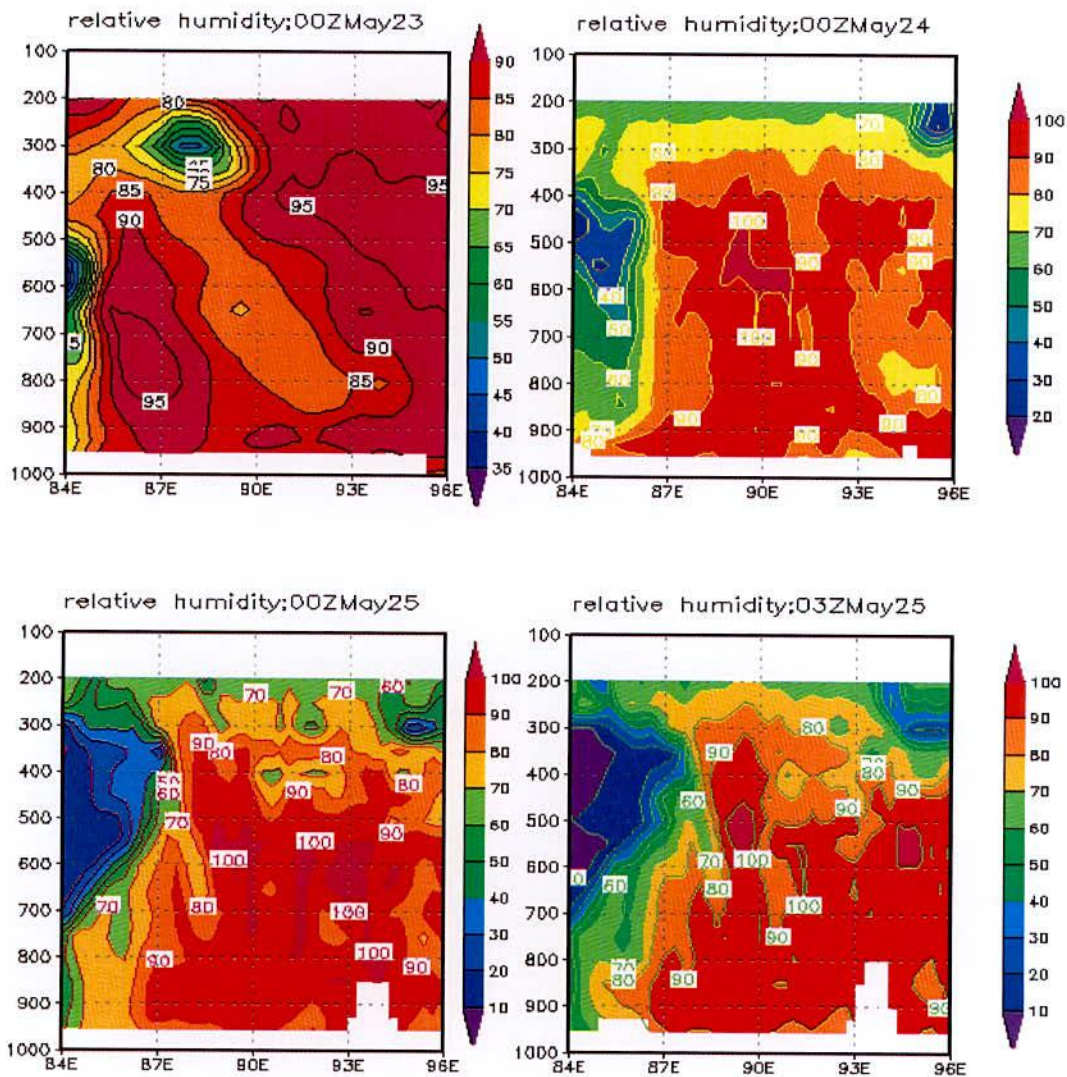


Figure 5.2.5.1a: MM5 model simulated vertical distribution of relative humidity along the east-west direction at 00 UTC on 23, 24, 25 May and at 09 UTC on 25 May 2009 of TC Aila.

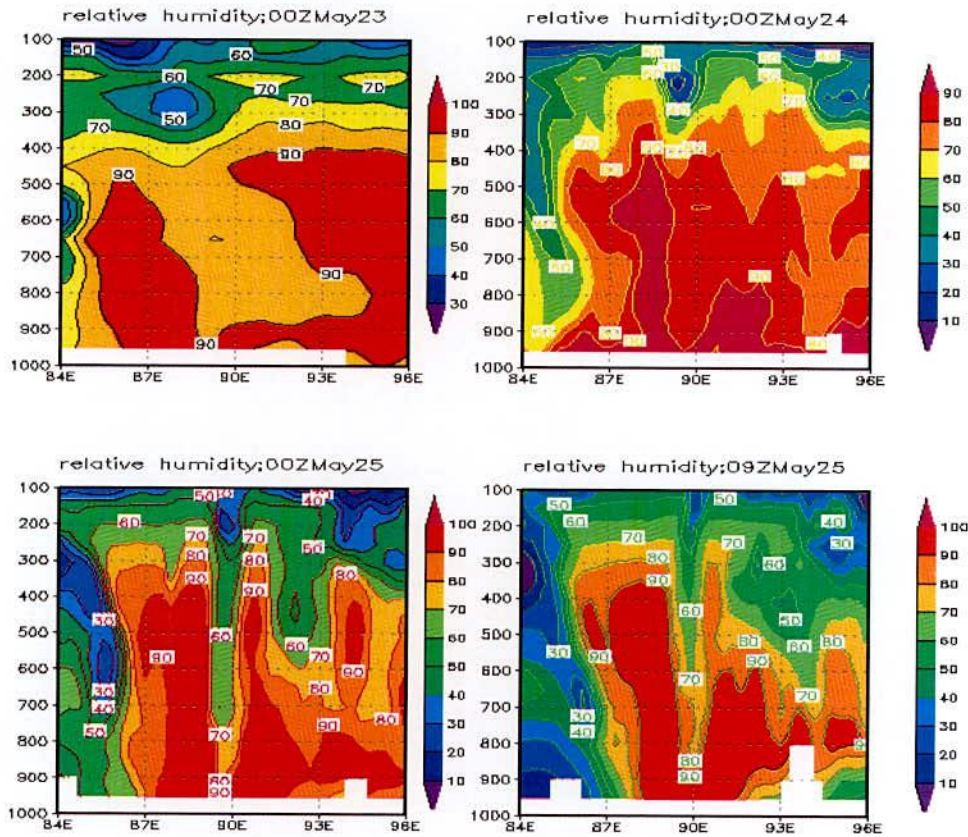


Figure 5.2.5.1b: WRF model simulated vertical distribution of relative humidity along the east-west direction at 00 UTC on 23, 24, 25 May and at 09 UTC on 25 May 2009 of TC Aila.

5.2.6 Water Vapor Mixing Ratio

The vertical distribution of water vapor mixing ratio obtained from MM5 along the east-west direction through the centre of the TC Aila at 00 UTC of 23, 24, 25 May and at 03 UTC on 25 May 2009 (i.e. its mature stage) from surface to 200 hPa level is shown in the Figure 5.2.6.1a and its values are tabulated in Table 5.2.6.1a. Again, the vertical distribution of water vapor mixing ratio obtained from WRF model along the east-west direction of the centre of the TC Aila at 00 UTC of 23, 24 and 25 May and at 09 UTC on 25 May 2009 (i.e. its mature stage) from surface to 100 hPa level is shown in the Figure 5.2.6.1b and its values are tabulated in Table 5.2.6.1b.

From the Figures 5.2.6.1a and 5.2.6.1b, it is seen clearly that the highest moisture content more than around 2.0 g/kg or more is found at the centre of the system at 950 hPa level (except for 00 UTC on 23 May 2009) than it decreases upwards up to 400 hPa or more. For the development of the system this upward level goes up to 300 hPa at 00 UTC on 25 May

and 03 UTC on May 2009 (i.e. its mature stage) for MM5 model and at 00 UTC on 25 May and at 03 UTC on May 2009 (i.e. its mature stage) for WRF model.

Table 5.2.6.1a: MM5 Model simulated maximum water vapour mixing ratio (kg/kg)*100 of TC Aila at 00 UTC on 23, 24, 25 May and at 03UTC on 25 May 2009.

| Simulated maximum value of water vapor mixing ratio (kg/kg)*100 | | | |
|---|--------------------|--------------------|--------------------|
| 00 UTC on 23May | 00 UTC on 24May | 00 UTC on 25May | 09 UTC on 25May |
| 1.8 | 2 | 2.2 | 2.2 |

Table 5.2.6.1b: WRF Model simulated maximum water vapour mixing ratio (kg/kg)*100 of TC Aila at 00 UTC on 23, 24, 25 May and 09 UTC on 25 May 2009.

| Simulated maximum value of water vapor mixing ratio (kg/kg)*100 | | | |
|---|--------------------|--------------------|--------------------|
| 00 UTC on 23May | 00 UTC on 24May | 00 UTC on 25May | 09 UTC on 25May |
| 2 | 2 | 2.2 | 2.4 |

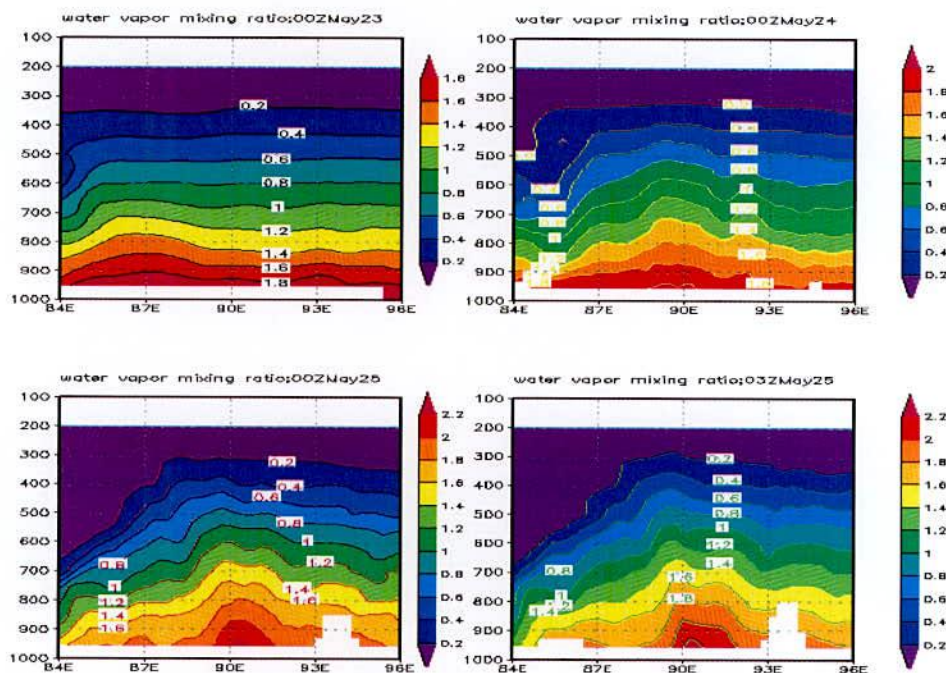


Figure 5.2.6.1a: Vertical distribution of MM5 model simulated water vapor mixing ratio along the east-west direction at 00 UTC on 23, 24, 25 May and 09 UTC on 25 May 2009 of TC Aila.

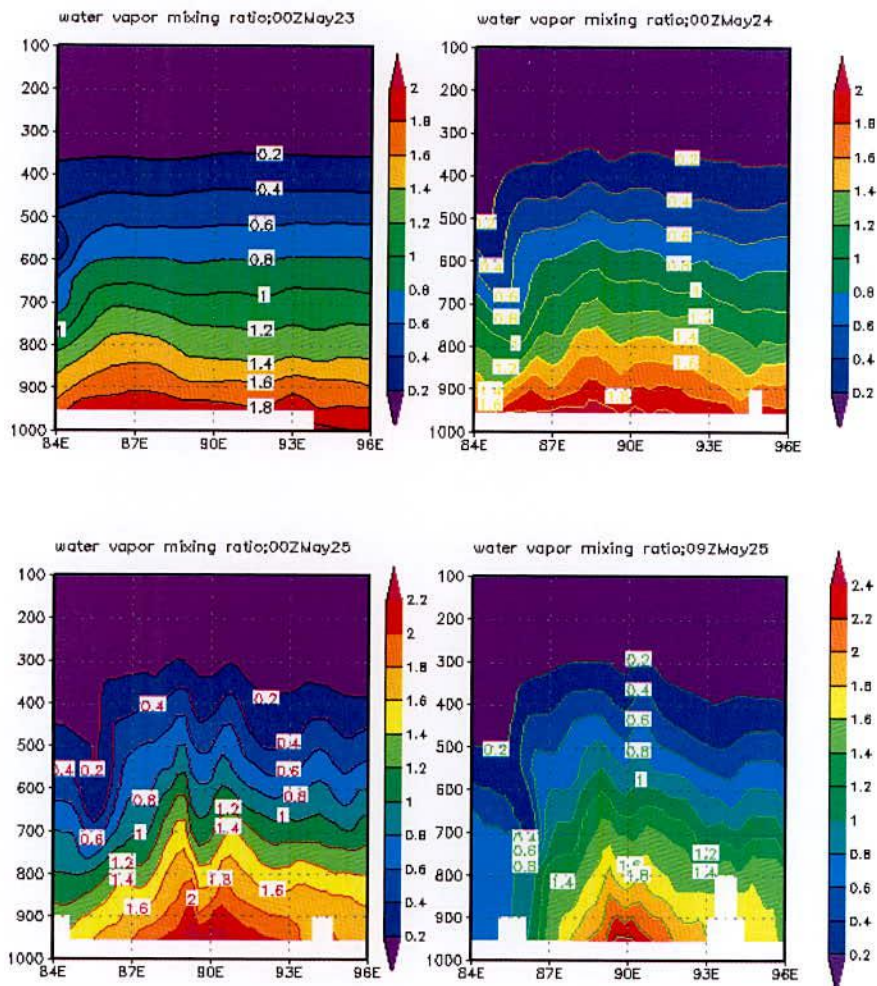


Figure 5.2.6.1b: Vertical distribution of WRF model simulated water vapor mixing ratio along the east-west direction at 00 UTC on 23, 24, 25 May and 09 UTC on 25 May 2009 of TC Aila.

The horizontal distribution of water vapor mixing ratio of TC Aila at 950 hPa level at 00 UTC on 23, 24, 25 May and at 03 UTC of May 2009 (i.e. its mature stage) obtained from MM5 model and at 00 UTC on 23, 24, 25 May and at 03 UTC on May 2009 (i.e. its mature stage) obtained from WRF model are shown in Figure 5.2.6.2a and 5.2.6.2b. It is noted that the high moisture flux comes from the southern side covering a large area of the Bay of Bengal which feeds the system along its south-eastern side through the boundary layer except for the initial time i.e. at 00 UTC on 23 May 2009, when high moisture flux is available at the northern side of the system. The value of high moisture flux increases slightly with development of the system.

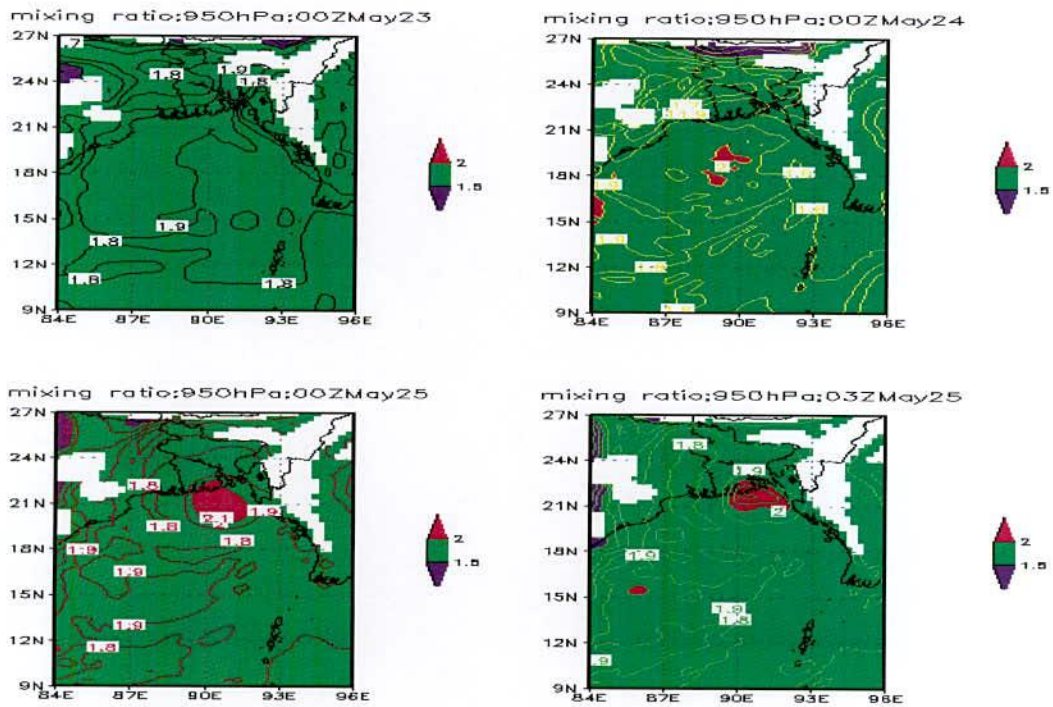


Figure 5.2.6.2a: MM5 model simulated water vapor mixing ratio ($\text{kg/kg} \times 10^{-2}$) at 950 hPa level of TC Aila at 00 UTC on 23, 24, 25 May and at 03 UTC on 25 May 2009.

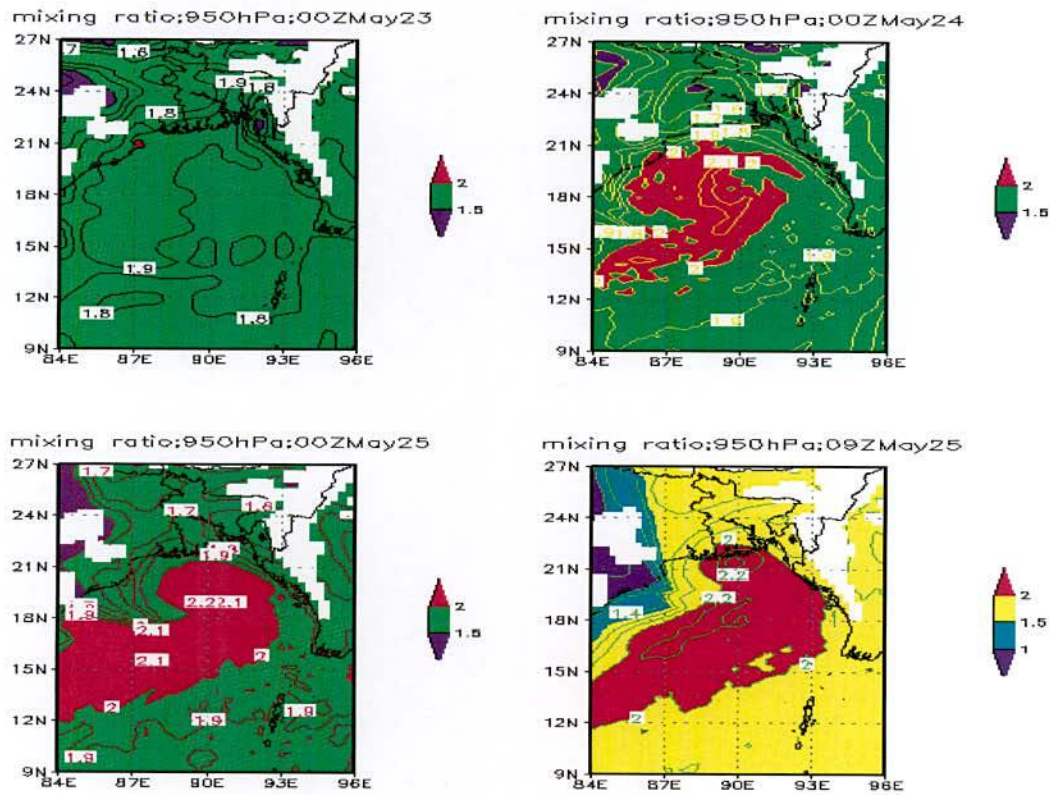


Figure 5.2.6.2b: WRF model simulated water vapor mixing ratio ($\text{kg/kg} \times 10^{-2}$) at 950 hPa level of TC Aila at 00 UTC of 23, 24, 25 May and 09 UTC of 25 May 2009

5.2.7 Rainfall Pattern

Figure 5.2.7.1 shows the MM5 and WRF models simulated 24 hrs accumulated rainfall along with rainfall obtained from TRMM data of TC Aila valid for the days 23, 24, and 25 May 2009 (i.e. ending at 00 UTC of 24, 25 and 26 May). The rainfall shows a highly asymmetric character in the horizontal distribution.

On 23 May 2009, the rainfall occurs mainly at the sea and a small amount of rain occurs over Bangladesh and its surrounding. MM5 model simulated rainfall is more than that simulated by WRF model. The simulated rainfall by MM5 and WRF models is comparable to the rainfall obtained from TRMM data with large spatial variability. On 24 May 2009, the rainfall occurs mainly at the sea. MM5 model simulated rainfall is more than that simulated by WRF model over Bangladesh and especially southern side of Bangladesh. Interestingly, there is no rain in some portion of Bangladesh simulated by WRF model. Rainfall simulated by WRF model is more than MM5 model at sea portion. Finally, the simulated rainfall by MM5 and WRF models is comparable to the rainfall obtained from TRMM data with large spatial variability. On 25 May 2009, the rainfall occurs mainly over Bangladesh and its surrounding. MM5 simulated heavy rainfall over middle and south and north sides whereas WRF model simulated heavy rainfall southwestern side. So, there is a spatial variability in the rainfall simulated by the two models. Rainfall obtained from TRMM is small in amount compared to the rainfall simulated by the two models. MM5 and WRF model simulated rainfall is comparable to the rainfall obtained from TRMM data with some spatial and temporal variability.

Figure 5.2.7.2 shows the MM5 and WRF models simulated 24 hrs accumulated rainfall of TC Aila along with rainfall obtained from BMD rain-gauge and TRMM data valid for the day 25 May 2009 (i.e. ending at 00 UTC of 26 May). Rainfall obtained from WRF mode is more than that obtained from MM5. Simulated rainfall matched more with rainfall obtained from rain-gauge data than the rainfall obtained from TRMM data. 24 hrs accumulated rainfall of TC Aila obtained from MM5 and WRF models are comparable with that obtained from TRMM and BMD rain-gauge data with spatial and temporal variability. The rainfall shows a highly asymmetric character in the horizontal distribution. It shows more rainfall (simulated by MM5) over north-eastern Bangladesh on 25 May 2009. It turns out that the model used in the present study is overestimated the 24 hrs rainfall of cyclone Aila valid for day 25 May 2009. It is noted that TRMM underestimates the pre-monsoon rainfall in this region.

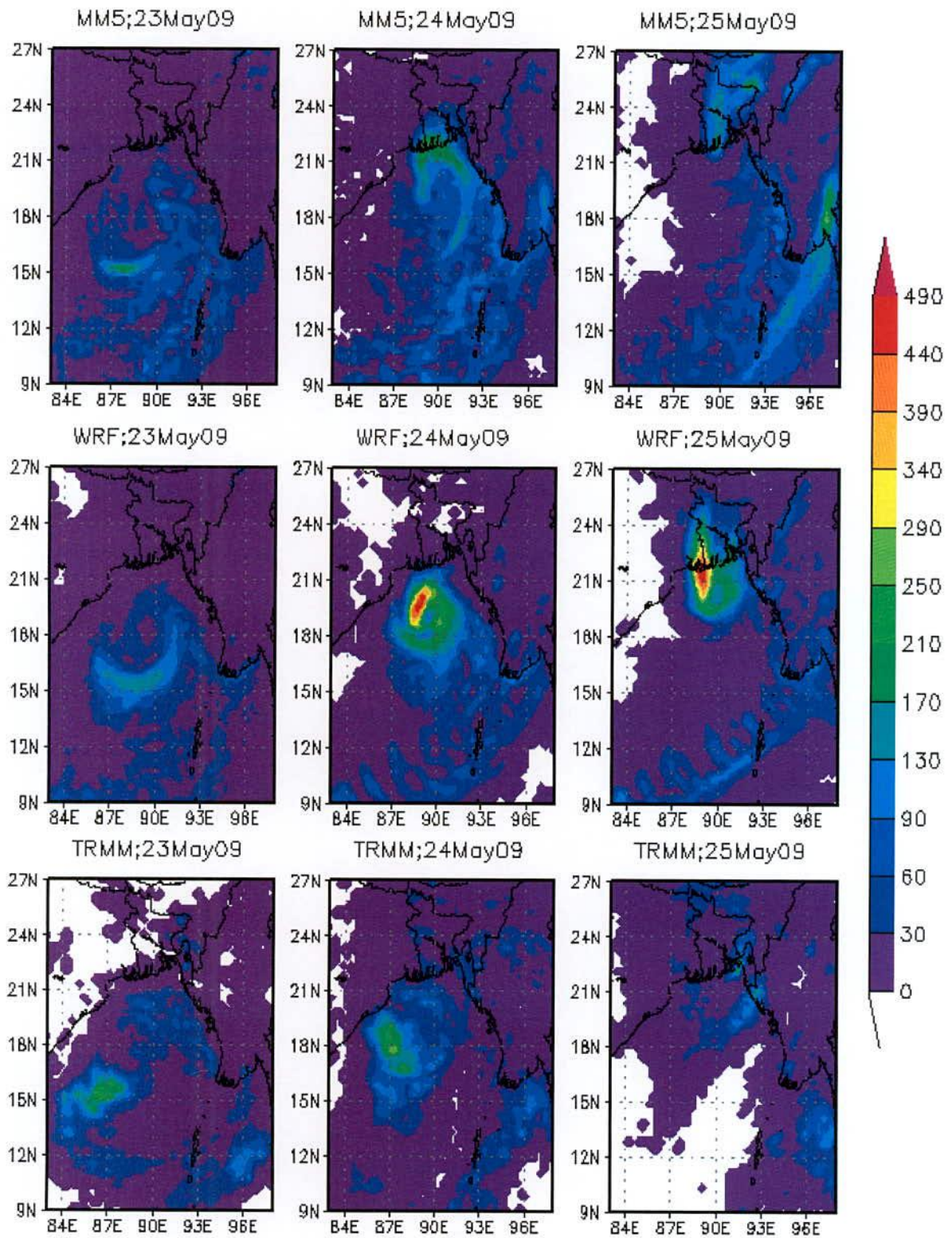


Figure 5.2.7.1: Accumulated rainfall of TC Aila for the days 23, 24 and 25 May 2009 simulated by MM5 and WRF Models along with that obtained from TRMM data.

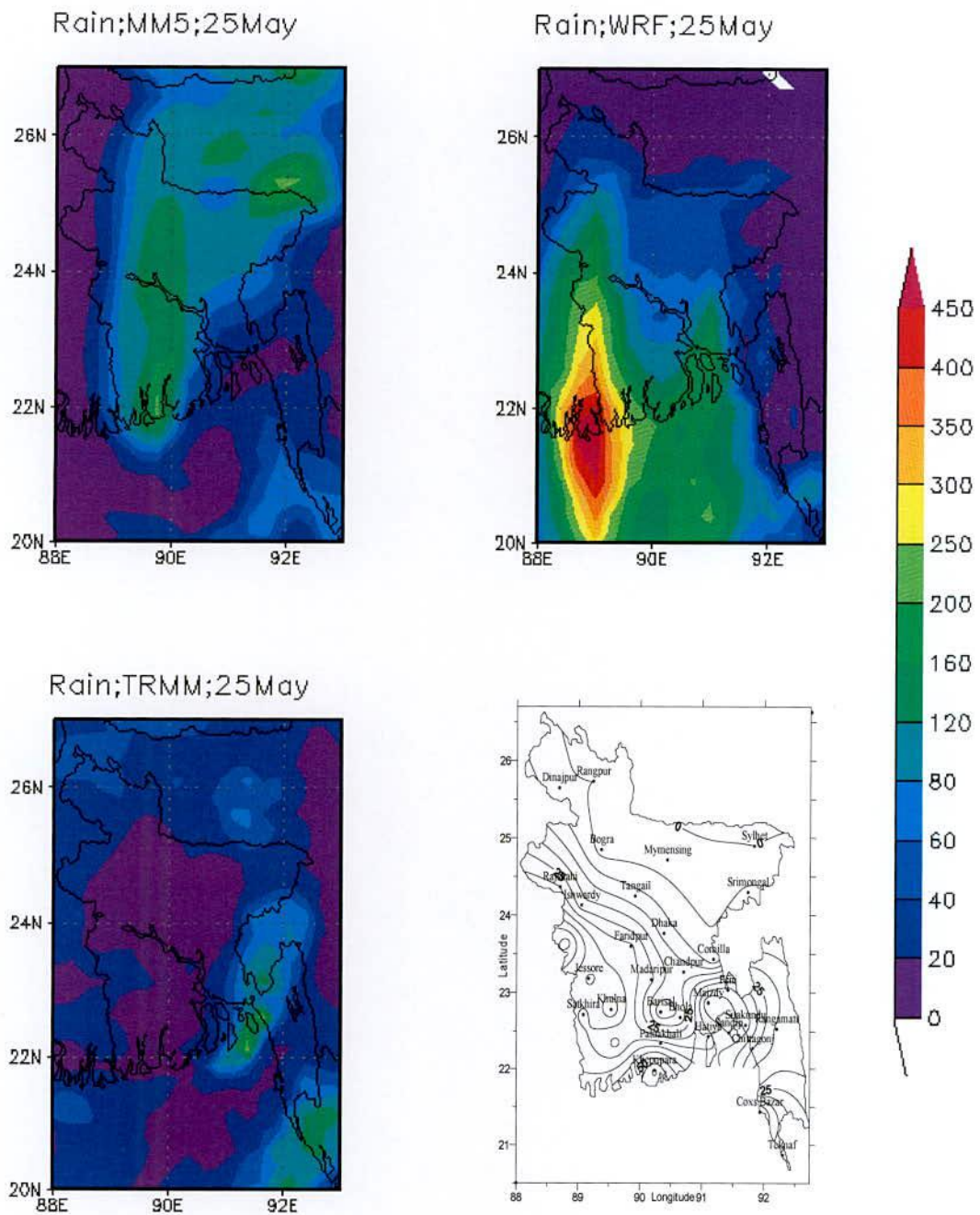


Figure 5.2.7.2: MM5 and WRF model simulated 24 hrs accumulated rainfall of TC Aila along with rainfall obtained from TRMM and BMD rain-gauge data valid for 25 May 2009.

5.2.8 Track Pattern

MM5 and WRF models simulated track of TC Aila along with observed track are plotted in the Figures 5.2.8.1a and 5.2.8.1b respectively. The track forecasts of TC Aila for 96, 72, 48 and 24 hrs are based on the initial fields of 00 UTC of 22 May, 00 UTC of 23 May, 00 UTC of 24 May, 12 UTC of 24 May respectively for MM5 model. Again, the track forecasts of TC Aila for 96, 72, 48 and 24 hrs are based on the initial fields of 18 UTC of 22 May, 00 UTC of 23 May, 00 UTC of 24 May, 12 UTC of 24 May respectively for WRF model. The change on initial field for 96 hrs simulation using WRF is for initial data problem. WRF model could not get sufficient data from initial field.

It is seen from Figure 5.2.8.1a that MM5 model simulated track for 96, 72, 48 and 24 hours model run are parallel to observed track but it is deviated east side of the observed track. It may be because of initial data error. Figure shows that model was able to generate northwest, north and northeast movement of the system very well. It reveals that tracks obtained from 24 and 48 hrs simulation of model are more close to the JTWC best track compared to tracks obtained from 72 and 96 hrs simulation of model. However, there are some errors in the positions with respect to time which shows some ahead in landfall. The track from 24 hours simulation track is better than that of any others simulation. The landfall position for 24 hrs simulation track is much closer to any other simulation. So, by changing initial data in simulated, track becomes close to the observed track.

It is seen from Figure 5.2.8.1a that WRF model simulated track for 96, 72, 48 and 24 hours model run are parallel to observed track but it is deviated east side of the observed track. It may be because of initial data error. Figure shows that model was able to generate northwest, north and northeast movement of the system very well. It reveals that tracks obtained from 24 and 48 hrs simulation of model are more close to the JTWC best track compared to tracks obtained from 72 and 96 hrs simulation of model. However, there are some errors in the positions with respect to time which shows some lag in landfall. The track from 48 hours simulation track is better than that of any other simulation. The landfall position for 48 hrs simulation track is much closer to any other simulation. So, by changing initial data in simulated, track becomes close to the observed track.

It is seen from the figure that simulated track obtained from MM5 and WRF model is parallel to observed track but it is deviated in the eastern side of the observed track. It is because of initial data problem. Again, track obtained from MM5 model for 24 hrs simulation is the best among other simulation whereas track obtained from WRF model for 48 hrs simulation is the best among other simulation.

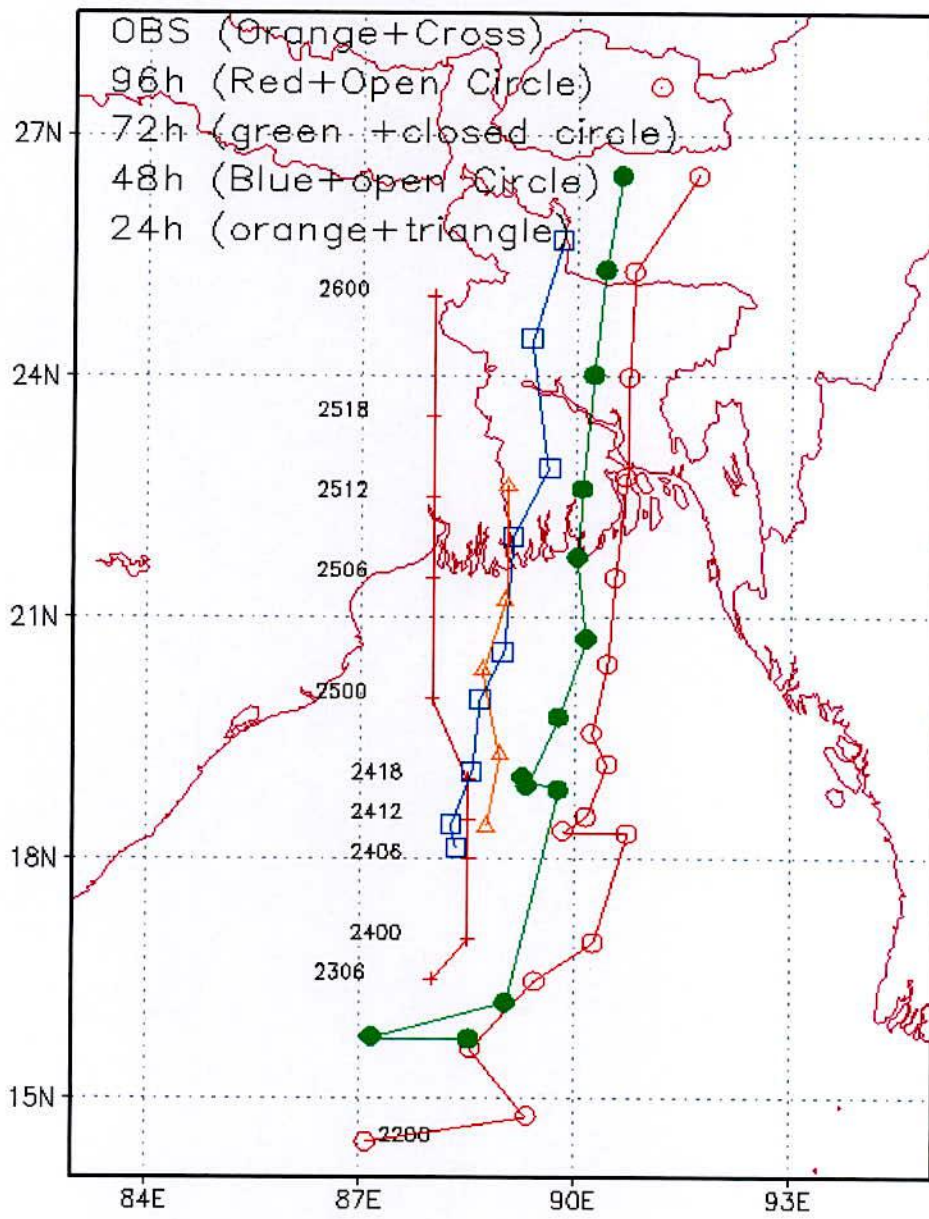


Figure 5.2.8.1a: MM5 simulated track and observed track of cyclone Aila

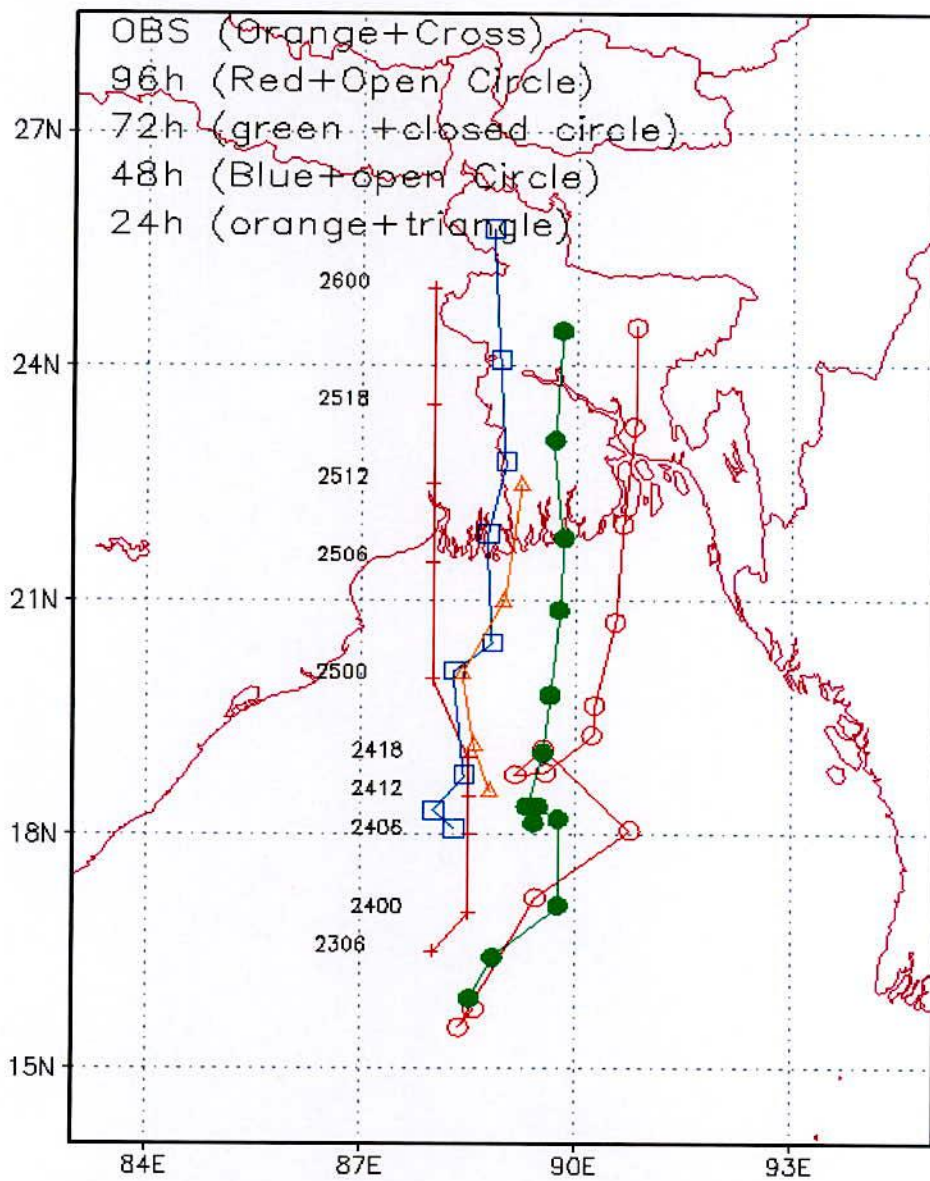


Figure 5.2.8.1b: WRF simulated track and observed track of cyclone Aila

5.3 Simulation of TC Rashmi (2008) using MM5 and WRF Models

To analyze the evolution and structure of TC Rashmi, the MM5 model is run for 96 hrs with the initial field at 00 UTC of 24 October 2008. But after 63 hrs of simulation at 15 UTC of 26 October 2008 for MM5 model and after 75 hrs of simulation at 03 UTC of 27 October 2008 for WRF model system attained at the state of highest intensity. Using MM5 and WRF models the different meteorological parameters are discussed for the evolution and structure of the TC Rashmi in the following sub-section. The MM5 and WRF model simulated data are compared with those obtained from Joint Typhoon Warning Centre (JTWC).

5.3.1 Pressure Field

Figure 5.3.1.1 shows the comparative evolution of observed MSLP and simulated MSLP of MM5 and WRF models of TC Rashmi. It appears from the figures 5.3.1.1 that MM5 model simulated and observed MSLP gradually drops with time and coincides with each other at 18 UTC of 24 October and 06 UTC of 25 October (i.e. 18 and 30 hours of simulation respectively). After that simulated MSLP decreases and finally reached the peak intensity with lowest pressure of 976 hPa just before landfall making an oscillation with higher MSLP 992 hPa and thereafter MSLP increases. The Model simulated MSLP of 976 hPa is obtained at 15 UTC of 26 October whereas the observed MSLP of 989 hPa is obtained at 18 UTC of 26 October 2008.

Again, the WRF model simulated and observed MSLP gradually drops with time and attains peak intensity just before the landfall and thereafter MSLP increases. The Model simulated MSLP of 979 hPa is obtained at 03 UTC of 27 October whereas the observed MSLP 989 hPa is obtained at 18 UTC of 26 October 2008. The model simulated MSLP at the centre of the cyclone after 09 hours from the observed MSLP. It is noted that landfall occurs faster for MM5 model than that for WRF model. The variation of MM5 and WRF models simulated MSLP compared to that of observed with time shows that both the models simulated realistic temporal variation of MSLP.

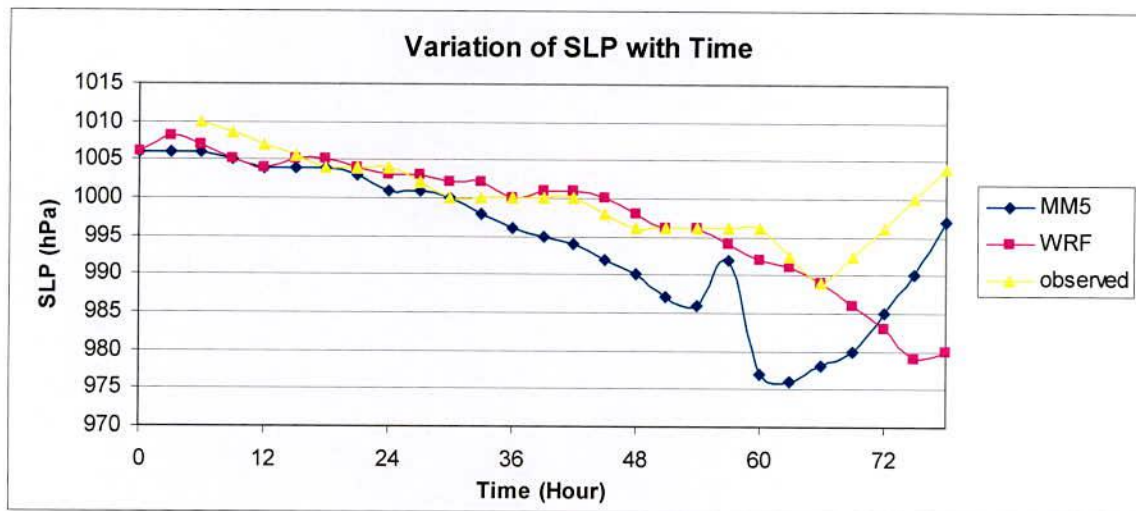


Figure 5.3.1.1: Evolution of MM5 and WRF models simulated minimum central pressure and observed minimum central pressure of the eye of the TC Rashmi with time.

The distribution of sea level pressure for the TC Rashmi obtained from MM5 model at 00 UTC on 24, 25, 26 October and at 15 UTC on 26 October 2008 (i.e. its mature stage) and obtained from WRF model at 00 UTC on 24, 25, 26 October and at 03 UTC on 27 October 2008 (i.e. its mature stage) is shown in Figure 5.3.1.2a. The figure demonstrates that the intensity of the TC increases as the MSLP drops with time up to its peak intensity and TC changes its position with time. The isobar has a circular arrangement around the TC centre with some asymmetric features in the outer periphery. The contour interval is different for different positions because of the different intensity of the system.

At mature stages the contour interval is 2.5 or 3 hPa for both the models. The lowest simulated MSLP of 976 hPa and 979 hPa for MM5 and WRF models respectively are obtained at 15 UTC on 26 October 2008 and at 03 UTC on 27 October 2008 whereas the observed lowest MSLP of 989 hPa is obtained at 18 UTC on 26 October 2008. According to the MM5 model, at the mature stage (at 15 UTC on 26 October 2008), considering the outermost closed isobar, the system's horizontal size is estimated as 7.5° in the east-west direction and 9.0° in the north-south, demonstrating a little bit of spatial asymmetry in its horizontal structure. Again, according to the WRF model, at the mature stage, considering the outermost closed isobar, the system's horizontal size is estimated as 7.5° in the east-west direction and 6.0° in the north-south, demonstrating a little bit of spatial asymmetry in its horizontal structure.

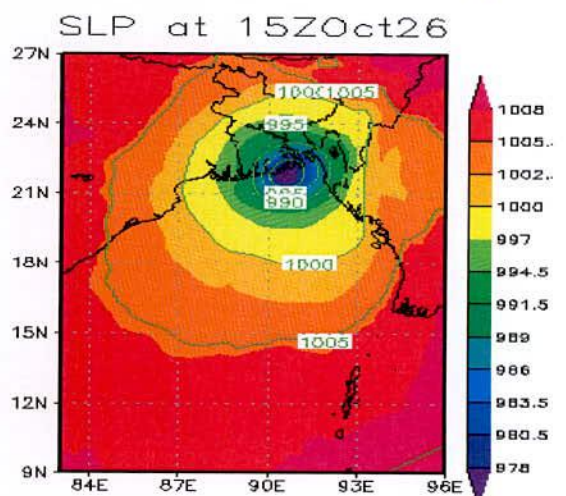
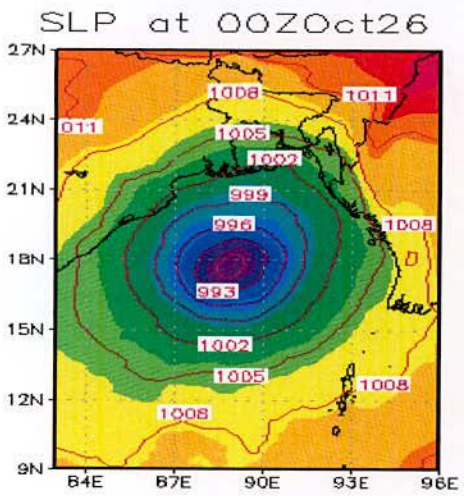
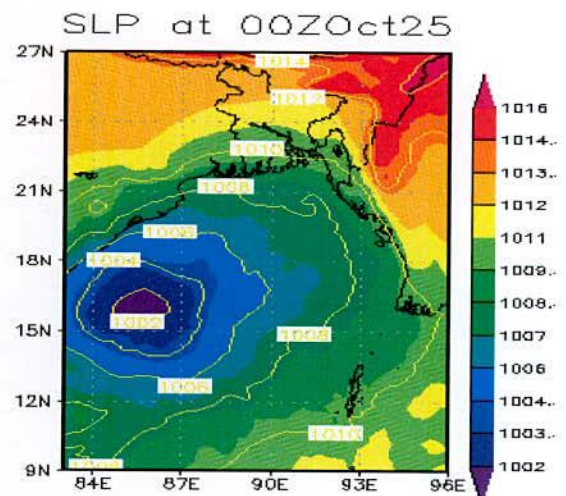
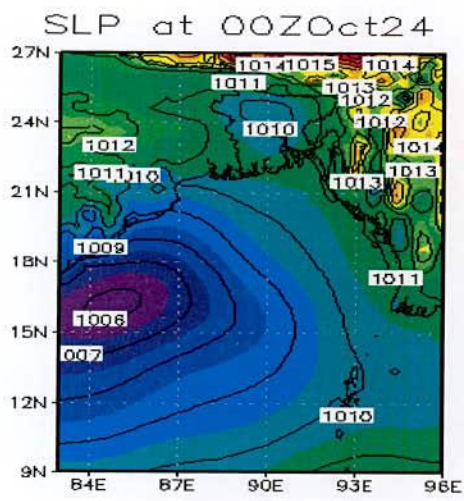


Figure 5.3.1.2a: MM5 Model simulated SLP of TC Rashmi at 00 UTC on 24, 25, 26 October and at 15 UTC on 26 October 2008.

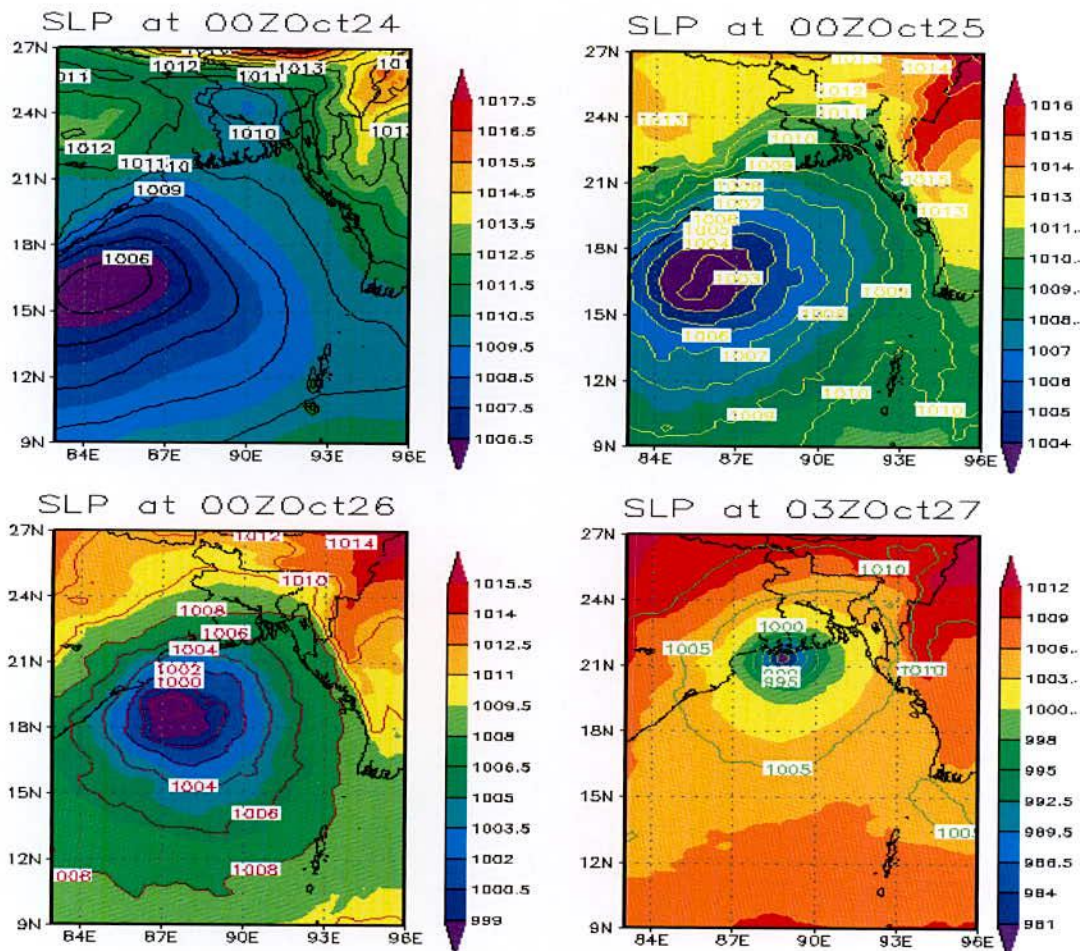


Figure 5.3.1.2b: WRF Model simulated SLP of TC Rashmi at 00 UTC of 24, 25, 26 October and 03 UTC of 27 October 2008.

The distribution of the sea level pressure of the TC Rashmi along east-west cross section passing through its centre (21.894°N and 90.607°E) for MM5 model and passing through its centre (21.357°N and 89.856°E) for WRF model are shown in Figure 5.3.1.3a and 5.3.1.3b respectively. The figures demonstrate the moderate pressure gradient around the centre with maximum gradient at around 80-90 km from the centre for MM5 and WRF models. Thus the radius of the TC eye is found to be below 90 km both for MM5 and WRF model according to the simulation.

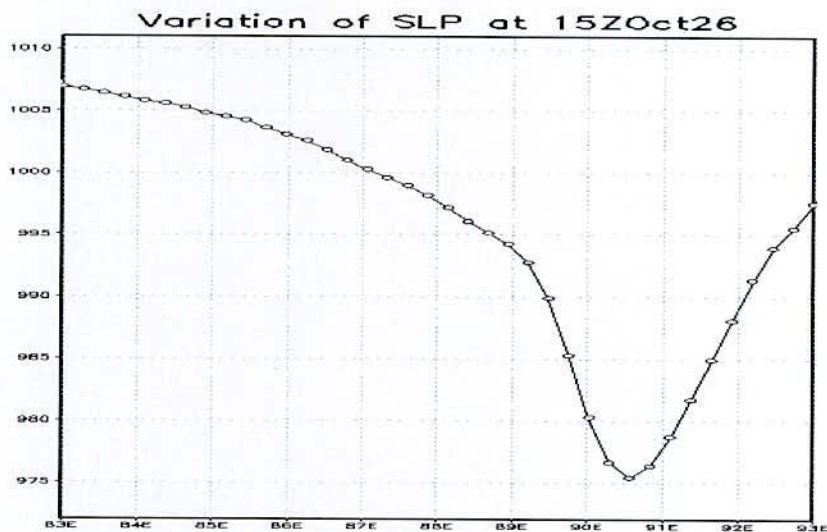


Figure 5.3.1.3a: East West cross sectional view of MM5 model simulated SLP of TC Rashmi through the centre (21.894°N and 90.6069°E) at 15 UTC on 26 October 2008.

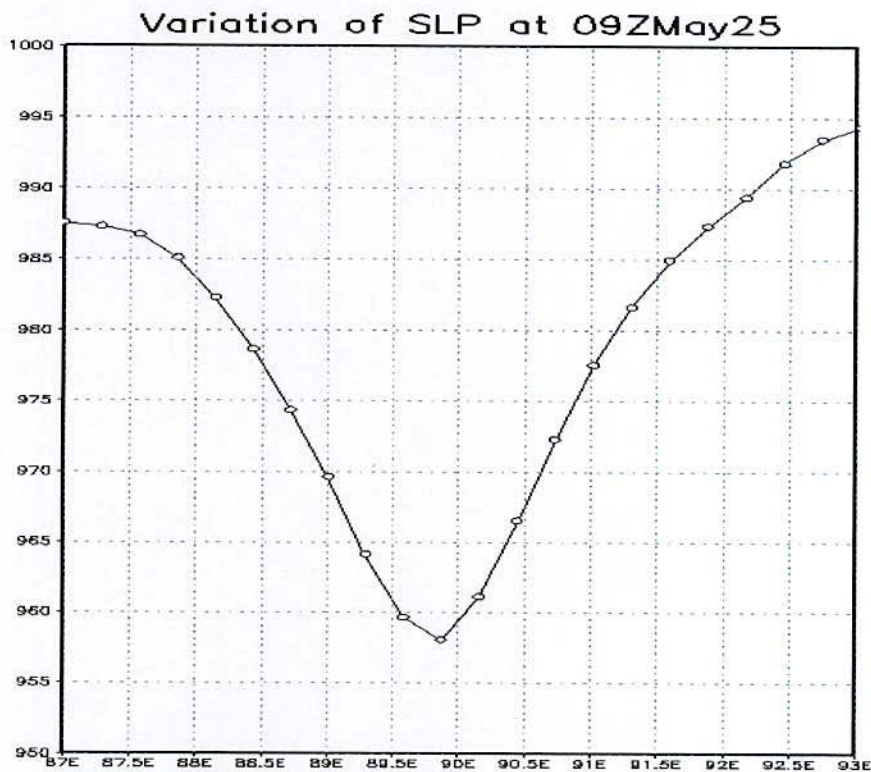


Figure 5.3.1.3b: East West cross sectional view of WRF model simulated SLP of TC Rashmi through the centre (21.331°N and 88.754°E) at 03 UTC on 27 October 2008.

5.3.2 Wind Field

Figure 5.3.2.1 shows the temporal variations of MM5 and WRF models simulated MWS and observed winds of TC Rashmi. The model simulated MWS are obtained at the standard meteorological height of 10 m. The MM5 and WRF Models simulated MWSs are higher than the observed values through almost full forecast hours without any exception. The simulated highest MWS are obtained at 15 UTC on 26 October and at 03 UTC on 27 October whereas that for observed MWS is obtained at 18 UTC on 26 October 2008. After that both the simulated winds by MM5 and WRF and observed winds decrease with time gradually.

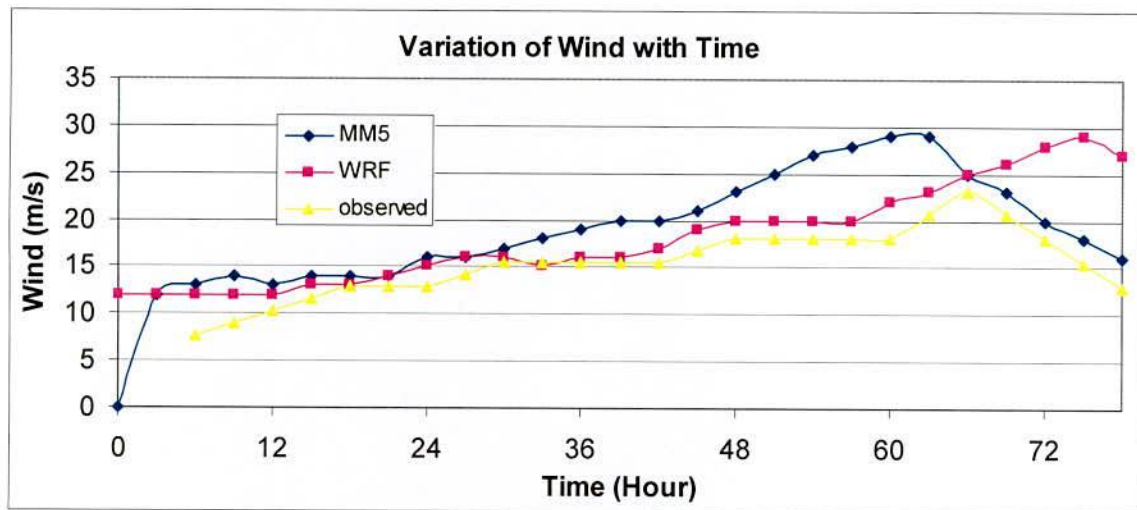


Figure 5.3.1.2.1: Observed and MM5 and WRF Models simulated wind speed (m/s) with time of TC Rashmi.

The distribution of surface (10 m) wind of Rashmi at 00 UTC of 24, 25, 26 October and at 15 UTC on 26 October 2008 (i.e. its mature stage) for MM5 model and at 00 UTC on 24, 25, 26 October and at 03 UTC on 27 October 2008 (i.e. its mature stage) for WRF model are shown in Figures 5.3.2.2a and 5.3.2.2b respectively. The Figure 5.3.2.2.a obtained from MM5 model shows that the wind field of the TC is highly asymmetric in the horizontal direction. At 00 UTC on 24 October 2008 (i.e. at the initial time of simulation) the TC is in the sea. The value of the wind is zero. At 00 UTC of 25 October 2008 (i.e. 24 hours of simulation), the figure shows that the pattern has an asymmetric wind distribution with strong wind bands in the front right side, rear left and front left sides far to the centre of northward moving storm. The wind flow in the core region shows a near circular feature with minimum wind speed at the centre. Similar pattern is also seen at 00 UTC on 26 October 2008 with strong wind bands at the front right side, rear and rear left sides. In this stage, TC is organized with strong wind bands around the wind flow and core region shows asymmetric feature with minimum wind speed at the centre. At 15 UTC on 26 October 2008 (i.e. at mature stage), a strong wind bands

(wind speed > 27 m/s) having strongest wind exceeding 29 m/s is found around the system centre with elongation in north-south direction. It may be noted that the model has generated slight higher winds of 29m/s (56 knot) than the observed winds of around 45 knot

Again, the Figure 5.3.2.2b obtained from WRF model shows that the wind field of the TC is highly asymmetric in the horizontal distribution. At 00 UTC of 24 October 2008 (i.e. at the initial time of simulation) the TC is in the sea. The figure shows that the pattern has an asymmetric wind distribution with strong wind bands in the front right side, rear left and rear right sides close to the centre of north directed moving storm. The wind flow in the core region shows a near circular feature with minimum wind speed at the centre. Similar pattern is also seen at 00 UTC of 25 October 2008 with strong wind bands at the front right side and rear and rear left sides. At 00 UTC of 26 October 2008, TC is organized with strong wind bands around and the wind flow in the core region shows asymmetric feature with minimum wind speed at the centre. At 03 UTC of 27 October 2008 (i.e. at mature stage), a strong wind bands (wind speed >27m/s) having strongest wind exceeding 29 m/s is found around the centre with elongation in east-west direction. It may be noted that the model has generated slightly higher winds of 29m/s (56 knot) than the observed winds of around 45 knot.

It is also noted that, due to friction of landmass, Figures 5.3.2.2a and 5.3.2.2b show the landfall feature of surface wind distribution where the winds is much less in the front side compared to others of the cyclonic system.

Figures 5.3.2.3a and 5.3.2.3b show the distribution of the surface wind of the TC Rashmi obtained from MM5 model along east-west cross section passing through its centre (21.894°N and 90.6074°E) at 15 UTC on 26 October 2008 and obtained from WRF model along east-west cross section passing through its centre (21.894°N and 90.6074°E) at 15 UTC on 26 October 2008. The figures demonstrate that a calm region is found inside the eye of the system and maximum wind was found in the eye wall. The radius of maximum wind of the TC Rashmi is found to be just lower than 100 km according to the simulation.

The horizontal distribution of vector wind field obtained from MM5 model at levels 850, 500, 300 and 200 hPa at time 15 UTC on 26 October 2008 (i.e. its mature stage) and field obtained from MM5 model at levels 850, 500, 300 and 200 hPa at 15 UTC on 26 October 2008 (i.e. its mature stage) are shown in the Figures 5.3.2.4a and 5.3.2.4b. MM5 and WRF Model derived maximum winds are tabulated in the Table 5.3.2.1a and 5.3.2.1b. A well organized TC circulation with strong winds encircling the centre is found at the 850 and 500 hPa levels. It is noted that the strong wind is confined to the right of the direction of the movement of the system. At 300 hPa wind shows cyclonic circulation in the right side of the TC and weak outflow in the left side. At 200 hPa level strong outflow is evident from the central part of the TC. So, using simulated results obtained from MM5 and WRF models, Figures 5.3.2.4a and 5.3.2.4b demonstrate inflow in the lower level and outflow in the upper level.

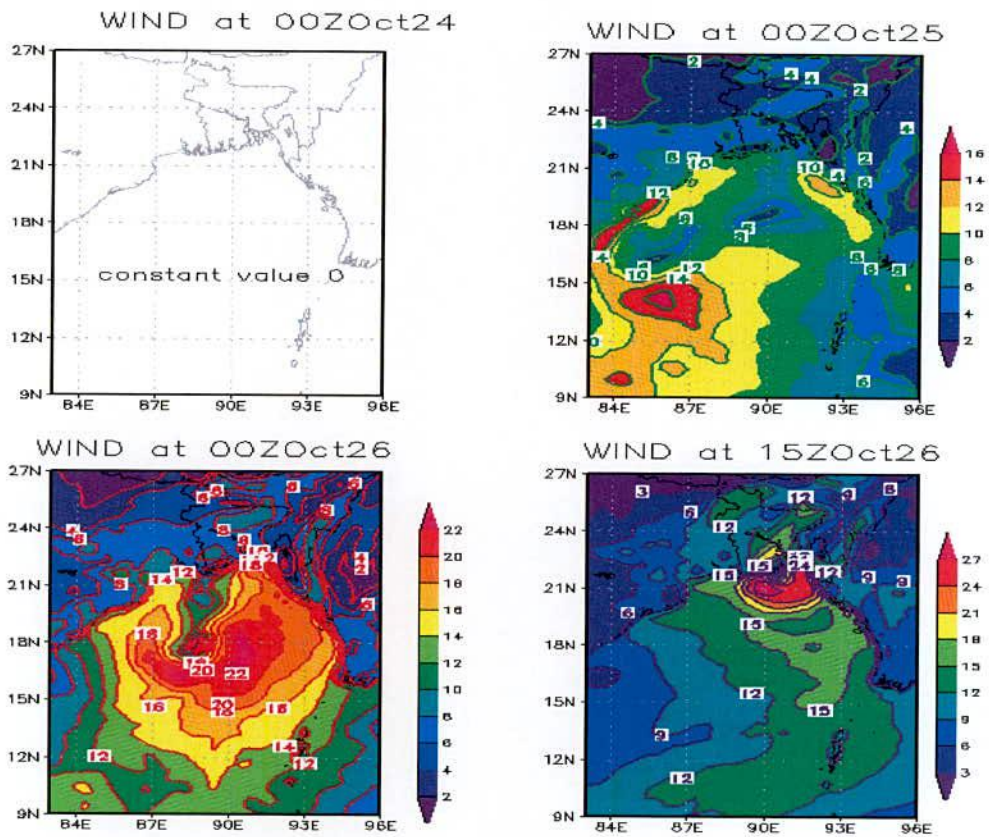


Figure 5.3.2.a: MM5 Model simulated Wind speed (m/s) of TC Rashmi at 00 UTC of 24, 25, 26 on October and at 15 UTC on 26 October 2008.

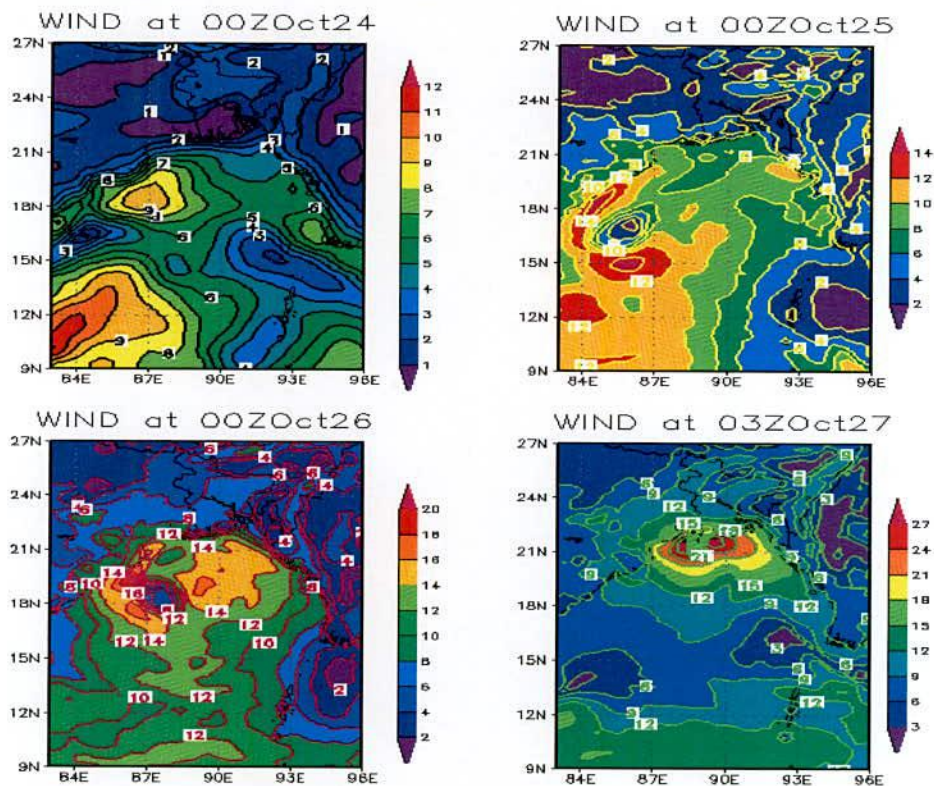


Figure 5.3.2.b: WRF model simulated Wind speed (m/s) of TC Rashmi at 00 UTC of 24, 25, 26 October and at 03 UTC on 27 October 2008.

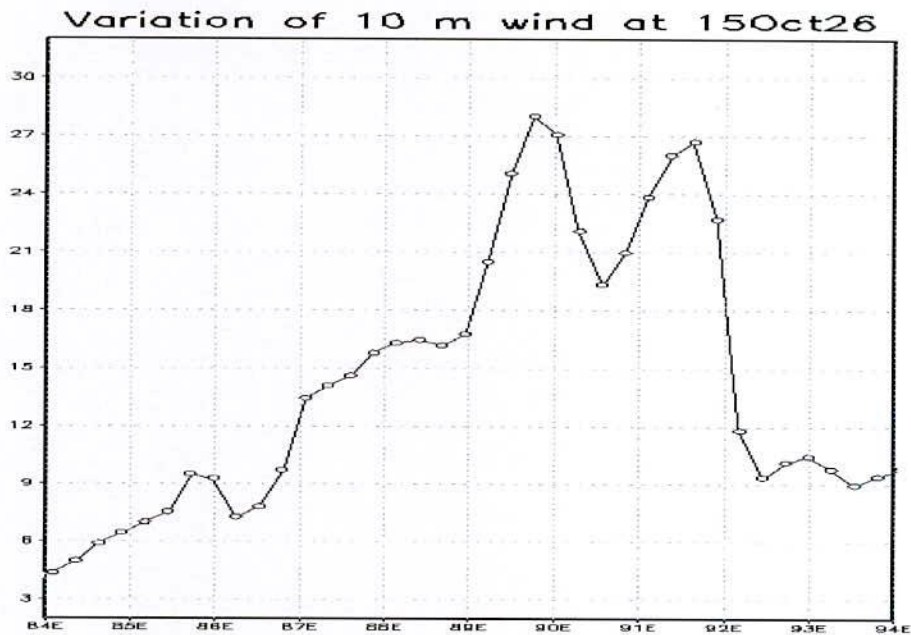


Figure 5.3.2.3a: East-West cross sectional view of MM5 model simulated wind speed (m/s) of TC Rashmi along its centre (21.894°N and 90.6069°E) at 15 UTC on 26 October 2008.

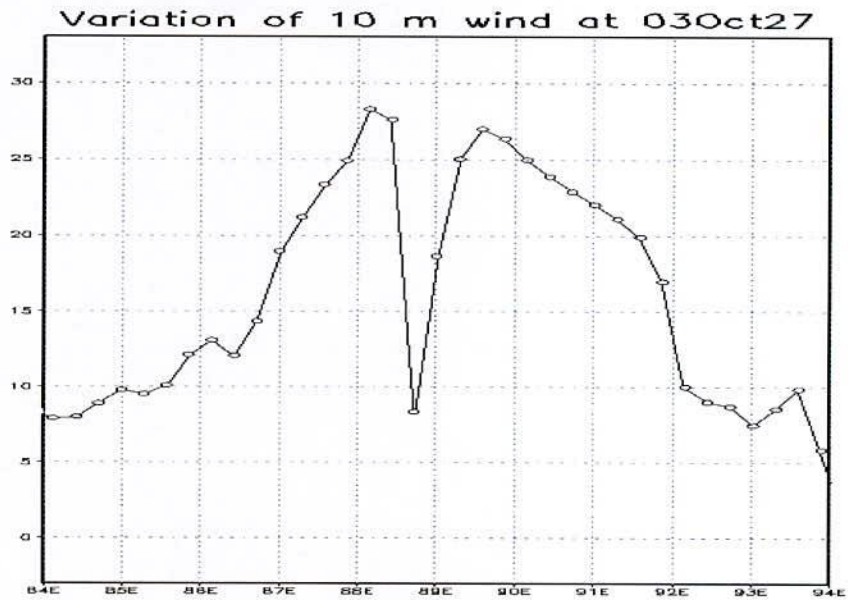


Figure 5.3.2.3b: East-West cross sectional view of WRF model simulated wind speed (m/s) of TC Rashmi along its centre (21.331°N and 88.754°E) at 03 UTC on 27 October 2008.

MM5 model derived maximum winds at the mature stage (15 UTC on 26 October 2008) are about 50, 60, 50 and 50 m/s at 850, 500, 300 and 200 hPa levels respectively. Again WRF model simulated maximum winds at the mature stage (03 UTC on 27 October 2008) are about 50, 40, 40 and 40 m/s at 850, 500, 300 and 200 hPa levels respectively. So, at mature stage maximum wind (at different levels) obtained from MM5 model is higher than or equal

to those obtained from WRF model and the mature stage obtained by MM5 model is earlier than that obtained by WRF model.

Table 5.3.2.1a: MM5 Model simulated wind speed (m/s) at 00 UTC on 24, 25, 26 October and at 15 UTC on 26 October 2008 at different pressure levels of TC Rashmi

| Pressure level (hPa) | Wind Speed (m/s) at different time | | | |
|----------------------|------------------------------------|----------------------|----------------------|----------------------|
| | 00 UTC on 24 October | 00 UTC on 25 October | 00 UTC on 26 October | 15 UTC on 26 October |
| 850 | 10 | 20 | 40 | 50 |
| 500 | 20 | 20 | 30 | 60 |
| 300 | 40 | 40 | 40 | 50 |
| 200 | 50 | 50 | 60 | 50 |

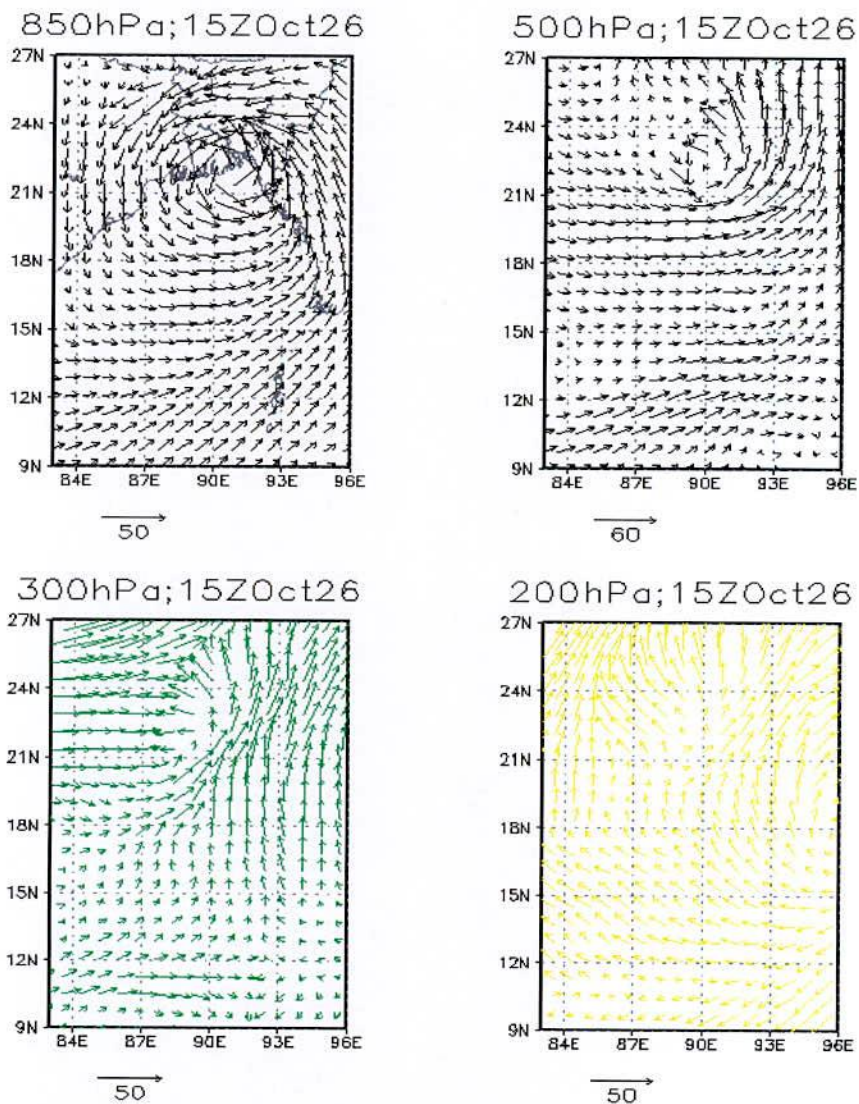
Table 5.3.2.1b: WRF model simulated wind speed (m/s) at 00 UTC on 24, 25, 26 October and at 03 UTC on 27 October 2008 at different pressure levels of TC Rashmi

| Pressure level (hPa) | Wind Speed (m/s) at different time | | | |
|----------------------|------------------------------------|----------------------|----------------------|----------------------|
| | 00 UTC on 24 October | 00 UTC on 25 October | 00 UTC on 26 October | 03 UTC on 27 October |
| 850 | 10 | 20 | 30 | 50 |
| 500 | 20 | 20 | 20 | 40 |
| 300 | 50 | 40 | 50 | 40 |
| 200 | 50 | 40 | 50 | 40 |

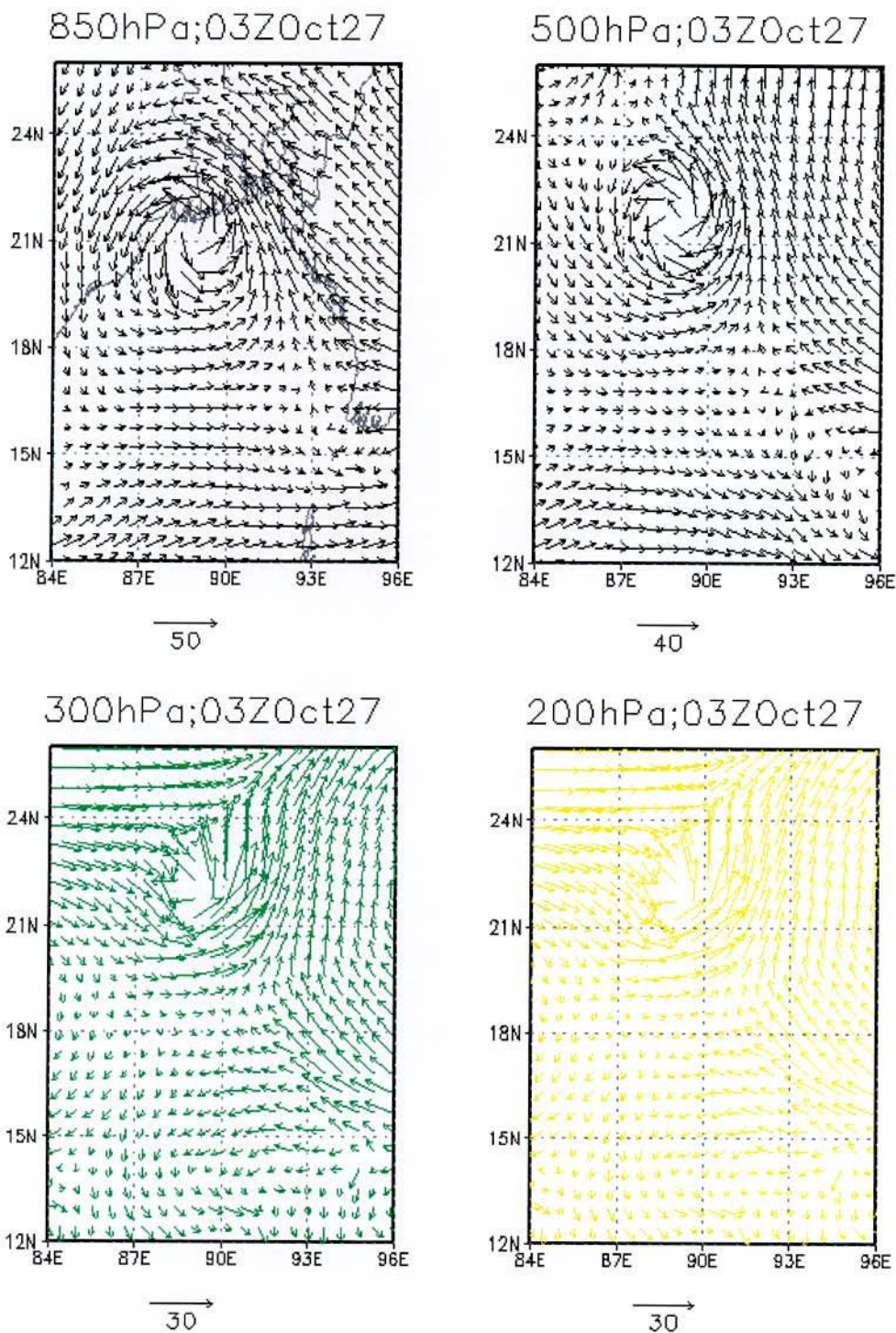
Figures 5.3.2.5a and 5.3.2.5b show the vertical profile of radial, tangential, vertical and horizontal winds of TC Rashmi obtained from MM5 model at 15 UTC of 26 October 2008 (i.e. its mature stage) and obtained from MM5 model at 15 UTC of 26 October 2008 (i.e. its mature stage) respectively. Results are also given in Tables 5.3.2.2a and 5.3.2.2b respectively for the models MM5 and WRF for different times mentioned in the Tables. From the tables it is clear that the value of the vertical profile of radial, tangential, vertical and horizontal wind of TC Rashmi obtained from MM5 and WRF models increases with the process of time.

From the figure it is found that vertical profile of radial wind is much more organized and it is also clearly seen that the system has strong inflow in the lower levels which bring the air to the system through the boundary level and lower level and outflow in the upper level. The maximum values of the radial component of wind at mature stage obtained from MM5 are higher than that obtained from WRF model (Tables 5.3.2.2a and 5.3.2.2b).

The tangential wind flows in a northerly direction at the eastern side of the system and in a southerly direction at the western side. The strong wind with different speeds (Table 5.3.1.2.2) is confined to the different levels in lower troposphere and extended up to 200 hPa level for MM5 and up to 100 for WRF model in the right and left side of the system. The value of the tangential wind in the eastern side is higher than that of western side.



5.3.2.4a: MM5 Model simulated wind vector at levels 850, 500, 300 and 200 hPa at 15 UTC on 26 October 2008.



5.3.2.4b: WRF Model simulated wind vector at levels 850, 500, 300 and 200 hPa at 3 UTC on 27 October 2008.

The values of the vertical motion are different in magnitude for different times and it reveals that strong upward motion of about 120 cm/s for MM5 model exists along the eye wall (at 15 UTC on 26 October 2008) and other parts of the system which feed moisture into the system. Again, this value is 650 cm/s for WRF model at 03 UTC on 27 October 2008. It is noted that

Rashmi has very weak updraft motion within 110 cm/s around at the eye wall in the west throughout mid and upper troposphere. The downward motion is visible in the central parts of the TC and other areas in between rain bands.

The vertical profile of horizontal wind of the system at its mature stage shows the distribution of strong winds up to 200 hPa and 100 hPa for MM5 and WRF models respectively around the centre of TC. It further confirms that the maximum winds are confined to the right of the direction of the movement of the system. This value decreases with the radial distance from both side of the eye. Calm wind zone is sharp and narrow and little bit tilted to the westward and get expanded towards upper levels. This is in agreement with the previous studies of Rao and Prasad (2006) and Goswami *et al.* (2006) on Orissa TC. Cyclonic circulation is generally seen up to about 300 hPa level and anticyclonic circulation with divergence fields aloft. In case of TC Rashmi, cyclonic circulation is also seen up to about 350, 300 hPa level for MM5 and WRF model respectively and anticyclonic circulation with divergence fields aloft.

Table 5.3.2.2a: MM5 model simulated radial wind, tangential wind, vertical velocity and horizontal wind (cm/s) of TC Rashmi at 00 UTC on 24, 25, 26 October and at 15 UTC on 26 October 2008.

| Component of wind | Simulated wind speed (cm/s) at different time | | | |
|-------------------|---|----------------------|----------------------|----------------------|
| | 00 UTC on 24 October | 00 UTC on 25 October | 00 UTC on 26 October | 15 UTC on 26 October |
| Radial wind | 400 | 600 | 1200 | 2500 |
| Tangential wind | 800 | 15 | 3000 | 4000 |
| Vertical velocity | 7 | 30 | 70 | 120 |
| Horizontal wind | 1000 | 1000 | 3000 | 4000 |

Table 5.3.2.2b: WRF model simulated radial wind, tangential wind, vertical velocity and horizontal wind (cm/s) of TC Rashmi at 00 UTC on 24, 25, 26 October and at 03 UTC on 27 October 2008.

| Component of wind | Simulated wind speed (cm/s) at different time | | | |
|-------------------|---|----------------------|----------------------|----------------------|
| | 00 UTC on 24 October | 00 UTC on 25 October | 00 UTC on 26 October | 03 UTC on 27 October |
| Radial wind | 400 | 600 | 1200 | 2000 |
| Tangential wind | 600 | 1200 | 2000 | 3000 |
| Vertical velocity | 0.10 | 45 | 650 | 120 |
| Horizontal wind | 1000 | 1000 | 3000 | 4000 |

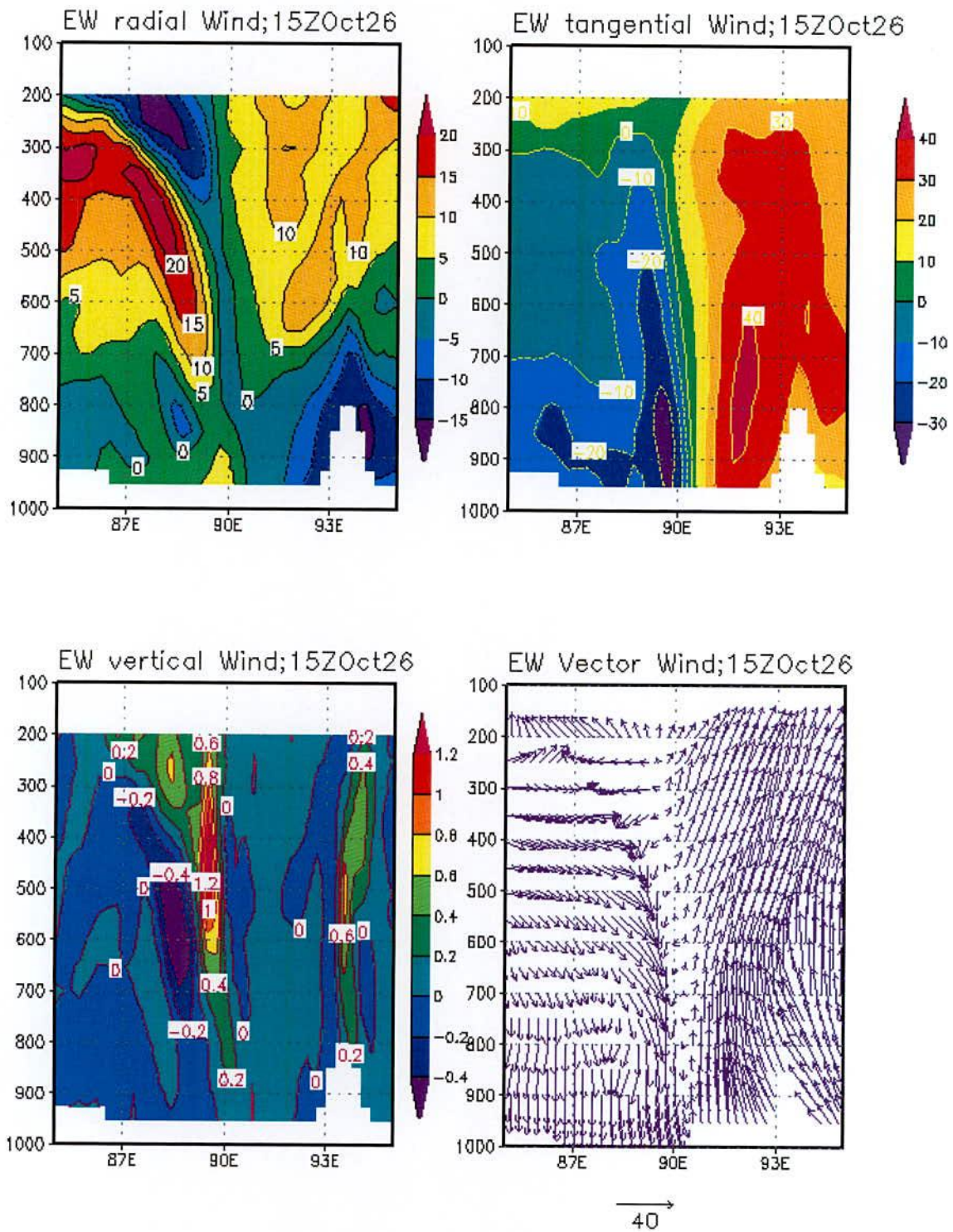


Figure 5.3.2.5a: MM5 model simulated radial wind, tangential wind, vertical velocity and horizontal wind (cm/s) of TC Rashmi at 00 UTC of 24, 25, 26 October and at 15 UTC of 26 October 2008.

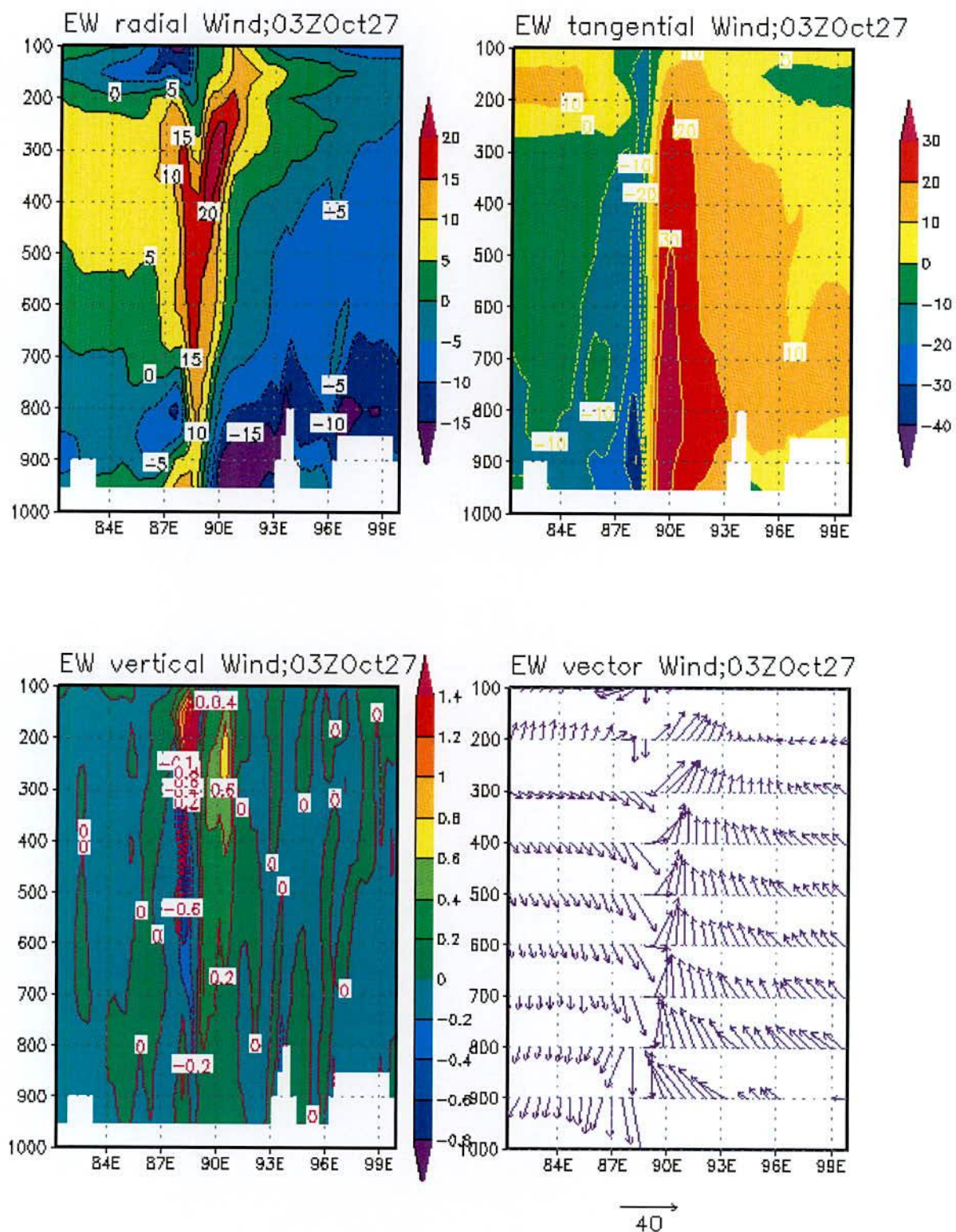


Figure 5.3.2.5b: WRF model simulated radial wind, tangential wind, vertical velocity and horizontal wind (cm/s) of TC Sidr at 00 UTC on 24, 25, 26 October and at 03 UTC on 27 October 2008.

5.3.3 Vorticity Field

To know the evolution, the MM5 and WRF model simulated relative vorticity at 850 hPa as a function of time is shown in Figure 5.1.3.1. From the figure it is observed for MM5 model that there is a gradually rise in the vorticity value in the first 63 hours of integration of the model. Thereafter the value shows a fall. Again, it is observed for WRF model that there is a gradually rise of vorticity in the first 48 hours of simulation of the model and sustains the maximum value for 9 hours duration (48 -54 hours of forecast). Thereafter the value shows a decreasing tendency and again increases up to 72 hours of simulation. Simulated vorticity obtained from WRF model is higher than that obtained from MM5 model.

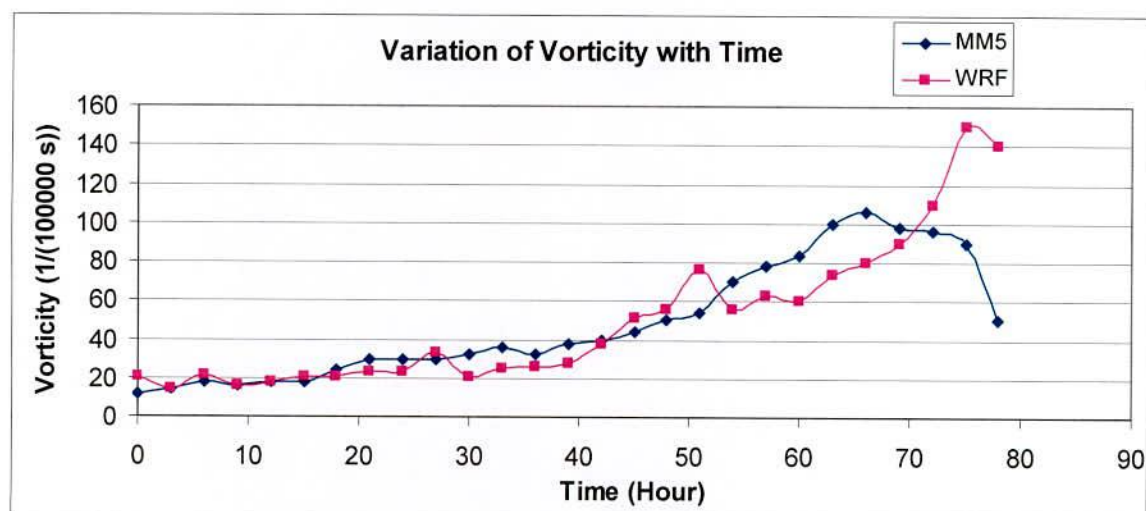


Figure 5.3.3.1: Evolution of model simulated vorticity with time of TC Rashmi

The horizontal distribution of the relative vorticity obtained from MM5 at 15 UTC of 26 October 2008 (i.e. its mature stage) of TC Rashmi for 850, 500, 300 and 200 hPa levels and obtained from WRF at 03 UTC of 27 October 2008 (i.e. its mature stage) of TC Rashmi for 850, 500, 300 and 200 hPa levels are shown in the Figures 5.3.3.2a and 5.3.3.2b respectively.

It is seen from the figures that the vorticity is distributed with maximum value at the centre and these values for the levels 850, 500, 300 and 200 hPa are tabulated in Tables 5.3.3.1a and 5.3.3.1b for MM5 and WRF models respectively. The values of relative vorticity are increased with the increase of time (i.e. in the development of the TC) at all levels. At 850 hPa, the distribution maintains circular pattern with some asymmetric features in the outer periphery. Negative vorticity field are situated far from the centre. This distance of the negative vorticity from the centre is increased due to development of TC (not shown). Low level relative vorticity fields confirm the strong cyclonic circulation at low levels with different time and distance in feeding the moisture into the system to sustain its intensity. At 500 and 300 hPa levels, the distribution of relative vorticity also shows a symmetric character

in the horizontal distribution. The values of relative vorticity are increased with the development of TC. At 200 hPa level, the weak positive vorticity embedded with negative vorticity field is visible at 200 hPa level. Negative vorticity is found at the centre of the TC.

It is clear from the figure that relative vorticity is more organized in the mature stage and the value of vorticity in this stage obtained from WRF model is higher than the value obtained from MM5 model.

Table 5.3.3.1a: MM5 Model simulated maximum vorticity ($\times 10^{-5} \text{ s}^{-1}$) at different pressure levels associated with TC Rashmi at 00 UTC on 24, 25, 25 October and at 15 UTC on 26 October 2008.

| Pressure level (hPa) | Vorticity ($\times 10^{-5} \text{ s}^{-1}$) at different times | | | |
|--------------------------|--|-------------------------|-------------------------|-------------------------|
| | 00 UTC on 24 October | 00 UTC on 25 October | 00 UTC on 26 October | 15 UTC on 26 October |
| 850 | 12 | 20 | 50 | 90 |
| 500 | 10 | 18 | 35 | 60 |
| 300 | 6 | 12 | 25 | 35 |
| 100 | 2 | 12 | 10 | 20 |
| Position of TC centre | 16.080°N, 84.677°E | 15.979°N, 85.677°E | 17.731°N, 88.892°E | 21.894°N, 90.607°E |
| Vertical distribution | | 24 | 40 | 90 |

Table 5.3.3.1b: WRF Model simulated maximum vorticity ($\times 10^{-5} \text{ s}^{-1}$) at different pressure levels associated with TC Rashmi at 00 UTC of 24, 25, 25 October and at 03 UTC on 27 October 2008.

| Pressure level (hPa) | Vorticity ($\times 10^{-5} \text{ s}^{-1}$) at different times | | | |
|--------------------------|--|---------------------------|--------------------------|--------------------------|
| | 00 UTC on 24 October | 00 UTC on 25 October | 00 UTC on 26 October | 03 UTC on 27 October |
| 850 | 20 | 20 | 50 | 140 |
| 500 | 40 | 20 | 60 | 90 |
| 300 | 6 | 15 | 40 | 80 |
| 200 | 15 | 12 | 35 | 70 |
| position of TC centre | 16.084°N and 84.719°E | 116.799°N and 85.895°E | 18.972°N and 87.293°E | 21.331°N and 88.754°E |
| Vertical distribution | 10 | 20 | 50 | 140 |

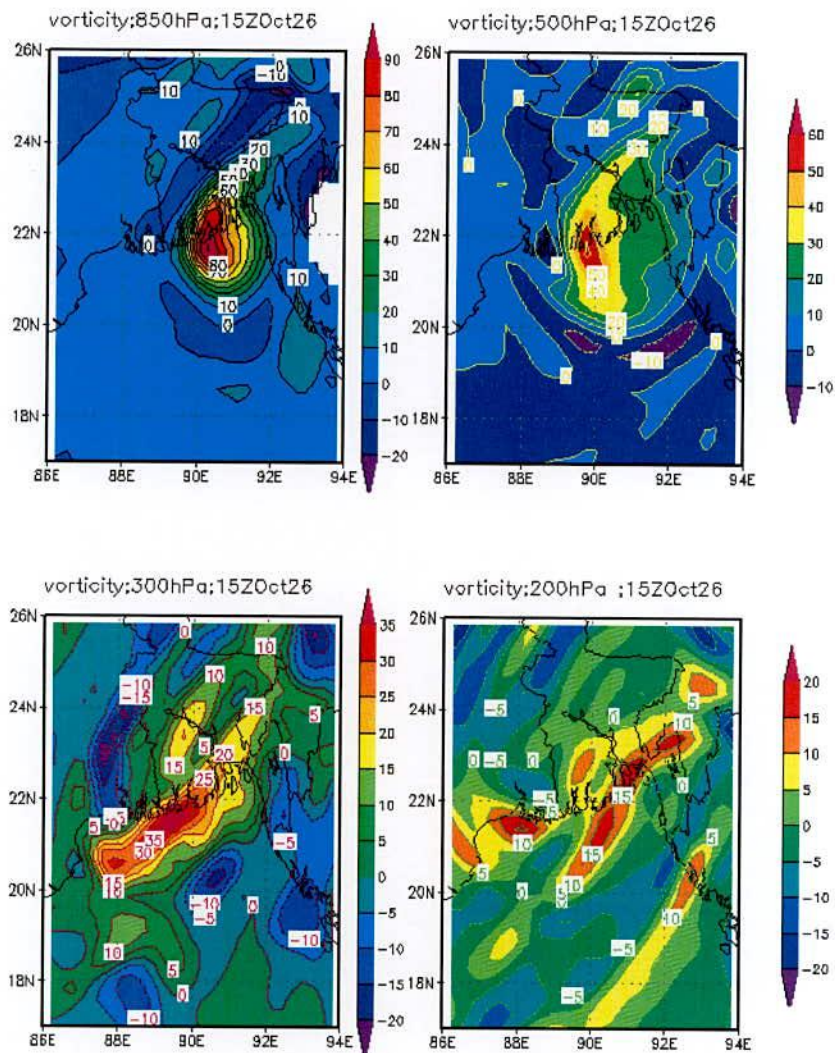


Figure 5.3.3.2a: MM5 Model simulated vorticity field of 850, 500, 300 and 200 hPa level at 15 UTC on 26 October 2008

Vertical distribution of the relative vorticity obtained from MM5 model along the centre in the east-west direction is shown in Figure 5.3.3.3a and the values at different pressure levels are tabulated in Table 5.3.3.1a. Similarly, vertical distribution of the relative vorticity obtained from WRF model along the centre in the east-west direction is shown in Figure 5.3.3.3b and the values at different pressure levels are tabulated in Table 5.3.3.1b.

According to the MM5 simulated results at 00 UTC on 24 October 2008 (i.e. the initial time), the positive vorticity is spread over a horizontal distance with strong vorticity at slightly westward of the centre (16.080°N 84.677°E). This pattern of distribution extends from surface to around 150 hPa level with the exception that the magnitude of the vorticity decreases with height. Similar pattern with higher positive value of vorticity is found at the centre after 24 hours of simulation at 00 UTC on 25 October 2008 along the centre (15.979°N and 85.677°E). At 00 UTC on 26 October 2008 the system has the positive vorticity along the

centre up to 200 hPa level with higher value (17.731°N and 88.892°E). At 15 UTC on 26 October 2008 the system has the highest value of positive vorticity along the centre (21.894°N and 90.607°E) up to 200 hPa with low magnitude.

According to the MM5 simulated results at 00 UTC on 24 October 2008 (i.e. the initial time), the positive vorticity is spread over a horizontal distance with strong vorticity at slightly western side of the centre (16.084°N and 84.719°E). This pattern of distribution extends from surface to around 150 hPa level with the exception that the magnitude of the vorticity decreases with height. Similar pattern with higher positive values of vorticity is found at the centre after 24 hours of simulation at 00 UTC on 25 October 2008 along the centre (16.799°N and 85.895°E). At 00 UTC on 26 October 2008, the system has the positive vorticity along the centre (19.847°N and 89.634°E) up to 200 hPa level with higher value. At 03 UTC on 27 October 2008, the system has the highest value of positive vorticity along the centre (21.357°N 89.856°E) up to 100 hPa with low magnitude.

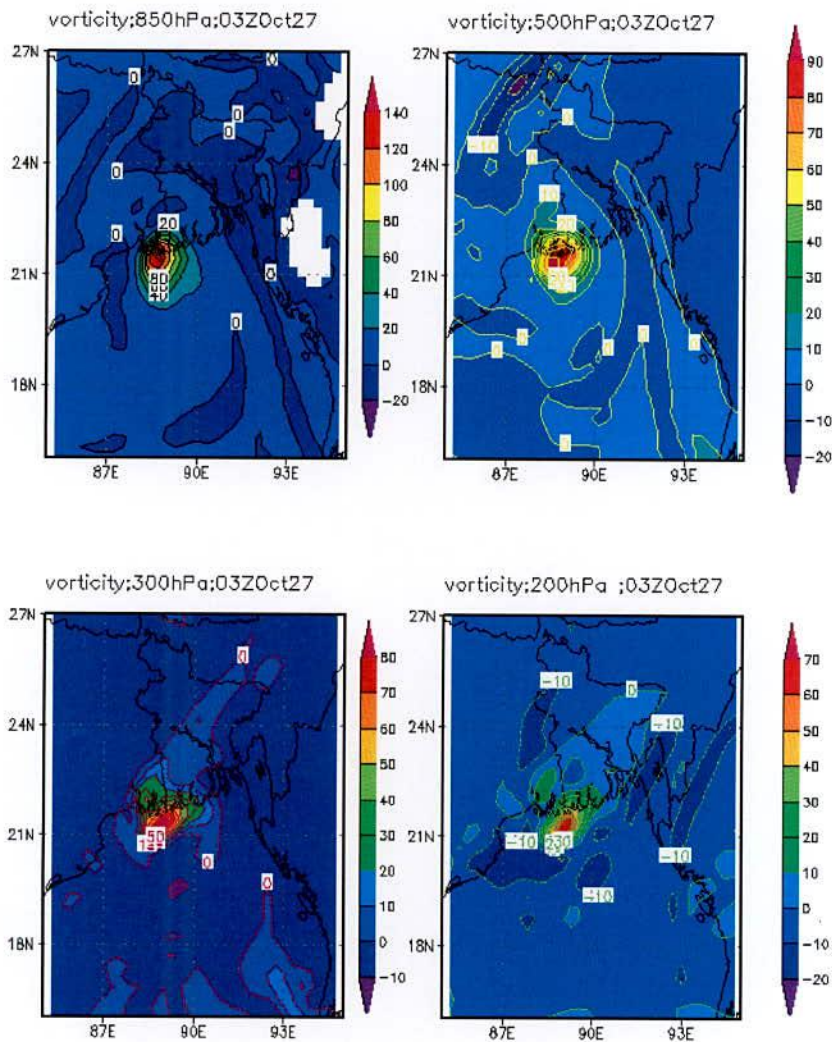


Figure 5.3.3.2b: WRF Model simulated vorticity fields of 850, 500, 300 and 200 hPa levels at 03 UTC on 27 October 2008.

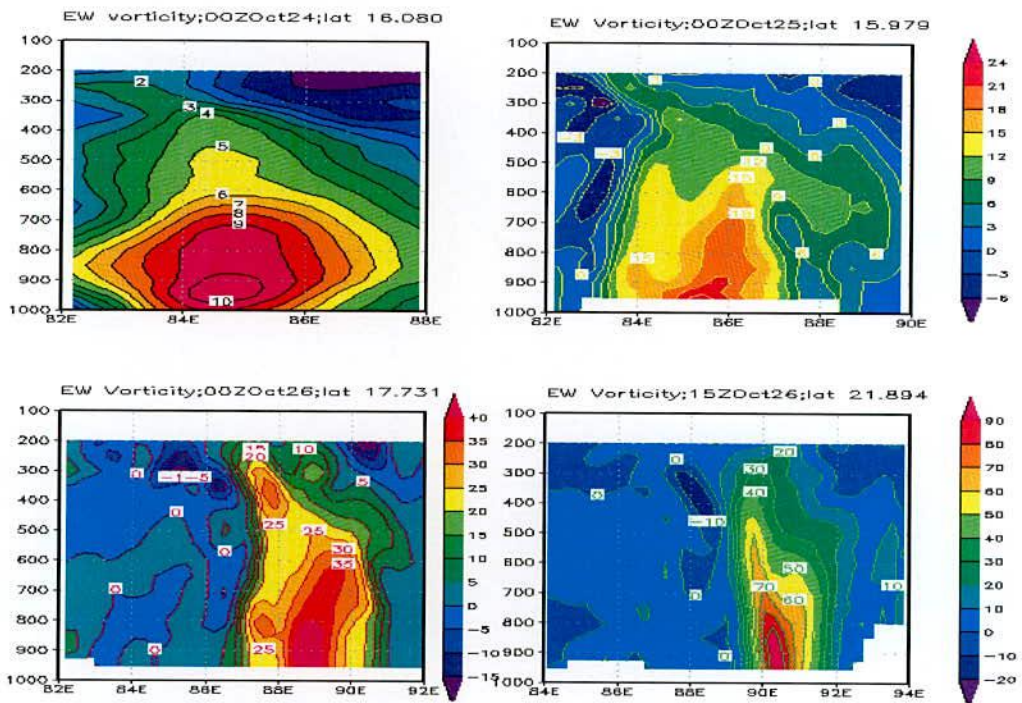


Figure 5.3.3.a: MM5 Model simulated east-west cross section of vertical distribution of relative vorticity of TC Rashmi through the centre at 00 UTC on 24, 25, 26 October and 15 UTC of 26 October 2008

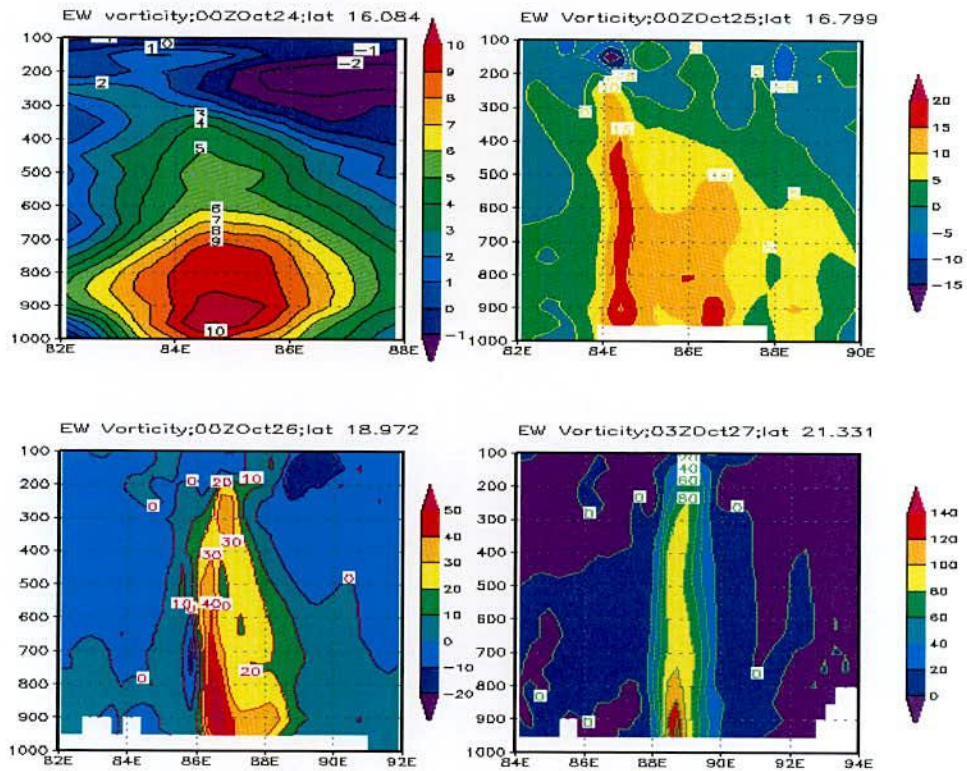


Figure 5.3.3.b: WRF Model simulated east-west vertical distribution of relative vorticity of TC Rashmi through the centre at 00 UTC of 24, 25, 26 October and 03 UTC of 27 October 2008

5.3.4 Temperature Anomaly

The MM5 model simulated temperature anomaly at 00 UTC of 24, 25, 26 October and 15 UTC of 26 October 2008 (i.e. its mature stage) of TC Rashmi from surface to 200 hPa levels is shown in Figure 5.3.4.1a and the values at different pressure levels are tabulated in Table 5.3.4.1a

At 00 UTC of 24 October 2008, maximum temperature is 6°C at around 450 hPa level. It is noted that the warm core region is largely expanded outward at 700-400 hPa level. The simulated temperature anomaly demonstrates that the warm core is visible mainly at upper troposphere. Negative temperature anomalies are also simulated at the upper and lower levels.

At 00 UTC of 25 October 2008, warm core is observed between 900-350 hPa level. It is noted that the warm core region is expanded outward at 900-350 hPa level. The highest 7°C temperature anomaly is simulated around 450 hPa level at the western side of the cyclone centre. The simulated temperature anomaly demonstrates that the warm core is visible mainly at upper troposphere. Negative temperature is also observed at the upper levels.

At 00 UTC of 26 October 2008, warm core is observed at 950-200 hPa layer. It is noted that the warm core region is expanded outward at 750-250 hPa level. The greatest anomaly of 9°C is found at around 450 hPa level in the western side of the eye of the cyclone. The simulated temperature anomaly demonstrates that the warm core is visible mainly in the upper troposphere. Negative temperature anomalies at lower levels are due to contamination by heavy precipitation.

At 15 UTC of 26 October 2008, warm core is observed in 950-150 hPa layer. It is noted that the warm core region is expanded outward at 700-300 hPa level. The greatest anomaly of 9°C is simulated at around 550-650 hPa level. The simulated temperature anomaly demonstrates that the warm core is visible mainly in the upper troposphere. Negative temperature anomalies at lower levels are due to contamination by heavy precipitation.

Maximum value of temperature anomaly obtained from WRF model is higher than that obtained from MM5 model.

Table 5.3.4.1a: MM5 Model simulated temperature anomaly (°C) associated with TC Rashmi at 00 UTC on 24, 25, 26 October and at 15 UTC on 26 October 2008.

| Temperature anomaly (°C) at time | | | |
|----------------------------------|-------------------------|-------------------------|-------------------------|
| 00 UTC on 24 October | 00 UTC on 25 October | 00 UTC on 26 October | 15 UTC on 26 October |
| 6 | 7 | 9 | 9 |

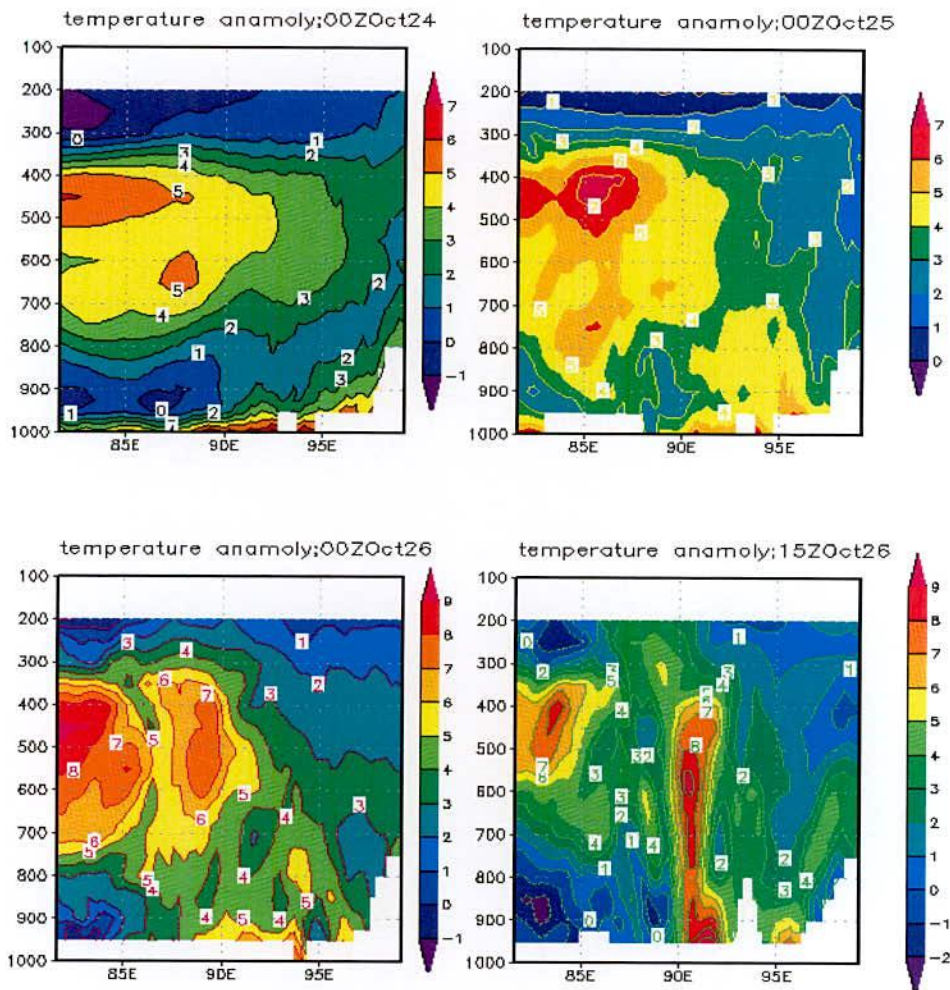


Figure 5.3.4.1a: MM5 model simulated vertical distribution of temperature anomaly in the east-west direction of TC Rashmi at 00 UTC on 24, 25, 26 October and at 15 UTC on 26 October 2008.

Again, the WRF model simulated temperature anomaly associated with TC Rashmi at 00 UTC on 24, 25, 26 October and at 03 UTC on 27 October 2008 (i.e. its mature stage) from surface to 100 hPa level is shown in Figure 5.3.4.1b and the values are tabulated in Table 5.3.4.1b. At 00 UTC on 24 October 2008, warm core with 9°C is observed in 800-250 hPa layer. It is noted that the warm core region is slightly expanded outward at 800-300 hPa level. The greatest anomaly is occurred around 450 hPa level. The simulated temperature anomaly demonstrates that the warm core is visible mainly at upper troposphere. Negative temperature anomalies is also seen at the upper levels.

At 00 UTC on 25 October 2008, warm core with 8°C is observed in 850-300 hPa layer. It is noted that the warm core region is expanded outward at 700-300 hPa level. The greatest anomaly is observed around 450 hPa level. The simulated temperature anomaly demonstrates that the warm core is visible mainly at upper troposphere.

At 00 UTC on 26 October 2008, a warm core with 12°C is observed in 950-150 hPa layer. It is noted that the warm core region is expanded outward at 750-250 hPa level. The greatest anomaly is observed around 500 hPa level. The simulated temperature anomaly demonstrates that the warm core is visible mainly at upper troposphere.

At 03 UTC on 27 October 2008, a warm core with 9°C is observed in 950-150 hPa layer. It is noted that the warm core region is expanded outward at 700-300 hPa level. The greatest anomaly is observed around 500 hPa level. The simulated temperature anomaly demonstrates that the warm core is visible mainly at upper troposphere.

At first the water vapour moves in the upward direction and transformed into liquid water and ice particle. The water vapour losses heat in the environment due to the transformation of liquid water and ice particle and then the temperature of the upper atmosphere increases.

Table 5.3.4.1b: WRF Model simulated temperature anomaly (°C) associated with TC Rashmi at 00 UTC on 24, 25, 26 October and at 03 UTC on 27 October 2008

| Temperature anomaly (°C) at different time | | | |
|--|-------------------------|-------------------------|-------------------------|
| 00 UTC of 24 October | 00 UTC of 25 October | 00 UTC of 26 October | 03 UTC of 27 October |
| 9 | 8 | 12 | 9 |

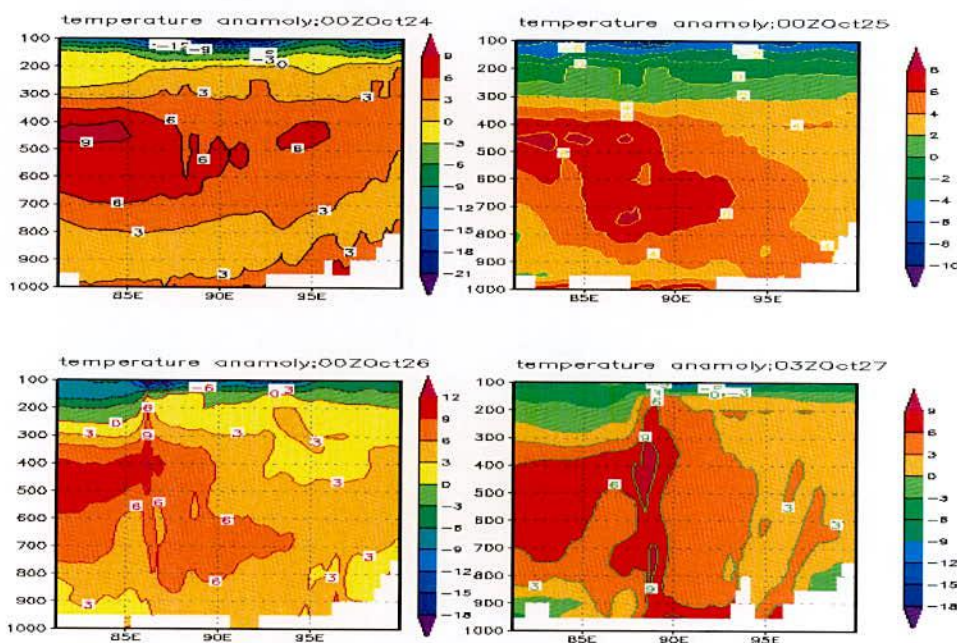


Figure 5.3.4.1b: WRF model simulated vertical distribution of temperature anomaly in the east-west direction of TC Rashmi at 00 UTC of 24, 25, 26 and 03 UTC of 27 October 2008.

5.3.5 Relative Humidity

The vertical section of relative humidity of TC Rashmi obtained from MM5 model at 00 UTC on 24, 25, 26 October and at 15 UTC on 26 October 2008 (i.e. its mature stage) from surface to 200 hPa level has shown in the Figure 5.3.5.1a and its values are tabulated in Table 5.3.5.1a. It is noted that high relative humidity (more than 90%) spreads in outer range of eye wall up to 750, 600, 550 and 300 hPa levels at 00 UTC on 24, 25, 26 October and at 15 UTC on 26 October 2008 respectively. High relative humidity bands are also found in the rain band of the system situated at both sides of the system throughout 950-750 hPa level.

The vertical cross section of relative humidity of TC Rashmi obtained from WRF model at 00 UTC on 24, 25, 26 October and at 03 UTC on 27 October 2008 (i.e. its mature stage) from surface to 100 hPa levels is shown in Figure 5.3.5.1b and its values are tabulated in Table 5.3.5.1b. It is noted that high relative humidity (more than 90%) spreads in outer range of eye wall up to 600, 450, 350 and 450 hPa levels at 00 UTC of 24, 25, 26 October and at 03 UTC on 27 October 2008 respectively. High relative humidity bands are also found in the rain band of the system situated at both sides of the system throughout 950-750 hPa level.

Table 5.3.5.1a: MM5 Model simulated maximum relative humidity (%) associate with TC Rashmi at 00 UTC on 24, 25, 26 October and at 15 UTC on 26 October 2008.

| Simulated maximum relative humidity (%) at different times | | | |
|--|-------------------------|-------------------------|-------------------------|
| 00 UTC on 24 October | 00 UTC on 25 October | 00 UTC on 26 October | 15 UTC on 26 October |
| 95 | 100 | 100 | 100 |

Table 5.3.5.1b: WRF Model simulated maximum relative humidity (%) associated with TC Rashmi at 00 UTC on 24, 25, 26 October and at 03 UTC on 27 October 2008.

| Simulated maximum relative humidity (%) at different times | | | |
|--|-------------------------|-------------------------|-------------------------|
| 00 UTC of 24 October | 00 UTC of 25 October | 00 UTC of 26 October | 03 UTC of 27 October |
| 90 | 90 | 100 | 100 |

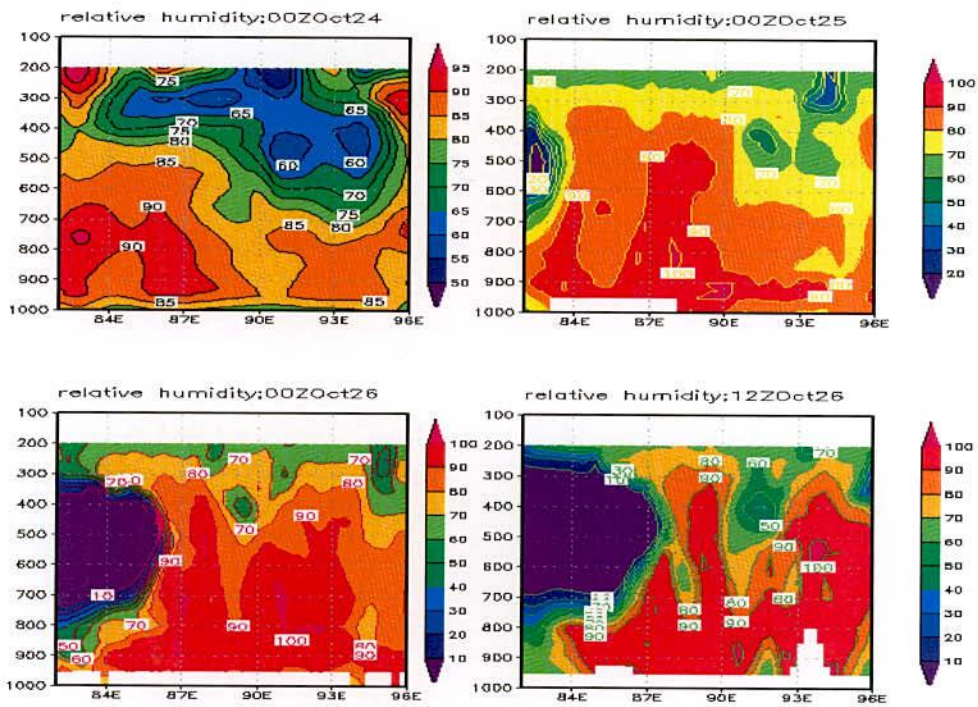


Figure 5.3.5.1a: MM5 model simulated vertical distribution of relative humidity (%) in the east-west direction of TC Rashmi at 00 UTC on 24, 25, 26 October and at 15 UTC on 26 October 2008.

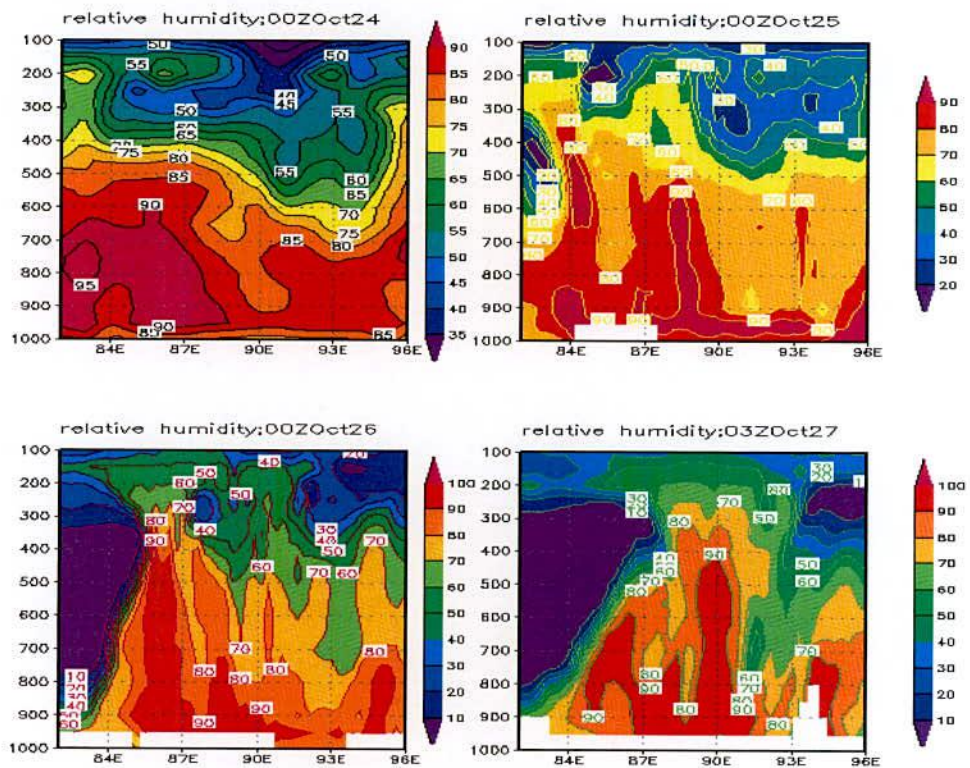


Figure 5.3.5.1b: WRF model simulated vertical distribution of relative humidity (%) in the east-west direction of TC Rashmi at 00 UTC on 24, 25, 26 October and 03 UTC on 27 October 2008.

5.3.6 Water Vapor Mixing Ratio

The vertical distribution of water vapor mixing ratio obtained from MM5 model in the east-west direction through the centre of TC at 00 UTC on 24, 25, 26 October and at 15 UTC on 26 October 2008 (i.e. its mature stage) of TC Rashmi from surface to 200 hPa level is shown in Figure 5.3.6.1a and its values are tabulated in Table 5.3.5.1a.

The analysis obtained from MM5 model shows that the highest moisture content more than around 2.0×10^{-2} kg/kg or more is found at the centre of the system at 950 hPa level and it decreases upwards to 400 hPa level or more. For the development of the system this upward level goes up to 350 and 300 hPa at 00 UTC on 26 October and at 15 UTC on 26 October 2008 (i.e. its mature stage) respectively.

The vertical distribution of water vapor mixing ratio obtained from WRF model along the east-west cross section of the centre at 00 UTC of 24, 25, 26 and 03 UTC of 27 October 2008 (i.e. its mature stage) of TC Rashmi from surface to 100 hPa level is shown in Figure 5.3.6.1b and its values are tabulated in Table 5.3.6.1b. It shows that the highest moisture content more than around 2.0×10^{-2} kg/kg or more is found at the centre of the system at 950 hPa level and it decreases upwards to 400 hPa level or more. For the development of the system this upward level goes up to 350 hPa at 00 UTC of 26 October and 03 UTC of 27 October 2008 (i.e. its mature stage).

The horizontal distribution of water vapor mixing ratio obtained from MM5 at 950 hPa level at 00 UTC of 24, 25, 26 October and 15 UTC of 26 October 2008 (i.e. its mature stage) and obtained from WRF model at 950 hPa level at 00 UTC of 24, 25, 26 October and 03 UTC of 27 October 2008 (i.e. its mature stage) associated with TC Rashmi is shown in the Figure 5.3.6.2a 5.3.6.2b respectively. It is noted that the high moisture flux comes from the southern side covering a large area of the Bay of Bengal which feeds the system along its southeastern side through the boundary layer. The value of high moisture flux increases slightly with development of the system.

Table 5.3.6.1a: MM5 model simulated maximum water vapour mixing ratio ($\text{kg/kg} \times 10^{-2}$) associated with TC Rashmi at 00 UTC on 24, 25, 26 October and at 15 UTC on 26 October 2008.

| Maximum value of Water vapor mixing ratio (%) at different time | | | |
|---|-------------------------|-------------------------|-------------------------|
| 00 UTC of 24 October | 00 UTC of 25 October | 00 UTC of 26 October | 15 UTC of 26 October |
| 1.8 | 2.0 | 2.0 | 2.0 |

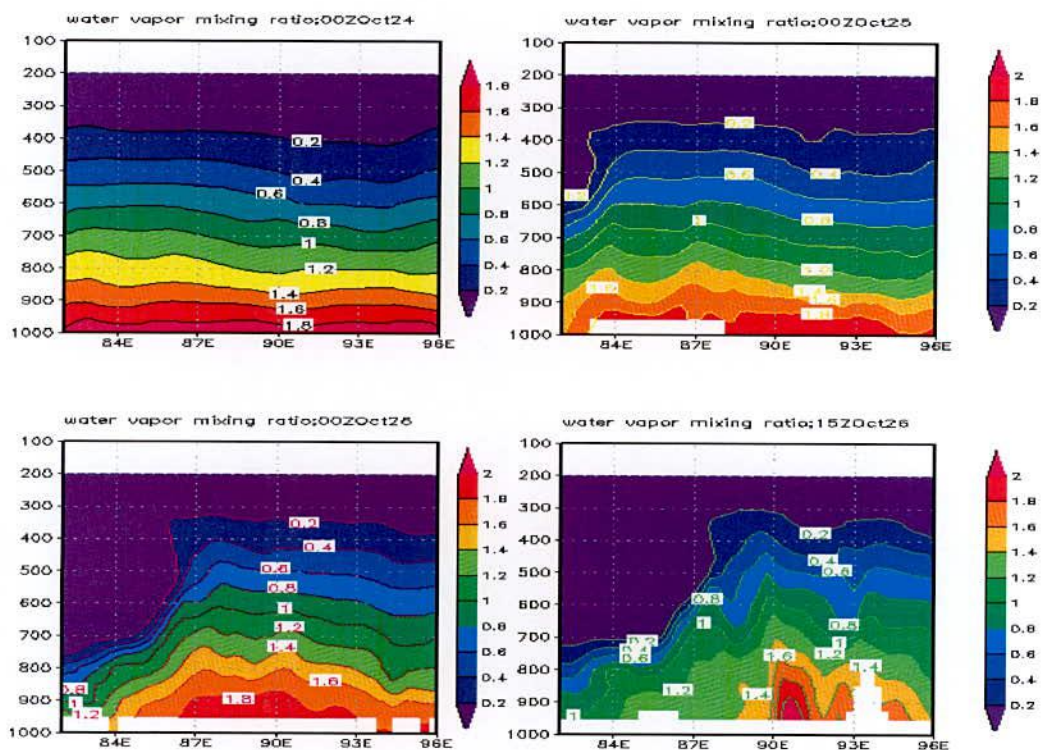


Figure 5.3.6.1a: MM5 model simulated vertical distribution of water vapor mixing ratio along the east-west cross section of the centre of TC Rashmi at 00 UTC of 24, 25, 26 October and 15 UTC of 26 October 2008.

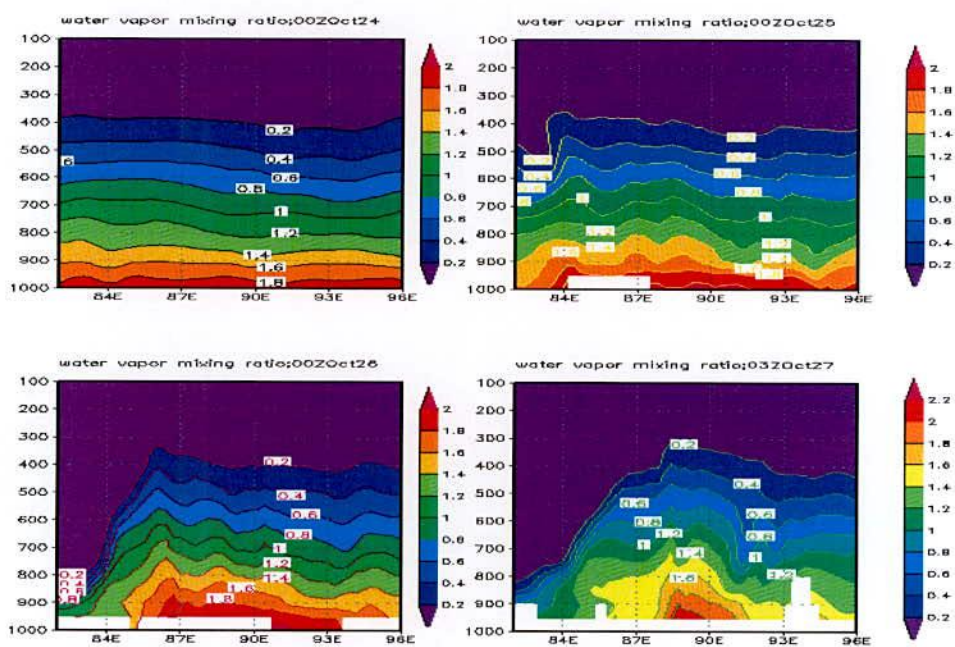


Figure 5.3.6.1b: WRF model simulated vertical distribution of water vapor mixing ratio along the east-west cross section of the centre of TC Rashmi at 00 UTC on 24, 25, 26 October and at 03 UTC on 27 October 2008.

Table 5.3.6.1b: WRF model simulated maximum water vapour mixing ratio ($\text{kg/kg} \times 10^{-2}$) associated with TC Rashmi at 00 UTC on 24, 25, 26 October and at 03 UTC on 27 October 2008.

| Maximum value of Water vapor mixing ratio (%) at different time | | | |
|---|-------------------------|-------------------------|-------------------------|
| 00 UTC of 24 October | 00 UTC of 25 October | 00 UTC of 26 October | 03 UTC of 27 October |
| 2.0 | 2.0 | 2.0 | 2.2 |

5.3.7 Rainfall Pattern

Figure 5.3.7.1 shows the MM5 and WRF models simulated 24 hrs accumulated rainfall along with rainfall obtained from TRMM data of TC Rashmi valid for the day 24, 25 and 26 October 2008 (i.e. ending at 00 UTC of 25, 26 October and 27 October). The rainfall shows a highly asymmetric character in the horizontal distribution.

On 24 October 2008, the rainfall occurs mainly at the sea and a small amount of rain occurs over Bangladesh and its surrounding. MM5 model simulated rainfall spreads on more area than that simulated by WRF model. The simulated rainfall by MM5 and WRF models is comparable to the rainfall obtained from TRMM data with large spatial variability.

On 25 October 2008, the rainfall occurs mainly at the sea. MM5 model simulated rainfall is more than that simulated by WRF model over Bangladesh and especially eastern side of Bangladesh. Finally, the simulated rainfall by MM5 and WRF models is comparable with the rainfall obtained from TRMM data with large spatial variability.

On 26 October 2008, the rainfall occurs mainly over Bangladesh and its surrounding. MM5 simulated heavy rainfall over whole Bangladesh whereas WRF model simulated heavy rainfall over south western side and sea. So, there is a spatial variability in the rainfall simulated by the two models. Rainfall obtained from TRMM is small in amount compared to the rainfall simulated by the two models. MM5 and WRF model simulated rainfall is comparable to the rainfall obtained from TRMM data with some spatial and temporal variability.

Figure 5.3.7.1 shows the model simulated 24 hrs accumulated rainfall of TC Rashmi for 26 October 2008 (i.e. ending at 00 UTC of 27 October 2008). The rainfall shows a highly asymmetric character in the horizontal distribution. Structure of rainfall simulated by MM5 is similar to the rainfall obtained from TRMM and BMD rain-gauge data. Structure of rainfall simulated by WRF model is differed than other simulated and observed rainfall. Simulated structure of rainfall by MM5 protrudes from the north to south for MM5.

It turns out that the model used in the present study is overestimated the 24 hrs rainfall of cyclone Rashmi than the rainfall obtained from TRMM and BMD rain-gauge data.

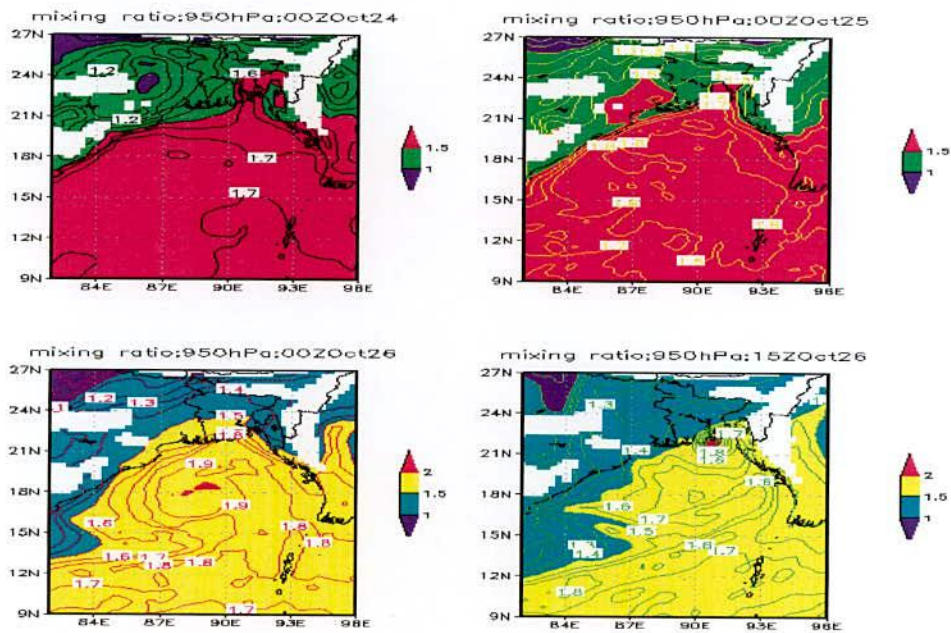


Figure 5.3.6.2a: MM5 model simulated horizontal distribution of water vapor mixing ratio ($\text{kg/kg} \times 10^{-2}$) associated with TC Rashmi at 950 hPa at 00 UTC on 24, 25, 26 October and at 15 UTC on 26 October 2008

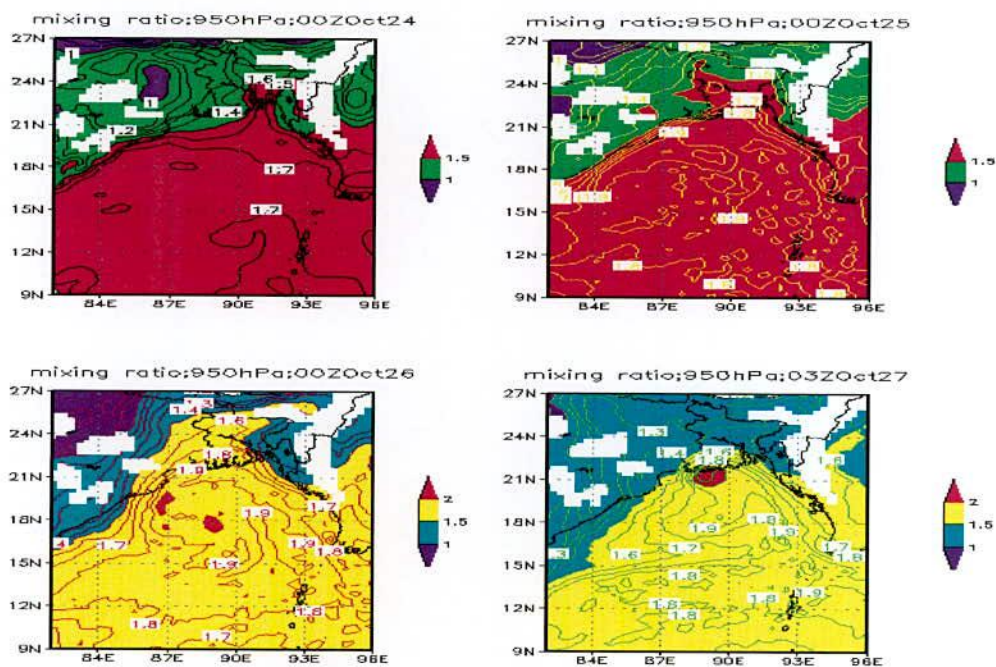


Figure 5.3.6.2b: MM5 model simulated horizontal distribution of water vapor mixing ratio ($\text{kg/kg} \times 10^{-2}$) associated with TC Rashmi at 950 hPa at 00 UTC on 24, 25, 26 October and at 03 UTC on 27 October 2008.

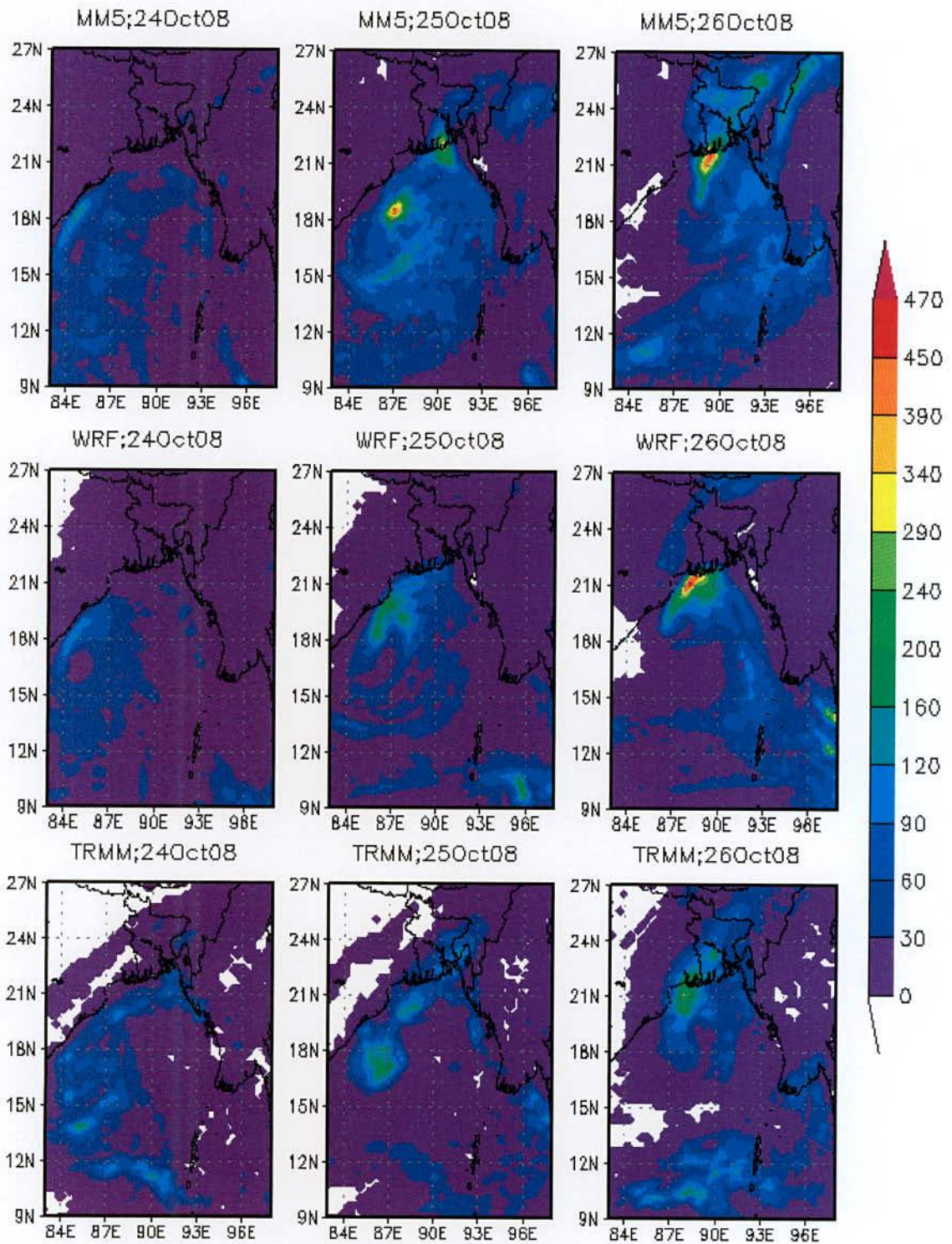


Figure 5.2.7.1:MM5 and WRF simulated 24 hrs accumulated rainfall (mm) of TC Rashmi along with rainfall obtained from TRMM data valid for 24, 25 and 26 October 2008.

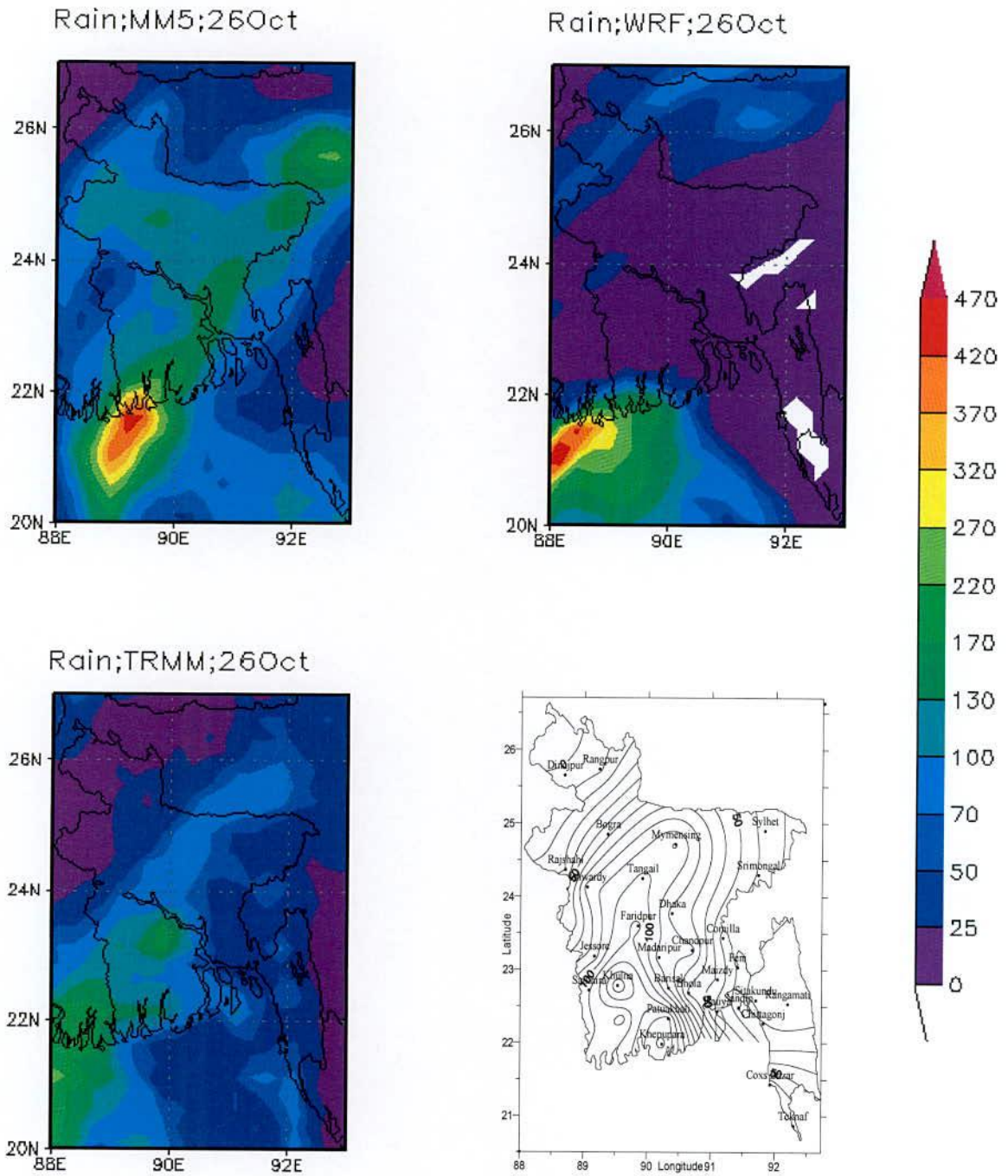


Figure 5.2.7.2:MM5 and WRF simulated 24 hrs accumulated rainfall (mm) of TC Rashmi along with rainfall obtained from TRMM and BMD rain-gauge data valid for 26 October 2008.

5.3.8 Track Pattern

MM5 and WRF models simulated track of TC Rashmi along with observed track are plotted in the Figures 5.3.8.1a and 5.3.8.1b respectively. The track forecasts of TC Rasmi for 96, 72, 48 and 24 hrs are based on the initial fields of 00 UTC of 24 October, 00 UTC of 25 October, 00 UTC of 26 October and 12 UTC of 26 October respectively for MM5 model.

It is seen from Figure 5.3.8.1a that the simulated track obtained by running the MM5 model for 96, 72, 48 and 24 hours are parallel to observed track but it is deviated to the east side of the observed track. It may be because of initial data error. Figure shows that model is able to generate northward movement of the system very well. It reveals that tracks obtained from 24 and 48 hrs simulation of model are more close to the JTWC best track compared to tracks obtained from 72 and 96 hrs simulation of model. However, there are some errors in the positions with respect to time which shows some ahead in landfall. The track from 48 hours simulation track is better than that of any others simulation. The landfall position for 48 hrs simulation track is much closer to that of observed track than any other simulation. So, by changing initial data in simulated, track becomes close to the observed track.

It is seen from Figure 5.3.8.1b that the simulated track obtained by running the WRF model for 96, 72, 48 and 24 hours is parallel to observed track but it is deviated east and west side of the observed track. It may be because of initial data error. Figure shows that model was able to generate northward movement of the system very well. It reveals that tracks obtained from 24 and 48 hrs simulation of model are more close to the JTWC best track compared to tracks obtained from 72 and 96 hrs simulation of model. However, there are some errors in the positions with respect to time which shows some ahead in landfall. The track from 48 hours simulation track is better than that of any others simulation. The landfall position for 48 hrs simulation track is much closer to the track obtained from JTWC observed data than any other simulation of model. So, by changing initial data in simulated, track becomes close to the observed track.

It is seen from the Figures 5.2.8.1a and 5.2.8.1b that simulated track obtained from MM5 and WRF model is parallel to observed track. But it is deviated eastern side of the observed track using MM5 model and eastern and western side of the observed track using WRF model. It may be because of initial data problem. Again, track obtained from MM5 and WRF model for 48 hrs simulation is the best among other simulations. By changing initial data we can improve this track.

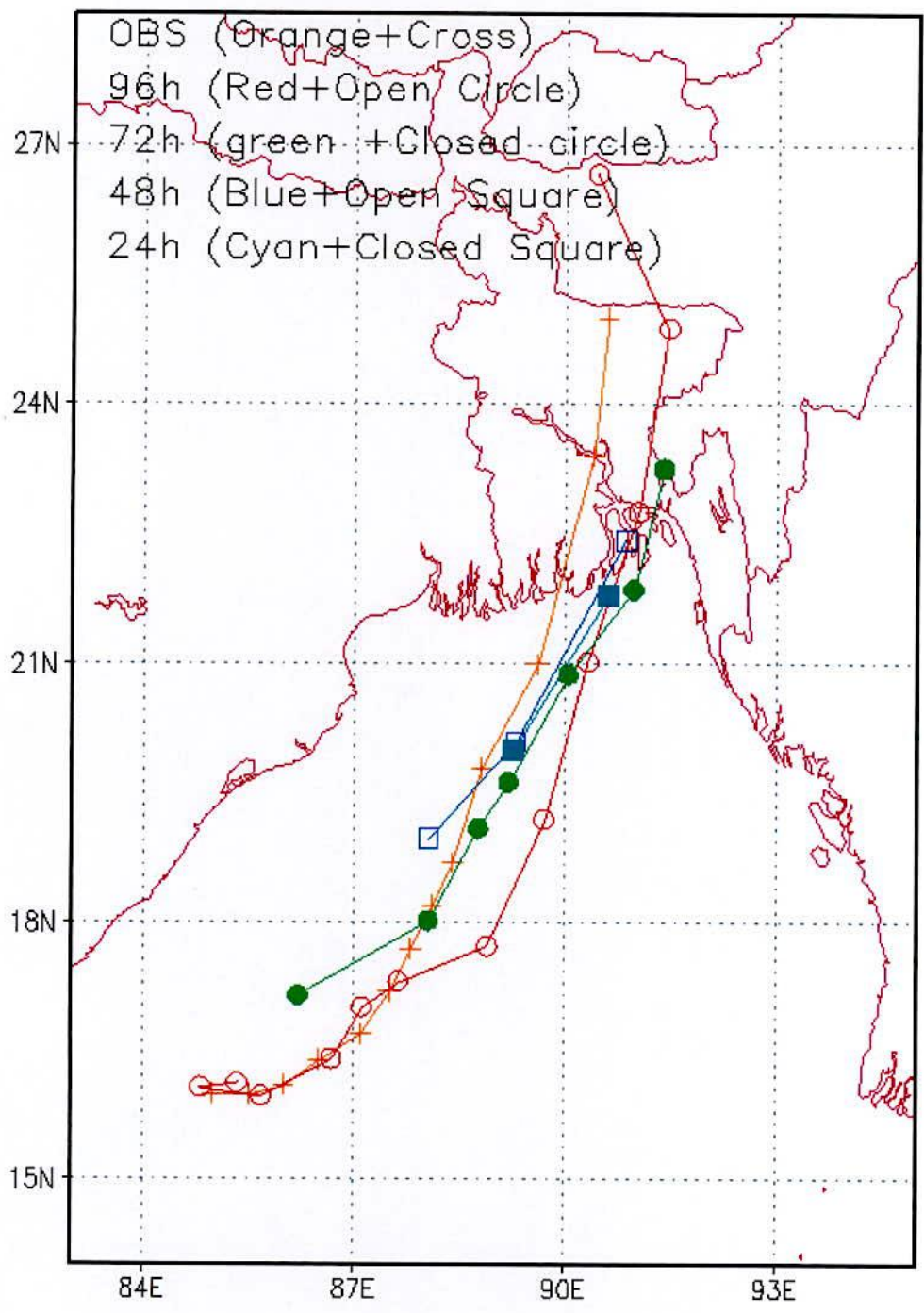


Figure 5.3.8.1a: MM5 model simulated and observed tracks of TC Rashmi.

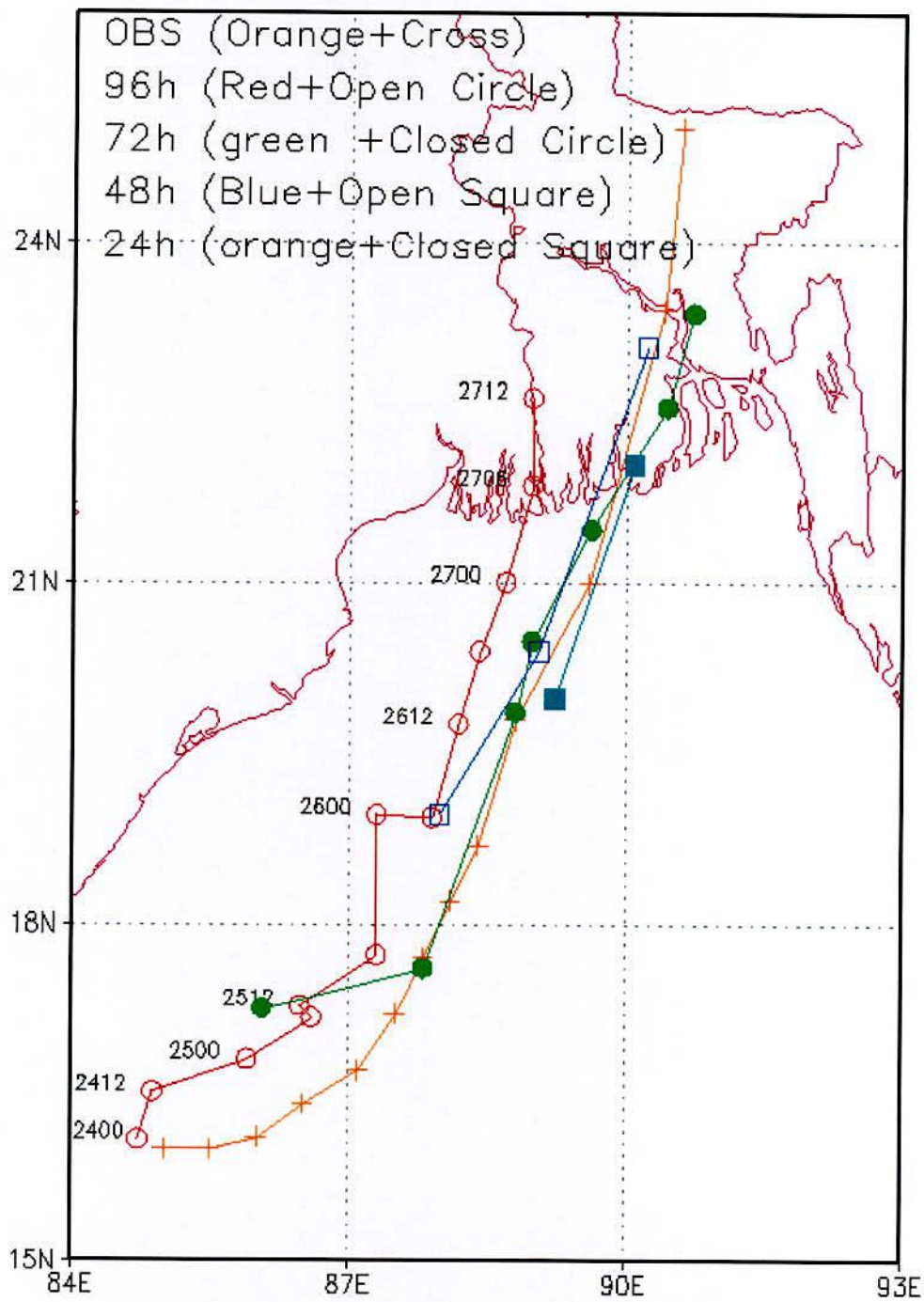


Figure 5.3.8.2b: WRF model simulated and observed tracks of TC Rashmi.

5.4: Summary of the Tropical Cyclone Events:

Both the models are able to simulate some salient features of TC such as pressure distribution, vertical motion around the centre, vertical and horizontal distribution of wind, vorticity, moisture field and temperature anomaly. Some of them are very close to the observations. Both of the models fail to simulate the SLP of TC Sidr. Simulated SLP is higher than that of observed SLP. Spatio temporal variation of minimum SLP obtained. But in all cases sharp pressure gradient in the vicinity of the centre of the TC are observed by the simulated pressure field at surface level (Table 5.4.1). Asymmetric patterns of surface wind distribution with well organized banded structure having the maximum about 40 to 240 km far from the centre and relatively weak winds at the centre are well simulated. Well organized circulation patterns are simulated at 850 hPa level confirming that maximum winds are confined to the right of the track of the TC movement. Anticyclonic circulation patterns at 200 hPa level or lower are visible in most of the cases. Model simulated MWS is nearly equal to the observed value (Table 5.4.1).

Table 5.4.1: Comparison of simulated, BMD and JTWC MSLP and Wind

| TC | parameters | Comparison of MSLP (hPa) | | | |
|--------|------------------|--------------------------|-----|------|---------|
| | | MM5 | WRF | JWTC | BMD |
| Sidr | MSLP | 961 | 977 | 918 | 942 |
| Rashmi | MSLP | 976 | 979 | 989 | 992 |
| Aila | MSLP | 974 | 955 | 974 | 987 |
| | | Comparison of MSLP (m/s) | | | |
| Sidr | wind at 10 m | 40 | 36 | 72 | 61-66 |
| | wind at 1000 hPa | 23 | 26 | | |
| | wind at 925 hPa | 53 | 51 | | |
| | wind at 850 hPa | 54 | 51 | | |
| | | | | | |
| Rashmi | wind at 10 m | 29 | 29 | 23 | 17 - 22 |
| | wind at 1000 hPa | 20 | 20 | | |
| | wind at 925 hPa | 42 | 43 | | |
| | wind at 850 hPa | 47 | 44 | | |
| | | | | | |
| Aila | wind at 10 m | 24 | 39 | 27 | 19 - 25 |
| | wind at 1000 hPa | 18 | 16 | | |
| | wind at 925 hPa | 35 | 60 | | |
| | wind at 850 hPa | 38 | 61 | | |

The model has successfully simulated the strong relative vorticity at lower level spreading over the strong convective region of each cyclone. For the very strong systems the positive vorticity is found to extend up to 100 hPa level. Simulated low level vorticity fields at 850 hPa level demonstrate the size of the system with strong convective regions of each cyclone,

which are in agreements with the observations. The warm core characteristics with maximum temperature anomaly of 3.5-14⁰C simulated in the middle and upper troposphere successfully by the models. This warm core has the vertical extends from the lower level to tropopause for strong system. The high relative humidity is found in the eye wall and rain bands of the TC and low relative humidity at the centre. From the analysis of water vapor maxing ratio it is found that high moisture flux comes from the southern side covering a large area of the Bay of Bengal which feeds the system along its southeastern side through the boundary layer.

For the simulation of rainfall, the simulated rainfall by the MM5 and WRF models are compared with that obtained from TRMM BMD rain-gauge data. Simulated rainfall is more than that obtained from TRMM and BMD rain-gauge data in most of the cases. These are tabulated in Table 5.4.2.

Table 5.4.2: Table for comparing rainfall of Tropical cyclone Sidr, Rashmi and Aila

| TC | date | domain size | Amount of rainfall (mm) | | | |
|--------|-------------------|------------------------|-------------------------|-----|------|------------|
| | | | MM5 | WRF | TRMM | Rain-gauge |
| Sidr | 13 November, 2007 | lat 9-27 lon 83-93 | 400 | 770 | 300 | x |
| | 14 November, 2007 | | 450 | 580 | 550 | x |
| | 15 November, 2007 | | 310 | 570 | 200 | x |
| | 15 November, 2007 | lat 20-27 lon 88-93 | 310 | 480 | 180 | 108 |
| | 16 November, 2007 | | 76 | 170 | 18 | 83 |
| Rashmi | 24 October, 2008 | lat 9-27 lon 83-93 | 66 | 12 | 180 | X |
| | 25 October, 2008 | | 320 | 200 | 230 | X |
| | 26 October, 2008 | | 440 | 470 | 250 | X |
| | 26 October, 2008 | lat 20-27 lon 88-93 | 440 | 470 | 250 | 153 |
| Aila | 23 May | lat 9-27 lon 83-93 | 190 | 170 | 240 | X |
| | 24 may | | 270 | 480 | 270 | X |
| | 25 May | | 260 | 490 | 220 | X |
| | 25 May | lat 20-27 lon 88-93 | 200 | 450 | 220 | 149 |

With regard to track predictions of selected TC, models are run for 24, 48, 72 and 48 hours forecast. Simulated track for 24 or 48 hours forecast are the best among other forecasts. One of the outstanding findings of the models is that the models has successfully predicted tracks, re- curvature and probable area and time of landfall of the selected tropical cyclones with high accuracy even in the 96 hours predictions. Again, WRF model simulates better track than that simulated by MM5 model. In case cyclone Sidr, WRF simulates very near to observed track. In maximum cases, simulated track deviated to the right of the observed

track. The landfall times and positions are tabulated in Table 5.4.3. The error of landfall and time are also summaries in table 5.4.4. Mean position error for 24, 48, 72 and 96 hours are 134, 136, 54 and 55 km respectively and respective mean time errors are 6.8, 13.5, 5.3 and 1.4 hours. Time of different stage (cyclonic storm, severe cyclonic storm and severe cyclonic storm with hurricane) of cyclone are tabulated in Table 5.4.5. Simulated time are compared with JTWC time. These are comparable in most of the cases.

Table 5.4.3: Landfall point and time error during cyclone Sidr (11-16 November 2007), Rashmi (24-28 October 2008) and Aila (23-27 May 2009)

| Cyclone | Forecast Hours | obs/model s | initial condition date/Time (UTC) | landfall time date/Time (UTC) | landfall position | | Error | |
|---------|----------------|-------------|-----------------------------------|-------------------------------|-------------------|-------|---------------|--------------|
| | | | | | lat°N | lon°E | Distance (km) | Time (hours) |
| Sidr | | Obs | | 15/1600 | 21.83 | 89.80 | | |
| | 96 | MM5 | 13 /0000 | 15/2000 | 22.54 | 91.65 | 203e | 4D |
| | 72 | | 14 /0000 | 17/0000 | 21.53 | 89.26 | 60w | 33D |
| | 48 | | 15/0000 | 16/0100 | 22.20 | 91.20 | 155e | 10D |
| | 24 | | 15/1200 | 15/18:00 | 22.07 | 90.58 | 87e | 2D |
| | 96 | WRF | 13 /0000 | 16/0200 | 21.80 | 89.52 | 31w | 11D |
| | 72 | | 14 /0000 | 16/1900 | 21.60 | 87.60 | 244w | 27D |
| | 48 | | 15/0000 | 15/2215 | 21.75 | 89.60 | 22w | 6.25D |
| | 24 | | 15/1200 | 15/1545 | 21.80 | 90.25 | 50e | 0.25E |
| | Rashmi | | | | 27/0000 | 22.50 | 90.00 | |
| 96 | | MM5 | 10/2400 | 26/1545 | 22.10 | 90.75 | 83e | 9.25E |
| 72 | | | 10/2500 | 26/1930 | 22.10 | 91.02 | 113e | 6.50E |
| 48 | | | 10/2600 | 26/2230 | 22.10 | 90.15 | 17e | 1.5W |
| 24 | | | 10/2612 | 27/0115 | 22.10 | 90.60 | 67e | 1.25D |
| | | | | | | | | |
| 96 | | WRF | 10/2400 | 27/0445 | 21.60 | 89.75 | 28w | 4.75D |
| 72 | | | 10/2500 | 26/1445 | 22.00 | 90.00 | 0 | 10.25E |
| 48 | | | 10/2600 | 26/1845 | 21.75 | 89.75 | 28w | 6.25E |
| 24 | | | 10/2612 | 26/2115 | 21.90 | 90.00 | 0 | 2.45E |
| Aila | | | ----- | 25/0830 | 21.80 | 88.30 | | |
| | 96 | MM5 | 05/2218 | 24/2330 | 22.00 | 90.52 | 246e | 10E |
| | 72 | | 05/2300 | 25/0600 | 22.00 | 90.45 | 239e | 2.50E |
| | 48 | | 05/2400 | 25/0300 | 21.60 | 89.05 | 83e | 5.5E |
| | 24 | | 05/2412 | 25/0715 | 21.60 | 89.00 | 78e | 0.45E |
| | | | | | | | | |
| | 96 | WRF | 05/2218 | 25/0630 | 20.00 | 90.55 | 250e | 2E |
| | 72 | | 05/2300 | 25/0645 | 21.65 | 90.30 | 222e | 1.75E |
| | 48 | | 05/2400 | 25/0600 | 21.65 | 88.50 | 22e | 2.5E |
| | 24 | | 05/2412 | 25/0915 | 21.6 | 89.00 | 78e | 2.25D |

D indicates forecast landfall time is delayed compared to actual time, W indicates west of the actual landfall position and E indicates forecast landfall time is earlier to actual landfall time.

Table 5.4.4: Mean landfall position and time errors of selected tropical cyclone

| Forecast Hours | Mean landfall Position Error (km) | Mean landfall Time Error (hrs) |
|----------------|-----------------------------------|--------------------------------|
| 96 hrs | 133.86 | 6.8 |
| 72 hrs | 135.71 | 13.5 |
| 48 hrs | 53.57 | 5.3 |
| 24 hrs | 54.86 | 1.4 |

Table 5.4.5: Development of cyclone Sidr (11-16 November 2007), Rashmi (24-28 October 2008) and Aila (23-27 May 2009)

| Cyclone | | time for the different stages of the cyclone | | |
|---------|------|--|-----------------|-----------------|
| | | CS | SCS | SCS(H) |
| Sidr | | date/time | | |
| | JTWC | 11 Nov/0600 UTC | 11 Nov/1800 UTC | 12 Nov/0600 UTC |
| | MM5 | 13 Nov/0300 UTC | 13 Nov/2100 UTC | 14 Nov/1200 UTC |
| | WRF | 13 Nov/1200 UTC | 13 Nov/2100 UTC | 15 Nov/0900 UTC |
| Rashmi | JTWC | 26 Oct/0000 UTC | ----- | ----- |
| | MM5 | 25 Oct/0900 UTC | 26 Oct/0300 UTC | ----- |
| | WRF | 25 Oct/2100 UTC | 26 Oct/1800 UTC | ----- |
| Aila | JTWC | 24 May/0000 UTC | 24 May/1800 UTC | 25 May/0600 UTC |
| | MM5 | 24 May/0300 UTC | 25 May/0000 UTC | ----- |
| | WRF | 24 May/0000 UTC | 24 May/1500 UTC | 25 May/0000 UTC |

CHAPTER 6
SENSITIVITY

6.1 Selection of Model

In the present study only the mesoscale models MM5 has been used to study the sensitivity of different PBL with cumulus, micro physics and radiation parameterization of MM5 model, model was run for different heavy precipitation events and tropical cyclone events and those have been discussed the following sections.

6.2 Experiments on Simulation of different Heavy Precipitation and TC events

Two types of events i.e. heavy rainfall and tropical cyclone events have been considered for the sensitivity test to understand their impact on simulation of different meteorological parameters and to understand the genesis, characteristics and structure of the systems. Two test cases have been considered for the heavy rainfall events and the events are Case 1 (1-3 May 2009), and Case 2 (9-11 June 2007). On the other hand, three test cases have been considered for the tropical cyclone events and the cases are Case 1 (Tropical Cyclone Aila, 23-27 May 2009), Case 2 (Tropical Cyclone Sidr, 11-17 November 2007) and Case 3 (Tropical Cyclone Rashmi 24-28 October 2008).

6.3 Initial Data Source

For the simulation of heavy precipitation events and tropical cyclone (TC) events, both of the models are run for 72 hours. Final Reanalysis (FNL) data ($1^{\circ} \times 1^{\circ}$) from National Centre for Environment Prediction (NCEP) is used as initial and lateral boundary conditions (LBCs) which is updated at six hourly interval i.e. the model is initialized with 00, 06, 12 and 18 UTC initial field of corresponding date.

6.4 Sensitivity Study of PBL with Cumulus Parameterization (CP)

6.4.1 Domain Set Up

For the heavy precipitation events and tropical cyclone (TC), two domains are taken: first one is mother domain and another one is nested domain inside the mother domain. Nested domain covers the Bangladesh region. Ratio of the resolution of the two domains is 3:1 respectively. The horizontal grid resolution of the mother domain is 90 km and nested domain is 30 km respectively. The dimension of the models MM5 and WRF are summarized in Table 6.4.1.

Table 6.4.1: Dimension of the domain for heavy precipitation events and TC

| Domain | heavy precipitation events | | TC | |
|--------|----------------------------|--------------|-------------|--------------|
| | Latitude °N | Longitude °E | Latitude °N | Longitude °E |
| 1 | 13.40-31.96 | 65.41-98.59 | 0.22-37.94 | 67.36-108.64 |
| 2 | 20.11-27.22 | 87.80-93.20 | 4.36-28.71 | 81.66-99.20 |

6.4.2 Model Physics

For the heavy rainfall events and TC cases, the MM5 model is run by using two types of Planetary Boundary Layer (MRF and Blackader) along with five types of cumulus parameterization schemes (AK, GR, KF, BM and KF2) making 10 independent run. The common physics options which are used, other than CP and PBL, includes: i) Dudhia Simple Ice microphysical Scheme for moisture anticipation, ii) Cloud Radiation Schemes for radiation calculation and iii) 5- Layer Soil model to predict soil temperature. Model physics are summarized in Table 6.4.2.1. Model equations in the surface flux form and solved on Arakawa B grid. Leapfrog time integration scheme with time splitting technique is used in model integration.

Table 6.4.2.1: Domain design of the model

Fifth generation Penn State/NCAR Mesoscale Model (MM5) Version 3.7

| | |
|-----------------------------------|---|
| Dynamics | Non-hydrostatic with three-dimensional Coriolis force |
| Main prognostic variables | u, v, w, T, p and q |
| Map projection | Lambert conformal mapping |
| Central point of the domain | 20° N, 88° E |
| Horizontal grid distance | 90 km and 30 km |
| Number of vertical levels | 23 half sigma levels |
| Horizontal grid system | Arakawa B grid |
| Time integration scheme | Leapfrog scheme with time-splitting technique |
| Radiation parameterization scheme | Cloud |
| PBL parameterization scheme | MRF, BKD |
| Cumulus parameterization schemes | AK, Grell, KF, KF-2 and BM |
| Microphysics | Simple Ice |
| Soil model | 5-layer soil model |

6.4.3 Results, Discussion and Conclusions of Sensitivity of PBL with CP on Heavy Rainfall Events

To understand the sensitivity on PBL with CP, the model is run for the rainfall case 1(May 1-3, 2009) and case 2(June 9-13, 2007). The simulated rainfalls are compared with that obtained from BMD observed Rain Gauge data and the best combinations of the parameterization schemes are chosen. They are shown in Figure 6.4.3.1(a-d) and Figure 6.4.3.2 (a-c) for the case 1 and 2 respectively. It is difficult to understand which combination is the best from the figures. Actually no one combination of PBL and CP perform better than others (Akhter *et. al.* [135]). To understand the performance more precisely and select the best run Root Mean Square (RMS) Error is also calculated for the case 1 only. Results are tabulated in the Table 6.4.3.1. From the Table, it is found that AK CP is better for daily rainfall prediction and KF2 is better for total rainfall prediction.

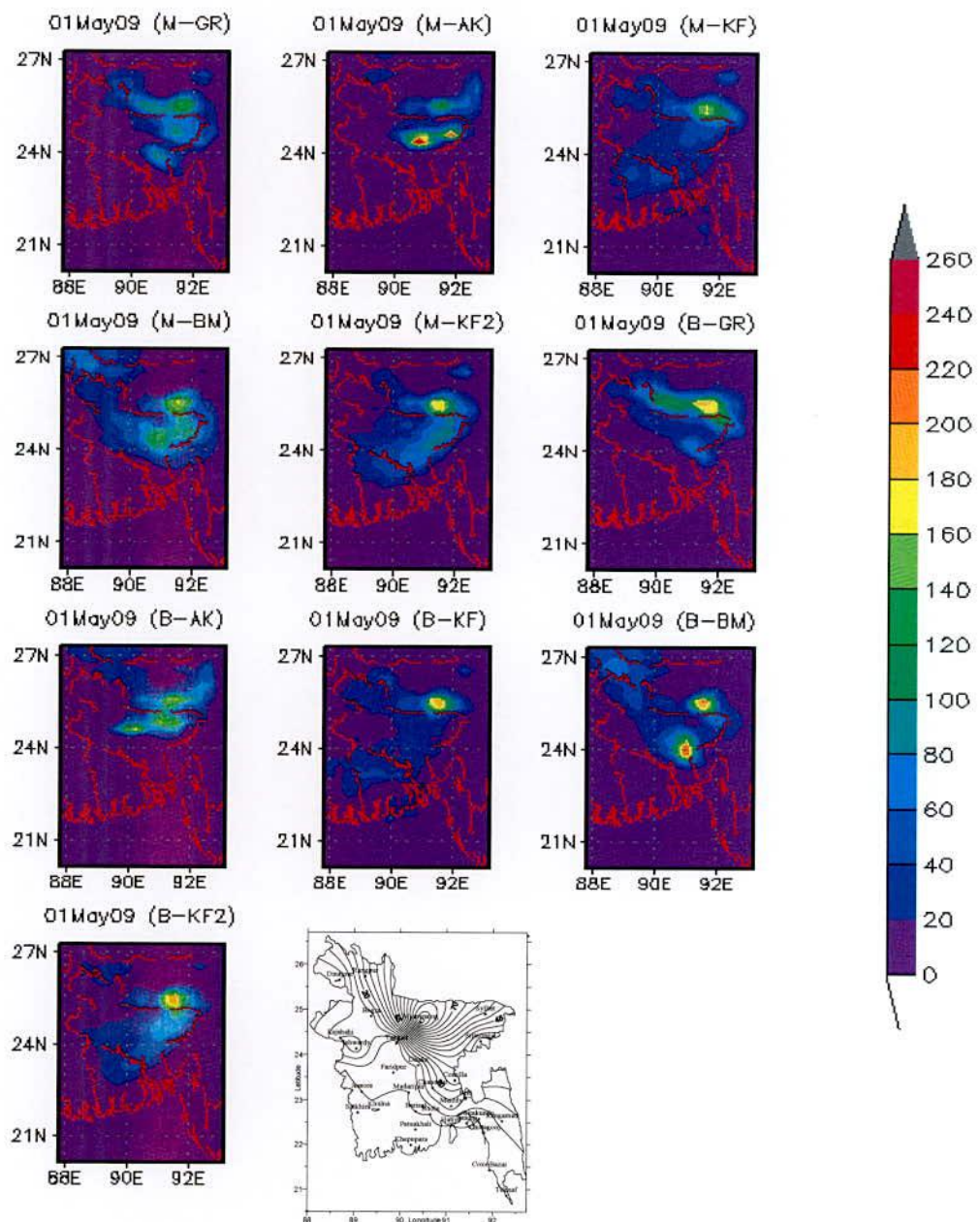


Figure 6.4.3.1a: MM5 model simulated 24 hours rainfall in combination with different PBL and cumulus parameterization and observed rain gauge rainfall data on 01 May 2009.

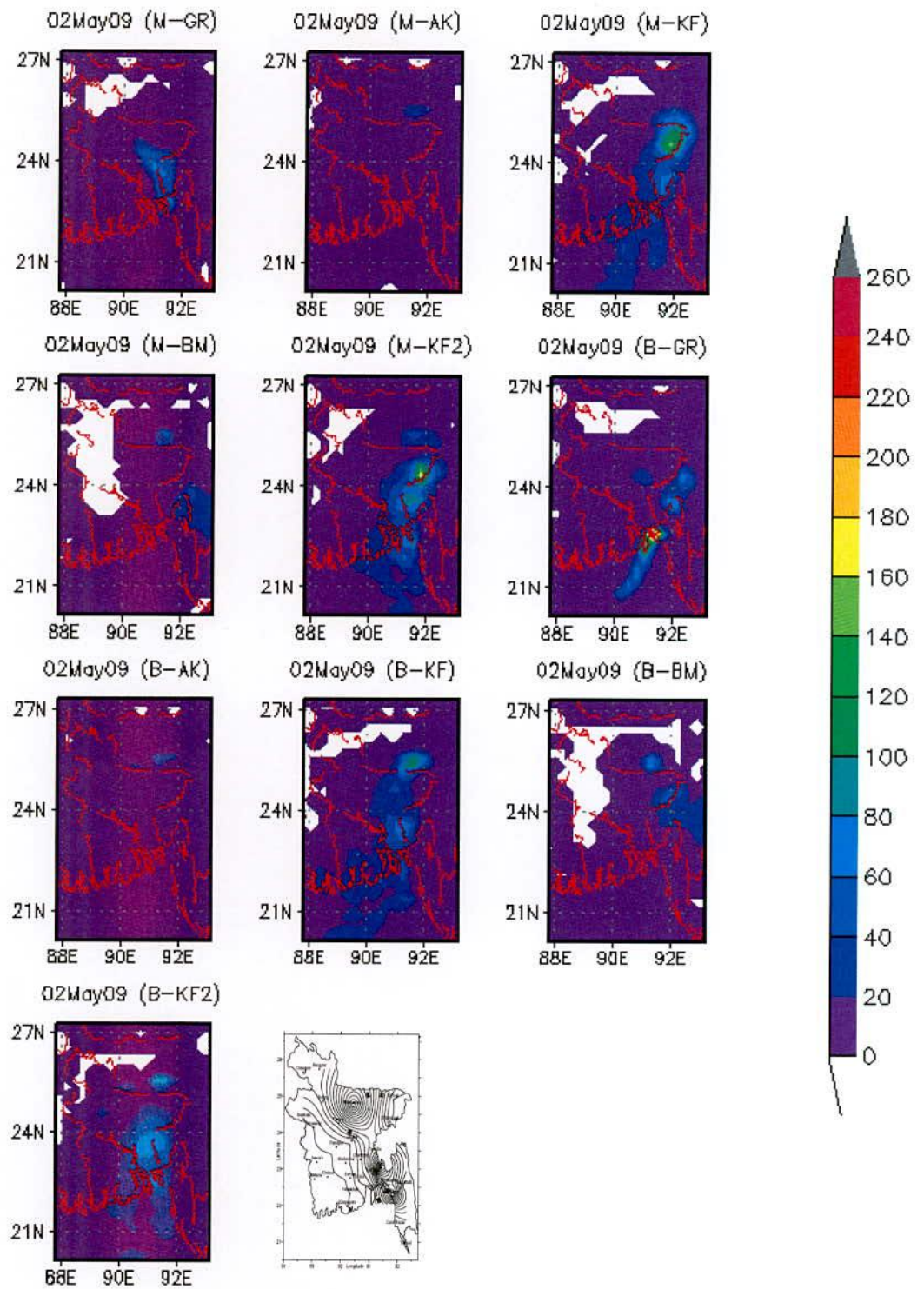


Figure 6.4.3.1b: MM5 model simulated 24 hours rainfall with observed rainfall on 02 May 2009.

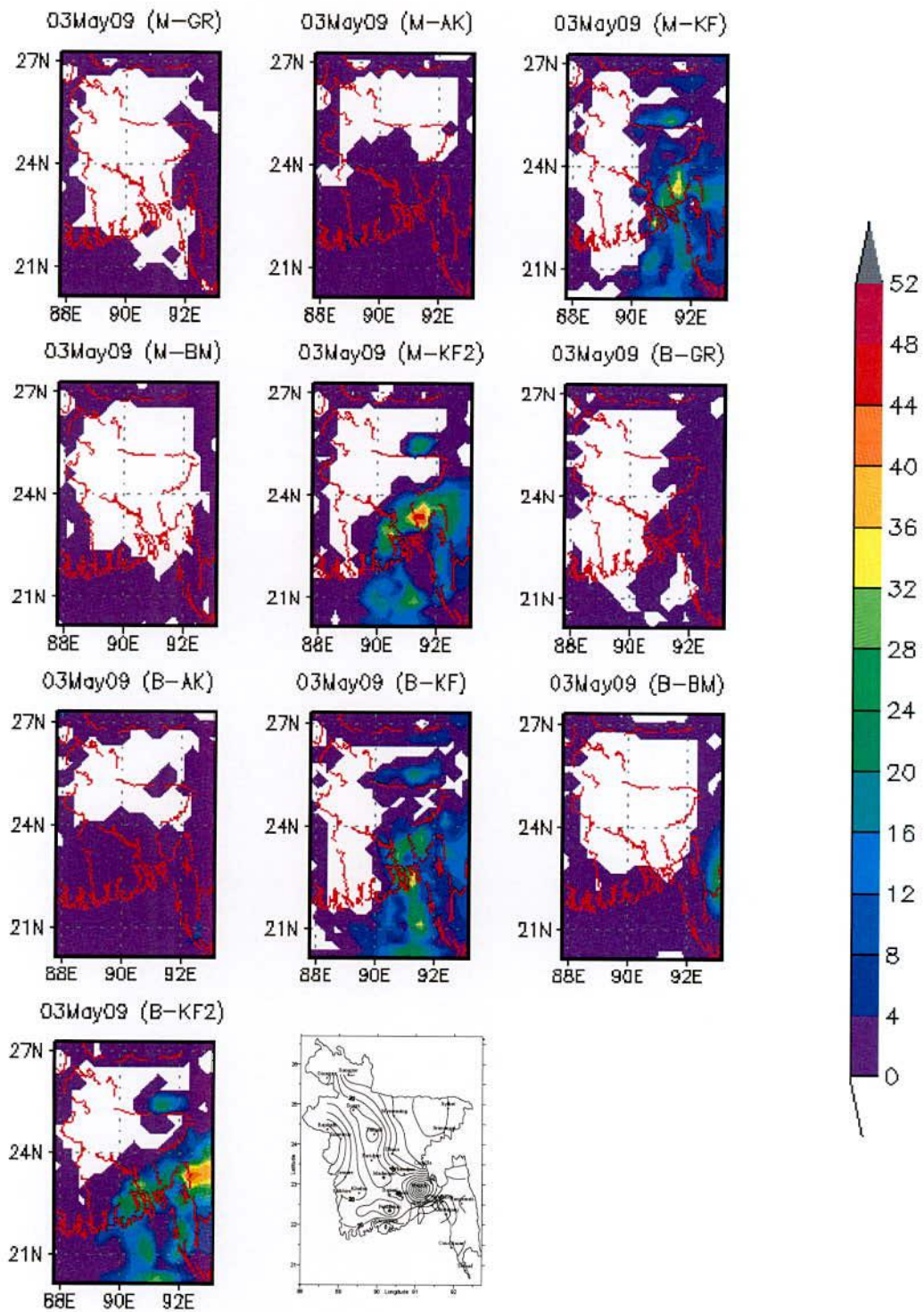


Figure 6.4.3.1c: MM5 model simulated 24 hours rainfall with observed rainfall on 03 May 2009.

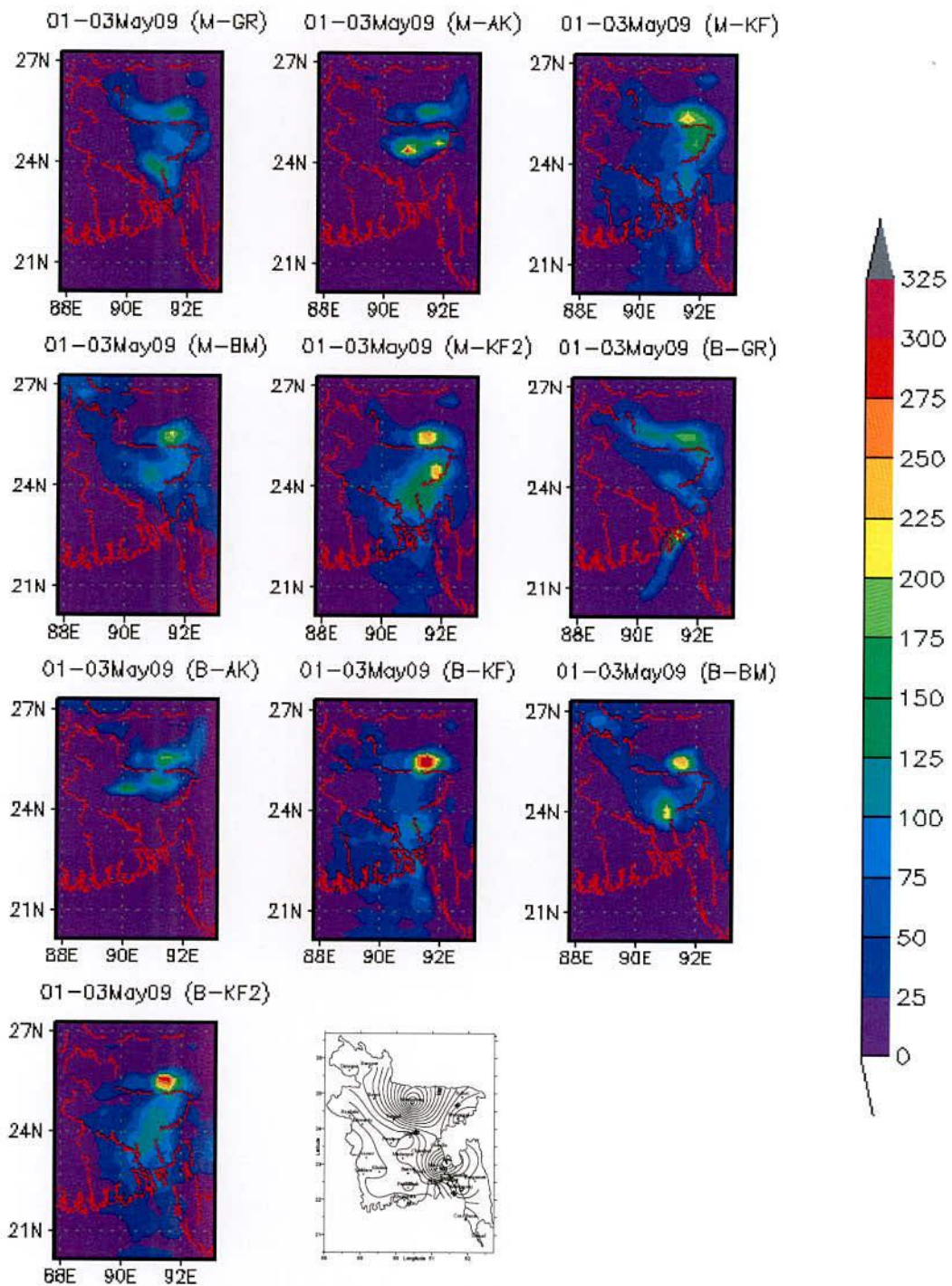
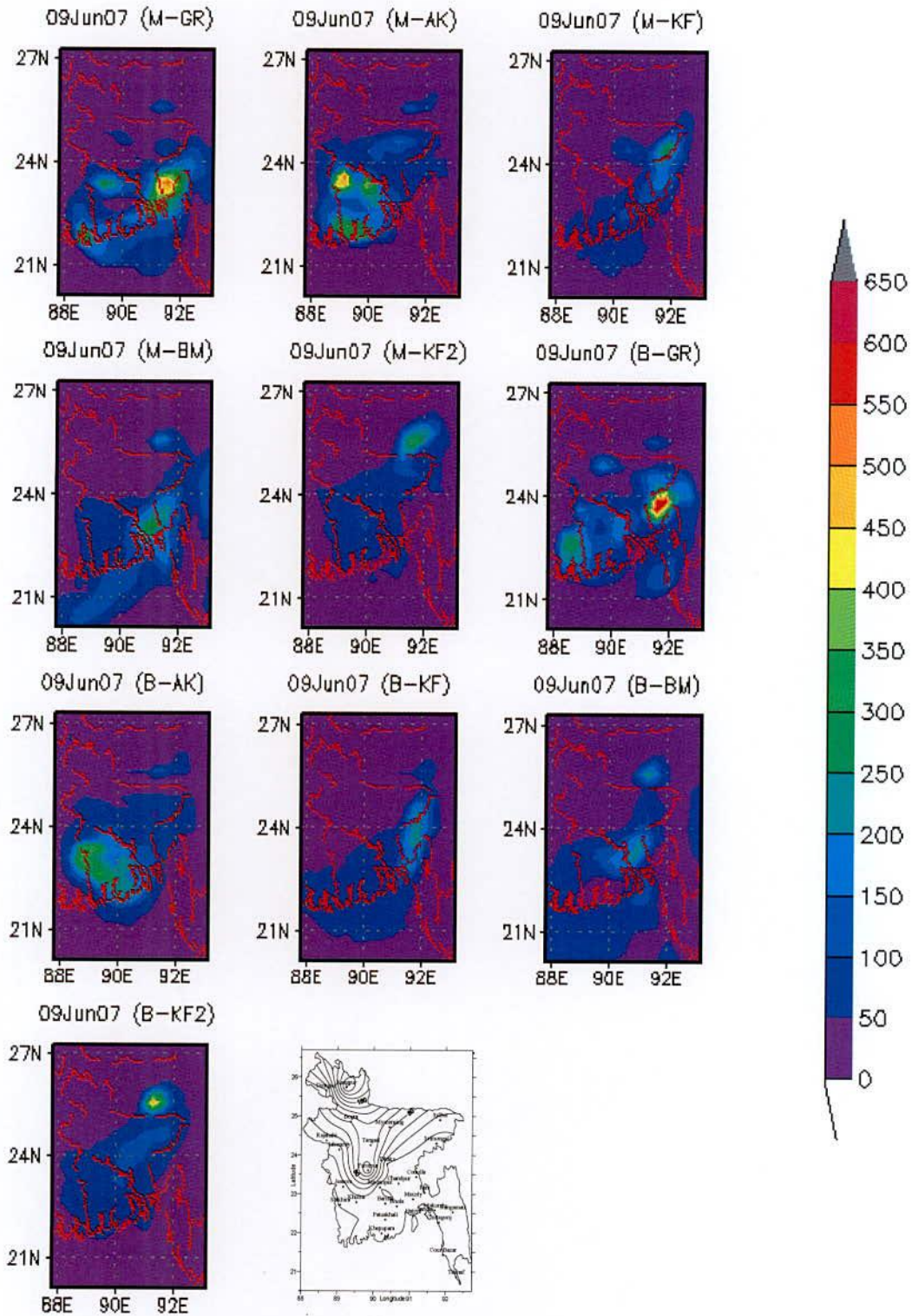


Figure 6.4.3.1d: MM5 model simulated 24-hours rainfall and observed rainfall on 01-03 May 2009.





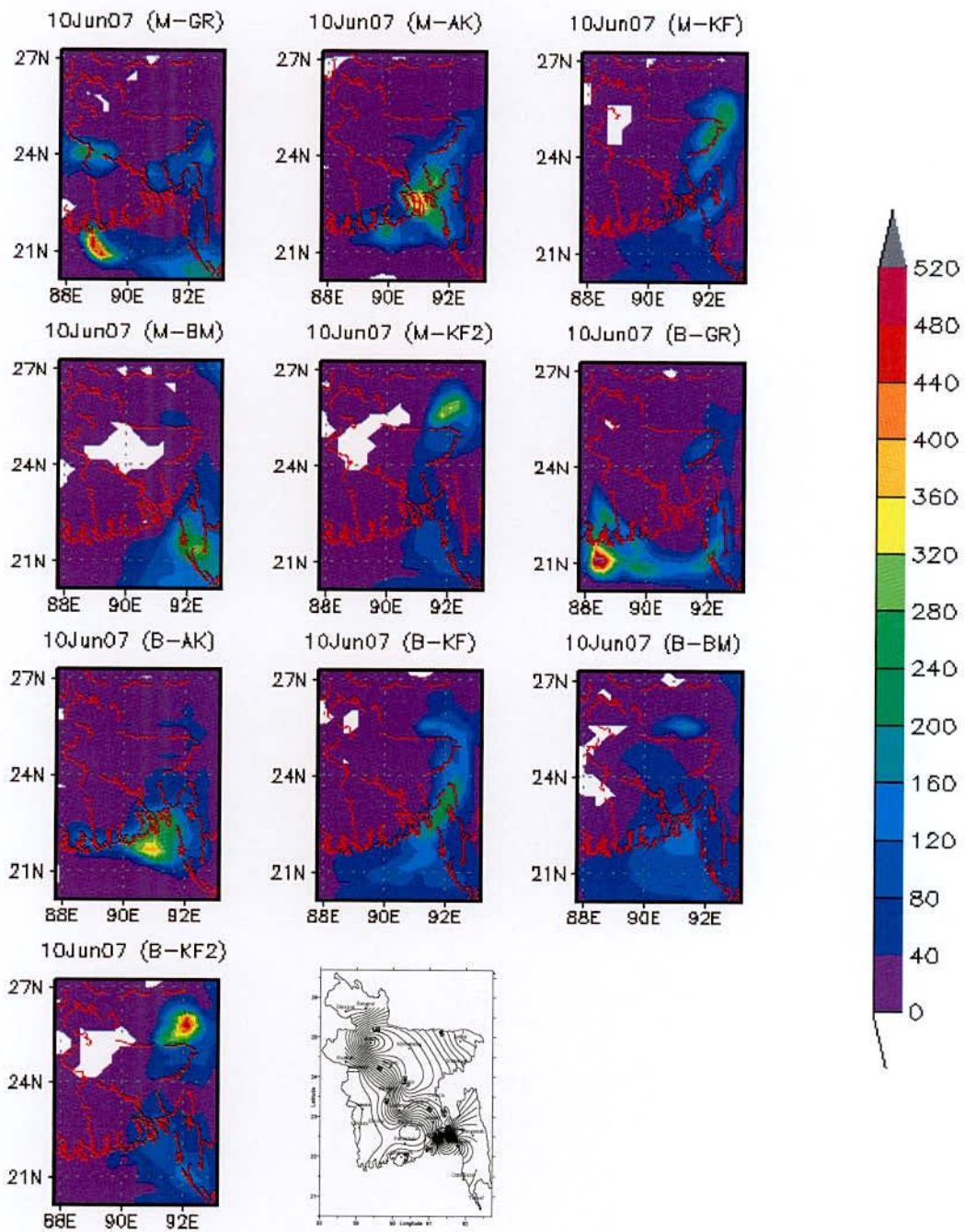


Figure 6.4.3.2b: MM5 model simulated 24-hours rainfall and observed rainfall on 10 June 2007.

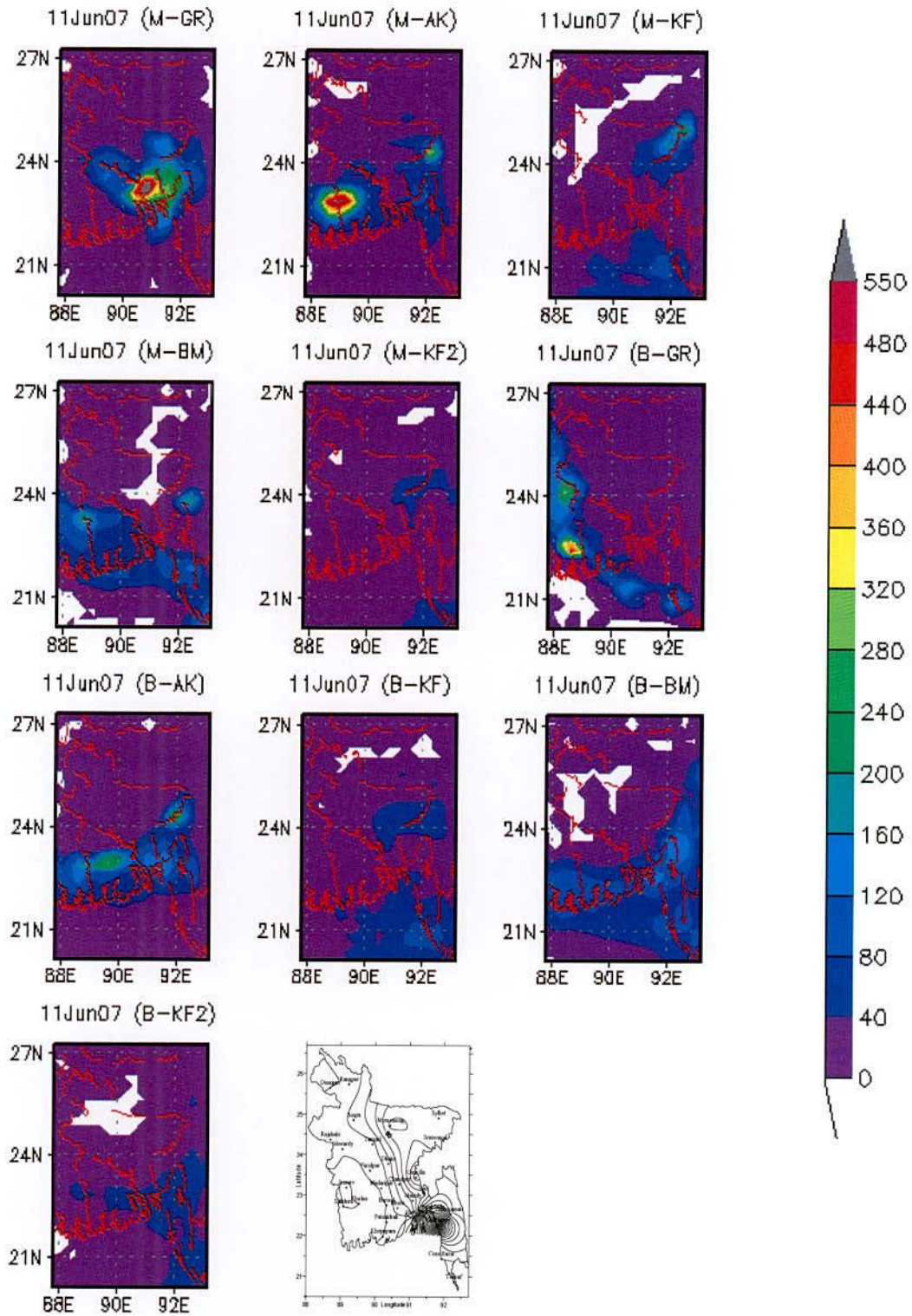


Figure 6.4.3.2c: MM5 model simulated 24-hours rainfall and observed rainfall on 11 June 2007.

6.4.4 Results, Discussion and Conclusions for the Sensitivity of PBL and CP on TC Events

For the tropical cyclone cases, at first the case 1 ((TC Aila) is taken and run the model MM5 using two types of Planetary Boundary Layer (PBL) along with five types of cumulus parameterization schemes making 10 independent run. The simulated track and intensity (pressure) are compared with data from IMD and choose the best combination of the parameterization schemes. The above mentioned procedure is repeated for other two cases (TC Sidr and Rashmi). The track of tropical cyclone Aila, Sidr and Rashmi are plotted in Figure 6.4.4.1(a-b), Figure 6.4.4.2(a-b) and Figure 6.4.4.3 (a-b) respectively. The central pressure of tropical cyclone Aila, Sidr and Rashmi are plotted in Figures 6.4.4.4(a-b), Figure 6.4.4.5(a-b) – 6.4.4.6(a-b) respectively. Performances of the PBL in combination with CP schemes are summarized in Table 6.4.4.1. Performances of each pair of PBL with a CP are not same for all TC. Simulated tracks are deviated mainly in the right or left of the observed tracks. Simulated SLP are more or less than that of observed. Considering the performance of PBL with CP for three TC, from the Figure and the Table, that no one combination of PBL and CP performs absolutely better than any other. But it seems that MRF PBL with KF CP performs better than any other. This combination of PBL and CP may be use as an operational purpose for the prediction of TC. But it is recommended that more combination may be done to search better option. Fortunately, it is used to analyze the evolution and structure of tropical cyclone. Pressure, wind (vector and scalar horizontal wind, radial, tangential and vertical wind), vorticity, temperature anomaly, relative humidity, water vapor mixing ratio, rainfall and track are studied. Combination of YSU PBL (upper version of MRF) with KF CP for WRF model is used to study the above mentioned cyclones.

Table 6.4.4.1: PBL in combination with CP schemes for best Track of different TC

| Sl. No. | Name of the TC | PBL | Name of the best two CP for Track, MSLP and Wind | | | |
|---------|----------------|-----|--|----------------|----------------|----------------|
| | | | Track | | MSLP | |
| | | | a ¹ | b ¹ | a ¹ | b ¹ |
| 1 | Aila | MRF | GR | KF | KF | GR |
| | | BKD | KF | GR | KF | GR |
| 2 | Sidr | MRF | KF | GR | KF | GR |
| | | BKD | KF | GR | BM | KF |
| 3 | Rashmi | MRF | BM | KF | GR | KF2 |
| | | BKD | KF | KF2 | KF | KF2 |

a¹ best performer; b¹ better than all except written in a¹

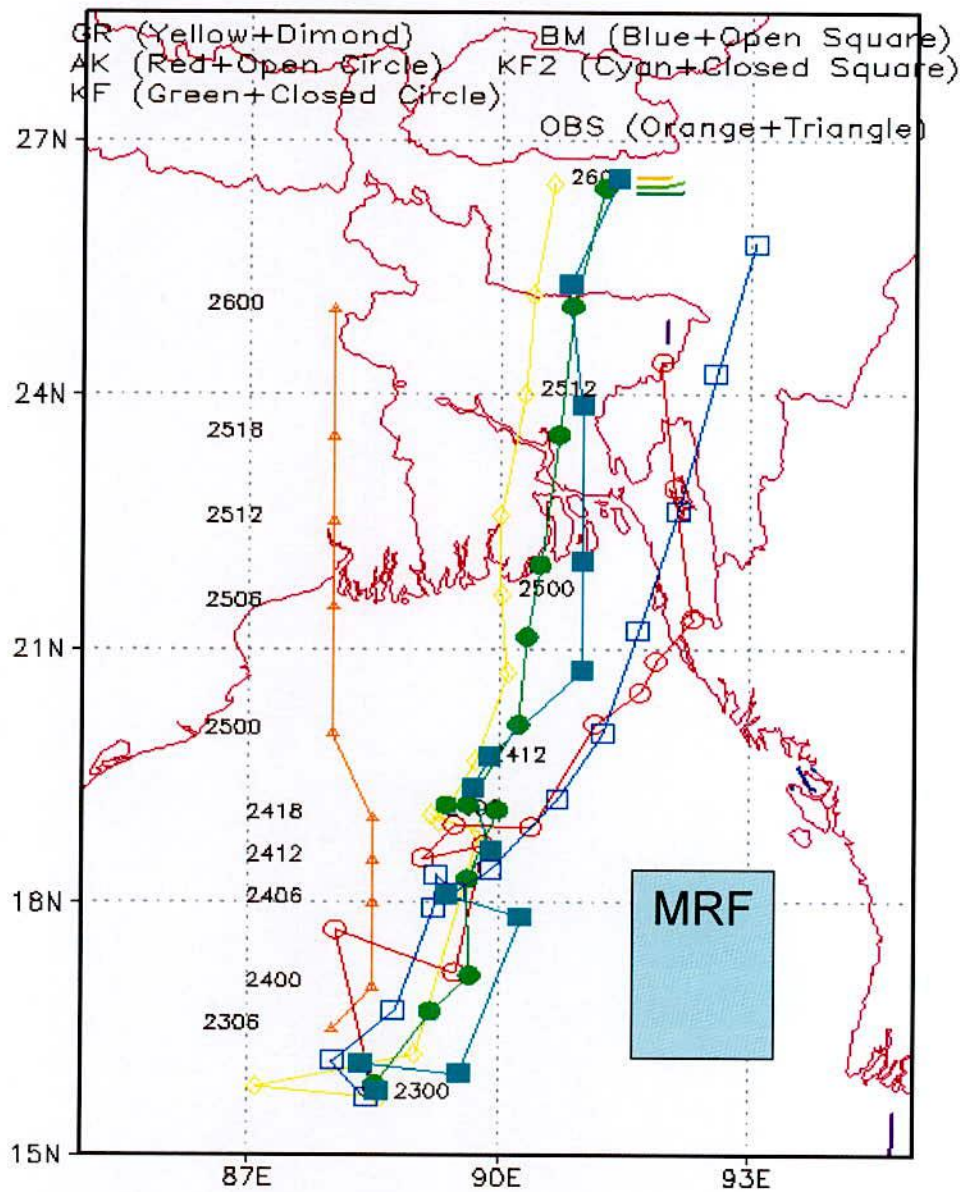
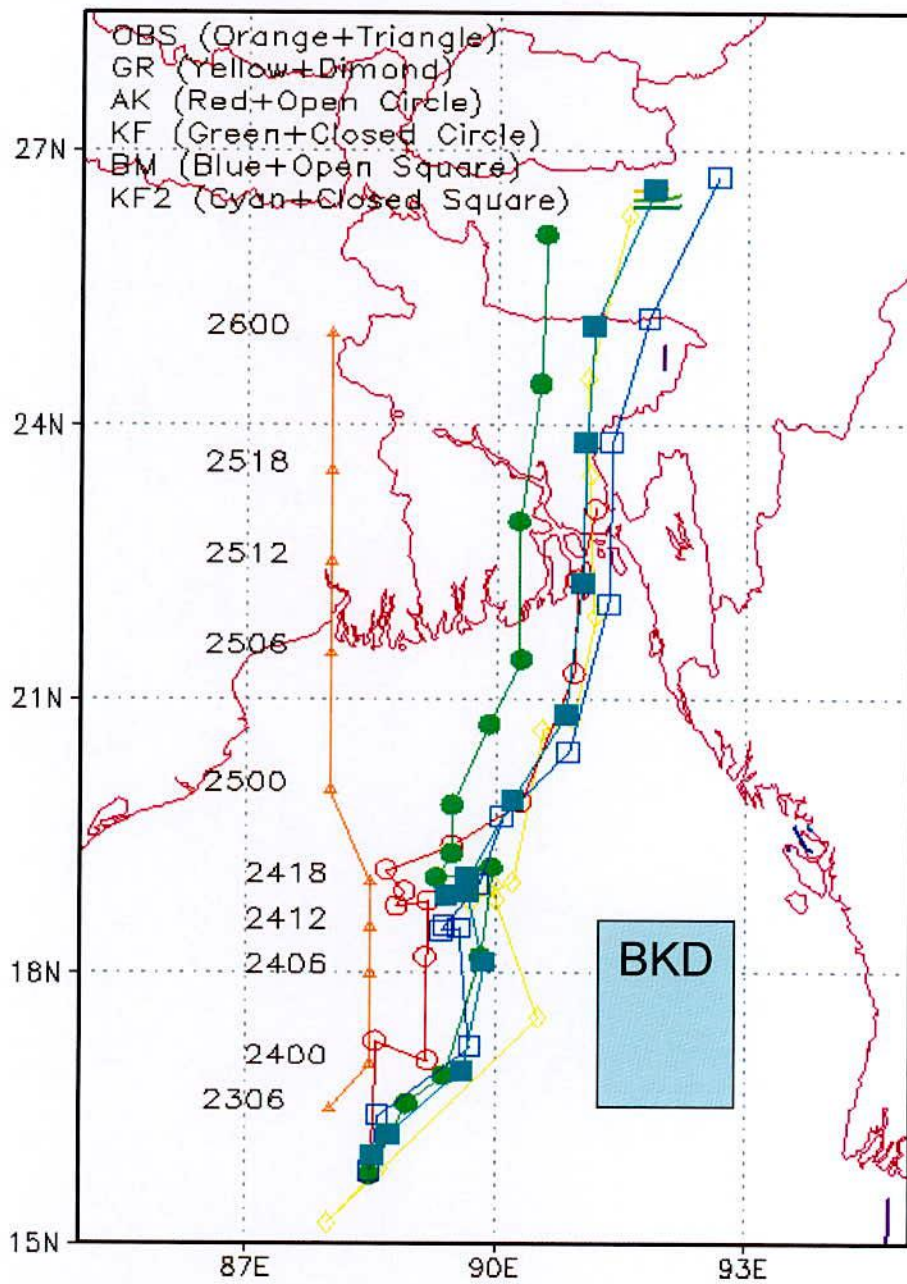


Figure 6.4.4.1a: MM5 Model simulated tracks of TC Aila using MRF PBL and different cumulus parameterization schemes.





GrADS: COLA/IGES

Figure 6.4.4.1b: MM5 Model simulated track of TC Aila using BKD PBL and different cumulus parameterization schemes.

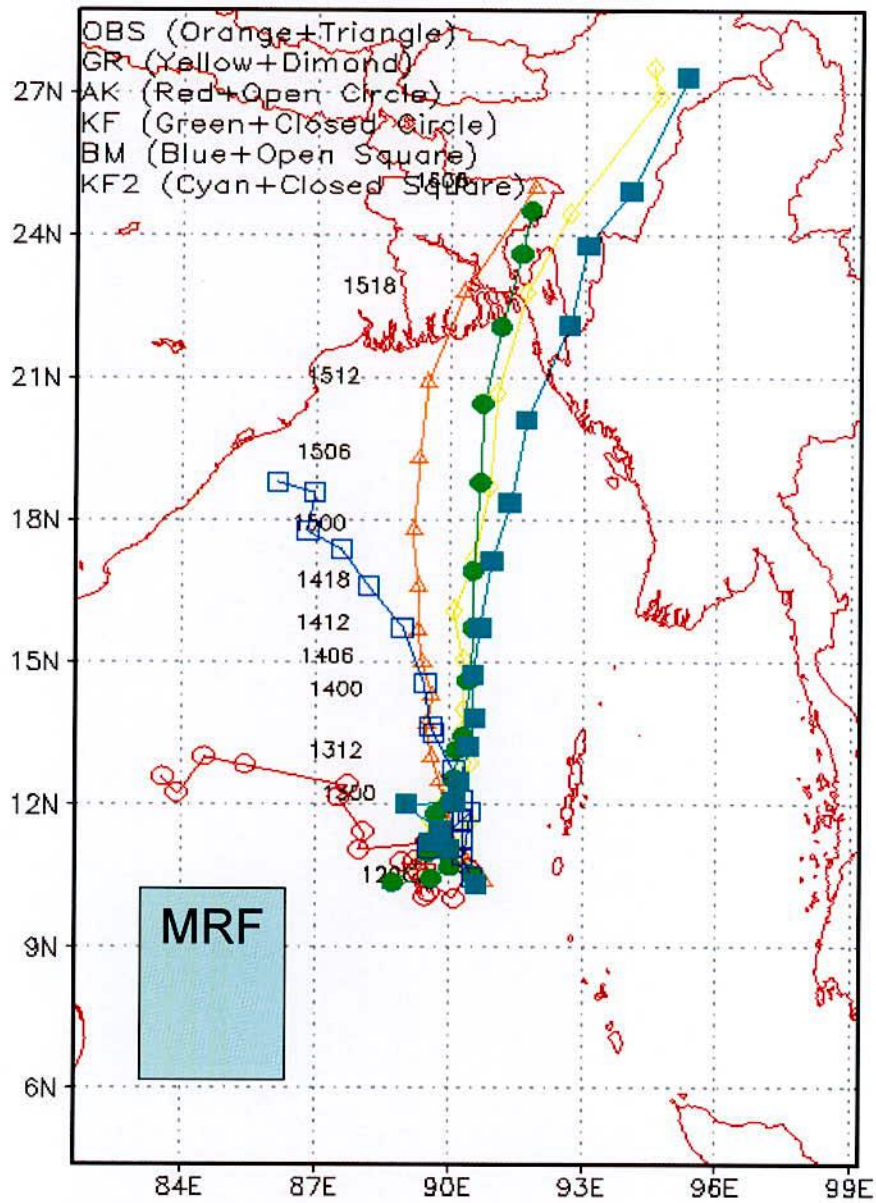
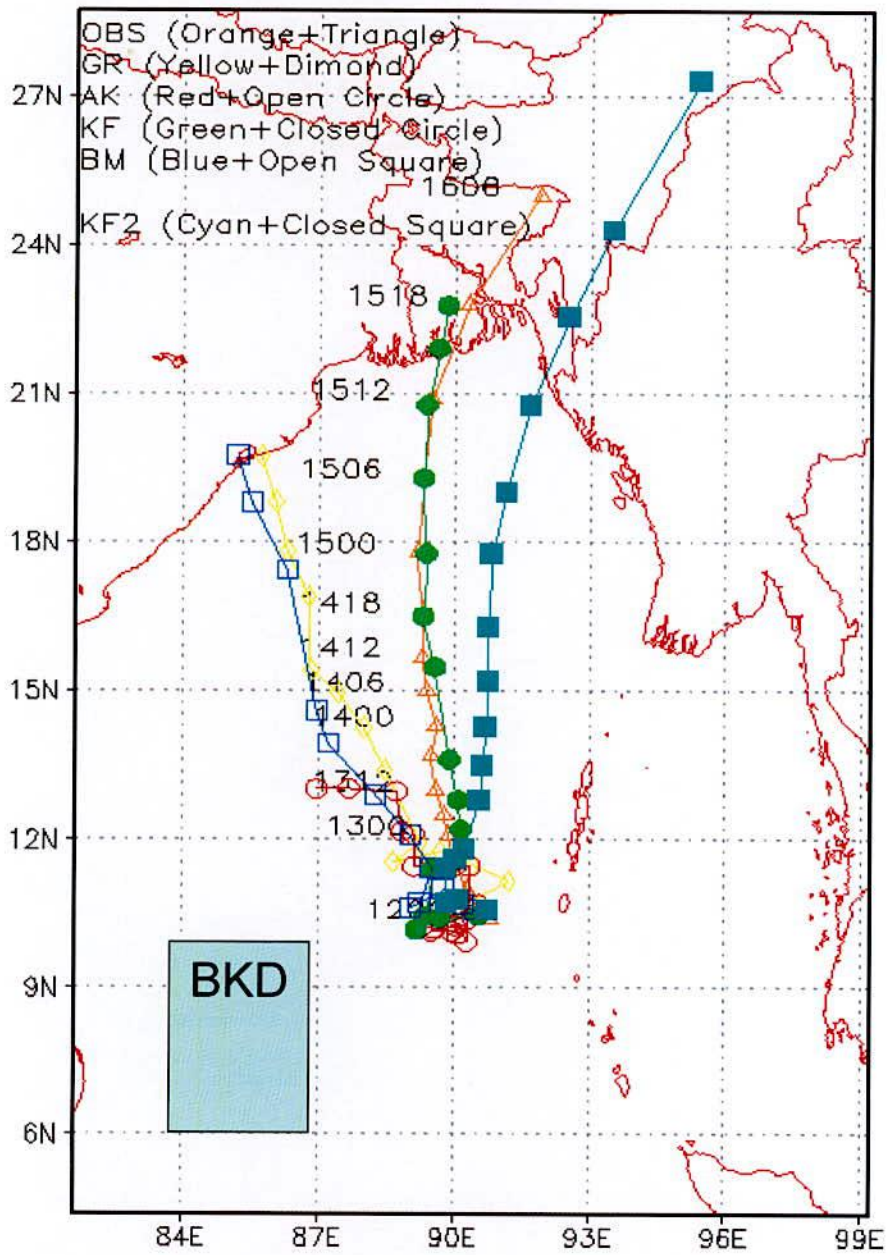


Figure 6.4.4.2a: MM5 Model simulated track of TC Sidr using MRF PBL and different cumulus parameterization schemes.



GrADS: COLA/IGES

Figure 6.4.4.2b: MM5 Model simulated track of TC Sidr using BKD PBL and different cumulus parameterization schemes.

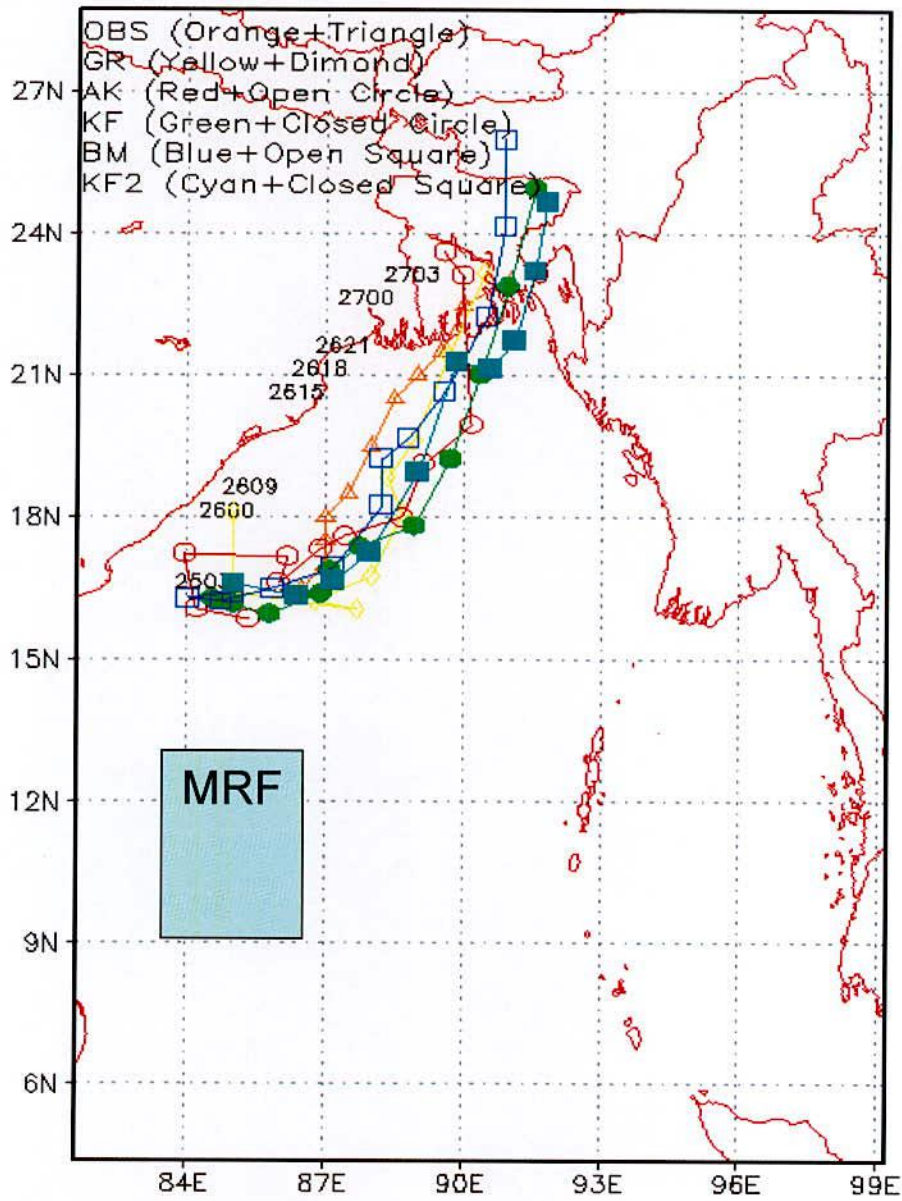
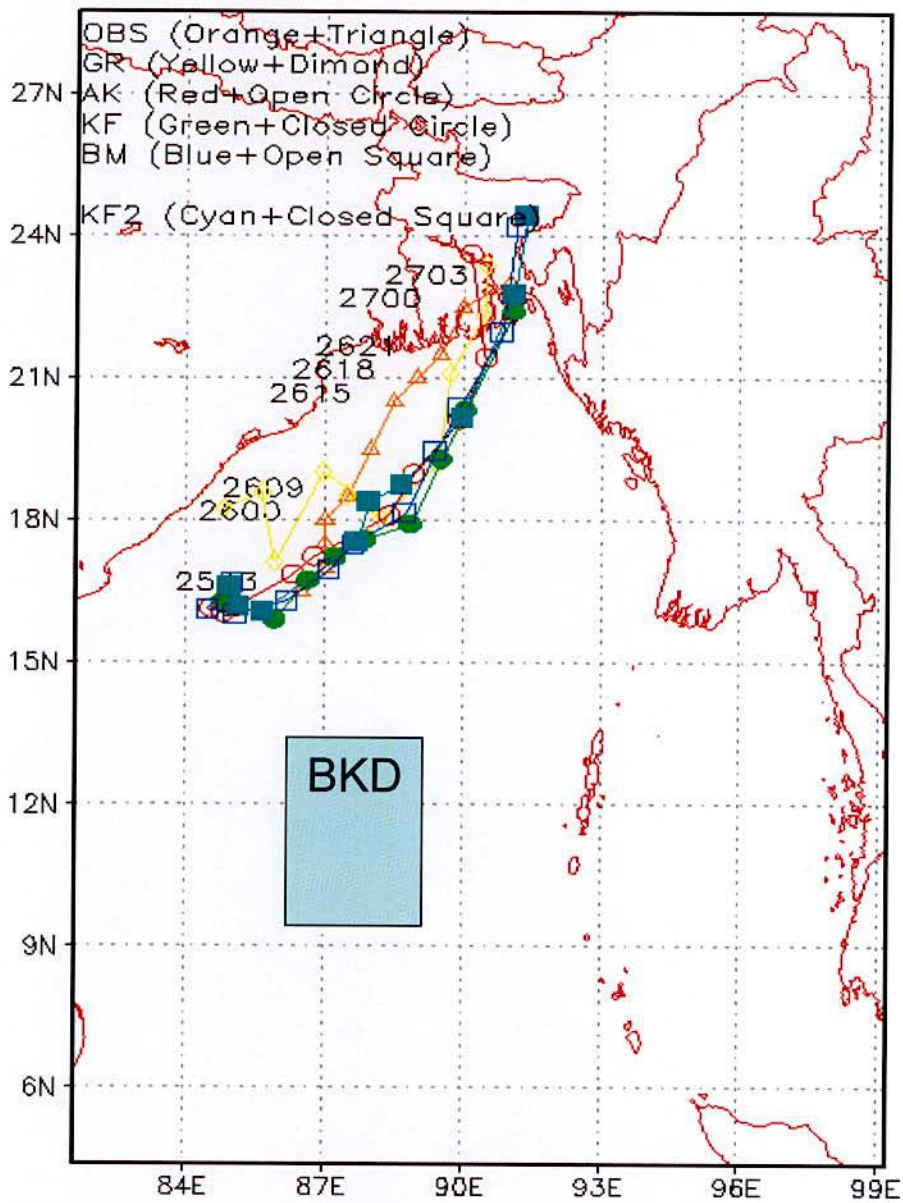


Figure 6.4.4.3a: MM5 Model simulated track of TC Rashmi using MRF PBL and different cumulus parameterization schemes.



GrADS: COLA/IGES

Figure 6.4.4.3b: MM5 Model simulated track of TC Rashmi using BKD PBL and different cumulus parameterization schemes.

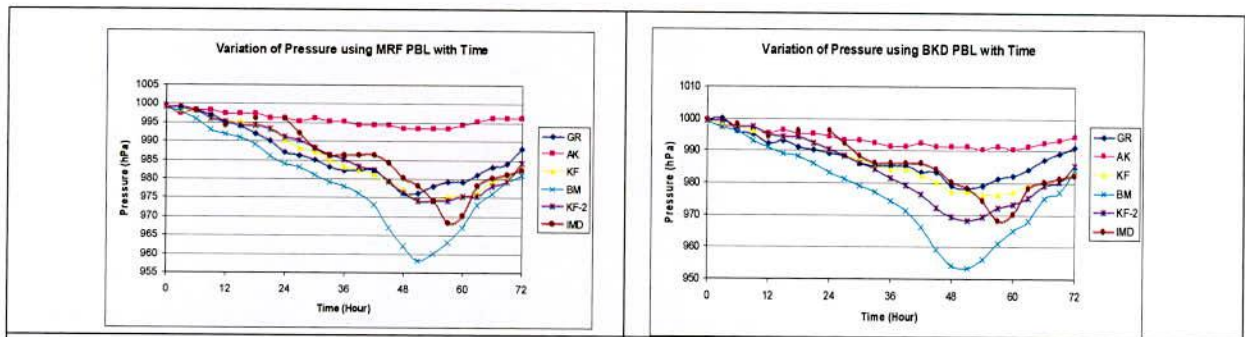


Figure 6.4.4.4a: SLP of cyclone Aila

Figure 6.4.4.4b: SLP of cyclone Aila

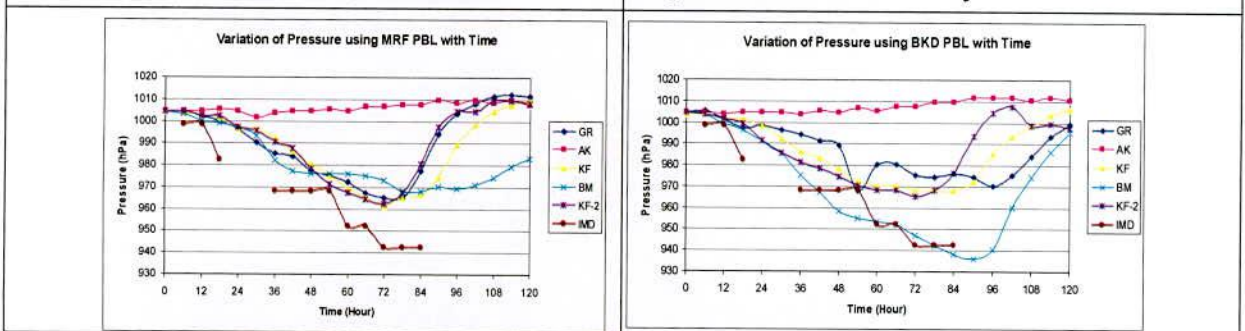


Figure 6.4.4.5a: SLP of cyclone Sidr

Figure 6.4.4.5b: SLP of cyclone Sidr

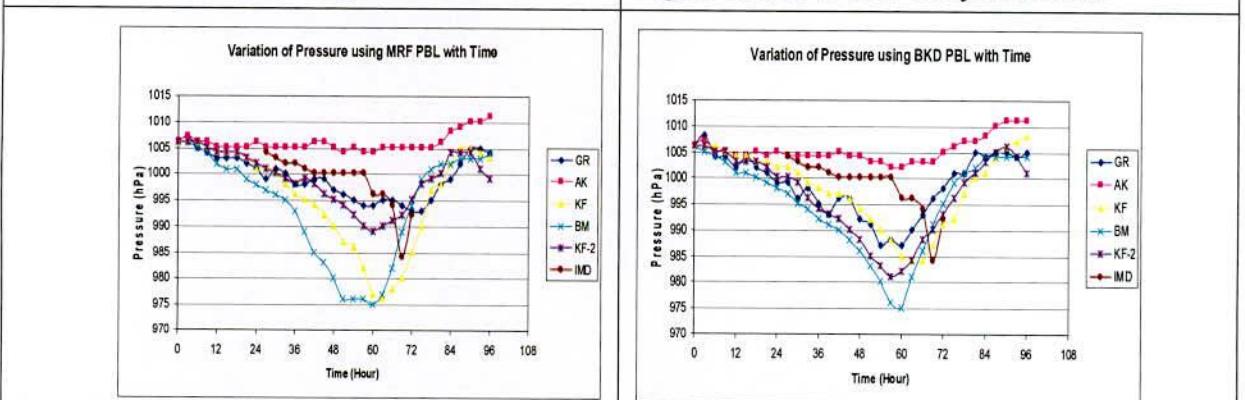


Figure 6.4.4.6a: SLP of cyclone Rashmi

Figure 6.4.4.6b: SLP of cyclone Rashmi

6.5. Sensitivity Study of Microphysics for Track and Intensity on TC Aila

6.5.1 Domain Set Up

For the tropical cyclone (TC), two domains is used: first one is mother domain and another one is nested domain inside the mother domain. Nested domain covers the Bangladesh region. Ratio of the resolution of the two domains is 3:1 respectively. The horizontal grid resolution of the mother domain is 90 km and nested domain is 30 km respectively. The dimension of the models MM5 and WRF are summaries in Table 6.4.1

Table 6.4.1: Dimension of the domain for heavy precipitation events and TC

| Domain | heavy precipitation events | | TC | |
|--------|----------------------------|--------------|-------------|--------------|
| | Latitude °N | Longitude °E | Latitude °N | Longitude °E |
| 1 | 13.40-31.96 | 65.41-98.59 | 0.22-37.94 | 67.36-108.64 |
| 2 | 20.11-27.22 | 87.80-93.20 | 4.36-28.71 | 81.66-99.20 |

6.5.2 Model Physics

To test the sensitivity of microphysics schemes for TC Aila, MM5 physics options which are used, other than microphysics, includes: i) MRF for Planetary Boundary Layer, ii) Grell for cumulus parameterization iii) Cloud Radiation Schemes for radiation calculation and iv) 5-Layer Soil model to predict soil temperature. Six microphysics options are used for six independent runs. The microphysics options are Warm Rain (WR), Simple Ice (SI), Mixed Phase –Reisner (MR1), Mixed phase with Graupel – Goddard (MG), Mixed phase with Graupel – Reisner (MR2) and Mixed phase with Graupel – Schultz (MS). Model physics are summaries in Table 6.5.2.1. Model equations in the surface flux form and solved on Arakawa B grid. Leapfrog time integration scheme with time splitting technique is used in model integration. All these options have been applied for both the domains. The model is run for 96 hours from 00 UTC of 23 May to 00 UTC of 27 May 2009 and their outputs are compared with those reported by India Meteorological Department (IMD).

Table 6.5.2.1: Domain design of the model
Fifth generation Penn State/NCAR Mesoscale Model (MM5) Version 3.7

| | |
|-----------------------------------|---|
| Dynamics | Non-hydrostatic with three-dimensional Coriolis force |
| Main prognostic variables | u, v, w, T, p and q |
| Map projection | Lambert conformal mapping |
| Central point of the domain | 20° N, 88° E |
| Horizontal grid distance | 90 km and 30 km |
| Number of vertical levels | 23 half sigma levels |
| Horizontal grid system | Arakawa B grid |
| Time integration scheme | Leapfrog scheme with time-splitting technique |
| Radiation parameterization scheme | Cloud |
| PBL parameterization scheme | MRF |
| Cumulus parameterization schemes | Grell |
| Microphysics | WR, SI, MRI, MG, MR2 and MS |
| Soil model | 5-layer soil model |

6.5.3 Results, Discussion and Conclusions

Model simulated Sea Level Pressure (SLP), wind and tracks are compared with those observed and shown in Figures 6.5.3.1, Figure 6.5.3.2 and Figure 6.5.3.3. The simulated minimum central pressure were found 966, 967, 976, 967, 974 and 974 hPa when warm rain (WR), simple ice (SI), mixed phase-Reisner1 (MR1), Goddard microphysics (MG), Reisner graupel - Reisner 2 (MR2) and Schultz microphysics (MS) respectively are incorporated and that for observed one is 968 hPa. At the formation stage tracks are different for different microphysics options. Landfall times are different for different microphysics options. The results indicate that the microphysical parameterization option have their own impact on the simulation of Aila.

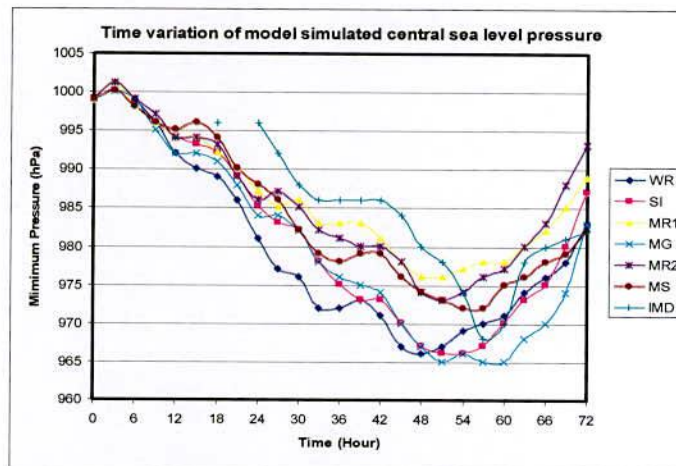


Figure 6.5.2.1: Comparison among simulated pressure using different microphysics and observed pressure of TC Aila

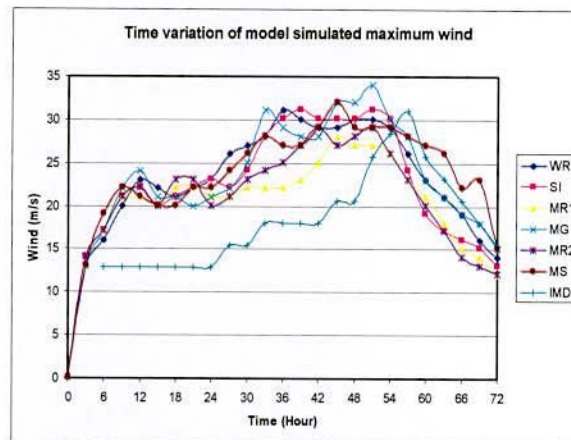


Figure 6.5.2.2: Comparison among simulated wind using different microphysics and observed wind of TC Aila



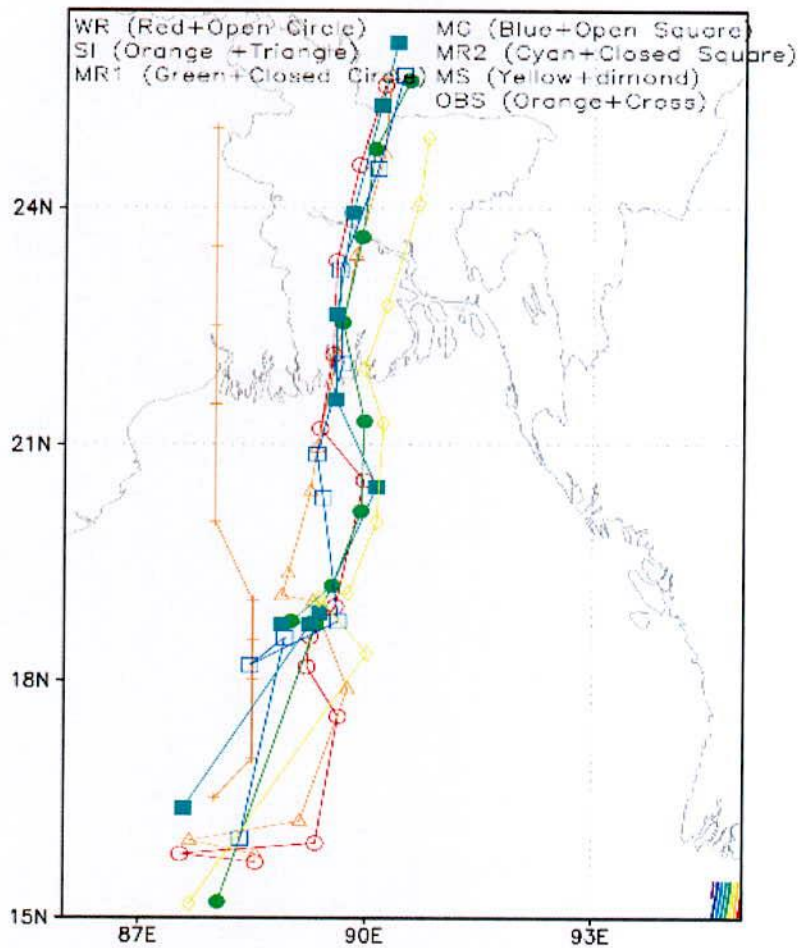


Figure 6.5.2.3: MM5 Model simulated Track of tropical cyclone Aila using different microphysics

6.6 Sensitivity Study of Radiation Parameterizations on Track and Intensity of TC Aila

6.6.1 Domain Set Up

For the tropical cyclone (TC), two domains are taken: first one is mother domain and another one is nested domain inside the mother domain. Nested domain covers the Bangladesh region. Ratio of the resolution of the two domains is 3:1 respectively. The horizontal grid resolution of the mother domain is 90 km and nested domain is 30 km respectively. The dimension of the models MM5 and WRF are summaries in Table 6.4.1

Table 6.4.1: Dimension of the domain for heavy precipitation events and TC

| Domain | heavy precipitation events | | TC | |
|--------|----------------------------|--------------|-------------|--------------|
| | Latitude °N | Longitude °E | Latitude °N | Longitude °E |
| 1 | 13.40-31.96 | 65.41-98.59 | 0.22-37.94 | 67.36-108.64 |
| 2 | 20.11-27.22 | 87.80-93.20 | 4.36-28.71 | 81.66-99.20 |

6.5.2 Model Physics

To test the sensitivity of RPS in the simulations of Aila by MM5, the following physics options are taken in all : i) MRF for Planetary Boundary Layer, ii) Grell for cumulus parameterization iii) Simple Ice Schemes for Microphysics and iv) 5 Layer Soil model to predict soil temperature. Five RPS options are used for five independent runs. The RPS options are None (i.e. no radiation parameterization schemes will be considered), Simple Cooling (SC) scheme, Cloud Radiation (CR) Scheme, Second generation Community Climate Model Radiation (CCM2) scheme and Rapid Radiation Transfer Model long wave (RRTM) scheme. All these options have been applied for both the domains. The model is run for 96 hours from 00 UTC of 23 May to 00 UTC of 27 May 2009 and their outputs are compared with those reported by India Meteorological Department (IMD).

Table 6.5.2.1: Domain design of the model
Fifth generation Penn State/NCAR Mesoscale Model (MM5) Version 3.7

| | |
|-----------------------------------|---|
| Dynamics | Non-hydrostatic with three-dimensional Coriolis force |
| Main prognostic variables | u, v, w, T, p and q |
| Map projection | Lambert conformal mapping |
| Central point of the domain | 20° N, 88° E |
| Horizontal grid distance | 90 km and 30 km |
| Number of vertical levels | 23 half sigma levels |
| Horizontal grid system | Arakawa B grid |
| Time integration scheme | Leapfrog scheme with time-splitting technique |
| Radiation parameterization scheme | None, SC, CR, CCM2 and RRTM |
| PBL parameterization scheme | MRF |
| Cumulus parameterization schemes | Grell |
| Microphysics | WR, SI, MRI, MG, MR2 and MS |
| Soil model | 5-layer soil model |

6.6.3 Results and Discussion and Conclusion

Model simulated MSLP, wind and track are compared with those observed and are shown in Figures 6.6.3.1, Figure 6.6.3.2 and Figure 6.6.3.3. Simulations with no (None) RPS, Simple Cooling (SC) Scheme, Cloud Radiation (CR) Scheme, second generation Community Climate Model Radiation (CCM2) Scheme and Rapid Radiation Transfer Model long wave (RRTM) Scheme have simulated 971, 983, 966, 969 and 967 hPa respectively as minimum SLP where as that for observed one is 968 hPa. Simulated track are parallel to each other and they are deviated mainly in the longitudinal position. Landfall times are different for different RPS options and those are obtained earlier than those of the observed. The results indicate that the radiation parameterization schemes (RPC) options have their own impact on the simulation of TC Aila.

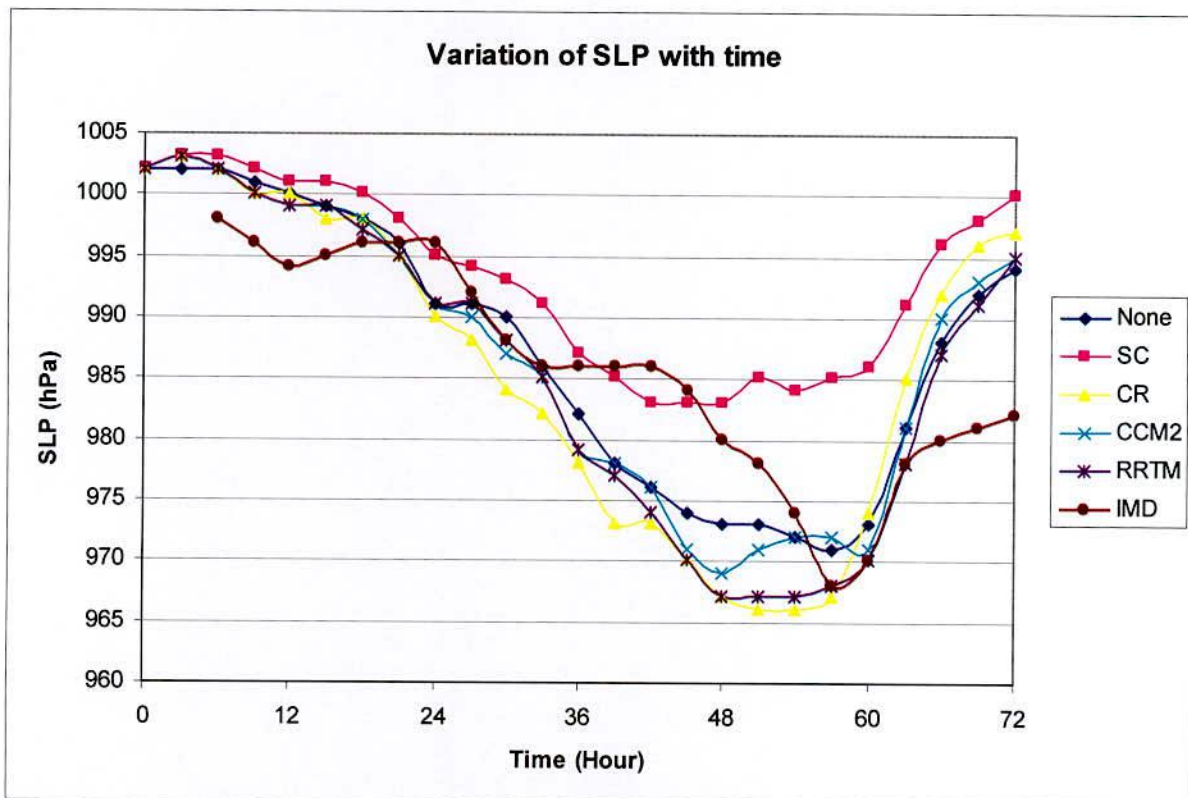


Figure 6.6.3.1: Comparison among simulated MSLP using different radiation parameters and observed MSLP of TC Aila

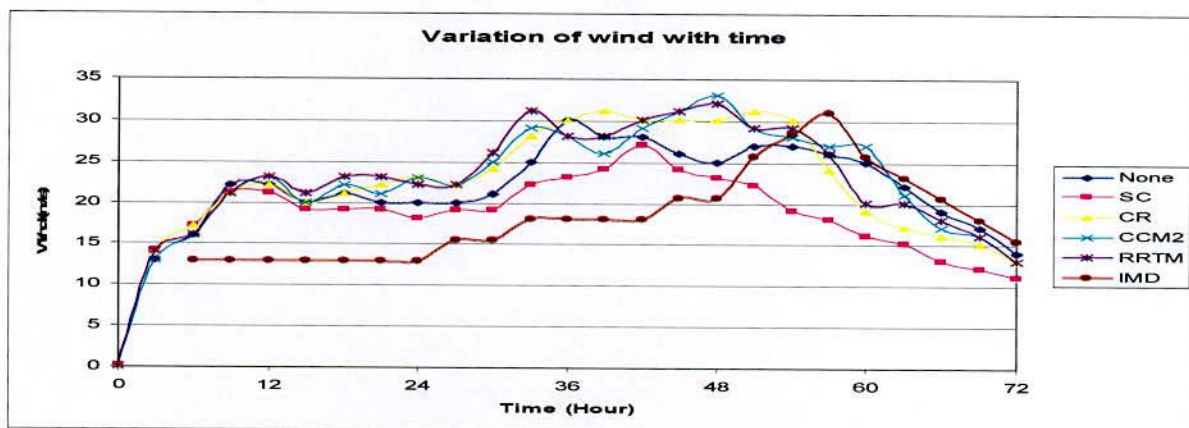


Figure 6.6.3.2: Comparison among simulated wind using different radiation parameters and observed wind of TC Aila

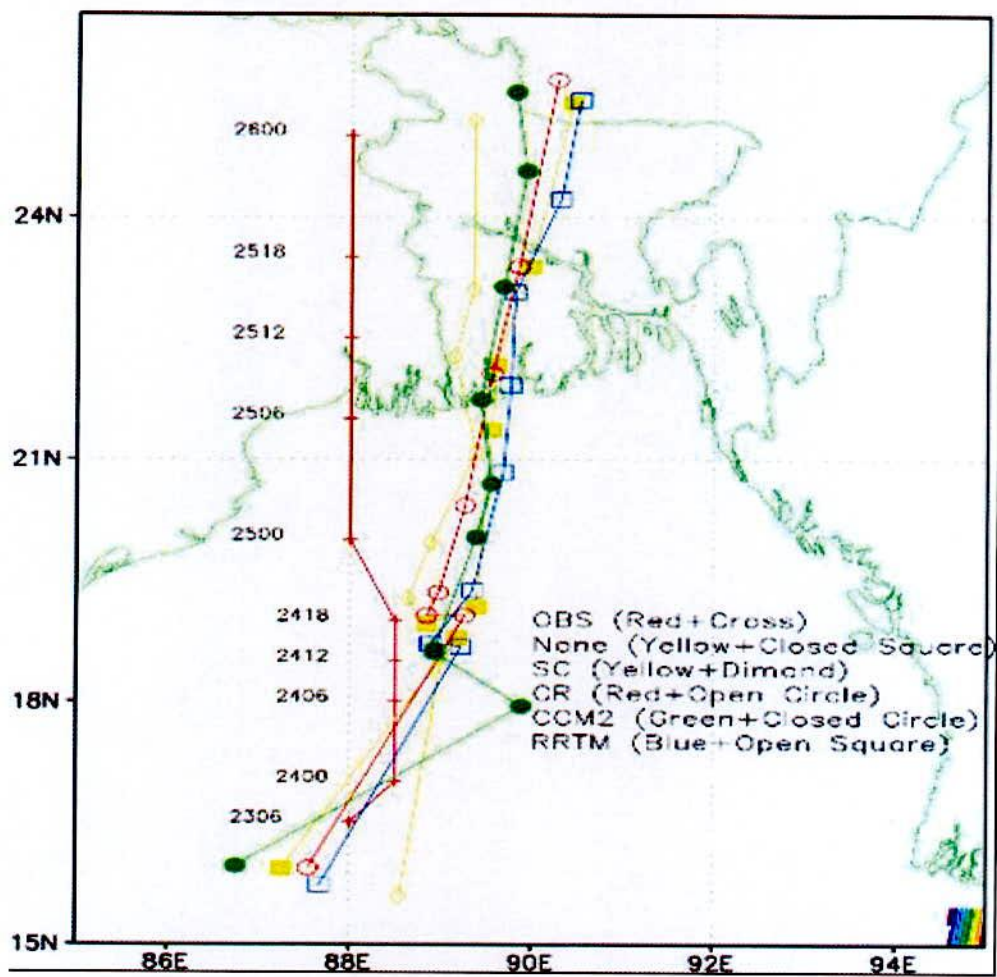


Figure 6.6.3.3: Comparison among simulated track using different RPS and observed track of TC Aila

CHAPTER 7
CONCLUSIONS

CONCLUSIONS

In the present study, two state-of-the-art mesoscale models MM5 and WRF-ARW have been used to evaluate their performances for the simulation of different heavy precipitation and TC events. Three test cases for the heavy precipitation events have been considered and the events are occurred during 9-14 June 2007, 1-3 July 2008 and 1-3 May 2009. On the other hand, three test cases of TC events are TC Aila, 23-27 May 2009; TC Rashmi, 24-28 October 2008; and TC Sidr, 11-17 November 2007.

To understand the knowledge about the sensitivity of various MP of the MM5 model, model was run for various sensitivity cases: sensitivity study on PBL with CP for heavy precipitation and TC events, sensitivity study on MP, radiation only for TC events.

For the heavy precipitation events MSLP, wind with rain, wind with humidity, rainfall and vertical structure of vertical velocity, divergence, relative vorticity, relative humidity (RH) and mixing ratio has been analyzed to understand the convective activity of the precipitation system by both the models.

MSLP simulated by MM5 and WRF models for all the heavy precipitation events are also same. Low pressure systems persist during the simulation period and satisfy the environment for convection. Southwesterly wind is the carrier of moisture from the Bay of Bengal and westerly in association with heat help the development of convective system. RH at 850 hPa levels is always equal or more than 90%. Cyclonic and anti-cyclonic circulations are simulated in all cases by both of the models at 850 and 200 hPa levels respectively. For heavy convective systems (June 07 and July 08) cyclonic circulation are also observed at 500 hPa where for the weak convective system (May 09) anti-cyclonic circulation is simulated by both of models. So, both of the modes can simulate synoptic features clearly and fairly.

Vertical structure of RH, mixing ratio, divergence, vorticity and vertical velocity simulated by both of the models are also consistence with the formation of convection. Both of the models can simulate the features well. Amount of precipitation simulated by both of the models are comparable with TRMM and Rain Gauge observational data. For different resolution of the domains, amount of rainfall are different for different domains. For increasing the resolution of the grid size rainfall obtained from WRF Model is also increased. Simulations of rainfalls are almost same for the two models. KF CP with MRF PBL in MM5 and YSU PBL in WRF Model can simulate the convective features fairly well.

On the other hand three TC events have been selected to simulate the structure, intensity, MSLP, wind (vector, radial, tangential, vertical wind), vorticity, temperature anomaly, RH,

mixing ratio, rainfall and track by both of the models. Simulated parameters are compared with the data obtained from Joint Typhoon Warning Centre (JTWC).

- Both the models are able to simulate some salient features of TC such as pressure distribution, vertical motion around the centre, vertical and horizontal distribution of wind, vorticity, moisture field and temperature anomaly. Some of them are very close to the observations.
- Both of the models fail to simulate the SLP of TC Sidr. Simulated SLP is higher than that of observed SLP. Spatio temporal variation of minimum SLP obtained. But in all cases sharp pressure gradient in the vicinity of the centre of the TC are observed by the simulated pressure field at surface level.
- Asymmetric patterns of surface wind distribution with well organized banded structure having the maximum about 40 to 240 km far from the centre and relatively weak winds at the centre are well simulated. Well organized circulation patterns are simulated at 850 hPa level confirming that maximum winds are confined to the right of the track of the TC movement. Anticyclonic circulation patterns at 200 hPa level or lower are visible in most of the cases. Model simulated MWS is nearly equal to the observed value.
- The model has successfully simulated the strong relative vorticity at lower level spreading over the strong convective region of each cyclone. For the very strong systems the positive vorticity is found to extend up to 100 hPa level. Simulated low level vorticity fields at 850 hPa level demonstrate the size of the system with strong convective regions of each cyclone, which are in agreements with the observations.
- The warm core characteristics with maximum temperature anomaly of 5-10⁰C simulated in the middle and upper troposphere successfully by the models. This warm core has the vertical extends from the lower level to tropopause for strong system.
- The high relative humidity is found in the eye wall and rain bands of the TC and low relative humidity at the centre. From the analysis of water vapor maxing ratio it is found that high moisture flux comes from the southern side covering a large area of the Bay of Bengal which feeds the system along its southeastern side through the boundary layer.
- With regard to track predictions of selected TC, models are run for 24, 48, 72 and 48 hours forecast. Simulated track for 24 or 48 hours forecast are the best among other forecasts. One of the outstanding findings of the models is that the models has successfully predicted tracks, re-curvedure and probable area and time of landfall of

the selected tropical cyclones with high accuracy even in the 96 hours predictions. Again, WRF model simulates better track than that simulated by MM5 model. In case cyclone Sidr, WRF simulates very near to observed track. In maximum cases, simulated track deviated to the right of the observed track.

- For the simulation of rainfall, the simulated rainfall by the MM5 and WRF models are compared with that obtained from TRMM BMD rain-gauge data. Simulated rainfall is more than that obtained from TRMM and BMD rain-gauge data in most of the cases.

Considering the above, it can be mentioned that both the models simulate convective system and the cyclonic feature well again the performance of WRF Model is better than that of MM5 Model. So, both of the models may be used as operational model by using the suitable microphysics and cumulus parameterization schemes.

All of the sensitivity tests are done using only NCAR MM5 model. In case of sensitivity on PBL with CP for heavy precipitation and TC events, 5 cumulus parameterization schemes Grell, AK, KF, BM and KF-2 are used with 2 PBL MRF and BKD for both the domains.

Simulated pattern of rainfall for individual option agrees with observable evidences. It is to be noted that the options for simulation rainfall using MM5 has been found dependable on resolution and location of the area. According to the study, no single option may be considered as the most suitable among the 10 options for the assessment of rainfall over Bangladesh but KF CP with MRF PBL may be consider as a better one. However further study is required to draw the final conclusion in choosing the best option of MM5.

- The central pressure and wind have been predicted with fair accuracy by 7 out of 10 runs. Few has over shooted and few PBL has under shooted the central pressure.
- Variations of tracks are observed mainly in the longitudinal position for all run.
- Use of suitable Bogussing Scheme may improve the predictability of track and intensity of TC.

It is clear that no one combination of PBL and CP performs better than any other combinations. But it seems that MRF PBL with KF CP performs better than any other combinations.

In case of sensitivity on microphysics for TC events, 6 different microphysics options are used, named warm rain (WR), simple ice (SI), mixed phase-Reisner1 (MR1), Goddard microphysics (MG), Reisner graupel-Reisner 2 (MR2) and Schultz microphysics (MS) to test the sensitivity of microphysics to simulate the severe cyclonic storm Aila that hit the Bangladesh coast on 25 May 2009.

From the simulations the following results come forward:

- Pressure drops are different for different microphysics options.
- Duration at the minimum CSLP is different for different microphysics options.
- At the formation stage tracks are different for different microphysics options.
- Landfall times are different for different microphysics options.

Hence it may be conclude that the microphysical parameterization options have their own impact on the simulation of TC Aila. The present study has investigated only one cyclone, and more cases should be examined to supplement these results. It is expected that it would be desirable to make sensitivity experiments with all possible combinations of the schemes of the physical processes.

To study the sensitivity/ role of the different radiation parameterization schemes (RPS) in the simulation of the severe cyclonic storm Aila MM5 model is used. Five RPS options are used for five independent runs. The RPS options are None (i.e. no radiation parameterization schemes will be considered), Simple Cooling (SC) scheme, Cloud Radiation (CR) Scheme, Second generation Community Climate Model Radiation (CCM2) scheme and Rapid Radiation Transfer Model long wave (RRTM) scheme. From the simulations the following results come forward:

- The central minimum SLP has been predicted with fair accuracy by None, CR, CCM2 and RRTM scheme, almost all except SC scheme.
- Durations at the minimum central SLP for different RPS options are different.
- Due to the weak presence of the system in the initial data, different RPS located the system at different location and at the formative stage the system moved in different direction.
- Simulated track are parallel to each other and they are deviated mainly in the longitudinal position.
- Landfall times are different for different RPS options and those are obtained earlier than those of the observed.

Hence it is conclude that the RPS options have their own impact on the simulation of Aila. The present study has investigated only one cyclone, and more cases should be examined to supplement these results. It is suggested that it would be desirable to make sensitivity experiments with all possible combinations of the schemes of the physical processes.

- ✦ Considering above simulations for the three heavy precipitation events and three TCs and sensitivity tests for different options in model on prediction of different parameters of heavy precipitation event and TC, both the models can be used may be used as operational model for further research.

REFERENCES

References

1. Lynch, Peter (March 2008). "The origins of computer weather prediction and climate modeling". *Journal of Computational Physics* (University of Miami) 227 (7) :34314 4. Bibcode 2008JCoPh.227.3431L. doi:10.1016/j.jcp.2007.02.034. Retrieved 2010-12-23.
2. Lynch, Peter (2006). "Weather Prediction by Numerical Process". *The Emergence of Numerical Weather Prediction*. Cambridge University Press. pp. 1–27. ISBN 978-0-521-85729-1.
3. Charney, Jule; Fjörtoft, Ragnar; von Neumann, John (November 1950). "Numerical Integration of the Barotropic Vorticity Equation". *Tellus* 2 (4). Bibcode 1950 Tell....2.. 23 7 C. doi:10.1111/j.2153-3490.1950.tb00336.x. Retrieved 2011-01-03.
4. Cox, John D. (2002). *Storm Watchers*. John Wiley & Sons, Inc.. p. 208. ISBN 0-471-38108-X.
5. Harper, Kristine; Uccellini, Louis W.; Kalnay, Eugenia; Carey, Kenneth; Morone, Lauren (May 2007). "2007: 50th Anniversary of Operational Numerical Weather Prediction". *Bulletin of the American Meteorological Society* 88 (5): 639–650. Bibcode 2007BAMS...88..639H. doi:10.1175/BAMS-88-5-639.
6. American Institute of Physics (2008-03-25). "Atmospheric General Circulation Modeling". Archived from the original on 2008-03-25. Retrieved 2008-01-13.
7. Phillips, Norman A. (April 1956). "The general circulation of the atmosphere: a numerical experiment". *Quarterly Journal of the Royal Meteorological Society* 82 (352):123–154. Bibcode 1956QJRMS..82..123P. doi: 10.1002/qj.49708235202.
8. Cox, John D. (2002). *Storm Watchers*. John Wiley & Sons, Inc. p. 210. ISBN 0-471-38108-X.
9. Lynch, Peter (2006). "The ENIAC Integrations". *The Emergence of Numerical Weather Prediction*. Cambridge University Press. pp. 206–208. ISBN 978-0-521-85729-1.
10. National Oceanic and Atmospheric Administration (2008-05-22). "The First Climate Model". Retrieved 2011-01-08.

11. Leslie, L.M.; Dietachmeyer, G.S. (December 1992). "Real-time limited area numerical weather prediction in Australia: a historical perspective". *Australian Meteorological Magazine* (Bureau of Meteorology) 41 (SP): 61–77. Retrieved 2011-01-03.
12. Shuman, Frederick G. (September 1989). "History of Numerical Weather Prediction at the National Meteorological Center". *Weather and Forecasting* 4 (3): 286–296. Bibcode 1989WtFor...4..286S.doi:10.1175/1520-0434(1989)004<0286:HONWPA>2.0.CO;2. Retrieved 2010-12-31.
13. Steyn, D. G. (1991). *Air pollution modeling and its application VIII, Volume 8*. Birkhäuser. pp. 241–242. ISBN 978-0-306-43828-8.
14. Xue, Yongkang; Fennessey, Michael J. (1996-03-20). "Impact of vegetation properties on U. S. summer weather prediction". *Journal of Geophysical Research* (American Geophysical Union) 101 (D3): 7419. Bibcode 1996JGR...101.7419X. doi:10.1029/95JD02169. Retrieved 2011-01-06.
15. Hughes, Harry (1976). *Model output statistics forecast guidance*. United States Air Force Environmental Technical Applications Center. pp. 1–16.
16. Best, D. L.; Pryor, S. P. (1983). *Air Weather Service Model Output Statistics Systems*. Air Force Global Weather Central. pp. 1–90.
17. Toth, Zoltan; Kalnay, Eugenia (December 1997). "Ensemble Forecasting at NCEP and the Breeding Method". *Monthly Weather Review* 125 (12): 3297–3319. Bibcode 1997MWRv..125.3297T. doi:10.1175/1520-0493(1997)125<3297:EFANAT>2.0.CO;2. Retrieved 2011-01-03.
18. "The Ensemble Prediction System (EPS)". ECMWF. Retrieved 2011-01-05.
19. Molteni, F.; Buizza, R.; Palmer, T.N.; Petroliagis, T. (January 1996). "The ECMWF Ensemble Prediction System: Methodology and validation". *Quarterly Journal of the Royal Meteorological Society* 122 (529): 73 – 119. Bibcode 1996QJRMS.122...73M. doi:10.1002/qj.49712252905. Retrieved 2010-01-03.
20. Anthes, R. A., and T. T. Warner, 1978: Development of hydrodynamic models suitable for air pollution and other mesometeorological studies. *Mon. Wea. Rev.*, 106, 1045-1078.

21. Grell GA, Dudhia J, Stauffer D. R. (1995) "A description of the fifth-generation Penn State/NCAR mesoscale model (MM5)" NCAR Technical Note 398. National Center for Atmospheric Research, Boulder, CO.
22. Dudhia J, Gill D, Manning K, Wang W, Bruyere C. (2004) "PSU/NCAR mesoscale modelling system tutorial class notes and users' guide (MM5 modelling system version 3)" National Center for Atmospheric Research, Boulder, CO. [http://www.mmm.ucar.edu/mm5/documents/\[27 September 2004\]](http://www.mmm.ucar.edu/mm5/documents/[27%20September%202004].).
23. Anthes RA. (1977) "A cumulus parameterization scheme utilizing a one-dimensional cloud model", *Monthly Weather Review*, Vol, 105, pp. 270–286.
24. Grell GA. (1993) "Prognostic evaluation of assumptions used by cumulus parameterizations" *Monthly Weather Review*, Vol, 121, pp.765–787.
25. Kain JS, Fritsch JM. (1990) "A one dimensional entraining/detraining plume model and its application in cumulus parameterization", *Journal of the Atmospheric Sciences*, Vol, 47, pp 2784–2802.
26. Kain, J.S. (2002) "The kain-Fritsch convective parameterization: An update" <http://www.mmm.ucar.edu/mm5/mm5-papers.html>, to be submitted to *J. Appl. Meteor.*
27. Betts AK, Miller MJ. (1986) "A new convective adjustment scheme: part II: single column tests using GATE wave, BOMEX, ATEX and Arctic air-mass data sets", *Quarterly Journal of the Royal Meteorological Society*, Vol, 112, pp.693–709.
28. Janjic, Zavisla I., 1994: The step-mountain eta coordinate model: Further development of the convection, viscous sublayer, and turbulent closure schemes. *Mon. Wea. Rev.*, 122, 927-945.
29. Hong, S.-Y., and H.-L. Pan, 1996: Nonlocal boundary layer vertical diffusion in a medium-range forecast model. *Mon. Wea. Rev.*, 124, 2322-2339.
30. Shamarock, W.C., J.B. Klemp, J. Dudhia, D.O. Gill, D.M. Barker, M.G. Duda, X.-Y. Huang, W. Wang and J.G. Powers, 2008: A description of the advanced Research WRF Version 3. NCAR Technical Notes, NCAR/TN-475+STR, Boulder, Colorado, USA.
31. Kessler, E., 1969: on the distribution and continuity of water substance in atmospheric circulation, *Meteor. Monopgr.*, 32, Amer. Meteor. Soc., 84 pp.

32. Lin, Y.-L., R.D. Farley, and H. D. Orville, 1983: Bulk parameterization of the snow field in a cloud model. *J. Climate Appl. Meteor.*, 22, 1065-1092.
33. Rutledge, S. A., and P. V. Hobbs, 1984: The mesoscale and microscale structure and organization of clouds and precipitation in midlatitude cyclones. XII: A diagnostic modeling study of precipitation development in narrow cloud-frontal rainbands. *J. Atmos. Sci.*, 20, 2949-2972.
34. Hong, S.-Y., J. Dudhia, and S.-H. Chen, 2004: A Revised Approach to Ice Microphysical Processes for the Bulk Parameterization of Clouds and Precipitation, *Mon. Wea. Rev.*, 132, 103-120.
35. Hong, S.-Y., and J.-O. J. Lim, the WRF Single-Moment 6-Class Microphysics Scheme (WSM6), *J. Korean Meteor. Soc.*, 42, 129-151.
36. TPB, 2001: Technical Procedures Bulletin (TPB) at <http://www.emc.ncep.noaa.gov/mmb/mmbpll/eta12tpb/> and on the CoMET Page at <http://meted.ucar.edu/nwp/pcu2/etapcp1/.htm>.
37. Dudhia, J., S.-Y. Hong, and K.-S. Lim, 2008: A new method for representing mixed-phase particle fall speeds in bulk microphysics parameterizations. *J. Met., Soc. Japan*, in press
38. Tao, W.-K., and J. Simpson, 1993: The Goddard cumulus ensemble model. Part I: Model description. *Terr. Atmos. Oceanic Sci.*, 4, 35-72.
39. Thompson, G., R. M. Rasmussen, and K. Manning, 2004: Explicit forecasts of winter precipitation using an improved bulk microphysics scheme. Part I: Description and sensitivity analysis. *Mon. Wea. Rev.*, 132, 519-542.
40. Morrison, H., G. G. Thompson, and V. Tatarskii, 2008: Impact of cloud microphysics on the development of trailing stratiform precipitation in a simulated squall line: Comparison of one- and two-moment schemes. Submitted to *Mon. Wea. Rev.*
41. Kain, J. S., 2004: The Kain-Fritsch convective parameterization: An update. *J. Appl. Meteor.*, 43, 170-181.
42. Kain, J. S., and J. M. Fritsch, 1990: A one-dimensional entraining/detraining plume model and its application in convective parameterization, *J. Atmos. Sci.*, 47, 2784-2802.

43. Kain, J. S., and J. M. Fritsch, 1993: Convective parameterization for mesoscale models: The Kain-Fritsch scheme, The representation of cumulus convection in numerical models, K.A. Emanuel and D.J. Raymond, Eds., Amer. Meteor. Soc., 246pp.
44. Janjic, Z. I., 1994: The step-mountain eta coordinate model: further developments of the convection, viscous sublayer and turbulence closure schemes, *Mon. Wea. Rev.*, 122, 927-745.
45. Janjic, Z. I., 2002: Comments on "Development and Evaluation of a Convection Scheme for Use in Climate Models", *J. Atmos. Sci.*, 57, p. 3686.
46. Grell, G. A., and D. Devenyi, 2002: A generalized approach to parameterizing convection combining ensemble and data assimilation techniques. *Geophys. Res. Lett.*, 29(14), Article 1693.
47. Monin, A.S. and A.M. Obukhov, 1954: Basic laws of turbulent mixing in the surface layer of the atmosphere. *Contrib. Geophys. Inst. Acad. Sci., USSR*, (151),163-187(in Russian).
48. Janjic, Z.I., 1996: the surface layer in the NCEP Eta Model, Eleventh Conference on Numerical Weather Prediction, Norfolk, VA. 19-23 August; Amer. Meteor. Soc., Boston, MA, 354-355.
49. Janjic, Z. I., 2002: Nonsingular Implementation of the Mellor-Yamada LEVEL 2.5 Scheme in the NCEP meso model, NCEP Office Note, No. 437, 61 pp .
50. Zilitinkevich, S. S., 1995: Non-local turbulent transport: pollution dispersion aspects of coherent structure of convective flows, *Air Pollution III- Volume I. Air Pollution Theory and Simulation*, Eds. H. Power, N. Moussiopoulos and C.A. Brebbia. Computational Mechanics Publications, Southampton Boston, 53-60.
51. Pleim, J. E., 2006: A simple, efficient solution of flux-profile relationships in the atmospheric surface layer, *J. Appl. Meteor. and Clim.*, 45, 341-347.
52. Chen, F., and J. Dudhia, 2001: Coupling an advanced land-surface/hydrology model with the penn State/NCAR MM5 modeling system. Part 1: Model description and implementation. *Mon. Wea. Rev.*, 129, 569-585.
53. Smirnova, T. G., J. M. Brown, and S. G. Benjamin, 1997: Performance of different soil model configurations in simulating ground surface temperature and surface fluxes. *Mon. Wea. Rev.*, 125, 1870-1884.

54. Smirnova, T. G., J. M. Brown, S. G. Benjamin, and D. Kim, 2009: Parameterization of coldseason processes in the MAPS land-surface scheme. *J. Geophys. Res.*, 105 (D3), 4077-4086.
55. Pleim, J. E. and A. Xiu, 1995: Development and testing of a surface flux and planetary boundary layer model for application in mesoscale models. *J. Appl. Meteor.*, 34, 16-32.
56. Xiu, A. and J. E. Pleim, 2001: Development of a land surface model part 1: Application in a mesoscale meteorology model. *J. Appl. Meteor.*, 40, 192-209.
57. Hoing, S.-Y., and H.-L. Pan, 1996: nonlocal planetary boundary layer vertical diffusion in the medium-range forecast model, *Mon. Wea. Rev.*, 124, 2322-2339.
58. Hong, S.-Y., Y. Noh, and J. Dudhia, 2006: A new vertical diffusion package with an explicit treatment of entrainment processes. *Mon. Wea. Rev.*, 134, 2318-2341.
59. Janjic, Z. I., 1990: The step-mountain coordinate: physical package, *Mon. Wea. Rev.*, 118, 1429-1443.
60. Pleim, J. E., 2007: A combined local and non-local closure model for the atmospheric boundary layer. Part 1: Model description and testing, *J. Appl. Meteor. and clim.*, 46, 1383-1395.
61. Mlawer, E. J., S. J. Taubman, P.D. Brown, M. J. Lacono, and S. A. Clough, 1997: Radiative transfer for inhomogeneous atmosphere: RRTM, a validated correlated-k model for the longwave. *J. Geophys. Res.*, 102(D14), 16663-16682.
62. Collins, W.D. et al., 2004: Description of the NCAR Community Atmosphere Model (CAM 3.0), NCAR Technical Note, NCAR/TN-464+STR, 226pp.
63. Dudhia, J., 1989: Numerical study of convection observed during the winter monsoon experiment using a mesoscale two-dimensional model, *J. Atmos. Sci.*, 46, 3077-3107.
64. Chou M.-D., and M. J. Suarez, 1994: An efficient thermal infrared radiation parameterization for use in general circulation models. NASA Tech. Memo. 104606, 3, 85pp.
65. Lacis, A. A., and J. E. Hansen, 1974: A parameterization for the absorption of solar radiation in the earth's atmosphere. *J. Atmos. Sci.*, 31, 118-133.
66. <http://www.atmosphere.mpg.de/enid/u7.html>

67. Gray, W.M., 1968, Global view of the origin of tropical disturbances and storms, *Mon. Wea. Rev.*, 96, 669-700.
68. Gray, W.M., 1975, Tropical cyclone genesis, Dept. of Atmos. Sci. Paper No. 323, Colorado State University, Ft. Collins, CO 80523, 121p.
69. Gray, W.M., 1978: Hurricanes: Their formation, structure, and likely role in the tropical circulation, *Meteorology over the tropical oceans*, D.B. Shaw (ed.), Royal Meteorological Society, London, 155-218.
70. Frank, W. M., 1987, Tropical cyclone formation. Chap. 3, *A Global View of Tropical Cyclones*, Office of Naval Research, Arlington, VA 22217, 53-90.
71. Palmen N, E., 1948: On the Formation and Structure of Tropical Hurricanes, *Geophysica*, 3, 26-38.
72. Raper, S., 1992: Observational data on the relationship between climatic change and frequency and magnitude of severe tropical storms. In *Climate and sea level change: Observations, projections and implications*, R. A. Warrick, E. M. Barrow, and T. M. L. Wigley (Eds.) Cambridge University Press, 192-212.
73. Riehl, H., 1948: On the formation of West Atlantic Hurricanes, Part I., *Miscellaneous Report 24*, Dept. of Met., University of Chicago, 1-64.
74. Hubert, L.F., 1955: A case study hurricane formation, *J. Meteor.*, 12, 486-492.
75. Yanai, J. I., and K. Emanuel, 1961: A detailed analysis of typhoon formation, *J. Meteor. Soc. Japan*, 39, 187-214.
76. Riehl, H., 1954: *Tropical Meteorology*, McGraw-Hill Book Company.
77. Ruprecht, E. and W. M. Gray, 1976a: Analysis of satellite-observed tropical cloud clusters. 1. Wind and dynamic fields. *Tellus*, 5, 391-413
78. Johnson, R. H., and R.A. Houze, 1987: Precipitation cloud systems of Asian monsoon. In *Monsoon Meteorology*, C.-P. Chang and T. N. Krishnamurti (Eds.), Oxford University Press, 298-353.
79. McBride, J. L., and W.M. Gray, 1980: Mass divergence in tropical weather systems. Part I: Diurnal variation. *Quart. J. Roy. Meteor. Soc.*, 106, 501-516.

80. Lee, C. A., 1989: Observational analysis of tropical cyclogenesis in the western North Pacific. Part I. Structural evolution of cloud clusters. *J. Atmos. Sci.*, 46, 2580-2598.
81. Tarakanov, G. G., 1980, *Tropical Meteorology*, Mir Publishers, Moscow, pp. 157-158.
82. Neumann, C.J., 1993: Global overview, *Global guide to tropical cyclone forecasting*, World Meteorological Organization, Geneva, 1.1-1.56.
83. Karmakar S., (Shrestha, M.L. ed.), 1998: Historical records of tropical cyclones which made landfall at the coastal areas of SAARC region, The impact of tropical cyclones on the coastal regions of SAARC countries and their influence in the region, SMRC-No. 1, SAARC Meteorological Research Centre, Dhaka, 69-318.
84. Alam, M.M., M.A. Hossain, and S. Shafee, 2002: Statistical analysis of cyclones and depressions in the Bay of Bengal during 1974-1999, *J. Bang. Ac. Sci.*, 26, 207-218.
85. Alam, M.M., M.A. Hossain, and S. Shafee, 2003: Frequency of Bay of Bengal cyclonic storms and depressions crossing different coastal zones, *Int. J. Climatol.*, 23, 1119-1125.
86. McBride, J. L., and H. E. Willoughby, 1986, Comment-An interpretation of Kurihara and Kwase's two dimensional tropical cyclone development model, *J. Atmos. Sci.*, 43, 3279-3283.
87. Ali, A., 1999a: Ghurnijhar, Bangla Academy, Dhaka.
88. Emanuel, K., 1994: *Tropical Cyclones*, Nikos Drakos, Computer Based Learning Unit, University of Leeds.
89. Neumann, C.J., 1972: An alternative to HURRAN tropical cyclone forecast system, Tech. Memo. NWS SR-52.
90. Leftwich, P.W., and C.J., Neumann, 1977: Statistical guidance on the prediction of eastern North Pacific tropical cyclone motion, Part II. NOAA Tech. Memo. NWS WR-125, 15pp.
91. Xu, Y., and C.J. Neumann, 1985: A statistical model for the prediction of western North Pacific tropical cyclone motion (WPCLPR). NOAA Tech. Memo. NWS-NHC 28, National Hurricane Centre, Miami, FL, 30pp.
92. Hope, J.R. and C.J. Neumann, 1970: An operational technique for relating the movement of existing tropical cyclones to past tracks, *Mon. Wea. Rev.*, 98, 925-933.

93. Frank, W. M. (1983) "The cumulus parameterization problem," *Mon, Wea. Rev.*, Vol. 111, pp. 1859-1871.
94. Molinari, J., Vollaro, D., Dudek, M. and Skubis, M. (1992) "Parameterization of the convective precipitation in mesoscale numerical models, A critical review", *Mon, Wea. Rev.*, Vol, 120, pp. 326-344.
95. Emanuel, K. A. and Raymond, D. J. (1993) "The representation of cumulus convection in numerical models", *Meteorol. Monogr. Ser., Am. Meteorol. Soc., Boston, MA*, Vol, 46, pp. 246.
96. Zhang, D. L., Kain, J.S., Fritsch, J. M. and Gao, K. (1994) "Comments on parameterization of convective precipitation in mesoscale numerical models, A critical review", *Mon, Wea. Rev.*, Vol, 122, pp. 2222-2231.
97. Kuo, Y. H., Bresch, J. F., Cheng, M. -D., Kain, J., Parsons, D. B., tao, W. K. and Zhang, D.-L.(1997) "Summary of miniworkshop on cumulus parameterization for mesoscale models, *Bull. Am. Meteorol. Soc.*, Vol, 78, pp. 475-491.
98. Dudhia, J. (1993) "A nonhydrostatic version of the Penn State- NCAR mesoscale model, Validation tests and simulation of an Atlantic cyclone and cold front" *Mon, Wea. Rev.*, Vol, 121, pp. 1493-1513.
99. Nitta, T. and Sekine, S. (1994) "Diurnal variation of convection activity over the tropical western Pacific, *Journal of Meteorological Society of Japan*, Vol, 72, pp 672-641.
100. Madden, R.A. and Julian, P. R. (1972) "Description of global -scale circulation cells in the tropics with a 40-50 day period," *Journal of Atmospheric Society*, Vol, 29, pp 1109-1123.
101. Yasunar, T. (1979) "Cloudness fluctuations associated with the Northern Hemisphere summer monsoon," *Journal of Meteorology Society of Japan*, Vol, 57, pp 227-242.
102. Kodama, Y. M., Ohta, A. Katsumata, M., Satoh, S. and Udeda, H. (2005) "Seasonal transition of predominant precipitation type and lightning activity over tropical monsoon area derived from TRMM observations," *Geophysical Research Letter*, Vol, 32, L14710. DOI: 10.1029/2005GL022986.
103. Matsumoto, J., Rahman, M. R., Hayashi, T., and Monji, N. (1996) "Rainfall distribution over the India Subcontinent during the 1987 and 1988 severe floods in Bangladesh," *Bulletin of Department of Geography University of Tokyo*, Vol, 28, pp 25-44.

104. Islam, M. N., Terao, T., Uyeda, H., Hayashi, T. and Kikuchi, K. (2005) "Spatial and temporal variation of the precipitation in and around Bangladesh," *Journal of Meteorological Society of Japan*, Vol, 83, pp 21-39.
105. Kataoka, A. and Satomura, T. (2005) "Numerical Simulation on the Diurnal Variation of Precipitation over Northeastern Bangladesh, A case study of an Active Period 14-21 June 1995," *Sola* Vol, 1, pp 205-208
106. Akhter, N., Islam, N. M., Teru, T. and Hayashi, T. (2007) "Selection of Parameterization in MM5 for the Estimation of Rainfall in Bangladesh," *Bangladesh Journal of Physics*, Vol, 3, pp. 75-83.
107. M. N. Ahsan, M. A. M. Chowdury and D. A. Quadir, Simulation of a Heavy rainfall event on 14 September over Dhaka, Bangladesh using MM5 model, *Journal of Scientific Research J. Sci.* 3(2), 261-270 (2011)
108. Odury S.R.U., Bhanu Kumar, Sai Ramalingeswara Rao, Kailasam Muni Krishna, Role of cumulus parameterization schemes in simulating heavy rainfall episodes of the coast of Maharashtra state during 28 June -4 July 2007, *Meteorol Atmos Phys* (2009) 105; 167-179
109. Ernst Kerrkhoven, Thaian Yew Gan, Michihara Shiiba, Gerhard Reuter and Kenji Tanaka, A comparison of cumulus parameterization schemes in a numerical weather prediction model for a monsoon rainfall event, *Hydrol. Process.* 20. 1961-1978 (2006)
110. K. Prasad, Monsoon Forecasting using Numerical Weather prediction Guidance, SAARC Meteorological Research Centre (SMRC), Report No. 11 (2005).
111. M. N. Islam and H. Uyeda, *Remote Sensing of Environment* 108, 264 (2006). doi:10.1016/j.rse.2006.11.011
112. Prasad, K., and Y.V. Rama Rao, 2006: *Simulation studies on cyclone track prediction by Quasi-Lagrangian model (QLM) in some historical and recent cases in the Bay of Bengal, using Global re-analysis and forecast Grid Point datasets*, SAARC Meteorological Research Centre publication No. 15, Dhaka, Bangladesh.
113. Charney, J.G., and A. Eliassen, 1964: On the growth of a hurricane depression, *J. Atmos. Sci.*, **21**, 68-75.
114. Trinh, V.T., and T.N. Krishnamurti, 1992: Vortex initialization for typhoon track prediction, *Meteor. Atmos. Phys.*, **47**, 117-126.

115. Kurihara, Y., M.A. Bender, R.E. Tuleya and R.J. Ross, 1995: Improvement in the GFDL automated prediction system, *Monthly Weather Review*, **123**, 2791-2801.
116. Leslie, L.M., and G.J. Holland, 1995: On the bogussing of tropical cyclones in numerical models: A comparison of vortex profiles, *Meteor. and Atmos. Phys.*, **56**, 101-110.
117. Prasad, K., 2004: *Cyclone track prediction experiments with a Quasi-Lagrangian model*, SAARC Meteorological Research Centre publication No. 9, Dhaka, Bangladesh.
118. Ashrit, R., M. Das Gupta and A.K. Bohra, 2006: MM5 simulation of the 1999 Orissa super cyclone: Impact of bogus vortex on track and intensity prediction, *Mausam*, **57**(1), 129-134.
119. Iwasaki, T., H. Nakano and M. Sugi, 1987: The performance of typhoon track prediction model with cumulus parameterization, *J. Meteor. Soc. Japan*, **65**, 555-570.
120. Mathur, M.B., 1991: The Meteorological Center's Quasi-Lagrangian Model for Hurricane Prediction, *Monthly Weather Review*, **119**, 1419-1447.
121. Rama Rao, Y.V., and K. Prasad, 2005: *Further evaluation of the Quasi-Lagrangian model for cyclone track prediction in the North Indian Ocean*, SAARC Meteorological Research Centre publication No. 12, Dhaka, Bangladesh.
122. Kurihara, Y., M.A. Bender and R.J. Ross, 1993: An initialization scheme of hurricane models by vortex specification, *Monthly Weather Review*, **121**, 2030-2045.
123. Puri, K., N.E. Davidson, L.M. Leslie and L.W. Lagan, 1992: The BMRC tropical limited area model, *Aust. Meteor. Mag.*, **40**, 81-104.
124. Liu, Y., D.-L. Zhang and M.K. Yau, 1997: A multiscale numerical study of Hurricane Andrew (1992). Part I: Explicit simulation and verification, *Monthly Weather Review*, **125**, 3073-3093.
125. Davis, C.A., and L.F. Bosart, 2001: Numerical simulations of the genesis of Hurricane Diana (1984), Part I: Control simulation, *Monthly Weather Review*, **129**, 1859-1881.
126. Barun, S.A., 2002: A cloud-Resolving simulation of Hurricane Bob (1991): Storm structure and eyewall buoyancy, *Monthly Weather Review*, **130**, 1573-1592.
127. Mohanty, U.C., M. Mandal and S. Raman, 2004: Simulation of Orissa super cyclone (1999) using PSU/NCAR meoscale model, *Natural Hazards*, **31**, 373-390.

128. Rao, G.V., and D.V.B. Rao, 2003: A review of some observed mesoscale characteristics of tropical cyclones and some preliminary numerical simulations of their kinematics features, *Proc. of Ind. Nat. Sci. Acad.*, **69A**, 5, 523-541.
129. Trivedi, D.K., J. Sanjay and S.S. Singh, 2002: Numerical simulation of a super cyclonic storm, Orissa (1999): Impact of initial conditions, *Meteorol. Appl.*, **9**, 367-376.
130. Yang, M-J., and L. Ching, 2005: A modeling study of typhoon Toraji (2001): Physical parameterization sensitivity and topographic effect, *Terrestrial, Atmospheric and Oceanic Sciences*, **16**(1), 177-213.
131. Lin, I.-I., C.H. Chen, I.F. Pun, W.T. Liu and C.C. Wu., 2008: Warm ocean anomaly, air sea fluxes, and the rapid intensification of tropical cyclone Nargis (2008), *Geophysical Research Letter*, **36**, L03817, doi: 10.1029/2008GL035815,2009.
132. Price, J.F., R.A. Weller and R. Pinkel, 1986: Diurnal cycling: Observations and models of the upper ocean response to diurnal heating, cooling, and wind mixing, *J. Geophysical Research*, **91**, 8411-8427.
133. K. Prasad, Monsoon Forecasting using Numerical Weather prediction Guidance, SAARC Meteorological Research Centre (SMRC), Report No. 11 (2005).
134. M. N. Islam and H. Uyeda, *Remote Sensing of Environment* 108, 264 (2006).
doi:10.1016/j.rse.2006.11.011
135. M. A. E. Akhter, M. A. Hossain and Md. Mahbub Alam, Sensitivity study of the comulus parameterization schemes with planetary boundary layer option in estimating rainfall in Bangladesh using MM5, *Prime University Journal of Multidisciplinary Quest*, Volume -5, Number-1, January-June 2011.

